

# **Application of Gold Catalysis in the Synthesis of Seven-Membered Ring Systems**

Dissertation zur Erlangung des mathematisch-naturwissenschaftlichen  
Doktorgrades

"Doctor rerum naturalium"

der Georg-August-Universität Göttingen

im Promotionsprogramm Chemie

der Georg-August University School of Science (GAUSS)

vorgelegt von

Kristin Sprenger

aus Göttingen

Göttingen, 2022

Betreuungsausschuss:

Prof. Dr. Manuel Alcarazo, Institut für Organische und Biomolekulare Chemie, Tammannstr. 2, 37077 Göttingen

Prof. Dr. Dietmar Stalke, Institut für Anorganische Chemie, Tammannstr. 4, 37077 Göttingen

Prof. Dr. Shoubik Das, Universität Antwerpen, Groenenborgerlaan 171, 2020 Antwerpen, Belgien

Mitglieder der Prüfungskommission:

Referent: Prof. Dr. Manuel Alcarazo, Institut für Organische und Biomolekulare Chemie, Tammannstr. 2, 37077 Göttingen

Korreferent: Prof. Dr. Dietmar Stalke, Institut für Anorganische Chemie, Tammannstr. 4, 37077 Göttingen

Weitere Mitglieder der Prüfungskommission:

Prof. Dr. Ricardo Mata, Institut für Physikalische Chemie, Tammannstr. 6, 37077 Göttingen

Jun.-Prof. Dr. Johannes C. L. Walker, Institut für Organische und Biomolekulare Chemie, Tammannstr. 2, 37077 Göttingen

Dr. Holm Frauendorf, Institut für Organische und Biomolekulare Chemie, Tammannstr. 2, 37077 Göttingen

Dr. Alessandro Bismuto, Institut für Organische und Biomolekulare Chemie, Tammannstr. 2, 37077 Göttingen

Tag der mündlichen Prüfung: 16. Februar 2023

Die vorliegende Arbeit entstand unter Anleitung von Prof. Dr. Manuel Alcarazo in der Zeit von April 2018 bis Dezember 2022 an der Georg-August-Universität zu Göttingen.

Teile dieser Arbeit wurden bereits veröffentlicht:

K. Sprenger, C. Golz, M. Alcarazo, *Eur. J. Org. Chem.* **2020**, 6245–6254.

M. Zhao, A.G. Barrado, K. Sprenger, C. Golz, R.A. Mata, M. Alcarazo, *Org. Lett.* **2020**, 22, 4932-4937.

Ich versichere, dass ich die eingereichte Dissertation selbstständig verfasst und keine anderen als die angegebenen Quellen und Hilfsmittel benutzt, sowie Zitate kenntlich gemacht habe.

---

Kristin Sprenger



## Danksagung

Zuallererst gilt mein Dank Prof. Dr. Manuel Alcarazo für die Aufnahme in seine Arbeitsgruppe und die Gelegenheit meine Promotion unter seiner Betreuung durchzuführen. Ich möchte ihm besonders dafür danken, dass er sich stets die Zeit genommen hat Ideen, aber auch eventuelle Probleme zu erörtern und mir mit hilfreichen Anregungen zur Seite zu stehen. Darüber hinaus hat er sich unermüdlich dafür eingesetzt die bestmöglichen Arbeitsbedingungen zu schaffen und durch die Organisation von Gruppenaktivitäten eine angenehme Atmosphäre innerhalb der Gruppe zu gestalten.

Außerdem möchte ich Prof. Dr. Dietmar Stalke danken, dass er die Rolle des Zweitbetreuers übernommen und stets reges Interesse an meinem Thema gezeigt hat. Mein Dank gilt auch Prof. Dr. Das, der trotz seines Umzugs nach Belgien stets ansprechbar war.

Des Weiteren möchte ich mich bei Prof. Dr. Ricardo Mata, Jun.-Prof. Johannes C. L. Walker, Dr. Holm Frauendorf und Dr. Alessandro Bismuto für die Teilnahme an meinem Disputationskomitee bedanken.

Weiterhin gilt mein Dank den Mitarbeitern des Arbeitskreises. Vor allem möchte ich mich bei Martina Pretor und Martin Simon bedanken, die mir jederzeit mit Rat und Tat zu Seite standen und eine einwandfreie technische Betreuung gewährleisteten. Darüber hinaus möchte ich mich bei Angela Heinemann und Sabine Schacht für die Hilfe mit organisatorischen Dingen und bürokratischen Hürden bedanken. Dr. Christopher Golz danke ich für die Messung meiner kristallographischen Proben und das Lösen der Strukturen.

Ich danke den Mitarbeitern der NMR- und Massenspektrometrie Abteilung für das Messen und die gewissenhafte Bearbeitung zahlreicher Proben.

Für das Korrekturlesen dieser Arbeit beziehungsweise Teilen davon und den damit verbundenen Anregungen und Verbesserungsvorschlägen möchte ich mich bei Dr. Christopher Golz, Dr. Valentina Pelliccioli, Simon Karnbrock und Martin Simon bedanken.

Mein Dank gilt außerdem allen derzeitigen und ehemaligen Mitgliedern der Alcarazo Gruppe für die angenehme Atmosphäre und die zahlreichen Unternehmungen, die ich die letzten Jahre sehr genossen habe. Besonders möchte ich mich bei meinen Laborkollegen Dr. Tim Johannsen, Dr. Christian Rugen, Hoang Dung Doan und Daniel Rösch bedanken. Die Auswahl der Musik und der Austausch über die verschiedensten Themen haben immer zu einer guten Stimmung beigetragen und für einen angenehmen Laboralltag gesorgt. Ich

möchte außerdem meinem Bachelorstudenten Kevin Klein und meiner Masterstudentin Mingyue Zhao für die großartige Zusammenarbeit und die Unterstützung im Labor danken.

Bedanken möchte ich mich auch bei meinen Freunden für die zahlreichen Erlebnisse, Aktivitäten und Urlaube. Diese Auszeiten fernab der Chemie habe ich sehr genossen und haben gutgetan, um mal abschalten zu können.

Schließlich gilt mein besonderer Dank meiner Familie, auf deren Unterstützung mich in den letzten Jahren uneingeschränkt verlassen konnte. Besonders bedanken möchte ich mich bei Alexander Marx, der mir immer den Rücken freigehalten hat und uneingeschränktes Verständnis zeigte.

## Abbreviations

[Au]	generic gold species	DFT	density functional theory
Å	Angstrom	<i>e.g.</i>	<i>exempli gratia</i> / for example
Ac	acetyl	EI	Electron impact ionization
aq.	aqueous	Et	ethyl
Ar	aryl	EtOH	ethanol
ATR	attenuated total reflection	<i>ee</i>	enantiomeric excess
Bn	benzyl	<i>eq</i>	equivalent
br	broad (NMR)	eV	electronvolt
Bu	butyl	<i>et al.</i>	<i>et alii</i> /and others
CAAC	cyclic(alkyl)(amino)carbene	EXSY	exchange spectroscopy
cat.	catalytic	h	hours
conc.	concentrated	HOMO	highest occupied molecular orbital
CO	carbon monoxide	HPLC	high performance liquid chromatography
COD	1,5-cyclooctadiene	HR-MS	high resolution mass spectrometry
Cy	cyclohexyl	Hz	hertz
δ	chemical shift	<i>iPr</i>	isopropyl
d	days	IR	infrared spectroscopy
d	doublet (NMR)	<i>J</i>	coupling constant (NMR)
dd	doublet of doublets (NMR)	J	Joule
ddd	doublet of doublet of doublets (NMR)	K	Kelvin
DCE	1,2-dichloroethane	L	ligand
DCM	dichloromethane	LUMO	lowest unoccupied molecular orbital
ddt	doublet of doublet of triplets (NMR)	M	generic metal

m	multiplet (NMR)	R	general residue
M	molar (mol L <sup>-1</sup> )	R <sub>f</sub>	retention factor
<i>m</i>	<i>meta</i>	rt	room temperature
min	minutes	s	singlet (NMR)
MeOH	methanol	sat.	saturated
Mes	mesityl	sext	sextet (NMR)
MHz	Megahertz	Sphos	2-Dicyclohexylphosphino-2',6'-dimethoxybiphenyl
m.p.	melting point	<i>t</i>	time
<i>m/z</i>	mass to charge ratio	<i>T</i>	temperature
$\tilde{\nu}$	wavenumber	t	triplet (NMR)
NBS	<i>N</i> -bromosuccinimide	<i>t</i> Bu	<i>tert</i> -butyl
<i>n</i> Bu	<i>n</i> -butyl	TADDOL	$\alpha,\alpha,\alpha',\alpha'$ -tetraaryl-1,3-dioxolane-4,5-dimethanol
NHC	<i>N</i> -heterocyclic carbene	td	triplet of doublets (NMR)
NMR	nuclear magnetic resonance	TEP	Tolman electronic parameter
NOE	nuclear overhauser effect	Tf	trifluoromethanesulfonyl
Nu	nucleophile	THF	tetrahydrofuran
N.R.	no reaction	TIPS	triisopropylsilyl
<i>o</i>	<i>ortho</i>	TLC	thin-layer chromatography
ovn	overnight	TMS	trimethylsilyl
<i>p</i>	<i>para</i>	tt	triplet of triplets (NMR)
<i>p</i> -TsOH	<i>p</i> -toluenesulfonic acid	UV-VIS	ultraviolet and visible light
Ph	phenyl	<i>v/v</i>	volume fraction
PPh <sub>3</sub>	triphenylphosphine	XPhos	dicyclohexyl[2',4',6'-tris(propan-2-yl)][1,1'-biphenyl]-2-yl]phosphane
Pr	propyl		
q	quartet (NMR)		
quant.	quantative		



# Table of contents

1. Introduction .....	1
1.1 Brønsted-Lowry vs. Lewis theory .....	1
1.2 $\pi$ -Acid catalysis based on gold and platinum.....	2
1.2.1 General properties of gold and platinum .....	2
1.2.2 Synthetic applications of gold and platinum catalysis.....	6
1.3 Cationic phosphines.....	12
1.3.1 Bonding situation .....	14
1.3.2 Evaluation of the donor abilities of $\alpha$ cationic phosphines.....	15
1.3.3 Synthesis of $\alpha$ cationic phosphines.....	18
1.3.4 Application of $\alpha$ cationic phosphines in catalysis .....	23
1.4 Seven-membered ring systems.....	30
1.4.1 Synthesis of seven-membered ring systems.....	31
1.4.2 Conformational stability of seven-membered ring systems .....	37
1.5 Planar-chiral ferrocenes .....	39
2. Project proposal .....	42
3. Results and discussion.....	44
3.1 Synthesis of seven-membered ring systems .....	44
3.1.1 Synthesis of precursors .....	45
3.1.2 Comparison between Brønsted acid and Au catalysis .....	54
3.1.3 Kinetic studies .....	59
3.1.4 Application of catalyst C in the synthesis of cycloheptatrienes, oxepines, thiepinines and silepinines .....	61
3.2 Structural analysis of seven-membered ring systems .....	66
3.3 Exploration of configurational stability of seven-membered ring systems .....	74
3.3.1 Dynamic HPLC experiments.....	74
3.3.2 Dynamic NMR spectroscopy .....	79
3.3.3 Density-functional theory (DFT) methods .....	83
4. Summary.....	95
5. Experimental .....	97

5.1 General remarks.....	97
5.2 Synthesis and characterization of new compounds .....	98
5.2.1 1-(benzyl)-2-ethynylbenzenes 150 .....	98
5.2.2 1-(oxyaryl)-2-ethynylbenzenes 151 .....	103
5.2.3 1-(thioaryl)-2-ethynylbenzenes 152.....	120
5.2.4 1-(silaaryl)-2-ethynylbenzenes 153 .....	125
5.2.5 Ferrocene-containing precursors .....	130
5.2.6 Intramolecular cyclization of precursors 150a-d, 151a and 152a employing Brønsted acid catalysis .....	134
5.2.7 Intramolecular cyclization of precursors 150, 151, 152 and 153 employing gold catalysis.....	137
5.3 Kinetic experiments <i>via</i> <sup>1</sup> H-NMR.....	148
5.4 Enantioselective dynamic HPLC.....	149
5.5 Dynamic NMR experiments.....	156
5.6 Computational details .....	162
6. References .....	163
7. Appendix.....	171
7.1 Crystallographic details .....	171
7.2 NMR spectra .....	195
7.3 Atomic coordinates for DFT calculations.....	304



# 1. Introduction

## 1.1 Brønsted-Lowry vs. Lewis theory

As an introduction to the topic of  $\pi$ -acid catalysis, basic concepts that allow the classification of substances into acids and bases will be considered first. In 1923, Johannes Brønsted<sup>[1]</sup> and Thomas Lowry<sup>[2]</sup> independently developed a concept for acids and bases. According to this theory, an acid is a proton ( $H^+$ ) donor and a base is a proton acceptor. Acids and bases can consist of molecules or ions. In a typical acid-base reaction (**Figure 1**), the acid HA loses a proton and becomes the corresponding base  $A^-$ , while the base B accepts the proton and becomes the corresponding acid  $BH^+$ . Since the reaction is reversible, an equilibrium is formed.

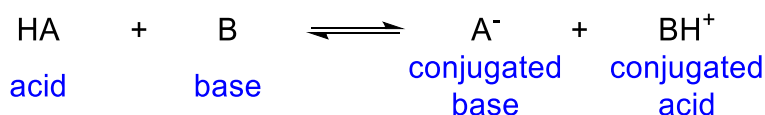


**Figure 1:** Example of an acid-base reaction according to the Brønsted-Lowry theory.

In the same year, Gilbert N. Lewis<sup>[3]</sup> introduced an extended acid-base concept that is independent of the  $H^+$  ion. According to Lewis, a base (molecule or ion) has a lone pair of electrons that can be used to form a coordinative covalent bond to another atom, molecule or ion. An acid contains an empty orbital and can accept an electron pair of a Lewis base to form a Lewis adduct. Therefore, Lewis acids are considered as electron pair acceptors and Lewis bases as electron pair donors. An example for a reaction that is not regarded as an acid-base reaction by the theory of Brønsted-Lowry is the reaction of boron trifluoride ( $BF_3$ ) with a base ( $F^-$ ).

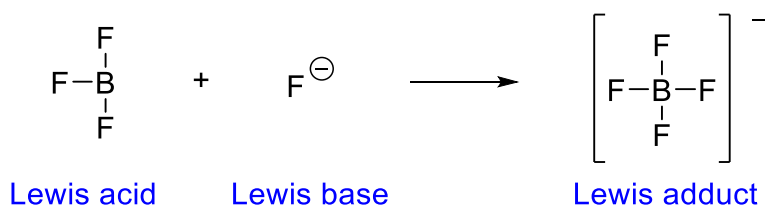


**Figure 2:** Reaction of a Lewis acid and a Lewis base resulting in a Lewis adduct.

While a substance defined as a base by Brønsted is also a base in the Lewis concept, acids according to Lewis comprise a much larger number of substances. A Lewis acid must have an empty orbital, which can be occupied by the electron pair of the base. Lewis acids include the following species: molecules or atoms with incomplete electron octet (e.g.  $BF_3$ ,  $AlCl_3$ ), simple cations (e.g.  $H^+$ ,  $Cu^{2+}$ ,  $Fe^{3+}$ ), atoms of some metals (e.g. Ni in the formation of nickel tetracarbonyl), and compounds of elements which valence shell can be extended beyond the electron octet (e.g.  $SiF_4$ ,  $SnCl_4$ ,  $PF_5$ ). To further classify Lewis acids and bases Ralph

## 1.2 $\pi$ -Acid catalysis based on gold and platinum

Pearson<sup>[4]</sup> implemented the concept of “hard and soft acids and bases” (HSAB). “Hard” in this context describes species (atoms, ions and molecules) that have a high charge density, i.e., a high charge and a small radius. “Soft”, on the other hand, refers to species with low charge density, i.e., with low charge and large radius. Moreover, “hard” species are difficult to polarize while “soft” species are easily polarizable. Based on this HSAB concept, a qualitative description of predominant factors controlling both reactions and chemical properties could be provided. Especially in transition metal chemistry, attempts have been made to relate the arrangement of ligands and transition metal ions to their softness and hardness.

### 1.2 $\pi$ -Acid catalysis based on gold and platinum

These fundamental principles described in the previous section play a very important role in the description of  $\pi$ -acid catalysis. Within this concept every metal cation and cationic metal complex bearing an available LUMO or reactive vacant orbital is categorized as “Lewis acid”.<sup>[3]</sup> The term “ $\pi$ -acid catalysis” describes the activation of  $\pi$  bonds using carbophilic Lewis acids such as Au(I) or Pt(II). More than 30 years ago, Ito and Hayashi were already able to achieve high selectivity with Lewis acids based on Au(I) in an asymmetric aldol reaction.<sup>[5]</sup> However, it took until the beginning of the 21st century until the research interest in Lewis acid catalysts based on noble metals, mainly Pt and Au, increased.<sup>[6,7]</sup> Prior to addressing the synthetic applications of gold and platinum catalysis, it is useful to take a closer look at the properties of the metals themselves.

#### 1.2.1 General properties of gold and platinum

In order to understand the electronic properties, which are closely related to the coordination behavior of heavy elements, such as the late transition metals gold and platinum, it is crucial to consider relativistic effects. In case of gold the relativistic effects are larger as for its neighbors in the periodic table and as for any element with  $Z < 100$ .<sup>[8]</sup> The mass increase caused by the high velocities of electrons when moving near a heavy nucleus leads to contraction of the atomic s and p orbitals. As a result of the contracted core orbitals the d and f orbitals are more shielded from the nuclear charge and expand in consequence.<sup>[8,9]</sup> The calculated relativistic contraction of the 6s orbital depending on the atomic number  $Z$  can be seen in **Figure 3** (left) and shows that, in addition to gold, platinum and mercury are also strongly affected. When comparing the orbital energies of gold and silver in their diatomic hydrides, the influence of relativistic effects become even clearer (**Figure 3**, right). The nonrelativistic energies (NR) of the 5s and 4d orbitals in AgH and the 6s and 5d orbitals

## 1. Introduction

in AuH are comparable. Hence, their chemical properties should be similar as well. In contrast, the relativistic (R) calculation yields for the 6s contraction and lowering in energy, while the  $5d_{5/2}$  is shifted higher in energy and becomes more diffuse. This results in a stronger  $\sigma$ -bond in AuH, since it is formed by the 6s orbital of the gold.<sup>[9]</sup>

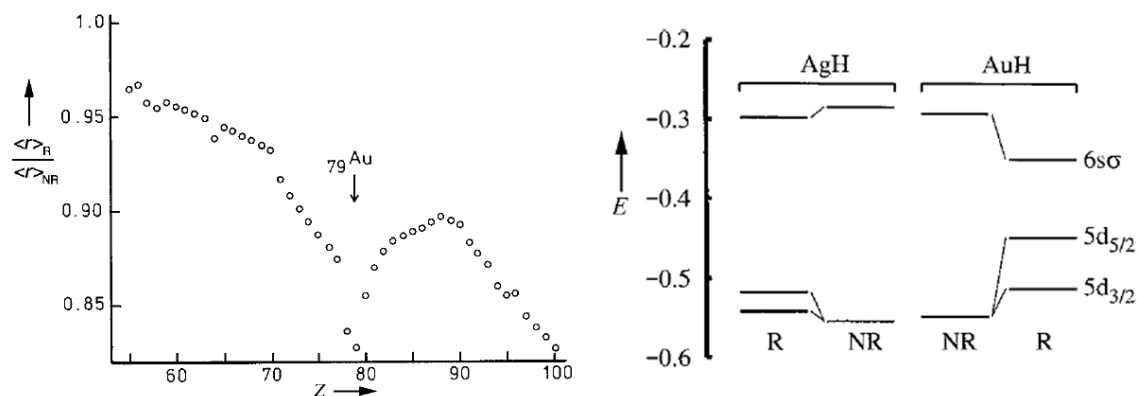


**Figure 3:** The ratio between relativistic (R) and nonrelativistic (NR) 6s orbital radii (left) and the comparison of AgH and AuH orbital energies with (R) and without (NR) relativistic effects (right).<sup>[9]</sup>

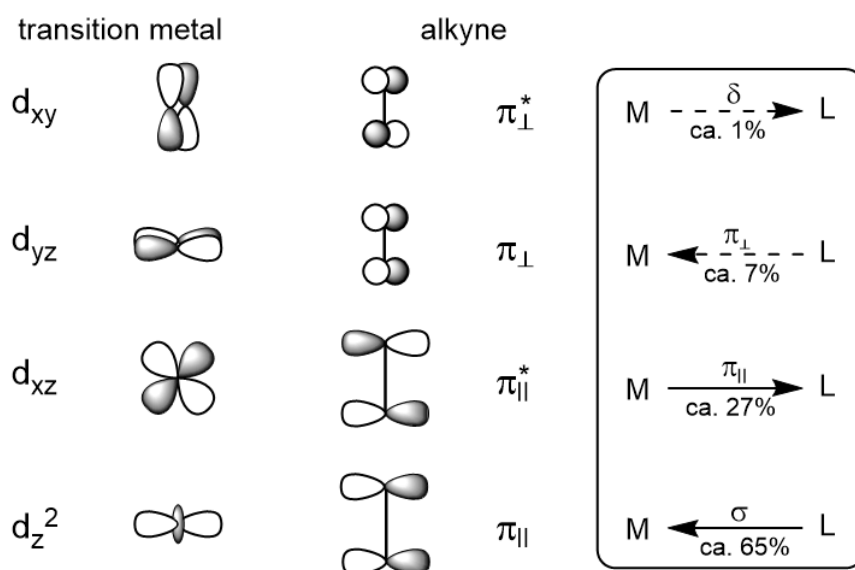
As a consequence of these relativistic effects, Au(I) and other related transition metal cations with the diffuse character of the d orbitals are considered as soft carbophilic Lewis acids. Such bond contractions can shorten the metal-ligand bond and thus improve the orbital overlap and increase the bond strength.<sup>[6]</sup>

The color of gold is also explained by relativistic effects. Excitation of the 5d electrons through absorption of blue light to Fermi level (bandgap 2.38 eV) results in the golden color. On the contrary, for silver the bandgap is much larger and no visible light is absorbed.<sup>[10]</sup>

Since gold/Au(I) and platinum/Pt(II) complexes are considered as soft nucleophiles they are predestined to activate soft nucleophiles, such as carbon-carbon multiple bonds.<sup>[10]</sup> The Dewar-Chatt-Duncanson model, which considers the bond as a donor-acceptor interaction between two closed shell fragments, can be utilized to interpret the bonding interactions between transition-metal complexes and alkynes or alkenes. According to this model a  $\sigma$  bond is formed by donation of electron density from the ligand to an empty orbital on the metal of appropriate symmetry and  $\pi$  interactions arise through back donation from filled metal orbitals to an antibonding  $\pi^*$  orbital. With computational analyses the contribution of the four interactions describing the bonding of alkynes as ligands in  $d^8$ -platinum and  $d^{10}$ -gold complexes could be investigated as shown in **Scheme 1** and deconvoluted into partial orbital-orbital interactions. The alkyne donates electron density from the in-plane  $\pi_{||}$  orbitals to the vacant  $d_z^2$  orbital of the metal forming a  $\sigma$  bond, which accounts for ca. 65% of the interactions. Moreover, back donation can occur between the  $d_{xy}$  orbital of the metal and the antibonding in-plane  $\pi_{||}^*$  orbital of the alkyne contributing with ca. 27%. The contribution

## 1.2 $\pi$ -Acid catalysis based on gold and platinum

of the orthogonal, out-of-plane  $M \leftarrow L$   $\pi$  interaction (ca. 7%) and the  $M \rightarrow L$   $\delta$  back donation (ca. 1%) resulting from mixing of the occupied  $d_{xy}$  orbital of the metal and the empty  $\pi_{\perp}^*$  of the alkyne can be neglected.



**Scheme 1:** Interaction between the orbitals of a transition metal and an alkyne ligand and the contributions of the individual term.<sup>[6]</sup>

In addition to describing the bonding situation of transition-metals and alkynes or alkenes with the Dewar-Chatt-Duncanson model, electrostatic interactions should not be ignored. High-level computational studies indicated that electrostatic interactions account for roughly half of the bonding force in  $[M^+(C_2H_4)]$  and  $[M^+(C_2H_2)]$  ( $M=Ag, Au$ ).<sup>[6]</sup> According to the Dewar-Chatt-Duncanson model electron density from the alkyne or alkene is donated to the metal and additionally the antibonding  $\pi^*$  orbital is populated resulting in an elongation of the carbon-carbon bond as well as a partial pyramidalization (alkynes) and bending (alkenes). This deviations from the idealized geometry compared to the uncoordinated ligand could be used to predict the extend of back bonding. The following structures were analyzed in the past to compare the differences between the free and the coordinated ligand in the resulting  $\pi$  complexes (**Figure 4**). The first example is Zeise's salt  $K[PtCl_3(C_2H_4)]$  (**1**) in which ethylene is coordinated to a  $Cl_3Pt^+$  fragment. Only minor changes in the geometry of ethylene are observed and a small increase of the bond length from 1.35 Å in free ethylene compared to 1.37 Å in the complex. These observations show that ethylene is a strong  $\sigma$  donor but a poor  $\pi$  acceptor.<sup>[11]</sup> In line with these results were the studies of Fürstner and coworkers on cyclododecyne (**2**) and the corresponding Au(I) complex **3**. They could show that upon coordination of Au(I) to cyclododecyne (**2**) structural changes were observed. The  $C\equiv C$  bond was elongated from 1.196(4) Å to 1.224(5) Å and the  $C\equiv C-CH_2$ -bond angle was decreased from 175.9(9)° to 165(1)°.<sup>[12]</sup>

## 1. Introduction

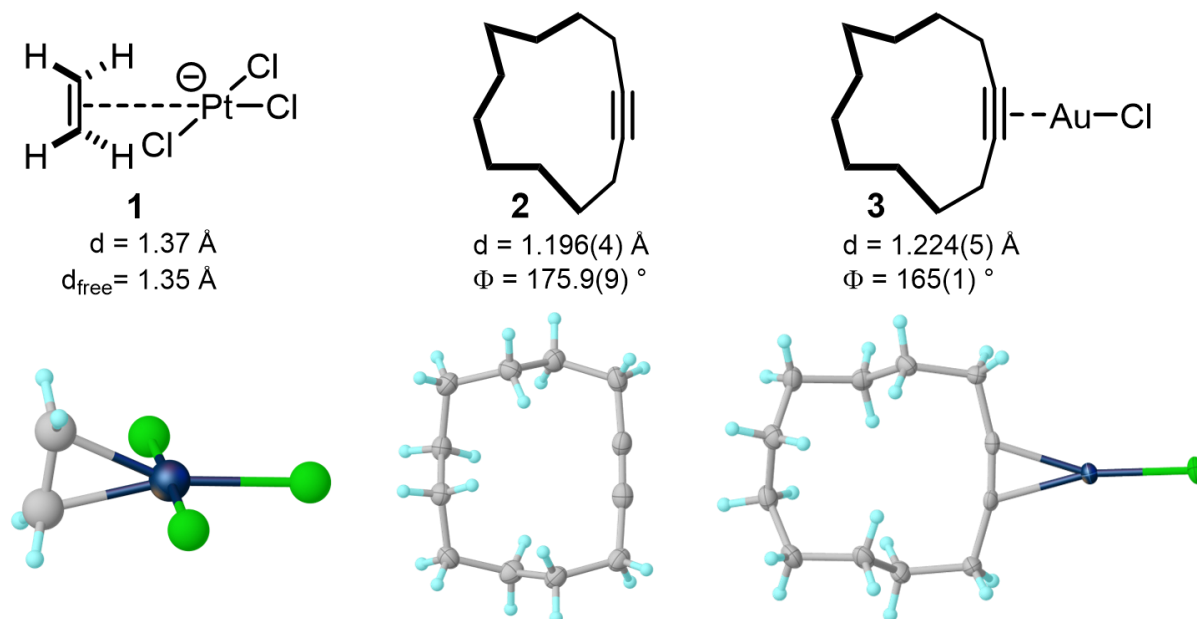
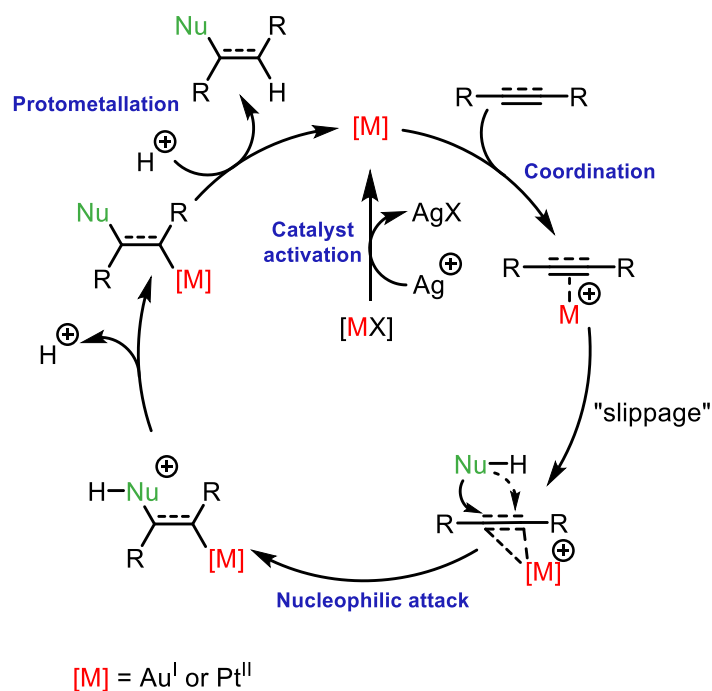


**Figure 4:** Schematic and solid state structures of Zeise's salt (**1**), cyclododecyne (**2**) and the corresponding Au(I) complex **3**,  $d$  denotes the C-C multiple bond length and  $\Phi$  refers to the C≡C-CH<sub>2</sub>-bond angle.

The general catalytic cycle of  $\pi$ -acid catalyzed transformations contains three elementary steps (**Scheme 2**). Often the active catalyst is generated by abstracting a ligand X to offer a coordination vacancy for the substrate to enter. Depending on the ligand X different types of activation are possible. When X is a halide it is typically scavenged *in situ* using a silver salt and the silver halide precipitates (as shown in **Scheme 2**).<sup>[6,13]</sup>



**Scheme 2:** General mechanism for the activation of multiple bonds by  $\pi$  acids as proposed by Fürstner<sup>[6,14]</sup> and Echavarren.<sup>[15]</sup>



## 1.2 $\pi$ -Acid catalysis based on gold and platinum

However, it should be remembered that silver additives do not act catalytically innocent and can change the outcome of  $\pi$ -acid catalyzed reactions in terms of selectivity and/or yield (“silver effect”).<sup>[16]</sup> To circumvent the use of silver salts, complexes can be used in which a weakly donating ligand such as acetonitrile<sup>[17]</sup> or bis(trifluoromethanesulfonyl)amide<sup>[18]</sup> is directly displaced by  $\pi$ -coordination of the substrate. Another silver-free method uses complexes such as [LAu(Me)] bearing an anionic ligand to generate the catalytically active species *via* protonation by a strong Brønsted acid.<sup>[19]</sup>

After activation of the precatalyst the catalytically active species coordinates the alkyne or alkene. By slippage of the metal, which means changing the coordination from  $\eta^2$  to  $\eta^1$ , partial carbocations are formed and the nucleophile attacks at one of these positions. The selectivity of this step is influenced by the substituents and the ancillary ligand. After the nucleophilic attack, a protodemetalation takes place. The product is released and the active catalyst is regenerated. Under aprotic conditions, the catalytic cycle could be completed by suitable electrophiles. No change in the oxidation state of the metal is observed along the complete catalytic cycle.<sup>[6,14]</sup>

Further investigations were conducted to explain the high selectivity in Au(I)- and Pt(II)-catalyzed reactions towards the nucleophilic attack on the alkyne compared to alkenes also called “alkynophilicity”. Computational studies on the bonding situation of Au(I)-ethylene and Au(I)-ethyne indicated that ethylene is a better  $\sigma$  donor and the ethylene complex is considered to be better stabilized than the ethyne complex. Thus, this effect of “alkynophilicity” is assumed to be kinetic in origin.<sup>[6,10]</sup>

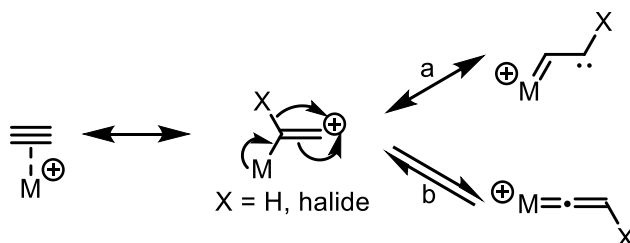
### 1.2.2 Synthetic applications of gold and platinum catalysis

From a preparative point of view these two noble metals combine several advantages. Transformations using gold or platinum catalysts are operationally safe and do not necessitate strict inert conditions in general. Furthermore, they show high functional group tolerance and outstanding chemoselectivity towards C-C multiple bonds. Thus, activated  $\pi$  systems in alkynes, alkenes and allenes have been shown to be subsequently attacked by several O-, N-, S- and C-centered nucleophiles underlining the broad application of this methodology.<sup>[6,13,20]</sup>

Initial work in this field was conducted with metal salts such as PtCl<sub>2</sub>, AuCl and AuCl<sub>3</sub>. As platinum and gold have different potential for backdonating electron density to the alkyne, diverging results could be observed for the same reaction by changing the oxidation state of the metal. Alkynes activated by Au(III) usually undergo direct nucleophilic attack at the

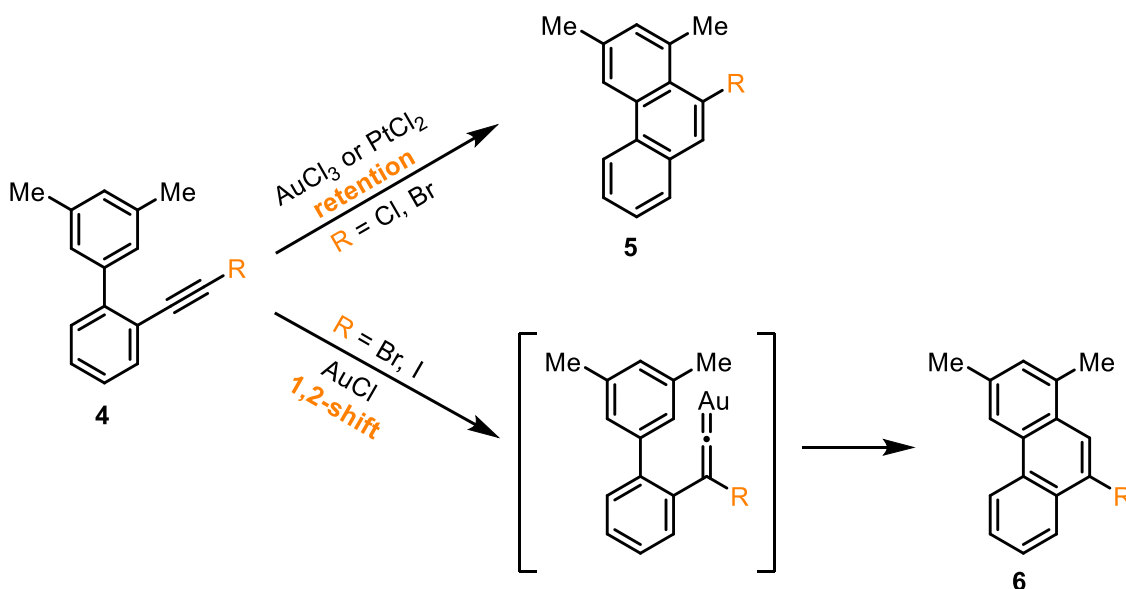
## 1. Introduction

vicinal position, whereas for Au(I) the formation of metal-vinylidene intermediates is enabled (**Scheme 3**, pathway b). As this formation is caused by a larger extent of  $\pi$ -backdonation, this results commonly in a 1,2-migration of a hydride or halide and the attack on the metal bound carbon atom leading to different regioisomeric outcomes as compared to Au(III).<sup>[6]</sup>



**Scheme 3:** Possible pathways in the activation of an alkyne by gold or platinum.

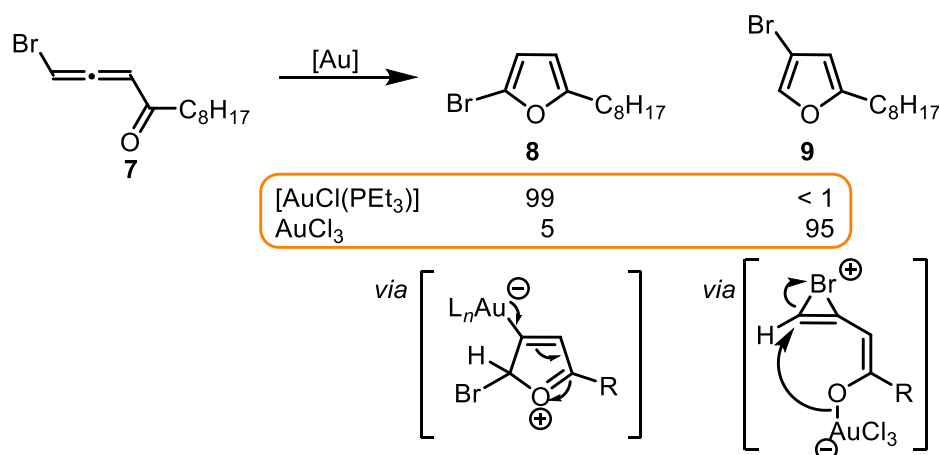
The Fürstner group published the first example in which different regioisomers were observed when gold catalysts in different oxidation states were used (**Scheme 4**).<sup>[21]</sup> For Au(III) the expected 10-halophenanthrenes **5** were obtained following a Friedel-Crafts-type hydroarylation of the triple bond in *ortho*-substituted biphenyls **4**. When utilizing Au(I) instead, the formation of 9-halophenanthrenes **6** was observed assuming a metal-vinylidene as intermediate. These results illustrate how sensitive a catalytic system can be in respect of apparently minor changes and that alternative reaction pathways can be generated.



**Scheme 4:** Regioisomeric outcomes in the synthesis of phenanthrenes depending on the oxidation state of Au.

Another example published by the group of Gevorgyan emphasizes the different properties of Au(I) and Au(III) as well. In their synthesis of halofurans **8** and **9** by cycloisomerization of bromoallenylketones **7** variable outcomes were discovered (**Scheme 5**).<sup>[22]</sup>

## 1.2 $\pi$ -Acid catalysis based on gold and platinum



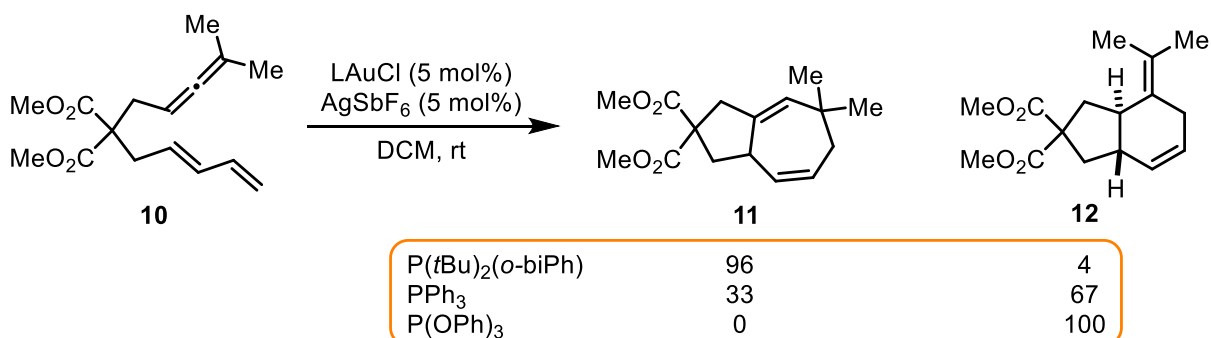
**Scheme 5:** Dichotomy in the behavior of Au(I) and Au(III) in the synthesis of halofuranes **8** and **9**.

Considering the HSAB concept the softer Au(I) activates the distal and soft double bond towards intramolecular attack of the oxygen to form regioisomer **8**. On the contrary, using Au(III) an intramolecular Michael addition of the bromine into the enone part generates a bromonium ion whereas the Au(III) coordinates to the oxygen and the other regioisomer **9** was obtained.

In addition to changing the oxidation state of the gold, the reactivity and regioselectivity can be tuned by the choice of ligands. Phosphines and *N*-heterocyclic carbenes are the most commonly used ligands. Their design can influence both the steric and electronic properties of the resulting gold complex. Compared to phosphine ligands, phosphites are less donating and generate more electrophilic catalysts, while *N*-heterocyclic carbenes are more donating and thus less electrophilic catalysts are obtained. In contrast, only a few ligands find application in platinum catalysis. Suitable ligands are mostly electron withdrawing and kinetically labile such as COD and CO.<sup>[6,13]</sup>

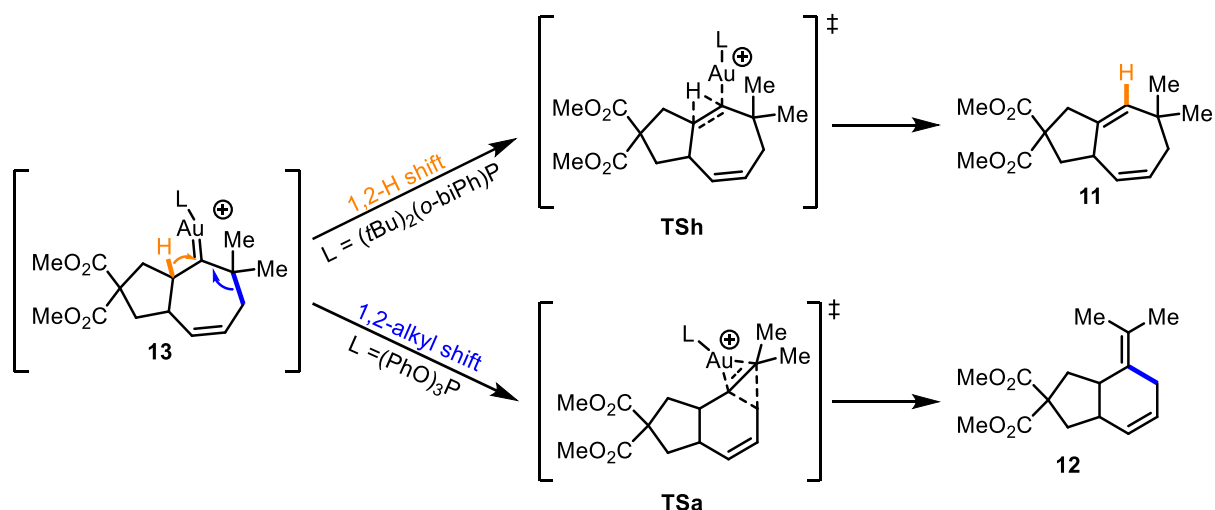
The Toste and the Mascareñas group studied the influence of steric and electronic properties of the ancillary ligand on Au(I)-catalyzed cycloadditions. By varying the ligands in the cycloaddition of allenedienes **10** either the [4+2] or the [4+3] cycloaddition could be favored (**Scheme 6**).<sup>[23,24]</sup> The Toste group assumed that the selectivity is dependent on the stability of the cationic transition states in the course of the reaction. When using the electron-rich di-*tert*-butylbiphenylphosphine  $\sigma$  donor ligand predominantly the [4+3] product **11** was obtained, whereas when an electron deficient phosphite ligand was employed the stability of the gold(I) carbenoid intermediate might be decreased leading exclusively to the [4+2] product **12**.<sup>[24]</sup> Similar observations regarding the selectivity were made by the group of Mascareñas who analyzed the divergence of allenedienes with a sulfonamide tether in cycloadditions.<sup>[23]</sup>

## 1. Introduction



**Scheme 6:** Product distribution dependent on the ligand in cycloaddition of allenediene **10**.

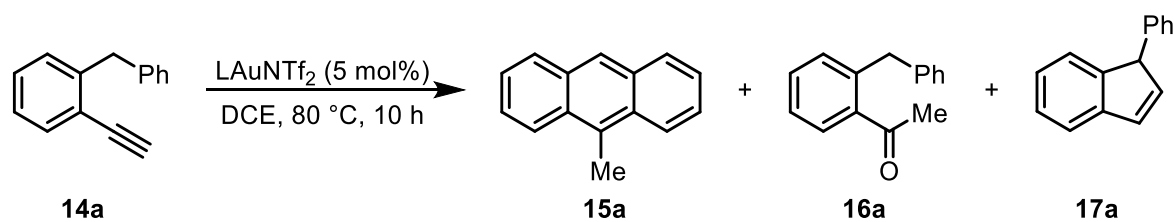
DFT calculations and mechanistic studies of both groups suggested a concerted [4+3] mechanism to form intermediate **13**, which is identical for both reaction pathways (**Scheme 7**). Moreover, electron-donating ligands were shown to favor the 1,2-hydride shift pathway, whereas  $\pi$  acceptor ligands such as phosphites facilitated 1,2-carbon migration. It was assumed that electronic factors such as interactions between the newly formed double bond in the transition states and the electrophilic gold atom might play a key role. The *exocyclic* double bond formed in the ring contraction pathway can simply change orientation in order to maximize the donation of electron density from the occupied  $\pi$  orbitals to the gold center, thus an acceptor ligand favors the transition state **TSa**. In contrast, the *endocyclic* double bond in **TSh** is more conformationally constrained, so this transition state is not specifically preferred by very electrophilic gold complexes. [23–25]



**Scheme 7:** Intermediate **13** for the [4+2] and [4+3] pathway.

Another interesting example where the choice of catalyst system led to different reaction results was published by Ye and coworkers.<sup>[26]</sup> They studied the cyclization of *o*-alkynyldiarylmethanes **14** by comparing different  $\pi$ -acid catalysts and also using a combination of Brønsted acid and Au catalysis. Starting from *o*-alkynyldiphenylmethane **14a** as a model substrate, they optimized the reaction conditions (**Scheme 8**).

## 1.2 $\pi$ -Acid catalysis based on gold and platinum



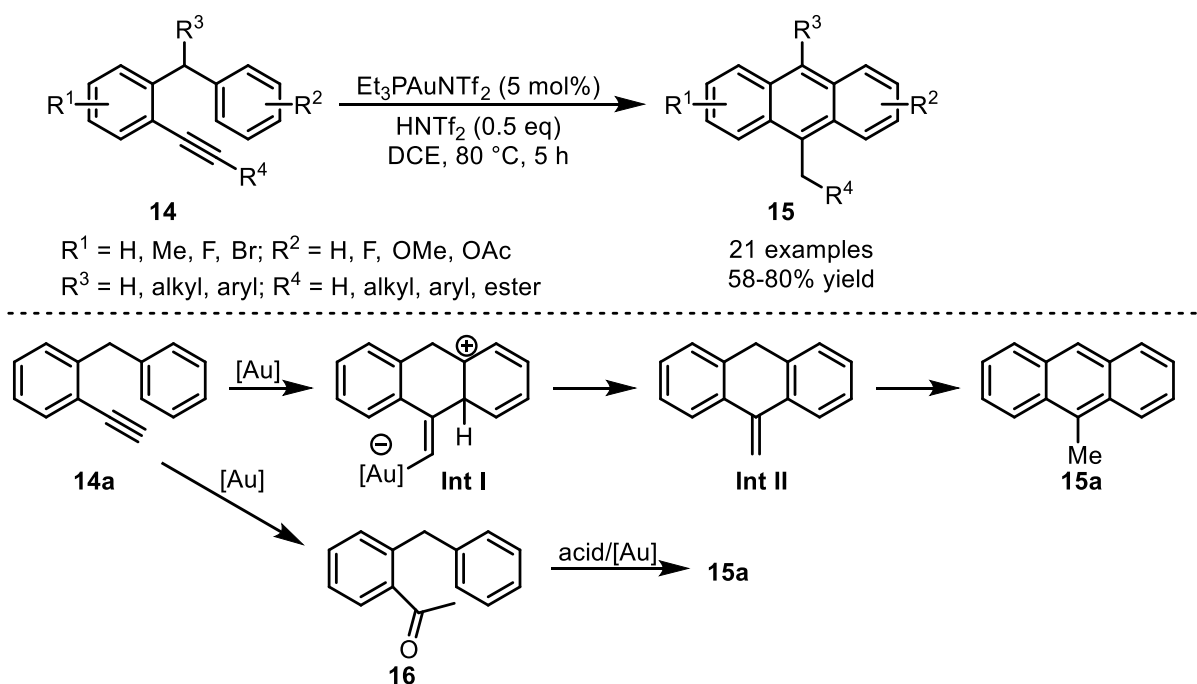
catalyst	acid	yield [%]		
		<b>15a</b>	<b>16a</b>	<b>17a</b>
$\text{Ph}_3\text{PAuNTf}_2$		51	17	6
XPhosAuNTf <sub>2</sub>		13	26	11
$(\text{C}_6\text{F}_5)_3\text{PAuNTf}_2$		53	12	<1
$\text{Et}_3\text{PAuNTf}_2$		65	10	<1
$\text{Et}_3\text{PAuNTf}_2$	0.5 eq. HNTf <sub>2</sub>	78	<1	<1
$\text{Et}_3\text{PAuNTf}_2$	0.5 eq. HNTf <sub>2</sub>	77	<1	<1
$\text{Et}_3\text{PAuNTf}_2$	0.5 eq. HNTf <sub>2</sub>	76	<1	<1
$\text{PtCl}_2$	0.5 eq. HNTf <sub>2</sub>	2	3	74

**Scheme 8:** Optimization of reaction conditions for the formation of anthracenes.<sup>[26]</sup>

While two major byproducts such as methyl ketone **16a**, from Au catalyzed hydration, and 1-substituted-1*H*-indene **17a** were observed with  $\text{Ph}_3\text{PAuNTf}_2$  as catalyst, the best yield and selectivity of the desired anthracene **15a** among the tested gold catalysts was obtained with  $\text{Et}_3\text{PAuNTf}_2$ . Through addition of 0.5 eq of the Brønsted acid HNTf<sub>2</sub> the Ye group could further improve the yield of the desired anthracene **14a** and reduce the formation of byproducts. Addition of larger amounts of the acid did not increase the yield. Without the gold catalyst no formation of the product **15a** was observed under the acidic reaction conditions. In contrast, when  $\text{PtCl}_2$  was used, 1-substituted-1*H*-indene **17a** was formed selectively.

Using their optimized reaction conditions, they examined several different substituted *o*-alkynyldiarylmethanes **14** and were able to apply their methodology to terminal as well as internal alkynes (**Scheme 9**). Interestingly, no 7-*endo-dig* cyclization was observed in all cases. The reactions were carried out under “open flask” conditions, excluding neither moisture nor air. The proposed mechanism of this transformation leading to the formation of the anthracene **15a** is presented in **Scheme 9** (bottom). According to Ye and co-workers, vinyl gold intermediate **I** could be initially generated by gold-catalyzed 6-*exo-dig* cyclization. Subsequent protodeauration forms intermediate **II**, which can be further isomerized by gold and/or protonic acid to give the desired **15a**. In addition, they propose that part of **15a** originates *via* a different pathway involving gold-catalyzed hydration followed by acid-catalyzed cyclodehydration. Since the acid is capable of converting **15a** into **15a**, it could be assumed that it acts as an accelerator of this minor reaction pathway.

## 1. Introduction



**Scheme 9:** Overview of the reaction scope for terminal and internal alkyne substrates (top) and proposed reaction mechanism (bottom).<sup>[26]</sup>

Besides the selectivity of gold catalyzed reactions, the reaction rate can be tuned as well by the design of a suitable ancillary ligand. In general, the following three stages in the catalytic cycle could be influenced by the ligand: (I) activation of the alkyne, (II) protodemetalation and (III) the deactivation of the gold catalyst. The Xu group among others intensively analyzed these effects of the ligand. If the rate determining step is the protodeauration which is usually expected to be a relatively fast step, electronic effects have a large influence and electron-rich ligands can accelerate the protodeauration. Furthermore, they recognized that steric effects also affect the rate of this step and sterically more demanding ligands reduce the speed. In case of weak nucleophiles and less reactive substrates such as allenes or alkenes, the activation of the carbon multiple bond is considered the rate determining step. By utilizing an electron deficient ligand, a stronger activation of the  $\pi$  system could be accomplished and the formation of the vinyl gold intermediate is facilitated.<sup>[27]</sup>

Toste and co-workers investigated the intermolecular hydroamination of allene **18** with hydrazide nucleophiles. Supporting the conclusions of the Xu group, their studies could show that the rate determining step is the electronic activation of the allene since allenes are less reactive than alkynes and electron-poor hydrazides are weak nucleophiles. The Toste group did a Hammett plot to compare the influence of the *para* substituent in triarylphosphine ligands on the rate constant of the hydroamination. As shown in **Figure 5** the reaction rates were increasing with electron withdrawing substituents at the ligand.<sup>[28]</sup>

### 1.3 Cationic phosphines

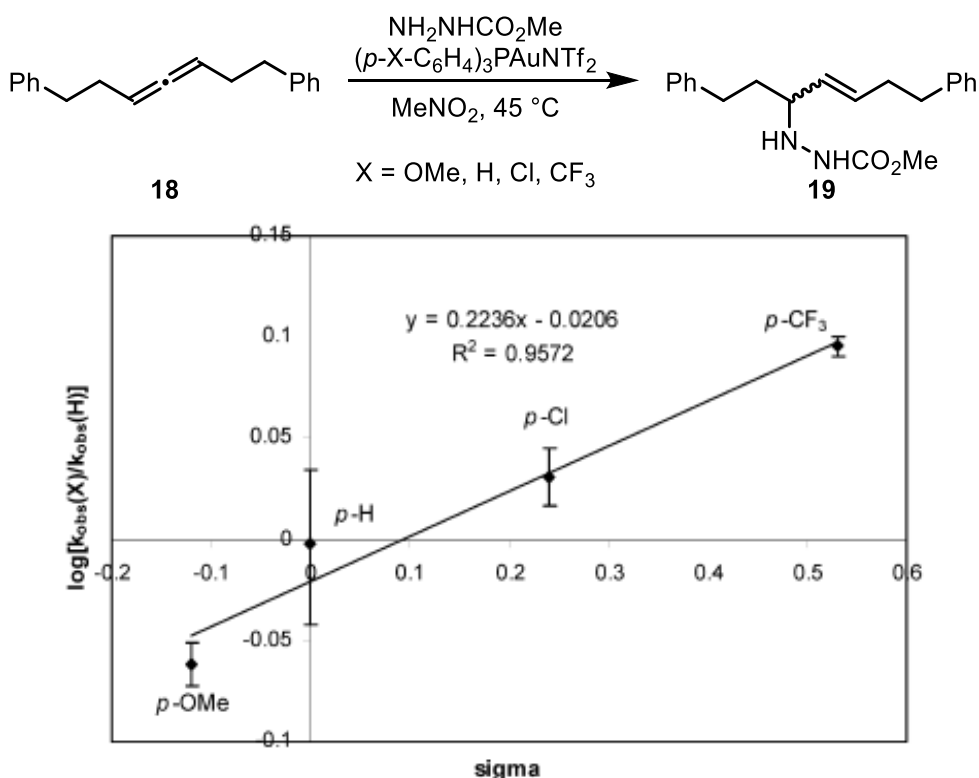


Figure 5: Hammett plot for the hydroamination of allene **18**.<sup>[28]</sup>

The examples depicted above have shown that careful choice of the ancillary ligand can influence the diastereoselectivity and the reaction rate of gold catalyzed transformations. Since electron deficient phosphine ligands delivered highly interesting results the Alcarazo group focused on the development of extremely electron poor phosphine ligands by introducing a positive charge in  $\alpha$  position to the phosphorus. The next chapter will deal with the synthesis of cationic phosphines and their application in  $\pi$ -acid catalysis.

### 1.3 Cationic phosphines

Phosphorus-based ligands are undisputedly the most widely used ligand class in homogeneous catalysis, since their physicochemical properties and donor abilities can be adjusted and modified quite simply by changing the substituents on the phosphorus. The vast majority of phosphine ligands are either neutral or anionic, which is obviously due to the superior ability of these systems to coordinate an electropositive metal center and stabilize a metal complex. Charged phosphines were used to alter the electrochemical properties, e.g. by introducing a charge on the phosphine ligand, the solubility in polar solvents can be improved and industrial processes can benefit.<sup>[29]</sup> In the Ruhrchemie/Rhône-Poulenc process a highly water-soluble metal complex with a sulfonated phosphine **20** was used in the hydroformylation of propene to allow a biphasic reaction and thus a better separation of the catalyst.<sup>[30]</sup> Complex **21** is utilized to identify

## 1. Introduction

reactive intermediates in alkene metathesis *via* electrospray ionization mass spectrometry.<sup>[31]</sup>

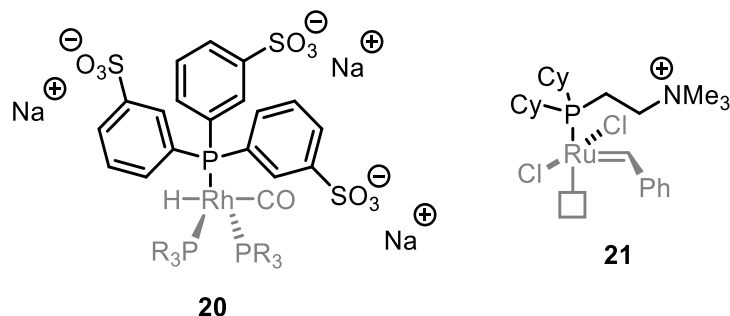


**Figure 6:** Examples of complexes with ionic ligands.

In both ligands the charged moieties are installed far away from the donating phosphorus atom. Although the charge influences the physicochemical properties it does not significantly affect the donor properties of the ionic phosphine ligand. In contrast, when the cationic charge is located neighboring to the phosphorus atom ( $\alpha$ -position) increased  $\pi$  acceptor properties were represented due to the strong electron withdrawing effect of the cationic ligand accompanied by a decreased  $\sigma$  donor ability.<sup>[29]</sup> This class of cationic ligands exhibit donor properties similar to those of the strong  $\pi$  accepting polyhalogenated phosphines, such as  $\text{PF}_3$ ,  $\text{P}(\text{CF}_3)_3$  or  $\text{PCl}_3$ . Since polyhalogenated phosphines are sensitive to moisture, highly toxic and difficult to handle because of their labile P-X bond, they are rarely used in coordination chemistry.<sup>[32]</sup> In comparison,  $\alpha$  cationic phosphines contain a relatively inert carbon phosphorus bond and can be easily handled under ambient conditions. In cases where catalytic processes require ancillary ligands outlining even stronger  $\pi$  accepting properties than phosphites  $\alpha$  cationic phosphines represent an excellent alternative.<sup>[29]</sup>

In the following sections the bonding situation, the donor ability, the synthesis and the applications of  $\alpha$  cationic phosphines will be discussed.



## 1.3 Cationic phosphines

### 1.3.1 Bonding situation

To understand how the properties of phosphine ligands can be tuned the bonding situation between the phosphine ligand and a transition metal should first be considered. The Dewar-Chatt-Duncanson model is applied to describe these bonding interactions (**Figure 7**).<sup>[33,34]</sup>

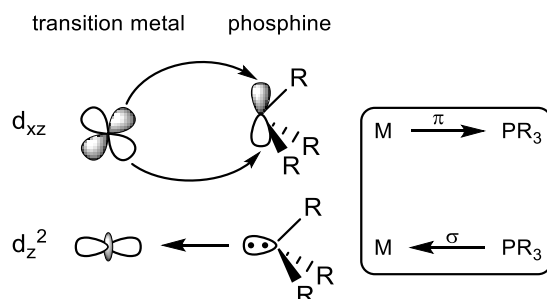


**Figure 7:** Interaction between the orbitals of a transition metal and a phosphine ligand.

The σ donor properties of a phosphine result from the interaction of the lone pair of the phosphorus and the vacant d<sub>z<sup>2</sup></sub> orbital of the metal. The π bond is formed by the overlap of an occupied metal d orbital with an empty antibonding σ\*(P-R) orbital. Calculations have shown that backbonding occurs into orbitals of the phosphorus with 3p character.<sup>[34]</sup> By replacing one of the R groups on the phosphorus with an electron withdrawing substituent, for example through introducing a positive charge in α position to the phosphorus, a lowering in energy of all the molecular orbitals of the corresponding phosphine would be expected, including the HOMO and the LUMO (**Figure 8**).

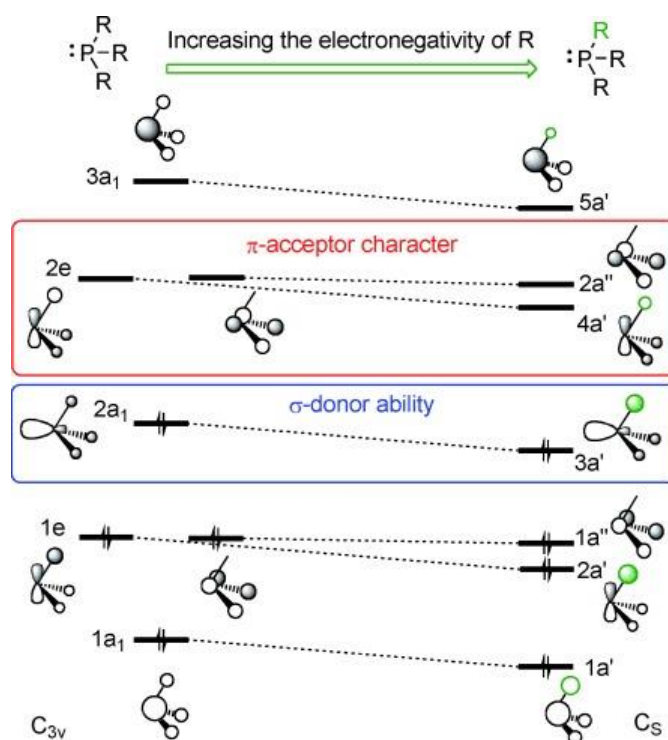


**Figure 8:** Effect of electron withdrawing substituents on the molecular orbitals of PR<sub>3</sub>.<sup>[29]</sup>

## 1. Introduction

Especially orbitals with a high contribution of the atomic orbitals of the positively charged substituent are affected ( $a'$  symmetry). As a result, the presence of a cationic charge diminishes the  $\sigma$  donor strength and enhances the  $\pi$  acceptor ability of the phosphine.<sup>[29]</sup>

Furthermore, the nature of the cationic substituent plays an important role. Since mainly aromatic compounds are employed to introduce a positively charged substituent to phosphines secondary orbital interactions should be included for the evaluation of the  $\pi$  donor character. Molecular orbitals of the phosphorus with adequate symmetry may interact with the vacant low lying  $\pi^*$  orbitals of the aromatic system. Through overlap of the  $3a'$  orbital of the phosphorus with the  $\pi^*$  orbitals delocalization of electron density on the aromatic system could be enabled resulting in the stabilization of the lone pair and weakening of the phosphorus-metal bond as a result of the decreased overlap with the orbitals of the metal (**Figure 9 a**)). Since this reduced  $\sigma$  donation from the phosphine could not be completely balanced by the increased  $\pi$  backdonation of the metal the corresponding complexes tend to decompose especially when di- or tricationic phosphines are considered. Additionally, interaction of the  $2a''$  orbital of the phosphorus with an empty  $\pi$  system on the page plane may occur. This overlap causes lowering of the  $2a''$  orbital and enhances the  $\pi$  accepting properties of the phosphine (**Figure 9 b**)). The strength of the secondary interactions is not equal for all cationic substituents and those bearing the lowest-lying LUMO are capable of maximizing both or at least one of these interactions. Besides secondary orbital interactions also electrostatic forces between the ligands or the ligand and the metal arising from partially charged moieties must be considered within the metal complex.<sup>[29,35]</sup>

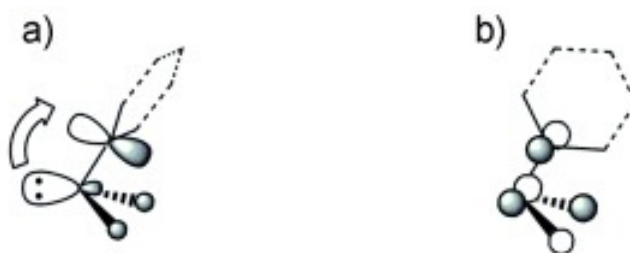


**Figure 9:** Secondary orbital interactions between the phosphorus and the cationic aromatic substituent.<sup>[29]</sup>

### 1.3.2 Evaluation of the donor abilities of $\alpha$ cationic phosphines

As mentioned in the previous section the introduction of a positive charge in  $\alpha$  position of the phosphorus in general diminishes the  $\sigma$  donor character of the phosphine while increasing the  $\pi$  acceptor ability. To experimentally evaluate this properties, Tolman studied the electronic and steric effects based on CO stretching frequencies ( $\tilde{\nu}$ ) in square-planar  $[\text{Ni}(\text{CO})_3(\text{L})]$  and ligand cone angles ( $\Theta$ ).<sup>[36]</sup>

### 1.3 Cationic phosphines

For determination of the so-called “Tolman’s electronic parameter” (TEP)  $\text{Ni}(\text{CO})_4$  was mixed with the ligand **L** to be studied and the carbonyl stretching frequency  $\tilde{\nu}$  was measured. The shift in the stretching frequency compared to free CO ( $2143\text{ cm}^{-1}$ ) can estimate the donor-acceptor properties in phosphines. CO as a ligand is an excellent  $\pi$  acceptor, which means that electron density from the metal is shifted to the C-O antibonding orbital. Population of this antibonding orbital weakens the carbon oxygen bond and reduces the stretching frequency. Therefore, strong  $\sigma$  donor ligands increase the electron density at the metal and reinforce the weakening of the C-O bond resulting in a decreased energy of the CO vibration. On the other hand,  $\pi$  accepting phosphines compete with the CO ligands for electron density of the metal and as a result the lowering of the stretching frequency is less pronounced.<sup>[37]</sup> To replace the highly toxic nickel carbonyl complexes the corresponding  $[\text{RhCl}(\text{CO})\text{L}_2]$  were utilized instead. In cases, where the ligand **L** is sterically demanding deviations from the square planar geometry can occur and the obtained stretching frequencies are not suitable for an exact comparison. Another practical problem in the determination of TEP by IR spectroscopy is the formation of the corresponding complex, which is not particularly favorable for certain ligands.<sup>[29,35]</sup> For its independence DFT studies are an adequate alternative to the experimental determination of the TEP.<sup>[38]</sup>

To classify the steric bulk of a given phosphine ligand Tolman introduced the cone angle  $\Theta$ . For symmetric phosphines  $\Theta$  is the apex angle of a cylindrical cone, centered  $2.28\text{ \AA}$  from the center of the phosphorus atom. The cone is tangential to the van-der-Waals radii of the outermost atoms of the ligand (**Figure 10**, left). In case of unsymmetrical phosphines, the cone angle  $\Theta$  is defined by this equation  $\Theta = \frac{2}{3} \sum_{i=1}^3 \theta_i/2$  and each half angle is measured independently for each substituent (**Figure 10**, right).<sup>[37]</sup>

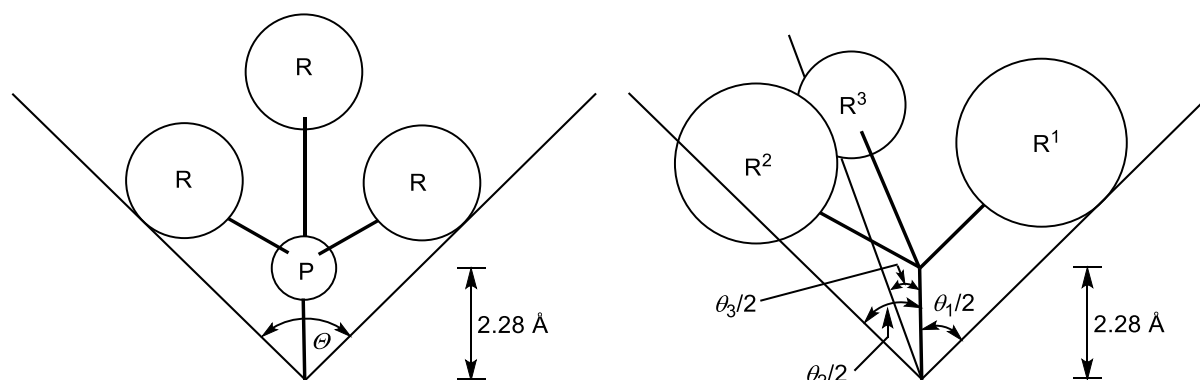


**Figure 10:** Definition of the cone angle  $\Theta$  for symmetrical phosphines (left) and determination of cone angles for unsymmetrical ligands (right).<sup>[37]</sup>

To relate the electronic and steric properties of phosphine ligands a Tolman stereoelectronic map including neutral and  $\alpha$  cationic phosphines is shown in **Figure 11**. Experimentally determined values are marked as red points, whereas calculated values using Gusev’s

## 1. Introduction

method<sup>[38]</sup> are shown as blue points. Monocationic phosphines arrange in the area between phosphites and polyhalogenated phosphines such as  $\text{PCl}_3$  or  $\text{P}(\text{CF}_3)_3$ , while introduction of two or three cationic substituents further increases the stretching frequency of the phosphines and places them at the top of the map. <sup>[29,35]</sup>

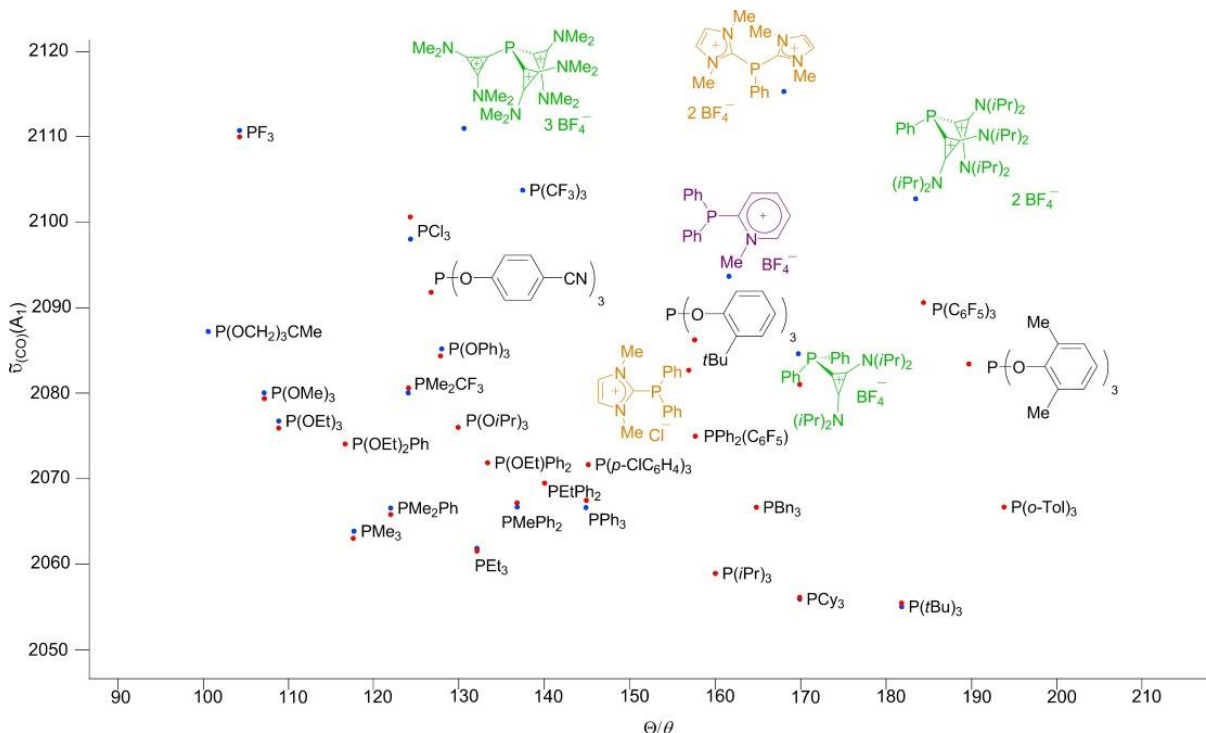


**Figure 11:** Tolman stereoelectronic map including neutral and cationic phosphines. Experimental TEPs are shown in red and calculated in blue.<sup>[29]</sup>

Another technique to classify the electronic properties of phosphines is cyclic voltammetry. Therefore, the oxidation potential of the free phosphine is measured, which makes this method independent from steric issues and no metal complexes have to be prepared. In this context, a lower oxidation potential correlates to electron-rich phosphines, which are considered as good  $\sigma$  donors, whereas higher oxidation potentials were obtained for electron poor ones. This results are in agreement with the TEPs and reveal the same ranking. <sup>[29,35]</sup>

To determine the relative contributions of the  $\sigma$  donor and  $\pi$  acceptor properties the Alcarazo group calculated the HOMO and the LUMO of cationic phosphines to study the effects of the cationic group (**Figure 12**).

### 1.3 Cationic phosphines

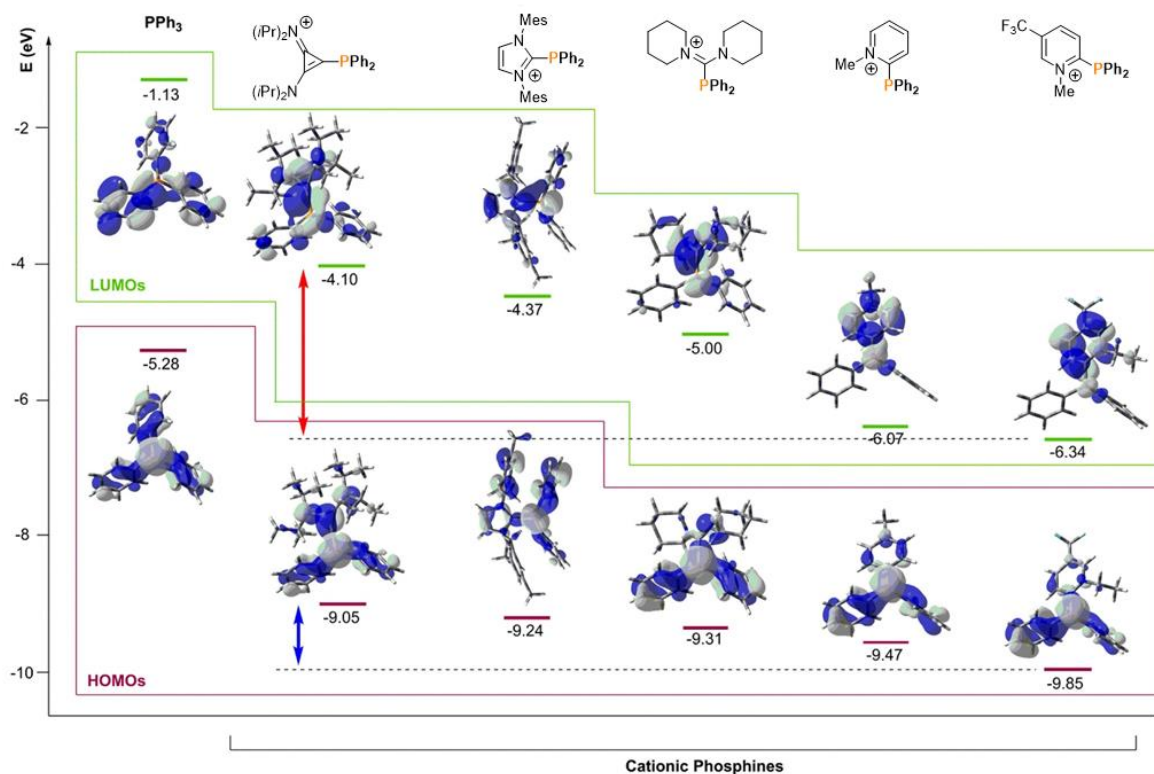


**Figure 12:** HOMO and LUMO energies for cationic phosphines calculated at the B3LYP-D3/def2-TZVP level of theory.<sup>[35]</sup>

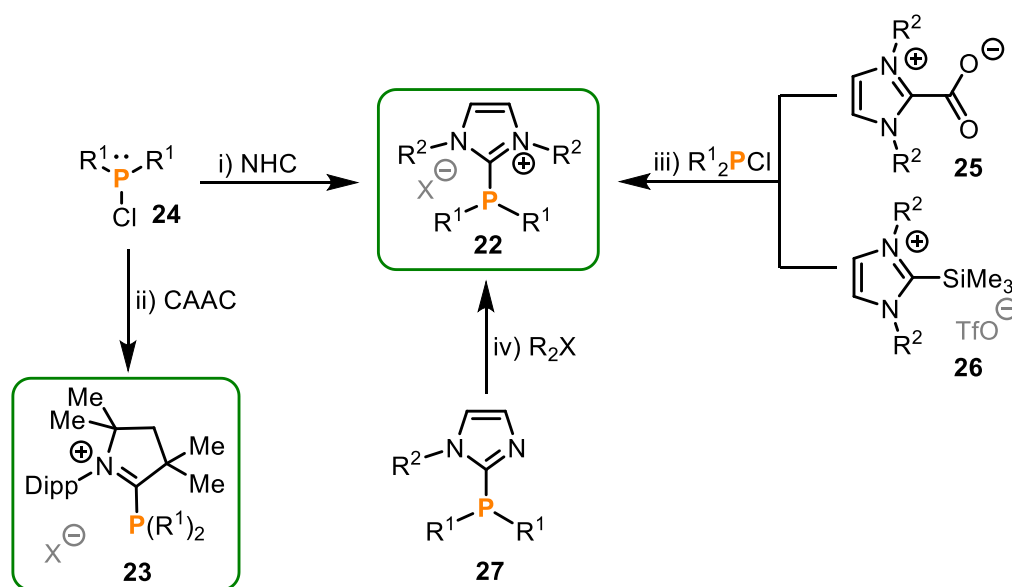
The HOMO energies were in a range between  $-9.05$  and  $-9.85$  eV and thus in a similar region for all cationic substituents, which indicates that the  $\sigma$  donor ability is comparable. In contrast, the LUMO is strongly influenced by the nature of the cationic group suggesting that  $\pi$  accepting ability has a greater dependency. The LUMO energy decreases from cyclopropenium ( $-4.10$  eV) to pyridinium ( $-6.34$  eV). However, the HOMO and LUMO energies of these cationic phosphines are significantly lower than those calculated for triphenylphosphine. In conclusion, it can be assumed that a diminution in the global donor strength leads to an increase of the acceptor abilities.<sup>[35]</sup>

#### 1.3.3 Synthesis of $\alpha$ cationic phosphines

The most prominent approach for the synthesis of  $\alpha$  cationic phosphines with the structure of **22** and **23** is the reaction of a di(alkyl/aryl)chlorophosphine **24** with an appropriate nucleophile, in this instance a carbene. In 1990 the first fully characterized imidazolium-based  $\alpha$  cationic phosphine **22** was described by Kuhn and coworkers. Following their methodology chlorodiphenylphosphine was reacted with an imidazolium carbene (**Scheme 10, i**).<sup>[39]</sup> Furthermore, this strategy has been extended using cyclic(alkyl)(amino)carbenes [(CAACs) (**Scheme 10, ii**)] by the Alcarazo group.<sup>[40]</sup> In cases where a free carbene is is

## 1. Introduction

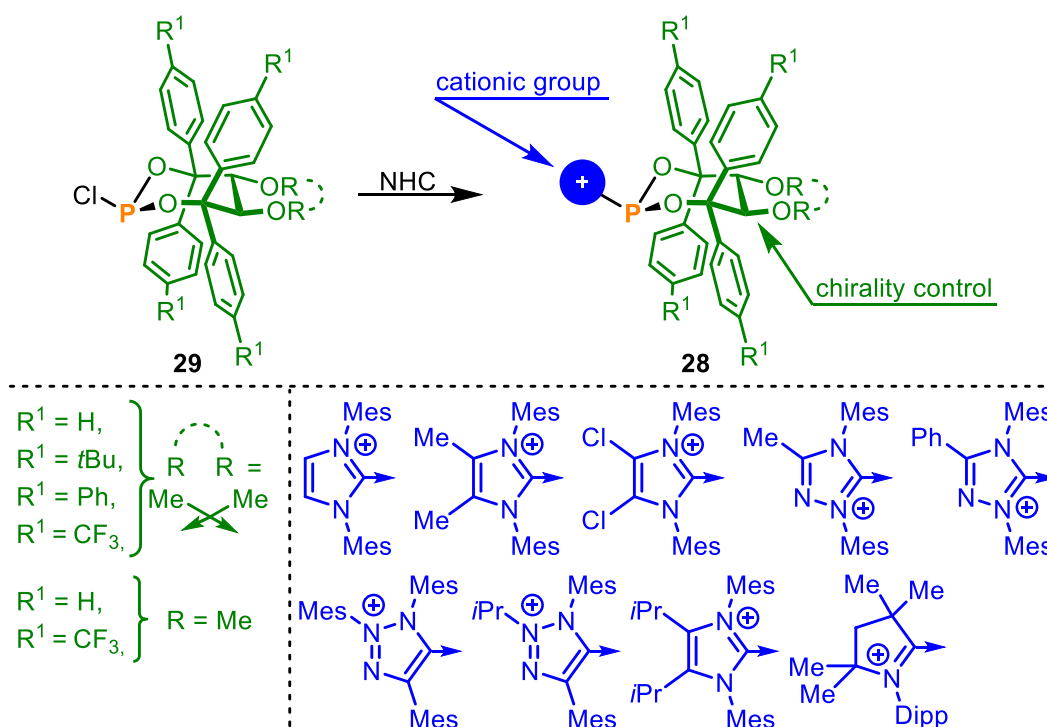
unstable under the reaction conditions, suitable precursors such as imidazolium-2-carboxylates **25**<sup>[41]</sup> or 2-silylimidazolium salts **26**<sup>[42]</sup> were employed (**Scheme 10** iii)). Another possibility is to transfer an already existing phosphine framework **27** via *N*-alkylation into a  $\alpha$  cationic phosphine **22** (**Scheme 10**, iv)). For this approach suitable alkylating agents such as Meerwein salts are necessary, whereas other alkylating agents, such as methyl iodide favor exclusively the alkylation of the phosphorus. The use of sulfates, e.g. dimethyl sulfate, resulted in a mixture of *N*- and *P*-alkylation.<sup>[43]</sup> To deal with the problem of *P*-alkylation Komarov *et. al.* described the coordination of the phosphine to tungsten pentacarbonyl and this way they could selectively alkylate the imidazole backbone when employing dimethyl sulfate, as the lone pair on the phosphorus is no longer available.<sup>[44]</sup>



**Scheme 10:** Routes for the synthesis of cationic phosphines.

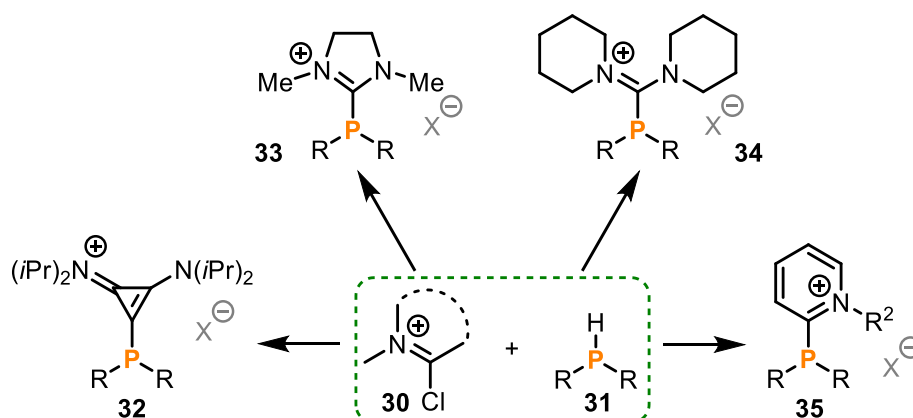
In addition to the synthesis of achiral  $\alpha$  cationic phosphines, the carbene route described in **Scheme 10**, a) was also applied by the Alcarazo group to introduce a large library of chiral analogues (**Scheme 11**). These cationic phosphonites **28** contain an imidazolium or triazolium unit and a TADDOL-derived moiety, which provides the chiral information, whereas both parts allow for electrical and sterical modification. Starting with the condensation of phosphorus trichloride and the TADDOL-derivative leading to the corresponding chirophosphonites **29** and subsequent reaction with a *N*-heterocyclic carbene gave the desired cationic phosphonites **28** in a two-step protocol.<sup>[45,46]</sup>

### 1.3 Cationic phosphines



**Scheme 11:** Synthesis of chiral cationic phosphonites **28**.

Since the previously described methods are either limited to imidazolium-based cationic phosphines or some of the desired architectures could not be realized *via* the carbene route, the Alcarazo group applied the condensation of Vielsmeier-type salts with secondary phosphines to circumvent this issue. With this methodology the library of  $\alpha$  cationic phosphines could be successfully expanded to cyclopropenio-<sup>[47]</sup>, imidazolinio-<sup>[48]</sup>, amidinio-<sup>[48]</sup> and pyridiniophosphines<sup>[49]</sup>, **32-35** (**Scheme 12**). In case of pyridiniophosphines **35** the stability of the phosphine is dependent on the nature of  $R^2$  and can be significantly increased by introduction of an aryl instead of an alkyl substituent.



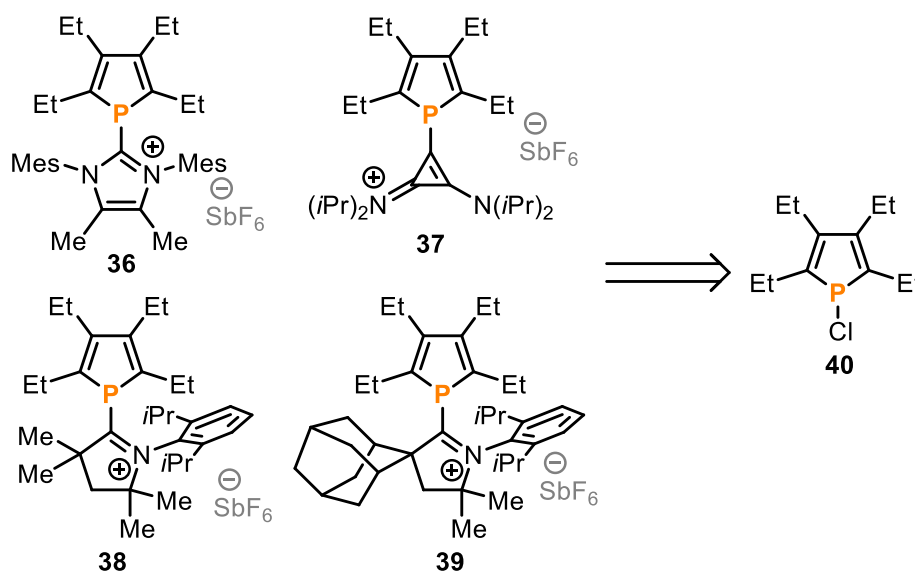
**Scheme 12:** Routes for the synthesis of cationic phosphines starting from di(alkyl/aryl)phosphines **31**.

Although the cationic charge depletes electron density from the phosphorus center a pyramidal environment was depicted in all cationic phosphines **22-23** and **32-35**, which

## 1. Introduction

indicates that the lone pair on the phosphorus is still available for the coordination of a metal. Complexes with Au, Ag, Cu, Pt, Ni, Ir, Pd, and Rh have been reported.<sup>[35]</sup>

Recently, the Alcarazo group introduced a new class of monocationic phosphines, namely  $\alpha$  cationic phospholes **36-39**, aiming for even stronger  $\pi$  accepting ligands than described before. The synthesis was carried out *via* reaction of the cyclic chlorophosphole **40** with the corresponding stable carbene and the  $\pi$  accepting properties were modulated by introducing cationic groups of different nature (**Scheme 13**).<sup>[50]</sup>

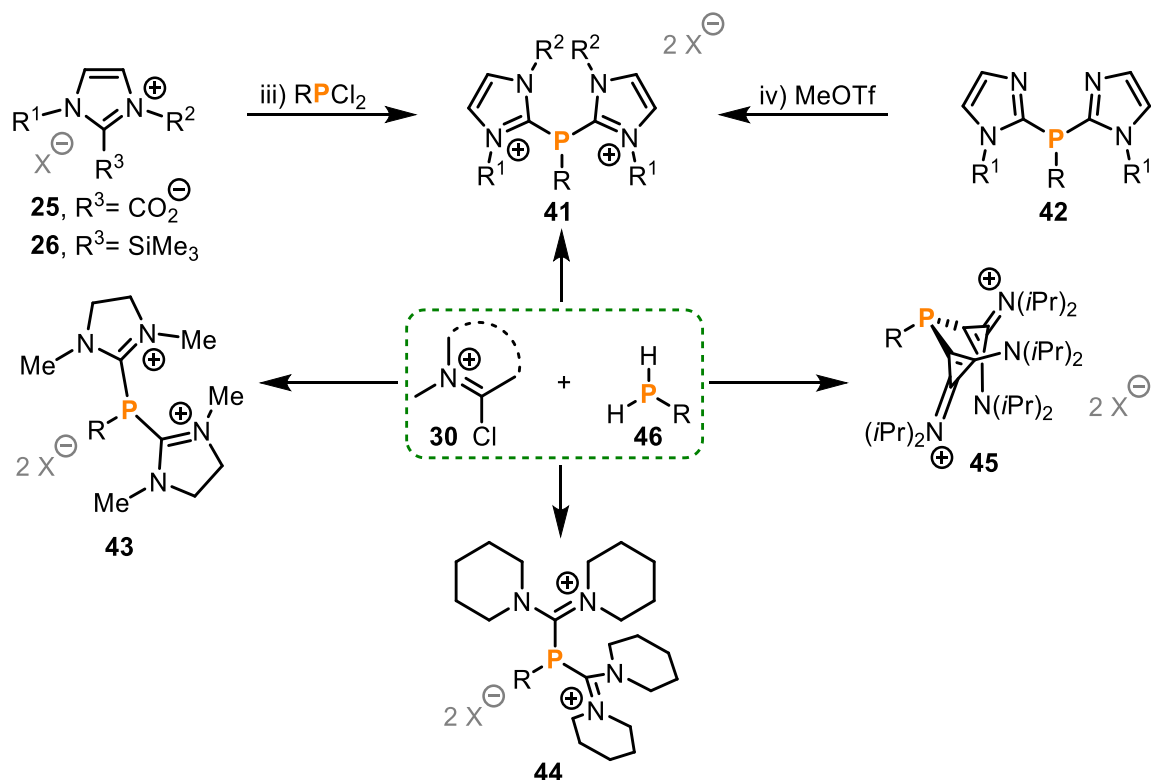


**Scheme 13:** Towards the synthesis of  $\alpha$  cationic phospholes **36-39**.

The synthetic approaches described previously towards monocationic phosphines find also application in the synthesis of polycationic phosphines. By using two equivalents of either imidazolium-2-carboxylates **25** or 2-silylimidazolium salts **26** and dichlorophosphines or phosphorus trichloride instead of chlorophosphines the groups of Weigand and Andrieu could obtain dicationic imidazolium-based phosphines **41** (**Scheme 14**, iii).<sup>[51,52]</sup> In addition, the double *N*-alkylation of already existing phosphine frameworks, such as **42**, with MeOTf is another suitable strategy to yield **41**, albeit very limited (**Scheme 14**, iv).<sup>[53]</sup> In contrast to monocationic phosphines, the procedure following **Scheme 10** i) for dicationic analogues is strongly dependent on the steric demand of the carbene and the direct reaction of the free carbene with phosphorus trichloride might result in the formation of phosphorus(I) cations instead of the desired product **41**.<sup>[54]</sup> To circumvent this problem, the strategy developed by the Alcarazo group to form dicationic phosphines with two imidazolidinium **43**, formamidinium **44**, and cyclopropenium **45** groups could be implemented. Starting from primary phosphines **46** a double condensation with the corresponding Vielsmeier-type salts **30** takes place, whereas in the case of the cyclopropenium species an additional base was required (**Scheme 14**, bottom).<sup>[48,55]</sup>

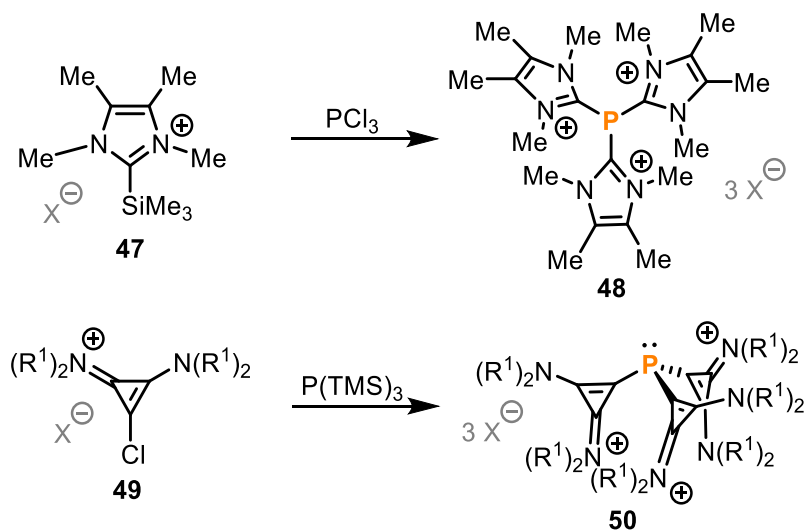


### 1.3 Cationic phosphines



**Scheme 14:** Routes for the synthesis of dicationic phosphines.

For tricationic phosphines only a few examples are described by the groups of Weigand<sup>[52]</sup> and Alcarazo<sup>[56]</sup>. Treatment of **47** with phosphorus trichloride led to the formation of tricationic **48** (**Scheme 15**, top). In the synthesis of **50** from **49** the steric bulk of the *N*-alkyl substituents limit the reaction and higher yields were observed for sterically less demanding substituents such as methyl groups (**Scheme 15**, bottom).



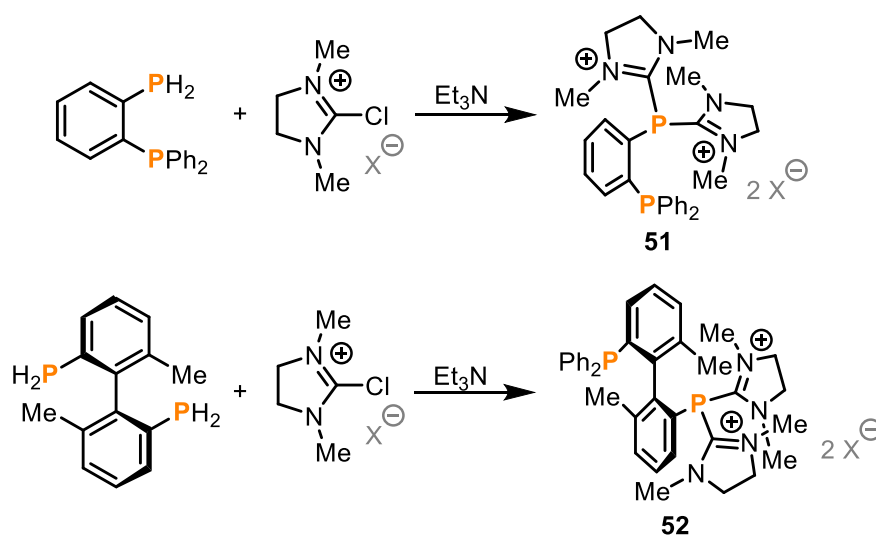
**Scheme 15:** Routes for the synthesis of tricationic phosphines.

Although no major structural changes were observed between monocationic phosphines and their polycationic analogues, the use of di- and tricationic phosphines is severely limited

## 1. Introduction

due to the decreased solubility in common organic solvents and the hindered coordination to metals. Whereas for the phosphorus center in **44** and **45** coordination to Pt(II), Pd(II) and Au(I) could be realized, ligand **50** is only able to form metal complexes with weak back donating fragments, such as  $[\text{PtCl}_3]^-$  and  $[\text{PdCl}_3]^-$ .<sup>[48,56,57]</sup> Since for **41** no coordination chemistry has been reported, it is not surprising that **48** is also incapable of coordinating a metal.<sup>[52]</sup>

To evaluate the full potential of polycationic phosphine ligands the coordination chemistry had to be expanded to enable a wider application. Gu *et. al.* synthesized a series of dicationic bidentate phosphine ligands containing a cationic moiety and an additional donating  $-\text{PPh}_2$  unit to induce the coordination of a metal. In **Scheme 16** two different examples of  $\alpha$  dicationic chelating phosphines are shown. Due to the distance between the two phosphorus atoms in **51** coordination to the same metal center would be favored, whereas phosphine **52** allows for higher flexibility and provides a platform for chiral analogues. In fact, various metal complexes including Rh(I), Pt(II), Pd(II) and Mo(0) could be realized with this type of chelating ligands.<sup>[58,59]</sup>



**Scheme 16:** Synthesis of  $\alpha$  cationic chelating phosphines **51** and **52**.

### 1.3.4 Application of $\alpha$ cationic phosphines in catalysis

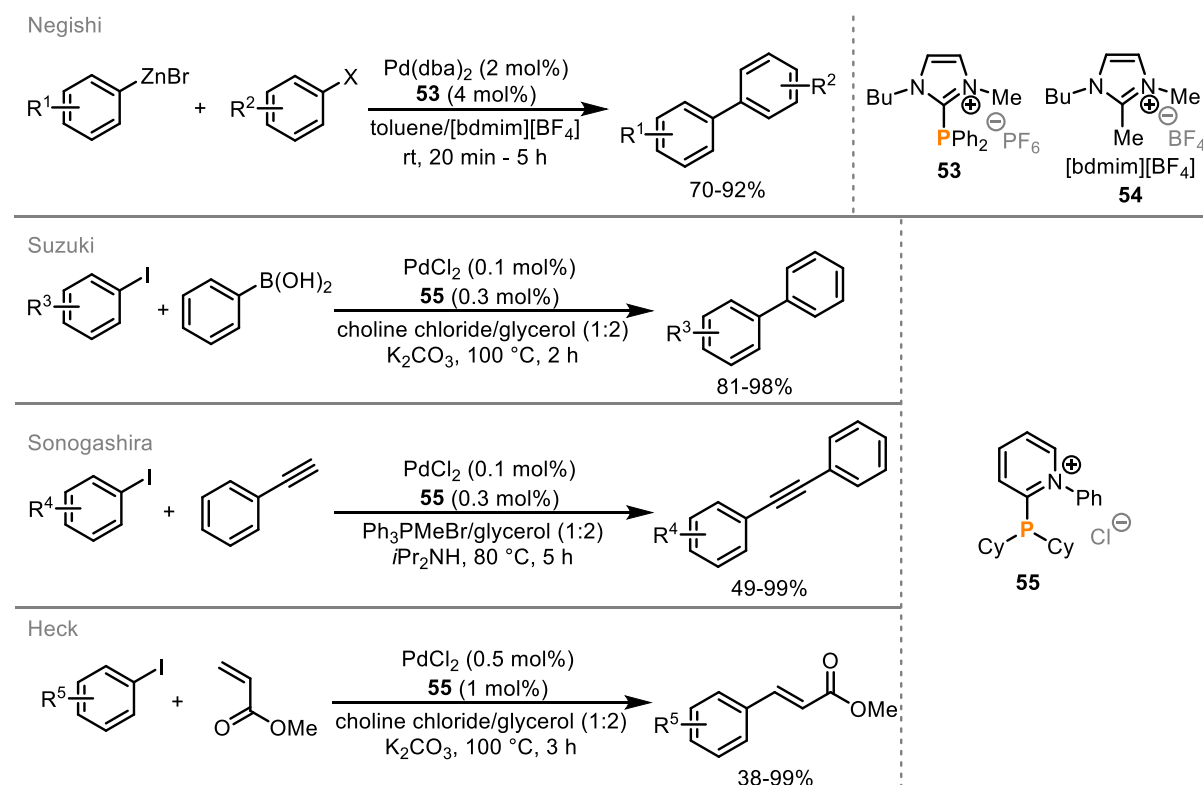
Initially, applications of cationic phosphines and the corresponding metal complexes were based on their modified physicochemical properties compared to neutral phosphines. Their high solubility in water and ionic liquids offered the possibility to be used as a transfer catalyst in polar or biphasic media, which can be easily recycled and separated from the reaction products by extraction or simple phase separation.<sup>[29,35]</sup> As a result, cationic

### 1.3 Cationic phosphines

phosphines were used in several catalytic transformations, including cross coupling reactions,<sup>[60–63]</sup> hydroformylation,<sup>[64]</sup> hydrosilylation,<sup>[65]</sup> and hydrogenations<sup>[61]</sup>.

In 2000 Knochel and co-workers studied a palladium-catalyzed Negishi type coupling, employing imidazolio-phosphine **53** as ligand and 1-butyl-2,3-dimethylimidazolium tetrafluoroborate ([bdmim][BF<sub>4</sub>]) (**54**) as ionic liquid. In a biphasic system with toluene, allowing recycling of the catalytic mixture for another cycle without losing catalytic activity, aryl zinc reagents were reacted with aryl iodides, bromides or nonaflates. The reaction proceeded at room temperature and was successfully extended to alkenyl iodides with excellent yields (**Scheme 17**, top).<sup>[60]</sup>

In addition, pyridinio phosphines **55** developed by the Alcarazo group found application as ancillary ligands in various cross coupling reactions. Using deep eutectic solvents, the groups of Alonso and Ramón could couple several aryl iodides and bromides with phenyl boronic acid in a Suzuki-type reaction. Moreover, this methodology was also applicable for Sonogashira- and Heck-type transformations with the catalyst system being recycled up to five times (**Scheme 17**).<sup>[63]</sup>



**Scheme 17:** Application of  $\alpha$  cationic phosphines in cross coupling reactions.

Catalytic processes can benefit from the use of  $\alpha$  cationic phosphines as ligands in two ways: first, they are very soluble in polar media, and second, their strong  $\pi$  acceptor ability increases the electrophilicity of the metal center. Over the last few years, the Alcarazo group has been intensively investigating the application of cationic phosphines in the field of  $\pi$

## 1. Introduction

acid catalysis with the aim of employing these methodologies towards the total synthesis of natural products.<sup>[29,35,66]</sup> Since di- and tricyclopropenio-substituted phosphines are strong  $\pi$  accepting ligands, application in the hydroarylation of *ortho*-alkynyl biphenyl **56** showed the outstanding catalytic activity compared to commercially available phosphines (**Figure 13**). Both, the tricationic Pt(II)<sup>[67]</sup> and the dicationic Au(I)<sup>[57]</sup> complex performed excellent in this transformation and gave almost exclusively the product of the 6-*endo* cyclization **57**. However, for the synthesis of highly strained phenanthrenes with internal substituents at positions 4 and 5 a stronger activation of the alkyne is necessary and only when employing the more  $\pi$  acidic Au(I) center the reaction proceeded. Additional DFT studies on the reaction mechanism suggested that the rate determining attack of the nucleophile (arene) towards the activated alkyne is facilitated when a cationic ligand is used.<sup>[57]</sup>

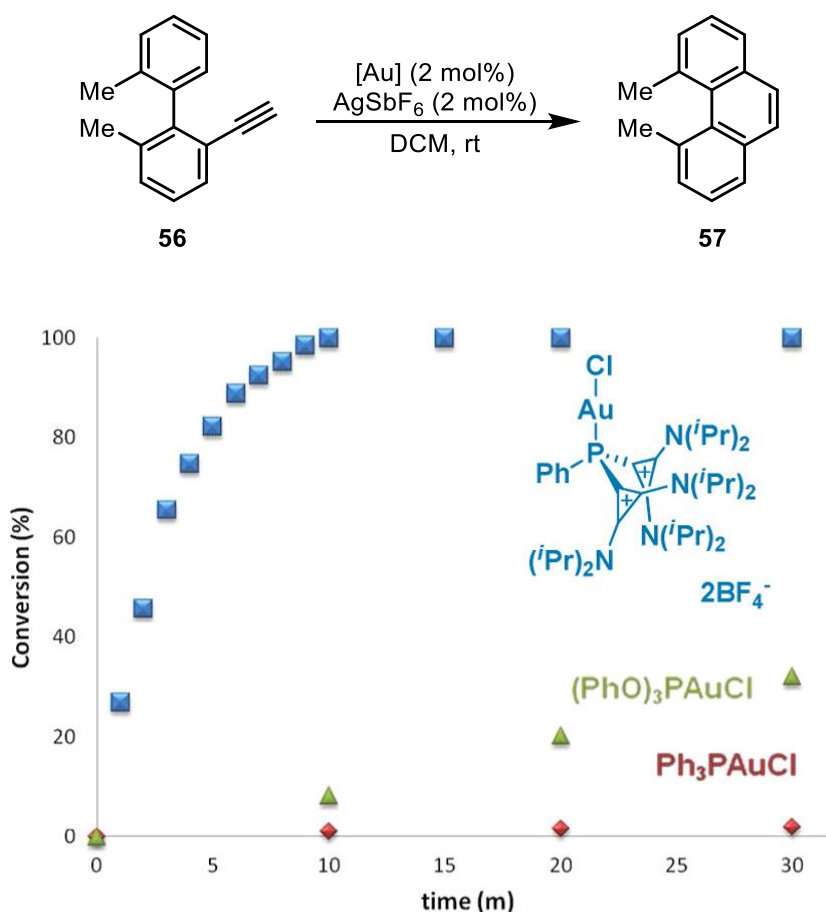


**Figure 13:** Effect of the ligand on the gold-catalyzed intramolecular hydroarylation of *o*-alkynylbiphenyl **56**.<sup>[57]</sup>

Furthermore, the synthesis of natural products bearing a phenanthrene moiety could be achieved using the developed strategy. This synthetic utility was shown amongst others for Bulbophyllantrin **58**, Coelognin **59** and Epimedoicarisoside A **60** (**Figure 14**).<sup>[57,68]</sup> Employing not only cyclopropenio-substituted but also other cationic phosphines reported by the Alcarazo group, several inter-<sup>[49]</sup> or intramolecular hydroarylations including

### 1.3 Cationic phosphines

arene,<sup>[57,67]</sup> furan,<sup>[55]</sup> thiophene<sup>[48]</sup> or pyrrole<sup>[47]</sup> based nucleophiles were realized to give access to numerous condensed aromatic and heteroaromatic systems with a high functional group tolerance.

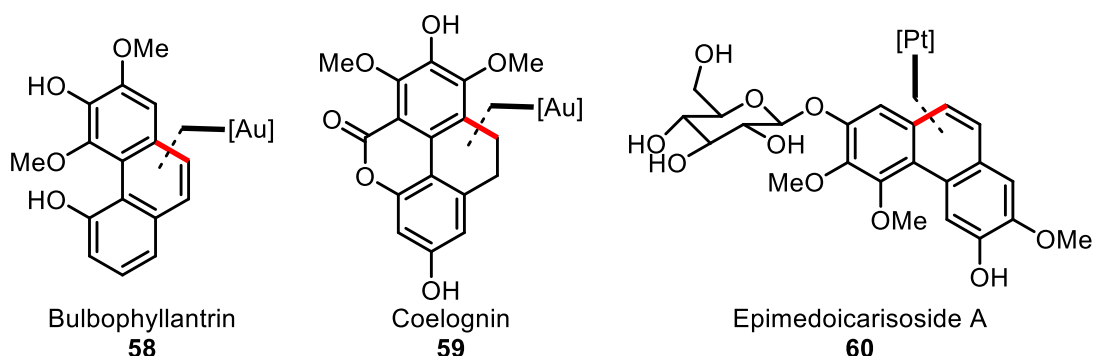
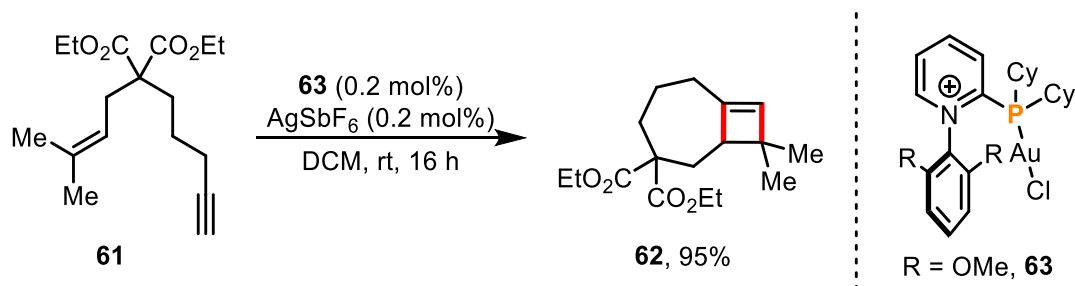


**Figure 14:** Accessible natural products using hydroarylations catalyzed by cationic phosphine ligands.

In addition to cross coupling reactions  $\alpha$  pyridinio phosphines as ancillary ligands show excellent reactivity in Au catalyzed cycloisomerizations as well. By exchanging the *N*-alkyl through an *N*-aryl substituent the stability of the corresponding Au(I) complex could be increased. Since *N*-arylpyridinio-phosphines are designed according to the architecture of Buchwald ligands the catalytic activity was compared in the [2+2] cycloaddition of 1,8-enyne **61** into cyclobutene **62**. When using XPhos (2 mol%) as ancillary ligand a yield of 48% was obtained after 24 h, whereas employing *N*-arylpyridinio-phosphine **63** gave **62** in 95% yield and additionally the catalyst loading was reduced to a tenth (**Scheme 18**).<sup>[69]</sup>

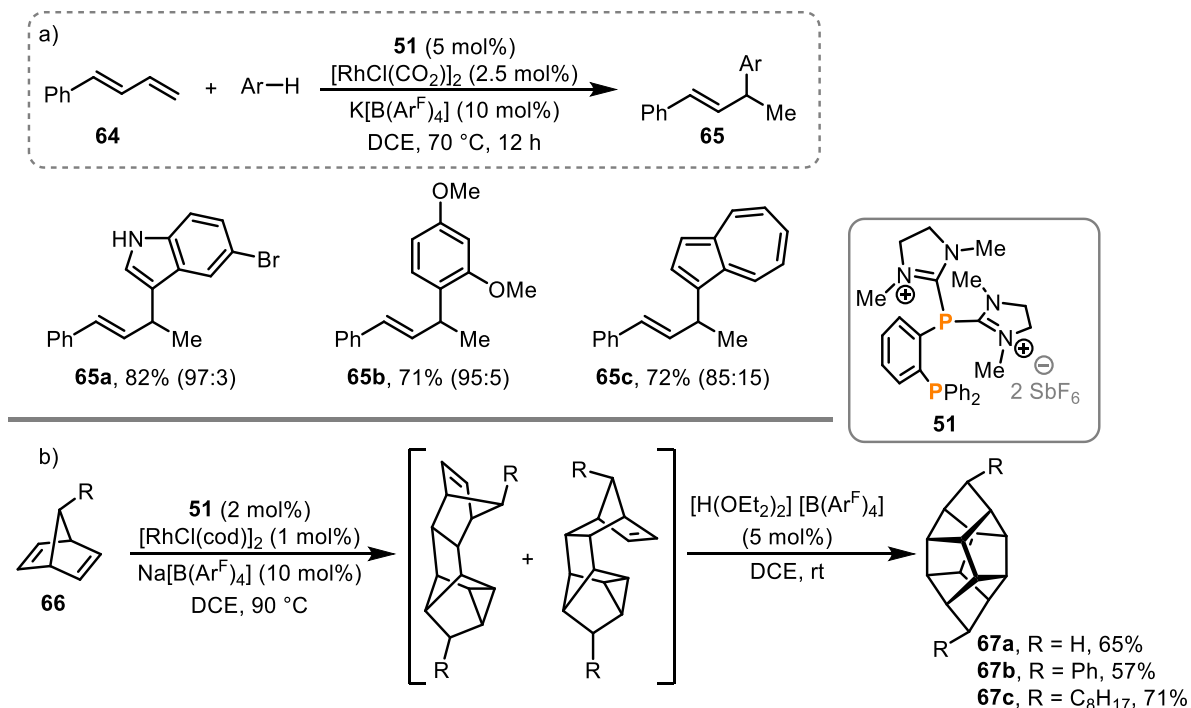


**Scheme 18:** [2+2] cycloaddition of 1,8-enyne **61** into cyclobutene **62**.

The dicationic chelating phosphine **51** turned out to be an excellent ligand in the Rh(I)-catalyzed hydroarylation of dienes with electron-rich arenes and heteroarenes. Several substituted indoles and also azulene derivatives, which exhibit a comparable lower nucleophilicity, could be converted with high regioselectivities (**Scheme 19, a**). The addition of  $K[B(Ar^F)]_4$  is essential for the reaction to proceed since it increases the solubility of the catalyst and therefore improves the conversion of the starting material.<sup>[58]</sup> Utilizing the same catalytic system the Alcarazo group reported recently the dimerization of norbornadiene resulting in the formation of thermodynamically more stable heptacyclo[6.6.0.0.2.6.0.3.13.0.4.11.0.5.9.0.10.14] tetradecane **67** (HCTD). After the Rh(I)-catalyzed

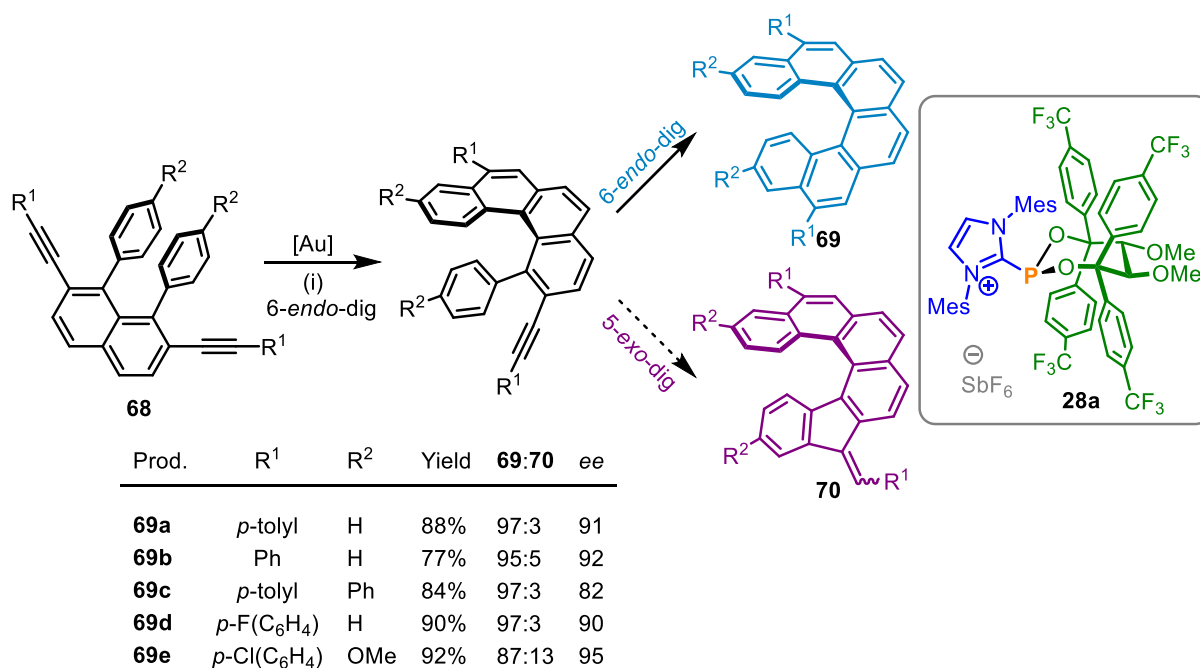
## 1. Introduction

dimerization of norbornadiene *via* a *homo*-Diels-Alder-cyclization mechanism, addition of a Brønsted acid facilitated cage closure to achieve the final product **67** (**Scheme 19**, b)).<sup>[70]</sup>



**Scheme 19:** a) Rh-catalyzed hydroarylation of dienes **64** and b) Rh-catalyzed two-step synthesis of HCTD **67**.

Among the above described achiral transformations, the group of Alcarazo demonstrated the application of chiral cationic phosphonites as suitable ancillary ligands in asymmetric Au(I) catalysis (**Scheme 20**).

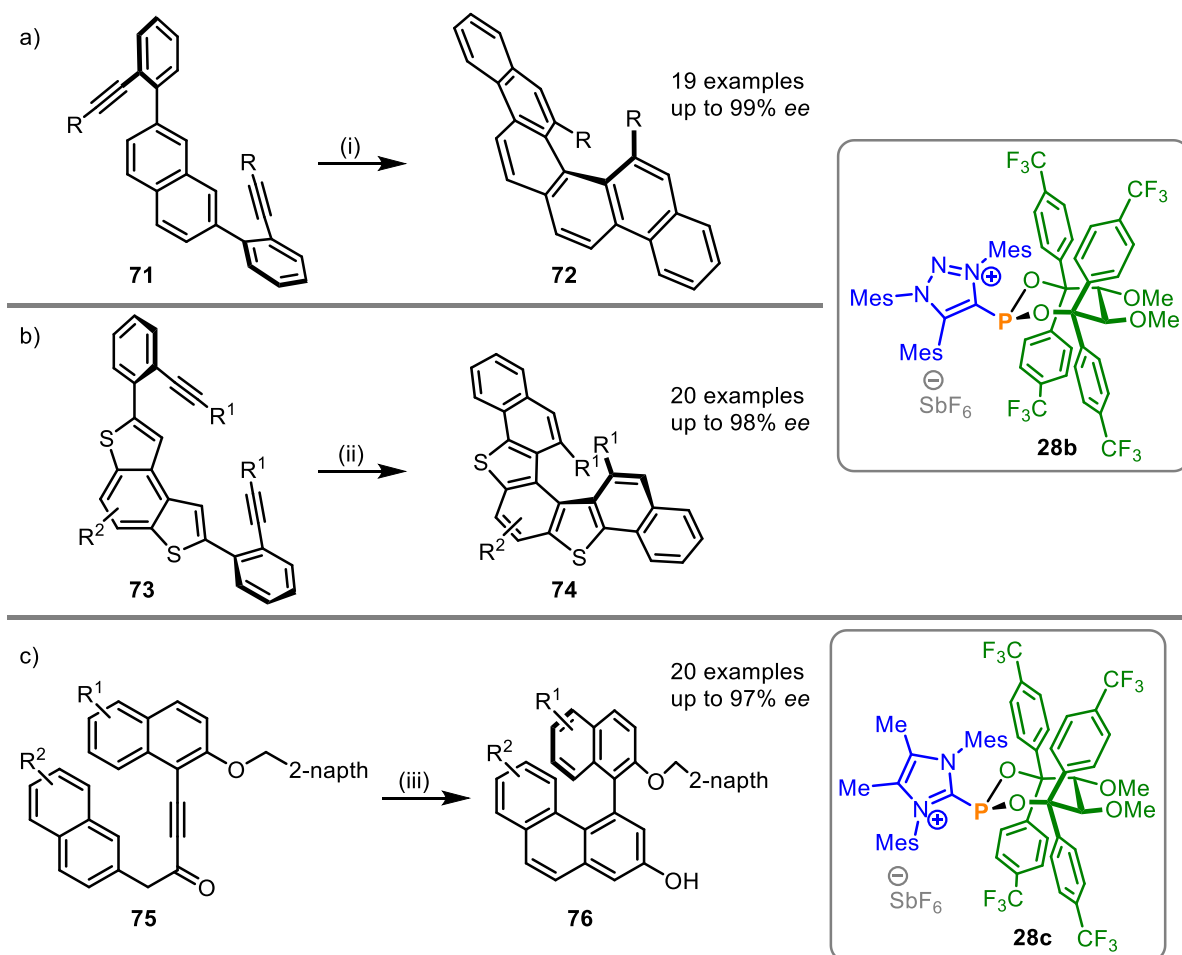


**Scheme 20:** Selected examples of [6]helicenes **69** from diynes **68**. *Reagents and conditions:* (i) **28a** (10 mol%), AgSbF<sub>6</sub> (10 mol%) in C<sub>6</sub>H<sub>5</sub>F, -20 °C, 72 h.<sup>[45]</sup>

### 1.3 Cationic phosphines

Starting with the asymmetric intramolecular hydroarylation of diynes **68** into [6]helicenes **69**, they could achieve high enantioselectivities up to 99% *ee* and mostly high *endo/exo* regioselectivities using catalyst **28a**. The enhanced reactivity caused by the cationic part of the catalyst is highly beneficial for high enantioselectivities, since the transformations also proceed at low temperatures.<sup>[45,46]</sup>

By replacing the cationic part with an 1,2,3-triazole the system finds application in the enantioselective synthesis of 1,12-disubstituted [4]helicenes **72**<sup>[71]</sup> (**Scheme 21**, a)) and dithia[5]helicenes **74**<sup>[72]</sup> (**Scheme 21**, b)) as well. While the configuration of the helicenes is defined after the hydroarylation step, more flexible systems can also be synthesized. Starting from a range of substituted benzyl alkynones **75**, the atroposelective preparation of 1,1'-binaphthyl-2,3'-diols **76** could be established (**Scheme 21**, c)).<sup>[73]</sup> To obtain high enantioselectivities, the existence of two methyl groups on the imidazolium group of the catalyst was crucial.



**Scheme 21:** a) Synthesis of 1,12-disubstituted [4]helicenes. b) Preparation of dithia[5]helicenes. c) Synthesis of 1,1'-binaphthyl-2,3'-diols. *Reagents and conditions:* (i) **28b** (10 mol%), AgSbF<sub>6</sub> (10 mol%), DCM, -20 °C, 96 h, (ii) **28b** (5 mol%), AgSbF<sub>6</sub> (5 mol%), DCM, -20 °C, 48 h, (iii) **28c** (5 mol%), AgSbF<sub>6</sub> (5 mol%), DCM, -30 °C, 12 h.

## 1. Introduction

As shown with selected examples in this chapter,  $\alpha$  cationic phosphines are a powerful and rapidly growing class of  $\pi$  accepting ligands. They exhibit a versatile coordination chemistry despite their electron deficiency. Many applications of these complexes rely on their solubility in aqueous media and ionic liquids making cationic phosphines excellent phase transfer catalysts. In addition, the influence of  $\alpha$  cationic phosphines as ancillary in the hydroarylation of *ortho*-alkynyl biphenyl systems was intensively studied by the Alcarazo group in recent years. Employing this methodology, the synthesis of various highly twisted phenanthrenes and corresponding natural products have been enabled. Furthermore, the strategy has been extended to enantioselective hydroarylation reactions by the development of chiral cationic phosphonites and their application in the formation of helicenes and hetero helicenes with excellent regio- and enantioselectivities.

Based on these examples, cationic phosphines were the natural choice for the planned transformations in this thesis. They have been widely used for achiral and enantioselective hydroarylation reactions. Due to their high reactivity, cationic phosphines are superior to conventional phosphine ligands.



## 1.4 Seven-membered ring systems

Medium-sized ring systems (7-11-membered) with mono- or dibenzannulated frameworks are the main motif in several biologically active compounds as well as in natural products. Among them, seven-membered rings with and without heteroatoms have been found in the pharmaceutical industry and in numerous natural products, exhibiting a wide range of biological and medicinal activities. A few selected examples are shown in **Figure 15**.

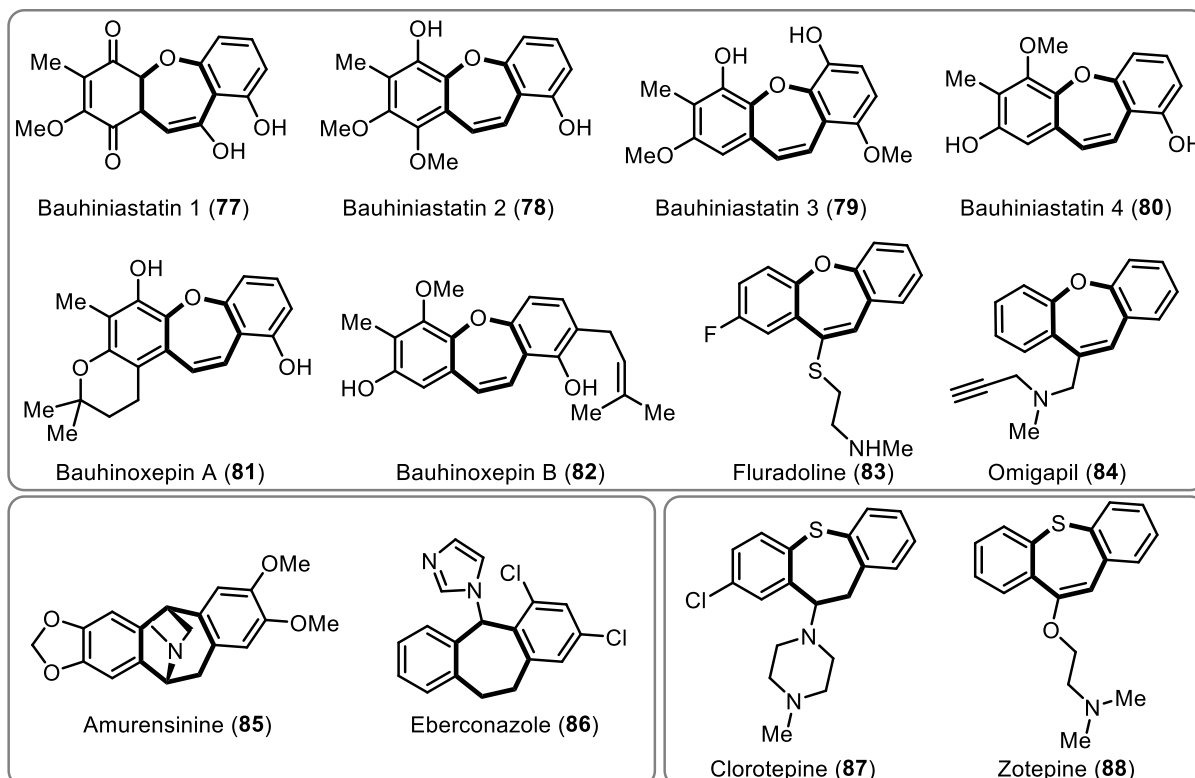


**Figure 15:** Selected examples for the dibenzo[*b,f*]oxepine, dibenzo[*a,e*]cycloheptatriene and dibenzo[*b,f*]thiepine motif in biological active compounds.

In particular, the tricyclic dibenzo[*b,f*]oxepine motif represents an important structural unit and has received significant attention from the medical community due to its potential biological properties. Pettit *et. al.* isolated Bauhiniastatins 1-4 (**77-80**) from leaves, stems and pods of *Bauhinia purpurea*, a well-known ornamental tree in Taiwan, and showed their activity in inhibiting the growth of cancer cell lines.<sup>[74]</sup> Bauhinoxepins A and B (**81, 82**), found in *Bauhinia saccocalyx*, and acting against mycobacteria, exhibit a similar structure.<sup>[75]</sup> The structural dibenzo[*b,f*]oxepine motif is also found in synthetic agents such as the painkiller and antidepressant fluradoline (**83**)<sup>[76]</sup> or Omigapil (**84**),<sup>[77]</sup> which has been tested in the treatment of Parkinson's disease and amyotrophic lateral sclerosis. Another important scaffold is the dibenzo[*a,e*]cycloheptatriene unit consisting of a cycloheptene with two adjacent benzene rings. This skeleton is present in a series of natural products and bioactive molecules. Amurensinine (**85**)<sup>[78]</sup> belongs to the isopavine family of alkaloids, with isopavines being used in the treatment of neurological functional disorders such as Parkinson's or Alzheimer's disease and eberconazole (**86**)<sup>[79]</sup> is an antifungal drug in the

## 1. Introduction

therapy of fungal skin infections. In addition, some dibenzo[*b,f*]thiepienes and their derivatives are also biologically active especially in the field of central nervous system drugs. Chlorotepine (**87**)<sup>[80]</sup> is a potent neuroleptic drug which has high affinity for serotonin and dopamine receptors and Zotepine (**88**)<sup>[81]</sup> acts as a dopaminergic receptor antagonist as well and is indicated in the treatment of acute and chronic schizophrenia.

### 1.4.1 Synthesis of seven-membered ring systems

To understand the biological properties and modes of action of molecules based on seven-membered ring systems, appropriate synthetic methods are required. Similar to five- and six-membered carbo- and heterocycles, there are several general methods to construct seven-membered rings, as shown in **Figure 16**. Depending on the nature of the ring, these include cyclization, ring closing, cycloaddition followed by cycloreversion and ring expansion reactions. The procedures for the preparation of oxepines, cycloheptatrienes, and thiepienes are considered separately below, and a selection of examples known from the literature is discussed. The focus is mainly on methods for the synthesis of dibenzannulated seven-membered ring systems with a double bond at the bottom.

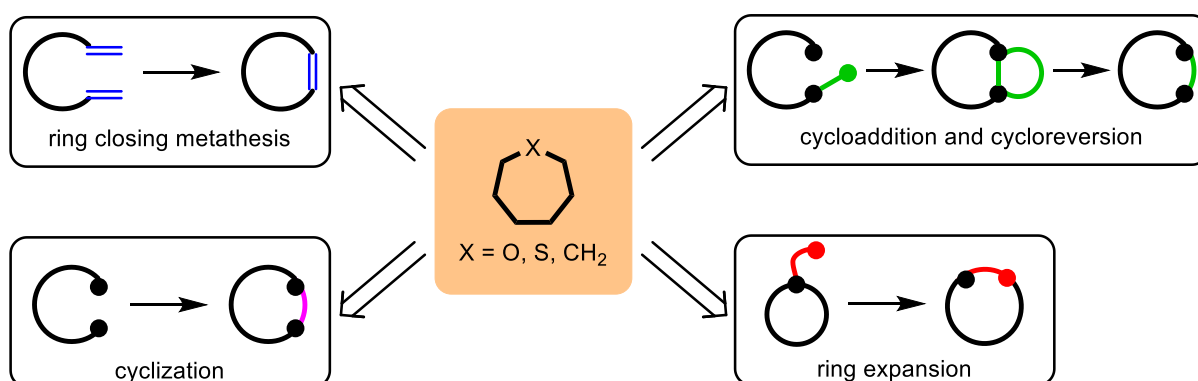
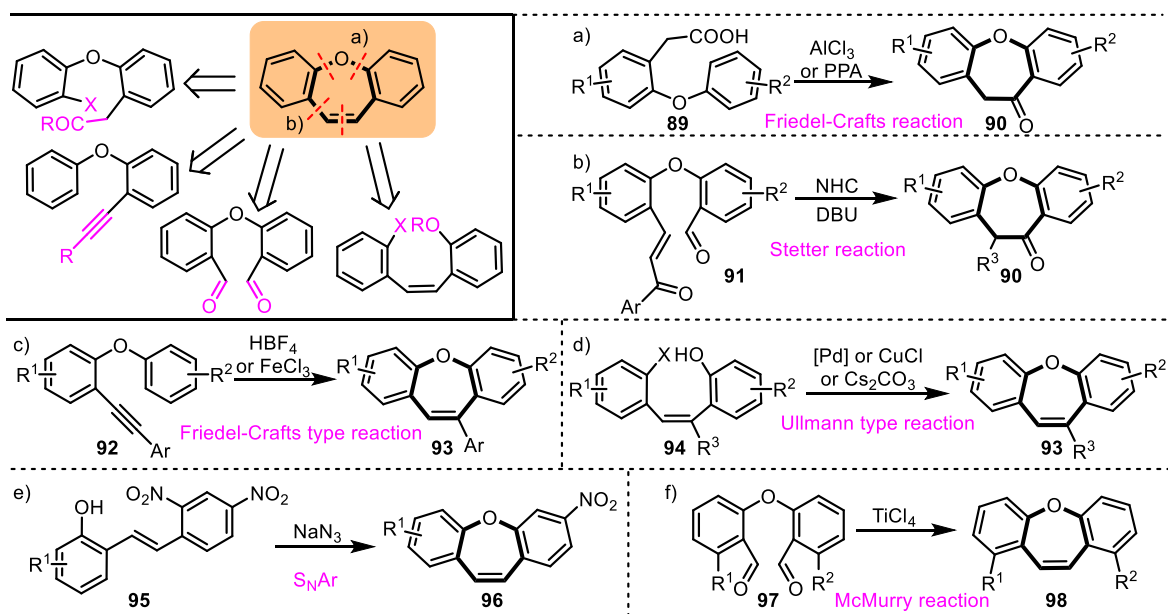


**Figure 16:** Synthetic approaches to seven-membered rings.

Starting with the dibenzo[*b,f*]oxepine framework, numerous different approaches have been described in the past. Methods that belong to the class of cyclizations can be largely divided into one of the classical synthesis paths: a) intramolecular C-O bond formation *via* Ullmann type reaction or S<sub>N</sub>Ar, or b) C-C bond formation *via* cyclodehydration or intramolecular McMurry coupling of intermediates with a preformed diaryl ether scaffold. Using the classical Friedel-Crafts acylation or an acid-mediated cyclodehydration, *o*-phenoxyphenylacetic acids **89** could be transformed into the corresponding dibenzo[*b,f*]oxepin-10(11H)-one **90**, which could be further functionalized (**Scheme 22, a**).<sup>[82,83]</sup> Recently, Suresh and co-workers described a novel NHC-catalyzed method in which a series of dibenzo[*b,f*]oxepine derivatives **90**, some at gram scale, were prepared *via* an intramolecular Stetter reaction. The obtained 1,4-dicarbonyl functionality can be further heterocyclized by a Paal-Knorr reaction (**Scheme 22, b**).<sup>[84]</sup> Another approach was

## 1.4 Seven-membered ring systems

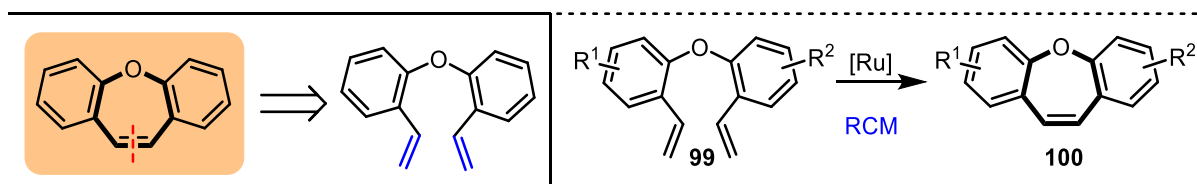
taken by Kitamura and Taniguchi when they described the acid-mediated annulation of *o*-(aryloxy)phenylalkynes **92**. The reaction proceeds *via* a vinyl cation formed by initial 1,2-addition of a suitable electrophile (e.g. H<sup>+</sup>). Subsequent intramolecular arylation yields the desired dibenzo[*b,f*]oxepine **93** (**Scheme 22**, c)). Unfortunately, this method yielded the desired product only in the case of 1-(*p*-methoxyphenyl)-2-(*o*-phenoxyphenyl)ethyne, where the carbocation generated can be sufficiently stabilized by the  $\alpha$  anisyl substituent.<sup>[85]</sup> Recently, a mild method was published using starting materials of similar structure but with FeCl<sub>3</sub> instead of a Brønsted acid (**Scheme 22**, c)). This enabled the development of a more widely applicable strategy that facilitates 7-*endo*-dig annulation of *o*-phenoxy diarylacetylenes **92** under mild reaction conditions. When the aromatic substituent at the triple bond was replaced by an aliphatic residue, no product formation was observed in this case either, and the starting material was quantitatively reisolated.<sup>[86]</sup> In terms of intramolecular C-O bond formation as key step to obtain the seven-membered oxepine **93** several Ullmann type reactions either catalyzed by a metal, such as palladium<sup>[87]</sup> or copper,<sup>[88]</sup> or transition-metal free and base-mediated reactions have been published (**Scheme 22**, d)).<sup>[89,90]</sup> Following the S<sub>N</sub>Ar approach, Krawczyk *et al.* published a NaN<sub>3</sub>-mediated cyclization of stilbenes **95** previously obtained from a condensation of 2,4-dinitrotoluene with various substituted methoxyaldehydes. The reaction also proceeds without NaN<sub>3</sub>, but the addition can significantly increase the yield (**Scheme 22**, e)).<sup>[91]</sup> Furthermore, starting from diaryl ether precursors **97**, intramolecular McMurry coupling is an additional option to generate dibenzo[*b,f*]oxepine **98** *via* C-C bond formation (**Scheme 22**, f)).<sup>[89]</sup>



**Scheme 22:** Cyclization methods for the synthesis of dibenzo[*b,f*]oxepines.

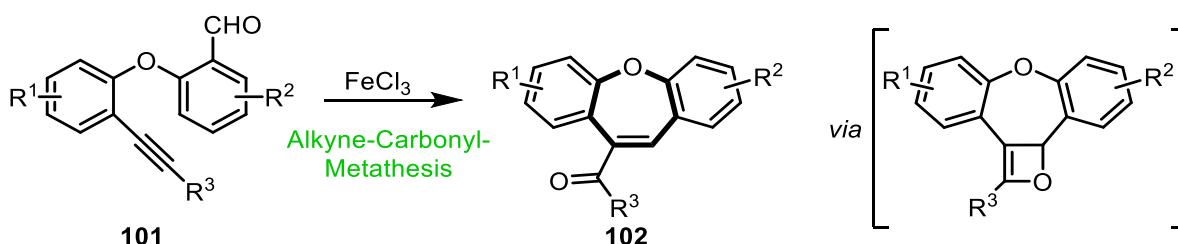
## 1. Introduction

Moreover, ring closing metathesis has also been successfully applied in the construction of medium-sized ring systems (**Scheme 23**). An approach was presented by the group of Mohapatra in the course of developing a synthesis route for Bauhiniastatins in which a Ullmann-type reaction was initially used to construct the biaryl ether **99** followed by an RCM reaction to obtain the final dibenzo[*b,f*]oxepine **100**. In the presence of the Grubbs II or Hoveyda-Grubbs II catalyst 2,2'-oxy-bis(vinylbenzenes) **99** were converted with high to excellent yields (82-96%).<sup>[92]</sup>



**Scheme 23:** Ring closing metathesis approach for the synthesis of dibenzo[*b,f*]oxepines.

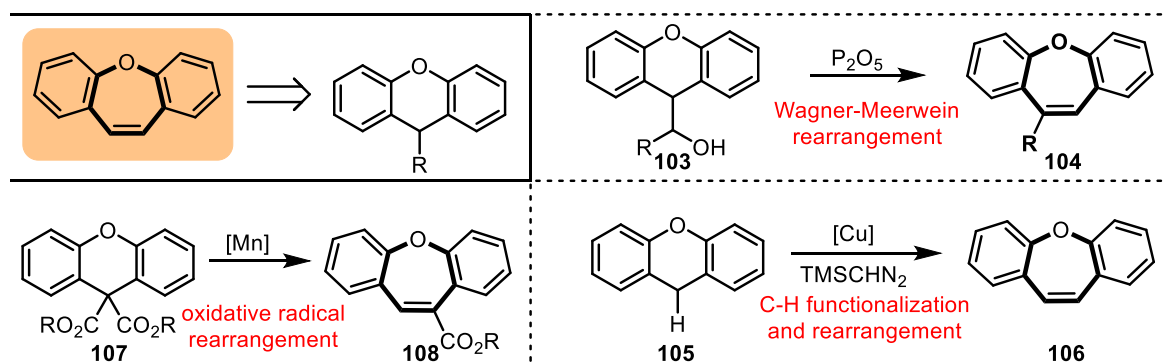
In addition, alkyne-carbonyl-metathesis proved to be a suitable method to build heterocycles and carbocycles under mild conditions. Normally, this reaction proceeds *via* a [2+2] cycloaddition followed by cycloreversion. By using FeCl<sub>3</sub> as a catalyst, Jana and co-workers were able to extend this strategy to the synthesis of seven-membered oxygen heterocycles **102** with outstanding chemo- and regioselectivity (**Scheme 24**).<sup>[93]</sup>



**Scheme 24:** Alkyne-Carbonyl Metathesis strategy towards dibenzo[*b,f*]oxepines.

Another classical approach is the Wagner-Meerwein rearrangement of xanthene derivatives **103**, which belongs to the class of ring expansions (**Scheme 25**, top right).<sup>[94]</sup> Since this rearrangement requires harsh conditions, such as large excess of strong acids or phosphorus pentoxide under heating and several steps to introduce the leaving group, the application is limited. Furthermore, the functional group tolerance is rather poor and only moderate yields of oxepine **104** have been obtained. To overcome these issues Stopka *et al.* developed a mild method that allows the direct C-H functionalization of xanthenes **105**. By using trimethylsilyldiazomethanes (TMSCHN<sub>2</sub>) in combination with a copper catalyst, a silicon leaving group is simultaneously incorporated to favor the subsequent *in situ* rearrangement to the corresponding oxepine **106** (**Scheme 25**, bottom right).<sup>[95]</sup> In this context of ring expansion, a Mn(III)-based oxidative 1,2-radical rearrangement has been published as well, which yields the desired dibenzo[*b,f*]oxepines **108** starting from 2-(9*H*-xanthenyl)malonates **107** (**Scheme 25**, bottom left).<sup>[96]</sup>

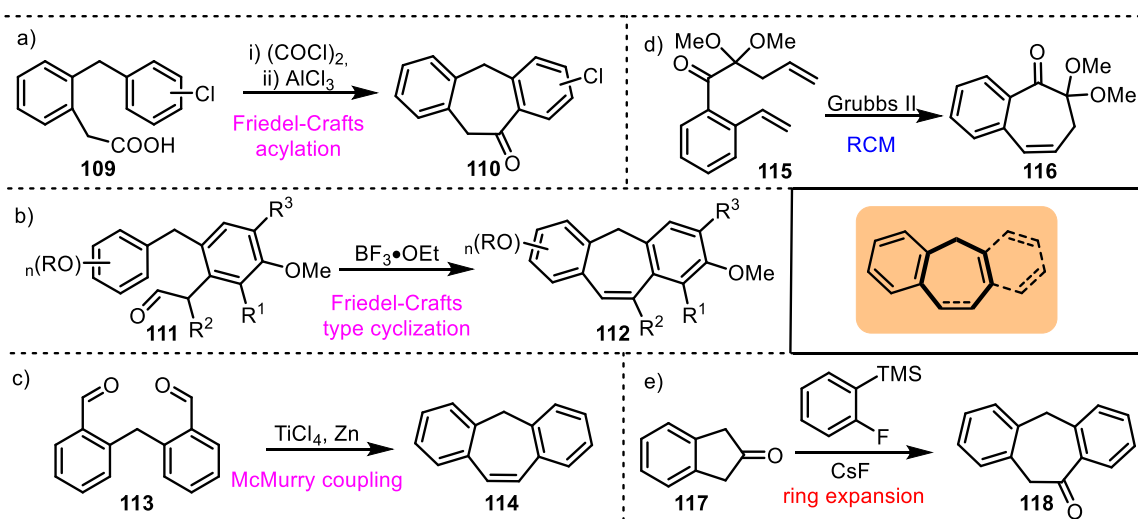
## 1.4 Seven-membered ring systems



**Scheme 25:** Ring expansion approach for the synthesis of dibenzo[b,f]oxepines.

Although the synthetic principles are similar, the literature on synthetic methods towards seven-membered carbocycles and thiepinines is less abundant compared to oxepines. Intramolecular Friedel-Crafts type reactions play a major role in the synthesis of dibenzocycloheptatrienes. As already described for the synthesis of dibenzoxepines, classical Friedel-Crafts acylation was used to convert 2-(2-benzylphenyl)acetic acids **109** into the corresponding 5,11-dihydro-dibenzo[a,d]cyclohepten-10-ones **110** which could be then further functionalized (**Scheme 26, a**).<sup>[97]</sup> Another approach was to prepare dibenzo[a,e]cycloheptatrienes **112** from substituted 2-allylbenzaldehydes **111** in an intramolecular Friedel-Crafts type cyclization in good to excellent yields. In summary, this is a formal [5+2] annulation, where the synthetic route starting from 2-allylbenzaldehyde **111** involves aldehyde reduction, intermolecular coupling, oxidative olefin cleavage and an intramolecular Friedel-Crafts reaction as a final ring closure step (**Scheme 26, b**).<sup>[98]</sup> Also an intramolecular McMurry coupling of dialdehyde **113** was recently applied in the synthesis of dibenzo[a,e]cycloheptatriene **114** (**Scheme 26, c**).<sup>[99]</sup> In ring-closing metathesis, only one example was found where this strategy was used in the construction of seven-membered carbocycles. Brückner and co-worker generated benzocycloheptadienedione monoketals **116** in the presence of Grubbs II catalyst from aromatic dienones **115**, which could be hydrolyzed to 3,4-benzotropolones (**Scheme 26, d**).<sup>[100]</sup> In addition to the previously described approaches, a protocol has recently been published in which ring expansion by cleavage of benzylic C-C bonds has allowed the preparation of medium ring-fused carbocycles. Employing fluoride anions to induce the insertion of arynes into benzylic C-C bonds of benzocyclic ketones **117** a strategy towards the synthesis of 5,11-dihydro-dibenzo[a,d]cyclohepten-10-ones **118** was proposed (**Scheme 26, e**).<sup>[101]</sup>

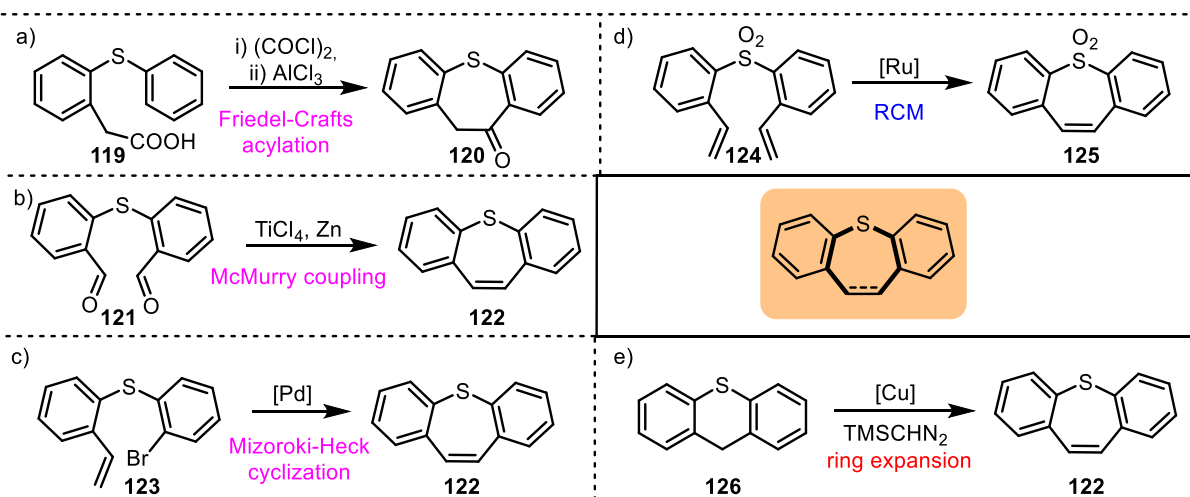
## 1. Introduction



**Scheme 26:** Synthetic approaches for the synthesis of seven-membered carbocycles.

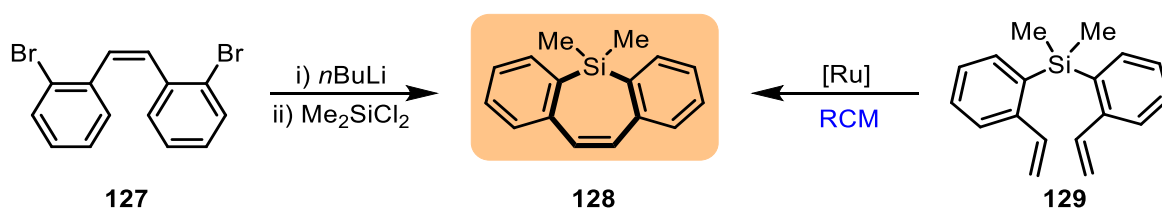
Continuing with the synthesis of dibenzo[*b,f*]thiepines, it is evident that the classical cyclization methods play the major role here as well. Usually, the sulfur bridge is established first and cyclization to the seven-membered ring is performed in the next step. Starting with a Hetero-Ullman coupling to form the thioether followed by an intramolecular Friedel-Crafts cyclization of **119** yielded the corresponding dibenzo[*b,f*]thiepin-10(11H)-one **120** (**Scheme 27**, a)). Further functionalization of the ketone functionality with *n*-butyllithium and a bromobenzene derivative and subsequent acidic dehydration led to the dibenzo[*b,f*]thiepines.<sup>[83]</sup> As already described for the dibenzo[*b,f*]oxepines the NHC-catalyzed intramolecular Stetter reaction could be also applied to generate a dibenzo[*b,f*]thiepin-10(11H)-one **120**.<sup>[84]</sup> In contrast, an intramolecular McMurry coupling provides the desired dibenzo[*b,f*]thiepine scaffold **122** without additional substituents (**Scheme 27**, b)).<sup>[102]</sup> Another protocol used a Pd-catalyzed intramolecular Mizoroki-Heck coupling, which was already applied in the synthesis of seven-membered nitrogen-containing heterocycles. Cyclization yielded both the 7-*endo* **122** (dibenzo[*b,f*]thiepine) and the 6-*exo* (thioxanthene) product, with a 7:3 *endo/exo* ratio providing the best selectivity with respect to the seven-membered ring (**Scheme 27**, c)).<sup>[103]</sup> Ring closing metathesis was demonstrated only for 2,2'-sulfonylbis(vinylbenzene) **124**, with the corresponding dibenzo[*b,f*]thiepin-5,5-dioxide **125** obtained in excellent yield (**Scheme 27**, d)).<sup>[104]</sup> The mild ring expansion strategy developed by Stopka *et. al.* and previously described for dibenzo[*b,f*]oxepines is also suitable for the synthesis of seven-membered sulfur heterocycles **122** (**Scheme 27**, e)).<sup>[95]</sup>

## 1.4 Seven-membered ring systems



**Scheme 27:** Synthetic strategies for the synthesis of dibenzo[*b,f*]thiepine.

Dibenzo[*b,f*]silepines show interesting optical properties. By incorporating varying donor groups with different donor strengths, the absorption and emission ranges can be changed. In addition, carbon is often exchanged by silicon to tune properties of drugs and to enhance the biological activity.<sup>[105]</sup> The unsubstituted dibenzo[*b,f*]silepine could be synthesized using a dibromostilbene precursor **127**. A dilithium halogen exchange using *n*-butyllithium was performed, allowing the aryl dilithium species generated *in situ* to be trapped with dichlorodimethylsilane give the desired silepine derivative **128**. For substituted dibenzo[*b,f*]silepines, a substitution with different halogens was necessary to achieve a selective dilithium halogen exchange and subsequent functionalization *via* cross-coupling reactions (**Scheme 28**, left).<sup>[106]</sup> The other strategy described in the literature is based on ring closing metathesis of bis(2-vinylphenyl)silanes **129** using the second generation Hoveyda-Grubbs catalyst (**Scheme 28**, right).<sup>[104]</sup>



**Scheme 28:** Synthetic approaches for the synthesis of dibenzo[*b,f*]silepine **128**.

However, some of these approaches have several limitations, partly requiring complex preparation of starting materials and sometimes harsh reaction conditions, like the Friedel-Crafts reaction or the Wagner-Meerwein rearrangement. In addition, lack of generality or unsatisfactory yields are further drawbacks. Therefore, due to the beneficial biological effects and applications of the seven-membered ring systems, it seems desirable to develop more general methods that proceed under mild conditions and exhibits high tolerance to functional groups.

### 1.4.2 Conformational stability of seven-membered ring systems

It was recognized early on that there is a close correlation between the conformational stability of compounds based on seven-membered ring systems and their pharmacological activity. The seven-membered ring adopts a boat-like conformation and, in particular, its conformational stability may have a major impact on the biological properties. This is due to the non-planar seven-membered ring adopting a geometry that behaves like enantiomers when mirrored. As can be seen in **Figure 17** a) the stereogenic element is the axis orthogonal to both arrows and intersecting them.<sup>[107,108]</sup> In addition, these conformers are often also considered as atropisomers, which is a special case of axial chirality. In atropisomers, the rotation around a single bond is so strongly hindered by sterically demanding substituents that conformers can be isolated. Both forms of isomerism can lead to enantiomers, diastereomers and cis-trans isomers, which in general could be equilibrated thermally (**Figure 17**). However, according to a definition by M. Oki, the half-life of isomerization for compounds to be considered as atropisomers (conversion of one rotamer into the other) at a given temperature must be higher than 1000 seconds.<sup>[109]</sup>

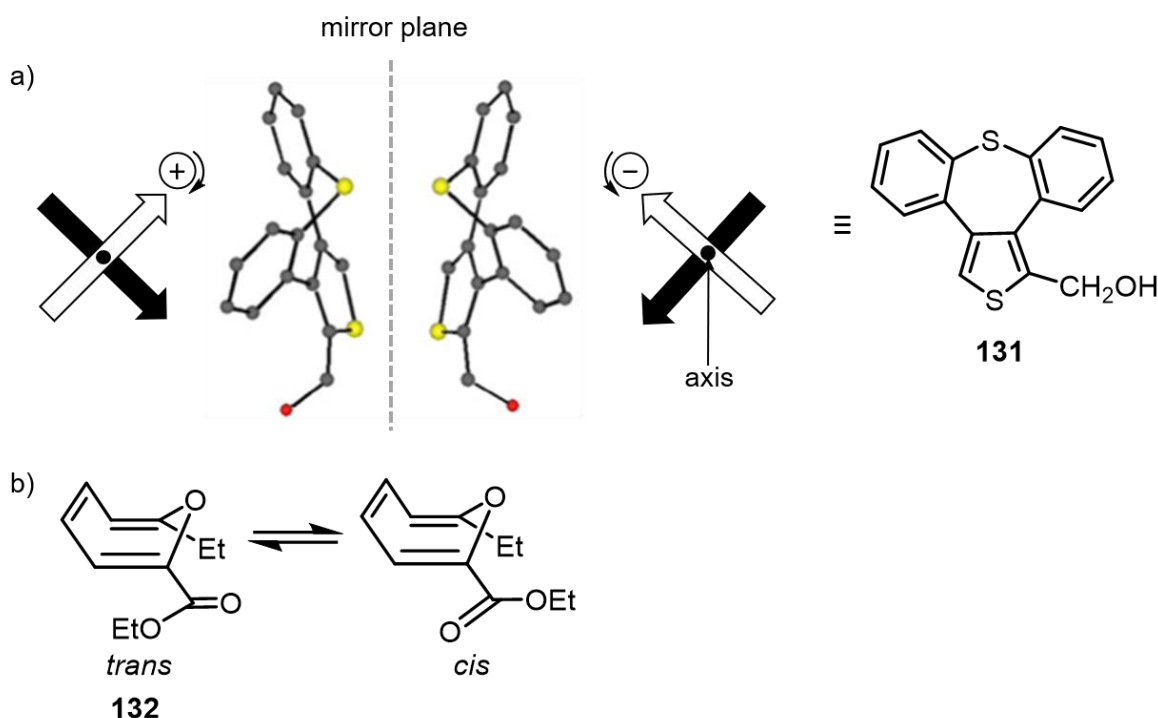


**Figure 17:** a) enantiomers of tetracyclic thiepine **131**, b) stereoisomers of oxepine **132**.<sup>[107]</sup>

Following the notion of axial chirality, the inversion of the central seven-membered ring is assumed to proceed *via* a planar achiral transition state. The energy of the inversion barrier can be of great pharmacological relevance. As soon as a rapid ring inversion can take place under physiological conditions, an equilibrium is reached and the appropriate conformer can be bound to the active site of an enzyme. Whereas if the inversion barrier is too high, only 50% of the conformers can be used. Therefore, conformational stability plays a major role in drug development. Either an interconvertible mixture might be developed when the



## 1.4 Seven-membered ring systems

inversion barrier of the seven-membered ring is low, or the planar chiral substance is employed as a single conformationally stable enantiomer.<sup>[107,110]</sup>

Based on these considerations, the conformational stability of some seven-membered ring systems was evaluated to investigate whether a separation of the enantiomers would be possible. Comparing the energy barriers for ring inversion of oxepines, thiepines and cycloheptatrienes reported in the literature, it is obvious that it is highly dependent on the number of annulated rings. A significant increase in the energy barrier from monocyclic **133** to tricyclic **134-137** analogues is observed, which is particularly high for tetracyclic representatives **138** (**Figure 18**). Due to the *gem*-dimethyl group in **137** and the associated steric repulsion with the *peri*-C-H bond, the barrier increases substantially in comparison to **134**. Furthermore, a significant difference can be noted between oxepine **135** and thiepine **136** derivatives, with little difference between **136** and the all-carbon analogue **137**. The non-bonding interactions between *peri*- and *ortho*-H atoms in tetracyclic tribenzocycloheptatriene **138** further enhance the barrier.<sup>[111]</sup>

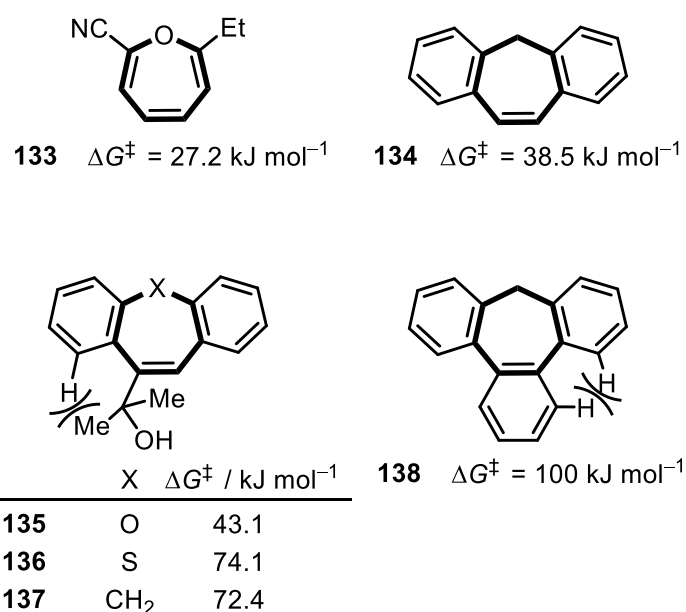


**Figure 18:** Overview of reported inversion barriers for oxepine, thiepine and cycloheptatriene derivatives.

Landek and co-workers studied the inversion barriers of tetracyclic derivatives with an oxepine or thiepine ring annulated to thiophene and the separability of the corresponding enantiomers. They demonstrated that molecules based on thiepines occur as a pair of enantiomers at room temperature and can be detected by variable temperature-dependent NMR spectroscopy as well as resolved by chiral HPLC analysis. Whereas none of the oxepine derivatives could be separated on chiral HPLC columns, due to a very fast enantiomerization process.<sup>[107]</sup> However, in all cases the inversion barrier is too low to ensure the stability of the individual enantiomers over a longer period at room temperature after a successful separation.

## 1.5 Planar-chiral ferrocenes

Within this thesis gold catalyzed transformations to generate seven-rings with annulated ferrocenes will be considered. Therefore, a brief introduction to planar-chiral ferrocenes will be given and conventional methods for the preparation as well as Au/Pt catalyzed asymmetric approaches will be discussed.

Planar-chiral ferrocenes represent an important framework in organic and organometallic chemistry and have been used as ligands, catalysts, or templates in a variety of asymmetric reactions. Their applications include, for example, asymmetric hydrogenations, allylic substitutions, conjugated additions, and pericyclic reactions.<sup>[112,113,114]</sup> Representative examples of planar-chiral ferrocenes are shown in **Figure 19**. In 1974, Hayashi *et al.* pioneered this field by presenting PPFA ((*S<sub>p</sub>*)- $\alpha$ -[(*R*)-2-diphenylphosphinoferrocenyl]ethyl)dimethylamine, **139**), the first planar-chiral ferrocenylphosphine ligand that exhibited both central and planar chirality and was prepared from Ugi's amine.<sup>[115]</sup> The structural motif of PPFA was adopted by Togni and collaborators in the development of Josiphos (**140**) in 1994 and found wide application.<sup>[116]</sup> Moreover a highly versatile catalyst was designed by the Fu group with the planar-chiral DMAP derivative **141**.<sup>[117]</sup>

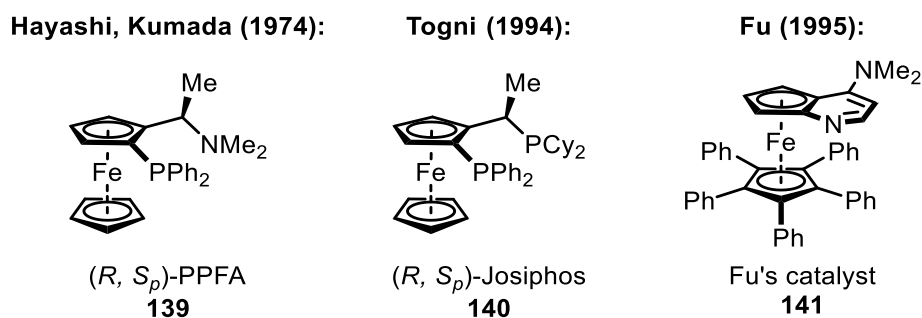
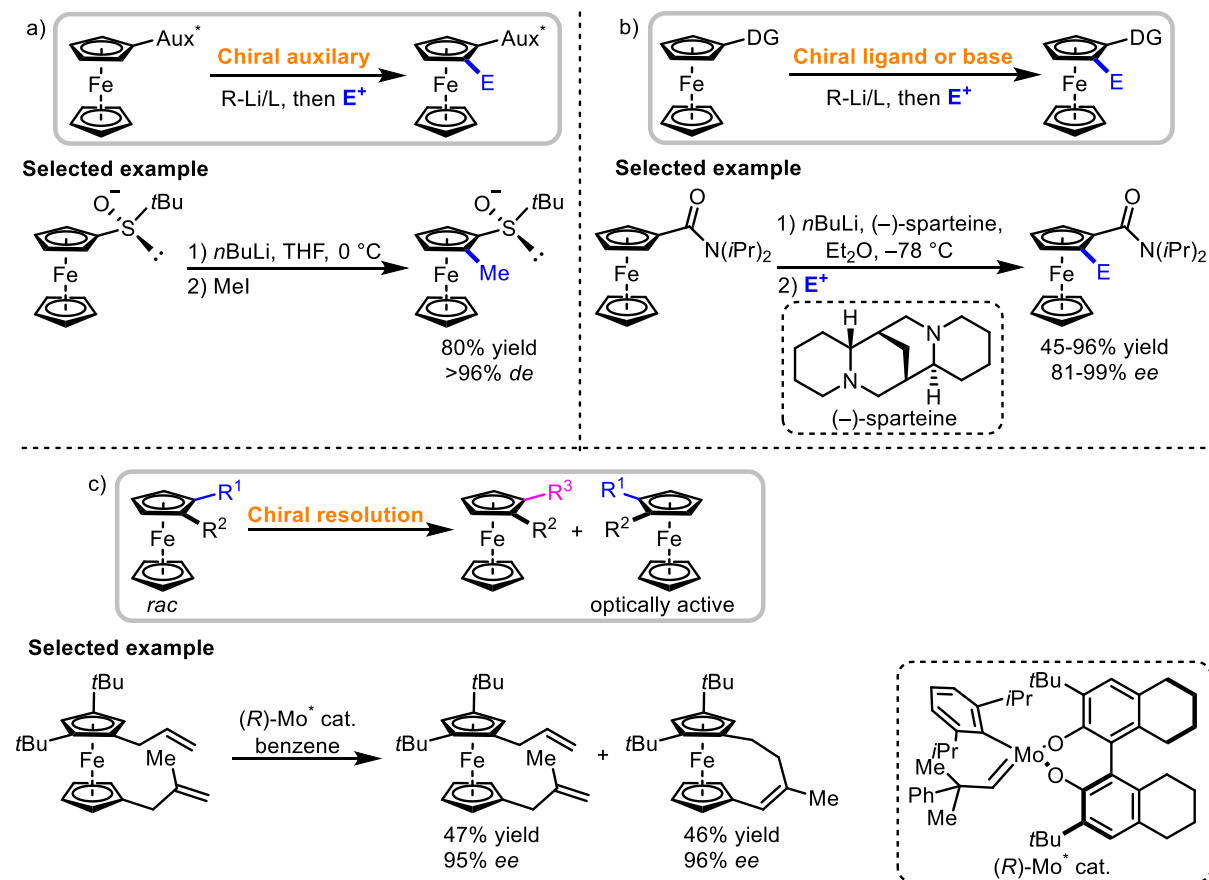


**Figure 19:** Representative planar-chiral ferrocene ligands and catalysts.

Diastereoselective directed *ortho*-metalation (DoM)<sup>[118]</sup> (**Scheme 29**, a)), enantioselective DoM<sup>[119]</sup> (**Scheme 29**, b)), and chiral resolution<sup>[120]</sup> (**Scheme 29**, c)) are well-established methods for introducing planar chirality into ferrocene frameworks. The aforementioned strategies often require stoichiometric amounts of preinstalled chiral auxiliaries or chiral bases and sensitive organometallic reagents, which hinders their practical application. An extremely efficient approach for the synthesis of planar chiral ferrocenes would be the development of versatile catalytic methods. Although transition metal-catalyzed asymmetric direct C-H functionalization has undergone tremendous development in recent decades,

## 1.5 Planar-chiral ferrocenes

there are relatively few studies on enantioselective C-H bond functionalization to introduce planar chirality into ferrocenes.



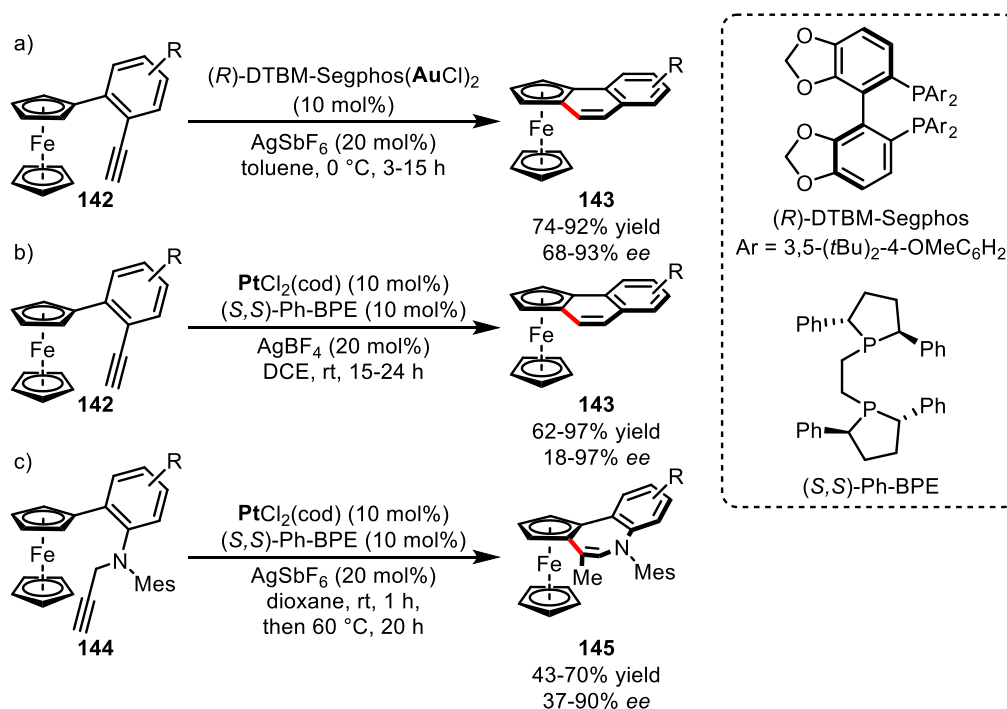
**Scheme 29:** Conventional methods to construct planar chiral ferrocenes.

In 1997, Siegel and Schmalz reported their pioneering work on a copper-catalyzed intramolecular asymmetric carbene C-H insertion reaction of ferrocenes with up to 78% *ee*.<sup>[121]</sup> After that, there was a surprisingly long period of no new developments in this field. Recently, a significant progress in the synthesis of planar chiral ferrocenes was achieved by the use of transition metals and C-H activation reactions.<sup>[112]</sup> However, the next section will focus only on Au/Pt-catalyzed asymmetric functionalization of C-H bonds.

Transition-metal catalyzed intramolecular hydroarylation has proven to be a powerful tool in the synthesis of phenanthrenes and helicenes and enantioselective versions have also been reported, as discussed previously in 1.3.4 *Application of  $\alpha$  cationic phosphines in catalysis*. Recently, Urbano and Carreño published an enantioselective Au(I)-catalyzed cycloisomerization reaction for the synthesis of *ortho*-condensed aromatic ferrocenes **143** under mild conditions. This is the first example of generating planar chirality using gold catalysts. Readily available *ortho*-alkynylaryl ferrocenes **142**, which can be prepared in only two steps from commercially available ferrocenyl boronic acids and 2-bromobenzaldehydes, serve as starting materials (**Scheme 30, a**).<sup>[122]</sup> Shortly thereafter,

## 1. Introduction

Shibata and coworkers reported a similar strategy to prepare planar chiral ferrocene frameworks **143** with up to 97% ee using a chiral Pt catalyst (**Scheme 30, b**).<sup>[123]</sup> In this context, Shibata and Ito were also able to extend their previously developed method to the enantioselective synthesis of azepine-fused planar-chiral ferrocenes **145** utilizing the same chiral Pt catalyst. It was the first enantioselective approach for the asymmetric synthesis of seven-membered ring fused planar-chiral ferrocenes (**Scheme 30, c**).<sup>[124]</sup>



**Scheme 30:** Au/Pt catalyzed asymmetric synthesis of planar-chiral ferrocenes.

Although a few examples of asymmetric synthesis of ring-fused planar-chiral ferrocenes are known the enantioselective approach is still challenging. Since planar-chiral ferrocene are important scaffolds in organic and organometallic chemistry it seems desirable to develop widely applicable methods.

## 2. Project proposal

Inspired by previous work of the Alcarazo group in the field of  $\pi$  acid catalysis and its application in the synthesis of phenanthrenes and carbohelicenes other classes of compounds will be addressed. As mentioned in the introduction seven-membered rings systems exhibit a wide range of biological and medicinal activities and have been found in numerous natural products as well as in the pharmaceutical industries. In order to realize the synthesis of these seven-membered ring systems, this work will attempt to transfer the annulation developed for *o*-ethynyl biphenyl substrates to 1-(benzyl-, oxyaryl-, thioaryl-, and silylaryl)-2-ethynylbenzenes, which differ only in the presence of a one-atom tether between the two rings (**Figure 20**). This includes the preparation of the respective starting materials and the selection of suitable  $\pi$  acidic catalysts, with cationic phosphine ligands also being considered. Since Ye and coworkers have described the cyclization of 1-benzyl-2-ethynylbenzenes to anthracenes *via* a combination of Brønsted acid and gold catalysis,<sup>[26]</sup> conditions must be found where the formation of the seven-membered ring *via* the 7-*endo*-dig process is preferred over the competing 6-*exo*-dig process and an additional comparison between Brønsted acid and gold catalysis will be conducted. In addition, the conformational stability of the seven-membered ring will be investigated by experimentally determining the inversion barrier and comparing it with the values obtained by complementary DFT calculations. Moreover, the effects of changing the tether will be investigated as well.

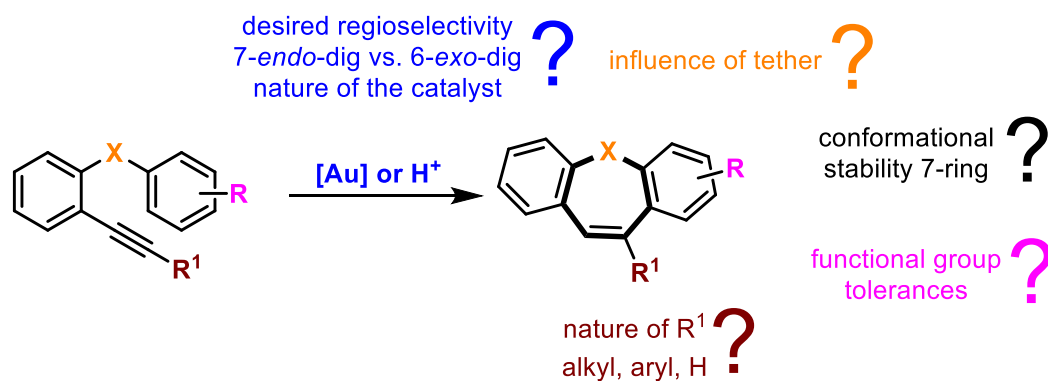


**Figure 20:** Challenges and questions towards the synthesis of seven-membered ring systems addressed in this work.

In addition to dibenzo compounds, the synthesis of seven-membered ring fused planar-chiral ferrocenes *via* asymmetric hydroarylation using previously developed chiral Au(I)<sup>[46,71]</sup> catalysts will be tried (**Figure 21**). Since this framework plays an important role as a ligand, catalyst or template in organic and organometallic chemistry, it would be desirable to further advance the development of asymmetric synthesis strategies. Following the preparation of the appropriate precursors, the optimization of the reaction conditions will be started based

## 2. Project proposal

on the racemic reaction. Subsequently, various chiral gold catalysts will be investigated and the most suitable representative will be selected. The exchange of benzene against ferrocene introduces another chiral element, that may help to control the configuration of the seven-membered ring (diastereomers).

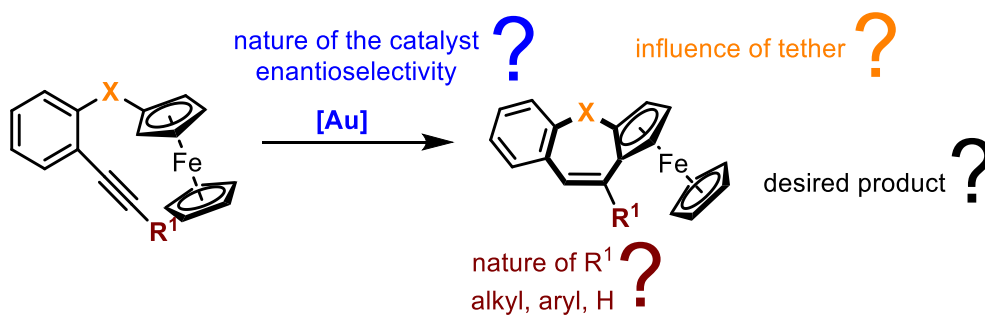
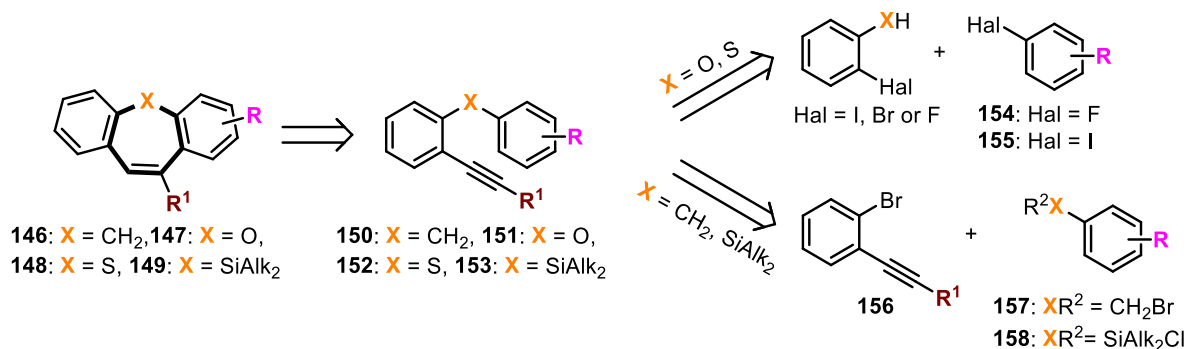


**Figure 21:** Challenges and questions towards the synthesis of seven-membered ring fused planar-chiral ferrocenes.

## 3. Results and discussion

### 3.1 Synthesis of seven-membered ring systems

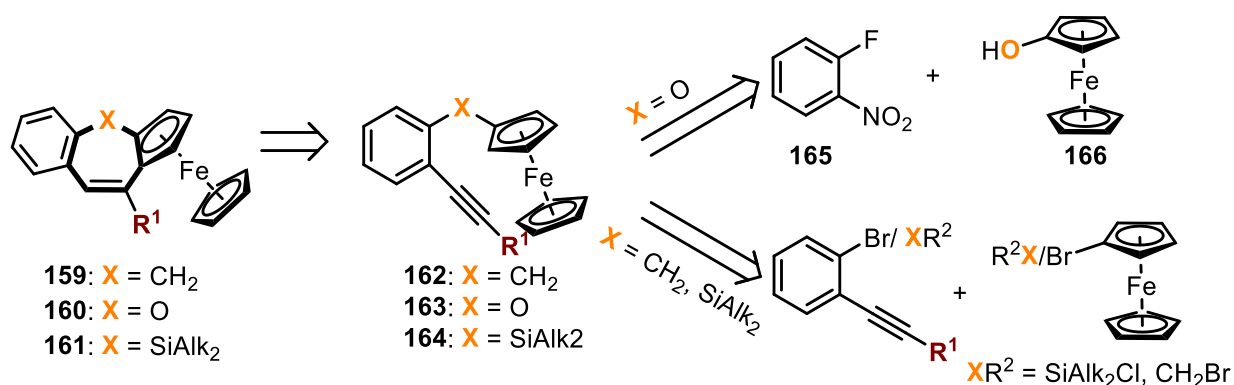
As mentioned in the project proposal, the desired dibenzo[*a,e*]cycloheptatrienes, dibenzo[*b,f*]oxepines, -thiepienes and silepienes should be realized *via* Au(I)-catalyzed cycloisomerization of the corresponding alkyne precursors. The respective synthesis strategy to obtain the precursors has to be adapted depending on the heteroatom in the seven-membered ring (**Scheme 31**).



**Scheme 31:** Retrosynthetic approach towards the synthesis of dibenzo[*a,e*]cycloheptatrienes **146**, dibenzo[*b,f*]oxepines **147**, -thiepienes **148** and silepienes **149**.

For -CH<sub>2</sub>- and -SiAlk<sub>2</sub>- as tethers, the alkyne was introduced prior to the connection between the two aromatics. For the oxygen and sulfur tethers, the linkage of the aromatic systems was conducted first and a halogen substituent was incorporated to allow for a later introduction of the alkyne. The obtained precursors could be converted to the desired seven-membered ring systems.

Retrosynthetic analysis was also performed for the synthesis of seven-membered ring fused planar-chiral ferrocenes to develop a suitable strategy for the synthesis of appropriate precursors (**Scheme 32**). Since Au(I)-catalyzed hydroarylation should be the key step of the synthesis, the presence of an alkyne in the precursor is mandatory.



**Scheme 32:** Retrosynthetic approach towards the synthesis of seven-membered ring fused planar-chiral ferrocenes.

### 3. Results and discussion

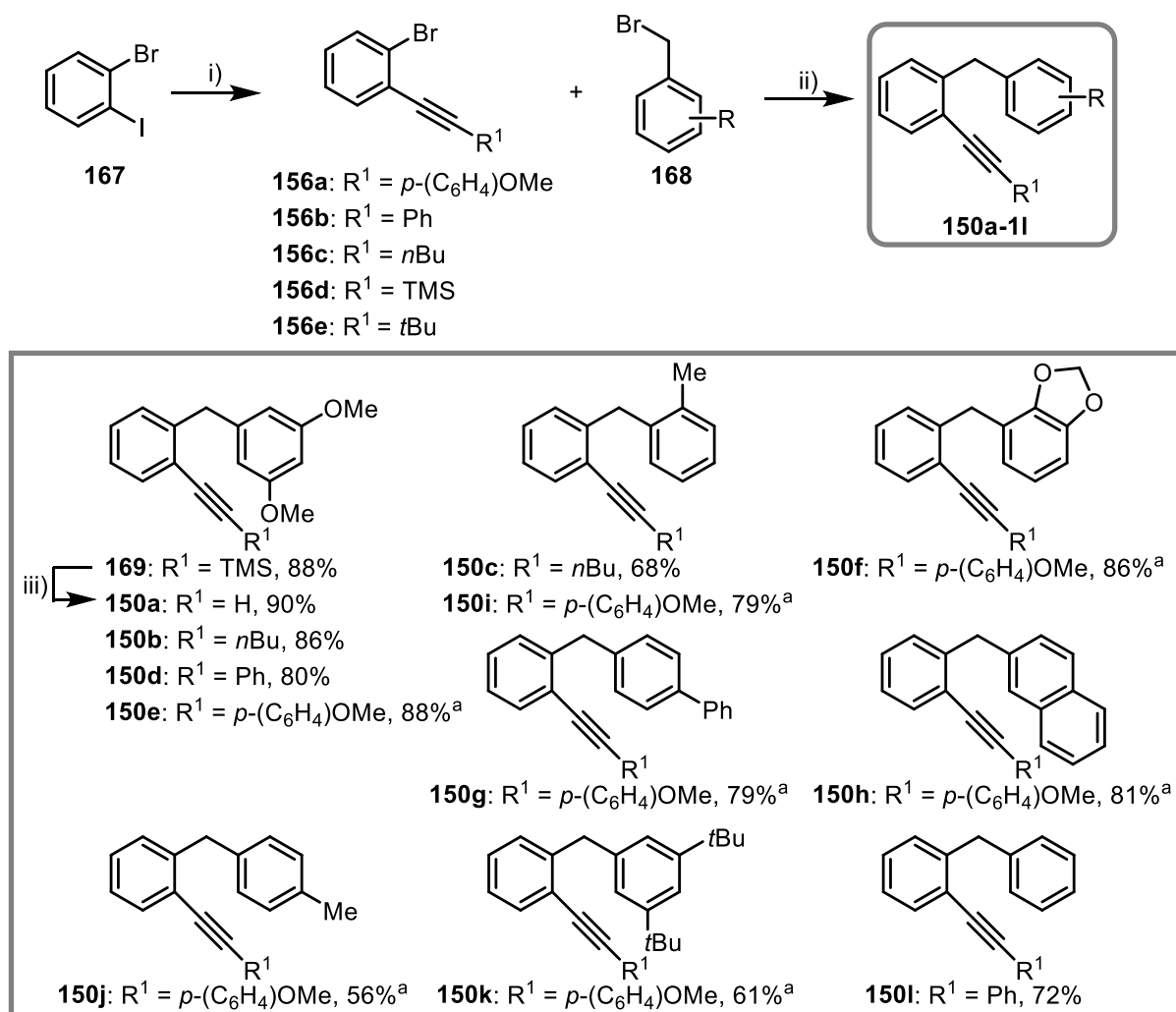
The precursors containing ferrocenes can be constructed from fragments similar to their dibenzo analogues. However, it must be considered that the respective reaction conditions cannot always be transferred directly to ferrocenes. Sulfur as a tether was not included since no suitable conditions for ferrocenes were found to realize the linkage.

#### 3.1.1 Synthesis of precursors

Depending on the tether, different synthetic routes were chosen for the respective precursors. The main focus was to require as few synthesis steps as possible while making the strategy variable enough to allow modulation of substituents on both the alkyne and aromatic systems.

##### 3.1.1.1 Cycloheptatriene precursors

For the synthesis of 1-(benzyl)-2-ethynylbenzene **150** precursors for cycloheptatrienes, a pathway we had previously applied was utilized (**Scheme 33**).<sup>[125]</sup>



**Scheme 33:** Synthesis of 1-(benzyl)-2-ethynylbenzenes. Reagents and conditions: i) alkyne (1.0 eq), PdCl<sub>2</sub>(PPh<sub>3</sub>)<sub>2</sub> (2 mol%), CuI (3 mol%), Et<sub>3</sub>N, rt, ovn, **156a** 96%, **156b** 99%, **156c** 88%, **156d** 96%, **156e** 99%, ii) *n*BuLi (1.05 eq), ZnBr<sub>2</sub> (1.05 eq), Pd(PPh<sub>3</sub>)<sub>4</sub> (5 mol%) THF, -78 °C, 30 min, then rt, 1 h, 65 °C, 15 h, iii) K<sub>2</sub>CO<sub>3</sub> (1.0 eq), DCM/MeOH (1:1), rt, ovn. <sup>a</sup>Compounds were prepared by M. Zhao.<sup>[125]</sup>

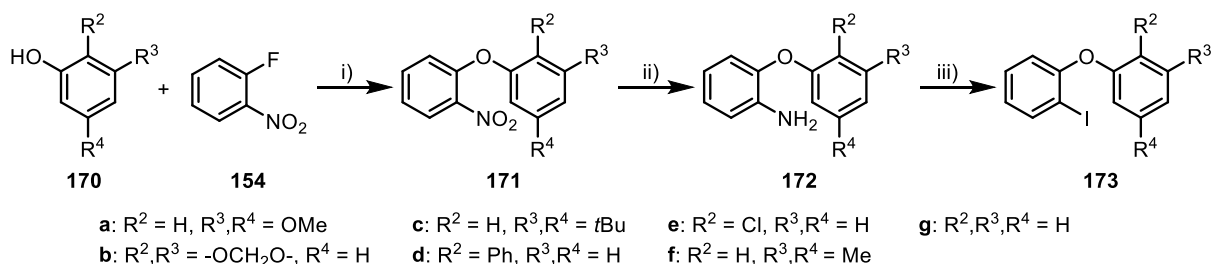


### 3.1 Synthesis of seven-membered ring systems

Through a Sonogashira coupling, 2-iodobromobenzene (**167**) was reacted with the respective terminal alkyne in presence of bis(triphenylphosphine)palladium(II)-dichloride and copper iodide to obtain **156a-e** in very good to excellent yields, which find also application in the synthesis of silepine precursors **153**. In order to yield the zincate for the following Negishi coupling a lithium halogen exchange on **156** was performed and zinc bromide was added. The desired cycloheptatriene precursors **150a-i** were isolated in 56 to 90% yield. To afford the free alkyne **150a** with a yield of 90%, the TMS protecting group of compound **169** was cleaved under basic conditions following a literature procedure.<sup>[126]</sup>

#### 3.1.1.2 Oxepine precursors

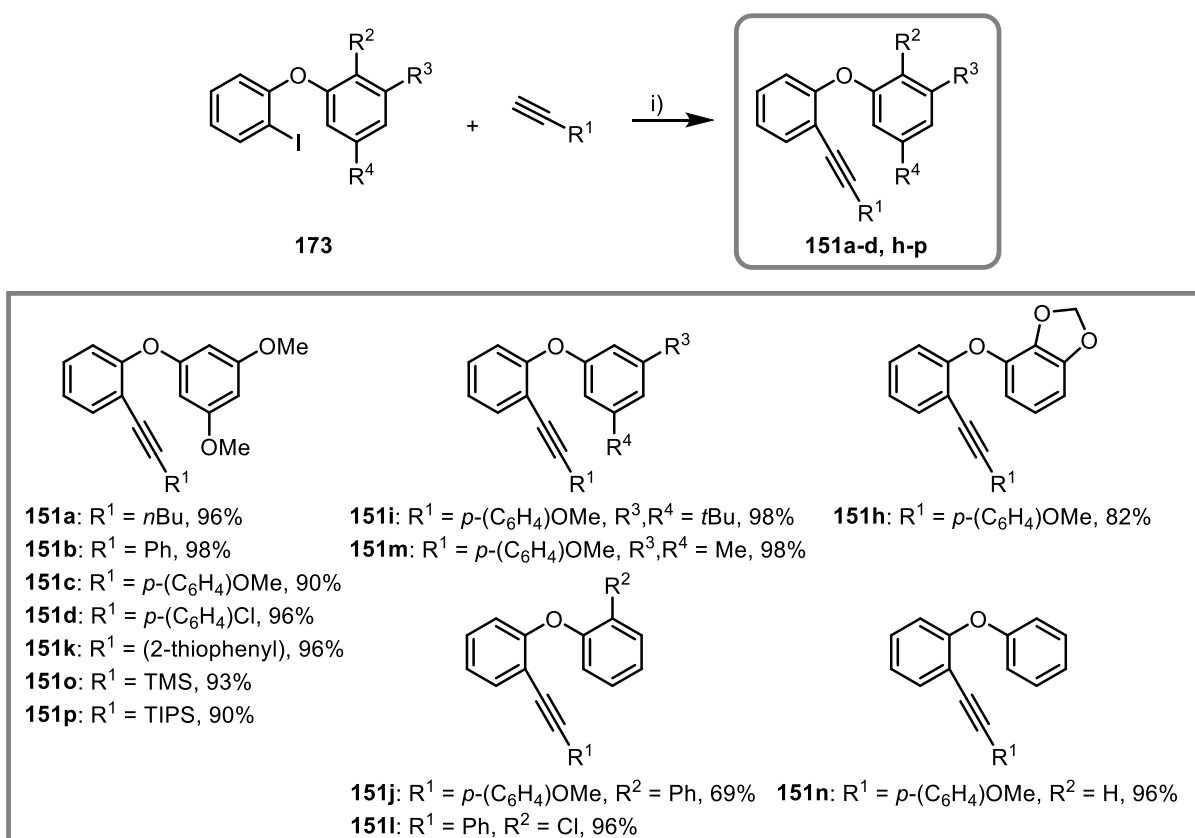
In the synthesis of 1-(oxyaryl)-2-ethynylbenzenes **151** as precursors for oxepines, the first step is a nucleophilic substitution of the respective phenol **170** to 1-fluoro-2-nitrobenzene (**165**) leading to biaryl ethers **171**. After reduction of the nitro group to obtain the corresponding amine **172**, a Sandmeyer-type reaction was carried out to generate the iodoaryl ethers **173** (**Scheme 34**). While the nucleophilic aromatic and subsequent reduction proceeded with nearly quantitative yields, the yields for the Sandmeyer-type reaction showed dependence on the substituents.



**Scheme 34:** Synthesis of iodoaryl ethers **173**. Reagents and conditions: i) K<sub>2</sub>CO<sub>3</sub> (2.0 eq), DMSO, 95 °C, 24 h, **171a** 98%, **171b** 93%, **171c** 99%, **171d** quant., **171e** 99%, **171f** 99%, **171g** quant., ii) Zn (68 eq), HCl/AcOH, EtOAc, 0 °C to rt, ovn, **172a** quant., **172b** 99%, **172c** quant., **172d** 95%, **172e** quant., **172f** quant., **172g** 94%, iii) *p*-TsOH·H<sub>2</sub>O (3.0 eq), KI (2.0 eq), NaNO<sub>2</sub> (2.0 eq), MeCN, H<sub>2</sub>O, rt, ovn, **173a** 70%, **173b** 81%, **173c** 76%, **173d** 54%, **173e** 91%, **173f** 98%, **173g** 89%.

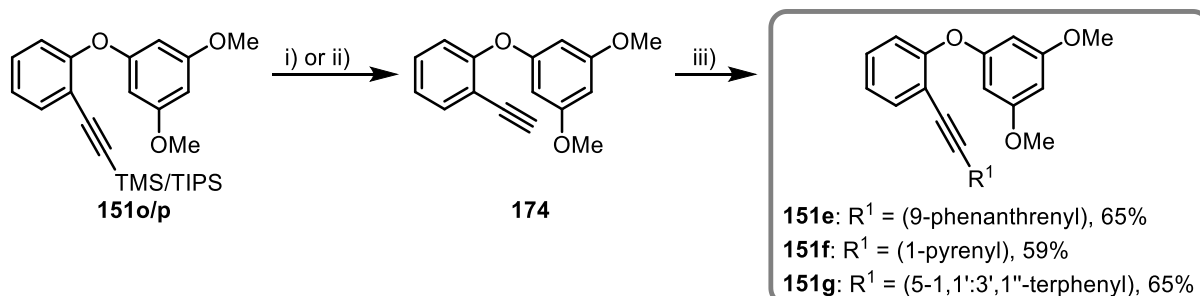
With the iodoaryl ethers **173** in hand, various substituted alkynes could be introduced *via* Sonogashira coupling, allowing in this way a certain flexibility of the synthetic route. The desired 1-(oxyaryl)-2-ethynylbenzenes **151** were obtained with high yields (**Scheme 35**). Changing the substituent R<sup>1</sup> and also substituents in *meta*-positions to the oxygen tether have no influence on the reactivity and excellent yields in the range of 90-98% were observed. When electron-donating substituents as for **151h** and **151j** are located in *ortho*-position to the oxygen tether, the yield is slightly decreased to 82% and 69%, respectively.

### 3. Results and discussion



**Scheme 35:** Sonogashira coupling to obtain **151a-d,h-p**. Reagents and conditions: i) alkyne (1.1 eq),  $\text{PdCl}_2(\text{PPh}_3)_2$  (2 mol%),  $\text{CuI}$  (3 mol%),  $\text{Et}_3\text{N}$ , rt, ovn.

Since the particular alkynes for the compounds **151e-g** were not commercially available, a different strategy was chosen. Starting with either **151o** or **151p**, the protecting group was first cleaved followed by Sonogashira coupling between the terminal alkyne **174** and the related commercially available bromides. Compared to the previously performed Songashira couplings, higher temperatures and higher catalyst loading were necessary to accomplish the reaction, due to the lower reactivity of bromides in contrast to iodides. In addition, the yields are also significantly lower with 59-65% (**Scheme 36**).

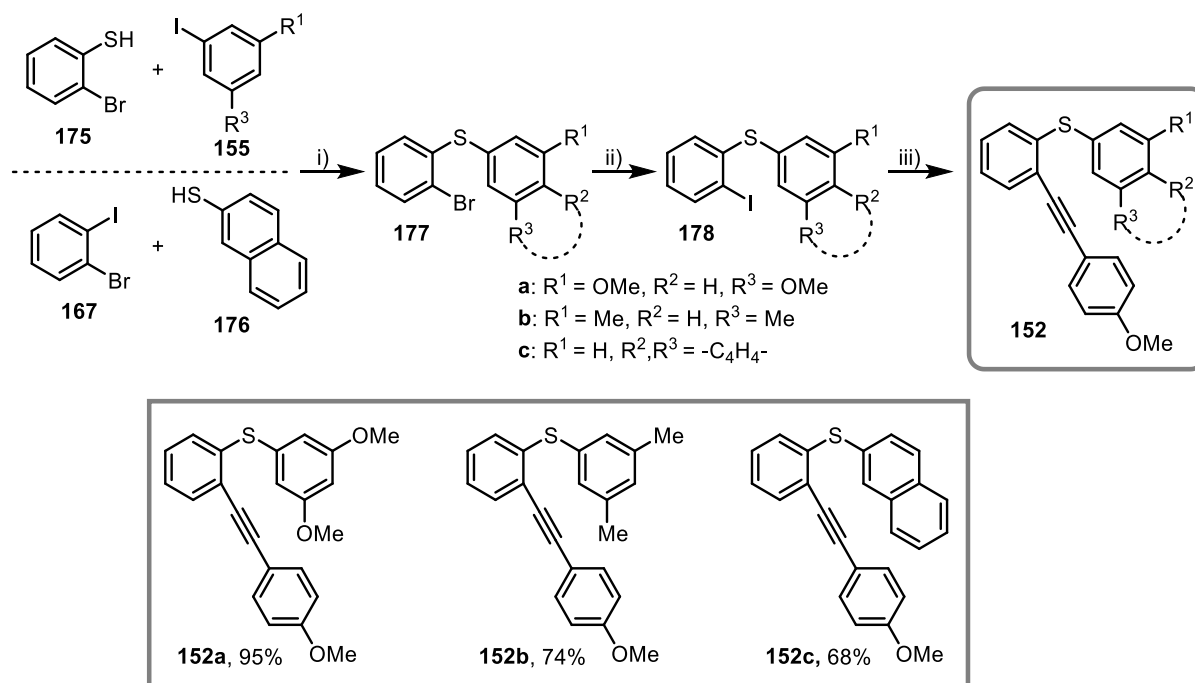


**Scheme 36:** Synthesis of precursors **151e-g**. Reagents and conditions: i)  $\text{K}_2\text{CO}_3$  (1.0 eq),  $\text{DCM}/\text{MeOH}$  (1:1), rt, 20 h, **174** quant., ii) TBAF (1 M in THF, 1.1 eq), THF, rt, 2 h, **174** 90%, iii) bromide (1.0 eq), alkyne (1.1 eq),  $\text{PdCl}_2(\text{PPh}_3)_2$  (5 mol%),  $\text{CuI}$  (10 mol%),  $\text{Et}_3\text{N}$ , 65 °C, 18-24 h, **151e** 65%, **151f** 59%, **151g** 65%.

### 3.1 Synthesis of seven-membered ring systems

#### 3.1.1.3 Thiepine precursors

According to a literature-known method, a copper-catalyzed approach was adopted for the preparation of thiepine precursors **152** and the associated C-S bond formation, in which thiols **175/176** are cross-coupled with aryl halides **167/155** (Scheme 37).<sup>[127]</sup>



**Scheme 37:** Synthesis of thiepine precursors. Reagents and conditions: i) thiophenol **175** or **176** (1.0 eq), aryl iodide **155** or **167** (1.1 eq), CuI (5 mol%), TBAB (1.0 eq), KOH (1.5 eq), H<sub>2</sub>O, 80 °C, 26-36 h, **177a** 71%, **177b** 85%, **177c** 88%, ii) 1) *n*BuLi (1.2 eq), THF, -78 °C, 30 min, 2) I<sub>2</sub> (1.5 eq), -78 °C to rt, 16 h, **178a** 75%, **178b** 99%, **178c** 99%, iii) 4-ethynylanisole (1.1 eq), PdCl<sub>2</sub>(PPh<sub>3</sub>)<sub>2</sub> (5 mol%), CuI (10 mol%), Et<sub>3</sub>N, rt, oven.

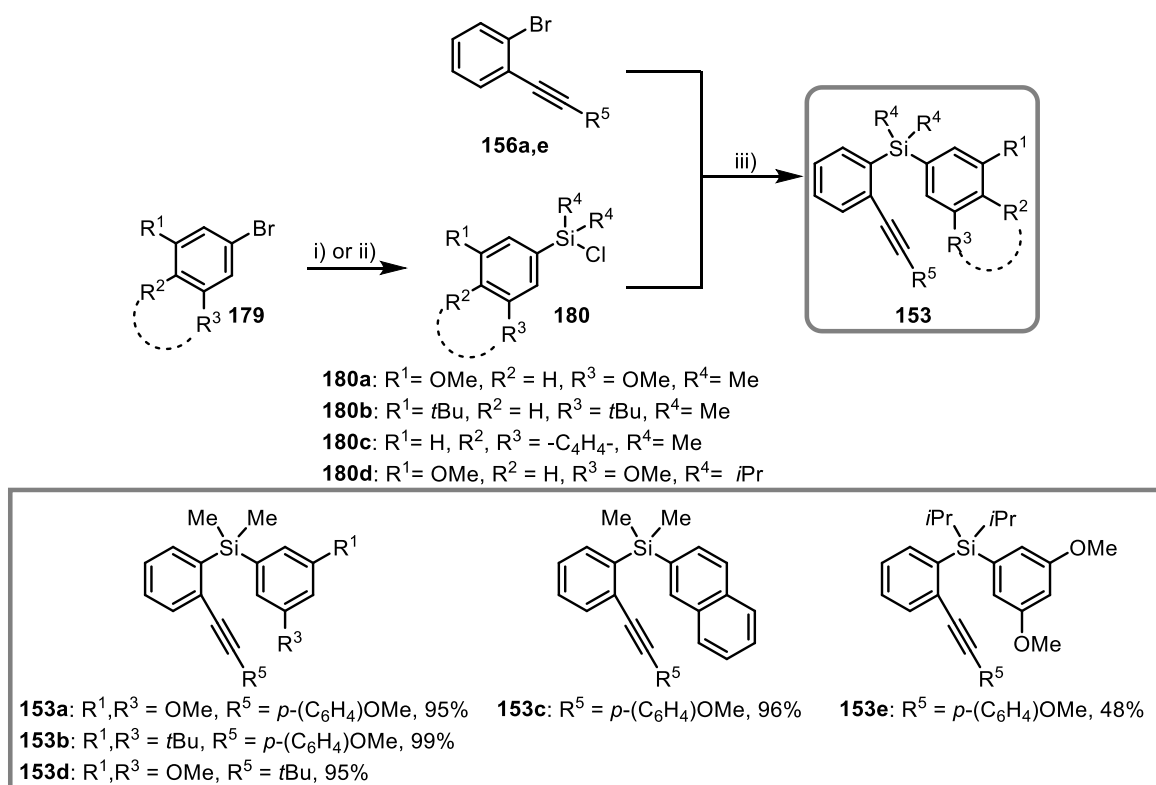
Depending on the commercial availability of the reactants, the respective coupling partners were selected. In addition to the iodo functionality for the cross-coupling, another halogen was also required to enable the later introduction of an alkyne moiety. Since the bromo compound **177b** gave low conversion in the Sonogashira coupling, iodine was introduced by a simple lithium-halogen exchange. With the iodoaryl thioethers **178**, the subsequent Sonogashira coupling proceeded smoothly and gave excellent yield for **152a** (95%) with electron-donating methoxy groups as substituents. For compounds **152b** and **152c** significantly lower yields were obtained (74% and 68%, respectively).

#### 3.1.1.4 Silepine precursors

The preparation of the silepine precursors **153** was straightforward (**Scheme 38**). First, chlorosilanes **180** were prepared from the desired aryl bromide **179** and dialkyldichlorosilanes. Depending on the dialkyldichlorosilane used, either the Grignard compound was synthesized from the aryl bromide **179** or a bromine-lithium exchange was performed. During our investigations we realized that dichlorodiisopropylsilane does not react with a Grignard compound and the desired chlorosilane **180d** cannot be formed. After

### 3. Results and discussion

a bromine-lithium exchange at compound **156**, which was already prepared for the synthesis of the cycloheptatriene precursors **150** (see **Scheme 33**), the chlorosilane **180** was added and the corresponding 1-(silaaryl)-2-ethynylbenzene **153** could be obtained. Excellent yields (95-99%) were observed for all precursors **153a-d** with methyl groups on the silicon tether. However, the dichlorodispropylsilane showed much lower reactivity, resulting in the desired precursor **153e** being obtained with a yield of only 48%.



**Scheme 38:** Preparation of 1-(silaaryl)-2-ethynylbenzenes. Reagents and conditions: i) 1) Mg (1.0 eq), THF, 65 °C, 3 h, 2) Me<sub>2</sub>SiCl<sub>2</sub> (1.0 eq), THF, 0 °C to rt, 24 h, **180a** 74%, **180b** 75%, **180c** 68%, ii) 1) *n*BuLi (1.0 eq), Et<sub>2</sub>O, 0 °C, 3 h, 2) *i*Pr<sub>2</sub>SiCl<sub>2</sub> (1.5 eq), Et<sub>2</sub>O, -78 °C to rt, 16 h, **180d** 48%, iii) 1) **156** (1.0 eq), *n*BuLi (1.1 eq), THF, -78 °C, 1 h, 2) **180** (1.1 eq), THF, -78 °C to rt, 16 h.

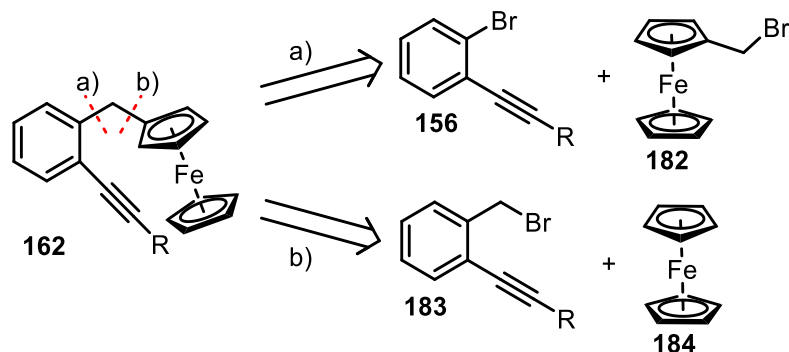
In summary, a variety of cycloheptatriene, oxepine, thiepine and silepine precursors were successfully synthesized. The synthetic routes allowed modularity and different substituents were incorporated. Moreover, the reactions proved to be general and afforded high yields regardless of the nature of the substituents, indicating that the synthetic pathways could be later extended to other substrates with similar results.

#### 3.1.1.5 Ferrocene-containing precursors

For precursors containing a -CH<sub>2</sub>- tether, the linkage of the two aromatic components should be achieved *via* a Negishi coupling as before (see section 3.1.1.1) and two possible disconnections can be taken into consideration (**Scheme 39**). Pathway a) starts from 1-bromo-2-ethynylbenzenes **156**, which are used to form the required zincates **181** and then coupled with (bromomethyl)ferrocene (**182**). In route b), the Negishi coupling is performed

### 3.1 Synthesis of seven-membered ring systems

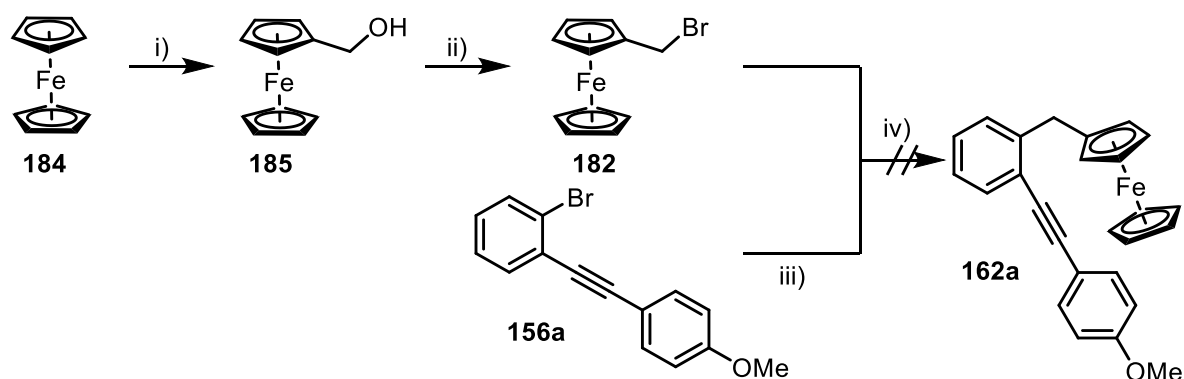
between the corresponding 1-(bromomethyl)-2-ethynylbenzene **183** and the zincate based on ferrocene (**184**). Both options were tried to find the best route towards compound **162**.



**Scheme 39:** Possible disconnections for the synthesis of compound **162** via Negishi coupling.

In pathway a) (**Scheme 40**), (bromomethyl)ferrocene (**182**) first had to be synthesized. For this purpose, ferrocene was lithiated using a procedure developed by Mueller-Westerhoff and Sanders<sup>[128]</sup> and was treated with paraformaldehyde to obtain ferrocenylmethanol (**185**). Subsequently, **185** was reacted in the presence of pyridine and phosphorus tribromide to give (bromomethyl)ferrocene (**182**), which was directly employed in the Negishi coupling with the zincate generated from **156a** without further purification. Unfortunately, the coupling was not successful under the conditions used and the desired product could not be isolated. In addition, **182** appeared to be relatively sensitive in solution, so it was decided to switch to pathway b).

#### Pathway a)

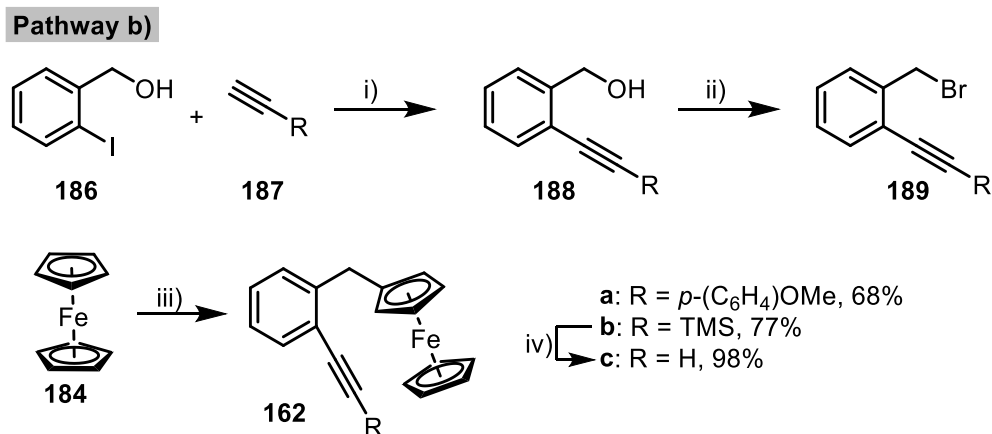


**Scheme 40:** Synthesis route a) towards compound **162a**. Reagents and conditions: i) 1) KO<sup>t</sup>Bu (0.1 eq), *t*BuLi (2.5 eq), THF, -78 °C, 2 h, 2) paraformaldehyde (2.5 eq), -78 °C to rt, 30 min, 74%; ii) 1) pyridine (1.0 eq), PBr<sub>3</sub> (1.0 eq), benzene/THF, 0 °C to rt, 4.5 h, 2) EtOH, rt, 30 min; iii) 1) *n*BuLi (1.05 eq), THF, -78 °C, 30 min, 2) ZnBr<sub>2</sub> (1.05 eq), rt, 1 h; iv) **182** (1.5 eq), Pd(PPh<sub>3</sub>)<sub>4</sub> (5 mol%), THF, 65 °C, 15 h.

According to pathway b) (**Scheme 41**), (2-iodophenyl)methanol (**186**) was reacted with the corresponding alkyne **187** in a Sonogashira coupling to give the benzyl alcohols **188** in very good yields, following literature-known procedures.<sup>[129,130]</sup> The benzyl alcohols **188** were converted to the benzylic bromides **189** in the presence of *N*-bromosuccinimide and

### 3. Results and discussion

triphenylphosphine, as described in the literature.<sup>[131,132]</sup> To form the zincate required for Negishi coupling, the ferrocene (**184**) was first lithiated followed by addition of zinc chloride.<sup>[133]</sup> After coupling with the benzyl bromides **189**, the desired precursor **162a** was obtained. To generate the free alkyne precursor **162c**, the TMS protecting group was cleaved under basic conditions.



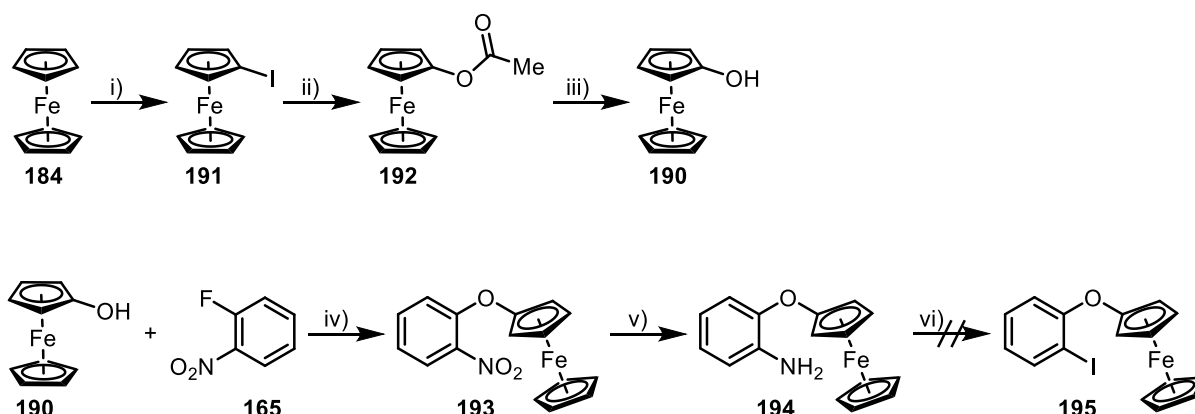
**Scheme 41:** Synthesis route b) for compound **162**. Reagents and conditions: i) **187a** (1.0 eq), PdCl<sub>2</sub>(PPh<sub>3</sub>)<sub>2</sub> (10 mol%), piperidine, 70 °C, 16 h or **187b** (1.3 eq), PdCl<sub>2</sub>(PPh<sub>3</sub>)<sub>2</sub> (5 mol%), CuI (10 mol%), Et<sub>3</sub>N, rt, 6 h, **188a** 87%, **188b** 95%, ii) NBS (1.16 eq), PPh<sub>3</sub> (1.16 eq), DCM, 0 °C, 40 min, **189a** 94%, **189b** 89%, iii) 1) KO<sup>t</sup>Bu (0.2 eq), *t*BuLi (2.0 eq), THF, -78 °C, 1.5 h, 2) ZnCl<sub>2</sub> (2.0 eq), THF, -78 °C to rt, 2 h, 3) **189** (1.0 eq), Pd(PPh<sub>3</sub>)<sub>4</sub> (5 mol%), THF, 65 °C, ovn, **162a** 68%, **162b** 77%, iv) K<sub>2</sub>CO<sub>3</sub> (1.0 eq), DCM/MeOH (1:1), rt, ovn, **162c** 98%.

Next, precursors should be synthesized incorporating the -O- tether. Therefore, it was considered which methods could be used to create an oxygen bridge between a phenyl substituent and ferrocene. On the one hand, the conditions previously used in the nucleophilic substitution to generate biaryl ethers **171** should be tested and, on the other hand, an Ullman-type protocol was published for the synthesis of different ferrocenyl aryl ethers as well.<sup>[134]</sup> In both cases, it is crucial that a halogen is located in the direct vicinity of the tether at the phenyl substituent allowing the alkyne, necessary for hydroarylation, to be introduced later.

Since the S<sub>N</sub>Ar between the corresponding phenol **170** and 1-fluoro-2-nitrobenzene (**165**) was proven to be effective in the synthesis of biarylethers **171**, it was decided to prepare hydroxyferrocene (**190**) based on literature-known procedures<sup>[135–137]</sup> and to submit it to the same reaction conditions (**Scheme 42**). Starting from ferrocene (**184**), lithiation was first performed and iodine was added to the lithiated species to obtain iodoferrocene (**191**), which was refluxed in the next step in acetonitrile with acetic acid in the presence of copper(I) oxide to give ferrocenyl acetate (**192**) in good yield. The conversion of **192** to hydroxyferrocene (**190**) was realized by treatment with aqueous sodium hydroxide solution followed by addition of aqueous hydrogen chloride solution. Subsequent S<sub>N</sub>Ar with 1-fluoro-2-nitrobenzene (**165**) was performed and yielded almost quantitative **193**. After reduction to the corresponding amine **194**, the Sandmeyer reaction was attempted to obtain **195**.

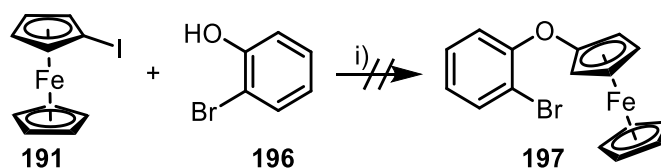
### 3.1 Synthesis of seven-membered ring systems

Unfortunately, the ferrocene did not survive the harsh reaction conditions and only decomposition could be observed.



**Scheme 42:** Synthesis route towards precursor **195** with a  $S_NAr$  as the key step. Reagents and conditions: i) 1) KO<sup>t</sup>Bu (0.1 eq), *t*BuLi (2.5 eq), THF,  $-78\text{ }^{\circ}\text{C}$ , 2 h, 2) iodine (2.5 eq),  $-78\text{ }^{\circ}\text{C}$  to rt, 30 min, 65%; ii) AcOH (1.2 eq), Cu<sub>2</sub>O (0.6 eq), MeCN, reflux, 3 h, 76%; iii) 1) aq. KOH (1.2 eq), EtOH,  $70\text{ }^{\circ}\text{C}$ , 15 min, 2) aq. HCl (1.2 eq), 98%; iv) K<sub>2</sub>CO<sub>3</sub> (1.0 eq), DMSO,  $95\text{ }^{\circ}\text{C}$ , 24 h, 98%; v) SnCl<sub>2</sub>·2H<sub>2</sub>O (4.0 eq), HCl (1 mL), *i*PrOH/H<sub>2</sub>O(2:1), reflux, 2 h, 87%; vi) NaNO<sub>2</sub> (2.0 eq), KI (2.0 eq), *p*TsOH·H<sub>2</sub>O (3.0 eq), MeCN, rt, 16 h.

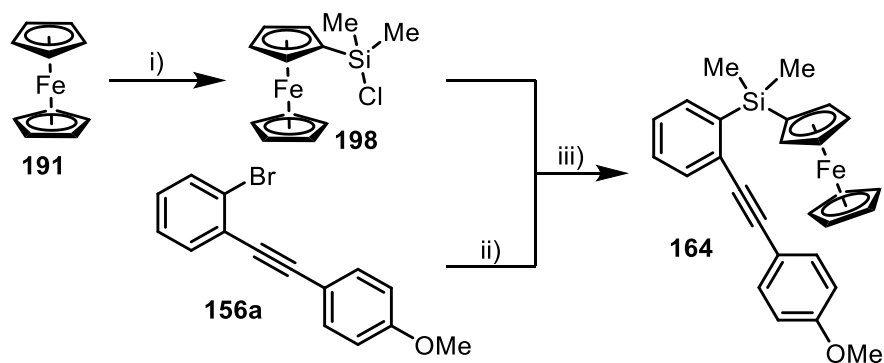
After the pathway *via* nucleophilic aromatic substitution failed the Ullmann-type protocol was tried (**Scheme 43**). According to the procedure published by Frey and Hoffmann several phenols could be coupled to iodoferrocene in the presence of copper(I)iodide and triphenylphosphine as the ligand.<sup>[134]</sup> Since in this case an additional halogen was necessary to allow the introduction of an alkyne moiety later, 2-bromophenol (**196**) was chosen as the coupling partner for iodoferrocene (**191**). After stirring the reaction mixture in a pressure Schlenk for 40 h there was still starting material left and the desired product **197** could not be isolated.



**Scheme 43:** Attempt to synthesize **197** *via* Ullmann-type reaction. Reagents and conditions: i) **191** (1.0 eq), **196** (2.0 eq), CuI (5 mol%), PPh<sub>3</sub> (15 mol%), CsCO<sub>3</sub> (2.0 eq), toluene,  $110\text{ }^{\circ}\text{C}$ , 40 h.

In contrast to the previously considered precursors, the incorporation of a -SiMe<sub>2</sub>- tether was straightforward and the conditions described in section 3.1.1.4 could be directly transferred (**Scheme 44**). First, ferrocene (**191**) was treated with *tert*-butyllithium and potassium *tert*-butoxide, followed by the addition of dichlorodimethylsilane to form and isolate the corresponding chlorodimethylsilyl-ferrocene (**198**). Subsequently, **156a** was also lithiated and reacted with **198**. The precursor **164** was obtained in good yield.

### 3. Results and discussion



**Scheme 44:** Synthesis of -SiMe<sub>2</sub>- precursor **164**. Reagents and conditions: i) 1) KO<sup>t</sup>Bu (0.1 eq), <sup>t</sup>BuLi (2.5 eq), THF, -78 °C, 2 h, 2) Me<sub>2</sub>SiCl<sub>2</sub>, THF, 0 °C to rt, 22 h, 83%; ii) *n*BuLi (1.1 eq), THF, -78 °C, 1 h; iii) **198** (1.1 eq), THF, 0 °C to rt, 78%.

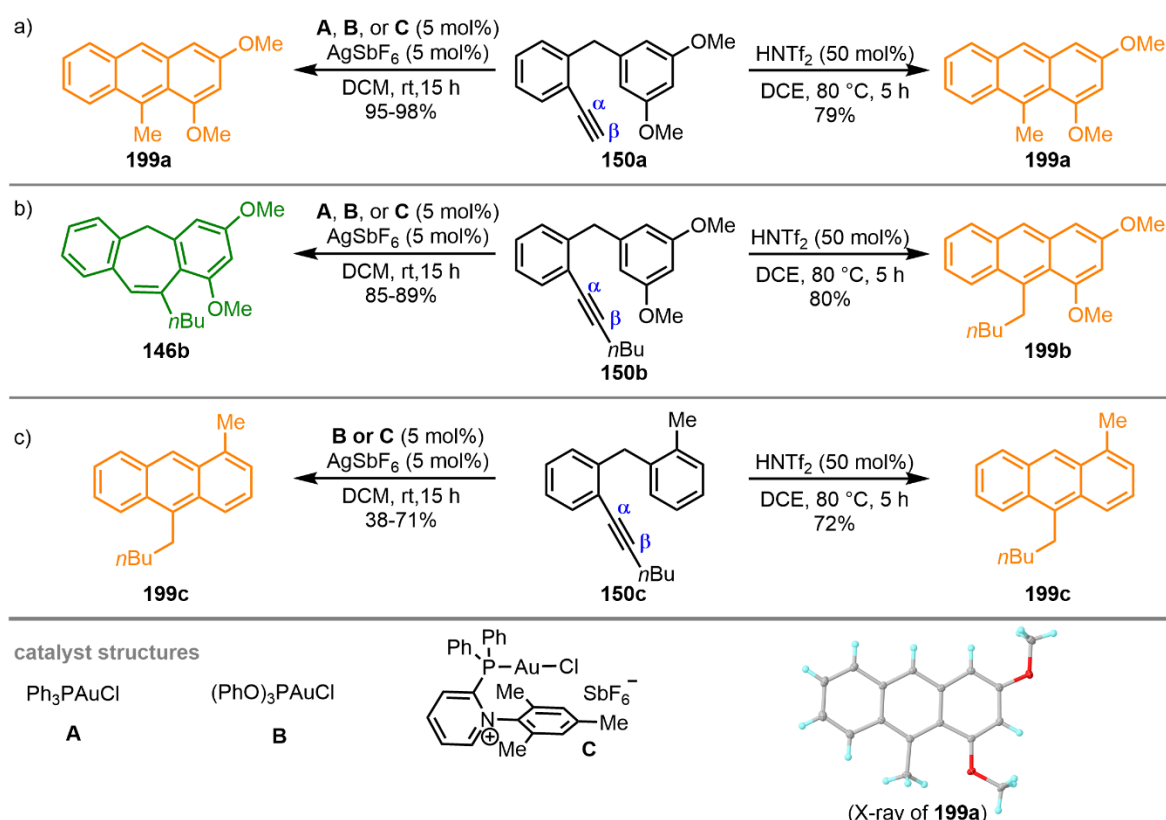
In summary, precursors containing a ferrocene moiety could be successfully synthesized with a -CH<sub>2</sub>- and -SiMe<sub>2</sub>- tether. Both internal and terminal alkynes could be incorporated, which are necessary for Au-catalyzed hydroarylation in the subsequent steps.



### 3.1 Synthesis of seven-membered ring systems

#### 3.1.2 Comparison between Brønsted acid and Au catalysis

Encouraged by the results of the Ye group, we decided to initially start our investigations with a comparison between Brønsted acid and Au catalysis. In addition, the influence exerted by the type of the catalyst and the substitution pattern of the substrates on the outcome of such transformations will be directly studied. As model substrates for our studies, 1-benzyl-2-ethynylbenzenes **150a-c** with terminal and butyl-substituted alkyne moieties were selected to evaluate their reactivity with respect to Au(I) catalysts, **A-C** (5 mol%), with ancillary ligands of different donor properties compared to HNTf<sub>2</sub> (50 mol%). The product distribution under the different reaction conditions is depicted in **Scheme 45**.



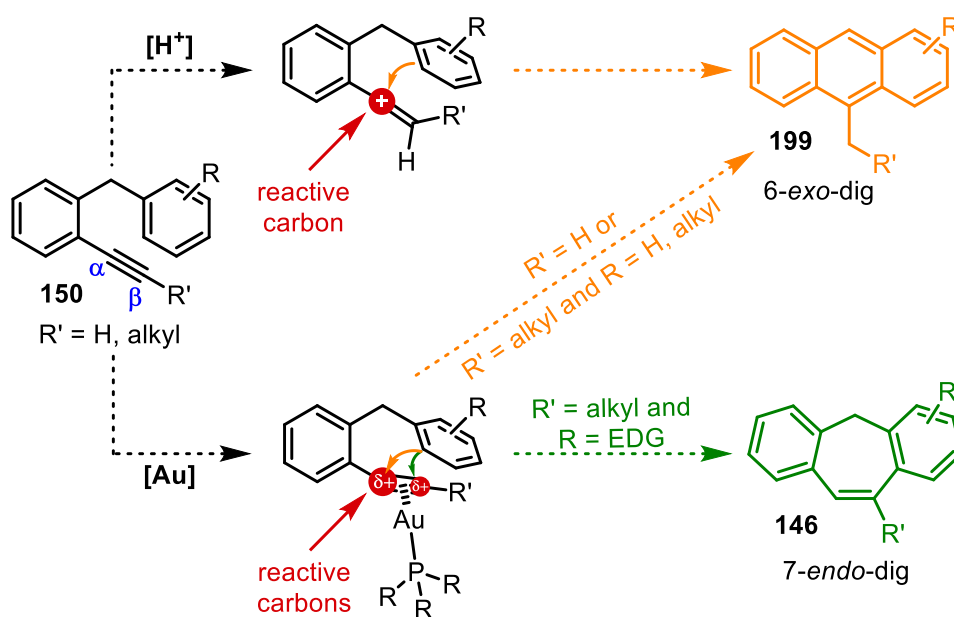
**Scheme 45:** Comparison between Brønsted acid and Au(I) catalysis in the hydroarylation of **150a-c**. X-ray of **199a**, displacement ellipsoids are drawn at 50% probability level.

Regardless of the nature of the catalyst utilized, hydroarylation of the terminal alkyne substrate **150a** exclusively affords the anthracene **199a** in good to excellent yields (**Scheme 45**, a)). The reaction proceeds *via* a 6-*exo*-dig mechanism followed by *in situ* tautomerization of the 9-methylene dihydroanthracene formed as intermediate shown previously in **Scheme 9**. NMR spectroscopy followed by X-ray crystallography was used to elucidate the structure of **199a**. A distinctly different reactivity is exhibited by substrate **150b**, which has a butyl-substituted alkyne functionality instead of the terminal alkyne. Employing the Brønsted acid HNTf<sub>2</sub>, the corresponding anthracene **199b** is obtained, as with **150a**, but the use of the three Au(I) catalysts investigated led to the formation of the kinetic

### 3. Results and discussion

product, which is cycloheptatriene **146b** (**Scheme 45**, b)). In addition, it was determined that the nucleophilicity of the aromatic ring performing the attack also plays a crucial role for the regioselectivity. For the substrate **150c**, which has the same butyl chain located on the alkyne terminus as **150b** but a less nucleophilic aromatic ring, the same reactivity pattern was observed as for **150a**. Both Brønsted and Au(I) catalysis yield the anthracene **199c** (**Scheme 45**, c)). However, major differences between the Au(I) catalysts were found in this case. While the reaction with Ph<sub>3</sub>PAuCl (**A**) does not proceed at all, a significantly worse conversion and resulting yield is obtained with (PhPO)<sub>3</sub>AuCl (**B**) compared to **C** (38% vs 71%, respectively), indicating that the substrate **150c** shows lower reactivity than **150a** or **150b**. This confirms the significant kinetic effect of the ancillary ligand, which is particularly evident in the case of weaker nucleophiles as **150c**, with precatalyst **C** showing by far the highest effectiveness. The catalyst loading of **C** could in fact be reduced to 2 mol% without any change being observed in the isolated yields. In contrast, the choice of Au catalyst does not seem to have any effect on regioselectivity.

Based on these results and the observations made for the model substrates **150a-c** the following mechanism was proposed (**Scheme 46**).



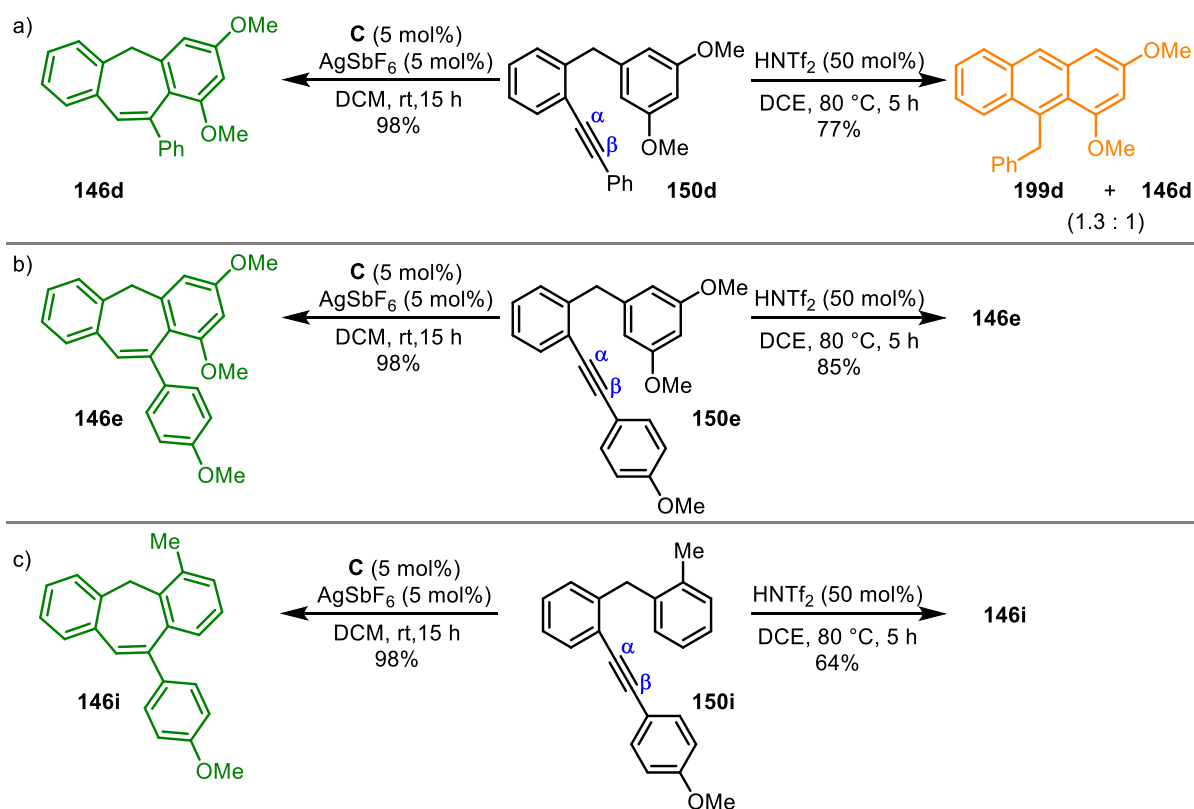
**Scheme 46:** Mechanistic proposal for the formation of **199a-c** and **146b**.

Since the resulting vinyl carbocation is better stabilized at the inner position of the alkyne, the initial protonation of **150** in acid-catalyzed reactions always occurs at the  $\beta$ -position. As a consequence, the attack of the lateral ring takes place at the carbon in  $\alpha$ -position and a dihydroanthracene intermediate is formed, which tautomerizes to the anthracene **199**. The catalytically active species in Au(I) catalysis, the fragment  $[R_3PAu]^+$ , is isolobal to  $H^+$ , therefore the alkyne **150** is preferentially activated at the  $\alpha$ -position explaining the formation

### 3.1 Synthesis of seven-membered ring systems

of **199a** and **199c** as products. However, coordination of Au(I) to alkynes **150b** and **150c** additionally allows activation of the  $\beta$ -position due to its softness and size. Since this position is sterically more accessible, this slight activation is sufficient to form the kinetic product **146b** via 7-*endo*-dig cyclization, if the entering nucleophile is reactive enough.

The mechanistic proposal can also be used to explain the following outcomes for substrate **150d-e,i** (**Scheme 47**). When examining **150d**, it is obvious that both carbon atoms of the alkyne are similarly electron-rich, which makes the formation of the vinyl carbocation not selective due to equal stabilization. Therefore, the use of HNTf<sub>2</sub> yields a mixture with almost identical ratios of **199d** and **146d** (ratio 1.3:1) (**Scheme 47, a**).



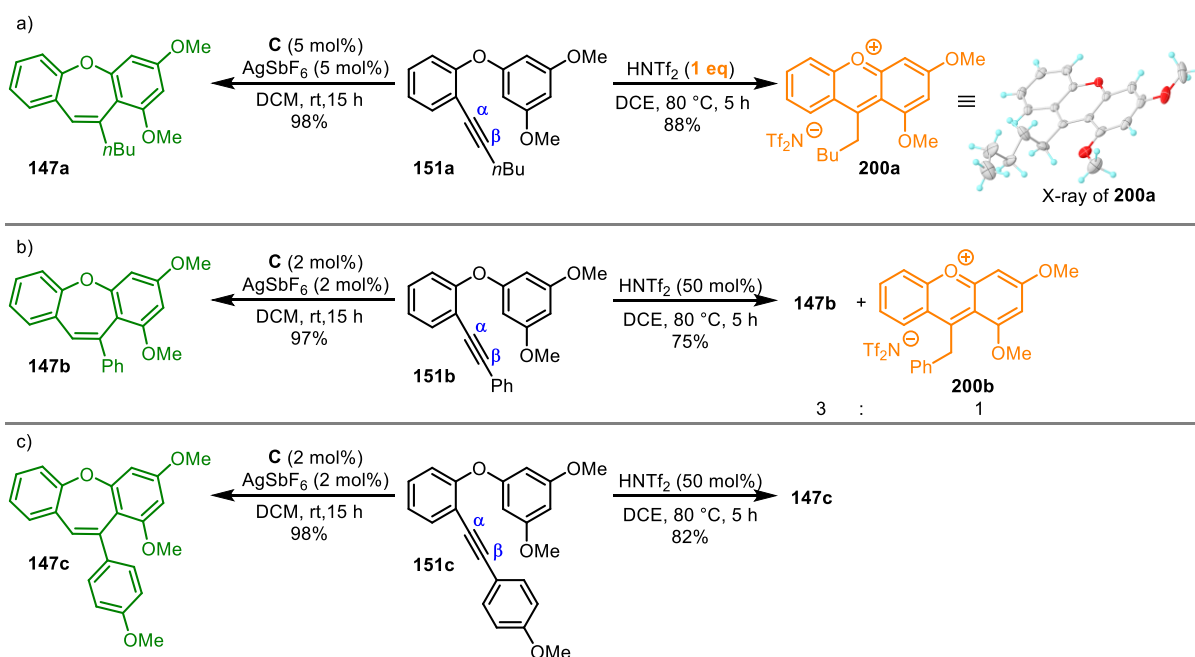
**Scheme 47:** Comparison between Brønsted acid and Au catalysis in the hydroarylation of **150d-e,i**.

In contrast, when **C** is used as a catalyst, selective 7-*endo*-dig cyclization and the formation of **146d** is observed in 98% yield. Although the Au(I) catalyst should activate both positions to the same extent, the nucleophilic attack occurs exclusively at the sterically more accessible  $\beta$ -position. If the terminal arene substituent on the alkyne contains a methoxy group, as in the case of **150e**, the polarization of the substrate changes completely (**Scheme 47, b**). As a result, regardless of the nature of the catalyst (Brønsted acid or Au), the vinyl carbocation is preferentially formed in the direct proximity of the anisyl residue and cycloheptatriene **146e** is the only product in both reactions. However, the yields for the Au catalyzed process are higher compared to the acid catalyzed reaction (98% vs 85%, respectively) The same observations were made for **150i**, although the lateral ring is a much

### 3. Results and discussion

weaker nucleophile. The significantly better stabilization of the vinyl carbocation is the decisive factor and ensures that the 7-*endo*-dig cyclization is the operating reaction pathway leading to the kinetic product **150i** (**Scheme 47**, c)).

Encouraged by the results on cycloheptatrienes, we wanted to gain further insight into the cyclization under investigation and also to evaluate the effects of the tether. Indeed, we set out to screen in order to verify if the synthetic approaches are also suitable for the preparation of oxepines from the corresponding diaryl ethers with substituted alkyne moieties (**Scheme 48**).



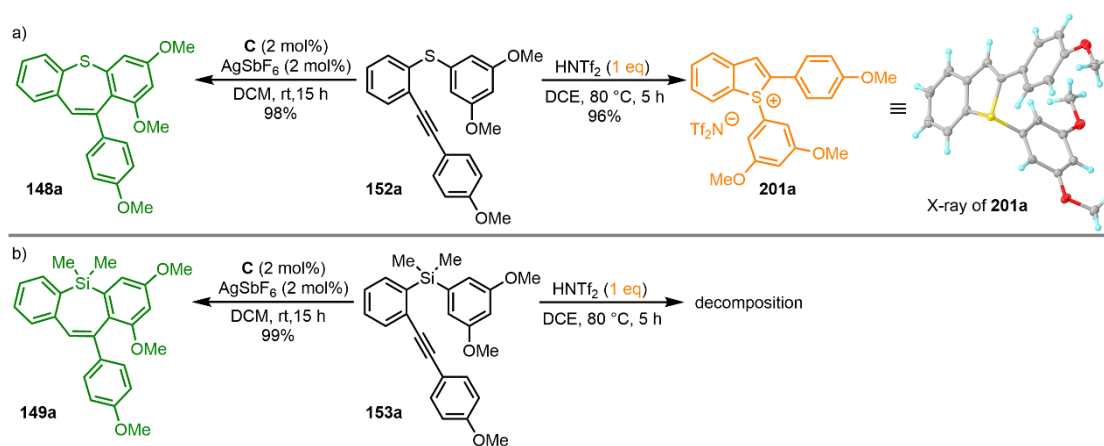
**Scheme 48:** Comparison between Brønsted acid and Au catalysis in the hydroarylation of **151a-c**. X-ray of **200a**, the Tf<sub>2</sub>N<sup>-</sup> anion was omitted for clarity; displacement ellipsoids are drawn at 30% probability level.

It should be stressed that changing the tether has a great influence on electronic properties of the substrate. By increasing the electron density, a clear polarization of the substrate is induced, which certainly affects the regioselectivity of the transformation. Moreover, there is no possibility to isomerize the 9-methylenexanthenes resulting from a 6-*exo*-dig process into a fully aromatic product. Fortunately, under Au catalyzed conditions, the oxepine **147a** was obtained in nearly quantitative yield (**Scheme 48**, a), left). The attack of the nucleophile occurs in the sterically more accessible  $\beta$ -position, with the soft Au(I) being able to activate both carbon atoms of the alkyne in **151a**. In contrast, the standard conditions used for acid catalysis resulted in the formation of a new product with about 50% conversion. However, as soon as 1 eq of HNTF<sub>2</sub> is used instead of 0.5 eq, complete conversion could be obtained (**Scheme 48**, a), right). Based on structure elucidation by X-ray, dibenzo[*b,d*]pyrylium salt **200a** could be confirmed as the product of the reaction. The formation of **200a** can be explained as follows: initial protonation activates the  $\alpha$ -position and subsequent 6-*exo*-dig

### 3.1 Synthesis of seven-membered ring systems

cyclization yields the corresponding 9-(methylene) xantheno intermediate. The aromatization is achieved by protonation of the *exo* double bond, illustrating that 1 eq of acid is obligatory for the reaction to be pushed to completeness. While with the use of catalyst **C**, only the product of 7-*endo*-dig cyclization is formed, under acid-catalyzed, a mixture is obtained. As previously discussed and showed in **Scheme 47** for **150d**, in the case of a phenyl substituted alkyne **151b** both carbon atoms are similarly electron-rich and the formation of the vinyl carbocation is not selective resulting in a mixture of **147b** and **200b** (**Scheme 48**, b)). Regardless of the catalyst, the hydroarylation of **151c** proceeds highly selectively via the 7-*endo*-dig reaction pathway and the oxepine **147c** is formed as the only product. As previously explained, the stabilization of the vinyl carbocation by the anisyl substituent is essential for the high selectivity (**Scheme 48**, c)).

Finally, we decided to study the applicability of the developed method in the synthesis of thiepines and silepines. Starting from the Au catalyzed approach, the prepared diaryl sulfide **152a** and silane **153a** were subjected to the standard conditions. For these substrates, successful conversion to the desired target compounds **148a** (**Scheme 49**, a)) and **149a** (**Scheme 49**, b)) was achieved with excellent yields and their structures were confirmed by X-ray analysis.



**Scheme 49:** Comparison between Brønsted acid and Au catalysis in the hydroarylation of diaryl sulfide **152a** a) and silane **153a**. b) X-ray of **201a**, the  $\text{OTf}_2^-$  anion is omitted for clarity; displacement ellipsoids are drawn at 50% probability level.

In contrast to the previously studied cycloheptatriene and oxepine precursors, it seems particularly important that the ring on which the Friedel-Craft alkenylation takes place is sufficiently electron-rich for a reaction to occur. Once the methoxy groups on the lateral ring are removed, the formation of the desired products can no longer be observed. When acid catalysis with one equivalent of  $\text{HNTf}_2$  is employed, the benzothiophenium salt **201a** is formed as the sole product. The reaction proceeds *via* a 5-*endo*-dig cyclization in which the sulfur atom adopts the role of the nucleophile and attacks the carbocation formed after

### 3. Results and discussion

protonation of the alkyne. The connectivity of **201a** was confirmed by X-ray crystallography. Acidic treatment of diarylsilane **153a** with HNTF<sub>2</sub> unfortunately leads to decomposition.

In order to consider not only by which factors the selectivity of the studied transformation can be influenced, but also to study how the reaction rate can be controlled by different ligands on Au(I), kinetic studies were performed.

#### 3.1.3 Kinetic studies

Simultaneously with the comparison of Brønsted acid and Au catalysis, additional kinetic studies were carried out to investigate the influence of the catalyst on the reaction rate and conversion of the 7-*endo*-dig cyclization. For this purpose, **152a** was chosen as the model substrate since it exhibits a reaction rate most suitable for this study. <sup>1</sup>H-NMR spectroscopy seemed to be the most appropriate method to monitor the conversion of **152a** into thiepine **148a**. Therefore, the reaction was carried out directly in a Young NMR tube in CD<sub>2</sub>Cl<sub>2</sub> and the ratio of educt to product was determined. After activation of the catalyst using an AgSbF<sub>6</sub> solution, the first <sup>1</sup>H-NMR spectrum was measured after 10 min and then at 5 min intervals. A catalyst concentration of 5 mol% was chosen to start the studies and the performance of commercially available Ph<sub>3</sub>PAuCl (**A**) was compared with our cationic phosphine Au complexes **C**, **D** and **E** (**Figure 22**, left). All the catalysts investigated outperform Ph<sub>3</sub>PAuCl (**A**), which is certainly due to the enhanced electrophilicity they confer to the Au center. Since full conversion was achieved with all cationic ligands and few measurement points were obtained in the initial range due to the high catalyst concentration and associated high reaction rates, it was decided to further examine this transformation at a catalyst concentration of 2 mol% and to test additional catalysts as well (**Figure 22**, right) and the catalysts **B** and **F** were including for further comparison as well as Et<sub>3</sub>PAuCl, which was used by Ye and coworkers in the synthesis of anthracenes.<sup>[26]</sup>

### 3.1 Synthesis of seven-membered ring systems

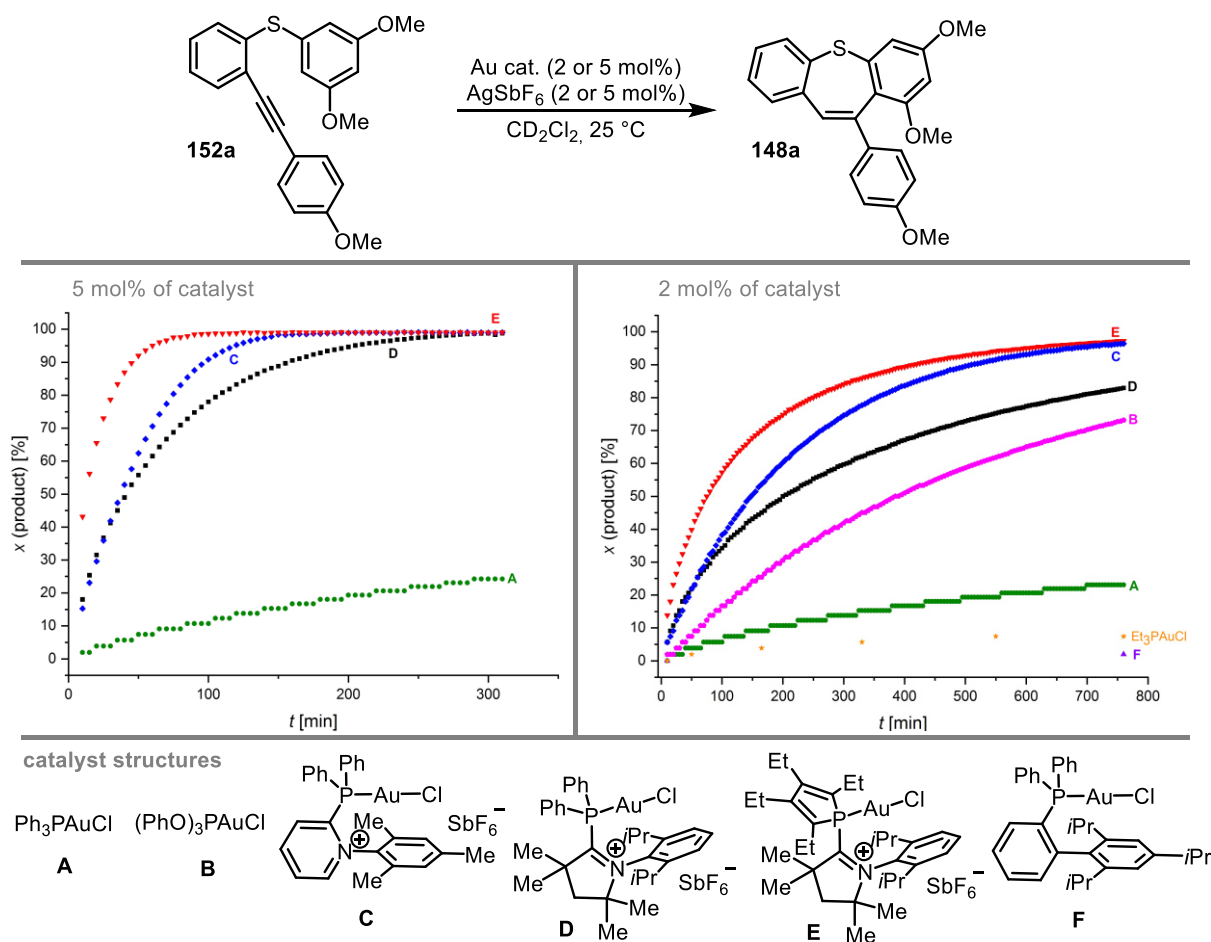


**Figure 22:** Ligand effect on the Au catalyzed hydroarylation of **152a** into thiepine **148a**. Conversions determined by  $^1\text{H-NMR}$ .

With 2 mol% of catalyst only catalyst **C** and **E** could reach full conversion of compound **152a**. The cationic complexes with a pyridinium-based **C** or CAAC-derived **D** cationic moiety showed similar initial reaction rates. After a reaction time of about 90 min and a conversion of 35%, the curve of **D** flattened much faster and reached only 83% conversion at the end. Complex **B** still comes closest to competing with Au complexes containing cationic ligands. In contrast, the worst catalytic performance was obtained when a neutral analogue **F** with a comparable structure to the cationic complex **C** was employed. The reaction basically does not proceed and the desired thiepine **148a** cannot be isolated. As expected all cationic precatalysts proved to be superior to the classical neutral ones namely  $\text{Et}_3\text{PAuCl}$ ,  $\text{Ph}_3\text{PAuCl}$  and  $(\text{PhO})_3\text{AuCl}$ . Among the neutral ancillary ligands, a clear trend in reactivity can also be seen. From  $\text{Et}_3\text{PAuCl}$  to  $\text{Ph}_3\text{PAuCl}$  to  $(\text{PhO})_3\text{AuCl}$ , the  $\pi$  acceptor ability of the ligand increases and thus also the reactivity of the corresponding Au complex. The best results and fastest reaction rates were provided by **E** containing the most  $\pi$  accepting ligand with a phosphole- and CAAC-derived cationic moiety.

After the kinetic studies, in addition to the comparative experiments described in the previous section, were able to confirm the selection of catalyst **C** as the most suitable

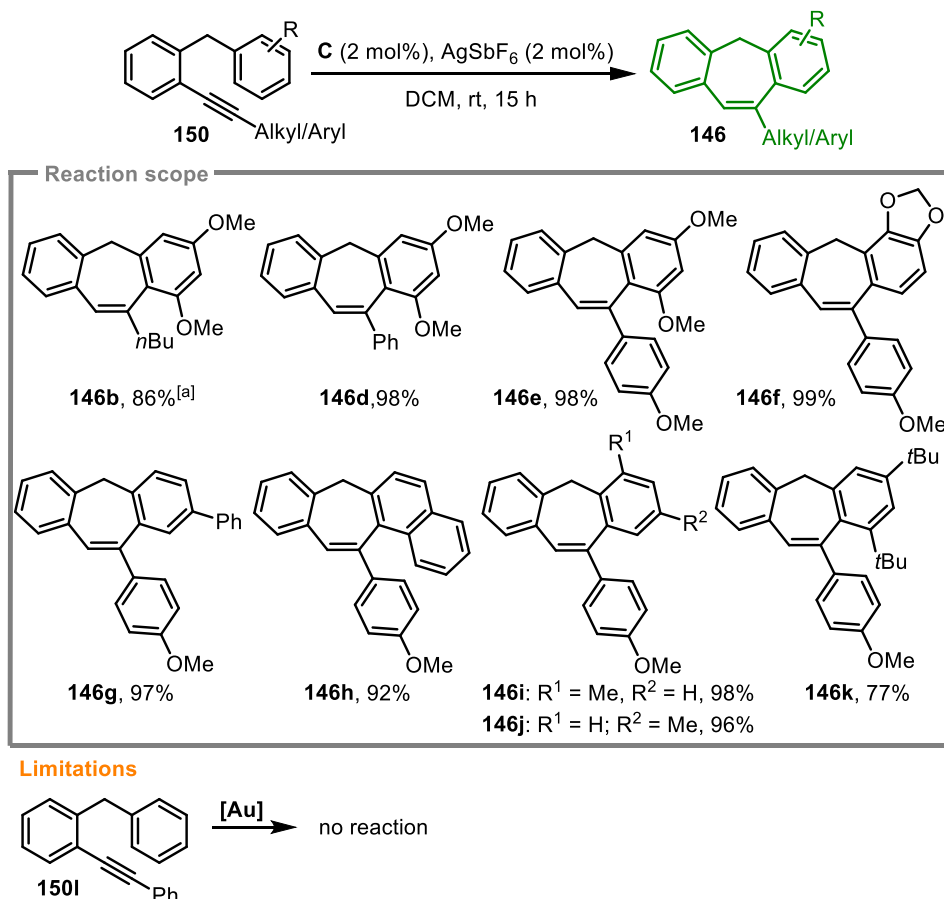
### 3. Results and discussion

catalyst and the reduction of the catalyst loading to 2 mol%, the scope of the transformation was investigated. In contrast to catalyst **E**, which showed higher reaction rates at the beginning, but comparable overall results, catalyst **C** is easier to prepare.

#### 3.1.4 Application of catalyst **C** in the synthesis of cycloheptatrienes, oxepines, thiepinines and silepinines

After determining the optimal catalyst and reaction conditions for the selective formation of the seven-membered ring, the scope and limitations of the Au catalyzed version of this transformation were investigated in the synthesis of cycloheptatrienes, oxepines, thiepinines, and silepinines.

Beginning with the preparation of cycloheptatrienes **146**, provided that the aromatic ring suffering the Friedel-Crafts alkenylation is electron-rich enough, the cyclization proceeds, regardless of the aliphatic or aromatic nature of the substituents on the alkyne (**Scheme 50**).



**Scheme 50:** Scope of the Au catalyzed 7-*endo*-dig cyclization of 1-(benzyl)-2-ethynylbenzenes **150** towards cycloheptatrienes **146**. [a] Reaction was carried out with 5 mol% of **C** and 5 mol% of AgSbF<sub>6</sub>.

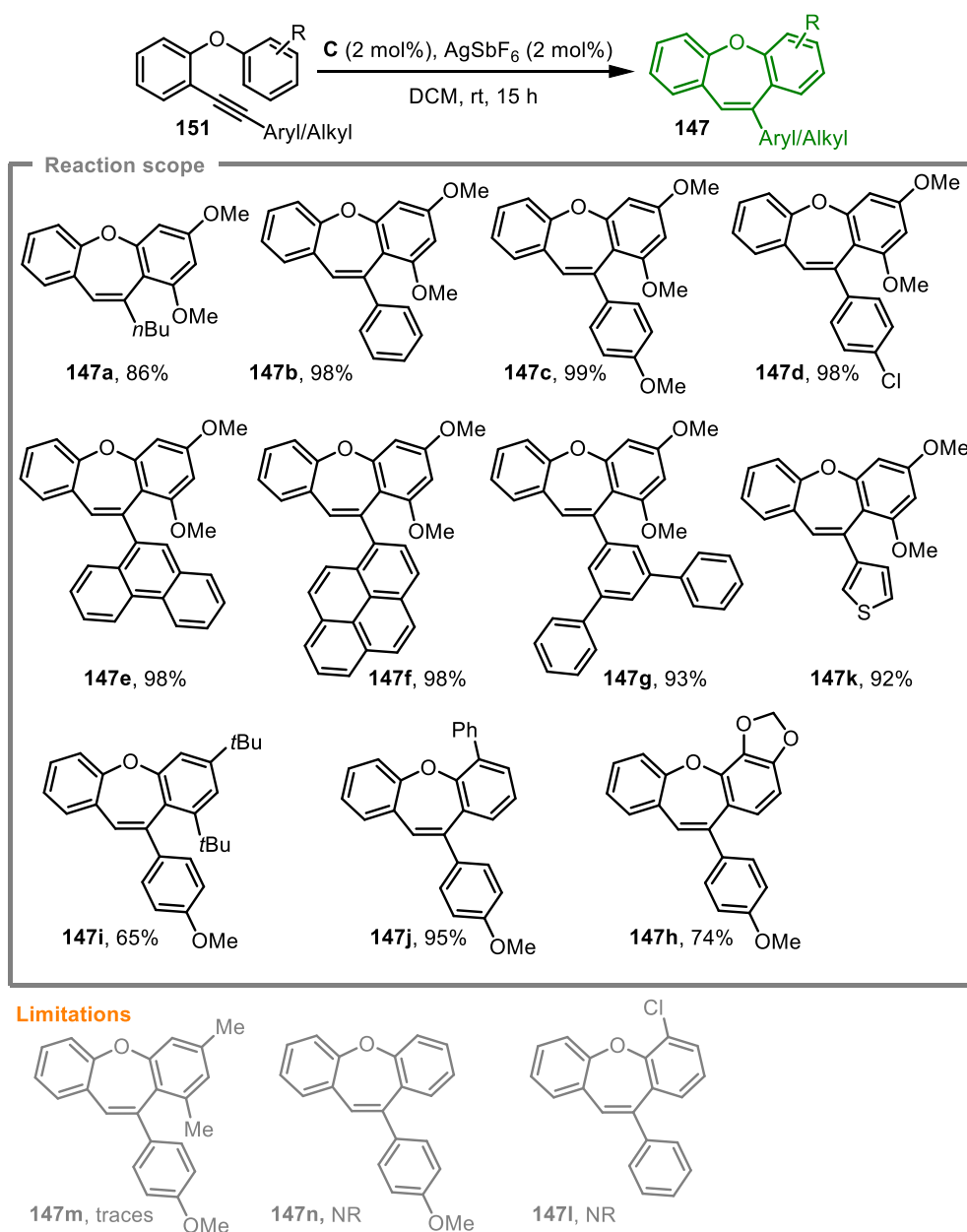
Electron donating substituents at the lateral ring, including methoxy groups **146d-e** and 1,3-dioxoles **146f**, were introduced in the precursors and successfully tolerated in the reaction.



### 3.1 Synthesis of seven-membered ring systems

Whereas electron neutral aryl groups bearing phenyl (**146g**), naphthyl substituents (**146h**), methyl (**146i-j**) or *tert*-butyl groups (**146k**), respectively, necessarily require an anisyl substituent on the alkyne for the cyclization to take place and the desired compounds were obtained in yield up to 98%. Unless neither the alkyne nor the arene is being activated as in **150i**, the desired transformation does not occur (**Scheme 50**) and the starting material was quantitatively recovered.

This transformation also proves to be extremely versatile in terms of substrate selection in the synthesis of oxepines **147**, since the nature of the substituents on the alkyne is not crucial for the Au catalyzed reaction to proceed smoothly (**Scheme 51**).

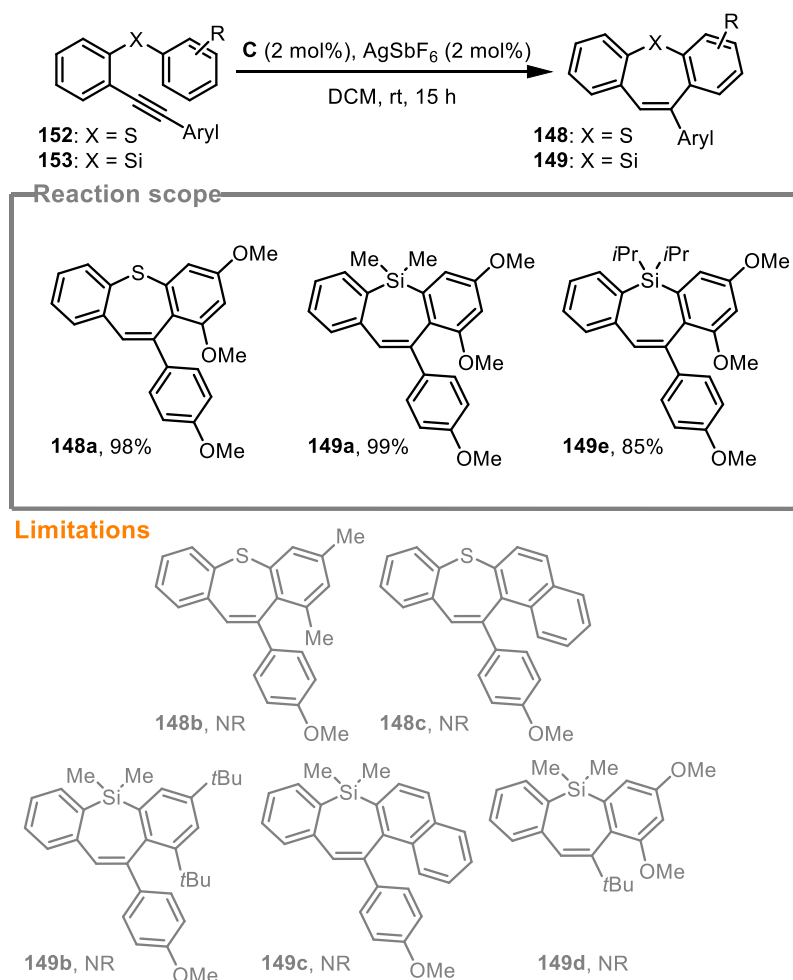


**Scheme 51:** Scope of the Au catalyzed 7-*endo*-dig cyclization of 1-(oxyaryl)-2-ethynylbenzenes **151** towards dibenzoxepines **147**.

### 3. Results and discussion

In addition to the butyl (**147a**), phenyl (**147b**) and anisyl substituents (**147c**) on the alkyne already demonstrated for the cycloheptatrienes, both a *p*-chloro phenyl moiety (**147d**), larger aromatic systems (**147e-g**) or a thiophene (**147k**) can be introduced. The formation of dibenzoxepines succeeded with excellent yields up to 99%, the seven-membered ring being the sole product. However, it should also be noted here that the ring suffering the electrophilic substitution must be at least electron-neutral **147i-j**, or better, electron-rich **147h**, as a prerequisite for the cyclization to occur. Once these requirements are no longer fulfilled, as in the case of substrates **147n,l**, no reaction can be observed. Even methyl substituents **147m** are not sufficient anymore and only traces of the desired product could be detected.

Compared to cycloheptatrienes **146** and oxepines **147**, the Au-catalyzed synthesis of thiepines **148** and silepines **149** is less versatile (**Scheme 52**). Electron donating substituents on the lateral ring, which acts as the incoming nucleophile, are essential for the reaction to proceed.



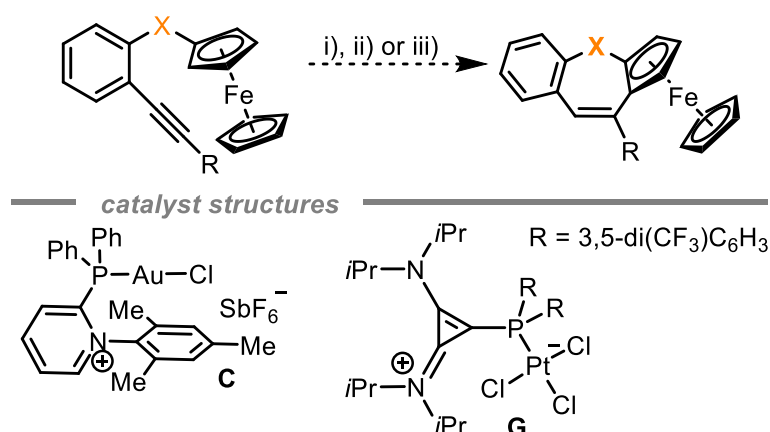
**Scheme 52:** Regioselective synthesis of thiepines **148** and silepines **149** via Au-catalysis.

### 3.1 Synthesis of seven-membered ring systems

As soon as the methoxy groups in the preparation of thiepinas as well as silepinas are replaced by other substituents such as methyl (**148b**), *tert*-butyl (**149b**) or aromatic groups (**148c** and **149c**), no cyclization is detected. In addition, the residue on the alkyne can also not easily be substituted by an alkyl moiety, as in the example of **149d**, without shutting down the reaction. However, in this case steric factors might not be completely excluded. The only possibility for variation in the synthesis of silepinas is provided by the alkyl groups on the silicon. With both methyl and isopropyl groups, the desired silepinas **149a** and **149b** can be obtained *via* 7-*endo*-dig cyclization in very good yields.

With the obtained precursors the method for the preparation of dibenzo seven-membered ring systems *via*  $\pi$ -acid catalyzed hydroarylation should be extended to the synthesis of seven-membered ring fused planar-chiral ferrocenes. The results of screening precursors **162a**, **162c** and **164** under application of different gold(I) and platinum(II) catalysts are summarized in **Table 1**.

**Table 1:** Results of screening for the cyclization of precursors **162a**, **162c** and **164**.



Entry	Precursor	X	R	Catalyst	Conversion <sup>[a]</sup>
1	<b>162a</b>	CH <sub>2</sub>	<i>p</i> -(C <sub>6</sub> H <sub>4</sub> )OMe	Ph <sub>3</sub> PAuCl	-
2	<b>162a</b>	CH <sub>2</sub>	<i>p</i> -(C <sub>6</sub> H <sub>4</sub> )OMe	<b>C</b>	-
3	<b>162a</b>	CH <sub>2</sub>	<i>p</i> -(C <sub>6</sub> H <sub>4</sub> )OMe	PtCl <sub>2</sub>	-
4	<b>162c</b>	CH <sub>2</sub>	H	Ph <sub>3</sub> PAuCl	-
5	<b>162c</b>	CH <sub>2</sub>	H	<b>C</b>	-
6	<b>162c</b>	CH <sub>2</sub>	H	PtCl <sub>2</sub>	decomposition
7	<b>162c</b>	CH <sub>2</sub>	H	<b>G</b>	decomposition
8	<b>164</b>	SiMe <sub>2</sub>	<i>p</i> -(C <sub>6</sub> H <sub>4</sub> )OMe	Ph <sub>3</sub> PAuCl	-
9	<b>164</b>	SiMe <sub>2</sub>	<i>p</i> -(C <sub>6</sub> H <sub>4</sub> )OMe	<b>C</b>	-
10	<b>164</b>	SiMe <sub>2</sub>	<i>p</i> -(C <sub>6</sub> H <sub>4</sub> )OMe	PtCl <sub>2</sub>	-

Reaction conditions: i) [Au] (5 mol%), AgSbF<sub>6</sub> (5 mol%), DCM (0.05 M), rt, 16-18 h; ii) PtCl<sub>2</sub> (10 mol%), toluene (0.05 M), 80 °C, 24 h; iii) **G** (5 mol%), AgSbF<sub>6</sub> (5 mol%), 1,2-DCE (0.05 M), 80 °C, 18 h. <sup>[a]</sup>The conversion was evaluated by <sup>1</sup>H-NMR of the crude mixture.

### 3. Results and discussion

The investigations were initiated with substrates containing a  $-\text{CH}_2-$  tether since these systems showed previously excellent results and reactivity (see **Scheme 50**). Beginning with compound **162a**, both  $\text{Ph}_3\text{PAuCl}$  (**A**) and the cationic gold complex **C** were first tried (entries 1, 2). Since no transformation of the starting material could be observed, an attempt was also made with platinum to see if the reaction would proceed at higher temperatures (entry 3). Subsequently, **162c**, a terminal alkyne that should exhibit higher reactivity, was studied. However, no reaction was detected with the gold catalysts again, although in both cases a green color was observed after addition of silver hexafluoroantimonate to activate the catalyst (entries 4, 5). The starting material could be reisolated after the reaction. This green color indicates unfavorable redox events at the ferrocene, which might disturb the desired reactivity. In addition, also platinum catalysts were applied. First  $\text{PtCl}_2$  and additionally a cationic platinum catalyst **G** to achieve maximum reactivity (entries 6, 7). Unfortunately, in both reactions a dark brown suspension was received and decomposition of the starting material was detected.

Since the intramolecular hydroarylation of both precursors with  $-\text{CH}_2-$  tether failed, compound **164** with  $-\text{SiMe}_2-$  tether was also tried. Again, suitable catalysts were screened starting with gold catalysts (entries 8, 9) and then  $\text{PtCl}_2$  (entry 10) was examined. No conversion to the desired product could be achieved in any of the three reactions and the starting material remained unchanged.

After all successfully synthesized precursors containing a ferrocene moiety have been investigated and in none of the experiments the desired target molecule could be obtained, it is likely that either ferrocene is not electron-rich enough for the reaction to proceed or might be too electron-rich since the color change to green indicating redox events, was observed. As mentioned before, the synthesis of seven-membered ring systems depends heavily on the electron richness of the ring undergoing the electrophilic substitution. Replacement of this part of the molecule by a ferrocene moiety might reveal the limitation of this method.

### 3.2 Structural analysis of seven-membered ring systems

In this chapter, the molecular structures of the cycloheptatrienes **146**, oxepines **147**, thiepinines **148** and silepinines **149** in the solid state will be presented and their structural characteristics compared. The central question is to what extent the tether and how the different substitution patterns affect the geometry of the central seven-membered ring.

Four cycloheptatriene structures could be crystallographically characterized, which differ only in the substituents on the right aromatic system and all exhibit an anisyl residue on the seven-membered ring (**Figure 23**).

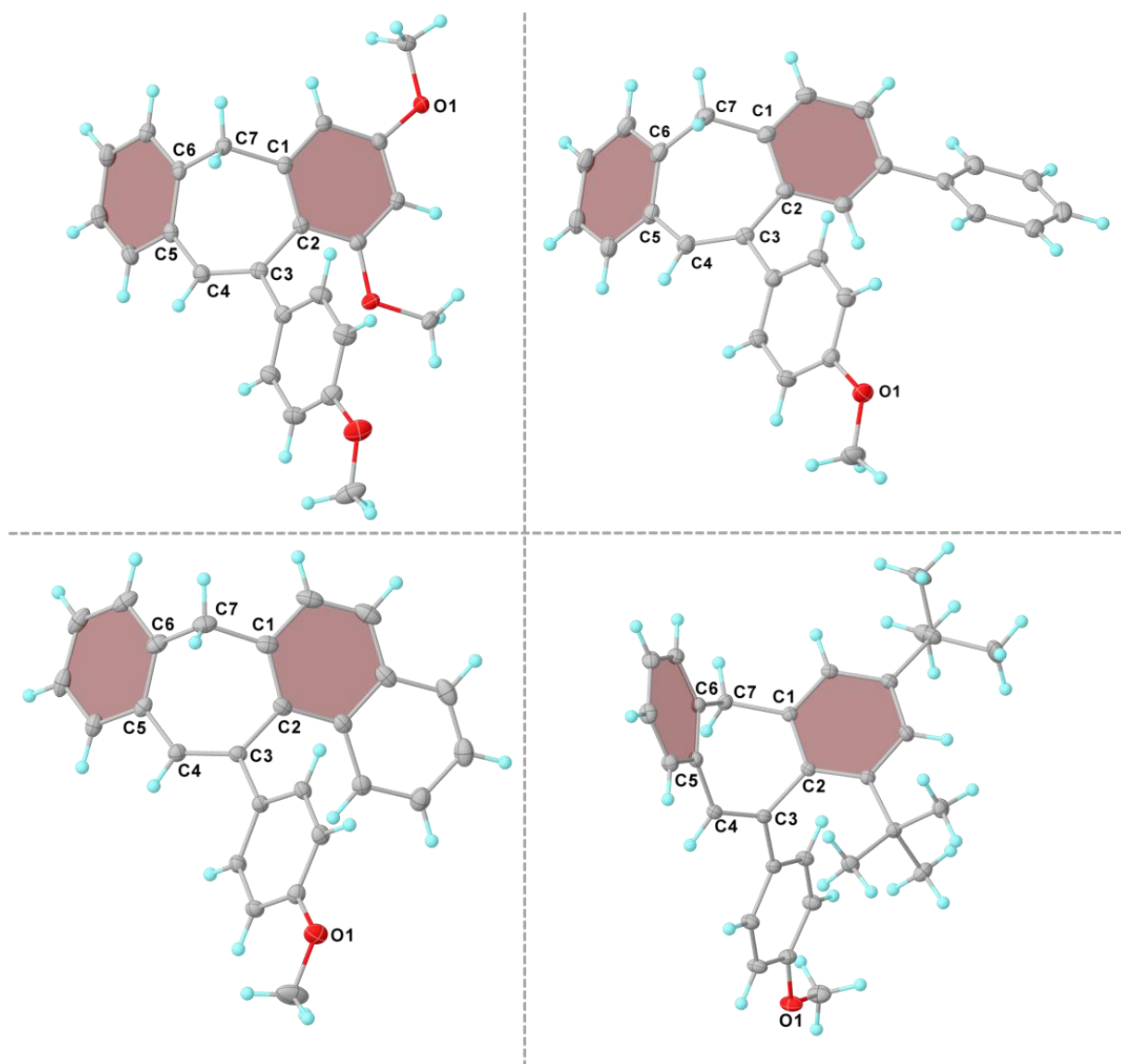


**Figure 23:** Molecular structures of **146e** (top left), **146g** (top right), **146h** (bottom left) and **146k** (bottom right) in the solid state. Anisotropic displacement parameters are depicted at the 50% probability level. Mean planes are highlighted in brown.

Compounds **146e** (**Figure 23**, top left) and **146g** (**Figure 23**, top right) crystallize from ethanol as colorless needles and as colorless blocks, respectively. Both crystallize in the monoclinic crystal system in space group  $P2_1/c$ . Single crystals of compound **146h** (**Figure**

### 3. Results and discussion

**23**, bottom left) suitable for X-ray analysis were obtained from DCM and hexane by diffusion crystallization. It crystallizes as colorless blocks in the orthorhombic crystal system in space group  $Pca2_1$ . Colorless blocks of compound **146k** (**Figure 23**, top right) were obtained by slow evaporation of chloroform. **146k** crystallizes in the monoclinic crystal system in space group  $P2_1/c$ .

With the molecular structures obtained, the differences in the structure of the central seven-membered ring caused by different substituents will now be examined. For this purpose, the bond lengths and the internal angles were analyzed in more detail. The bond lengths of the compounds considered are given in **Table 2** and the bond angles are shown in **Table 3**. In summary, all bond lengths are in the range of the classical C-C single (1.54 Å) and C-C double bond (1.34 Å).<sup>[138]</sup> A closer look reveals that the distances of C1-C2 and C5-C6 are generally close to the typical bond length of 1.39 Å for benzene, C2-C3 and C4-C5 are in the range of  $sp^2$ - $sp^2$  hybridized carbon atoms (1.47 Å), C3-C4 correspond to the typical bond length of alkenes (1.34 Å), and C6-C7 and C7-C1 are in the range of  $sp^2$ - $sp^3$  hybridized carbon atoms (1.50 Å).<sup>[138]</sup> Deviating from these trends, outliers can be observed in some positions depending on the substituents. The phenyl substituent in **146g** appears to have the greatest influence on the geometry of the central seven-membered ring and thus the bond lengths; a shortening of the C1-C2 bond and, at the same time, a significant lengthening of the C2-C3 bond are noted. Also noticeable is the large difference in the distance between C7-C1 and C6-C7, which is almost identical in comparison for the other molecules. In addition, the *tert*-butyl groups in **146h**, being sterically very demanding substituents, do not seem to significantly affect the geometry of the central seven-membered ring.

**Table 2:** Bond lengths of the central seven-membered ring in dibenzo[*a,e*]cycloheptatrienes **146**.

	C7-C1 [Å]	C1-C2 [Å]	C2-C3 [Å]	C3-C4 [Å]	C4-C5 [Å]	C5-C6 [Å]	C6-C7 [Å]
<b>146e</b>	1.507(1)	1.398(1)	1.484(1)	1.351(1)	1.470(1)	1.408(2)	1.507(1)
<b>146g</b>	1.492(1)	1.377(1)	1.531(1)	1.365(1)	1.461(1)	1.405(1)	1.546(2)
<b>146h</b>	1.503(2)	1.394(2)	1.488(2)	1.359(2)	1.467(2)	1.407(2)	1.506(2)
<b>146k</b>	1.514(1)	1.412(1)	1.496(1)	1.349(1)	1.470(1)	1.409(1)	1.513(1)

The bond angles of C6-C7-C1, which include the tether and thus a  $sp^3$  hybridized carbon atom, are close to the classical tetrahedral angle of  $109.5^\circ$  with values ranging from  $108.3(1)^\circ$  to  $110.5(1)^\circ$ . In general, it can be observed that the bond angles between C7-C1-C2, C1-C2-C3, C4-C5-C6, and C5-C6-C7 roughly correspond to the classical value of  $120^\circ$  for  $sp^2$  hybridized carbon atoms, whereas larger deviations can be observed for C2-C3-C4 and C3-C4-C5. The substituents seem to have the greatest influence on the angle between C1-C2-C3. With two sterically demanding *tert*-butyl substituents as in **146k** the smallest

### 3.2 Structural analysis of seven-membered ring systems

(117.0(1)°) and with one phenyl substituent as in **146g** on the right aromatic system the largest angle (123.6(1)°) is obtained. This shows that the angle at C2 is the most flexible and exhibits the greatest deformation due to the substitution pattern. All the dibenzo[*a,e*]cycloheptatrienes **146** considered exhibit a boat-like conformation of the central seven-membered ring.

**Table 3:** Bond angles in the central seven-membered ring in dibenzo[*a,e*]cycloheptatrienes **146**.

	C6-C7-C1 [°]	C7-C1-C2 [°]	C1-C2-C3 [°]	C2-C3-C4 [°]	C3-C4-C5 [°]	C4-C5-C6 [°]	C5-C6-C7 [°]
<b>146e</b>	108.3(1)	118.7(1)	122.0(1)	122.3(1)	126.7(1)	121.2(1)	119.1(1)
<b>146g</b>	110.1(1)	117.1(1)	123.6(1)	125.2(1)	126.4(1)	120.9(1)	119.8(1)
<b>146h</b>	110.5(1)	120.8(1)	120.3(1)	124.0(1)	128.4(1)	121.3(1)	118.1(1)
<b>146k</b>	109.9(1)	120.2(1)	117.0(1)	122.4(1)	124.7(1)	119.1(1)	119.0(1)

In addition, four structures of the obtained oxepines could be crystallographically studied. The oxepines characterized differed in the substituents on the right ring system as well as in the residues at the bottom of the seven-membered ring. Compounds **147b** and **147c** crystallize from ethanol as colorless blocks and colorless plates in the orthorhombic crystal system, **147b** (**Figure 24**, top left) in space group  $P2_12_12_1$  and **147c** (**Figure 24**, top right) in space group  $Pna2_1$ . The flack parameter for **147b** is [ $x = 0.011(16)$ ], indicating that the crystals are truly enantiopure. Since the racemic compound was crystallized, it is the result of a spontaneous resolution into a racemic conglomerate. Compounds **147i** and **147k** were crystallized from ethanol as colorless needles and colorless plates. **147i** crystallizes in the monoclinic crystal system in space group  $P2_1/n$  and the asymmetric unit contains one molecule (**Figure 24**, bottom left). **147k** crystallizes in the orthorhombic crystal system in space group  $P2_12_12_1$  (**Figure 24**, bottom right). Resulting from a spontaneous resolution into a racemic conglomerate truly enantiopure crystals of **147k** with a flack parameter of [ $x = 0.04(3)$ ] were obtained. Dynamic disorder of the thiophenyl moiety was observed, with both possible molecular structures occurring with similar probability, which is a typical behavior for unsubstituted thiophenes.

### 3. Results and discussion

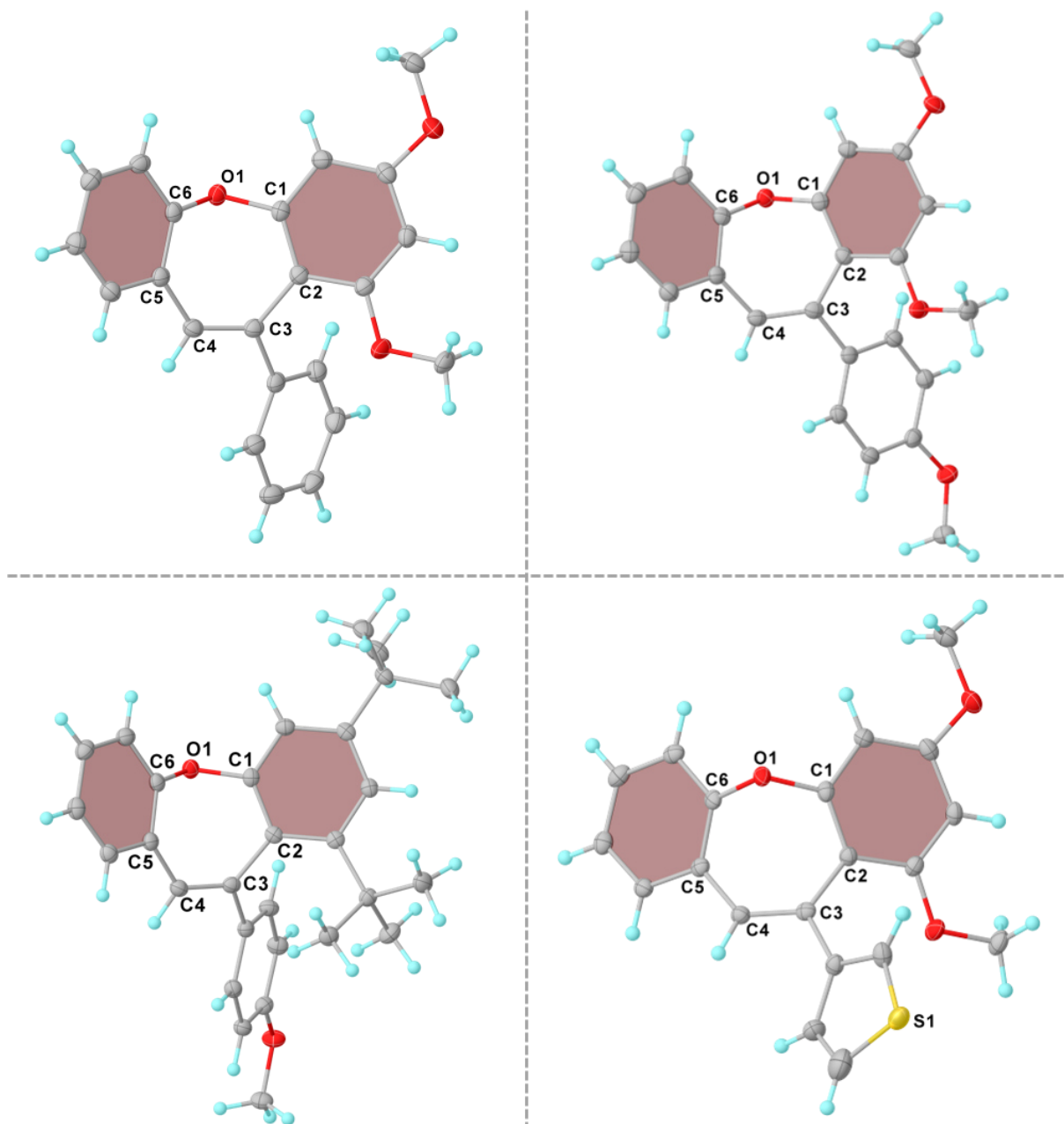


**Figure 24:** Molecular structures of **147b** (top left), **147c** (top right), **147i** (bottom left) and **147k** (bottom right) in the solid state. Anisotropic displacement parameters are depicted at the 50% probability level. Mean planes are highlighted in brown.

To continue the investigation of the influence of substituents on the geometry of the central seven-membered ring for dibenzo[*a,e*]oxepines **147**, the bond lengths (**Table 4**) and bond angles (**Table 5**) were also studied in more detail. In general, similar trends as for the previously discussed dibenzo[*a,e*]cycloheptatrienes **146** could be observed and the C-C bond lengths stay in comparable ranges. The C1-C2 and C5-C6 bond length corresponds to the typical 1.39 Å reported for benzene, for C2-C3 and C4-C5 it is in the range of sp<sup>2</sup>-sp<sup>2</sup> hybridized carbon atoms (1.47 Å), and for C3-C4 it is in agreement with the typical bond length of alkenes (1.34 Å). The oxygen-carbon bonds O1-C1 and C6-O1 contained in the seven-membered ring are shorter than the 1.43 Å reported in literature.<sup>[138]</sup> When comparing



### 3.2 Structural analysis of seven-membered ring systems

the dibenzo[*b,f*]oxepines **146** with each other, it is striking that the influence of the different substituents on the bond lengths is vanishingly small. A change of the residue at the former triple bond does not influence the bond lengths significantly. Only when the methoxy groups are replaced by sterically more demanding *tert*-butyl groups in **147i** minor changes and an elongation of the C2-C3 bond can be observed.

**Table 4:** Bond lengths of the central seven-membered ring in dibenzo[*b,f*]oxepines **147**.

	O1-C1 [Å]	C1-C2 [Å]	C2-C3 [Å]	C3-C4 [Å]	C4-C5 [Å]	C5-C6 [Å]	C6-O1 [Å]
<b>147b</b>	1.398(2)	1.392(2)	1.483(2)	1.347(2)	1.462(2)	1.399(2)	1.396(2)
<b>147c</b>	1.397(2)	1.390(2)	1.485(2)	1.350(2)	1.464(2)	1.399(2)	1.401(2)
<b>147i</b>	1.399(1)	1.399(1)	1.501(1)	1.346(1)	1.468(1)	1.402(1)	1.392(1)
<b>147k</b>	1.397(2)	1.389(2)	1.483(2)	1.352(2)	1.460(2)	1.397(2)	1.394(2)

Considering the bond angles, a noticeable finding is that the C6-O1-C1 angles of 112-114° are slightly larger than the classical tetrahedral angle (109.5°). Based on the VSEPR model, the angle should actually be around 104°, since the free electron pairs on oxygen would occupy more space and thus lead to a decrease in the C6-O1-C1 angle. However, the ring strain of the seven-membered ring might be the reason why the actual C6-O1-C1 angle is larger with 112-114°. The remaining bond angles are close to the usual value of 120° for sp<sup>2</sup> hybridized carbon atoms, with the angles between O1-C1-C2, C4-C5-C6, and C5-C6-O1 hitting the value fairly close, and the deviations increasing from C1-C2-C3 through C2-C3-C4 and C3-C4-C5. As was already the case for the bond angles, only very small influences by the substitution patterns considered can be observed for the bond angles. However, the rather small angle of 117° for C1-C2-C3 in compound **147i** is remarkable and can be explained by the steric demand of the *tert*-butyl groups. The typical boat-like conformation of seven-membered rings was observed in all structures of the dibenzo[*a,e*]oxepines **147** regardless of the substituents.

**Table 5:** Bond angles in the central seven-membered ring in dibenzo[*b,f*]oxepines **147**.

	C6-O1-C1 [°]	O1-C1-C2 [°]	C1-C2-C3 [°]	C2-C3-C4 [°]	C3-C4-C5 [°]	C4-C5-C6 [°]	C5-C6-O1 [°]
<b>147b</b>	114.2(1)	119.9(1)	122.5(1)	122.9(1)	127.2(1)	122.0(1)	119.9(1)
<b>147c</b>	112.1(1)	119.2(1)	121.9(1)	122.3(1)	125.7(1)	121.4(1)	119.5(1)
<b>147i</b>	113.5(1)	120.1(1)	117.0(1)	123.2(1)	126.7(1)	119.4(1)	119.3(1)
<b>147k</b>	113.9(1)	120.2(1)	122.2(1)	123.6(1)	127.6(2)	121.9(2)	119.3(1)

Only one structure of the heavier homologue to oxepines **147** was characterized by single crystal X-ray diffraction. Colorless plates of compound **148a** were obtained from a mixture

### 3. Results and discussion

of ethanol and ethyl acetate. **148a** crystallizes in the monoclinic crystal system in space group  $P2_1/n$  (**Figure 25**).

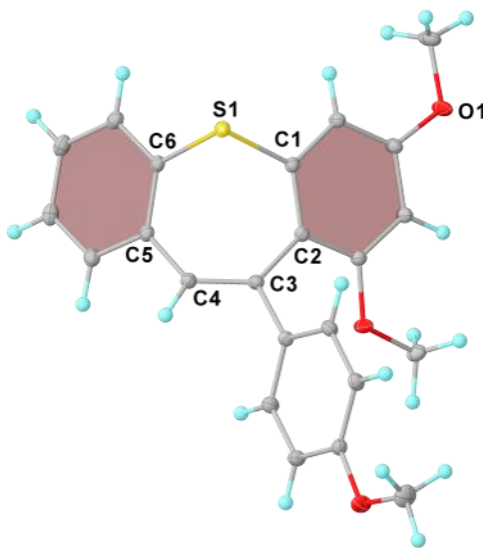


**Figure 25:** Molecular structure of **148a** in the solid state. Anisotropic displacement parameters are depicted at the 50% probability level. Mean planes are highlighted in brown. Selected bond lengths [Å] and angles [°]: S1-C1 1.778(1), C1-C2 1.398(1), C2-C3 1.480(1), C3-C4 1.353(1), C4-C5 1.466(1), C5-C6 1.405(1), C6-S1 1.776(1), C6-S1-C1 99.3(4), S1-C1-C2 120.4(1), C1-C2-C3 123.9(1), C2-C3-C4 124.6(1), C3-C4-C5 128.8(1), C4-C5-C6 123.0(1), C5-C6-S1 120.3(1).

When the bond lengths in compound **148a** are considered, the S1-C1 and C6-S1 distance fits perfectly with the value of 1.77 Å reported in the literature for a sulfur atom bonded to two aromatic carbon atoms.<sup>[138]</sup> Moreover, for the bond lengths between carbon atoms, the same trends as for the dibenzo[*a,e*]cycloheptatrienes and dibenzo[*b,f*]oxepines can be observed and they are in agreement with the ranges tabulated in the literature. For the bond angles, a significant decrease is observed for the C6-S1-C1 angle compared to the oxygen analogue. Due to the lower hybridization tendency of sulfur, there is an approximation to 90°, which corresponds to the angle between the p orbitals. All other bond angles within the central seven-membered ring reflect similar observations as for the previously discussed molecules and a boat-like conformation was adopted.

Compound **149a** exhibits polymorphism and gives colorless needles or plates with slightly different molecular structures depending on the solvent used for crystallization. From methanol, **149a** crystallizes in the monoclinic system in the space group  $C2/c$  with one molecule in the asymmetric unit (**Figure 26**, left). When a mixture of methanol and ethyl acetate is used, crystallization of **149a** occurs in the triclinic crystal system in space group  $P\bar{1}$ . The asymmetric unit consists of two molecules, and in one molecule a disorder of the methoxy group at the anisyl moiety is found. The structure of the seven-membered ring is the same in each molecular structure and a boat-like conformation was observed but orientation of the methoxy groups differs depending on the solvent. An overlay of the

### 3.2 Structural analysis of seven-membered ring systems

molecular structures obtained from methanol and a mixture of methanol and ethyl acetate is shown in **Figure 26** (right).

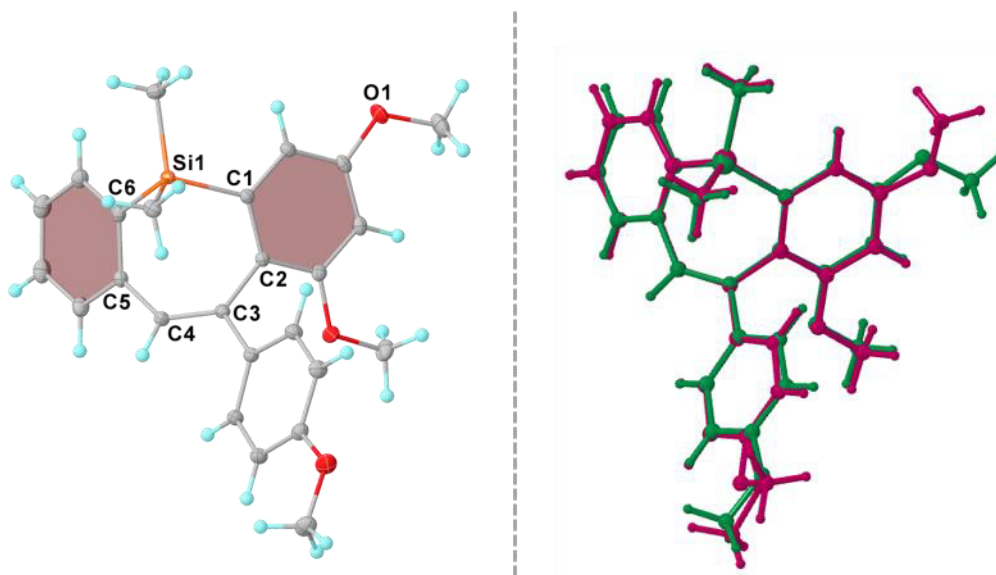


**Figure 26:** Molecular structure of **149a** in the solid state crystallized from methanol. Anisotropic displacement parameters are depicted at the 50% probability level. Mean planes are highlighted in brown (left). Overlay of molecular structures obtained from methanol (green) and a mixture of methanol and ethyl acetate (pink) (right). Selected bond lengths [Å] and angles [°]: Si1-C1 1.867(1), C1-C2 1.403(2), C2-C3 1.493(2), C3-C4 1.353(2), C4-C5 1.474(2), C5-C6 1.410(2), C6-Si1 1.871(1), C6-Si1-C1 100.7(1), Si1-C1-C2 118.5(1), C1-C2-C3 122.4(1), C2-C3-C4 125.0(1), C3-C4-C5 129.4(1), C4-C5-C6 121.4(1), C5-C6-Si1 119.6(1).

The carbon-silicon bonds Si1-C1 and C6-Si1 are almost equal in length and correspond to the value of 1.86 Å for a C-Si single bond reported in the literature.<sup>[138]</sup> The carbon-carbon bonds in the central seven-membered ring of **149a** are nearly identical to the structures considered previously although a different heteroatom is located in the tether. Compared to the carbon representative **147**, a significant decrease of the C6-Si1-C1 bond angle can be found. Due to the lower tendency to hybridize of the silicon s valence orbital, the angle is closer to 90°, which corresponds to the angle of the p orbitals to each other.

To further investigate the effects that the geometry of the central seven-ring has on the bending of the whole molecule, in addition to the bond lengths and angles, the phenyl rings on the right and left side were used to define mean planes (marked in brown) and the intersecting angles of the planes' normals were considered (**Table 6**). These range from 51-60° for an oxygen, 60-70° for a carbon, 67° for a sulfur, and 74° for a silicon tether. In addition, it is noticeable that the molecules are bent to different degrees depending on the substituent and tether, indicating a certain flexibility of the seven-membered ring. In comparison, the respective heavier homologue has a larger angle, which means that it is less bent. The bending angles for the sulfur **148a** and the silicon compound **149a** are larger, since they prefer C-X-C angles around 90° due to the lower tendency of hybridization. To see if packing effects in the solid state have a significant effect on the bending angles of the studied molecules, a comparison was made with the bending angles obtained from the

### 3. Results and discussion

theoretically optimized structures. Significant deviations are seen except for the sulfur compound **148a**, indicating that packing effects may influence the structures.

**Table 6:** Observed bending angles in dibenzo[*a,e*]cycloheptatrienes **146**, dibenzo[*b,f*]oxepines **147**, dibenzo[*b,f*]thiepine **148a** and dibenzo[*b,f*]silepine **149a**.

Identifier	X	Bending angle [°] (X-ray)	Bending angle [°] (calc. B3LYP-D3/6-31+g(d))
<b>146e</b>	CH <sub>2</sub>	69.9	64.1
<b>146g</b>	CH <sub>2</sub>	65.7	60.2
<b>146h</b>	CH <sub>2</sub>	59.9	65.9
<b>146k</b>	CH <sub>2</sub>	66.9	67.9
<b>147b</b>	O	51.9	55.1
<b>147c</b>	O	60.1	55.4
<b>147i</b>	O	51.6	59.8
<b>147k</b>	O	51.4	56.3
<b>148a</b>	S	67.3	66.8
<b>149a</b>	SiMe <sub>2</sub>	74.1	66.5

In summary, the atom in the tether does not greatly affect the bond lengths and bond angles of the remaining carbon atoms in the seven-membered ring. However, the distances of the aromatic systems in the region of the tether and the degree of bending of the entire molecule are significantly influenced, depending on the size of the tether atom and the C6-X-C1 angle.

In section 3.3.3 the DFT calculations are discussed and the flexibilities observed in the molecules could be related to the calculated interconversion barriers.

## 3.3 Exploration of configurational stability of seven-membered ring systems

As described in the introduction in section 1.4.2, the central seven-membered ring adopts a boat-like conformation, that forms chiral enantiomers. Since conformational stability can have a major impact on the biological activity and appropriate application of cycloheptatrienes, oxepines, thiepinines, and silepinines, the interconversion barriers should be determined using suitable methods.

The following complementary methods have been applied in order to evaluate the conformational stability and to determine the interconversion barriers of the molecules synthesized within this thesis:

1. Dynamic high-performance liquid chromatography (HPLC) experiments
2. Dynamic nuclear magnetic resonance (NMR) spectroscopy
3. Density-functional theory (DFT) methods

The application of DFT methods is intended to be an addition to the experimental results. Since not every molecule fulfills the requirements for the application of the chosen experimental methods, a differentiated consideration is necessary and the suitability is discussed in the following subchapters. The decisive factor is always how fast the interconversion proceeds and whether it can be visualized on the time scale of the selected methods.

### 3.3.1 Dynamic HPLC experiments

Dynamic HPLC on enantioselective stationary phases has become an established technique in order to study chiral molecules with internal motions that lead to stereoinversion. To determine enantiomerization barriers using this technique, it is crucial that the enantiomers can be separated on appropriate chiral stationary phases and that this occurs on the timescale of the separation process. The HPLC time scale ranges from seconds for fast HPLC on short columns to hours when using standard columns and low flow rates of the eluent. Depending on the technical requirements of the HPLC system used, barriers in the range of 59 to 105 kJ mol<sup>-1</sup> can be obtained in the temperature range from -80 to 80 °C. Usually, the characteristic peak shape for an interconversion of enantiomers shows two resolved peaks and an in between plateau. The elution profiles contain all necessary information to extract the kinetic parameters, e.g., the rate constant or the Gibbs free energy for this exchange process. Several methods based on different theoretical frameworks describing the dynamic system have been applied to derive the kinetic parameters from experimental elution profiles.<sup>[139]</sup> In the context of this work, the unified equation developed by Oliver Trapp<sup>[140]</sup> was utilized, since it does not require complex

### 3. Results and discussion

computer-simulated elution profiles. Using the unified equation, interconversion barriers can be determined from the obtained chromatograms. This allows the calculation of rate constants for first order reactions that take place during a chromatographic separation. The rate constant can be derived directly from chromatographic parameters such as retention times of the interconverting species A and B, the peak width at half maximum and the relative plateau height, independent of the initial concentrations of the converting analytes A and B and the equilibrium constant. If the process being investigated is an enantiomerization, the unified equation can be solved analytically. For this purpose, Trapp and co-workers<sup>[140]</sup> implemented the analytical solution of the unified equation into the computer program DCXplorer, which calculates the required chromatographic parameters and also the rate constant directly from the elution profiles of the dynamic chromatography experiments. Subsequently, the Gibbs free activation energy was determined using the Eyring equation. The unified equation and the other formulas used to calculate the interconversion barriers are given in the experimental part.

In order to gain insight into the interconversion barriers of the synthesized seven-membered ring systems, the cycloheptatrienes **146h** and **146k** with the comparatively most sterically demanding substituents were first investigated and temperature-dependent chiral separations were conducted. Representative elution profiles are shown in **Figure 27** and **Figure 28**, respectively.

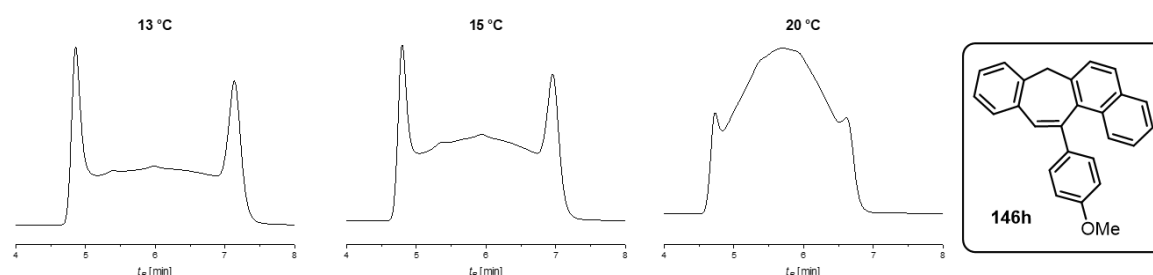


**Figure 27:** Elution profiles of the temperature-dependent chiral separation of **146h**. Separation conditions: column: Chiralpak<sup>®</sup> IA-3; *n*-hexane/*iso*-propanol 99/1 (V/V); flow: 1.0 mL/min.

For **146h** (**Figure 27**), no baseline separation of the enantiomers could be achieved as a distinct plateau formation was already observed at a temperature of 13 °C. Once the plateau exceeds a height of 50%, determination of peak widths at half maximum and column efficiencies with sufficient precision becomes impossible, therefore the elution profile at 20 °C, which shows strong coalescence, was not included in the interconversion barrier analysis. Since the height of the plateau at a temperature of 15 °C is 49%, just below the 50% threshold, the elution profile was included and the free Gibbs activation energy  $\Delta G^\ddagger$  could be determined to be 82.8 kJ mol<sup>-1</sup> at both 13 °C and 15 °C. However, with only two

### 3.3 Exploration of configurational stability of seven-membered ring systems

values, an Eyring plot could not be constructed and the activation enthalpy and entropy could not be calculated.

Next, **146k** was investigated, whose two *tert*-butyl groups should exhibit a significantly greater steric hindrance compared to **146h** with only one naphthyl substituent. It was possible to partially separate the enantiomers but no complete baseline separation of the peaks could be achieved and tailing was observed at all temperatures (**Figure 28**).

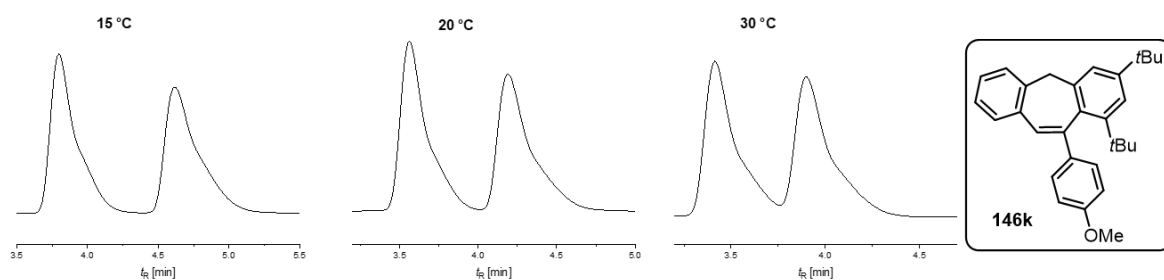


**Figure 28:** Elution profiles of the temperature-dependent chiral separation of **146k**. Separation conditions: column: Chiralpak® IA-3; *n*-hexane/*iso*-propanol 99/1 (V/V); flow: 1.0 mL/min.

This may be due to the fact that interconversion already takes place at that temperature and baseline separation is prevented due to plateau formation, or because the stationary phase used is not able to provide better separation efficiency under the investigated conditions. The temperature dependence of these effects, especially chromatographic tailing, has a negative influence on the separation factor, and makes reliably assigning the correct height to the plateau impossible. In addition, the asymmetry of the peaks prevents the half-width from being properly determined. Therefore, no reliable conclusions can be drawn regarding the value of the interconversion barrier using HPLC.

Subsequently, oxepine **147i** was analyzed (**Figure 29**), which has the same sterically demanding *tert*-butyl substituents as **146k**.

### 3. Results and discussion

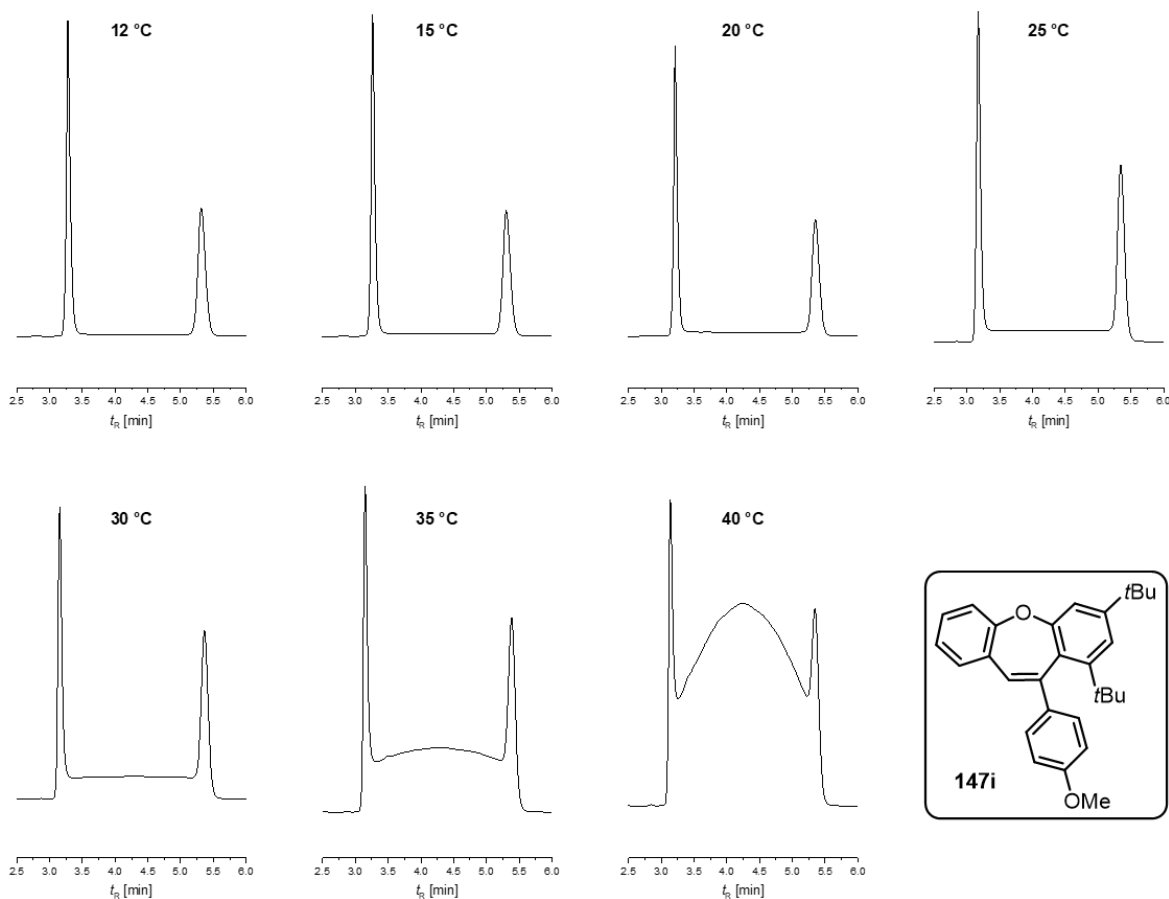


**Figure 29:** Elution profiles of the temperature-dependent chiral separation of **147i**. Separation conditions: column: Chiralpak® IA-3; *n*-hexane/*iso*-propanol 98/2 (V/V); flow: 1.0 mL/min.

However, significantly lower barriers have been observed in the past for oxepines with the same substitution pattern when compared to the corresponding cycloheptatrienes.<sup>[107]</sup> For determination of the enantiomerization barriers, the temperature-dependent measurements from 15-35 °C were considered. Below a temperature of 15 °C a plateau is hardly detectable and at 40 °C a plateau height of 50% is exceeded, thus peak width at half height and efficiencies cannot be reliably determined.

For compound **149e**, sufficient separation of the enantiomers could be achieved by HPLC (**Figure 30**). The elution profiles from 12-20 °C were used to calculate the Gibbs free activation energy  $\Delta G^\ddagger$ . Distinct plateau formation caused by the dynamic enantiomerization at elevated temperatures and peak coalescence for temperatures above 25 °C were observed.



### 3.3 Exploration of configurational stability of seven-membered ring systems

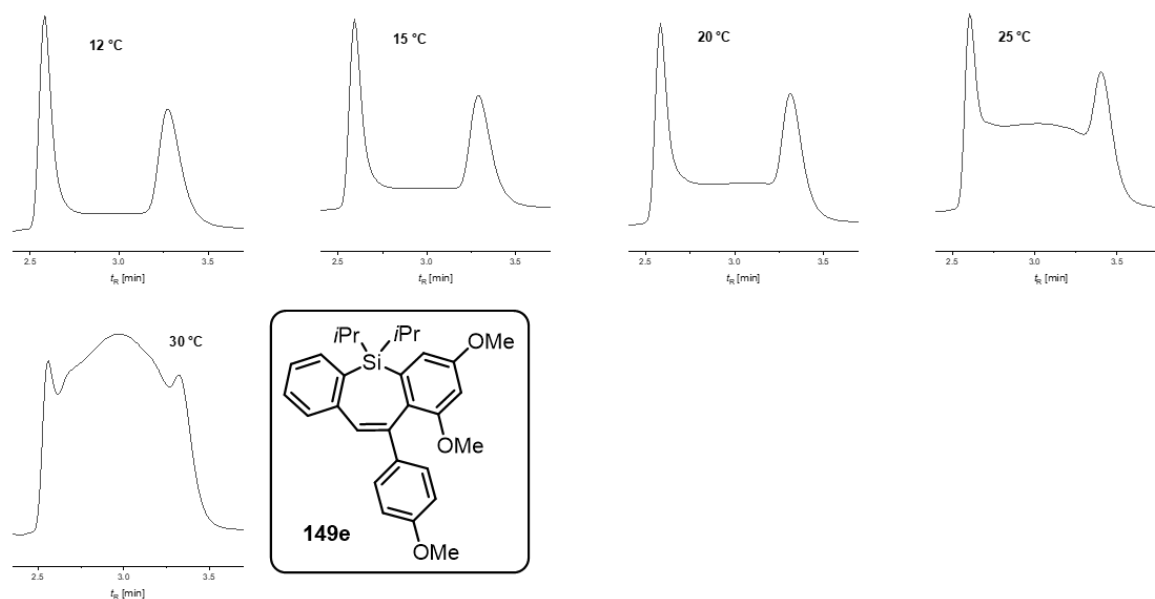


**Figure 30:** Elution profiles of the temperature-dependent chiral separation of **149e**. Separation conditions: column: Chiralpak® IC-3; *n*-hexane/ethyl acetate 96/4 (V/V) (12-35 °C); flow: 1.0 mL/min.

With these data in hand Eyring Plot analyses were performed for compounds **147i** and **149e** to provide the activation parameters  $\Delta H^\ddagger$  and  $\Delta S^\ddagger$ . **Figure 31** depicts the Eyring plots, showing the high precision in the determination of the rate constants.

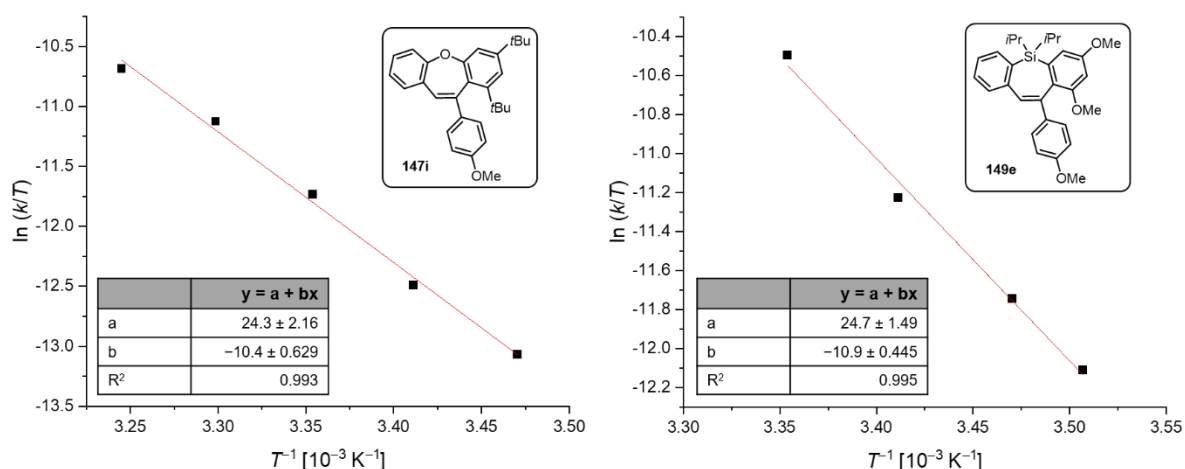


**Figure 31:** Eyring plots for **147i** (left) and **149e** (right).

The experimentally determined activation parameters of the investigated compounds are summarized in **Table 7**. Only small differences can be found for the calculated activation barriers of the enantiomerization of compounds **147i** and **149e**, despite significant structural differences. In addition to the steric bulk of the substituent in the direct vicinity of the seven-membered ring, sterically demanding substituents on the tether appear to markedly increase the interconversion barrier. Therefore, a relatively high Gibbs free activation energy was observed for **149e** despite the comparatively "small" methoxy substituents. However, in both cases the enantiomerization barriers are too low to realize isolation of the respective enantiomers.

### 3. Results and discussion

**Table 7:** Activation parameters of the enantiomerization of compounds **148i** and **149e**.

Compd.	$\Delta G^{\ddagger}_{298\text{ K}}$ [kJ mol <sup>-1</sup> ]	$\Delta H^{\ddagger}$ [kJ mol <sup>-1</sup> ]	$\Delta S^{\ddagger}_{298\text{ K}}$ [J K <sup>-1</sup> mol <sup>-1</sup> ]
<b>147i</b>	88.0	90.5	8.55
<b>149e</b>	84.9	86.3	4.49

Unfortunately, the enantiomers of the thiepine derivative **148a** could not be separated using available chiral HPLC columns, suggesting a barrier too low for HPLC timescale and a very rapid enantiomerization process. Although similar interconversion barriers could be expected for thiepines as for cycloheptatrienes, the methoxy substituents are not sterically demanding enough to prevent interconversion and allow isolation of the enantiomers.

#### 3.3.2 Dynamic NMR spectroscopy

Besides dynamic HPLC, dynamic NMR spectroscopy was used as a complementary experimental technique to investigate interconversions of enantiomers that are on a different time scale. As for dynamic HPLC, the rate constants and the resulting thermodynamic parameters, such as the activation barrier of the interconversion, can be determined. Dynamic NMR spectroscopy can be used to study medium-fast exchange processes (milliseconds to seconds) and slow to medium-fast exchange (seconds up to a minute). A medium-fast exchange is characterized by line broadening and splitting. Using temperature-dependent NMR at low temperature separated signals can be observed, which merge into one broad signal at the coalescence temperature. Above this temperature a single resonance is visible in the spectrum. The rate constant and the other kinetic parameters can be derived at the coalescence point.<sup>[141]</sup>

Another NMR method for analyzing exchange processes is the two-dimensional NMR technique called EXSY, which stands for EXchange Spetroscopy. This technique is particularly suitable for the study of slow exchange. It is a variant of the nuclear overhauser enhanced spectroscopy (NOESY) that can be used to obtain information about chemical exchange processes in a straightforward fashion before line distortion occurs. All protons exchanging with each other become visible as cross peaks.<sup>[142,143]</sup> The applicability of this approach assumes that the signal from each species in the exchange process is conveniently separated from the others in the NMR spectrum. Thus, the silepines **149a** and **149e** proved to be particularly suitable for this method of investigation, since separated signals were obtained for each of the two methyl and two isopropyl groups on the silicon, respectively.

For the evaluation of the EXSY experiments the free program EXSYCALC was used, which calculates the magnetization exchange rates  $k'$  of the exchange equilibrium through a quantitative analysis of the obtained NMR peaks. The calculations are performed based on

### 3.3 Exploration of configurational stability of seven-membered ring systems

a full relaxation matrix analysis of the peak intensities. Further details and background on the assumptions on which the program is based are given in the experimental section.

For silepine **149a**, 2D-EXSY spectra were recorded at  $-25\text{ }^{\circ}\text{C}$ ,  $0\text{ }^{\circ}\text{C}$ ,  $25\text{ }^{\circ}\text{C}$ , and  $50\text{ }^{\circ}\text{C}$ . From the obtained spectra, the required intensities of the cross and diagonal peaks were determined by integration and, at the respective temperatures, the rate constants were calculated using the program EXSYCALC (**Figure 32**).

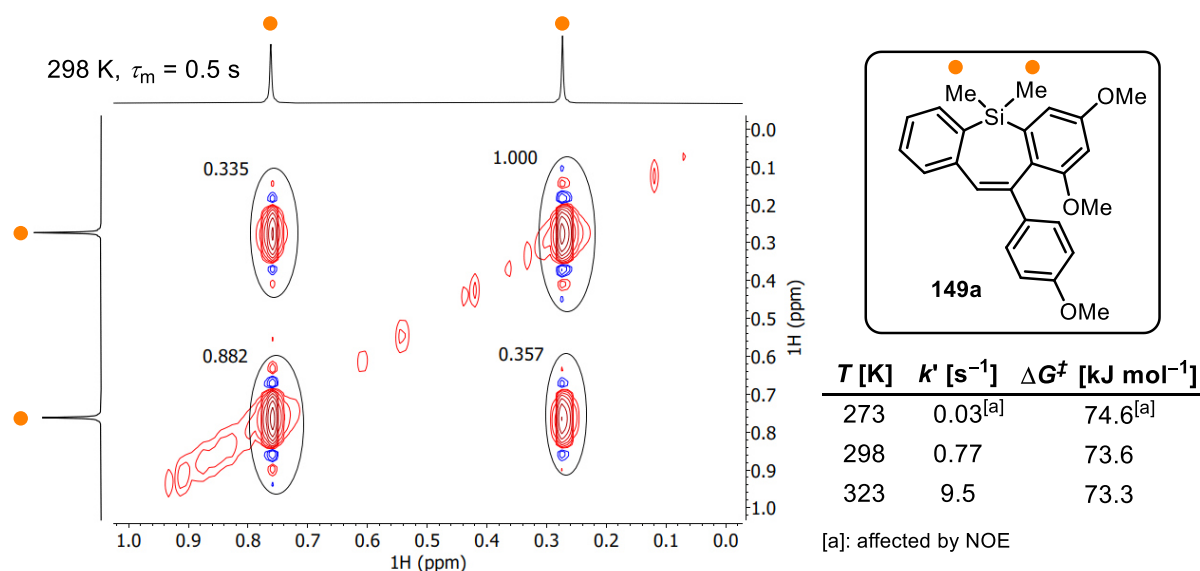


**Figure 32:** Detail view of the 2D-EXSY spectrum of silepine **149a** at 298 K showing the exchanging methyl groups (marked with orange dots), the calculated rate constants  $k$  and the corresponding Gibbs free energies  $\Delta G^\ddagger$ .

At a temperature of  $-25\text{ }^{\circ}\text{C}$ , no exchange between the methyl groups was observed and the predominating nuclear Overhauser effect (NOE) could be assumed to  $0.014\text{ s}^{-1}$ . At  $0\text{ }^{\circ}\text{C}$ , the corresponding EXSY spectrum results in a rate constant of  $0.016\text{ s}^{-1}$ , but the interfering NOE is probably in the same order of magnitude (negative) as the desired exchange effect (positive). Thus, if the previously estimated value for the NOE is considered, the "correct value" for the rate constant is more likely in the range of  $0.03\text{ s}^{-1}$  or even higher, since the NOE effect is also temperature dependent. Nevertheless, a value of  $0.03\text{ s}^{-1}$  is approximated for the rate constant at  $0\text{ }^{\circ}\text{C}$  and used for the further calculations.

With the obtained rate constants, the Gibbs free energy  $\Delta G^\ddagger$  could be calculated. It can be seen that the Gibbs free energy at  $0\text{ }^{\circ}\text{C}$  shows a larger deviation than the other two values among themselves, which is due to the assumptions made earlier to estimate the rate constant at this temperature. In summary, a value of  $73.6\text{ kJ mol}^{-1}$  for the Gibbs free activation energy at 298 K corresponds to a half-life of 890 s, indicating that separation of the enantiomers is pointless. Moreover, to determine the other activation parameters for the

### 3. Results and discussion

interconversion of **149a**, an Eyring plot was created and a linear regression was performed, which provided a very good fit to the data (**Figure 33**).

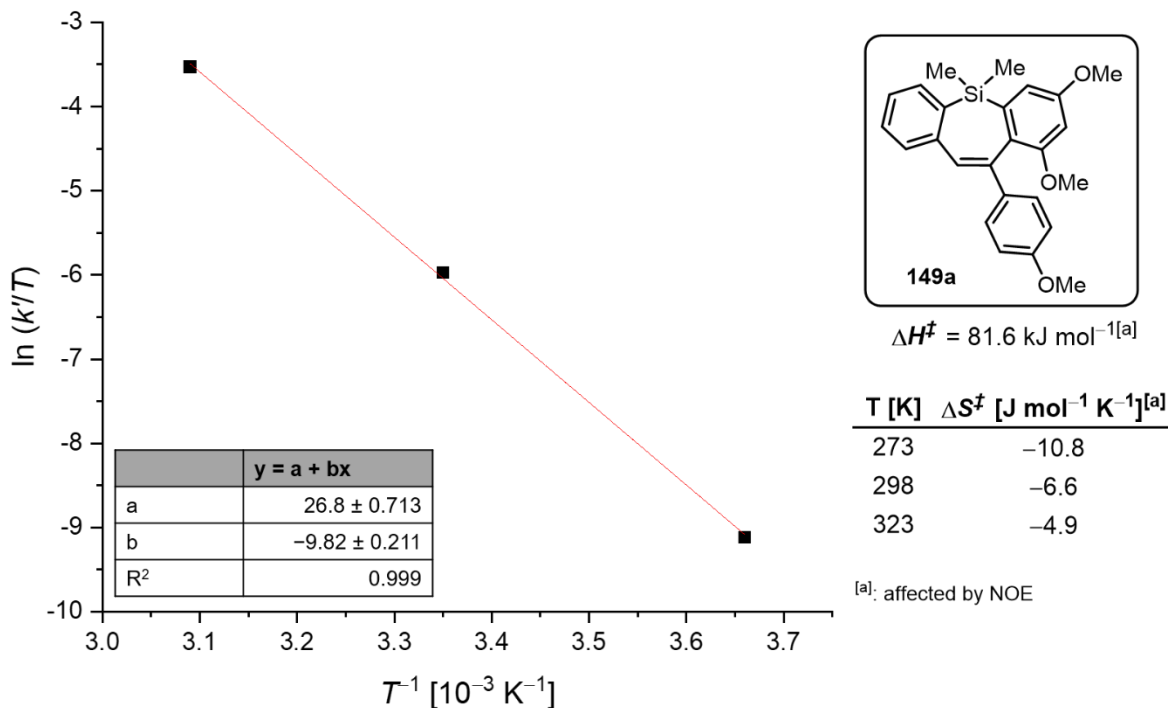


**Figure 33:** Eyring plot of silepine **149a** and the calculated activation enthalpy  $\Delta H^\ddagger$  and entropy  $\Delta S^\ddagger$ .

Although  $k'$  was approximated for 25 °C, it is consistent with the data obtained from the other measurements and shows no deviations from the linear fit. The activation enthalpy  $\Delta H^\ddagger$  could be obtained from the slope of the linear regression curve, and the activation entropy  $\Delta S^\ddagger$  could be obtained as a function of temperature.

In contrast to **149a**, where the exchange of the methyl groups on the NMR time scale could already be observed at 0 °C, it seems to be slower for **149e**. At temperatures of 25 °C and 50 °C, exchange signals for the isopropyl groups could be observed (see **Figure 34**), but the interfering NOE distorts the determination of the correct intensities of the peaks.

### 3.3 Exploration of configurational stability of seven-membered ring systems

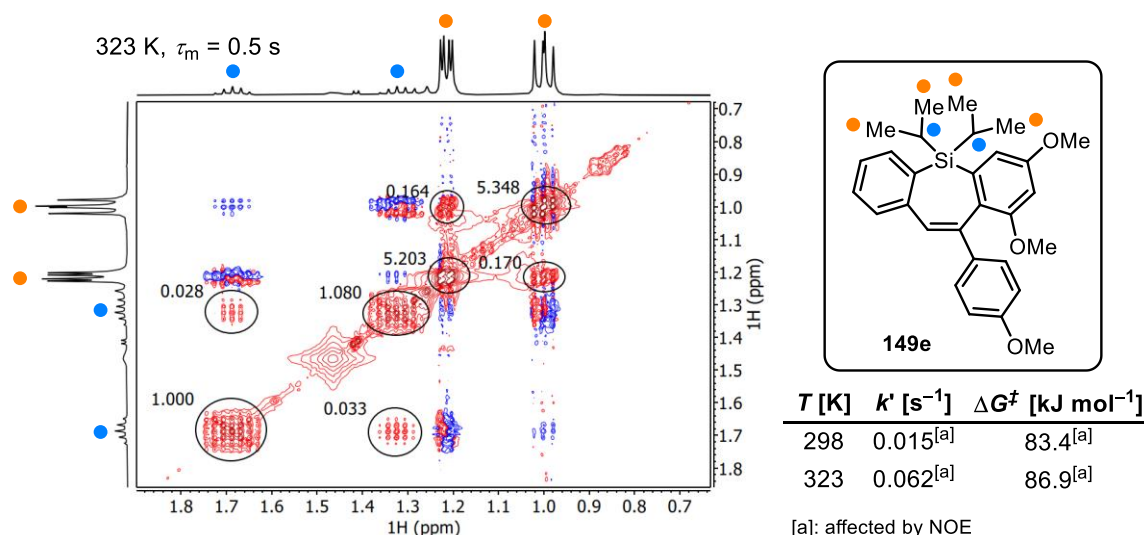


**Figure 34:** Detail view of the 2D-EXSY spectrum of silepine **149e** at 323 K showing the exchanging methyl groups (marked with orange dots) and the protons on the tertiary carbon atom of the isopropyl substituent (marked with blue dots), the calculated rate constants  $k'$  and the corresponding Gibbs free energies  $\Delta G^\ddagger$ .

Therefore, it can be assumed that the "correct values" of the rate constants are higher than the determined ones. Consequently, the estimation of the Gibbs free energy is also subject to errors explaining the different values obtained for 25 °C and 50 °C (**Figure 34**). The same rate constants were obtained regardless of whether the intensities of the cross and diagonal peaks of the methyl groups or the protons at the tertiary carbon atom of the isopropyl substituents were considered. Nevertheless, the tendency of increasing the interconversion barrier due to the higher steric demand of the isopropyl substituents on the silicon compared to **149a** can be observed. Although the determined barrier with 83.4  $kJ\ mol^{-1}$  for the Gibbs free energy of **149e** is significantly higher, the corresponding half-life with 46 s at 298 K is not sufficient enough to allow a separation of the enantiomers.

Within this chapter the applicability of dynamic NMR spectroscopy, namely 2D-EXSY, for the determination of the interconversion barriers of seven-membered ring systems was investigated. The method has been proven to be successful for silepines **149a** and **149e**, since the groups exchanging upon interconversion show clearly separated signals at 298 K. The obtained Gibbs free energies are summarized in **Table 8**. Despite the interfering NOE, comparison of the two experimental techniques shows for compound **149e** a rather good agreement.

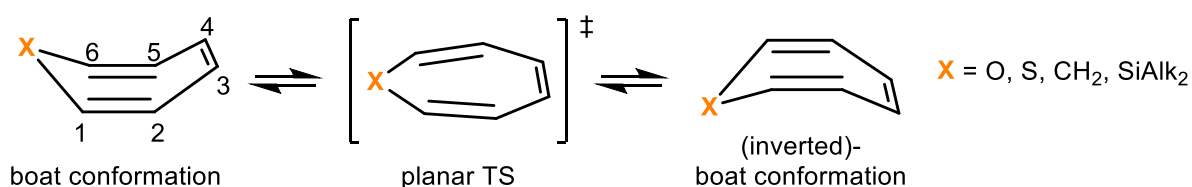
**Table 8:** Comparison of the Gibbs free energies for the enantiomerization of compounds **149a** and **149e** determined by DNMR and DHPLC at 298 K.

Compd.	$\Delta G^\ddagger_{298\ K}$ [ $kJ\ mol^{-1}$ ] (NMR)	$\Delta G^\ddagger_{298\ K}$ [ $kJ\ mol^{-1}$ ] (HPLC)
<b>149a</b>	73.6	-
<b>149e</b>	83.4	84.9

### 3.3.3 Density-functional theory (DFT) methods

This chapter deals with the estimation of interconversion barriers for seven-membered ring systems using DFT methods. First, a suitable model is developed to describe the chemical process underlying this transformation, using an appropriate level of theory. Subsequently, this model is applied to determine the barriers of selected molecules and to investigate which factors have a direct influence.

Based on structural analyses in the past and also in the context of this work (see section 3.2), it is known that seven-membered cyclic molecules adopt a non-planar, boat-shaped conformation independently of X and as mentioned before, the possible boat conformations are enantiomerically related. The interconversion to the other enantiomer is assumed to proceed *via* a planar transition state (TS) (**Scheme 53**).



**Scheme 53:** Model for the interconversion of the boat-like seven-membered ring *via* a planar TS.

The energy difference between the boat conformation and the planar TS corresponds to the barrier to be determined. The barrier is obviously dependent on the stability of the respective structures. The more stable the boat conformation and the less stable the TS, the larger the energy difference. Steric/geometric factors are one type of influence on these stabilities, e.g., by introducing sterically demanding substituents that induce destabilizing interactions in the planar transition state and thereby increase its energy. In addition, electronic effects influencing the energy barriers should also be included, especially in the context of the TS aromaticity since it can be considered to fulfill Hückel's rule.

To gain a deeper insight into the stabilization of the planar and boat conformations, the nucleus-independent chemical shift (NICS), based on magnetic shielding of a ghost atom at the ring centers, was used in the past to estimate the stability of the respective conformations for X = CH<sub>2</sub> and X = SiMe<sub>2</sub>.<sup>[144]</sup> The values obtained allow conclusions to be drawn about the extent of conjugative stabilization. Positive NICS values (3.1 for silepine and 8.2 for cycloheptatriene), denote antiaromaticity for the planar form according to the definition of Schleyer.<sup>[145]</sup> Whereas the boat form of cycloheptatriene with a NICS value of -4.2 was considered as weakly aromatic and the one of silepine with -0.5 as almost non-aromatic. The weak aromaticity of the boat form for cycloheptatrienes was reasoned by the assumption of homoconjugative interactions between the p-orbitals of C-1 and C-6, which result in stabilization of the boat form. In contrast, in the silepine the distance between C-1

### 3.3 Exploration of configurational stability of seven-membered ring systems

and C-6 is longer, and therefore homoconjugative stabilization is nearly absent. In conclusion, based on the NICS, it was assumed that in the silepine there is no stabilization of the boat form and a relative destabilization of the planar form compared to the boat form. In the cycloheptatriene, the boat form is stabilized by homoconjugation and there is destabilization of the planar form, which in total results in a larger barrier compared to the silepine.<sup>[144]</sup>

In order to validate the described model for determining the interconversion barriers, the structures of the boat conformations of compounds **146h** and **146k** were first optimized using the functional B3LYP in combination with two different basis sets (6-31+g(d) and def2-TZVP). By comparing the bond lengths and angles in the central seven-membered ring of the obtained optimized geometries with the solid state structures, a verification could be made whether the chosen theory level provides a good adaptation (**Table 9**).

**Table 9:** Comparison of the bond lengths and angles in the central seven-membered ring obtained from the solid state structures to the values computed at the B3LYP/6-31+g(d) and B3LYP/def2-TZVP level of theory including the D3 version of Grimme's dispersion with Becke-Johnson damping (GD3BJ).



Bond lengths [Å]	146h					146k				
	X-ray	6-31+g(d)	$\Delta$	def2-TZVP	$\Delta$	X-ray	6-31+g(d)	$\Delta$	def2-TZVP	$\Delta$
C7-C1	1.503(2)	1.510	0.007	1.505	0.002	1.514(1)	1.513	0.001	1.508	0.005
C1-C2	1.394(2)	1.394	0	1.387	0.007	1.412(1)	1.417	0.005	1.411	0.001
C2-C3	1.488(2)	1.488	0	1.484	0.004	1.496(1)	1.495	0.001	1.491	0.005
C3-C4	1.359(2)	1.360	0.001	1.351	0.008	1.349(1)	1.355	0.006	1.346	0.003
C4-C5	1.466(2)	1.464	0.002	1.459	0.007	1.470(1)	1.467	0.003	1.462	0.008
C5-C6	1.407(2)	1.413	0.006	1.406	0.001	1.409(1)	1.413	0.004	1.406	0.003
C6-C7	1.506(2)	1.511	0.005	1.506	0	1.513(1)	1.513	0	1.508	0.005
Bond angles [°]	146h					146k				
C6-C7-C1	110.5(1)	109.6	0.9	109.5	1.0	109.9(6)	110.0	0.1	109.9	0
C7-C1-C2	120.8(1)	120.1	0.7	120.1	0.7	120.2(7)	119.6	0.6	119.5	0.7
C1-C2-C3	120.3(1)	120.3	0	120.4	0.1	117.0(6)	117.2	0.2	117.3	0.3
C2-C3-C4	124.0(1)	122.8	1.2	122.7	1.3	122.4(7)	123.2	0.8	123.2	0.8
C3-C4-C5	128.4(1)	127.6	0.8	127.7	0.7	124.9(7)	125.9	1.0	126.0	1.1
C4-C5-C6	121.3(1)	120.9	0.4	120.9	0.4	119.1(7)	119.4	0.3	119.5	0.1
C5-C6-C7	118.1(1)	118.5	0.4	118.6	0.5	118.7(7)	118.7	0	118.7	0

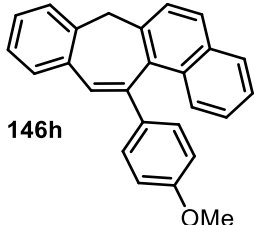
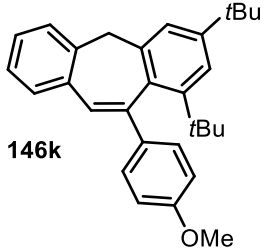
The comparison of the basis sets 6-31+g(d) and def2-TZVP shows that there are only minor differences between the two methods. Bond lengths are very well represented in the optimized geometries for compound **146h** and are in the range of three sigma with two exceptions. For compound **146k**, the standard deviations sigma of the bond lengths

### 3. Results and discussion

obtained from the solid state structures are smaller, so only a few of the calculated bond lengths are found in the range of three sigma. However, the deviations are still to be considered small. The bond angles show deviations smaller than 1 ° in most cases, but only in a few cases in the 3σ range. How well the individual angles are approximated also seems to depend on the particular substituents. For **146h**, the C1-C2-C3 angle in the solid structure shows perfect agreement with the model, whereas the C2-C3-C4 and C6-C7-C1 angle exhibits the largest variation. In contrast, for compound **146k**, the C6-C7-C1 angle is perfectly approximated and C3-C4-C5 angle deviates the farthest, which might be a consequence of a deformation resulting from the direct vicinity of the *tert*-butyl and the *para*-anisyl substituent on the seven-membered ring.

In order to finalize the selection of a suitable basis set and to further validate the model shown in **Scheme 53**, a comparison of the interconversion barriers of the compounds **146h** and **146k** was also performed. From this comparison with the experimentally determined barrier for **146h**, it can be concluded whether the structure of the planar transition state was also sufficiently depicted by the respective method. Furthermore, additional corrections were applied in order to achieve a better adaptation. The calculated interconversion barriers are summarized in **Table 10**.

**Table 10:** Overview of the computed interconversion barriers for **146h** and **146k** depending on different basis sets and corrections. The “tight” option involves the use of the superfine grid, GD3BJ denotes the empirical dispersion correction as the D3 version of Grimme’s dispersion with Becke-Johnson damping, and the solvent correction SCRF was performed using the conductor-like polarizable continuum model (CPCM) for chloroform.

	functional/ basis set	$\Delta G^\ddagger$ [kJ mol <sup>-1</sup> ]				Exp.	
		Tight	GD3BJ	SCRF	GD3, SCRF		
 <b>146h</b>	B3LYP/6-31+g(d)	84.4	84.3	86.2	84.9	86.8	82.8
	B3LYP/def2-TZVP	83.5	83.4	85.3	83.8	85.7	
 <b>146k</b>	B3LYP/6-31+g(d)	93.0	93.0	95.0	93.1	94.7	
	B3LYP/def2-TZVP	92.8	92.5	94.6	93.1	94.3	

The tightening of the cutoffs on forces and step size has no influence on the determined barrier and did not lead to a different transition state. In general, it can be observed that the difference between the two basis sets used is small and is at most 1 kJ mol<sup>-1</sup> for all the options chosen. Adding a dispersion correction increases the obtained barrier by almost 2 kJ mol<sup>-1</sup>, whereas a solvent correction with chloroform only accounts for about 0.5 kJ mol<sup>-1</sup> for **146h** or even less for **146k**. These small deviations are all within the



### 3.3 Exploration of configurational stability of seven-membered ring systems

chemical accuracy. All in all, the calculated barrier for **146h** is in the same range as the experimentally determined one and thus validates this model as a suitable method for estimating the interconversion barriers of seven-membered ring systems. In addition, the basis set 6-31+g(d) is, considering the significantly shorter calculation time, quite sufficient to predict trends for the interconversion barriers and to estimate to what extent they are high enough to allow resolution of the enantiomers at room temperature.

To verify that the transition states correspond to saddle points, intrinsic reaction coordinate (IRC) scans were performed. This approach is effective when transitions between conformational isomers are considered and only one reaction coordinate may exist. The IRC calculation starts with the transition state, will step forward to the reactants, and then backwards to the product. It is useful to demonstrate that the transition state found is undoubtedly connected to both reactant and product. These IRC scans have proven to be suitable in regions where the potential energy surface is not too flat. In very flat regions, IRC scans sometimes terminated prematurely because the change in energy per step was too small. This phenomenon occurred for compounds **146h** and **146k** and only incomplete IRC profiles were obtained (**Figure 35**).

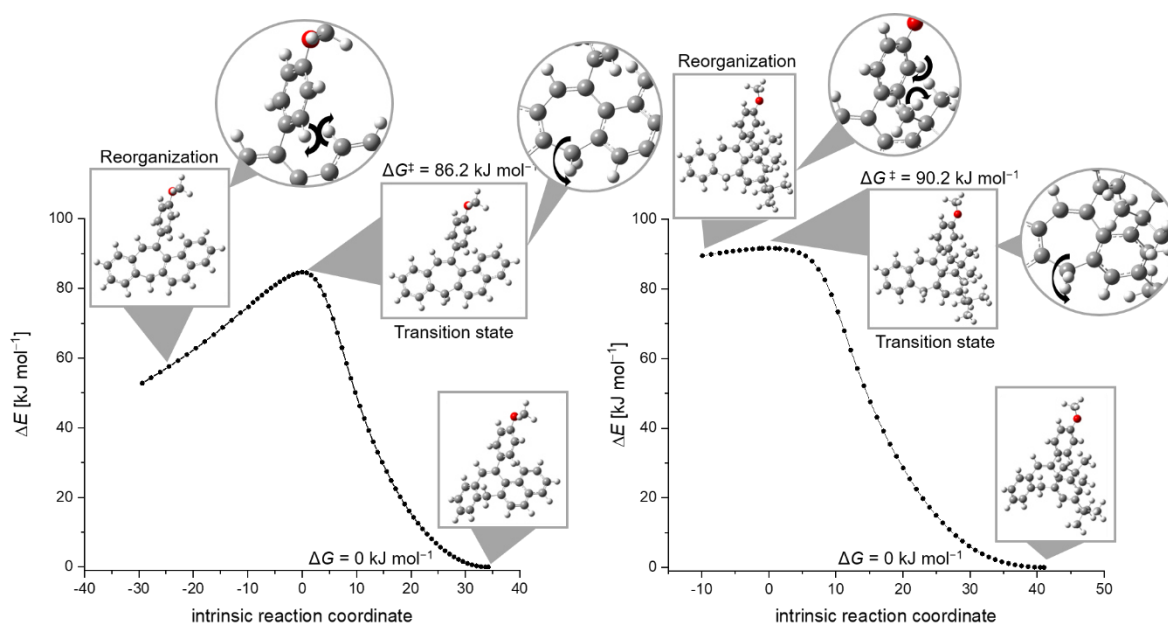


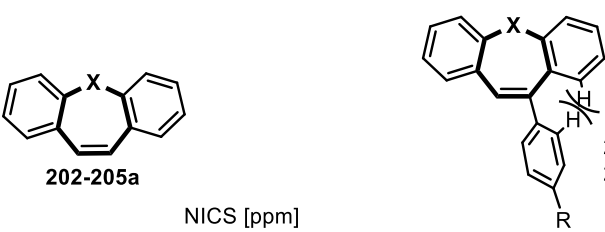
**Figure 35:** Incomplete IRC profiles for the inversion of **146h** (left) and **146k** (right) under the local quadratic approximation calculated with B3LYP-D3/6-31+g(d).

Due to low gradients the scans stop too early, but nonetheless describe the reaction path and thus validate the transition states. In addition, the last point on the IRC scans was taken and a geometry optimization was conducted to check the optimized geometry for consistency with the expected minimum. Although the IRCs profiles are incomplete, it can be assumed that the reaction paths consist of two rather independent movements along the interconversion of the enantiomers. One movement is the flipping of the tether into or

### 3. Results and discussion

through the seven-membered ring and the second is the reorganization of the substituent at C3 position. The overlap of these two movements along the intrinsic reaction coordinate lead to a flat gradient and a broad IRC profile. In both cases, the flipping of the -CH<sub>2</sub>- tether corresponds to the point with the highest energy and thus denotes the rate-determining step. On the left flank the *para*-anisyl substituent on the seven-membered ring rotates past the adjacent substituents while simultaneously flipping the -CH<sub>2</sub>- group in the cycloheptatriene ring. Once the transition state (maximum of the curve) is reached, the *para*-anisyl substituent nearly retains its position and the aromatic backbone bends while the tether oscillates to the other side of the seven-membered ring to give the opposite enantiomer. In addition, the shape of the IRC profile appears to depend on the nature of the substituents in close proximity to the seven-membered ring. For **146h**, bearing sterically demanding *tert*-butyl groups, the potential energy surface around the transition state is significantly flatter than for **146k** and seems to exhibit a plateau.

With the validated model for the description of the interconversion barriers of seven-membered ring systems in hand, simple molecules were selected to start the investigations on the influence of the tether and to evaluate how different substitution patterns affect the barrier. The interconversion barrier  $\Delta G^\ddagger$  of simple dibenzo compounds **202-205** were calculated at the B3LYP-D3/6-31+g(d) level (with Becke–Johnson damping) and are shown in **Figure 36**.



X	$\Delta G^\ddagger$ [kJ mol <sup>-1</sup> ]	NICS [ppm]		
		Boat	Planar	
<b>202a</b>	O	20.5	4.4	13.6
<b>203a</b>	S	40.2	1.2	11.1
<b>204a</b>	CH <sub>2</sub>	44.4	0.8	7.2
<b>205a</b>	SiMe <sub>2</sub>	22.5	1.6	3.9

X	R	$\Delta G^\ddagger$ [kJ mol <sup>-1</sup> ]	NICS [ppm]		
			Boat	Planar	
<b>202b</b>	O	H	32.2	3.7	13.4
<b>202c</b>	O	OMe	33.0	3.1	13.4
<b>203b</b>	S	H	57.8	0.9	11.2
<b>203c</b>	S	OMe	59.9	0.8	11.1
<b>204b</b>	CH <sub>2</sub>	H	59.0	0.7	7.3
<b>204c</b>	CH <sub>2</sub>	OMe	59.6	0.7	7.3
<b>205b</b>	SiMe <sub>2</sub>	H	43.1	1.8	4.3
<b>205c</b>	SiMe <sub>2</sub>	OMe	44.3	1.7	4.3

**Figure 36:** Comparison of calculated interconversion barriers and NICS values for simple molecules with and without substituents at the seven-membered ring. All Gibbs free activation energies were computed at the B3LYP-D3/6-31+g(d) level. The NICS values were calculated at the B3LYP/6-31+g\* level and the ghost atom was placed at the center of the seven-membered ring.

The lowest Gibbs free activation energy was computed for the dibenzoxepine compound **202a** bearing with oxygen the smallest tether. Furthermore, a remarkable difference can be noted between oxepine **202a** and thiepine **203a**, with only small difference to the all-carbon analogue **204a**. The calculated trends are consistent with the literature.<sup>[107]</sup> Despite the

### 3.3 Exploration of configurational stability of seven-membered ring systems

difference in tether size, the barrier for the silicon derivative **205a** is within the range of the dibenzoxepine compound **202a**. By introducing a phenyl substituent in the lower region of the seven-membered ring, the steric hindrance and thus the barriers can be increased by  $\sim 10 \text{ kJ mol}^{-1}$ . A small change in the nature of the substituent also appears to have an effect. When the phenyl is replaced by an electron donating *para*-anisyl residue, the barrier increases further, albeit comparatively less ( $\sim 5 \text{ kJ mol}^{-1}$ ). Furthermore, the barriers of the oxepine and silepine derivatives show a larger difference after a substituent was implemented. This electron donating substituent shows that the electronic properties have also an impact on the barrier by affecting the stability of the boat or the planar structure of the seven-membered ring. It can be assumed that the increased electron density either stabilizes the boat shape, destabilizes the planar shape, or both simultaneously, resulting in a larger energy difference as well as interconversion barrier, respectively. To range the effect of the substituents on the stabilities the NICS of a ghost atom placed at the ring center of the seven-membered ring was calculated. All values obtained were positive denoting antiaromaticity for the boat as well as the planar forms. As expected the planar forms show higher antiaromaticity compared to the boat forms. In general, it can be seen that the nature of the substituent hardly influences the destabilization of the transition state. In contrast, the NICS of the boat form slightly decreases for a *para*-anisyl instead of a phenyl substituent indicating that an electron donating group destabilizes the boat form less. Thus, a slightly higher barrier is obtained when an additional methoxy group was introduced although the steric effect stays the same. To draw further conclusions and show that the position of the probe used is suitable, further calculations would be necessary.

In addition to the calculated barriers and the NICS values, the IRC scans of compounds **204a** and **204b** were studied (**Figure 37**). After the developed model for the determination of interconversion barriers in seven-membered ring systems could be successfully validated and applied to simple molecules, compounds synthesized within this thesis were subsequently investigated. In addition to the interconversion barriers for dibenzo[*a,e*]cycloheptatrienes **146h** and **146k** (**Table 10**), the barriers for **146i**, **146j** and **146e** could be calculated (**Figure 38**). The Gibbs free activation energy was also used to estimate half-lives at 25 °C.

### 3. Results and discussion

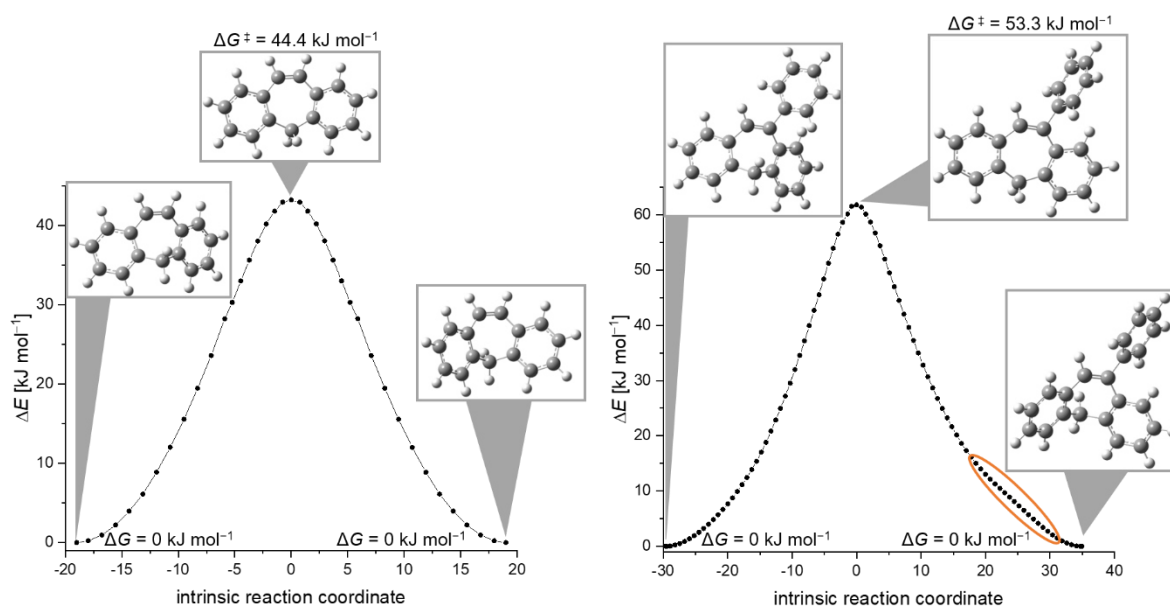


**Figure 37:** IRC profiles for the inversion of **204a** (left) and **204b** (right) under the local quadratic approximation calculated with B3LYP-D3/6-31+g(d).

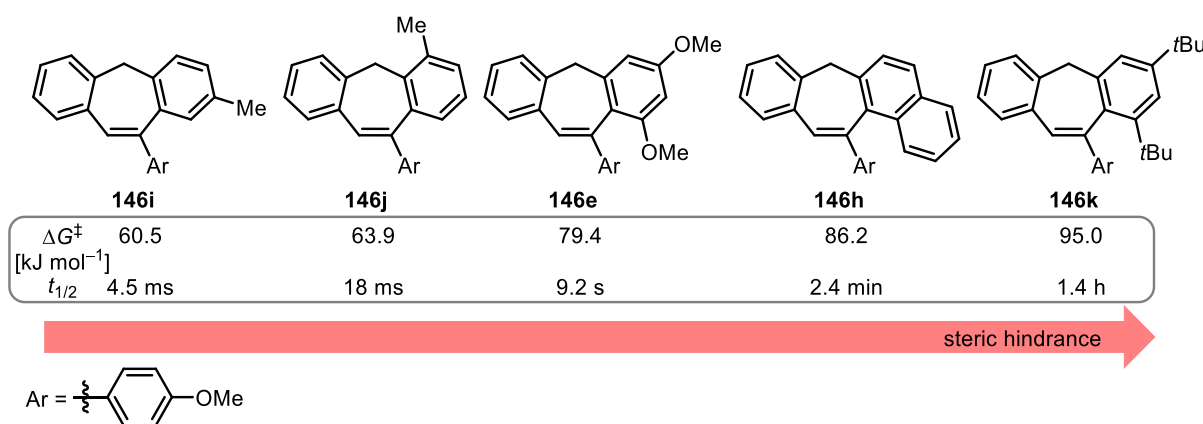


**Figure 38:** Overview of the barriers obtained for dibenzo[*a,e*]cycloheptatrienes **146** and the corresponding half-lives at 25 °C depending on the steric demand of the substituents. All Gibbs free activation energies were computed at the B3LYP-D3/6-31+g(d) level.

As expected the interconversion barriers for dibenzo[*a,e*]cycloheptatrienes **146** increase with the steric demand of the substituents. In **146i**, the methyl substituent is relatively far from the seven-membered ring and hardly affects the inversion at all, resulting in a similar value as for the unsubstituted dibenzo compound **204c**. The barrier is slightly higher for **146j**, since the methyl group is in close proximity to the tether. However, the substituents in direct vicinity of the *para*-anisyl moiety at the bottom of the seven-membered ring have the greatest influence on the interconversion barrier leading to an increase of around 15 kJ mol<sup>-1</sup> between **146j** and **146e**. From the methoxy to the naphthyl to the *tert*-butyl group, the steric demand increases further and so does the barrier. Thus, the barrier with the *tert*-butyl substituents is significantly higher than with the more electron-donating methoxy groups. To draw further conclusions how the steric and electronic properties of the

### 3.3 Exploration of configurational stability of seven-membered ring systems

substituents on the backbone influence the barrier in detail calculations of more substitution pattern are necessary.

In addition, to the determined barriers the IRC scan for compound **146e** (**Figure 39**) was analyzed and compared to the incomplete profiles of **146h** and **146k**.

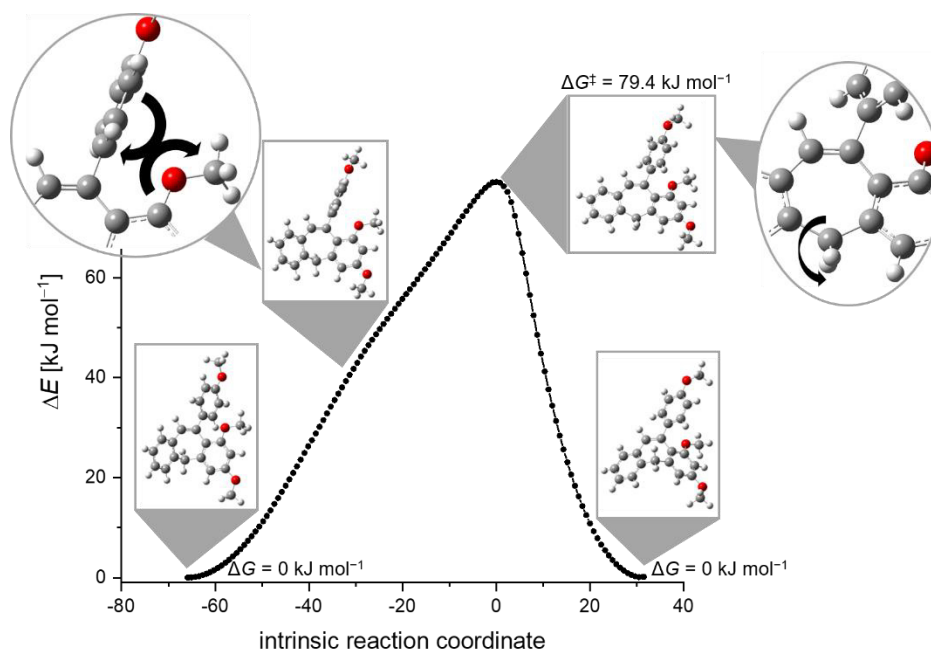


**Figure 39:** IRC profile for the inversion of **146e** under the local quadratic approximation calculated with B3LYP-D3/6-31+g(d).

As mentioned earlier, the methoxy groups are less sterically demanding, which also influences the shape of the IRC profile. In comparison to **146h** and **146k**, it appears less flat in the region of the transition state. Additionally, a distinct shoulder is visible approximately halfway between the minimum and the transition state, which further illustrates the occurrence of two movements along the reaction path of interconversion.

In addition, the interconversion barriers of selected dibenzo[*b,f*]oxepines **147c** and **147i** and dibenzo[*b,f*]thiepine **148a** could be calculated successfully using the developed method (**Figure 40**). Based on the computed Gibbs free activation energies, the respective half-lives were determined at 25 °C. The example of dibenzo[*b,f*]oxepines shows once again how crucial the influence of sterically demanding substituents in the direct vicinity of the seven-membered ring can be. The replacement of the methoxy groups by bulky *tert*-butyl groups significantly increases the barrier by 35 kJ mol<sup>-1</sup>. This exchange of substituents is also directly reflected in the half-life: instead of 227 μs for **147c**, it is already 4.9 min for **147i**.

### 3. Results and discussion

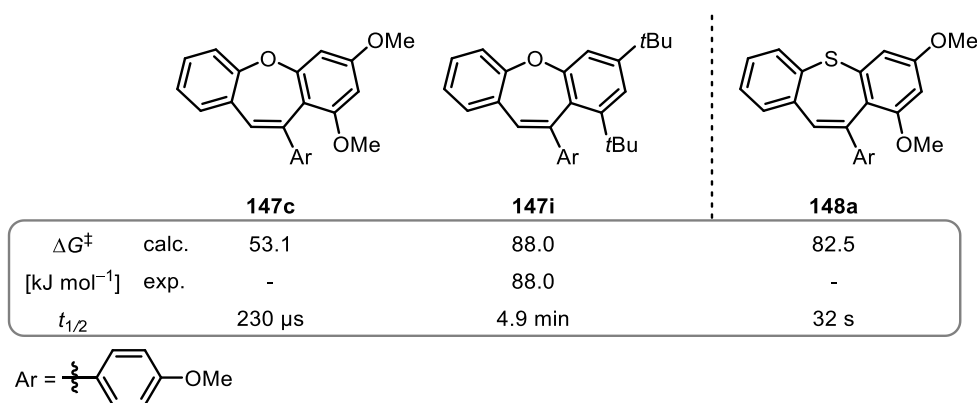


**Figure 40:** Overview of the barriers obtained for dibenzo[*b,f*]oxepines **147c** and **147i** and dibenzo[*b,f*]thiepine **148a**. All Gibbs free activation energies were computed at the B3LYP-D3/6-31+g(d) level. The corresponding half-lives were calculated based on the theoretical barriers at 25 °C.

Nevertheless, it is still insufficient to allow isolation of the enantiomers. However, comparing the calculated value for the Gibbs free energy of **147i** with the value obtained from dynamic HPLC, a perfect agreement between theory and experiment is found. In case the heteroatom in the seven-membered ring is a sulfur atom, as in **148a**, the barrier increases by 30 kJ mol<sup>-1</sup> in comparison the oxygen analogue **147c**, which is consistent with the trends observed for unsubstituted dibenzo compounds (see **Figure 36**).

For compounds **147c** and **148a**, additional IRC scans (see **Figure 41**) were performed both to confirm the transition states found and to allow comparison of the IRC profiles with the carbon analogue **146e**.

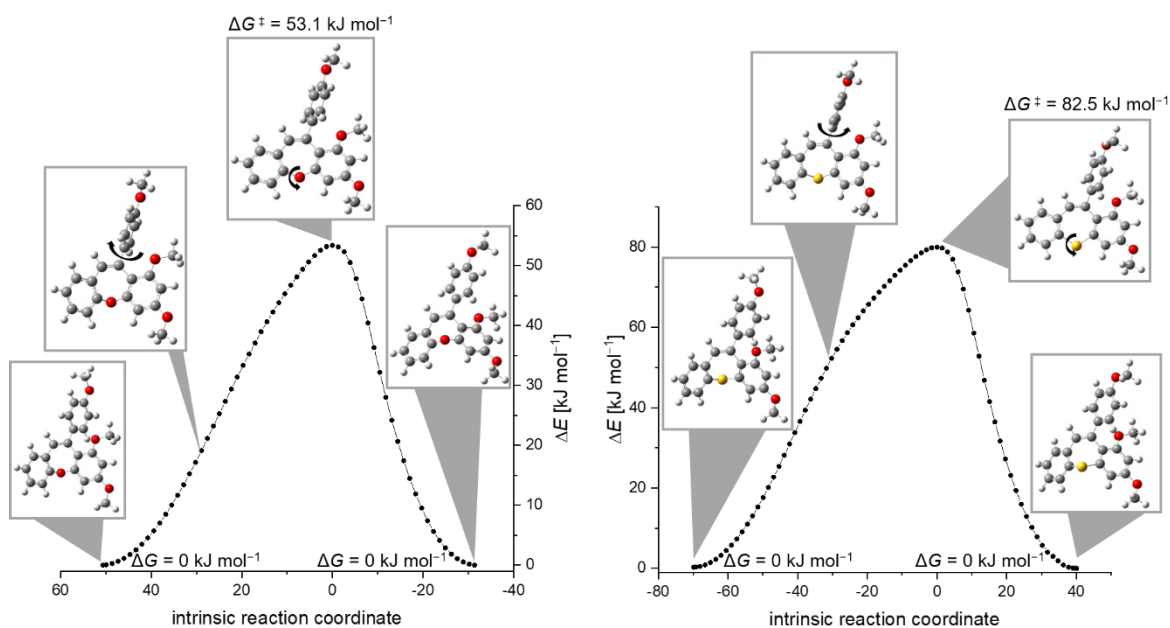


**Figure 41:** IRC profile for the inversion of **147c** (left) and **148a** (right) under the local quadratic approximation calculated with B3LYP-D3/6-31+g(d). The x-axis in the IRC profile of **147c** is shown inverted for better comparison.

### 3.3 Exploration of configurational stability of seven-membered ring systems

For dibenzo[*b,f*]oxepine **147c** (**Figure 41**, left), a shoulder is barely discernible on the left flank. In addition, the overall IRC profile appears narrower and more even on both sides of the transition state compared to **146e**. In case of dibenzo[*b,f*]thiepine **148a** (**Figure 41**, right), the shoulder underlining that the reorganization of the substituents on the seven-membered ring and the flip of the tether are different in energy, is clearly visible. Nevertheless, the flip is in both cases the rate-determining step. In comparison to **146e**, the IRC profile is significantly broader. Therefore, it can be stated that not only the substituents have an influence on the pathway along the intrinsic reaction coordinate, but also the tether. From -O- via -CH<sub>2</sub>- to -S- the interconversion barrier increases and the IRC profile becomes continuously broader. In contrast to the compounds considered previously, the rate-determining step in the interconversion of **147i** appears to be the reorganization of the substituents rather than flipping of the tether, which is indicated by the obtained transition state (**Figure 42**, right). The transition state of **147i** was compared to the transition state of an analogous structure containing a methyl instead of a *tert*-butyl group (**Figure 42**, left) to illustrate the differences when the steric hindrance of the substituents changes.

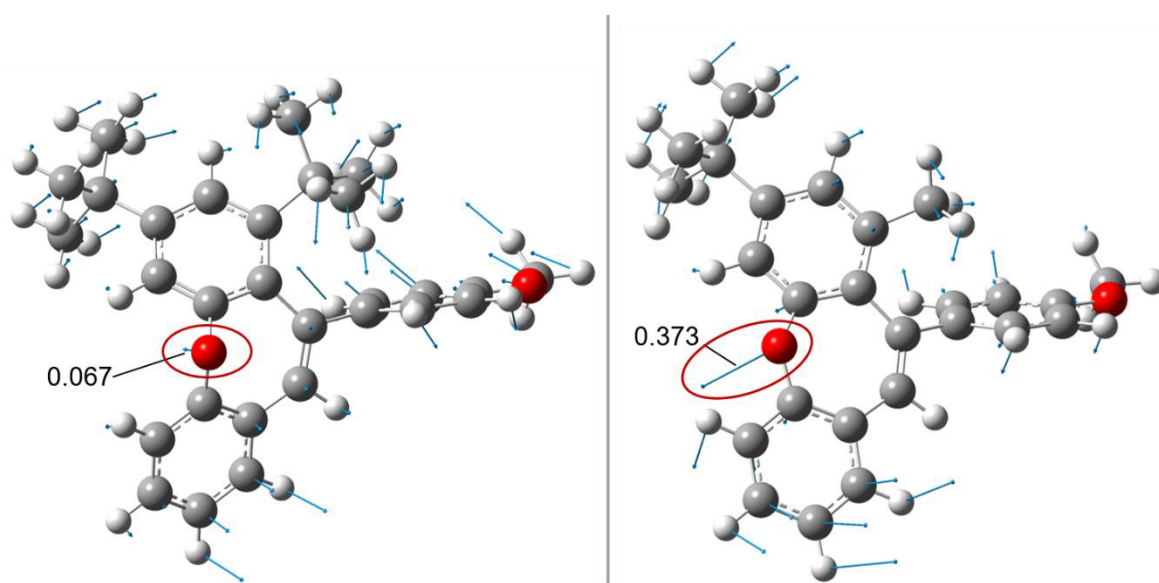


**Figure 42:** Transition state of **147i** with displacement vectors (right) and transition state of an analogous structure in which one *tert*-butyl is replaced by a methyl group (right) calculated with B3LYP-D3/6-31+g(d). Crucial displacement vectors are highlighted with red circles.

Based on the displacement vectors, it can be seen that with increasing steric demand, the vectors describing the reorganization of the *para*-anisyl and the neighboring *tert*-butyl substituent are comparatively longer than the vector representing the flipping of the tether. This indicates that the transition state is mostly defined by the reorganization of the substituents rather than by flipping of the tether. In contrast, for sterically less demanding substituents, a significantly larger displacement of the tether is observed (0.373 vs. 0.067), suggesting that the flipping of the tether affects the rate-determining step to a larger extent. Furthermore, the seven-membered ring is more planar when only one *tert*-butyl group is

### 3. Results and discussion

attached to the molecule. Since the barrier for the reorganization and the flip of the tether in **147i** is assumed to be equally high, a broad plateau in the energy profile is expected making the IRC scan particularly troublesome.

To complete the study of the interconversion barriers for the synthesized seven-membered ring systems, dibenzo[*b,f*]silepines **149a** and **149e** were investigated. These two examples will be used specifically to evaluate the steric effect in the tether region more closely. The interconversion barriers for **149a** and **149e** are depicted in **Figure 43** and the corresponding half-lives at 25 °C were calculated based on the experimental values.

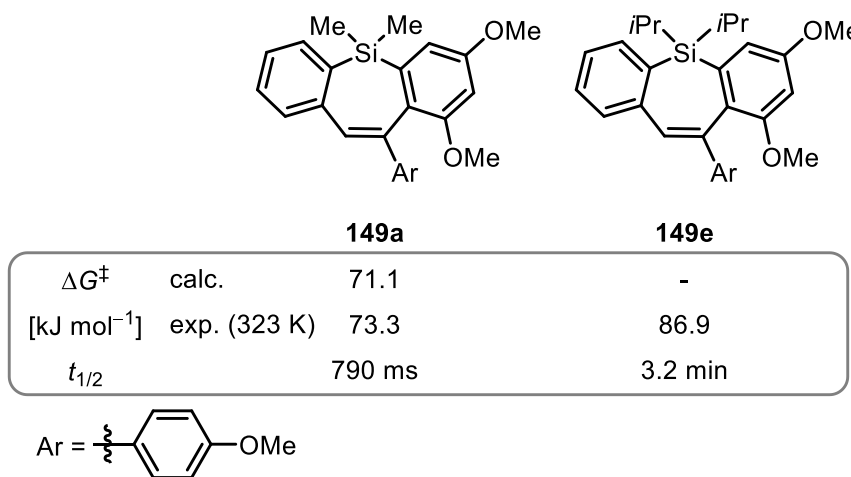


**Figure 43:** Comparison of experimentally determined barriers with calculated barriers for dibenzo[*b,f*]silepines **149a** and **149e**. The Gibbs free activation energy for **149a** was computed at the B3LYP-D3/6-31+g(d) level and an additional solvent correction for chloroform was applied. The corresponding half-lives were calculated based on the experimental barriers at 25 °C.

For **149a** a barrier could be computed, which gives a good agreement with the experimental value and shows only a difference of  $\sim 2$  kJ mol<sup>-1</sup>. Unfortunately, for compound **149e**, difficulties were encountered in finding the transition state. On the one hand, more rotations are possible due to the isopropyl groups on the silicon and on the other hand, the potential seems to be extremely flat. Therefore, several states with similar energy were present and finding the saddle point was unsuccessful with the methods used. However, based on the experimentally determined conversion barriers, it is clear that an increased steric demand of the alkyl substituents on the silicon tether also leads to a significant increase of the barrier by almost 15 kJ mol<sup>-1</sup>. Although the interconversion of the enantiomers is hindered by the isopropyl groups, the determined barrier of 86.9 kJ mol<sup>-1</sup> is still far too low to allow separation of the enantiomers.

The IRC profile for the interconversion of **149a** (**Figure 44**) shows a more broad shape as observed for dibenzo[*a,e*]cycloheptatrienes **146**, dibenzo[*b,f*]oxepines **147** and dibenzo[*b,f*]thiepine **148a**.



### 3.3 Exploration of configurational stability of seven-membered ring systems

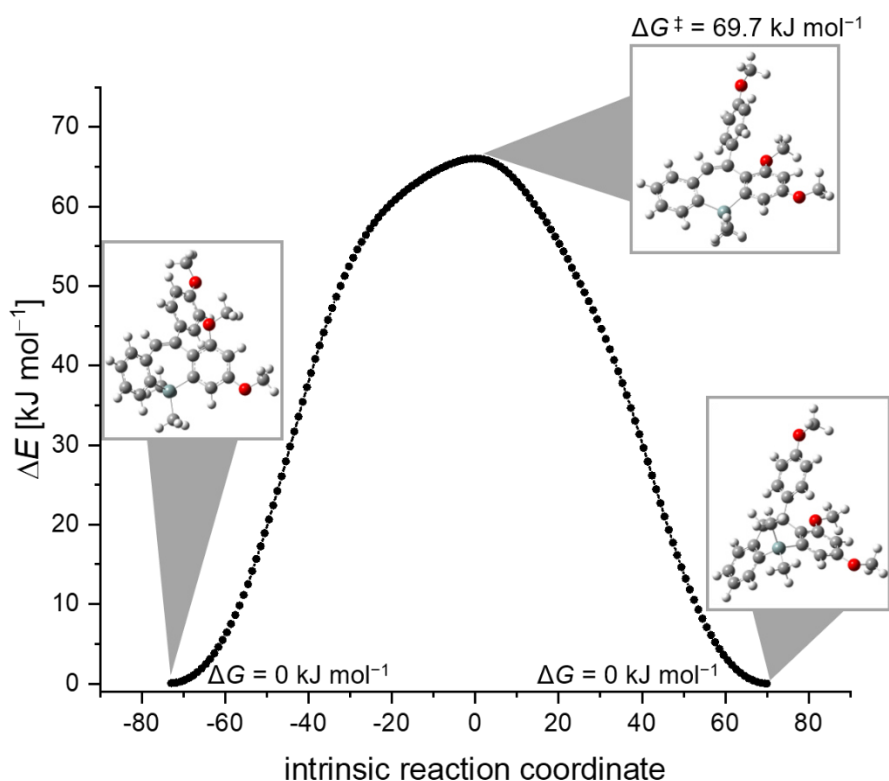


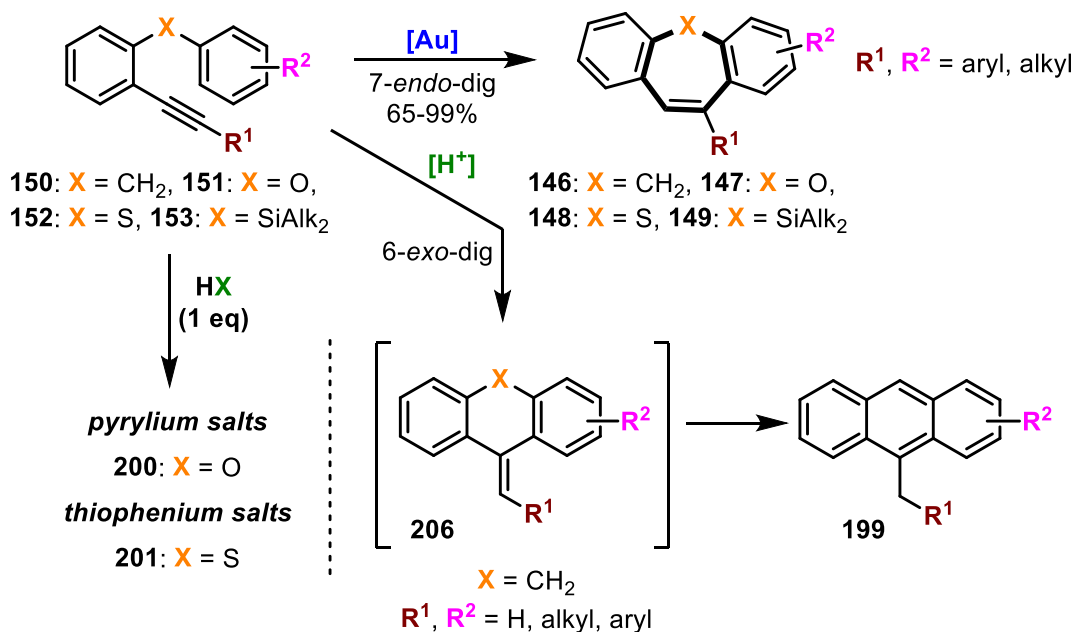
**Figure 44:** IRC profile for the interconversion of **149a** under the local quadratic approximation calculated with B3LYP-D3/6-31+g(d).

The curve is nearly symmetrical on both sides of the transition state and a shoulder is only barely visible. The two processes seem to be energetically closer in the case of **149a**. On the first half (left) of the profile the reorganization process of the *para*-anisyl substituent and the oscillation of the silicon into the seven-membered ring takes place, whereas on the other half (right) mainly the silicon oscillates.

After experimental and computational investigation of the interconversion barriers of the seven-membered ring, it is clear that the greatest potential for separating and isolating the enantiomers lies with compounds having a  $-\text{CH}_2-$  or  $-\text{S}-$  tether. In both cases, the highest barriers have been determined even for undecorated molecules or with sterically less demanding substituents such as methoxy groups. However, in the case of sulfur, reactivity of the precursors poses a drawback, since only electron-rich substituents, on the ring that is suffering the Friedel-Craft alkylation, guarantee the desired reactivity. For this reason, it was not possible to incorporate more sterically demanding substituents to further increase the barrier and to expand the scope of dibenzo[*b,f*]thiepinines. With the molecules synthesized within this thesis it was not possible to obtain an interconversion barrier above  $110 \text{ kJ mol}^{-1}$ , which is at least necessary to allow isolation of the enantiomers and to consider an enantioselective synthesis of the seven-membered ring. Another substituent on the C4 position of the seven-membered ring seems to be required to exceed the  $110 \text{ kJ mol}^{-1}$  as shown by the Alcarazo group in the past with an additional CN-group.<sup>[125]</sup>

## 4. Summary

To conclude, a new synthetic strategy for the synthesis of seven-membered ring systems with and without heteroatoms applying an Au(I)-based catalyst was successfully established (**Scheme 54**). The developed methodology led to the formation of the desired seven-membered ring with excellent yields and regioselectivities.



**Scheme 54:** Different pathways in the cyclization of 1-(benzyl-, oxyaryl-, thioaryl-, and silaaryl)-2-ethynylbenzenes.

The selectivity in the cyclization of 1-(benzyl-, oxyaryl-, thioaryl-, and silaaryl)-2-ethynylbenzenes was investigated through a comparison between Brønsted acid and Au(I) catalysis. Brønsted acid catalysis invariably favored the pathway in which the most stable carbocation intermediate was formed by protonation of the alkyne. This preferentially facilitated 6-*exo*-dig cyclization and the generation of anthracene **199** and anthracene-like structures for the substrates studied. Whereas Au(I) catalysis generally preferred seven-membered ring formation *via* 7-*endo*-dig cyclization. Subsequent kinetic studies allowed the selection of a suitable catalytic system. Using an *N*-arylpyridiniophosphine as an ancillary ligand, the benefit of this  $\alpha$  cationic phosphine could be proven and a series of structurally differentiated dibenzo cycloheptatrienes **146**, -oxepines **147**, -thiepinines **148** and -silepinines **149** were successfully synthesized. Although seven-membered ring fused planar-chiral ferrocenes would exhibit an interesting and desirable motif, the optimized reaction conditions could not be transferred to the ferrocene-containing precursors. Nonetheless, the developed synthesis strategy could be further understood through these experiments and limitations could be identified.<sup>[125]</sup>

In addition to the synthetic part of this thesis, the configurational stability of the seven-membered ring system was investigated. The influence of the tether as well as of the substituents was considered in detail. Single crystal X-ray diffraction analysis was employed to provide initial valuable insights into the flexibility of the seven-membered ring, which is closely related to the interconversion barrier. In addition to the successful application of experimental methods such as DHPLC and EXSY spectroscopy, complementary DFT methods were also utilized to assess the interconversion barriers of the central seven-membered ring. To our delight, a very good agreement between the applied experimental and theoretical methods was observed (**Figure 45**).

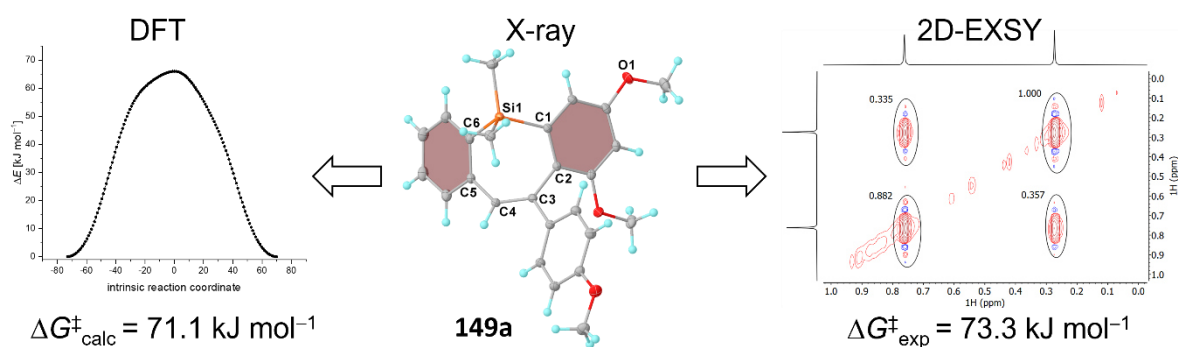


**Figure 45:** Comparison of the complementary methods used to determine the interconversion barrier of **149a**.

Through this comprehensive investigation of the configurational stability of the seven-membered ring system, clear trends have been identified. It can be stated that as the steric demand of the substituents increases and the flexibility of the seven-membered ring decreases, the barrier at interconversion also rises. Although in none of the molecules studied the interconversion barrier allowed isolation of the enantiomers, the pool of experience has grown significantly with the knowledge that another substituent at the C4 position of the seven-membered ring is required to ensure the desired stability as was shown previously.

## 5. Experimental

### 5.1 General remarks

**Working methods:** Unless stated otherwise, all reactions were carried out using pre-dried glassware under an inert atmosphere (nitrogen or argon if specifically noted) using Standard Schlenk techniques or under nitrogen atmosphere in a MBraun UNIlab plus glovebox. Dry and degassed solvents (THF, dichloromethane, toluene, diethyl ether, pentane, acetonitrile) were obtained with the MBraun Solvent Purification System (MB-SPS-800) or by distillation over the drying agents as and stored under a protective gas atmosphere. Flash chromatography was either performed Macherey Nagel 60 (40-63  $\mu\text{m}$ ) silica gel. Thin-layer chromatography (TLC) analysis was performed using polygram SIL G/UV254 TLC plates from Macherey Nagel and visualized by UV irradiation and/or phosphomolybdic acid or  $\text{KMnO}_4$  dip.

**Starting materials:** All commercially available reagents (Acros Organics, ABCR, Alfa Aesar, Sigma Aldrich, Fluorochem, TCI, J and K Scientific, Chempur GmbH, BLDpharm, Thermo Fisher Scientific) were used as received. **189a**<sup>[129,131]</sup>, **189b**<sup>[130,132]</sup>, **190**<sup>[114,136,137]</sup> and catalysts **C**<sup>[69]</sup>, **D**<sup>[68]</sup>, **E**<sup>[50]</sup> and **G** were prepared according to literature procedures. **150e**, **150f**, **150g**, **150h**, **150i**, **150k** were prepared by M. Zhao.<sup>[125]</sup>

**NMR:** Spectra were recorded on Bruker Avance Neo 600, Avance Neo 400, Avance III HD 400, Avance III 400 or Avance III HD 300.  $^1\text{H}$  and  $^{13}\text{C}$  chemical shifts ( $\delta$ ) are reported in ppm relative to TMS using the solvent signals as reference in  $\text{CDCl}_3$  (1H: 7.26 ppm,  $^{13}\text{C}$ : 77.16 ppm) or  $\text{C}_6\text{D}_6$  (1H: 7.16 ppm,  $^{13}\text{C}$ : 128.1 ppm). Coupling constants ( $J$ ) are given in Hertz (Hz).  $^{29}\text{Si}$  spectra were measured as  $^{29}\text{Si}$  INEPT.

**HRMS:** Bruker Daltonik maXis Q-TOF (ESI), Bruker Daltonik micrOTOF (ESI), Thermo Scientific LTQ Orbitrap XL (ESI), Thermo Scientific Exactive GC-Orbitrap-MS (EI) or Jeol AccuTOF (EI). Dimensionless mass-to-charge ratios ( $m/z$ ) are given.

**IR:** Infrared spectra were recorded on FT/IR-4600 spectrometer and reported in wavenumbers ( $\text{cm}^{-1}$ ).

**Melting point:** Melting points were measured with a Büchi M-560 apparatus and a heating rate of  $5^\circ\text{C}/\text{min}$ .

**Chiral HPLC:** chiral HPLC measurements were performed using a Shimadzu Prominence-i LC2030C 3D Plus with integrated downstream UV/Vis PDA detector. System control and chromatogram analysis were carried out with LabSolutions software version 5.92. Enantioselective separations were conducted on a Chiralpak<sup>®</sup> IA-3 (150 mm, i.d. 4.6 mm, particle size 3  $\mu\text{m}$ ) or a Chiralpak<sup>®</sup> IC-3 (150 mm, i.d. 4.6 mm, particle size 3  $\mu\text{m}$ ) column, which were bought from Daicel Chiral Technologies. The solvents used (*n*-hexane, *iso*-propanol, ethyl acetate) were purchased from Fisher Scientific or Sigma-Aldrich in HPLC-

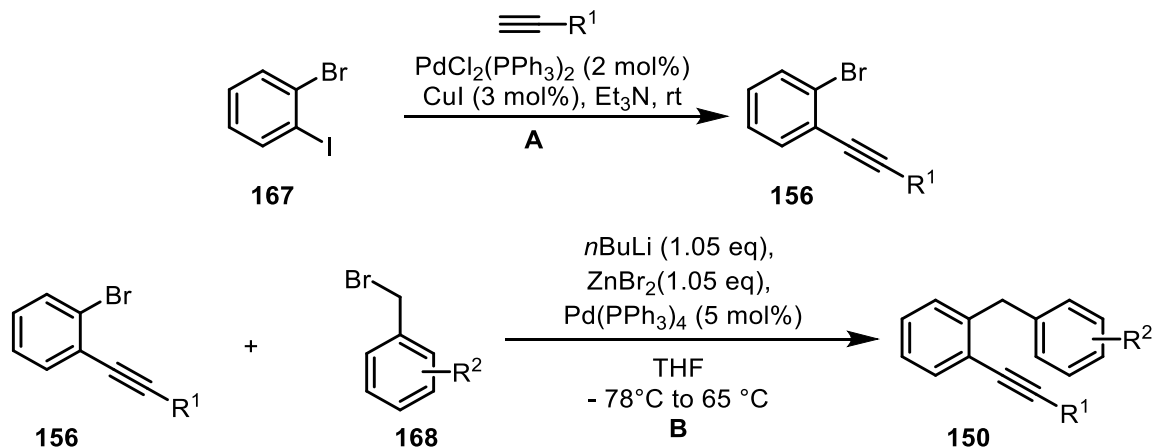
## 5.2 Synthesis and characterization of new compounds

grade quality. Specific conditions, such as eluent mixtures, flow rates and temperatures are provided for each compound individually.

**Single crystal X-ray diffraction analysis:** Data collection was done on two dual source equipped Bruker D8 Venture four-circle-diffractometer from Bruker AXS GmbH; used X-ray sources: microfocus  $\text{I}\mu\text{S}$  2.0 Cu/Mo and microfocus  $\text{I}\mu\text{S}$  3.0 Ag/Mo from Incoatec GmbH with mirror optics HELIOS and single-hole collimator from Bruker AXS GmbH; used detector: Photon III CE14 (Cu/Mo) and Photon III HE (Ag/Mo) from Bruker AXS GmbH. Used programs: *APEX3 Suite* (v2019.11-0) for data collection and therein integrated programs *SAINTV8.40A* (Integration) und *SADABS 2016/2*<sup>[146]</sup> (Absorption correction) from *Bruker AXS GmbH*; structure solution was done with *SHELXT*<sup>[147]</sup>, refinement with *SHELXL-2018/3*<sup>[147]</sup>; *OLEX*<sup>2</sup> was used for data finalization<sup>[148]</sup>. Special Utilities: *SMZ1270* stereomicroscope from *Nikon Metrology GmbH* was used for sample preparation; crystals were mounted on *MicroMounts* or *MicroLoops* from *MiTeGen* in NVH oil; for sensitive samples the *X-TEMP 2 System* was used for picking of crystals<sup>[149]</sup>; crystals were cooled to given temperature with *Cryostream 800* from *Oxford Cryosystems*.

## 5.2 Synthesis and characterization of new compounds

### 5.2.1 1-(benzyl)-2-ethynylbenzenes 150



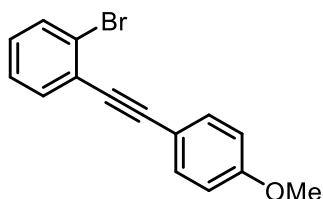
Scheme S1: Synthesis of 1-benzyl-2-ethynylbenzenes 150.

### General procedure A for Sonogashira-Hagihara coupling

According to a modified literature procedure<sup>[150]</sup>, a suspension of the aryl iodide or bromide (1.0 eq),  $\text{PdCl}_2(\text{PPh}_3)_2$  (2 or 5 mol%),  $\text{CuI}$  (3 or 10 mol%) in dry  $\text{Et}_3\text{N}$  (0.1-0.3 M) was degassed for 15 min with nitrogen. The corresponding alkyne (1.1 eq or 1.2 eq) was added and the reaction mixture was stirred at the depicted temperature for the appropriate time. After completion, the reaction mixture was filtered through a pad of silica and eluted with dichloromethane. The volatiles were removed under reduced pressure and the residue was purified by column chromatography ( $\text{SiO}_2$ ,  $\text{EtOAc}$  in hexane).

## 5. Experimental

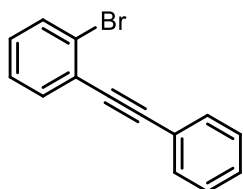
### 1-bromo-2-((4-methoxyphenyl)ethynyl)benzene (**156a**)



Prepared from 2-bromiodobenzene (4.00 g, 14.1 mmol, 1.0 eq), PdCl<sub>2</sub>(PPh<sub>3</sub>)<sub>2</sub> (199 mg, 283 μmol, 2 mol%), CuI (80.8 mg, 424 μmol, 3 mol%) and 4-ethynylanisole (2.06 g, 15.6 mmol, 1.1 eq) in Et<sub>3</sub>N (45 mL) at room temperature for 19 h according to general procedure **A**. Column chromatography (SiO<sub>2</sub>, hexane/EtOAc, 50:1, R<sub>f</sub> = 0.30) yielded **156a** (3.89 g, 13.6 mmol, 96%) as a white solid.

<sup>1</sup>H-NMR (400 MHz, CDCl<sub>3</sub>): δ = 7.61 (dd, J = 8.1, 1.2 Hz, 1H), 7.56 – 7.49 (m, 3H), 7.28 (td, J = 7.4; 1.3 Hz, 1H), 7.16 (ddd, J = 8.1, 7.4, 1.7 Hz, 1H), 6.92 – 6.86 (m, 2H), 3.84 (s, 3H). <sup>13</sup>C{<sup>1</sup>H}-NMR (101 MHz, CDCl<sub>3</sub>) δ = 160.1, 133.3, 133.2, 132.5, 129.2, 127.1, 125.9, 125.6, 115.2, 114.2, 94.2, 87.0, 55.5 ppm. The analytical data were in accordance to the literature.<sup>[151]</sup>

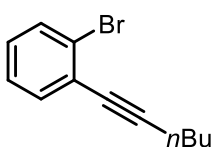
### 1-bromo-2-(phenylethynyl)benzene (**156b**)



Prepared from 2-bromiodobenzene (1.50 g, 5.30 mmol, 1.0 eq), PdCl<sub>2</sub>(PPh<sub>3</sub>)<sub>2</sub> (74.4 mg, 106 μmol, 2 mol%) and CuI (30.3 mg, 159 μmol, 3 mol%) and phenyl acetylene (596 mg, 5.83 mmol, 1.1 eq) in dry Et<sub>3</sub>N (17 mL) at rt for 18 h according to general procedure **A**. After column chromatography (SiO<sub>2</sub>, hexane, R<sub>f</sub> = 0.42) **156b** (1.35 g, 5.25 mmol, 99%) was obtained as a yellow liquid.

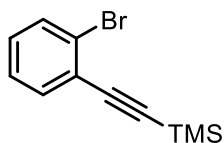
<sup>1</sup>H-NMR (300 MHz, CDCl<sub>3</sub>): δ = 7.68 – 7.51 (m, 4H), 7.41 – 7.34 (m, 3H), 7.30 (td, J = 7.6, 1.3 Hz, 1H), 7.18 (ddd, J = 8.0, 7.4, 1.7 Hz, 1H) ppm. <sup>13</sup>C{<sup>1</sup>H}-NMR (75 MHz, CDCl<sub>3</sub>): δ = 133.4, 132.6, 131.8, 129.5, 128.8, 128.5, 127.2, 125.8, 125.6, 123.1, 94.1, 88.2 ppm. The analytical data were in accordance to literature<sup>[152]</sup>.

### 1-bromo-2-(hex-1-yn-1-yl)benzene (**156c**)



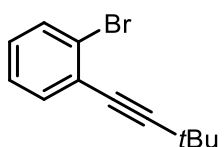
Prepared from 2-bromiodobenzene (1.55 g, 5.48 mmol, 1.0 eq), PdCl<sub>2</sub>(PPh<sub>3</sub>)<sub>2</sub> (76.9 mg, 110 μmol, 2 mol%) and CuI (31.3 mg, 164 μmol, 3 mol%) and 1-hexyne (495 mg, 6.03 mmol, 1.1 eq) in dry Et<sub>3</sub>N (18 mL) at rt for 18 h according to general procedure **A**. After column chromatography (SiO<sub>2</sub>, hexane, R<sub>f</sub> = 0.39) **156c** (1.15 g, 4.83 mmol, 88%) was obtained as a yellow liquid.

<sup>1</sup>H-NMR (400 MHz, CDCl<sub>3</sub>): δ = 7.55 (dd, J = 8.1, 1.3 Hz, 1H), 7.42 (dd, J = 7.7, 1.8 Hz, 1H), 7.22 (td, J = 7.5, 1.3 Hz, 1H), 7.11 (td, J = 7.7, 1.8 Hz, 1H), 2.47 (t, J = 6.9 Hz, 2H), 1.70 – 1.59 (m, 2H), 1.58 – 1.46 (m, 2H), 0.96 (t, J = 7.2 Hz, 3H) ppm. <sup>13</sup>C{<sup>1</sup>H}-NMR (101 MHz, CDCl<sub>3</sub>): δ = 133.4, 132.4, 128.8, 127.0, 126.2, 125.6, 95.7, 79.5, 30.8, 22.1, 19.4, 13.8 ppm. Analytical data are in accordance to literature<sup>[151]</sup>.

**((2-bromophenyl)ethynyl)trimethylsilane (156d)**

Following general procedure **A**, to a suspension of 2-bromiodobenzene (1.50 g, 5.30 mmol, 1.0 eq), PdCl<sub>2</sub>(PPh<sub>3</sub>)<sub>2</sub> (74.4 mg, 106 μmol, 2 mol%) and CuI (30.3 mg, 159 μmol, 3 mol%) in dry Et<sub>3</sub>N (17 mL) TMS-acetylene (573 mg, 5.83 mmol, 1.1 eq) was added and the reaction was stirred at rt for 15 h. After column chromatography (SiO<sub>2</sub>, hexane, *R<sub>f</sub>* = 0.41) **156d** (1.29 g, 5.10 mmol, 96%) was obtained as a yellow liquid.

<sup>1</sup>H-NMR (300 MHz, CDCl<sub>3</sub>): δ = 7.57 (dd, *J* = 7.9, 1.4 Hz, 1H), 7.49 (dd, *J* = 7.8, 1.8 Hz, 1H), 7.28 – 7.20 (m, 1H), 7.15 (td, *J* = 7.7, 1.8 Hz, 1H), 0.28 (s, 9H) ppm. <sup>13</sup>C{<sup>1</sup>H}-NMR (101 MHz, CDCl<sub>3</sub>): δ = 133.7, 132.5, 129.7, 127.0, 125.9, 125.4, 103.2, 99.8, 0.0 ppm. The analytical data were in accordance to literature<sup>[151]</sup>.

**1-bromo-2-(3,3-dimethylbut-1-yn-1-yl)benzene (156e)**

Prepared from 2-bromiodobenzene (5.00 g, 17.7 mmol, 1.0 eq), PdCl<sub>2</sub>(PPh<sub>3</sub>)<sub>2</sub> (248 mg, 353 μmol, 2 mol%), CuI (101 mg, 530 μmol, 3 mol%) and 3,3-dimethylbutyne (1.60 g, 19.4 mmol, 1.1 eq) in Et<sub>3</sub>N (50 mL) at 80 °C for 15 h according to general procedure **A**. Column chromatography (SiO<sub>2</sub>, hexane, *R<sub>f</sub>* = 0.42) yielded **156e** (4.17 g, 17.6 mmol, 99%) as a pale yellow liquid.

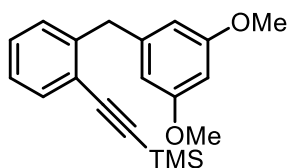
<sup>1</sup>H-NMR (400 MHz, CDCl<sub>3</sub>): δ = 7.55 (dd, *J* = 8.0, 1.3 Hz, 1H), 7.41 (dd, *J* = 7.7, 1.7 Hz, 1H), 7.21 (td, *J* = 7.6, 1.3 Hz, 1H), 7.10 (ddd, *J* = 8.1, 7.4, 1.7 Hz, 1H), 1.35 (s, 9H) ppm. <sup>13</sup>C{<sup>1</sup>H}-NMR (101 MHz, CDCl<sub>3</sub>): δ = 133.2, 132.4, 128.7, 127.0, 126.2, 125.9, 103.7, 78.1, 31.0, 28.4 ppm. The analytical data were in accordance to literature.<sup>[153]</sup>

**General procedure B for Negishi coupling**

A Schlenk flask was charged with the bromoalkyne **156** (1.00 eq) and dry THF (0.4 M) under nitrogen atmosphere. The solution was cooled down to –78 °C and *n*BuLi (2.5 M, 1.05 eq) was added. The reaction mixture was stirred at –78 °C for 30 min, then a solution of zinc bromide (1.05 eq) in dry THF (0.8 M) was added dropwise. The reaction mixture was allowed to slowly warm up to room temperature. After 1 h, the organozinc reagent was added to a solution of the corresponding benzylic bromide (1.00 eq) and Pd(PPh<sub>3</sub>)<sub>4</sub> (5 mol%) in dry THF (0.5 M) in a pressure Schlenk. The reaction mixture was heated to 65 °C for 15 h. After cooling down to room temperature, the reaction was quenched with sat. aq. NH<sub>4</sub>Cl solution, diluted with diethyl ether and water and extracted with diethyl ether three times. The combined organic layers were washed with water, dried over Na<sub>2</sub>SO<sub>4</sub> and concentrated *in vacuo*. The crude product was purified by flash chromatography (SiO<sub>2</sub>, ethyl acetate in hexane).

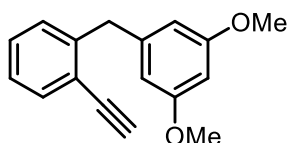
## 5. Experimental

### ((2-(3,5-dimethoxybenzyl)phenyl)ethynyl)trimethylsilane (**169**)



According to general procedure **B**, the organozinc reagent, prepared from **156d** (500 mg, 1.97 mmol, 1.00 eq), *n*BuLi (2.5 M, 830  $\mu$ L, 2.07 mmol, 1.05 eq) in dry THF (5 mL) and zinc bromide (467 mg, 2.07 mmol, 1.05 eq) in dry THF (2.5 mL), was added to a solution of 3,5-dimethoxybenzyl bromide (480 mg, 1.97 mmol, 1.00 eq) and Pd(PPh<sub>3</sub>)<sub>4</sub> (114 mg, 98.7  $\mu$ mol, 5 mol%) in dry THF (4 mL). Purification by flash chromatography (SiO<sub>2</sub>, hexane/EtOAc, 30:1, *R<sub>f</sub>* = 0.17) yielded **169** (563 mg, 1.73 mmol, 88%) as a colorless oil. **<sup>1</sup>H-NMR** (300 MHz, CDCl<sub>3</sub>):  $\delta$  = 7.52 – 7.46 (m, 1H), 7.28 – 7.21 (m, 1H), 7.20 – 7.12 (m, 2H), 6.45 (d, *J* = 2.2 Hz, 2H), 6.34 (t, *J* = 2.3 Hz, 1H), 4.13 (s, 2H), 3.78 (s, 6H), 0.27 (s, 9H) ppm. **<sup>13</sup>C{<sup>1</sup>H}-NMR** (101 MHz, CDCl<sub>3</sub>):  $\delta$  = 160.9, 143.3, 143.1, 132.7, 129.3, 128.9, 126.2, 122.8, 107.3, 104.2, 98.6, 98.2, 55.4, 40.5, 0.2 ppm. **HR-MS** (ESI): calculated *m/z* for C<sub>20</sub>H<sub>25</sub>O<sub>2</sub>Si<sup>+</sup> ([M+H]<sup>+</sup>): 325.1618; found 325.1622. **FTIR** (ATR, neat):  $\tilde{\nu}$  = 3064, 2998, 2956, 2898, 2835, 2154, 1594, 1461, 1428, 1346, 1322, 1291, 1249, 1204, 1154, 1095, 1065, 937, 866, 839, 757, 692, 646 cm<sup>-1</sup>.

### 1-(2-ethynylbenzyl)-3,5-dimethoxybenzene (**150a**)



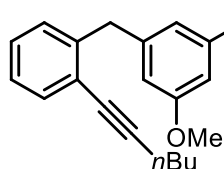
Following a literature procedure,<sup>[126]</sup> potassium carbonate (226 mg, 1.63 mmol, 1.0 eq) was added to a solution of **169** (530 mg, 1.63 mmol, 1.0 eq) in dichloromethane (25 mL) and methanol (25 mL). The reaction mixture was stirred at room temperature for 15 h. After removal of the volatiles, the residue was redissolved in dichloromethane (25 mL) and washed with sat. aq. NaHCO<sub>3</sub> solution (50 mL) followed by extraction with dichloromethane (3 x 40 mL). The combined organic phases were dried over MgSO<sub>4</sub> and concentrated under reduced pressure yielding the desired product **150a** (369 mg, 1.46 mmol, 90%) as a colorless liquid. **<sup>1</sup>H-NMR** (300 MHz, CDCl<sub>3</sub>):  $\delta$  = 7.54 – 7.47 (m, 1H), 7.26 (td, *J* = 7.3, 1.6 Hz, 1H), 7.20 – 7.12 (m, 2H), 6.41 (d, *J* = 2.3 Hz, 2H), 6.32 (t, *J* = 2.3 Hz, 1H), 4.13 (s, 2H), 3.76 (s, 6H), 3.28 (s, 1H) ppm. **<sup>13</sup>C{<sup>1</sup>H}-NMR** (75 MHz, CDCl<sub>3</sub>):  $\delta$  = 160.9, 143.4, 142.9, 133.0, 129.4, 129.2, 126.3, 121.9, 107.3, 98.2, 82.7, 81.3, 55.4, 40.3 ppm. **HR-MS** (ESI): calculated *m/z* for C<sub>17</sub>H<sub>17</sub>O<sub>2</sub><sup>+</sup> ([M+H]<sup>+</sup>): 253.1223; found 253.1223. **FTIR** (ATR, neat):  $\tilde{\nu}$  = 3285, 3062, 3000, 2955, 2935, 2907, 2836, 1592, 1459, 1428, 1345, 1324, 1290, 1203, 1147, 1092, 1057, 936, 907, 826, 757, 729, 690, 648, 617, 532 cm<sup>-1</sup>.

### 1-(2-(hex-1-yn-1-yl)benzyl)-3,5-dimethoxybenzene (**150b**)

According to general procedure **B**, the zinc reagent, prepared from **156c** (500 mg, 2.11 mmol, 1.00 eq), *n*BuLi (2.5 M, 885  $\mu$ L, 2.21 mmol, 1.05 eq) in dry THF (5.5 mL) and zinc bromide (499 mg, 2.21 mmol, 1.05 eq) in dry THF (2.7 mL), was added to a solution of 3,5-dimethoxybenzyl bromide (487 mg, 2.11 mmol, 1.00 eq) and Pd(PPh<sub>3</sub>)<sub>4</sub> (122 mg,



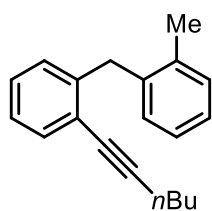
## 5.2 Synthesis and characterization of new compounds



105  $\mu\text{mol}$ , 5 mol%) in dry THF (4.2 mL). Purification by flash chromatography ( $\text{SiO}_2$ , hexane/EtOAc, 30:1,  $R_f = 0.21$ ) yielded **150b** (561 mg, 1.82 mmol, 86%) as a colorless oil.

$^1\text{H NMR}$  (300 MHz,  $\text{CDCl}_3$ ):  $\delta = 7.45 - 7.36$  (m, 1H), 7.22 – 7.08 (m, 3H), 6.41 (d,  $J = 2.2$  Hz, 2H), 6.31 (t,  $J = 2.3$  Hz, 1H), 4.09 (s, 2H), 3.75 (s, 6H), 2.44 (t,  $J = 6.9$  Hz, 2H), 1.66 – 1.38 (m, 4H), 0.93 (t,  $J = 7.2$  Hz, 3H) ppm.  $^{13}\text{C}\{^1\text{H}\}\text{-NMR}$  (101 MHz,  $\text{CDCl}_3$ ):  $\delta = 160.9, 143.3, 142.6, 132.3, 129.3, 127.8, 126.1, 123.9, 107.3, 98.1, 94.6, 79.6, 55.4, 40.5, 31.1, 22.2, 19.4, 13.8$  ppm. **HR-MS** (ESI): calculated  $m/z$  for  $\text{C}_{21}\text{H}_{25}\text{O}_2^+$  ( $[\text{M}+\text{H}]^+$ ): 309.1849; found 309.1851. **FTIR** (ATR, neat):  $\tilde{\nu} = 3063, 2998, 2956, 2932, 2871, 2836, 1594, 1461, 1428, 1345, 1324, 1291, 1204, 1155, 1098, 1065, 935, 827, 757, 690$   $\text{cm}^{-1}$ .

### 1-(hex-1-yn-1-yl)-2-(2-methylbenzyl)benzene (150c)

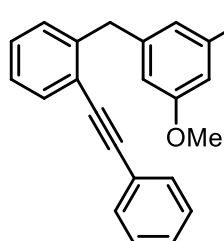


According to General procedure **B**, the organozinc reagent, prepared from **156c** (215 mg, 907  $\mu\text{mol}$ , 1.00 eq),  $n\text{BuLi}$  (2.5 M, 380  $\mu\text{L}$ , 952  $\mu\text{mol}$ , 1.05 eq) in dry THF (2.4 mL) and zinc bromide (214 mg, 952  $\mu\text{mol}$ , 1.05 eq) in dry THF (1.2 mL), was added to a solution of 2-methylbenzyl bromide (168 mg, 907  $\mu\text{mol}$ , 1.00 eq) and  $\text{Pd}(\text{PPh}_3)_4$  (52.4 mg,

45.3  $\mu\text{mol}$ , 5 mol%) in dry THF (1.8 mL). Purification by flash chromatography ( $\text{SiO}_2$ , hexane,  $R_f = 0.22$ ) yielded **150c** (162 mg, 617  $\mu\text{mol}$ , 68%) as a pale yellow liquid.

$^1\text{H-NMR}$  (300 MHz,  $\text{CDCl}_3$ ):  $\delta = 7.49 - 7.36$  (m, 1H), 7.21 – 7.10 (m, 5H), 7.08 – 7.01 (m, 1H), 6.92 – 6.83 (m, 1H), 4.14 (s, 2H), 2.43 (t,  $J = 6.9$  Hz, 2H), 2.24 (s, 3H), 1.62 – 1.50 (m, 2H), 1.50 – 1.37 (m, 2H), 0.92 (t,  $J = 7.2$  Hz, 3H) ppm.  $^{13}\text{C}\{^1\text{H}\}\text{-NMR}$  (101 MHz,  $\text{CDCl}_3$ ):  $\delta = 142.2, 138.8, 136.9, 132.1, 130.3, 130.0, 128.6, 127.8, 126.5, 126.1, 125.9, 124.0, 95.0, 79.4, 37.8, 31.0, 22.1, 19.7, 19.4, 13.8$  ppm. **HR-MS** (EI): calculated  $m/z$  for  $\text{C}_{20}\text{H}_{22}^+$  ( $[\text{M}]^+$ ): 262.1716; found 262.1722. **FTIR** (ATR, neat):  $\tilde{\nu} = 3064, 3018, 2956, 2929, 2871, 2837, 1598, 1483, 1448, 1429, 1378, 1327, 1107, 1050, 948, 917, 864, 809, 755, 741, 715, 623, 591$   $\text{cm}^{-1}$ .

### 1,3-dimethoxy-5-(2-(phenylethynyl)benzyl)benzene (150d)



Prepared from iodobenzene (100 mg, 490  $\mu\text{mol}$ , 1.0 eq),  $\text{PdCl}_2(\text{PPh}_3)_2$  (6.7 mg, 9.8  $\mu\text{mol}$ , 2 mol%) and  $\text{CuI}$  (2.8 mg, 14.7  $\mu\text{mol}$ , 3 mol%) and **150a** (136 mg, 539  $\mu\text{mol}$ , 1.1 eq) in dry  $\text{Et}_3\text{N}$  (1.6 mL) at rt for 18 h according to general procedure **A**. After column chromatography ( $\text{SiO}_2$ , hexane/EtOAc, 50:1,  $R_f = 0.11$

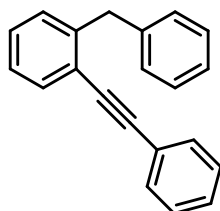
(hexane/EtOAc, 30:1)) **150d** (129 mg, 393  $\mu\text{mol}$ , 80%) was obtained as a colorless oil.

$^1\text{H-NMR}$  (400 MHz,  $\text{CDCl}_3$ ):  $\delta = 7.59 - 7.48$  (m, 3H), 7.38 – 7.31 (m, 3H), 7.29 – 7.24 (m, 1H), 7.24 – 7.18 (m, 2H), 6.46 (d,  $J = 2.3$  Hz, 2H), 6.32 (t,  $J = 2.3$  Hz, 1H), 4.19 (s, 2H), 3.72 (s, 6H) ppm.  $^{13}\text{C}\{^1\text{H}\}\text{-NMR}$  (101 MHz,  $\text{CDCl}_3$ ):  $\delta = 160.9, 143.1, 142.9, 132.4, 131.7, 129.5,$

## 5. Experimental

128.7, 128.5, 128.4, 126.4, 123.5, 123.0, 107.3, 98.3, 93.6, 88.6, 55.4, 40.8 ppm. **HR-MS** (ESI): calculated  $m/z$  for  $C_{23}H_{21}O_2^+$  ( $[M+H]^+$ ): 329.1536; found 329.1534. **FTIR** (ATR, neat):  $\tilde{\nu}$  = 3058, 2999, 2957, 2934, 2836, 1593, 1493, 1459, 1428, 1344, 1324, 1290, 1204, 1152, 1089, 1064, 993, 936, 905, 830, 795, 755, 727, 688, 648, 602, 536  $cm^{-1}$ .

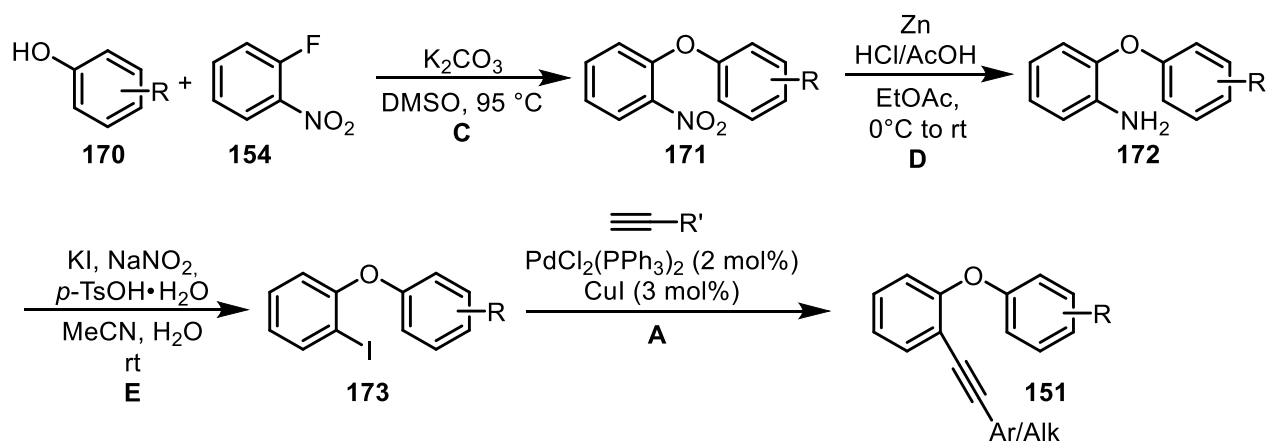
### 1-benzyl-2-(phenylethynyl)benzene (150k)



According to general procedure **B**, the organozinc reagent, prepared from **156b** (500 mg, 1.94 mmol, 1.00 eq), *n*BuLi (2.5 M, 820  $\mu$ L, 2.04 mmol, 1.05 eq) in dry THF (5 mL) and zinc bromide (460 mg, 2.04 mmol, 1.05 eq) in dry THF (2.5 mL), was added to a solution of benzyl bromide (333 mg, 1.94 mmol, 1.00 eq) and Pd(PPh<sub>3</sub>)<sub>4</sub> (112 mg, 97.2  $\mu$ mol, 5 mol%) in dry THF (4 mL). Purification by flash chromatography (SiO<sub>2</sub>, pentane,  $R_f$  = 0.11) yielded **150k** (375 mg, 1.40 mmol, 72%) as a pale colorless liquid.

**<sup>1</sup>H-NMR** (300 MHz, CDCl<sub>3</sub>):  $\delta$  = 7.56 – 7.51 (m, 1H), 7.50 – 7.43 (m, 2H), 7.36 – 7.29 (m, 3H), 7.28 – 7.24 (m, 4H), 7.24 – 7.14 (m, 2H), 4.24 (s, 2H) ppm. **<sup>13</sup>C{<sup>1</sup>H}-NMR** (75 MHz, CDCl<sub>3</sub>):  $\delta$  = 143.2, 140.7, 132.4, 131.6, 129.6, 129.1, 128.7, 128.6, 128.5, 128.4, 126.3, 126.2, 123.5, 123.1, 93.5, 88.5, 40.5 ppm. The analytical data were in accordance to the literature<sup>[152]</sup>

### 5.2.2 1-(oxyaryl)-2-ethynylbenzenes **151**



**Scheme S2:** Synthetic strategy for of 1-(oxyaryl)-2-ethynylbenzenes **151**.

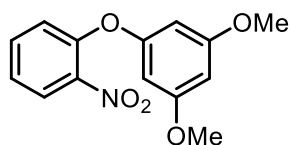
#### General procedure **C** for nucleophilic substitution

According to a literature procedure,<sup>[154]</sup> a mixture of 1-fluoro-2-nitrobenzene (1.0 eq), the corresponding phenol (1.0 eq) and K<sub>2</sub>CO<sub>3</sub> (2.0 eq) in DMSO (~0.4 M) were heated to 95 °C under air for the specified time. After cooling to room temperature, water was added and the mixture was extracted with diethyl ether. The combined organic phases were washed

## 5.2 Synthesis and characterization of new compounds

with brine, dried over Na<sub>2</sub>SO<sub>4</sub> and concentrated in *vacuo*. The desired product **171** was used without further purification in the next step.

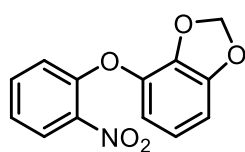
### 1,3-dimethoxy-5-(2-nitrophenoxy)benzene (**171a**)



Prepared using 1-fluoro-2-nitrobenzene (2.25 mL, 21.3 mmol, 1.0 eq), 3,5-dimethoxy phenol (3.28 g, 21.3 mmol, 1.0 eq) and K<sub>2</sub>CO<sub>3</sub> (5.88 g, 42.5 mmol, 2.0 eq) in DMSO (50 mL) at 95 °C for 26 h according to general procedure **C**. The desired product **171a** (5.76 g, 20.9 mmol, 98%) was obtained as an orange oil.

**<sup>1</sup>H-NMR** (300 MHz, CDCl<sub>3</sub>): δ = 7.95 (dd, *J* = 8.2, 1.7 Hz, 1H), 7.51 (ddd, *J* = 8.4, 7.4, 1.7 Hz, 1H), 7.20 (ddd, *J* = 8.1, 7.4, 1.3 Hz, 1H), 7.09 (dd, *J* = 8.4, 1.2 Hz, 1H), 6.28 (t, *J* = 2.2 Hz, 1H), 6.20 (d, *J* = 2.2 Hz, 2H), 3.76 (s, 6H) ppm. **<sup>13</sup>C{<sup>1</sup>H}-NMR** (101 MHz, CDCl<sub>3</sub>): δ = 161.9, 157.7, 150.4, 141.5, 134.3, 125.8, 123.5, 121.1, 97.8, 96.8, 55.7 ppm. **HR-MS** (ESI): calculated *m/z* for C<sub>14</sub>H<sub>14</sub>NO<sub>5</sub><sup>+</sup> ([M+H]<sup>+</sup>): 298.0686; found: 298.0688. **FTIR** (ATR, neat):  $\tilde{\nu}$  = 3101, 3005, 2960, 2941, 2840, 1586, 1524, 1472, 1429, 1348, 1267, 1236, 1204, 1151, 1127, 1089, 1051, 988, 974, 825, 778, 746, 704, 669 cm<sup>-1</sup>.

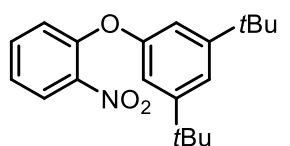
### 4-(2-nitrophenoxy)benzo[d][1,3]dioxole (**171b**)



Prepared using 1-fluoro-2-nitrobenzene (2.55 mL, 24.2 mmol, 1.0 eq), 4-(2-nitrophenoxy)benzo[d][1,3]dioxole (3.35 g, 24.2 mmol, 1.0 eq) and K<sub>2</sub>CO<sub>3</sub> (6.69 g, 48.4 mmol, 2.0 eq) in DMSO (60 mL) at 95 °C for 24 h according to general procedure **C**. The desired product **171b** (5.84 g, 22.5 mmol, 93%) was obtained as an off-white solid.

**<sup>1</sup>H-NMR** (400 MHz, CDCl<sub>3</sub>): δ = 7.96 (dd, *J* = 8.2, 1.7 Hz, 1H), 7.50 (ddd, *J* = 8.7, 7.4, 1.7 Hz, 1H), 7.18 (ddd, *J* = 8.5, 7.4, 1.2 Hz, 1H), 7.02 (dd, *J* = 8.4, 1.2 Hz, 1H), 6.84 (t, *J* = 8.1 Hz, 1H), 6.73 (dd, *J* = 7.8, 1.1 Hz, 1H), 6.63 (dd, *J* = 8.5, 1.1 Hz, 1H), 5.96 (s, 2H) ppm. **<sup>13</sup>C{<sup>1</sup>H}-NMR** (101 MHz, CDCl<sub>3</sub>): δ = 150.5, 150.0, 140.5, 138.0, 137.9, 134.3, 126.0, 123.1, 122.6, 118.9, 114.6, 106.0, 102.0 ppm. **HR-MS** (ESI): calculated *m/z* for C<sub>13</sub>H<sub>10</sub>NO<sub>5</sub><sup>+</sup> ([M+H]<sup>+</sup>): 260.0553; found 260.0559. **FTIR** (ATR, neat):  $\tilde{\nu}$  = 3078, 3047, 2907, 1627, 1612, 1598, 1586, 1524, 1482, 1461, 1351, 1310, 1249, 1221, 1165, 1118, 1091, 1060, 1041, 1014, 925, 863, 820, 777, 739, 717, 702, 671, 604 cm<sup>-1</sup>.

### 1,3-di-*tert*-butyl-5-(2-nitrophenoxy)benzene (**171c**)

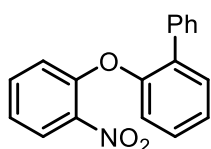


Prepared using 1-fluoro-2-nitrobenzene (2.25 mL, 21.3 mmol, 1.0 eq), 3,5-di-*tert*-butylphenol (4.39 g, 21.3 mmol, 1.0 eq) and K<sub>2</sub>CO<sub>3</sub> (5.88 g, 42.5 mmol, 2.0 eq) in DMSO (50 mL) at 95 °C for 24 h according to general procedure **C**. The desired product **171c** (6.90 g, 21.1 mmol, 99%) was obtained as a yellow oil.

## 5. Experimental

**<sup>1</sup>H-NMR** (300 MHz, CDCl<sub>3</sub>):  $\delta$  = 7.94 (dd,  $J$  = 8.2, 1.7 Hz, 1H), 7.46 (ddd,  $J$  = 8.4, 7.4, 1.7 Hz, 1H), 7.26 (d,  $J$  = 1.8 Hz, 1H), 7.13 (ddd,  $J$  = 8.4, 7.4, 1.2 Hz, 1H), 6.96 (dd,  $J$  = 8.5, 1.2 Hz, 1H), 6.91 (d,  $J$  = 1.7 Hz, 2H), 1.30 (s, 18H) ppm. **<sup>13</sup>C{<sup>1</sup>H}-NMR** (75 MHz, CDCl<sub>3</sub>):  $\delta$  = 154.8, 153.4, 151.9, 134.1, 125.8, 122.2, 119.2, 119.1, 114.4, 35.2, 31.5 ppm. **HR-MS** (ESI): calculated  $m/z$  for C<sub>20</sub>H<sub>26</sub>NO<sub>3</sub><sup>+</sup> ([M+H]<sup>+</sup>): 328.1907; found 328.1910. **FTIR** (ATR, neat):  $\tilde{\nu}$  = 2962, 2904, 2870, 1603, 1583, 1528, 1479, 1421, 1351, 1296, 1266, 1245, 1162, 1090, 960, 876, 858, 777, 745, 707 cm<sup>-1</sup>.

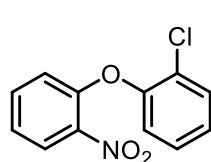
### 2-(2-nitrophenoxy)-1,1'-biphenyl (171d)



Prepared using 1-fluoro-2-nitrobenzene (1.25 mL, 11.8 mmol, 1.0 eq), [1,1'-biphenyl]-2-ol (2.00 g, 11.8 mmol, 1.0 eq) and K<sub>2</sub>CO<sub>3</sub> (3.25 g, 23.5 mmol, 2.0 eq) in DMSO (35 mL) at 95 °C for 24 h according to general procedure C. The desired product **171d** (3.42 g, 11.8 mmol, quant.) was obtained as a yellow oil.

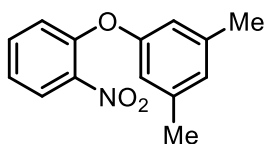
**<sup>1</sup>H-NMR** (400 MHz, CDCl<sub>3</sub>):  $\delta$  = 7.84 (dd,  $J$  = 8.2, 1.7 Hz, 1H), 7.57 – 7.52 (m, 2H), 7.49 (dd,  $J$  = 7.5, 1.9 Hz, 1H), 7.41 – 7.29 (m, 5H), 7.29 – 7.23 (m, 1H), 7.10 (dd,  $J$  = 8.0, 1.4 Hz, 1H), 7.02 (ddd,  $J$  = 8.4, 7.3, 1.3 Hz, 1H), 6.77 (dd,  $J$  = 8.5, 1.2 Hz, 1H) ppm. **<sup>13</sup>C{<sup>1</sup>H}-NMR** (101 MHz, CDCl<sub>3</sub>):  $\delta$  = 151.9, 151.2, 140.4, 136.9, 134.2, 134.1, 131.7, 129.2, 129.2, 128.4, 127.7, 125.8, 125.7, 122.3, 120.8, 119.0 ppm. **HR-MS** (ESI): calculated  $m/z$  for C<sub>18</sub>H<sub>14</sub>NO<sub>3</sub><sup>+</sup> ([M+H]<sup>+</sup>): 292.0968; found 292.0967. **FTIR** (ATR, neat):  $\tilde{\nu}$  = 3060, 3033, 1604, 1583, 1524, 1475, 1453, 1433, 1348, 1308, 1255, 1238, 1193, 1161, 1112, 1087, 1044, 1009, 884, 844, 801, 764, 742, 700, 665, 614 cm<sup>-1</sup>.

### 2-(2-nitrophenoxy)-1,1'-biphenyl (171e)



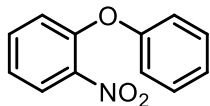
Prepared using 1-fluoro-2-nitrobenzene (0.86 mL, 8.17 mmol, 1.0 eq), 2-chlorophenol (0.85 mL, 8.17 mmol, 1.0 eq) and K<sub>2</sub>CO<sub>3</sub> (2.26 g, 16.3 mmol, 2.0 eq) in DMSO (20 mL) at 95 °C for 24 h according to general procedure C. The desired product **171e** (2.02 g, 8.10 mmol, 99%) was obtained as a yellow liquid.

**<sup>1</sup>H-NMR** (300 MHz, CDCl<sub>3</sub>):  $\delta$  = 7.98 (dd,  $J$  = 8.1, 1.7 Hz, 1H), 7.53 – 7.44 (m, 2H), 7.28 (td,  $J$  = 7.6, 1.7 Hz, 1H), 7.24 – 7.14 (m, 2H), 7.08 (dd,  $J$  = 8.0, 1.6 Hz, 1H), 6.84 (dd,  $J$  = 8.4, 1.2 Hz, 1H) ppm. **<sup>13</sup>C{<sup>1</sup>H}-NMR** (101 MHz, CDCl<sub>3</sub>):  $\delta$  = 151.0, 150.5, 140.6, 134.4, 131.2, 128.4, 126.4, 126.3, 126.0, 123.3, 121.6, 119.0 ppm. **HR-MS** (ESI): calculated  $m/z$  for C<sub>12</sub>H<sub>9</sub>ClNO<sub>3</sub><sup>+</sup> ([M+H]<sup>+</sup>): 250.0265; found 250.0265. **FTIR** (ATR, neat):  $\tilde{\nu}$  = 3102, 3073, 3043, 2867, 1606, 1580, 1523, 1471, 1446, 1347, 1308, 1262, 1241, 1209, 1161, 1129, 1089, 1060, 1036, 945, 884, 844, 797, 774, 742, 683, 661 cm<sup>-1</sup>.

**1,3-dimethyl-5-(2-nitrophenoxy)benzene (171f)**

Prepared using 1-fluoro-2-nitrobenzene (0.86 mL, 8.19 mmol, 1.0 eq), 3,5-dimethylphenol (1.00 g, 8.19 mmol, 1.0 eq) and  $K_2CO_3$  (2.26 g, 16.4 mmol, 2.0 eq) in DMSO (20 mL) at 95 °C for 26 h according to general procedure **C**. The desired product **171f** (1.96 g, 8.07 mmol, 99%) was obtained as a yellow liquid.

**$^1H$ -NMR** (300 MHz,  $CDCl_3$ ):  $\delta$  = 7.94 (dd,  $J$  = 8.1, 1.7 Hz, 1H), 7.48 (ddd,  $J$  = 8.3, 7.4, 1.7 Hz, 1H), 7.17 (ddd,  $J$  = 8.4, 7.4, 1.2 Hz, 1H), 7.01 (dd,  $J$  = 8.4, 1.2 Hz, 1H), 6.82 (s, 1H), 6.67 (s, 2H), 2.30 (s, 6H) ppm.  **$^{13}C\{^1H\}$ -NMR** (101 MHz,  $CDCl_3$ ):  $\delta$  = 155.7, 151.2, 141.4, 140.1, 134.2, 126.5, 125.8, 122.9, 120.5, 117.1, 21.4 ppm. **HR-MS** (ESI): calculated  $m/z$  for  $C_{14}H_{14}NO_3^+$  ( $[M+H]^+$ ): 244.0968; found 244.0972. **FTIR** (ATR, neat):  $\tilde{\nu}$  = 3102, 3071, 3017, 2952, 2919, 2864, 1604, 1585, 1523, 1472, 1347, 1292, 1268, 1235, 1161, 1133, 1089, 1037, 1022, 999, 949, 894, 858, 840, 810, 775, 745, 703, 666  $cm^{-1}$ .

**1-nitro-2-phenoxybenzene (171g)**

Prepared using 1-fluoro-2-nitrobenzene (1.68 mL, 15.9 mmol, 1.0 eq), phenol (1.50 g, 15.9 mmol, 1.0 eq) and  $K_2CO_3$  (4.10 g, 31.9 mmol, 2.0 eq) in DMSO (40 mL) at 95 °C for 24 h according to general procedure **C**. The desired product **171g** (3.43 g, 15.9 mmol, quant.) was obtained as a yellow liquid.

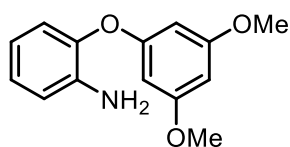
**$^1H$ -NMR** (400 MHz,  $CDCl_3$ ):  $\delta$  = 7.95 (dd,  $J$  = 8.1, 1.7 Hz, 1H), 7.50 (ddd,  $J$  = 8.7, 7.4, 1.7 Hz, 1H), 7.42 – 7.34 (m, 2H), 7.22 – 7.15 (m, 2H), 7.09 – 7.03 (m, 2H), 7.01 (dd,  $J$  = 8.4, 1.2 Hz, 1H) ppm.  **$^{13}C\{^1H\}$ -NMR** (101 MHz,  $CDCl_3$ ):  $\delta$  = 155.9, 150.9, 141.5, 134.2, 130.2, 125.8, 124.7, 123.2, 120.6, 119.4 ppm. **HR-MS** (ESI): calculated  $m/z$  for  $C_{12}H_{10}NO_3^+$  ( $[M+H]^+$ ): 216.0655; found 216.0653. **FTIR** (ATR, neat):  $\tilde{\nu}$  = 3070, 3041, 1607, 1586, 1521, 1487, 1475, 1348, 1265, 1240, 1194, 1160, 1087, 1071, 1038, 1023, 881, 841, 794, 775, 741, 689, 662  $cm^{-1}$ .

**General procedure D for the reduction to amines**

Following a literature known procedure,<sup>[154]</sup> to a solution of the biaryl ether **171** (1.0 eq) in EtOAc (~0.16 M) conc. HCl (8.5-9.5 mL/mmol) and conc. AcOH (8.5-9.5 mL/mmol) were added dropwise at 0 °C. Zinc powder (68 eq) was added in portions at 0 °C and the reaction mixture was stirred at room temperature for 16 h. After cooling to 0 °C, the reaction mixture was treated dropwise with aq. ammonia solution (33%, 17-19 mL/mmol) and the remaining zinc was filtered off. The solution was extracted with EtOAc three times and the combined organic phases were dried over  $Na_2SO_4$ . The volatiles were removed and the amines **172** were used without further purification in the next step.

## 5. Experimental

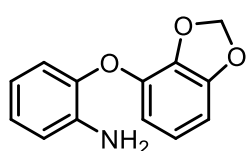
### 2-(3,5-dimethoxyphenoxy)aniline (**172a**)



Using general procedure **D**, **171a** (5.76 g, 20.9 mmol, 1.00 eq) in EtOAc (130 mL) was treated with conc. HCl (195 mL), conc. AcOH (195 mL), zinc powder (93.0 g, 1.42 mol, 68.0 eq) and aq. ammonia solution (33%, 390 mL). Extraction yielded **172a** (5.13 g, 20.9 mmol, quant.) as a brown oil.

**<sup>1</sup>H-NMR** (400 MHz, CDCl<sub>3</sub>):  $\delta$  = 6.99 (ddd,  $J$  = 7.9, 7.3, 1.5 Hz, 1H), 6.91 (dd,  $J$  = 8.0, 1.4 Hz, 1H), 6.82 (dd,  $J$  = 7.9, 1.6 Hz, 1H), 6.72 (ddd,  $J$  = 8.0, 7.3, 1.6 Hz, 1H), 6.18 (t,  $J$  = 2.2 Hz, 1H), 6.15 (d,  $J$  = 2.2 Hz, 2H), 3.74 (s, 6H) ppm. **<sup>13</sup>C{<sup>1</sup>H}-NMR** (101 MHz, CDCl<sub>3</sub>):  $\delta$  = 161.8, 159.6, 142.7, 138.8, 125.3, 120.8, 119.0, 116.7, 95.8, 95.0, 55.5 ppm. **HR-MS** (ESI): calculated  $m/z$  for C<sub>14</sub>H<sub>16</sub>NO<sub>3</sub><sup>+</sup> ([M+H]<sup>+</sup>): 246.1127; found: 246.1125. **FTIR** (ATR, neat):  $\tilde{\nu}$  = 3466, 3374, 3002, 2960, 2940, 2838, 1595, 1499, 1472, 1458, 1442, 1427, 1303, 1270, 1198, 1150, 1130, 1063, 1052, 990, 976, 930, 824, 750, 682 cm<sup>-1</sup>.

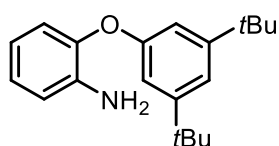
### 2-(benzo[d][1,3]dioxol-4-yloxy)aniline (**172b**)



Using general procedure **D**, **171b** (5.67 g, 21.9 mmol, 1.00 eq) in EtOAc (150 mL) was treated with conc. HCl (200 mL), conc. AcOH (200 mL), zinc powder (97.2 g, 1.49 mol, 68.0 eq) and aq. ammonia solution (33%, 400 mL). Extraction yielded **172b** (4.96 g, 21.6 mmol, 99%) as a white solid.

**<sup>1</sup>H-NMR** (400 MHz, CDCl<sub>3</sub>):  $\delta$  = 6.96 (ddd,  $J$  = 7.8, 7.3, 1.5 Hz, 1H), 6.83 (ddd,  $J$  = 9.7, 8.0, 1.5 Hz, 2H), 6.76 (dd,  $J$  = 8.5, 7.9 Hz, 1H), 6.70 (ddd,  $J$  = 8.0, 7.3, 1.6 Hz, 1H), 6.64 (dd,  $J$  = 7.9, 1.1 Hz, 1H), 6.50 (dd,  $J$  = 8.4, 1.1 Hz, 1H), 5.99 (s, 2H), 3.81 (br s, 2H) ppm. **<sup>13</sup>C{<sup>1</sup>H}-NMR** (101 MHz, CDCl<sub>3</sub>):  $\delta$  = 149.6, 143.7, 140.4, 137.9, 137.2, 124.7, 122.2, 118.8, 118.5, 116.6, 112.9, 104.4, 101.7 ppm. **HR-MS** (ESI): calculated  $m/z$  for C<sub>13</sub>H<sub>12</sub>NO<sub>3</sub><sup>+</sup> ([M+H]<sup>+</sup>): 230.0812; found 230.0815. **FTIR** (ATR, neat):  $\tilde{\nu}$  = 3454, 3370, 2903, 1618, 1586, 1496, 1480, 1458, 1355, 1307, 1259, 1246, 1174, 1146, 1054, 1037, 1008, 918, 832, 796, 774, 743, 716, 685, 606, 540 cm<sup>-1</sup>.

### 2-(3,5-di-*tert*-butylphenoxy)aniline (**172c**)



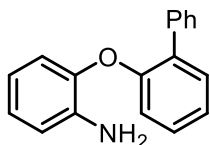
Using general procedure **D**, **171c** (6.36 g, 21.3 mmol, 1.00 eq) in EtOAc (130 mL) was treated with conc. HCl (200 mL), conc. AcOH (200 mL), zinc powder (94.5 g, 1.45 mol, 68.0 eq) and aq. ammonia solution (33%, 400 mL). Extraction yielded **172c** (6.32 g, 21.3 mmol, quant.) as a yellow oil.

**<sup>1</sup>H-NMR** (300 MHz, CDCl<sub>3</sub>):  $\delta$  = 7.15 (t,  $J$  = 1.7 Hz, 1H), 6.95 (td,  $J$  = 8.0, 1.7 Hz, 1H), 6.86 (d,  $J$  = 1.7 Hz, 2H), 6.83 (dt,  $J$  = 8.0, 1.7 Hz, 2H), 6.73-6.66 (m, 1H), 3.86 (br s, 2H), 1.30 (s, 18H) ppm. **<sup>13</sup>C{<sup>1</sup>H}-NMR** (75 MHz, CDCl<sub>3</sub>):  $\delta$  = 156.6, 152.8, 144.2, 138.2, 124.1, 118.9, 118.8, 117.2, 116.4, 112.5, 35.1, 31.5 ppm. **HR-MS** (ESI): calculated  $m/z$  for C<sub>20</sub>H<sub>28</sub>NO<sup>+</sup>

## 5.2 Synthesis and characterization of new compounds

([M+H]<sup>+</sup>): 298.2165; found: 298.2169. **FTIR** (ATR, neat):  $\tilde{\nu}$  = 3473, 3383, 2961, 2903, 2868, 1617, 1580, 1499, 1478, 1460, 1421, 1393, 1362, 1297, 1271, 1245, 1211, 1154, 1136, 1119, 1029, 961, 862, 744, 708 cm<sup>-1</sup>.

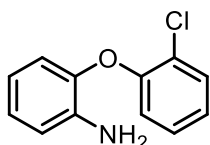
### 2-([1,1'-biphenyl]-2-yloxy)aniline (**172d**)



Using general procedure **D**, **171d** (3.41 g, 11.7 mmol, 1.00 eq) in EtOAc (75 mL) was treated with conc. HCl (110 mL), conc. AcOH (110 mL), zinc powder (52.0 g, 796 mmol, 68.0 eq) and aq. ammonia solution (33%, 220 mL). Extraction yielded **172d** (2.91 g, 11.1 mmol, 95%) as a white solid.

**<sup>1</sup>H-NMR** (400 MHz, CDCl<sub>3</sub>):  $\delta$  = 7.65 – 7.57 (m, 2H), 7.45 (dd,  $J$  = 7.6, 1.8 Hz, 1H), 7.43 – 7.37 (m, 2H), 7.36 – 7.30 (m, 1H), 7.30 – 7.24 (m, 1H), 7.18 (dt,  $J$  = 7.5, 1.4 Hz, 1H), 6.98 – 6.89 (m, 2H), 6.84 (dd,  $J$  = 8.0, 1.6 Hz, 1H), 6.78 (dd,  $J$  = 7.9, 1.6 Hz, 1H), 6.73 – 6.66 (m, 1H), 3.72 (br s, 2H) ppm. **<sup>13</sup>C{<sup>1</sup>H}-NMR** (101 MHz, CDCl<sub>3</sub>):  $\delta$  = 154.0, 144.1, 138.4, 138.0, 132.6, 131.3, 129.4, 128.8, 128.3, 127.3, 124.4, 123.5, 119.3, 118.9, 118.0, 116.5 ppm. **HR-MS** (ESI): calculated  $m/z$  for C<sub>18</sub>H<sub>16</sub>NO<sup>+</sup> ([M+H]<sup>+</sup>): 262.1226; found 262.1229. **FTIR** (ATR, neat):  $\tilde{\nu}$  = 3463, 3375, 3058, 3030, 1616, 1579, 1498, 1475, 1457, 1431, 1301, 1270, 1251, 1209, 1189, 1155, 1135, 1113, 1074, 1047, 1031, 1010, 908, 881, 822, 772, 736, 697, 611, 558, 524 cm<sup>-1</sup>.

### 2-(2-chlorophenoxy)aniline (**172e**)



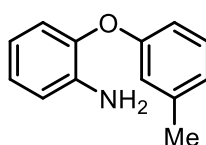
Using general procedure **D**, **171e** (1.89 g, 7.55 mmol, 1.00 eq) in EtOAc (50 mL) was treated with conc. HCl (70 mL), conc. AcOH (70 mL), zinc powder (33.6 g, 514 mmol, 68.0 eq) and aq. ammonia solution (33%, 140 mL). Extraction yielded **172e** (1.66 g, 7.55 mmol, quant.) as brown oil.

**<sup>1</sup>H-NMR** (400 MHz, CDCl<sub>3</sub>):  $\delta$  = 7.45 (dd,  $J$  = 7.9, 1.6 Hz, 1H), 7.18 (ddd,  $J$  = 8.2, 7.4, 1.6 Hz, 1H), 7.08 – 6.96 (m, 2H), 6.89 (dd,  $J$  = 8.2, 1.5 Hz, 1H), 6.84 (dd,  $J$  = 7.9, 1.6 Hz, 1H), 6.80 (dd,  $J$  = 8.0, 1.5 Hz, 1H), 6.72 (ddd,  $J$  = 8.0, 7.2, 1.6 Hz, 1H), 3.87 (br s, 2H) ppm. **<sup>13</sup>C{<sup>1</sup>H}-NMR** (101 MHz, CDCl<sub>3</sub>):  $\delta$  = 152.9, 143.2, 138.2, 130.8, 128.0, 125.2, 124.5, 124.0, 119.4, 119.0, 118.5, 116.8 ppm. **HR-MS** (ESI): calculated  $m/z$  for C<sub>12</sub>H<sub>11</sub>ClNO<sup>+</sup> ([M+H]<sup>+</sup>): 220.0524; found 220.0528. **FTIR** (ATR, neat):  $\tilde{\nu}$  = 681, 743, 783, 822, 884, 930, 1035, 1057, 1130, 1155, 1189, 1230, 1264, 1303, 1445, 1499, 1579, 1619, 3035, 3067, 3379, 3466 cm<sup>-1</sup>.

### 2-(3,5-dimethylphenoxy)aniline (**172f**)

Using general procedure **D**, **171f** (1.89 g, 7.78 mmol, 1.00 eq) in EtOAc (50 mL) was treated with conc. HCl (75 mL), conc. AcOH (75 mL), zinc powder (34.6 g, 529 mmol, 68.0 eq) and

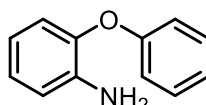
## 5. Experimental



33% aq. ammonia solution (150 mL). Extraction yielded **172f** (1.66 g, 7.76 mmol, quant.) as brown liquid.

**<sup>1</sup>H-NMR** (400 MHz, CDCl<sub>3</sub>):  $\delta$  = 6.98 (td,  $J$  = 7.6, 1.5 Hz, 1H), 6.91 – 6.80 (m, 2H), 6.76 – 6.72 (m, 1H), 6.71 (s, 1H), 6.60 (s, 2H), 3.82 (br s, 2H), 2.28 (s, 6H) ppm. **<sup>13</sup>C{<sup>1</sup>H}-NMR** (101 MHz, CDCl<sub>3</sub>):  $\delta$  = 157.6, 143.5, 139.7, 138.7, 124.8, 124.6, 120.4, 119.0, 116.6, 115.0, 21.5 ppm. **HR-MS** (ESI): calculated  $m/z$  for C<sub>14</sub>H<sub>16</sub>NO<sup>+</sup> ([M+H]<sup>+</sup>): 214.1226; found 214.1230. **FTIR** (ATR, neat):  $\tilde{\nu}$  = 3469, 3377, 3033, 2917, 1616, 1584, 1499, 1459, 1309, 1296, 1270, 1200, 1136, 1032, 950, 838, 782, 749, 687 cm<sup>-1</sup>.

### 2-phenoxyaniline (**172g**)



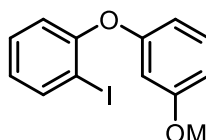
Using general procedure **D**, **171g** (3.42 g, 15.9 mmol, 1.00 eq) in EtOAc (100 mL) was treated with conc. HCl (150 mL), conc. AcOH (150 mL), zinc powder (70.7 g, 1.08 mol, 68.0 eq) and 33% aq. ammonia solution (300 mL). Extraction yielded **172g** (2.76 g, 14.9 mmol, 94%) as a green solid.

**<sup>1</sup>H-NMR** (400 MHz, CDCl<sub>3</sub>):  $\delta$  = 7.36 – 7.27 (m, 2H), 7.10 – 7.03 (m, 1H), 7.03 – 6.95 (m, 3H), 6.88 (dd,  $J$  = 8.1, 1.7 Hz, 1H), 6.84 (dt,  $J$  = 8.1, 1.7 Hz, 1H), 6.78 – 6.69 (m, 1H), 3.84 (br s, 2H) ppm. **<sup>13</sup>C{<sup>1</sup>H}-NMR** (101 MHz, CDCl<sub>3</sub>):  $\delta$  = 157.6, 143.3, 138.7, 129.9, 125.0, 122.8, 120.3, 119.1, 117.3, 116.7 ppm. **HR-MS** (ESI): calculated  $m/z$  for C<sub>12</sub>H<sub>12</sub>NO<sup>+</sup> ([M+H]<sup>+</sup>): 186.0915; found 186.0913. **FTIR** (ATR, neat):  $\tilde{\nu}$  = 3429, 3351, 3236, 3047, 1618, 1582, 1485, 1456, 1301, 1265, 1210, 1191, 1165, 1150, 1071, 1024, 933, 898, 877, 812, 786, 744, 632 cm<sup>-1</sup>.

### General procedure E for Sandmeyer reaction

Adapted from a literature procedure,<sup>[154]</sup> to a solution of the amine **172** (1.0 eq) and *p*-toluenesulfonic acid monohydrate (3.0 eq) in acetonitrile (~0.6 M with respect to the amine) was added a solution of potassium iodide (2.0 eq) and sodium nitrite (2.0 eq) in water (2–3 M) at room temperature. The reaction mixture was stirred for 16 h. Sat. aq. NaHCO<sub>3</sub> solution was added, followed by the addition of water until the precipitate was dissolved. The mixture was extracted with diethyl ether three times. The combined organic phases were washed with a sat. aq. Na<sub>2</sub>S<sub>2</sub>O<sub>3</sub> solution, dried over Na<sub>2</sub>SO<sub>4</sub> and concentrated in *vacuo*. The residue was purified by column chromatography (SiO<sub>2</sub>, EtOAc in hexane).

### 1-(2-iodophenoxy)-3,5-dimethoxybenzene (**173a**)



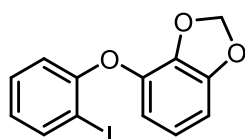
Following general procedure **E**, **172a** (5.13 g, 20.9 mmol, 1.0 eq) and *p*-toluenesulfonic acid monohydrate (11.9 g, 62.8 mmol, 3.0 eq) in acetonitrile (130 mL) were treated with potassium iodide (6.94 g, 41.8 mmol, 2.0 eq) and sodium nitrite (2.89 g, 41.8 mmol, 2.0 eq) in water (15 mL). After column chromatography (SiO<sub>2</sub>, hexane/EtOAc, 30:1,  $R_f$  = 0.24 (hexane/EtOAc, 20:1)) **173a** (5.71 g, 16.0 mmol, 70%) was obtained as a colorless oil.



## 5.2 Synthesis and characterization of new compounds

**<sup>1</sup>H-NMR** (300 MHz, CDCl<sub>3</sub>):  $\delta$  = 7.85 (dd,  $J$  = 7.9, 1.6 Hz, 1H), 7.30 (ddd,  $J$  = 8.2, 7.3, 1.6 Hz, 1H), 6.97 (dd,  $J$  = 8.2, 1.4 Hz, 1H), 6.88 (ddd,  $J$  = 7.9, 7.3, 1.5 Hz, 1H), 6.23 (t,  $J$  = 2.2 Hz, 1H), 6.13 (d,  $J$  = 2.2 Hz, 2H), 3.76 (s, 6H) ppm. **<sup>13</sup>C{<sup>1</sup>H}-NMR** (101 MHz, CDCl<sub>3</sub>):  $\delta$  = 161.8, 158.9, 156.2, 140.0, 129.8, 125.7, 120.2, 97.0, 95.7, 89.2, 55.6 ppm. **HR-MS** (ESI): calculated  $m/z$  for C<sub>14</sub>H<sub>13</sub>IO<sub>3</sub><sup>+</sup> ([M]<sup>+</sup>): 356.9982; found: 356.9985. **FTIR** (ATR, neat):  $\tilde{\nu}$  = 3062, 3000, 2958, 2935, 2833, 1597, 1571, 1459, 1433, 1258, 1223, 1201, 1149, 1129, 1048, 1020, 988, 973, 929, 820, 752, 721, 679, 645, 604, 534 cm<sup>-1</sup>.

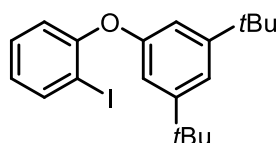
### 4-(2-iodophenoxy)benzo[d][1,3]dioxole (173b)



Following general procedure **E**, **172b** (4.95 g, 19.1 mmol, 1.0 eq) and *p*-toluenesulfonic acid monohydrate (10.9 g, 57.3 mmol, 3.0 eq) in acetonitrile (120 mL) were treated with potassium iodide (6.34 g, 38.2 mmol, 2.0 eq) and sodium nitrite (2.64 g, 38.2 mmol, 2.0 eq) in water (20 mL). After column chromatography (SiO<sub>2</sub>, hexane/EtOAc, 50:1,  $R_f$  = 0.19) **173b** (5.26 g, 15.4 mmol, 81%) was obtained as a white solid.

**<sup>1</sup>H-NMR** (400 MHz, CDCl<sub>3</sub>):  $\delta$  = 7.84 (dd,  $J$  = 8.2, 1.6 Hz, 1H), 7.26 (td,  $J$  = 7.8, 1.7 Hz, 1H), 6.87 – 6.82 (m, 2H), 6.80 (dd,  $J$  = 8.4, 7.8 Hz, 1H), 6.69 (dd,  $J$  = 7.8, 1.1 Hz, 1H), 6.53 (dd,  $J$  = 8.4, 1.1 Hz, 1H), 5.98 (s, 2H) ppm. **<sup>13</sup>C{<sup>1</sup>H}-NMR** (101 MHz, CDCl<sub>3</sub>):  $\delta$  = 156.3, 149.8, 139.9, 139.3, 137.8, 129.6, 125.2, 122.3, 117.4, 114.2, 105.2, 101.8, 87.3 ppm. **HR-MS** (EI): calculated  $m/z$  for C<sub>13</sub>H<sub>9</sub>IO<sub>3</sub><sup>+</sup> ([M]<sup>+</sup>): 339.9596; found 339.9596. **FTIR** (ATR, neat):  $\tilde{\nu}$  = 3056, 2954, 2916, 2850, 1625, 1608, 1573, 1496, 1482, 1456, 1434, 1359, 1263, 1245, 1209, 1173, 1117, 1047, 1018, 951, 922, 873, 845, 822, 780, 743, 719, 685, 656, 604, 557, 526, 504 cm<sup>-1</sup>.

### 1,3-di-*tert*-butyl-5-(2-iodophenoxy)benzene (173c)

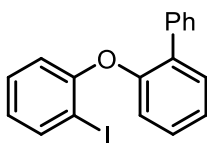


Following general procedure **E**, **172c** (6.36 g, 21.3 mmol, 1.0 eq) and *p*-toluenesulfonic acid monohydrate (12.2 g, 64.2 mmol, 3.0 eq) in acetonitrile (135 mL) were treated with potassium iodide (7.10 g, 42.8 mmol, 2.0 eq) and sodium nitrite (2.95 g, 42.8 mmol, 2.0 eq) in water (14 mL). After column chromatography (SiO<sub>2</sub>, hexane,  $R_f$  = 0.30) **173c** (6.78 g, 16.6 mmol, 76%) was obtained as a white solid.

**<sup>1</sup>H-NMR** (300 MHz, CDCl<sub>3</sub>):  $\delta$  = 7.89 – 7.81 (m, 1H), 7.29 – 7.17 (m, 2H), 6.87 (d,  $J$  = 1.7 Hz, 2H), 6.85 – 6.77 (m, 2H), 1.30 (s, 18H) ppm. **<sup>13</sup>C{<sup>1</sup>H}-NMR** (75 MHz, CDCl<sub>3</sub>):  $\delta$  = 157.5, 155.9, 153.0, 139.8, 129.5, 124.5, 118.1, 117.8, 113.9, 87.9, 35.2, 31.5 ppm. **HR-MS** (EI): calculated  $m/z$  for C<sub>20</sub>H<sub>25</sub>IO<sup>+</sup> ([M]<sup>+</sup>): 408.0950; found 408.0948. **FTIR** (ATR, neat):  $\tilde{\nu}$  = 3064, 2961, 2903, 2867, 1606, 1594, 1574, 1463, 1437, 1421, 1393, 1362, 1297, 1261, 1235, 1159, 1119, 1042, 1019, 961, 900, 875, 750, 706, 647 cm<sup>-1</sup>.

## 5. Experimental

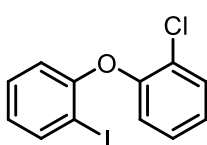
### 2-(2-iodophenoxy)-1,1'-biphenyl (173d)



Following general procedure **E**, **172d** (2.78 g, 10.6 mmol, 1.0 eq) and *p*-toluenesulfonic acid monohydrate (6.07 g, 31.9 mmol, 3.0 eq) in acetonitrile (70 mL) were treated with potassium iodide (3.53 g, 21.3 mmol, 2.0 eq) and sodium nitrite (1.47 g, 21.3 mmol, 2.0 eq) in water (8 mL). After column chromatography (SiO<sub>2</sub>, hexane/EtOAc, 50:1, *R<sub>f</sub>* = 0.24) **173d** (2.13 g, 5.72 mmol, 54%) was obtained as a pale pink oil.

**<sup>1</sup>H-NMR** (400 MHz, CDCl<sub>3</sub>): δ = 7.77 (dd, *J* = 7.9, 1.6 Hz, 1H), 7.68 – 7.60 (m, 2H), 7.48 (dd, *J* = 7.5, 1.8 Hz, 1H), 7.42 – 7.34 (m, 2H), 7.34 – 7.26 (m, 2H), 7.26 – 7.21 (m, 1H), 7.16 (ddd, *J* = 8.7, 7.3, 1.5 Hz, 1H), 6.93 (dd, *J* = 8.1, 1.3 Hz, 1H), 6.75 (td, *J* = 7.6, 1.4 Hz, 1H), 6.68 (dd, *J* = 8.2, 1.4 Hz, 1H) ppm. **<sup>13</sup>C{<sup>1</sup>H}-NMR** (101 MHz, CDCl<sub>3</sub>): δ = 156.8, 153.1, 139.8, 137.5, 133.4, 131.6, 129.5, 129.5, 128.8, 128.2, 127.4, 124.6, 124.5, 119.6, 117.9, 88.0 ppm. **HR-MS** (ESI): calculated *m/z* for C<sub>18</sub>H<sub>13</sub>IONa<sup>+</sup> ([M+Na]<sup>+</sup>): 394.9903; found 394.9905. **FTIR** (ATR, neat):  $\tilde{\nu}$  = 3059, 3027, 1577, 1502, 1476, 1462, 1431, 1250, 1227, 1196, 1157, 1117, 1074, 1042, 1018, 878, 799, 748, 737, 697, 647, 611 cm<sup>-1</sup>.

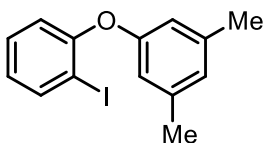
### 1-chloro-2-(2-iodophenoxy)benzene (173e)



Following General procedure **E**, **172e** (1.61 g, 7.31 mmol, 1.0 eq) and *p*-toluenesulfonic acid monohydrate (4.17 g, 21.9 mmol, 3.0 eq) in acetonitrile (45 mL) were treated with potassium iodide (2.43 g, 14.6 mmol, 2.0 eq) and sodium nitrite (1.01 g, 14.6 mmol, 2.0 eq) in water (5 mL). After column chromatography (SiO<sub>2</sub>, hexane/EtOAc, 50:1, *R<sub>f</sub>* = 0.37) **173e** was obtained as a colorless liquid.

**<sup>1</sup>H-NMR** (400 MHz, CDCl<sub>3</sub>): δ = 7.87 (dd, *J* = 7.9, 1.5 Hz, 1H), 7.48 (dd, *J* = 7.9, 1.7 Hz, 1H), 7.33 – 7.18 (m, 2H), 7.11 (td, *J* = 7.7, 1.6 Hz, 1H), 6.94 – 6.84 (m, 2H), 6.76 (dd, *J* = 8.2, 1.4 Hz, 1H) ppm. **<sup>13</sup>C{<sup>1</sup>H}-NMR** (101 MHz, CDCl<sub>3</sub>): δ = 156.2, 152.2, 140.1, 131.0, 129.7, 128.1, 125.7, 125.5, 125.0, 120.3, 118.2, 88.0 ppm. **HR-MS** (ESI): calculated *m/z* for C<sub>12</sub>H<sub>9</sub>ClIO<sup>+</sup> ([M+Na]<sup>+</sup>): 352.9201; found 352.9205. **FTIR** (ATR, neat):  $\tilde{\nu}$  = 3062, 3019, 1572, 1474, 1462, 1437, 1259, 1236, 1158, 1128, 1115, 1060, 1038, 1019, 940, 877, 795, 746, 725, 682, 646 cm<sup>-1</sup>.

### 1-(2-iodophenoxy)-3,5-dimethylbenzene (173f)

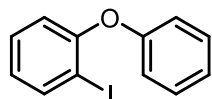


Following general procedure **E**, **172e** (1.65 g, 6.79 mmol, 1.0 eq) and *p*-toluenesulfonic acid monohydrate (3.88 g, 20.4 mmol, 3.0 eq) in acetonitrile (45 mL) were treated with potassium iodide (2.25 g, 13.6 mmol, 2.0 eq) and sodium nitrite (937 mg, 13.6 mmol, 2.0 eq) in water (8 mL). After column chromatography (SiO<sub>2</sub>, hexane, *R<sub>f</sub>* = 0.20) **173f** (2.19 g, 6.74 mmol, 98%) was obtained as a colorless liquid.

## 5.2 Synthesis and characterization of new compounds

**<sup>1</sup>H-NMR** (300 MHz, CDCl<sub>3</sub>):  $\delta$  = 7.85 (dd,  $J$  = 7.8, 1.6 Hz, 1H), 7.32 – 7.23 (m, 1H), 6.92 – 6.81 (m, 2H), 6.76 (s, 1H), 6.60 (s, 2H), 2.29 (s, 6H) ppm. **<sup>13</sup>C{<sup>1</sup>H}-NMR** (101 MHz, CDCl<sub>3</sub>):  $\delta$  = 156.9, 156.8, 139.9, 139.8, 129.7, 125.4, 125.2, 119.4, 116.3, 88.9, 21.5 ppm. **HR-MS** (ESI): calculated  $m/z$  for C<sub>14</sub>H<sub>14</sub>IO<sup>+</sup> ([M+H]<sup>+</sup>): 325.0084; found 325.0082. **FTIR** (ATR, neat):  $\tilde{\nu}$  = 3060, 3016, 2917, 2862, 1615, 1595, 1575, 1463, 1437, 1296, 1264, 1228, 1137, 1041, 1019, 951, 854, 838, 753, 720, 685, 648 cm<sup>-1</sup>.

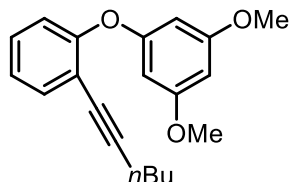
### 1-iodo-2-phenoxybenzene (173g)



Following general procedure **E**, **172g** (2.67 g, 14.4 mmol, 1.0 eq) and *p*-toluenesulfonic acid monohydrate (8.24 g, 43.3 mmol, 3.0 eq) in acetonitrile (90 mL) were treated with potassium iodide (4.79 g, 28.9 mmol, 2.0 eq) and sodium nitrite (1.99 g, 28.9 mmol, 2.0 eq) in water (10 mL). After column chromatography (SiO<sub>2</sub>, hexane/EtOAc, 50:1,  $R_f$  = 0.39) **173g** (3.81 g, 12.9 mmol, 89%) was obtained as a white solid.

**<sup>1</sup>H-NMR** (400 MHz, CDCl<sub>3</sub>):  $\delta$  = 7.87 (dd,  $J$  = 7.8, 1.5 Hz, 1H), 7.40 – 7.32 (m, 2H), 7.29 (ddd,  $J$  = 8.6, 7.3, 1.5 Hz, 1H), 7.16 – 7.09 (m, 1H), 7.00 – 6.96 (m, 2H), 6.93 – 6.83 (m, 2H) ppm. **<sup>13</sup>C{<sup>1</sup>H}-NMR** (101 MHz, CDCl<sub>3</sub>):  $\delta$  = 157.0, 156.7, 140.0, 129.9, 129.8, 125.5, 123.6, 119.6, 118.6, 89.1 ppm. **HR-MS** (EI): calculated  $m/z$  for C<sub>12</sub>H<sub>9</sub>IO<sup>+</sup> ([M]<sup>+</sup>): 295.9698; found 296.9690. **FTIR** (ATR, neat):  $\tilde{\nu}$  = 3060, 3038, 1591, 1573, 1488, 1462, 1437, 1258, 1232, 1198, 1162, 1117, 1072, 1040, 1020, 868, 796, 747, 715, 689, 646 cm<sup>-1</sup>.

### 1-(2-(hex-1-yn-1-yl)phenoxy)-3,5-dimethoxybenzene (151a)

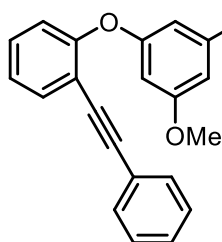


Prepared from **173a** (150 mg, 421  $\mu$ mol, 1.0 eq), PdCl<sub>2</sub>(PPh<sub>3</sub>)<sub>2</sub> (5.9 mg, 8.4  $\mu$ mol, 2 mol%), CuI (2.4 mg, 13  $\mu$ mol, 3 mol%), 1-hexyne (38.1 mg, 463  $\mu$ mol, 1.1 eq) in dry Et<sub>3</sub>N (2 mL) at room temperature for 16 h utilizing general procedure **C**. Column chromatography (SiO<sub>2</sub>, hexane/EtOAc, 50:1,  $R_f$  = 0.15) yielded **151a** (126 mg, 40.6  $\mu$ mol, 96%) as a colorless oil.

**<sup>1</sup>H-NMR** (300 MHz, CDCl<sub>3</sub>):  $\delta$  = 7.44 (dd,  $J$  = 7.6, 1.8 Hz, 1H), 7.27 – 7.19 (m, 1H), 7.07 (td,  $J$  = 7.6, 1.2 Hz, 1H), 6.97 (dd,  $J$  = 8.2, 1.2 Hz, 1H), 6.19 (t,  $J$  = 2.2 Hz, 1H), 6.14 (d,  $J$  = 2.2 Hz, 2H), 3.74 (s, 6H), 2.35 (t,  $J$  = 6.9 Hz, 2H), 1.53 – 1.29 (m, 4H), 0.87 (t,  $J$  = 7.2 Hz, 3H) ppm. **<sup>13</sup>C{<sup>1</sup>H}-NMR** (101 MHz, CDCl<sub>3</sub>):  $\delta$  = 161.6, 159.7, 156.8, 133.8, 128.9, 124.0, 120.1, 117.2, 96.7, 95.8, 95.2, 76.1, 55.5, 30.8, 22.0, 19.5, 13.8 ppm. **HR-MS** (ESI): calculated  $m/z$  for C<sub>20</sub>H<sub>23</sub>O<sub>2</sub><sup>+</sup> ([M+H]<sup>+</sup>): 311.1642; found 311.1636. **FTIR** (ATR, neat):  $\tilde{\nu}$  = 3001, 2956, 2932, 2871, 2838, 1594, 1570, 1486, 1473, 1441, 1324, 1253, 1204, 1152, 1133, 1105, 1065, 991, 977, 944, 930, 822, 770, 748, 682, 539 cm<sup>-1</sup>.

## 5. Experimental

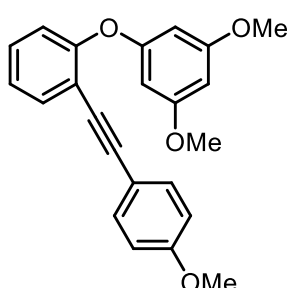
### 1,3-dimethoxy-5-(2-(phenylethynyl)phenoxy)benzene (**151b**)



Prepared from **173a** (300 mg, 842  $\mu\text{mol}$ , 1.0 eq),  $\text{PdCl}_2(\text{PPh}_3)_2$  (11.8 mg, 16.9  $\mu\text{mol}$ , 2 mol%),  $\text{CuI}$  (4.8 mg, 25  $\mu\text{mol}$ , 3 mol%), phenylacetylene (94.6 mg, 927  $\mu\text{mol}$ , 1.1 eq) in dry  $\text{Et}_3\text{N}$  (4 mL) at room temperature for 18 h utilizing general procedure **C**. Column chromatography ( $\text{SiO}_2$ , hexane/ $\text{EtOAc}$ , 30:1,  $R_f = 0.23$  (hexane/ $\text{EtOAc}$ , 10:1)) yielded **151b** (274 mg, 829  $\mu\text{mol}$ , 98%) as a yellow oil.

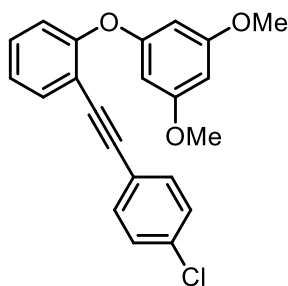
**$^1\text{H-NMR}$**  (400 MHz,  $\text{CDCl}_3$ ):  $\delta = 7.57$  (dd,  $J = 7.7, 1.7$  Hz, 1H), 7.40 – 7.38 (m, 2H), 7.33 – 7.28 (m, 4H), 7.13 (td,  $J = 7.5, 1.2$  Hz, 1H), 7.03 (dd,  $J = 8.2, 1.3$  Hz, 1H), 6.22 (t,  $J = 2.2$  Hz, 1H), 6.20 (d,  $J = 2.1$  Hz, 2H), 3.75 (s, 6H) ppm.  **$^{13}\text{C}\{^1\text{H}\}\text{-NMR}$**  (101 MHz,  $\text{CDCl}_3$ ):  $\delta = 161.7, 159.5, 157.0, 133.7, 131.8, 129.8, 128.4, 128.3, 124.0, 123.4, 120.0, 116.3, 97.0, 95.5, 94.5, 85.2, 55.6$  ppm. **HR-MS** (ESI): calculated  $m/z$  for  $\text{C}_{22}\text{H}_{19}\text{O}_3^+$  ( $[\text{M}+\text{H}]^+$ ): 331.1329; found 331.1335. **FTIR** (ATR, neat):  $\tilde{\nu} = 3059, 3000, 2957, 2938, 2836, 1590, 1569, 1495, 1471, 1439, 1427, 1263, 1215, 1202, 1149, 1097, 1051, 989, 975, 929, 822, 752, 687, 537$   $\text{cm}^{-1}$ .

### 1,3-dimethoxy-5-(2-((4-methoxyphenyl)ethynyl)phenoxy)benzene (**151c**)



Prepared from **173a** (1.00 g, 2.81 mmol, 1.0 eq),  $\text{PdCl}_2(\text{PPh}_3)_2$  (98.5 mg, 140  $\mu\text{mol}$ , 5 mol%),  $\text{CuI}$  (53.5 mg, 281  $\mu\text{mol}$ , 10 mol%), 4-ethynylanisole (408 mg, 3.09 mmol, 1.1 eq) in dry  $\text{Et}_3\text{N}$  (30 mL) at room temperature for 18 h utilizing general procedure **C**. Column chromatography ( $\text{SiO}_2$ , hexane/ $\text{EtOAc}$ , 30:1,  $R_f = 0.09$  (hexane/ $\text{EtOAc}$ , 20:1)) followed by recrystallization from ethanol yielded **151c** (912 mg, 2.53 mmol, 90%) as colorless needles. Mp: 69–71  $^\circ\text{C}$ .

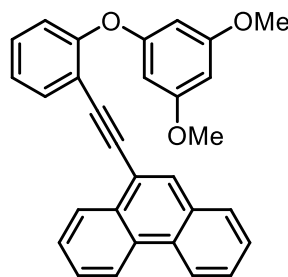
**$^1\text{H-NMR}$**  (300 MHz,  $\text{CDCl}_3$ ):  $\delta = 7.54$  (dd,  $J = 7.7, 1.8$  Hz, 1H), 7.35 – 7.28 (m, 2H), 7.29 – 7.24 (m, 2H), 7.12 (td,  $J = 7.6, 1.2$  Hz, 1H), 7.02 (dd,  $J = 8.2, 1.1$  Hz, 1H), 6.86 – 6.72 (m, 2H), 6.27 – 6.10 (m, 3H), 3.81 (s, 3H), 3.74 (s, 6H) ppm.  **$^{13}\text{C}\{^1\text{H}\}\text{-NMR}$**  (75 MHz,  $\text{CDCl}_3$ ):  $\delta = 161.7, 159.7, 159.6, 156.8, 133.5, 133.2, 129.4, 124.0, 120.1, 116.7, 115.5, 114.0, 96.9, 95.4, 94.5, 83.8, 55.6, 55.4$  ppm. **HR-MS** (ESI): calculated  $m/z$  for  $\text{C}_{20}\text{H}_{23}\text{O}_3^+$  ( $[\text{M}]^+$ ): 361.1434; found 361.1437. **FTIR** (ATR, neat):  $\tilde{\nu} = 3004, 2960, 2953, 2837, 1605, 1512, 1473, 1441, 1288, 1249, 1218, 1204, 1153, 1132, 1064, 1032, 975, 913, 831, 764, 746, 681, 669, 654$   $\text{cm}^{-1}$ .

**1-(2-((4-chlorophenyl)ethynyl)phenoxy)-3,5-dimethoxybenzene (151d)**

Prepared from **173a** (250 mg, 702  $\mu\text{mol}$ , 1.0 eq),  $\text{PdCl}_2(\text{PPh}_3)_2$  (9.9 mg, 14  $\mu\text{mol}$ , 2 mol%),  $\text{CuI}$  (4.0 mg, 21  $\mu\text{mol}$ , 3 mol%), 1-chloro-4-methoxybenzene (105 mg, 772  $\mu\text{mol}$ , 1.1 eq) in dry  $\text{Et}_3\text{N}$  (2.5 mL) at room temperature for 16 h utilizing general procedure **C**. Column chromatography ( $\text{SiO}_2$ , hexane/ $\text{EtOAc}$ , 50:1,  $R_f = 0.16$  (hexane/ $\text{EtOAc}$ , 30:1)) yielded **151d** (245 mg, 672  $\mu\text{mol}$ , 96%) as

a yellow liquid.

**$^1\text{H-NMR}$**  (400 MHz,  $\text{CDCl}_3$ ):  $\delta = 7.55$  (dd,  $J = 7.7, 1.5$  Hz, 1H), 7.35 – 7.23 (m, 5H), 7.13 (td,  $J = 7.6, 1.2$  Hz, 1H), 7.03 (dd,  $J = 8.2, 1.2$  Hz, 1H), 6.22 (t,  $J = 2.0$  Hz, 1H), 6.19 (d,  $J = 2.2$  Hz, 2H), 3.75 (s, 6H).  **$^{13}\text{C}\{^1\text{H}\}\text{-NMR}$**  (101 MHz,  $\text{CDCl}_3$ ):  $\delta = 161.7, 159.4, 157.1, 134.4, 133.7, 133.0, 130.1, 128.7, 124.0, 121.9, 120.0, 115.9, 97.0, 95.5, 93.3, 86.2, 55.6$  ppm. **HR-MS** (ESI): calculated  $m/z$  for  $\text{C}_{22}\text{H}_{18}\text{ClO}_3^+$  ( $[\text{M}+\text{H}]^+$ ): 365.0939; found 369.0939. **FTIR** (ATR, neat):  $\tilde{\nu} = 3066, 3000, 2959, 2940, 2838, 1595, 1569, 1495, 1473, 1440, 1263, 1219, 1204, 1152, 1131, 1090, 1064, 1013, 991, 976, 944, 930, 826, 750, 720, 682$   $\text{cm}^{-1}$ .

**9-((2-((3,5-dimethoxyphenoxy)phenyl)ethynyl)phenanthrene (151e)**

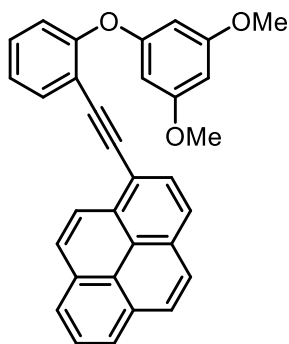
Prepared from 9-bromophenanthrene (150 mg, 590  $\mu\text{mol}$ , 1.0 eq),  $\text{PdCl}_2(\text{PPh}_3)_2$  (20.7 mg, 29.5  $\mu\text{mol}$ , 5 mol%),  $\text{CuI}$  (11.2 mg, 60.0  $\mu\text{mol}$ , 10 mol%), **174** (496 mg, 5.05 mmol, 1.1 eq) in dry  $\text{Et}_3\text{N}$  (2 mL) 65  $^\circ\text{C}$  for 24 h utilizing general procedure **C**. Column chromatography ( $\text{SiO}_2$ , hexane  $\rightarrow$  hexane/ $\text{EtOAc}$  9:1,  $R_f = 0.21$  (hexane/ $\text{EtOAc}$ , 10:1)) yielded **151e** (150 mg, 348  $\mu\text{mol}$ , 65%) as

a yellow solid.

**$^1\text{H-NMR}$**  (600 MHz,  $\text{CDCl}_3$ ):  $\delta = 8.70 - 8.61$  (m, 2H), 8.35 (ddd,  $J = 8.1, 1.5, 0.6$  Hz, 1H), 7.95 (s, 1H), 7.84 (ddt,  $J = 7.9, 1.4, 0.6$  Hz, 1H), 7.72 (ddd,  $J = 7.7, 1.7, 0.4$  Hz, 1H), 7.66 (dddd,  $J = 8.3, 6.9, 2.9, 1.4$  Hz, 2H), 7.59 (ddd,  $J = 8.0, 6.9, 1.1$  Hz, 1H), 7.55 (ddd,  $J = 8.1, 6.9, 1.2$  Hz, 1H), 7.37 (ddd,  $J = 8.2, 7.4, 1.7$  Hz, 1H), 7.22 (td,  $J = 7.5, 1.2$  Hz, 1H), 7.13 (ddd,  $J = 8.2, 1.2, 0.4$  Hz, 1H), 6.28 (d,  $J = 2.2$  Hz, 2H), 6.26 (t,  $J = 2.2$  Hz, 1H), 3.75 (s, 6H) ppm.  **$^{13}\text{C}\{^1\text{H}\}\text{-NMR}$**  (151 MHz,  $\text{CDCl}_3$ ):  $\delta = 161.8, 159.8, 156.8, 133.7, 132.0, 131.4, 131.2, 130.5, 130.1, 130.0, 128.7, 127.6, 127.4, 127.2, 127.1, 127.0, 124.3, 122.74, 122.72, 120.6, 119.9, 116.8, 96.6, 95.4, 92.9, 89.7, 55.6$  ppm. **HR-MS** (ESI): calculated  $m/z$  for  $\text{C}_{30}\text{H}_{23}\text{O}_3^+$  ( $[\text{M}+\text{H}]^+$ ): 431.1642; found 431.1646. **FTIR** (ATR, neat):  $\tilde{\nu} = 3054, 3004, 2957, 2936, 2901, 2836, 1591, 1569, 1472, 1438, 1381, 1257, 1219, 1202, 1150, 1129, 1051, 990, 975, 945, 891, 820, 744, 723, 680, 617$   $\text{cm}^{-1}$ .

## 5. Experimental

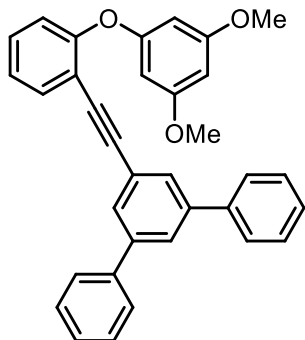
### 1-((2-(3,5-dimethoxyphenoxy)phenyl)ethynyl)pyrene (151f)



Prepared from 1-bromopyrene (151 mg, 536  $\mu\text{mol}$ , 1.0 eq),  $\text{PdCl}_2(\text{PPh}_3)_2$  (18.8 mg, 26.8  $\mu\text{mol}$ , 5 mol%),  $\text{CuI}$  (10.2 mg, 53.6  $\mu\text{mol}$ , 10 mol%), **174** (150 mg, 590  $\mu\text{mol}$ , 1.1 eq) in dry  $\text{Et}_3\text{N}$  (2 mL) 65 °C for 18 h utilizing general procedure **C**. Column chromatography ( $\text{SiO}_2$ , hexane/ $\text{EtOAc}$ , 30:1,  $R_f$  = 0.17 (hexane/ $\text{EtOAc}$ , 30:1)) yielded **151f** (144 mg, 315  $\mu\text{mol}$ , 59%) as a yellow solid.

**$^1\text{H-NMR}$**  (600 MHz,  $\text{CDCl}_3$ ):  $\delta$  = 8.45 (d,  $J$  = 9.0 Hz, 1H), 8.23 – 8.14 (m, 2H), 8.10 – 8.06 (m, 3H), 8.05 – 7.99 (m, 3H), 7.77 (ddd,  $J$  = 7.6, 1.7, 0.5 Hz, 1H), 7.38 (ddd,  $J$  = 8.2, 7.4, 1.7 Hz, 1H), 7.24 (td,  $J$  = 7.5, 1.2 Hz, 1H), 7.15 (ddd,  $J$  = 8.2, 1.2, 0.4 Hz, 1H), 6.33 (d,  $J$  = 2.2 Hz, 2H), 6.28 (t,  $J$  = 2.2 Hz, 1H), 3.77 (s, 6H) ppm.  **$^{13}\text{C}\{^1\text{H}\}\text{-NMR}$**  (151 MHz,  $\text{CDCl}_3$ ):  $\delta$  = 161.9, 159.9, 156.7, 133.7, 132.2, 131.41, 131.36, 131.2, 130.0, 129.7, 128.4, 128.3, 127.4, 126.3, 126.0, 125.7, 125.6, 124.5, 124.4, 124.3, 120.5, 118.0, 117.0, 96.7, 95.4, 93.8, 90.9, 55.6 ppm. **HR-MS** (ESI): calculated  $m/z$  for  $\text{C}_{32}\text{H}_{23}\text{O}_3^+$  ( $[\text{M}+\text{H}]^+$ ): 455.1642; found 455.1647. **FTIR** (ATR, neat):  $\tilde{\nu}$  = 3074, 3042, 2962, 2939, 2838, 2005, 1587, 1568, 1506, 1473, 1441, 1424, 1324, 1302, 1266, 1240, 1218, 1192, 1150, 1132, 1092, 1060, 1050, 989, 972, 951, 926, 905, 874, 843, 818, 786, 765, 747, 716, 679, 653, 610, 583, 532  $\text{cm}^{-1}$ .

### 5'-((2-(3,5-dimethoxyphenoxy)phenyl)ethynyl)-1,1':3',1''-terphenyl (151g)

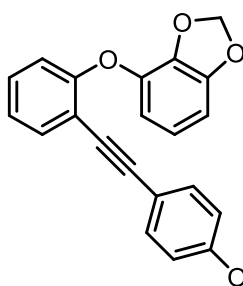


Prepared from 5'-bromo-1,1':3',1''-terphenyl (166 mg, 536  $\mu\text{mol}$ , 1.0 eq),  $\text{PdCl}_2(\text{PPh}_3)_2$  (18.8 mg, 26.8  $\mu\text{mol}$ , 5 mol%),  $\text{CuI}$  (10.2 mg, 53.6  $\mu\text{mol}$ , 10 mol%), **174** (150 mg, 590  $\mu\text{mol}$ , 1.1 eq) in dry  $\text{Et}_3\text{N}$  (2 mL) 65 °C for 18 h utilizing general procedure **C**. Column chromatography ( $\text{SiO}_2$ , hexane/ $\text{EtOAc}$ , 30:1,  $R_f$  = 0.27 (hexane/ $\text{EtOAc}$ , 10:1)) yielded **151g** as an off-white solid.

**$^1\text{H-NMR}$**  (600 MHz,  $\text{CDCl}_3$ ):  $\delta$  = 7.73 (t,  $J$  = 1.8 Hz, 1H), 7.65 – 7.58 (m, 5H), 7.56 (d,  $J$  = 1.7 Hz, 2H), 7.50 – 7.43 (m, 4H), 7.40 – 7.37 (m, 2H), 7.34 (ddd,  $J$  = 8.2, 7.4, 1.7 Hz, 1H), 7.17 (td,  $J$  = 7.5, 1.2 Hz, 1H), 7.09 (dd,  $J$  = 8.3, 1.1 Hz, 1H), 6.24 – 6.16 (m, 3H), 3.69 (s, 6H) ppm.  **$^{13}\text{C}\{^1\text{H}\}\text{-NMR}$**  (151 MHz,  $\text{CDCl}_3$ ):  $\delta$  = 161.7, 159.7, 156.9, 142.0, 140.5, 133.7, 130.0, 129.3, 129.0, 127.8, 127.4, 126.2, 124.2, 124.2, 120.5, 116.4, 96.7, 95.3, 94.7, 85.4, 77.4, 77.2, 76.9, 55.5 ppm. **HR-MS** (ESI): calculated  $m/z$  for  $\text{C}_{34}\text{H}_{27}\text{O}_3^+$  ( $[\text{M}+\text{H}]^+$ ): 483.1955; found 483.1956. **FTIR** (ATR, neat):  $\tilde{\nu}$  = 3080, 3059, 3034, 3003, 2968, 2941, 2839, 1592, 1497, 1474, 1450, 1412, 1254, 1208, 1201, 1146, 1133, 1097, 101065, 1052, 978, 926, 909, 887, 873, 829, 815, 772, 756, 695, 678, 651, 614, 602, 533  $\text{cm}^{-1}$ .

## 5.2 Synthesis and characterization of new compounds

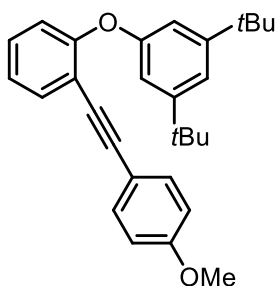
### 4-(2-((4-methoxyphenyl)ethynyl)phenoxy)benzo[d][1,3]dioxole (151h)



Prepared from **173b** (500 mg, 1.47 mmol, 1.0 eq), PdCl<sub>2</sub>(PPh<sub>3</sub>)<sub>2</sub> (20.6 mg, 29.4 μmol, 2 mol%), CuI (8.4 mg, 44 μmol, 3 mol%), 4-ethynylanisole (214 mg, 1.62 mmol, 1.1 eq) in dry Et<sub>3</sub>N/THF (2:1, 9 mL) at room temperature for 16 h utilizing general procedure **C**. Column chromatography (SiO<sub>2</sub>, hexane → hexane/EtOAc, 9:1, R<sub>f</sub> = 0.18 (hexane/EtOAc, 10:1)) yielded **151h** (466 mg, 1.35 mmol, 92%) as a colorless liquid.

**<sup>1</sup>H-NMR** (400 MHz, CDCl<sub>3</sub>): δ = 7.54 (dd, *J* = 7.7, 1.7 Hz, 1H), 7.40 – 7.32 (m, 2H), 7.29 – 7.22 (m, 1H), 7.10 (td, *J* = 7.5, 1.2 Hz, 1H), 6.96 (d, *J* = 8.2 Hz, 1H), 6.83 (d, *J* = 8.7 Hz, 2H), 6.79 (t, *J* = 8.2 Hz, 1H), 6.66 (d, *J* = 7.9 Hz, 1H), 6.56 (d, *J* = 8.5 Hz, 1H), 5.95 (s, 2H), 3.81 (s, 3H) ppm. **<sup>13</sup>C{<sup>1</sup>H}-NMR** (101 MHz, CDCl<sub>3</sub>): δ = 159.7, 157.0, 149.6, 140.2, 137.5, 133.6, 133.2, 129.3, 123.6, 122.1, 118.1, 115.6, 115.5, 114.0, 113.8, 104.6, 101.7, 94.6, 83.7, 55.4 ppm. **HR-MS** (ESI): calculated *m/z* for C<sub>22</sub>H<sub>17</sub>O<sub>4</sub><sup>+</sup> ([M+H]<sup>+</sup>): 345.1121; found 345.1120. **FTIR** (ATR, neat):  $\tilde{\nu}$  = 3067, 3004, 2957, 2896, 2837, 2776, 1630, 1606, 1570, 1510, 1482, 1459, 1442, 1357, 1286, 1245, 1207, 1173, 1100, 1058, 1012, 928, 866, 830, 783, 747, 712, 657, 604 cm<sup>-1</sup>.

### 1,3-di-*tert*-butyl-5-(2-((4-methoxyphenyl)ethynyl)phenoxy)benzene (151i)



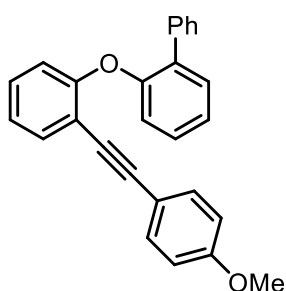
Prepared from **173c** (2.00 g, 4.90 mmol, 1.0 eq), PdCl<sub>2</sub>(PPh<sub>3</sub>)<sub>2</sub> (68.8 mg, 98 μmol, 2 mol%), CuI (28.0 mg, 147 μmol, 3 mol%), 4-ethynylanisole (712 mg, 5.39 mmol, 1.1 eq) in dry Et<sub>3</sub>N (25 mL) at room temperature for 12 h utilizing general procedure **C**. Column chromatography (SiO<sub>2</sub>, hexane/EtOAc, 30:1, R<sub>f</sub> = 0.24) yielded **151i** (1.98 g, 4.80 mmol, 98%) as a colorless oil.

**<sup>1</sup>H-NMR** (400 MHz, CDCl<sub>3</sub>): δ = 7.56 (dt, *J* = 7.8, 1.2 Hz, 1H), 7.30 – 7.23 (m, 3H), 7.21 – 7.18 (m, 1H), 7.08 (td, *J* = 7.5, 1.2 Hz, 1H), 6.96 – 6.91 (m, 3H), 6.83 – 6.78 (m, 2H), 3.80 (s, 3H), 1.31 (s, 18H) ppm. **<sup>13</sup>C{<sup>1</sup>H}-NMR** (75 MHz, CDCl<sub>3</sub>): δ = 159.6, 157.8, 156.5, 152.7, 133.5, 133.2, 129.4, 123.0, 118.6, 117.4, 115.7, 115.6, 113.9, 113.2, 94.6, 84.3, 55.4, 35.1, 31.5 ppm. **HR-MS** (ESI): calculated *m/z* for C<sub>29</sub>H<sub>32</sub>O<sub>2</sub><sup>+</sup> ([M+H]<sup>+</sup>): 413.2475; found 413.2475. **FTIR** (ATR, neat):  $\tilde{\nu}$  = 3067, 2954, 2902, 2866, 2836, 1605, 1585, 1569, 1510, 1481, 1442, 1419, 1362, 1287, 1245, 1227, 1173, 1158, 1099, 1031, 961, 904, 873, 858, 830, 806, 774, 753, 732, 707, 649 cm<sup>-1</sup>.

### 2-(2-((4-methoxyphenyl)ethynyl)phenoxy)-1,1'-biphenyl (151j)

Prepared from **173d** (250 mg, 672 μmol, 1.0 eq), PdCl<sub>2</sub>(PPh<sub>3</sub>)<sub>2</sub> (9.4 mg, 13 μmol, 2 mol%), CuI (3.8 mg, 20 μmol, 3 mol%), 4-ethynylanisole (97.7 mg, 739 μmol, 1.1 eq) in dry Et<sub>3</sub>N (3 mL) at room temperature for 18 h utilizing general procedure **C**. Column chromatography

## 5. Experimental

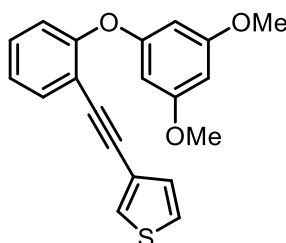


(SiO<sub>2</sub>, hexane/EtOAc, 50:1, *R*<sub>f</sub> = 0.16 (hexane/ EtOAc, 30:1)) yielded **151j** (174 mg, 462 μmol, 69%) as a colorless oil.

**<sup>1</sup>H-NMR** (300 MHz, CDCl<sub>3</sub>): δ = 7.77 – 7.68 (m, 2H), 7.49 (td, *J* = 7.6, 1.8 Hz, 2H), 7.42 – 7.32 (m, 2H), 7.34 – 7.13 (m, 6H), 7.05 (td, *J* = 7.5, 1.2 Hz, 1H), 6.91 (ddd, *J* = 11.0, 8.1, 1.2 Hz, 2H), 6.85 – 6.76 (m, 2H), 3.80 (s, 3H) ppm. **<sup>13</sup>C{<sup>1</sup>H}-NMR** (101 MHz, CDCl<sub>3</sub>):

δ = 159.7, 157.1, 154.2, 137.9, 133.5, 133.1, 132.4, 131.3, 129.6, 129.3, 128.6, 128.2, 127.2, 123.6, 123.4, 119.3, 118.2, 116.1, 115.6, 114.0, 94.5, 84.3, 55.4 ppm. **HR-MS** (ESI): calculated *m/z* for C<sub>27</sub>H<sub>20</sub>O<sub>2</sub>Na<sup>+</sup> ([M+Na]<sup>+</sup>): 377.1536; found 377.1533. **FTIR** (ATR, neat):  $\tilde{\nu}$  = 3060, 3033, 2957, 2933, 2836, 1606, 1568, 1511, 1476, 1443, 1432, 1288, 1250, 1227, 1174, 1108, 1031, 1011, 884, 831, 802, 752, 699 cm<sup>-1</sup>.

### 3-((2-(3,5-dimethoxyphenoxy)phenyl)ethynyl)thiophene (**151k**)

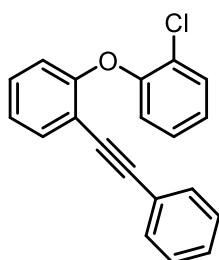


Prepared from **173a** (250 mg, 702 μmol, 1.0 eq), PdCl<sub>2</sub>(PPh<sub>3</sub>)<sub>2</sub> (9.9 mg, 14 μmol, 2 mol%), CuI (4.0 mg, 21 μmol, 3 mol%), 3-ethynylthiophene (83.5 mg, 772 μmol, 1.1 eq) in dry Et<sub>3</sub>N (3 mL) at room temperature for 18 h utilizing general procedure **C**. Column chromatography (SiO<sub>2</sub>, hexane/EtOAc, 30:1, *R*<sub>f</sub> = 0.21

(hexane/EtOAc, 10:1)) yielded **151k** (226 mg, 672 μmol, 96%) as an orange oil.

**<sup>1</sup>H-NMR** (400 MHz, CDCl<sub>3</sub>): δ = 7.55 (dd, *J* = 7.6, 1.7 Hz, 1H), 7.39 (dd, *J* = 3.0, 1.1 Hz, 1H), 7.29 (ddd, *J* = 8.4, 7.4, 1.7 Hz, 1H), 7.24 (dd, *J* = 5.0, 3.0 Hz, 1H), 7.12 (td, *J* = 7.6, 1.2 Hz, 1H), 7.06 (dd, *J* = 5.0, 1.1 Hz, 1H), 7.02 (dd, *J* = 8.2, 1.2 Hz, 1H), 6.22 (t, *J* = 2.2 Hz, 1H), 6.19 (d, *J* = 2.2 Hz, 2H), 3.74 (s, 6H) ppm. **<sup>13</sup>C{<sup>1</sup>H}-NMR** (101 MHz, CDCl<sub>3</sub>): δ = 161.7, 159.5, 157.0, 133.6, 130.0, 129.7, 128.9, 125.3, 123.9, 122.4, 119.9, 116.2, 97.1, 95.5, 89.6, 84.7, 55.6 ppm. **HR-MS** (ESI): calculated *m/z* for C<sub>20</sub>H<sub>17</sub>O<sub>3</sub>S<sup>+</sup> ([M+H]<sup>+</sup>): 337.0893; found 337.0896. **FTIR** (ATR, neat):  $\tilde{\nu}$  = 3104, 3000, 2956, 2938, 2836, 1591, 1570, 1523, 1471, 1439, 1356, 1260, 1217, 1200, 1149, 1126, 1097, 1050, 989, 975, 940, 930, 869, 844, 820, 777, 750, 681, 624, 577, 539 cm<sup>-1</sup>.

### 1-chloro-2-(2-(phenylethynyl)phenoxy)benzene (**151l**)



Prepared from **173e** (230 mg, 696 μmol, 1.0 eq), PdCl<sub>2</sub>(PPh<sub>3</sub>)<sub>2</sub> (9.8 mg, 14 μmol, 2 mol%), CuI (4.0 mg, 21 μmol, 3 mol%), phenylacetylene (78.2 mg, 765 μmol, 1.1 eq) in dry Et<sub>3</sub>N (3 mL) at room temperature for 18 h utilizing general procedure **C**. Column chromatography (SiO<sub>2</sub>, hexane/EtOAc, 50:1, *R*<sub>f</sub> = 0.29 (hexane/ EtOAc, 30:1)) yielded **151l**

(202 mg, 663 μmol, 95%) as a yellow oil.

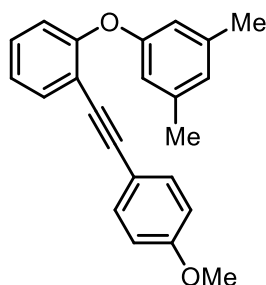
**<sup>1</sup>H-NMR** (400 MHz, CDCl<sub>3</sub>): δ = 7.59 (dd, *J* = 7.6, 1.7 Hz, 1H), 7.47 (dd, *J* = 7.9, 1.7 Hz, 1H), 7.42 – 7.35 (m, 2H), 7.33 – 7.27 (m, 4H), 7.23 – 7.12 (m, 2H), 7.04 (td, *J* = 7.7, 1.5 Hz,



## 5.2 Synthesis and characterization of new compounds

1H), 6.96 (dd,  $J = 8.2, 1.1$  Hz, 1H), 6.89 (dd,  $J = 8.1, 1.5$  Hz, 1H) ppm.  $^{13}\text{C}\{^1\text{H}\}$ -NMR (101 MHz,  $\text{CDCl}_3$ ):  $\delta = 156.7, 153.2, 133.9, 131.7, 130.8, 129.8, 128.4, 128.3, 127.9, 124.9, 124.17, 124.16, 123.3, 119.4, 119.2, 116.0, 94.9, 84.7$  ppm. **HR-MS** (ESI): calculated  $m/z$  for  $\text{C}_{20}\text{H}_{14}\text{ClO}^+$  ( $[\text{M}+\text{H}]^+$ ): 305.0728; found 305.0728. **FTIR** (ATR, neat):  $\tilde{\nu} = 3061, 3032, 2954, 2923, 1585, 1569, 1496, 1474, 1443, 1261, 1235, 1201, 1158, 1129, 1098, 1059, 1035, 942, 915, 885, 838, 795, 750, 689$   $\text{cm}^{-1}$ .

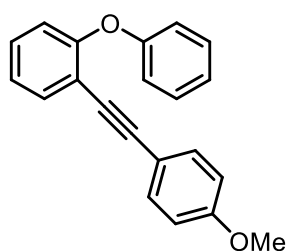
### 1-(2-((4-methoxyphenyl)ethynyl)phenoxy)-3,5-dimethylbenzene (151m)



Prepared from **173f** (500 mg, 1.54 mmol, 1.0 eq),  $\text{PdCl}_2(\text{PPh}_3)_2$  (21.7 mg, 30.9  $\mu\text{mol}$ , 2 mol%),  $\text{CuI}$  (8.8 mg, 46  $\mu\text{mol}$ , 3 mol%), 4-ethynylanisole (224 mg, 1.70 mmol, 1.1 eq) in dry  $\text{Et}_3\text{N}$  (8 mL) at room temperature for 16 h utilizing general procedure **C**. Column chromatography ( $\text{SiO}_2$ , hexane/ $\text{EtOAc}$ , 50:1,  $R_f = 0.15$ ) yielded **151m** (507 mg, 1.52 mmol, 98%) as a white solid.

$^1\text{H}$ -NMR (300 MHz,  $\text{CDCl}_3$ ):  $\delta = 7.54$  (dd,  $J = 7.6, 1.7$  Hz, 1H), 7.37 – 7.26 (m, 2H), 7.32 – 7.20 (m, 1H), 7.09 (td,  $J = 7.6, 1.1$  Hz, 1H), 6.95 (dd,  $J = 8.2, 1.1$  Hz, 1H), 6.85 – 6.78 (m, 2H), 6.73 (s, 1H), 6.66 (s, 2H), 3.81 (s, 3H), 2.29 (s, 6H).  $^{13}\text{C}\{^1\text{H}\}$ -NMR (101 MHz,  $\text{CDCl}_3$ ):  $\delta = 159.7, 157.6, 139.6, 133.5, 133.2, 129.4, 124.9, 123.4$  (2 C), 119.5, 116.29, 116.25, 115.6, 114.0, 94.4, 84.1, 55.4, 21.5. **HR-MS** (ESI): calculated  $m/z$  for  $\text{C}_{23}\text{H}_{21}\text{O}_2^+$  ( $[\text{M}+\text{H}]^+$ ): 329.1536; found 329.1532. **FTIR** (ATR, neat):  $\tilde{\nu} = 3008, 2955, 2918, 2835, 2218, 1606, 1589, 1568, 1511, 1482, 1443, 1294, 1248, 1224, 1136, 1100, 1032, 948, 832, 760, 686$   $\text{cm}^{-1}$ .

### 1-((4-methoxyphenyl)ethynyl)-2-phenoxybenzene (151n)

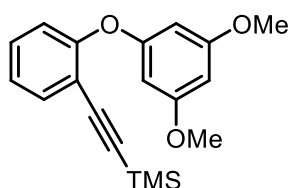


Prepared from **173g** (200 mg, 675  $\mu\text{mol}$ , 1.0 eq),  $\text{PdCl}_2(\text{PPh}_3)_2$  (9.5 mg, 14  $\mu\text{mol}$ , 2 mol%),  $\text{CuI}$  (3.9 mg, 20  $\mu\text{mol}$ , 3 mol%), 4-ethynylanisole (98.2 mg, 743  $\mu\text{mol}$ , 1.1 eq) in dry  $\text{Et}_3\text{N}$  (3 mL) at room temperature for 18 h utilizing general procedure **C**. Column chromatography ( $\text{SiO}_2$ , hexane/ $\text{EtOAc}$ , 50:1,  $R_f = 0.17$  (hexane/ $\text{EtOAc}$ , 30:1)) yielded **151n** (195 mg, 649  $\mu\text{mol}$ , 96%) as a white solid.

$^1\text{H}$ -NMR (400 MHz,  $\text{CDCl}_3$ ):  $\delta = 7.57$  (dd,  $J = 7.7, 1.7$  Hz, 1H), 7.38 – 7.32 (m, 2H), 7.32 – 7.24 (m, 3H), 7.16 – 7.06 (m, 2H), 7.06 – 6.98 (m, 3H), 6.84 – 6.78 (m, 2H), 3.81 (s, 3H) ppm.  $^{13}\text{C}\{^1\text{H}\}$ -NMR (101 MHz,  $\text{CDCl}_3$ ):  $\delta = 159.7, 157.7, 157.0, 133.6, 133.2, 129.7, 129.5, 123.8, 123.0, 119.9, 118.2, 116.6, 115.5, 114.0, 94.7, 83.9, 55.4$  ppm. **HR-MS** (ESI): calculated  $m/z$  for  $\text{C}_{21}\text{H}_{17}\text{O}_2^+$  ( $[\text{M}+\text{H}]^+$ ): 301.1223; found 301.1220. **FTIR** (ATR, neat):  $\tilde{\nu} = 3068, 3037, 3006, 2934, 2908, 2836, 1605, 1569, 1510, 1481, 1444, 1288, 1248, 1231, 1174, 1161, 1099, 1072, 1031, 882, 831, 799, 780, 750, 691$   $\text{cm}^{-1}$ .

## 5. Experimental

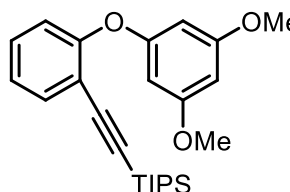
### **((2-(3,5-dimethoxyphenoxy)phenyl)ethynyl)trimethylsilane (151o)**



Prepared from **173a** (1.50 g, 4.21 mmol, 1.0 eq), PdCl<sub>2</sub>(PPh<sub>3</sub>)<sub>2</sub> (73.9 mg, 105 μmol, 2 mol%), CuI (40.1 mg, 211 μmol, 3 mol%), TMS-acetylene (496 mg, 5.05 mmol, 1.2 eq) in dry Et<sub>3</sub>N (27 mL) at room temperature for 18 h utilizing general procedure **C**. Column chromatography (SiO<sub>2</sub>, hexane/EtOAc, 40:1, *R<sub>f</sub>* = 0.20 (hexane/EtOAc, 30:1)) yielded **151o** (1.28 g, 3.91 mmol, 93%) as a pale yellow oil.

**<sup>1</sup>H-NMR** (400 MHz, CDCl<sub>3</sub>): δ = 7.49 (dd, *J* = 7.7, 1.7 Hz, 1H), 7.33 – 7.22 (m, 1H), 7.08 (ddd, *J* = 8.2, 7.5, 1.2 Hz, 1H), 6.99 (dd, *J* = 8.2, 1.2 Hz, 1H), 6.20 (t, *J* = 2.2 Hz, 1H), 6.14 (d, *J* = 2.2 Hz, 2H), 3.74 (d, *J* = 1.1 Hz, 6H), 0.14 (s, 9H) ppm. **<sup>13</sup>C{<sup>1</sup>H}-NMR** (101 MHz, CDCl<sub>3</sub>): δ = 161.6, 159.6, 157.3, 134.1, 130.0, 123.9, 120.2, 116.2, 100.4, 100.0, 96.8, 95.3, 55.6, -0.1 ppm. **HR-MS** (ESI): calculated *m/z* for C<sub>19</sub>H<sub>23</sub>O<sub>3</sub>Si<sup>+</sup> ([M+H]<sup>+</sup>): 327.1411; found 327.1410. **FTIR** (ATR, neat):  $\tilde{\nu}$  = 3001, 2957, 2898, 2838, 2160, 1592, 1472, 1439, 1237, 1197, 1150, 1130, 1101, 1053, 990, 976, 943, 930, 865, 838, 823, 757, 698, 680, 643, 539 cm<sup>-1</sup>.

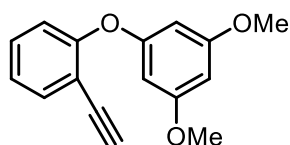
### **((2-(3,5-dimethoxyphenoxy)phenyl)ethynyl)triisopropylsilane (151p)**



Prepared from **173a** (250 mg, 702 μmol, 1.0 eq), PdCl<sub>2</sub>(PPh<sub>3</sub>)<sub>2</sub> (12.3 mg, 17.6 μmol, 2 mol%), CuI (6.7 mg, 35 μmol, 3 mol%), TIPS-acetylene (154 mg, 842 μmol, 1.2 eq) in dry Et<sub>3</sub>N (5 mL) at room temperature for 18 h utilizing general procedure **C**. Column chromatography (SiO<sub>2</sub>, hexane/EtOAc, 50:1, *R<sub>f</sub>* = 0.27 (hexane/ EtOAc, 30:1)) yielded **151p** (259 mg, 631 μmol, 90%) as a pale yellow oil.

**<sup>1</sup>H-NMR** (400 MHz, CDCl<sub>3</sub>): δ = 7.52 (dd, *J* = 7.5, 1.8 Hz, 1H), 7.29 (td, *J* = 8.0, 1.9 Hz, 1H), 7.11 (td, *J* = 8.0, 1.7 Hz, 1H), 7.06 – 6.99 (m, 1H), 6.15 (t, *J* = 2.2 Hz, 1H), 6.08 (d, *J* = 2.3 Hz, 2H), 3.73 (s, 6H), 1.03 (s, 21H). **<sup>13</sup>C{<sup>1</sup>H}-NMR** (101 MHz, CDCl<sub>3</sub>): δ = 161.6, 159.8, 156.8, 134.3, 129.9, 124.2, 120.8, 117.2, 102.1, 96.4, 96.2, 94.9, 55.5, 18.7, 11.4 ppm. **HR-MS** (ESI): calculated *m/z* for C<sub>25</sub>H<sub>35</sub>O<sub>3</sub>Si<sup>+</sup> ([M+H]<sup>+</sup>): 411.2350; found 411.2348. **FTIR** (ATR, neat):  $\tilde{\nu}$  = 3000, 2942, 2891, 2864, 2159, 1594, 1569, 1472, 1441, 1239, 1204, 1152, 1133, 1065, 994, 978, 882, 856, 822, 793, 766, 747, 678, 663, 637 cm<sup>-1</sup>.

### **1-(2-ethynylphenoxy)-3,5-dimethoxybenzene (174)**



Following a literature procedure,<sup>[126]</sup> potassium carbonate (527 mg, 3.81 mmol, 1.0 eq) was added to a solution of **151o** (1.25 g, 3.81 mmol, 1.0 eq) in dichloromethane (60 mL) and methanol (60 mL). The reaction mixture was stirred at room temperature for 20 h. After removal of the volatiles, the residue was redissolved in dichloromethane (60 mL) and washed with sat. aq.

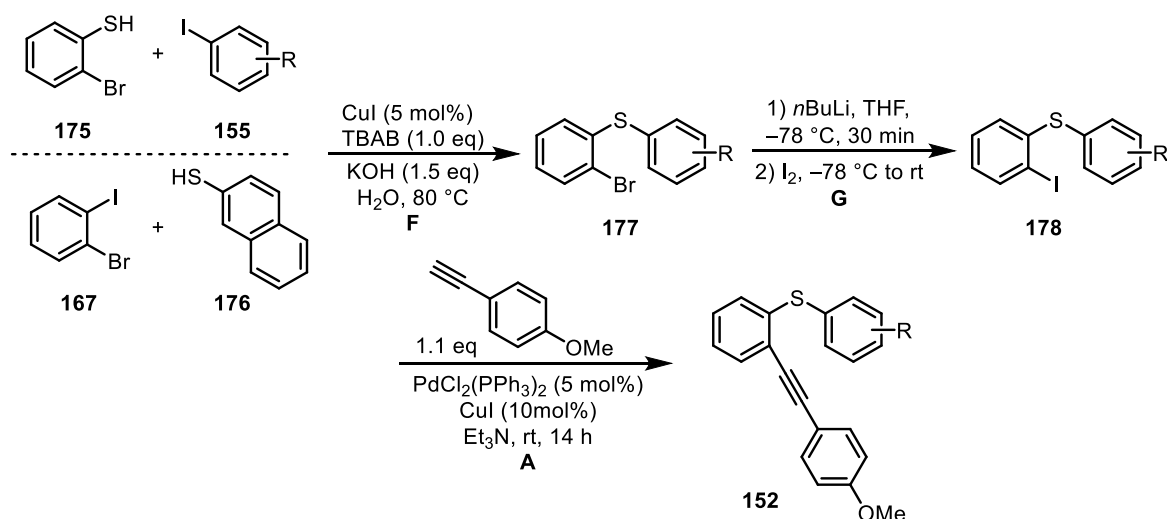
## 5.2 Synthesis and characterization of new compounds

NaHCO<sub>3</sub> solution followed by extraction with dichloromethane (3 x 80 mL). The combined organic phases were dried over MgSO<sub>4</sub> and concentrated under reduced pressure yielding the desired product **174** (966 mg, 3.80 mmol, quant.) as an orange oil.

Following another procedure, to a solution of **151p** (205 mg, 499 μmol, 1.0 eq) in dry THF (5 mL) was added a solution of TBAF (1 M in THF, 0.55 mL, 550 μmol, 1.1 eq). The reaction mixture was stirred at room temperature for 2 h. After completion of the reaction, water (10 mL) was added and the aqueous phase was extracted with diethyl ether (3 x 20 mL). The combined organic layers were dried over Na<sub>2</sub>SO<sub>4</sub> and concentrated in *vacuo*. The residue was purified by column chromatography (hexane/EtOAc, 30:1, *R<sub>f</sub>* = 0.15) to obtain **174** (122 mg, 480 μmol, 96%) as a pale yellow oil.

**<sup>1</sup>H-NMR** (400 MHz, CDCl<sub>3</sub>): δ = 7.54 (dd, *J* = 7.7, 1.7 Hz, 1H), 7.33 – 7.27 (m, 1H), 7.08 (td, *J* = 7.6, 1.1 Hz, 1H), 6.94 (dd, *J* = 8.3, 1.0 Hz, 1H), 6.23 (t, *J* = 2.2 Hz, 1H), 6.18 (d, *J* = 2.2 Hz, 2H), 3.75 (s, 6H), 3.23 (s, 1H) ppm. **<sup>13</sup>C{<sup>1</sup>H}-NMR** (101 MHz, CDCl<sub>3</sub>): δ = 161.7, 159.0, 158.0, 134.4, 130.3, 123.6, 119.1, 114.6, 97.5, 95.9, 81.9, 79.4, 55.6 ppm. **HR-MS** (ESI): calculated *m/z* for C<sub>16</sub>H<sub>15</sub>O<sub>3</sub><sup>+</sup> ([M+H]<sup>+</sup>): 255.1016; found 255.1020. **FTIR** (ATR, neat):  $\tilde{\nu}$  = 3278, 3001, 2958, 2939, 2837, 1591, 1568, 1481, 1471, 1439, 1427, 1270, 1229, 1203, 1187, 1150, 1100, 1050, 989, 975, 929, 822, 750, 657, 620, 537 cm<sup>-1</sup>.

### 5.2.3 1-(thioaryl)-2-ethynylbenzenes **152**



**Scheme S3:** Synthetic strategy for 1-(thioaryl)-2-ethynylbenzenes **152**.

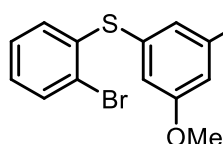
#### General procedure F for the preparation of 2-bromo biaryllic thiols **177**

Following a modified literature known procedure,<sup>[127]</sup> CuI (5 mol%) was added to a stirred suspension of 2-bromothiophenol (1.0 eq), the aryl iodide (1.1 eq), TBAB (1.0 eq) and KOH (1.5 eq) in water (1 mL). The suspension was heated in a closed vessel to 80 °C under air

## 5. Experimental

for the appropriate time. The reaction was monitored by TLC. After full conversion, the reaction mixture was cooled to room temperature and EtOAc (10 mL) was added. The layers were separated and the aqueous layer was extracted with EtOAc three times. The combined organic phases were washed with brine, water, dried over Na<sub>2</sub>SO<sub>4</sub> and concentrated in *vacuo*. The residue was purified by column chromatography (SiO<sub>2</sub>, EtOAc in hexane).

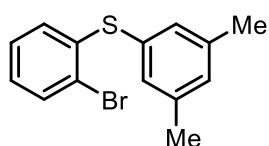
### (2-bromophenyl)(3,5-dimethoxyphenyl)sulfane (177a)



Using general procedure **F**, 2-bromothiophenol (190 mg, 1.00 mmol, 1.0 eq), 3,5-dimethoxy iodobenzene (292 mg, 1.11 mmol, 1.1 eq), TBAB (324 mg, 1.00 mmol, 1.0 eq), KOH (85 mg, 1.51 mmol, 1.5 eq), CuI (9.6 mg, 50.3 μmol, 5 mol%) in water (1 mL) were heated to 80 °C for 26 h. Column chromatography (SiO<sub>2</sub>, hexane/EtOAc, 30:1, *R<sub>f</sub>* = 0.21 (hexane/EtOAc, 20:1)) yielded compound **177a** (230 mg, 0.85 mmol, 71%) as a colorless oil.

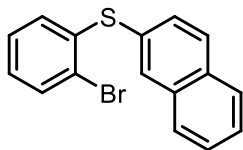
**<sup>1</sup>H-NMR** (300 MHz, CDCl<sub>3</sub>): δ = 7.57 (dd, *J* = 8.2, 1.4 Hz, 1H), 7.21 – 7.14 (m, 1H), 7.09 – 7.01 (m, 2H), 6.59 (d, *J* = 2.3 Hz, 2H), 6.44 (t, *J* = 2.3 Hz, 1H), 3.77 (s, 6H) ppm. **<sup>13</sup>C{<sup>1</sup>H}-NMR** (75 MHz, CDCl<sub>3</sub>): δ = 161.5, 138.2, 134.9, 133.2, 130.5, 128.0, 127.7, 123.6, 110.7, 101.0, 55.6 ppm. **HR-MS** (ESI): calculated *m/z* for C<sub>14</sub>H<sub>14</sub><sup>79</sup>BrO<sub>2</sub>S<sup>+</sup> ([M+H]<sup>+</sup>): 324.9892; found 324.9895. **FTIR** (ATR, neat):  $\tilde{\nu}$  = 3081, 3054, 3004, 2957, 2935, 2832, 1580, 1445, 1416, 1332, 1298, 1281, 1247, 1202, 1152, 1104, 1063, 1041, 1019, 989, 926, 830, 745, 711, 682, 651, 619, 590, 538 cm<sup>-1</sup>.

### (2-bromophenyl)(3,5-dimethylphenyl)sulfane (177b)



Using general procedure **F**, 2-bromothiophenol (190 mg, 1.00 mmol, 1.0 eq), 3,5-dimethyl iodobenzene (257 mg, 1.11 mmol, 1.1 eq), TBAB (324 mg, 1.00 mmol, 1.0 eq), KOH (85 mg, 1.51 mmol, 1.5 eq), CuI (9.6 mg, 50.3 μmol, 5 mol%) in water (1 mL) were heated to 80 °C for 26 h. Column chromatography (SiO<sub>2</sub>, hexane, *R<sub>f</sub>* = 0.35) yielded compound **177b** (250 mg, 0.85 mmol, 85%) as a colorless liquid.

**<sup>1</sup>H-NMR** (300 MHz, CDCl<sub>3</sub>): δ = 7.55 (dd, *J* = 7.9, 1.4 Hz, 1H), 7.19 – 7.09 (m, 3H), 7.06 – 6.96 (m, 2H), 6.89 (dd, *J* = 7.9, 1.6 Hz, 1H), 2.32 (s, 6H) ppm. **<sup>13</sup>C{<sup>1</sup>H}-NMR** (101 MHz, CDCl<sub>3</sub>): δ = 139.6, 139.5, 133.0, 132.0, 131.7, 130.6, 129.4, 127.9, 127.0, 122.6, 21.33 ppm. **HR-MS** (EI): calculated *m/z* for C<sub>14</sub>H<sub>13</sub><sup>79</sup>BrS<sup>+</sup> ([M]<sup>+</sup>): 291.9916; found: 291.9916. **FTIR** (ATR, neat):  $\tilde{\nu}$  = 3057, 2956, 2918, 2856, 1600, 1576, 1557, 1445, 1427, 1376, 1253, 1103, 1037, 1020, 848, 744, 710, 688, 651 cm<sup>-1</sup>.

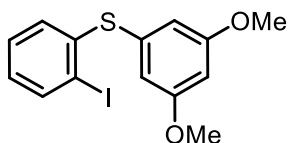
**(2-bromophenyl)(naphthalen-2-yl)sulfane (177c)**

Using general procedure **F**, 2-naphthalenethiol (170 mg, 1.06 mmol, 1.0 eq), 1-bromo-2-iodobenzene (330 mg, 1.17 mmol, 1.1 eq), TBAB (342 mg, 1.06 mmol, 1.0 eq), KOH (89 mg, 1.59 mmol, 1.5 eq), CuI (10.1 mg, 53.1  $\mu$ mol, 5 mol%) in water (1 mL) were heated to 80 °C for 36 h. Column chromatography (SiO<sub>2</sub>, hexane,  $R_f$  = 0.24) yielded compound **177c** (294 mg, 93.3  $\mu$ mol, 88%) as a colorless oil.

**<sup>1</sup>H-NMR** (300 MHz, CDCl<sub>3</sub>):  $\delta$  = 8.00 (s, 1H), 7.92 – 7.75 (m, 3H), 7.64 – 7.45 (m, 4H), 7.13 (td,  $J$  = 7.6, 1.5 Hz, 1H), 7.04 (td,  $J$  = 7.6, 1.8 Hz, 1H), 6.96 (dd,  $J$  = 7.7, 1.8 Hz, 1H) ppm. **<sup>13</sup>C{<sup>1</sup>H}-NMR** (75 MHz, CDCl<sub>3</sub>):  $\delta$  = 138.9, 134.1, 133.2, 133.1, 133.0, 130.4, 130.3, 130.0, 129.5, 128.0, 127.9, 127.9, 127.4, 127.0, 126.9, 123.1 ppm. **HR-MS** (EI): calculated  $m/z$  for C<sub>16</sub>H<sub>11</sub><sup>79</sup>BrS<sup>+</sup> ([M]<sup>+</sup>): 313.9765; found 313.9759. **FTIR** (ATR, neat):  $\tilde{\nu}$  = 3052, 2955, 2926, 1909, 1624, 1570, 1498, 1444, 1425, 1340, 1252, 1195, 1131, 1102, 1072, 1018, 943, 895, 850, 812, 740, 711, 648, 633, 601, 526 cm<sup>-1</sup>.

**General procedure G**

To a solution of *n*BuLi (2.5 M in hexane, 1.2 eq) in THF (~0.5 M) was added a solution of the **177** (1.0 eq) in THF (0.25 M) at –78 °C. After stirring for 30 min at –78 °C, I<sub>2</sub> (1.5 eq) was added. The reaction mixture was slowly warmed up to room temperature and was stirred for the depicted time. Then, sat. aq. Na<sub>2</sub>S<sub>2</sub>O<sub>3</sub> solution was added and the layers were separated. The aqueous layer was extracted with diethyl ether two times. The combined organic phases were washed with brine, water, dried over Na<sub>2</sub>SO<sub>4</sub> and concentrated under reduced pressure. The crude product was purified by column chromatography (SiO<sub>2</sub>, EtOAc in hexane).

**(3,5-dimethoxyphenyl)(2-iodophenyl)sulfane (178a)**

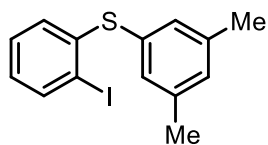
Prepared from **177a** (900 mg, 2.77 mmol, 1.0 eq) in THF (11 mL), *n*BuLi (2.5 M in hexane, 3.35 mL, 5.53 mmol, 1.2 eq) in THF (10 mL) and I<sub>2</sub> (1.05 g, 4.15 mmol, 1.5 eq) according to general procedure **G**. The reaction mixture was stirred for 22 h at room temperature. After column chromatography (SiO<sub>2</sub>, hexane/EtOAc, 20:1,  $R_f$  = 0.22), the desired product **178a** (770 mg, 2.07 mmol, 75%) was obtained as a pale yellow oil.

**<sup>1</sup>H-NMR** (300 MHz, CDCl<sub>3</sub>):  $\delta$  = 7.84 (dd,  $J$  = 7.9, 1.3 Hz, 1H), 7.28 – 7.19 (m, 1H), 7.08 (dd,  $J$  = 7.9, 1.6 Hz, 1H), 6.95 – 6.83 (m, 1H), 6.56 (d,  $J$  = 2.2 Hz, 2H), 6.43 (t,  $J$  = 2.3 Hz, 1H), 3.76 (s, 6H). **<sup>13</sup>C{<sup>1</sup>H}-NMR** (101 MHz, CDCl<sub>3</sub>):  $\delta$  = 161.5, 141.7, 139.8, 135.9, 130.2, 129.0, 127.9, 110.3, 100.9, 100.1, 55.6 ppm. **HR-MS** (ESI): calculated  $m/z$  for C<sub>14</sub>H<sub>14</sub>I<sub>2</sub>O<sub>2</sub>S<sup>+</sup> ([M+H]<sup>+</sup>): 372.9754; found 372.9754. **FTIR** (ATR, neat):  $\tilde{\nu}$  = 3005, 2960, 2933, 2829, 1583,

## 5. Experimental

1561, 1466, 1452, 1438, 1421, 1337, 1281, 1254, 1207, 1160, 1116, 1092, 1065, 1034, 1006, 988, 926, 866, 853, 834, 811, 745, 702, 676, 641, 620, 582, 539  $\text{cm}^{-1}$ .

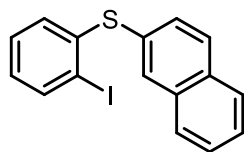
### (3,5-dimethylphenyl)(2-iodophenyl)sulfane (**178b**)



Prepared from **177b** (500 mg, 1.71 mmol, 1.0 eq) in THF (6 mL), *n*BuLi (2.5 M in hexane, 0.82 mL, 2.05 mmol, 1.2 eq) in THF (4.1 mL) and  $\text{I}_2$  (649 mg, 2.56 mmol, 1.5 eq) according to general procedure **G**. The reaction mixture was stirred for 16 h at room temperature. After column chromatography ( $\text{SiO}_2$ , hexane,  $R_f = 0.32$ ), the desired product **178b** (580 mg, 1.70 mmol, 99%) was obtained as a colorless oil.

**$^1\text{H-NMR}$**  (400 MHz,  $\text{CDCl}_3$ ):  $\delta = 7.82$  (dd,  $J = 7.8, 1.4$  Hz, 1H), 7.23 – 7.14 (m, 1H), 7.10 – 7.07 (m, 2H), 7.03 – 6.99 (m, 1H), 6.91 (dd,  $J = 8.0, 1.6$  Hz, 1H), 6.85 (td,  $J = 7.6, 1.6$  Hz, 1H), 2.31 (s, 6H) ppm.  **$^{13}\text{C}\{^1\text{H}\}\text{-NMR}$**  (101 MHz,  $\text{CDCl}_3$ ):  $\delta = 143.1, 139.6, 139.5, 133.1, 131.3, 130.5, 129.0, 128.8, 127.2, 98.7, 21.3$  ppm. **HR-MS** (EI): calculated  $m/z$  for  $\text{C}_{14}\text{H}_{13}\text{IS}^+$  ( $[\text{M}]^+$ ): 339.9783; found: 339.9786. **FTIR** (ATR, neat):  $\tilde{\nu} = 3048, 2913, 2856, 1598, 1578, 1565, 1438, 1422, 1375, 1296, 1251, 1113, 1093, 1035, 1007, 846, 742, 706, 686, 641$   $\text{cm}^{-1}$ .

### (2-iodophenyl)(naphthalen-2-yl)sulfane (**178c**)



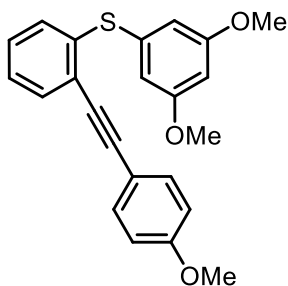
Prepared from **177c** (1.15 g, 3.64 mmol, 1.0 eq) in THF (15 mL), *n*BuLi (2.5 M in hexane, 1.75 mL, 4.36 mmol, 1.2 eq) in THF (9 mL) and  $\text{I}_2$  (1.38 g, 5.45 mmol, 1.5 eq) according to general procedure **F**. The reaction mixture was stirred for 16 h at room temperature. After column chromatography ( $\text{SiO}_2$ , hexane,  $R_f = 0.20$ ), the desired product **178c** (580 mg, 1.70 mmol, 99%) was obtained as a pale yellow oil.

**$^1\text{H-NMR}$**  (400 MHz,  $\text{CDCl}_3$ ):  $\delta = 7.97$  (d,  $J = 1.8$  Hz, 1H), 7.90 – 7.82 (m, 3H), 7.82 – 7.76 (m, 1H), 7.57 – 7.49 (m, 2H), 7.46 (dd,  $J = 8.6, 1.9$  Hz, 1H), 7.18 (td,  $J = 7.6, 1.4$  Hz, 1H), 6.98 (dd,  $J = 7.9, 1.6$  Hz, 1H), 6.89 (td,  $J = 7.6, 1.6$  Hz, 1H) ppm.  **$^{13}\text{C}\{^1\text{H}\}\text{-NMR}$**  (101 MHz,  $\text{CDCl}_3$ ):  $\delta = 142.4, 139.8, 134.1, 133.0, 132.6, 131.3, 130.1, 129.7, 129.5, 128.9, 127.9, 127.8, 127.7, 126.9, 126.9, 99.4$  ppm. **HR-MS** (EI): calculated  $m/z$  for  $\text{C}_{16}\text{H}_{11}\text{IS}^+$  ( $[\text{M}]^+$ ): 361.9621; found 361.9620. **FTIR** (ATR, neat):  $\tilde{\nu} = 3050, 2964, 1623, 1605, 1587, 1565, 1498, 1438, 1421, 1360, 1341, 1302, 1267, 1251, 1193, 1160, 1131, 1070, 1034, 1007, 943, 894, 856, 811, 741, 705, 644$   $\text{cm}^{-1}$ .

### (3,5-dimethoxyphenyl)(2-((4-methoxyphenyl)ethynyl)phenyl)sulfane (**152a**)

Following general procedure **C**, **152a** (773 mg, 1.96 mmol, 95%) was prepared from **178a** (764 mg, 2.05 mmol, 1.0 eq),  $\text{PdCl}_2(\text{PPh}_3)_2$  (72.02 mg, 103  $\mu\text{mol}$ , 5 mol%), CuI (39.1 mg, 205  $\mu\text{mol}$ , 10 mol%) and 4-ethynylanisole (407 mg, 3.08 mol, 1.5 eq) [rt, 14h] as a white

## 5.2 Synthesis and characterization of new compounds

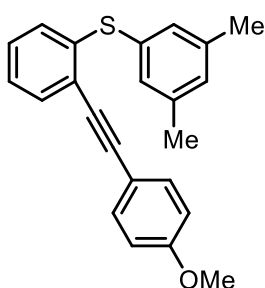


solid after column chromatography (SiO<sub>2</sub>, hexane/EtOAc, 10:1, *R<sub>f</sub>* = 0.18 (hexane/EtOAc, 9:1)).

**<sup>1</sup>H-NMR** (300 MHz, CDCl<sub>3</sub>): δ = 7.54 – 7.49 (m, 1H), 7.48 – 7.42 (m, 2H), 7.20 – 7.09 (m, 3H), 6.90 – 6.83 (m, 2H), 6.63 (d, *J* = 2.2 Hz, 2H), 6.41 (t, *J* = 2.3 Hz, 1H), 3.83 (s, 3H), 3.75 (s, 6H) ppm.

**<sup>13</sup>C{<sup>1</sup>H}-NMR** (101 MHz, CDCl<sub>3</sub>): δ = 161.3, 159.9, 139.3, 135.7, 133.3, 132.5, 129.3, 128.6, 126.3, 123.7, 115.4, 114.1, 110.5, 100.7, 95.9, 86.1, 55.6, 55.5 ppm. **HR-MS** (ESI): calculated *m/z* for C<sub>23</sub>H<sub>21</sub>O<sub>3</sub>S<sup>+</sup> ([M+H]<sup>+</sup>): 377.1206; found 377.1213. **FTIR** (ATR, neat):  $\tilde{\nu}$  = 3060, 3005, 2957, 2934, 2832, 2210, 1596, 1579, 1508, 1448, 1433, 1416, 1335, 1283, 1249, 1204, 1174, 1157, 1106, 1066, 1041, 1024, 988, 929, 869, 834, 818, 785, 761, 719, 683, 620, 534 cm<sup>-1</sup>.

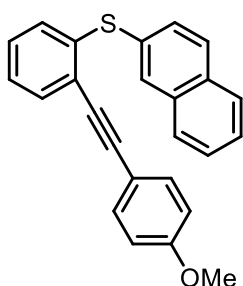
### (3,5-dimethylphenyl)(2-((4-methoxyphenyl)ethynyl)phenyl)sulfane (152b)



Following general procedure **C**, **152b** (242 mg, 703 μmol, 74%) was prepared from **178b** (254 mg, 747 μmol, 1.0 eq), PdCl<sub>2</sub>(PPh<sub>3</sub>)<sub>2</sub> (26.2 mg, 37.3 μmol, 5 mol%), CuI (14.2 mg, 74.7 μmol, 10 mol%) and 4-ethynylanisole (148 mg, 1.12 mol, 1.5 eq) [rt, 16h] as a white solid after column chromatography (SiO<sub>2</sub>, hexane → hexane/EtOAc, 98:2, *R<sub>f</sub>* = 0.20 (hexane/EtOAc, 98:2)).

**<sup>1</sup>H-NMR** (300 MHz, CDCl<sub>3</sub>): δ = 7.52 – 7.47 (m, 2H), 7.47 – 7.44 (m, 1H), 7.18 – 7.09 (m, 4H), 7.02 – 6.95 (m, 2H), 6.90 – 6.84 (m, 2H), 3.83 (s, 3H), 2.31 (s, 6H) ppm. **<sup>13</sup>C{<sup>1</sup>H}-NMR** (101 MHz, CDCl<sub>3</sub>): δ = 159.9, 140.7, 139.2, 133.3, 132.7, 132.3, 131.3, 130.1, 128.5, 128.3, 125.6, 122.9, 115.5, 114.1, 95.8, 86.1, 55.4, 21.3 ppm. **HR-MS** (ESI): calculated *m/z* for C<sub>23</sub>H<sub>21</sub>OS<sup>+</sup> ([M+H]<sup>+</sup>): 345.1308; found: 345.1313. **FTIR** (ATR, neat):  $\tilde{\nu}$  = 3049, 3004, 2957, 2918, 2835, 2215, 1605, 1578, 1510, 1461, 1437, 1288, 1249, 1173, 1148, 1106, 1060, 1032, 831, 753, 688 cm<sup>-1</sup>.

### (2-((4-methoxyphenyl)ethynyl)phenyl)(naphthalen-2-yl)sulfane (152c)



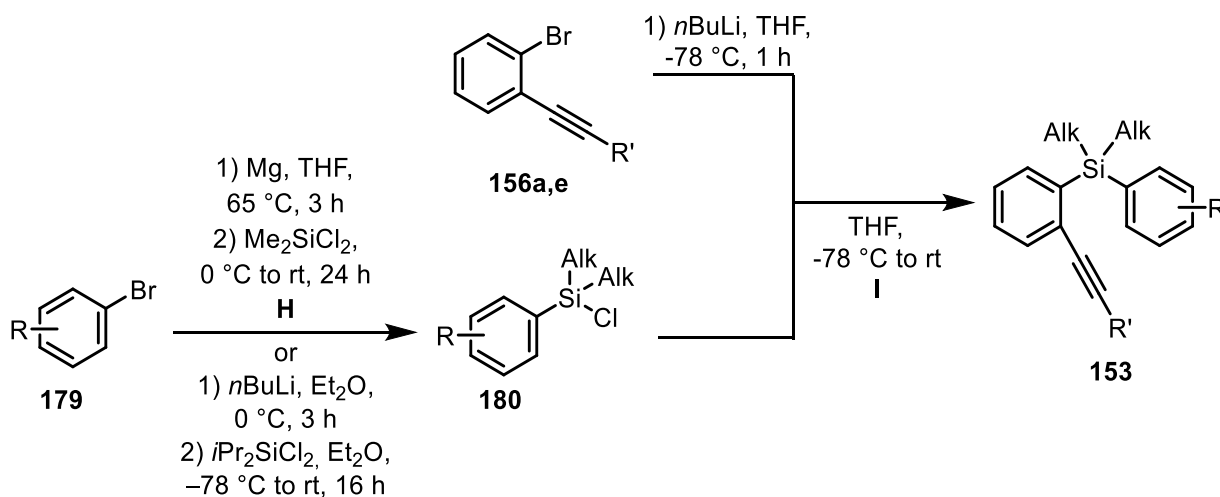
Following general procedure **C**, **152c** (796 mg, 2.17 mmol, 68%) was prepared from **178c** (1.15 g, 3.19 mmol, 1.0 eq), PdCl<sub>2</sub>(PPh<sub>3</sub>)<sub>2</sub> (44.7 mg, 63.7 μmol, 2 mol%), CuI (18.2 mg, 95.6 μmol, 3 mol%) and 4-ethynylanisole (463 mg, 3.50 mol, 1.1 eq) [rt, 17h] as white solid after column chromatography (SiO<sub>2</sub>, hexane/EtOAc, 30:1, *R<sub>f</sub>* = 0.15).

**<sup>1</sup>H-NMR** (400 MHz, CDCl<sub>3</sub>): δ = 7.99 (d, *J* = 1.7 Hz, 1H), 7.86 – 7.79 (m, 2H), 7.78 – 7.72 (m, 1H), 7.55 – 7.45 (m, 4H), 7.44 – 7.36 (m, 2H), 7.19 – 7.08 (m, 2H), 7.05 – 6.99 (m, 1H), 6.87 – 6.77 (m, 2H), 3.82 (s, 3H) ppm. **<sup>13</sup>C{<sup>1</sup>H}-NMR** (75 MHz, CDCl<sub>3</sub>): δ = 159.9, 139.9, 134.0, 133.3, 132.8, 132.5, 132.5, 131.1, 130.3, 129.2, 128.9, 128.6, 127.9, 127.8, 126.7, 126.7, 126.1, 123.4, 115.3, 114.1, 96.0, 86.1, 55.4 ppm. **HR-MS** (ESI):

## 5. Experimental

calculated  $m/z$  for  $C_{25}H_{29}OS^+$  ( $[M+H]^+$ ): 367.1151; found 367.1152. **FTIR** (ATR, neat):  $\tilde{\nu} = 3049, 2972, 2935, 2839, 1602, 1580, 1507, 1456, 1431, 1287, 1244, 1173, 1146, 1103, 1059, 1021, 943, 895, 851, 831, 812, 782, 754, 743, 718, 693 \text{ cm}^{-1}$ .

### 5.2.4 1-(silaaryl)-2-ethynylbenzenes **153**

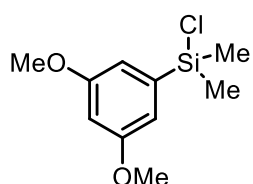


**Scheme S4:** Synthetic strategy for the synthesis of 1-(silaaryl)-2-ethynylbenzenes **153**.

#### General Procedure H for the synthesis of chlorosilanes

Adapted from literature procedures,<sup>[155]</sup> a solution of the bromide (1.0 eq) in dry THF (~1.2 M) was added over 30 min to a suspension of activated Mg turnings (1.0 eq) in dry THF (~2 M) under nitrogen atmosphere. The reaction mixture was heated to reflux for 3 h. After cooling down to room temperature, the resulting Grignard reagent was added dropwise to a solution of dichlorodimethylsilane (1.0 eq) in THF (~1.9 M) at 0 °C. The reaction mixture was allowed to warm up to room temperature and stirred for 24 h. The solvent was removed *in vacuo*, dry pentane (5 mL) was added, the resulting precipitate was filtered off and washed with pentane (3 x 5 mL). The solvent was evaporated and the crude product was purified by Kugelrohr distillation under argon atmosphere.

#### chloro(3,5-dimethoxyphenyl)dimethylsilane (**180a**)



Following general procedure **H**, **180a** (1.58 g, 6.83 mmol, 74%) was synthesized from 3,5-dimethoxybromobenzene (2.00 g, 9.21 mmol, 1.0 eq) in dry THF (6 mL), activated Mg turnings (246 mg, 10.1 mmol, 1.1 eq) in dry THF (5 mL) and dichlorodimethylsilane (1.19 g, 1.10 mL, 9.21 mmol, 1.0 eq) in dry THF (5 mL). Kugelrohr distillation yielded the desired product as a colorless liquid.

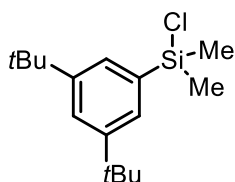
**<sup>1</sup>H-NMR** (300 MHz, C<sub>6</sub>D<sub>6</sub>):  $\delta = 6.92$  (d,  $J = 2.3$  Hz, 2H), 6.58 (t,  $J = 2.3$  Hz, 1H), 3.32 (s, 6H), 0.46 (s, 6H) ppm. **<sup>13</sup>C{<sup>1</sup>H}-NMR** (101 MHz, CDCl<sub>3</sub>):  $\delta = 161.5, 138.6, 111.1, 102.9, 54.9,$



## 5.2 Synthesis and characterization of new compounds

2.0 ppm.  $^{29}\text{Si-NMR}$  (80 MHz,  $\text{C}_6\text{D}_6$ ):  $\delta = 20.5$  ppm. **FTIR** (ATR, neat):  $\tilde{\nu} = 3000, 2957, 2902, 2834, 1580, 1456, 1403, 1331, 1284, 1254, 1202, 1153, 1124, 1061, 988, 925, 827, 784, 686, 607, 542$   $\text{cm}^{-1}$ . Compound **180a** was too sensitive to obtain good HRMS data. As expected for this compound class only hydrolysis products could be observed.

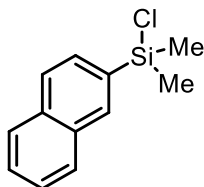
### chloro(3,5-di-*tert*-butylphenyl)dimethylsilane (**180b**)



Following general procedure **H**, **180b** (3.15 g, 8.34 mmol, 75%) was synthesized from 1-bromo-3,5-di-*tert*-butylbenzene (3.00 g, 11.1 mmol, 1.0 eq) in dry THF (7 mL), activated Mg turnings (298 mg, 12.3 mmol, 1.1 eq) in dry THF (5 mL) and dichlorodimethylsilane (1.44 g, 1.35 mL, 11.1 mmol, 1.0 eq) in dry THF (6 mL). Kugelrohr distillation yielded the desired product as a colorless liquid.

$^1\text{H-NMR}$  (300 MHz,  $\text{C}_6\text{D}_6$ ):  $\delta = 7.69$  (d,  $J = 1.9$  Hz, 2H), 7.62 (d,  $J = 1.9$  Hz, 1H), 1.29 (s, 18H), 0.54 (s, 6H).  $^{13}\text{C}\{^1\text{H}\}\text{-NMR}$  (101 MHz,  $\text{CDCl}_3$ ):  $\delta = 150.7, 135.9, 127.4, 124.9, 35.0, 31.6, 2.3$  ppm.  $^{29}\text{Si-NMR}$  (79 MHz,  $\text{CDCl}_3$ ):  $\delta = 20.5$  ppm. **FTIR** (ATR, neat):  $\tilde{\nu} = 3054, 2961, 2903, 2867, 2588, 1475, 1410, 1392, 1362, 1252, 1202, 1149, 1025, 872, 832, 809, 710, 671$   $\text{cm}^{-1}$ . Compound **180b** was too sensitive to obtain good HRMS data. As expected for this compound class only hydrolysis products could be observed.

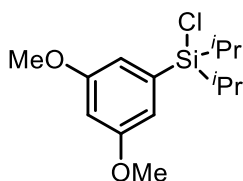
### chlorodimethyl(naphthalen-2-yl)silane (**180c**)



Following general procedure **H**, **180c** (1.44 g, 6.51 mmol, 68%) was synthesized from 2-bromonaphthalene (2.00 g, 9.66 mmol, 1.0 eq) in dry THF (8 mL), activated Mg turnings (258 mg, 10.6 mmol, 1.1 eq) in dry THF (5 mL) and dichlorodimethylsilane (1.25 g, 1.15 mL, 9.66 mmol, 1.0 eq) in dry THF (5 mL). Kugelrohr distillation yielded the desired product as a colorless liquid.

$^1\text{H-NMR}$  (400 MHz,  $\text{C}_6\text{D}_6$ ):  $\delta = 8.07$  (s, 1H), 7.67 – 7.56 (m, 4H), 7.30 – 7.22 (m, 2H), 0.51 (s, 6H) ppm.  $^{13}\text{C}\{^1\text{H}\}\text{-NMR}$  (75 MHz,  $\text{C}_6\text{D}_6$ ):  $\delta = 134.8, 134.7, 133.9, 133.3, 129.2, 128.7, 128.0, 127.3, 126.5, 2.0$  ppm.  $^{29}\text{Si-NMR}$  (99 MHz,  $\text{C}_6\text{D}_6$ ):  $\delta = 20.2$  ppm. Compound **180c** was too sensitive to obtain good HRMS data. As expected for this compound class only hydrolysis products could be observed.

### chloro(3,5-dimethoxyphenyl)diisopropylsilane (**180d**)



Following a modified literature procedure,<sup>[156]</sup> to a solution of 1-bromo-3,5-dimethoxybenzene (1.60 g, 7.37 mmol, 1.0 eq) in dry diethyl ether (15 mL) was added *n*BuLi (2.5 M in hexane, 2.95 mL, 7.37 mmol, 1.0 eq) at 0 °C under nitrogen atmosphere. The reaction mixture was stirred at 0 °C for 3 h. The prepared 3,5-dimethoxyphenyllithium solution was added slowly to a solution of *i*Pr<sub>2</sub>SiCl<sub>2</sub> (2.05 g, 2.00 mL, 11.1 mmol, 1.5 eq) in dry diethyl ether (10 mL)

## 5. Experimental

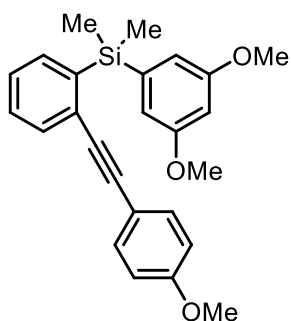
under nitrogen atmosphere at  $-78\text{ }^{\circ}\text{C}$ . The reaction mixture was allowed to warm up to room temperature over 16 h. The solvent was removed in *vacuo* and the residue was washed with dry pentane three times. After evaporation of the solvent, the crude product was purified by Kugelrohr distillation under argon atmosphere to obtain **180d** (1.01 g, 3.53 mmol, 48%) as a colorless liquid.

**$^1\text{H-NMR}$**  (300 MHz,  $\text{CDCl}_3$ ):  $\delta$  = 6.73 (d,  $J$  = 2.4 Hz, 2H), 6.52 (t,  $J$  = 2.3 Hz, 1H), 3.81 (s, 6H), 1.44 – 1.31 (m, 2H), 1.12 – 0.96 (m, 18H) ppm.  **$^{13}\text{C-NMR}$**  (75 MHz,  $\text{CDCl}_3$ ):  $\delta$  = 160.5, 134.7, 112.1, 101.9, 55.4, 17.2, 16.9, 14.0 ppm. Compound **180d** was too unstable to obtain good IR or HRMS data. As expected for this compound class only hydrolysis products could be observed.

### General procedure I for the synthesis of dialkyldiphenylsilanes

According to a modified literature procedure,<sup>[157]</sup> *n*BuLi (2.5 M in hexane, 1.08 eq) was added to a solution of **156** (1.0 eq) in dry THF ( $\sim 0.1\text{ M}$ ) at  $-78\text{ }^{\circ}\text{C}$  under nitrogen atmosphere. After stirring at  $-78\text{ }^{\circ}\text{C}$  for 1 h, the chlorosilane **180** (1.08 eq) was added dropwise. The reaction mixture was warmed up to room temperature and stirred for 16 h. After the addition of water, the aqueous layer was extracted with diethyl ether twice. The combined organic phases were washed with sat. aq.  $\text{NH}_4\text{Cl}$  solution, brine, dried over  $\text{Na}_2\text{SO}_4$  and concentrated under reduced pressure. The residue was purified by column chromatography ( $\text{SiO}_2$ , DCM in hexane or EtOAc in hexane).

### (3,5-dimethoxyphenyl)(2-((4-methoxyphenyl)ethynyl)phenyl)dimethylsilane (**153a**)

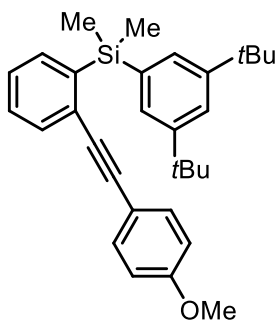


Prepared from **156a** (2.89 g, 10.1 mmol, 1.0 eq) in dry THF (80 mL), *n*BuLi (2.5 M in hexane, 4.35 mL, 10.9 mmol, 1.08 eq) and **180a** (2.51 g, 10.9 mmol, 1.08 eq) following general procedure I. After column chromatography ( $\text{SiO}_2$ , hexane/DCM, 2:1  $\rightarrow$  1:1,  $R_f$  = 0.16 (hexane/DCM, 2:1)) **153a** (3.87 g, 9.60 mmol, 95%) was obtained as a colorless amorphous solid.

**$^1\text{H-NMR}$**  (300 MHz,  $\text{CDCl}_3$ ):  $\delta$  = 7.54 (dd,  $J$  = 7.6, 0.8 Hz, 1H), 7.42 (dd,  $J$  = 7.3, 1.0 Hz, 1H), 7.35 (td,  $J$  = 7.5, 1.6 Hz, 1H), 7.31 – 7.22 (m, 3H), 6.89 – 6.81 (m, 2H), 6.73 (d,  $J$  = 2.4 Hz, 2H), 6.47 (t,  $J$  = 2.3 Hz, 1H), 3.82 (s, 3H), 3.74 (s, 6H), 0.68 (s, 6H) ppm.  **$^{13}\text{C}\{^1\text{H}\}\text{-NMR}$**  (101 MHz,  $\text{CDCl}_3$ ):  $\delta$  = 160.5, 159.7, 140.8, 140.0, 135.4, 132.9, 132.5, 129.3, 129.3, 127.3, 115.7, 114.1, 112.0, 101.1, 92.6, 89.9, 55.5, 55.4,  $-2.0$  ppm.  **$^{29}\text{Si-NMR}$**  (79 MHz,  $\text{CDCl}_3$ ):  $\delta$  =  $-6.34$  ppm **HR-MS** (ESI): calculated  $m/z$  for  $\text{C}_{25}\text{H}_{27}\text{O}_3\text{Si}^+$  ( $[\text{M}+\text{H}]^+$ ): 403.1724; found 403.1723. **FTIR** (ATR, neat):  $\tilde{\nu}$  = 3048, 3000, 2954, 2934, 2902, 2834, 2111, 1604, 1579, 1509, 1457, 1403, 1336, 1283, 1246, 1202, 1174, 1153, 1123, 1062, 1030, 864, 828, 798, 774, 725, 661, 646  $\text{cm}^{-1}$ .

### (3,5-di-*tert*-butylphenyl)(2-((4-methoxyphenyl)ethynyl)phenyl)dimethylsilane (**153b**)

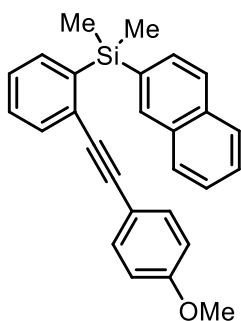
## 5.2 Synthesis and characterization of new compounds



Prepared from **156a** (2.17 g, 7.54 mmol, 1.0 eq) in dry THF (80 mL), *n*BuLi (2.5 M in hexane, 3.25 mL, 8.14 mmol, 1.08 eq) and **180b** (2.30 g, 8.14 mmol, 1.08 eq) following general procedure I. After column chromatography (SiO<sub>2</sub>, hexane/EtOAc, 50:1, *R<sub>f</sub>* = 0.34 (hexane/EtOAc, 30:1)) **153b** (3.43 g, 7.53 mmol, 99%) was obtained as a colorless highly viscous oil.

**<sup>1</sup>H-NMR** (400 MHz, CDCl<sub>3</sub>): δ = 7.59 – 7.56 (m, 1H), 7.48 – 7.45 (m, 3H), 7.43 (ddd, *J* = 7.3, 1.5, 0.6 Hz, 1H), 7.36 (td, *J* = 7.5, 1.5 Hz, 1H), 7.30 – 7.25 (m, 1H), 7.17 – 7.11 (m, 2H), 6.83 – 6.77 (m, 2H), 3.81 (s, 3H), 1.31 (s, 18H), 0.70 (s, 6H) ppm. **<sup>13</sup>C{<sup>1</sup>H}-NMR** (126 MHz, CDCl<sub>3</sub>): δ = 159.6, 149.7, 140.6, 136.8, 135.5, 132.8, 132.3, 129.4, 129.1, 128.6, 127.2, 123.2, 115.7, 114.0, 92.7, 90.2, 55.4, 35.0, 31.6, –1.6 ppm. **<sup>29</sup>Si-NMR** (99 MHz, CDCl<sub>3</sub>): δ = –6.7 ppm. **HR-MS** (ESI): calculated *m/z* for C<sub>31</sub>H<sub>39</sub>OSi<sup>+</sup> ([M+H]<sup>+</sup>): 455.2765; found 455.2762. **FTIR** (ATR, neat):  $\tilde{\nu}$  = 3048, 2953, 2901, 2866, 2834, 1605, 1581, 1509, 1460, 1407, 1391, 1361, 1285, 1246, 1173, 1146, 1122, 1069, 1031, 864, 829, 811, 758, 712, 694, 659, 645 cm<sup>-1</sup>.

### (2-((4-methoxyphenyl)ethynyl)phenyl)dimethyl(naphthalen-2-yl)silane (**153c**)



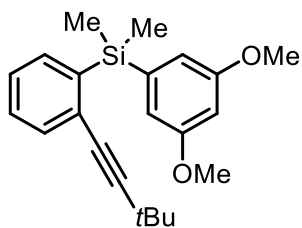
Prepared from **156a** (1.68 g, 5.85 mmol, 1.0 eq) in dry THF (50 mL), *n*BuLi (2.5 M in hexane, 2.53 mL, 6.32 mmol, 1.08 eq) and **180c** (1.40 g, 6.32 mmol, 1.08 eq) following general procedure I. After column chromatography (SiO<sub>2</sub>, hexane/EtOAc, 40:1, *R<sub>f</sub>* = 0.21 (hexane/EtOAc, 30:1)) **153c** (2.22 g, 5.64 mmol, 96%) was obtained as a white solid.

**<sup>1</sup>H-NMR** (400 MHz, CDCl<sub>3</sub>): δ = 8.10 (s, 1H), 7.87-7.76 (m, 3H), 7.64 (d, *J* = 8.2 Hz, 1H), 7.56 (ddd, *J* = 7.8 Hz, 1H), 7.52 – 7.43 (m, 3H), 7.37 (td, *J* = 7.5, 1.4 Hz, 1H), 7.31 – 7.23 (m, 1H), 7.19 – 7.13 (m, 2H), 6.80 – 6.72 (m, 2H), 3.80 (s, 3H), 0.78 (s, 6H) ppm. **<sup>13</sup>C{<sup>1</sup>H}-NMR** (75 MHz, CDCl<sub>3</sub>): δ = 159.7, 140.2, 135.8, 135.4, 135.2, 133.9, 133.1, 132.8, 132.6, 130.8, 129.4, 129.3, 128.3, 127.8, 127.3, 127.0, 126.4, 125.9, 115.5, 114.0, 92.7, 89.9, 55.4, –1.9 ppm. **<sup>29</sup>Si-NMR** (79 MHz, CDCl<sub>3</sub>): δ = –6.9 ppm. **HR-MS** (ESI): calculated *m/z* for C<sub>27</sub>H<sub>25</sub>OSi<sup>+</sup> ([M+H]<sup>+</sup>): 393.1669; found 393.1660. **FTIR** (ATR, neat):  $\tilde{\nu}$  = 3048, 2951, 2895, 2834, 1604, 1567, 1509, 1463, 1438, 1402, 1287, 1244, 1178, 1147, 1109, 1080, 1029, 952, 854, 830, 802, 763, 739, 724, 697, 665, 643, 585 cm<sup>-1</sup>.

### (3,5-dimethoxyphenyl)(2-(3,3-dimethylbut-1-yn-1-yl)phenyl)dimethylsilane (**153d**)

Prepared from **156e** (1.48 g, 6.23 mmol, 1.0 eq) in dry THF (50 mL), *n*BuLi (2.5 M in hexane, 2.70 mL, 6.73 mmol, 1.08 eq) and **180a** (1.55 g, 6.73 mmol, 1.08 eq) following general

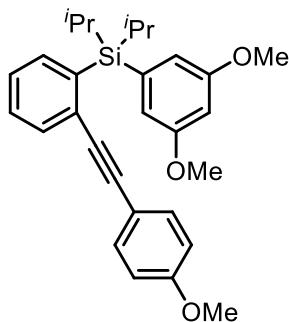
## 5. Experimental



procedure I. After column chromatography (SiO<sub>2</sub>, hexane/EtOAc, 30:1,  $R_f$  = 0.18) **153d** (1.99 g, 5.64 mmol, 90%) was obtained as a colorless liquid.

**<sup>1</sup>H-NMR** (400 MHz, CDCl<sub>3</sub>):  $\delta$  = 7.45 – 7.40 (m, 1H), 7.34 – 7.31 (m, 1H), 7.29 (td,  $J$  = 7.6, 1.6 Hz, 1H), 7.19 (td,  $J$  = 7.4, 1.3 Hz, 1H), 6.70 (d,  $J$  = 2.3 Hz, 2H), 6.48 (t,  $J$  = 2.4 Hz, 1H), 3.79 (s, 6H), 1.20 (s, 9H), 0.64 (s, 6H) ppm. **<sup>13</sup>C{<sup>1</sup>H}-NMR** (101 MHz, CDCl<sub>3</sub>):  $\delta$  = 160.5, 141.0, 139.3, 135.3, 132.8, 129.9, 129.1, 126.8, 112.2, 101.5, 100.9, 80.9, 55.4, 30.7, 28.1, -1.9 ppm. **<sup>29</sup>Si-NMR** (80 MHz, CDCl<sub>3</sub>):  $\delta$  = -6.1 ppm. **HR-MS** (ESI): calculated  $m/z$  for C<sub>22</sub>H<sub>29</sub>O<sub>2</sub>Si<sup>+</sup> ([M+H]<sup>+</sup>): 353.1931; found 353.1933. **FTIR** (ATR, neat):  $\tilde{\nu}$  = 2997, 2964, 2901, 2866, 2831, 1580, 1458, 1402, 1361, 1329, 1282, 1244, 1202, 1153, 1124, 1061, 922, 863, 830, 799, 759, 722, 688, 660, 644 cm<sup>-1</sup>.

### (3,5-dimethoxyphenyl)diisopropyl(2-((4-methoxyphenyl)ethynyl)phenyl)silane (**153e**)

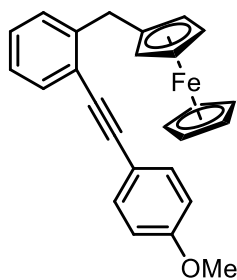


Prepared from **156a** (940 mg, 3.27 mmol, 1.0 eq) in dry THF (50 mL), *n*BuLi (2.5 M in hexane, 1.40 mL, 3.53 mmol, 1.08 eq) and **180d** (1.01 g, 3.53 mmol, 1.08 eq) following general procedure I. After column chromatography (SiO<sub>2</sub>, hexane/EtOAc, 50:1,  $R_f$  = 0.05 (hexane/EtOAc, 30:1) and toluene,  $R_f$  = 0.33) **153e** (619 mg, 1.35 mmol, 41%) was obtained as a white solid.

**<sup>1</sup>H-NMR** (500 MHz, CDCl<sub>3</sub>):  $\delta$  = 7.58 (ddd,  $J$  = 7.7, 1.3, 0.6 Hz, 1H), 7.50 (ddd,  $J$  = 7.5, 1.5, 0.6 Hz, 1H), 7.36 (td,  $J$  = 7.6, 1.4 Hz, 1H), 7.26 (td,  $J$  = 7.5, 1.3 Hz, 1H), 7.16 – 7.12 (m, 2H), 6.82 – 6.79 (m, 2H), 6.71 (d,  $J$  = 2.3 Hz, 2H), 6.47 (t,  $J$  = 2.3 Hz, 1H), 3.81 (s, 3H), 3.75 (s, 6H), 1.81 (hept,  $J$  = 7.4 Hz, 2H), 1.08 (d,  $J$  = 7.4 Hz, 6H), 0.98 (d,  $J$  = 7.4 Hz, 6H) ppm. **<sup>13</sup>C{<sup>1</sup>H}-NMR** (126 MHz, CDCl<sub>3</sub>):  $\delta$  = 160.1, 159.6, 137.7, 136.4, 135.6, 133.4, 132.7, 130.5, 129.0, 126.7, 115.8, 113.9, 113.9, 100.8, 91.6, 91.0, 77.4, 77.2, 76.9, 55.4, 18.3, 18.1, 11.0 ppm. **<sup>29</sup>Si-NMR** (99 MHz, CDCl<sub>3</sub>):  $\delta$  = 3.0 ppm. **HR-MS** (ESI): calculated  $m/z$  for C<sub>29</sub>H<sub>35</sub>O<sub>3</sub>Si<sup>+</sup> ([M+H]<sup>+</sup>): 459.2350; found 459.2351. **FTIR** (ATR, neat):  $\tilde{\nu}$  = 3073, 3049, 2998, 2940, 2862, 2832, 2212, 1604, 1579, 1509, 1459, 1402, 1328, 1281, 1246, 1202, 1173, 1153, 1120, 1061, 1031, 994, 923, 881, 829, 786, 760, 694, 659, 626 cm<sup>-1</sup>.

### 5.2.5 Ferrocene-containing precursors

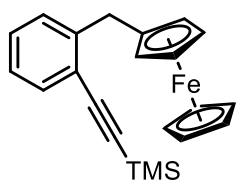
#### 2-[(4-methoxyphenyl)ethynyl]benzylferrocene (**162a**)



The synthesis of the (chlorozincio)ferrocene was performed according to a literature known procedure.<sup>[133]</sup> To a solution of ferrocene (158 mg, 0.847 mmol, 1.0 eq) and potassium *tert*-butoxide (19 mg, 0.169 mmol, 0.2 eq) in dry THF (5 mL) was added *t*BuLi (1.7 M in pentane, 1 mL, 1.7 mmol, 2.0 eq) at  $-78\text{ }^{\circ}\text{C}$  under argon atmosphere. After stirring at  $-78\text{ }^{\circ}\text{C}$  for 1.5 h, a solution of zinc chloride (2 M in THF, 0.85 mL, 1.7 mmol, 2.0 eq) was added. The reaction mixture was stirred at room temperature for 2 h. The resulting (chlorozincio)ferrocene was added to **189a** (255 mg, 0.847 mmol, 1.0 eq) and Pd(PPh<sub>3</sub>)<sub>4</sub> (49 mg, 0.042 mmol, 5 mol%) in dry THF (5 mL) and the reaction mixture was stirred at  $65\text{ }^{\circ}\text{C}$  overnight. After cooling down to room temperature, the reaction was quenched through addition of an aq. sat. NH<sub>4</sub>Cl solution. The mixture was diluted with water and diethyl ether and the layers were separated. The aqueous phase was extracted with diethyl ether twice. The combined organic phases were washed with water, dried over Na<sub>2</sub>SO<sub>4</sub> and concentrated under reduced pressure. The residue was purified by column chromatography (SiO<sub>2</sub>, hexane/EtOAc, 50:1,  $R_f = 0.23$ ) yielding **162a** (235 mg, 0.578 mmol, 68%) as a yellow solid.

**<sup>1</sup>H-NMR** (300 MHz, CDCl<sub>3</sub>):  $\delta = 7.65 - 7.40$  (m, 3H),  $7.24 - 7.06$  (m, 3H),  $7.03 - 6.81$  (m, 2H),  $4.22$  (s, 2H),  $4.13$  (s, 5H),  $4.07$  (s, 2H),  $3.94$  (s, 2H),  $3.85$  (s, 3H) ppm. **<sup>13</sup>C{<sup>1</sup>H}-NMR** (101 MHz, CDCl<sub>3</sub>):  $\delta = 159.8, 143.9, 133.1, 132.0, 128.8, 128.3, 126.1, 122.7, 115.9, 114.3, 93.5, 87.8, 87.5, 69.0, 68.8, 67.6, 55.5, 34.6$  ppm. **HR-MS** (ESI): calculated  $m/z$  for C<sub>26</sub>H<sub>22</sub>FeO<sup>+</sup> ([M]<sup>+</sup>): 406.1015; found 406.1012. **FTIR** (ATR, neat):  $\tilde{\nu} = 3049, 2936, 2910, 2837, 1606, 1566, 1510, 1481, 1454, 1417, 1317, 1291, 1254, 1173, 1148, 1104, 1084, 1030, 998, 936, 839, 820, 808, 752, 700\text{ cm}^{-1}$ .

#### 2-[(trimethylsilyl)ethynyl]benzylferrocene (**162b**)



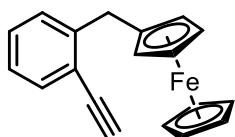
The synthesis of the (chlorozincio)ferrocene was performed according to a literature known procedure.<sup>[133]</sup> To a solution of ferrocene (244 mg, 1.31 mmol, 1.0 eq) and potassium *tert*-butoxide (29 mg, 0.262 mmol, 0.2 eq) in dry THF (5.5 mL) was added *t*BuLi (1.7 M in pentane, 1.55 mL, 2.6 mmol, 2.0 eq) at  $-78\text{ }^{\circ}\text{C}$  under argon atmosphere. After stirring at  $-78\text{ }^{\circ}\text{C}$  for 1.5 h, a solution of zinc chloride (2 M in THF, 1.3 mL, 2.6 mmol, 2.0 eq) was added. The reaction mixture was stirred at room temperature for 2 h. The resulting (chlorozincio)ferrocene was added to **189b** (350 mg, 1.31 mmol, 1.0 eq) and Pd(PPh<sub>3</sub>)<sub>4</sub> (76 mg, 0.065 mmol, 5 mol%) in dry THF (5.5 mL) and the reaction mixture was stirred at  $65\text{ }^{\circ}\text{C}$  overnight. After cooling down to room temperature, the reaction was quenched

## 5. Experimental

through addition of an aq. sat.  $\text{NH}_4\text{Cl}$  solution. The mixture was diluted with water and diethyl ether and the layers were separated. The aqueous phase was extracted with diethyl ether twice. The combined organic phases were washed with water, dried over  $\text{Na}_2\text{SO}_4$  and concentrated under reduced pressure. The residue was purified by column chromatography ( $\text{SiO}_2$ , hexane/ EtOAc, 50:1,  $R_f = 0.39$ ) yielding **162b** (373 mg, 1.00 mmol, 77%) as an orange solid.

**$^1\text{H-NMR}$**  (400 MHz,  $\text{CDCl}_3$ ):  $\delta = 7.43$  (dd,  $J = 7.9, 1.5$  Hz, 1H), 7.20 (td,  $J = 7.5, 1.5$  Hz, 1H), 7.15 – 7.06 (m, 2H), 4.20 (t,  $J = 1.8$  Hz, 2H), 4.14 (s, 5H), 4.08 (t,  $J = 1.8$  Hz, 2H), 3.88 (s, 2H), 0.33 (s, 9H) ppm.  **$^{13}\text{C}\{^1\text{H}\}\text{-NMR}$**  (101 MHz,  $\text{CDCl}_3$ ):  $\delta = 144.5, 132.4, 128.8, 128.6, 125.9, 122.2, 104.5, 98.4, 87.8, 69.0, 68.8, 67.6, 34.5, 0.3$  ppm. **HR-MS** (ESI): calculated  $m/z$  for  $\text{C}_{22}\text{H}_{25}\text{FeSi}^+$  ( $[\text{M}+\text{H}]^+$ ): 373.1070; found 373.1060. **FTIR** (ATR, neat):  $\tilde{\nu} = 3095, 3019, 2958, 2899, 1479, 1449, 1423, 1323, 1272, 1244, 1218, 1159, 1105, 1036, 1022, 998, 926, 843, 820, 758, 702, 647$   $\text{cm}^{-1}$ .

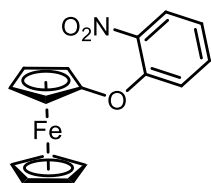
### 2-(ethynyl)benzylferrocene (**162c**)



Potassium carbonate (100 mg, 0.725 mmol, 1.0 eq) was added to a solution of **162b** (270 mg, 0.725 mmol, 1.0 eq) in DCM/methanol (1:1, 24 mL) and the reaction mixture was stirred overnight. The solvent was removed under reduced pressure. The residue was redissolved in DCM and washed with aq. sat.  $\text{NaHCO}_3$  solution. The layers were separated and the aqueous phase was extracted with DCM twice. The combined organic phases were dried over  $\text{Na}_2\text{SO}_4$  and all volatiles were removed under reduced pressure to obtain **162c** (213 mg, 0.710 mmol, 98%) as an orange solid.

**$^1\text{H-NMR}$**  (300 MHz,  $\text{CDCl}_3$ ):  $\delta = 7.47$  (d,  $J = 7.9$  Hz, 1H), 7.23 (d,  $J = 7.6$  Hz, 1H), 7.17 – 7.10 (m, 2H), 4.17 (s, 2H), 4.14 (s, 5H), 4.08 (s, 2H), 3.89 (s, 2H), 3.33 (s, 1H) ppm.  **$^{13}\text{C}\{^1\text{H}\}\text{-NMR}$**  (101 MHz,  $\text{CDCl}_3$ ):  $\delta = 144.5, 132.9, 129.0, 128.8, 126.0, 121.3, 87.5, 82.8, 81.2, 69.1, 68.8, 67.6, 34.3$  ppm. **HR-MS** (ESI): calculated  $m/z$  for  $\text{C}_{19}\text{H}_{17}\text{Fe}^+$  ( $[\text{M}+\text{H}]^+$ ): 301.0674; found 301.0659. **FTIR** (ATR, neat):  $\tilde{\nu} = 3264, 3098, 3064, 3018, 2946, 2914, 2858, 1644, 1596, 1565, 1480, 1445, 1404, 1321, 1270, 1227, 1176, 1154, 1103, 1039, 1024, 994, 956, 926, 909, 850, 817, 754, 702, 661, 634$   $\text{cm}^{-1}$ .

### 1-nitro-2-ferrocenyloxybenzene (**193**)



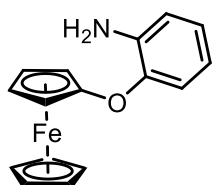
Adapted from a literature procedure,<sup>[154]</sup> a mixture of 1-fluoronitrobenzene (409 mg, 2.90 mmol, 1.0 eq), ferrocenol (586 mg, 2.90 mmol, 1.0 eq) and potassium carbonate (401 mg, 2.90 mmol, 1.0 eq) in degassed DMSO (10 mL) was stirred at 95 °C for 24 h. After cooling to room temperature, water was added and the mixture was extracted with diethyl ether three times. The combined organic phases were washed with brine, dried over

## 5.2 Synthesis and characterization of new compounds

$\text{Na}_2\text{SO}_4$  and concentrated under reduced pressure affording **193** (914 mg, 2.83 mmol, 98%) as an orange crystalline solid. Mp: 107-109 °C (5 °C/min).

**$^1\text{H-NMR}$**  (400 MHz,  $\text{CDCl}_3$ ):  $\delta$  = 7.87 (d,  $J$  = 8.1 Hz, 1H), 7.42 (t,  $J$  = 7.9 Hz, 1H), 7.07 (t,  $J$  = 7.7 Hz, 1H), 7.01 (d,  $J$  = 8.5 Hz, 1H), 4.32 (s, 7H), 4.01 (s, 2H) ppm.  **$^{13}\text{C}\{^1\text{H}\}\text{-NMR}$**  (101 MHz,  $\text{CDCl}_3$ ):  $\delta$  = 153.0, 140.2, 134.0, 125.5, 121.9, 120.8, 117.7, 69.9, 63.7, 61.0 ppm. **HR-MS** (ESI): calculated  $m/z$  for  $\text{C}_{16}\text{H}_{13}\text{FeNO}_3^+$  ( $[\text{M}]^+$ ): 323.0239; found 323.0232. **FTIR** (ATR, neat):  $\tilde{\nu}$  = 3100, 3046, 2955, 2923, 2856, 1602, 1587, 1520, 1480, 1447, 1347, 1310, 1277, 1250, 1168, 1106, 1090, 1047, 1016, 929, 861, 812, 773, 737, 695, 673, 610  $\text{cm}^{-1}$ .

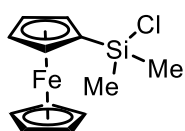
### 2-ferrocenyloxyaniline (**194**)



Adapted from a literature procedure,<sup>[158]</sup> a mixture of **193** (200 mg, 0.619 mmol, 1.0 eq), tinn(II) chloride dihydrate (559 mg, 2.48 mmol, 4.0 eq) and an aqueous hydrochloric acid solution (conc., 1 mL, 0.619 mmol, 1.0 eq) in 2-propanol/water (2:1, 30 mL) was heated to reflux for 2 h. After cooling down to room temperature, the mixture was treated with sodium carbonate until obtaining pH 7. 2-Propanol was removed under reduced pressure using a rotary evaporator and the remaining suspension was extracted with DCM three times. The combined organic layers were dried over  $\text{Na}_2\text{SO}_4$  and the volatiles were removed under reduced pressure yielding **194** (158 mg, 0.539 mmol, 87%) as a brownish oil, which was used without further purification directly in the next step.

**$^1\text{H-NMR}$**  (400 MHz,  $\text{CDCl}_3$ ):  $\delta$  = 6.95 (dd,  $J$  = 8.0, 1.4 Hz, 1H), 6.89 (td,  $J$  = 7.5, 1.3 Hz, 1H), 6.77 (dd,  $J$  = 7.8, 1.6 Hz, 1H), 6.67 (td,  $J$  = 7.7, 1.5 Hz, 1H), 4.26 (s, 5H), 4.22 (t,  $J$  = 2.0 Hz, 2H), 3.92 (t,  $J$  = 2.0 Hz, 2H) ppm.  **$^{13}\text{C}\{^1\text{H}\}\text{-NMR}$**  (101 MHz,  $\text{CDCl}_3$ ):  $\delta$  = 145.8, 137.5, 123.8, 123.3, 118.5, 117.4, 116.1, 69.4, 62.8, 59.1 ppm. **HR-MS** (ESI): calculated  $m/z$  for  $\text{C}_{16}\text{H}_{15}\text{FeNO}^+$  ( $[\text{M}]^+$ ): 293.0498; found 293.0494. **FTIR** (ATR, neat):  $\tilde{\nu}$  = 3452, 3371, 3091, 1703, 1615, 1499, 1455, 1410, 1373, 1300, 1268, 1237, 1190, 1105, 1031, 1000, 932, 818, 787, 740  $\text{cm}^{-1}$ .

### dichloromethylsilylferrocene (**198**)



Ferrocene was lithiated using a literature known procedure.<sup>[128]</sup> Ferrocene (1.25 g, 6.72 mmol, 1.0 eq) and potassium *tert*-butoxide (75 mg, 0.67 mmol, 10 mol%) were dissolved in dry THF (63 mL) under argon atmosphere. The solution was cooled to  $-78$  °C and *t*BuLi (1.7 M in pentane, 9.9 mL, 16.8 mmol, 2.5 eq) was added over 15 min. After stirring at  $-78$  °C for 2 h, the lithiated ferrocene was added to a solution of dimethyldichlorosilane (1.30 g, 1.25 mL, 10.1 mmol, 1.5 eq) in dry THF (10 mL) at 0 °C. The reaction mixture was warmed up to room temperature and stirred overnight. The volatiles were removed *in vacuo* and the residue

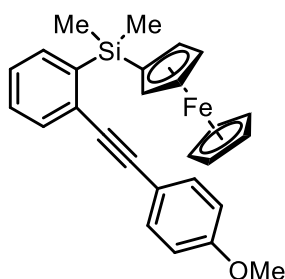
## 5. Experimental

was extracted with pentane (3 x 5 mL). After concentrating *in vacuo*, the residue was purified *via* Kugelrohr distillation yielding **198** (1.56 g, 5.61 mmol, 83%) as an orange oil.

**<sup>1</sup>H-NMR** (300 MHz, CDCl<sub>3</sub>): δ = 4.43 (s, 2H), 4.22 (s, 2H), 4.18 (s, 5H), 0.66 (s, 6H) ppm.

The <sup>1</sup>H-NMR data correspond to those reported in literature.<sup>[159]</sup>

### (2-((4-methoxyphenyl)ethynyl)phenyl)dimethyl(ferrocenyl)silane (**164**)



To a solution of 1-bromo-2-((4-methoxyphenyl)ethynyl)benzene (**156a**) (477 mg, 1.66 mmol, 1.0 eq) in dry THF (25 mL) was added *n*BuLi (2.5 M, 0.73 mL, 1.83 mmol, 1.1 eq) at -78 °C under nitrogen atmosphere. After stirring at -78 °C for 1 h, a solution of **198** (510 mg, 1.83 mmol, 1.1 eq) in dry THF (5 mL) was added dropwise. The reaction mixture was warmed up to room

temperature and stirred for 22 h. Water was added and the aqueous layer was extracted with diethyl ether three times. The combined organic phases were washed with sat. aq. NH<sub>4</sub>Cl solution, brine and dried over Na<sub>2</sub>SO<sub>4</sub>. After evaporation of all volatiles, the residue was purified by column chromatography (SiO<sub>2</sub>, hexane → hexane/EtOAc, 95:5, *R*<sub>f</sub> = 0.14 (hexane/EtOAc, 50:1)) affording **164** (585 mg, 1.30 mmol, 78%) as an orange crystalline solid. Mp: 139-141 °C (5 °C/min).

**<sup>1</sup>H-NMR** (300 MHz, CDCl<sub>3</sub>): δ = 7.56 – 7.46 (m, 3H), 7.35 – 7.26 (m, 2H), 7.18 (td, *J* = 7.3, 1.3 Hz, 1H), 6.96 – 6.88 (m, 2H), 4.40 (t, *J* = 1.7 Hz, 2H), 4.24 (t, *J* = 1.7 Hz, 2H), 4.13 (s, 5H), 3.85 (s, 3H), 0.72 (s, 6H) ppm. **<sup>13</sup>C{<sup>1</sup>H}-NMR** (101 MHz, CDCl<sub>3</sub>): δ = 159.8, 142.2, 135.1, 132.9, 132.4, 128.9, 128.6, 127.2, 115.9, 114.3, 92.2, 90.4, 74.0, 71.2, 69.9, 68.4, 55.5, -1.5 ppm. **<sup>29</sup>Si-NMR** (79 MHz, CDCl<sub>3</sub>): δ = -6.21 ppm. **HR-MS** (ESI): calculated *m/z* for C<sub>27</sub>H<sub>26</sub>FeOSi<sup>+</sup> ([M]<sup>+</sup>): 450.1097; found 450.1092. **FTIR** (ATR, neat):  $\tilde{\nu}$  = 3044, 3021, 2965, 2937, 2905, 2840, 1605, 1580, 1566, 1509, 1455, 1415, 1302, 1284, 1243, 1174, 1160, 1120, 1105, 1069, 1028, 1004, 895, 864, 832, 805, 769, 721, 694, 659 cm<sup>-1</sup>.

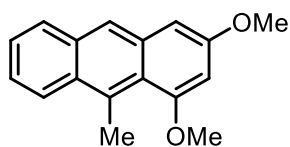


### 5.2.6 Intramolecular cyclization of precursors **150a-d**, **151a** and **152a** employing Brønsted acid catalysis

#### General procedure J

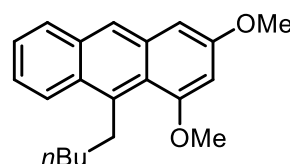
HNTf<sub>2</sub> (0.5 eq, 0.05 M in DCE, 1 mL) was added to a solution of the alkyne (100 μmol, 1.0 eq) in dry DCE (1 mL) in a dried Schlenk equipped with a stirring bar at room temperature under nitrogen atmosphere. The reaction mixture was heated to 80 °C for 5 h. After cooling down to room temperature, DCM was added and the organic phase was washed with sat. aq. NaHCO<sub>3</sub> solution twice. The resulting solution was again extracted with DCM. The combined organic phases were dried over Na<sub>2</sub>SO<sub>4</sub> and were concentrated under reduced pressure. The residue was purified by column chromatography (SiO<sub>2</sub>, EtOAc in hexane).

#### 1,3-dimethoxy-9-methylanthracene (**199a**)



Following general procedure **J**, **199a** (19.9 mg, 78.9 μmol, 79%) was prepared from **150a** (25.2 mg, 100 μmol, 1.0 eq) and HNTf<sub>2</sub> (0.05 M in DCE, 1 mL, 50.0 μmol, 50 mol%) in DCE (1 mL). Purification by column chromatography (SiO<sub>2</sub>, hexane/EtOAc, 30:1, *R<sub>f</sub>* = 0.22 (hexane/EtOAc, 30:1)) afforded **199a** as a yellow crystalline solid. Single crystals suitable for X-ray analysis were obtained by evaporation of hexane/EtOAc. Mp: 107-110 °C. **<sup>1</sup>H-NMR** (300 MHz, CDCl<sub>3</sub>): δ = 8.40 – 8.22 (m, 1H), 8.08 (s, 1H), 7.92 – 7.80 (m, 1H), 7.54 – 7.37 (m, 2H), 6.78 (d, *J* = 2.4 Hz, 1H), 6.45 (d, *J* = 2.2 Hz, 1H), 3.98 (s, 3H), 3.95 (s, 3H), 3.30 (s, 3H) ppm. **<sup>13</sup>C{<sup>1</sup>H}-NMR** (101 MHz, CDCl<sub>3</sub>): δ = 159.7, 156.8, 134.4, 132.4, 132.3, 130.1, 128.1, 125.4, 125.1, 124.2, 123.4, 121.3, 98.9, 97.5, 55.6, 55.4, 18.0 ppm. **HR-MS** (ESI): calculated *m/z* for C<sub>17</sub>H<sub>17</sub>O<sub>2</sub><sup>+</sup> ([M+H]<sup>+</sup>): 253.1223; found 253.1220. **FTIR** (ATR, neat):  $\tilde{\nu}$  = 3082, 3034, 2994, 2937, 2831, 1628, 1560, 1529, 1447, 1405, 1347, 1289, 1248, 1234, 1204, 1167, 1146, 1099, 1065, 1053, 1033, 1007, 945, 865, 836, 802, 778, 745, 726, 620, 599, 561, 528, 510 cm<sup>-1</sup>.

#### 1,3-dimethoxy-9-pentylanthracene (**199b**)



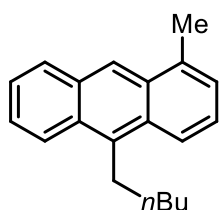
Following general procedure **J**, **199b** (24.6 mg, 79.8 μmol, 80%) was prepared from **150b** (30.8 mg, 100 μmol, 1.0 eq) and HNTf<sub>2</sub> (0.05 M in DCE, 1 mL, 50.0 μmol, 50 mol%) in DCE (1 mL). Purification by column chromatography (SiO<sub>2</sub>, hexane/EtOAc, 50:1, *R<sub>f</sub>* = 0.27 (hexane/EtOAc, 30:1)) afforded **199b** as a yellow solid.

**<sup>1</sup>H NMR** (300 MHz, CDCl<sub>3</sub>): δ = 8.38 – 8.19 (m, 1H), 8.09 (s, 1H), 7.95 – 7.77 (m, 1H), 7.52 – 7.34 (m, 2H), 6.79 (d, *J* = 2.4 Hz, 1H), 6.47 (d, *J* = 2.4 Hz, 1H), 3.99 (s, 3H), 3.95 (s, 3H), 3.80 (br s, 2H), 1.95 – 1.76 (m, 2H), 1.68 – 1.39 (m, 4H), 0.99 (t, *J* = 7.2 Hz, 3H) ppm.

## 5. Experimental

**<sup>13</sup>C{<sup>1</sup>H}-NMR** (101 MHz, CDCl<sub>3</sub>):  $\delta$  = 159.3, 156.6, 137.5, 134.5, 132.4, 129.6, 128.2, 125.4, 125.0, 124.4, 123.8, 120.6, 98.9, 97.7, 55.6, 55.4, 33.1, 32.4, 31.0, 22.8, 14.4 ppm. **HR-MS** (ESI): calculated  $m/z$  for C<sub>21</sub>H<sub>25</sub>O<sub>2</sub><sup>+</sup> ([M+H]<sup>+</sup>): 309.1849; found 309.1846. **FTIR** (ATR, neat):  $\tilde{\nu}$  = 3069, 3015, 2948, 2925, 2857, 2831, 1626, 1565, 1529, 1486, 1447, 1407, 1353, 1316, 1292, 1247, 1231, 1204, 1164, 1146, 1096, 1055, 1038, 946, 882, 846, 818, 794, 749, 738, 644, 627, 597, 563, 549, 515 cm<sup>-1</sup>.

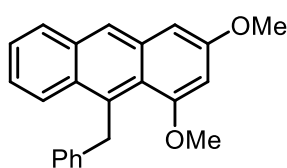
### 1-methyl-10-pentylanthracene (**199c**)



Following general procedure **J**, **199c** (18.9 mg, 72.0  $\mu$ mol, 72%) was prepared from **150c** (26.2 mg, 100  $\mu$ mol, 1.0 eq) and HNTf<sub>2</sub> (0.05 M in DCE, 1 mL, 50.0  $\mu$ mol, 50 mol%) in DCE (1 mL). Purification by column chromatography (SiO<sub>2</sub>, pentane,  $R_f$  = 0.59 (hexane/EtOAc, 50:1)) afforded **199c** as a pale yellow oil.

**<sup>1</sup>H-NMR** (300 MHz, CDCl<sub>3</sub>):  $\delta$  = 8.47 (s, 1H), 8.32 – 8.23 (m, 1H), 8.17 (d,  $J$  = 8.9 Hz, 1H), 8.05 (dd,  $J$  = 8.4, 1.5 Hz, 1H), 7.56 – 7.44 (m, 2H), 7.41 (dd,  $J$  = 8.9, 6.6 Hz, 1H), 7.31 (dt,  $J$  = 6.6, 1.1 Hz, 1H), 3.67 – 3.56 (m, 2H), 2.83 (s, 3H), 1.90 – 1.76 (m, 2H), 1.66 – 1.52 (m, 3H), 1.52 – 1.37 (m, 2H), 0.96 (t,  $J$  = 7.2 Hz, 3H) ppm. **<sup>13</sup>C{<sup>1</sup>H}-NMR** (101 MHz, CDCl<sub>3</sub>):  $\delta$  = 136.1, 135.0, 131.6, 131.4, 129.8, 129.7, 129.4, 125.5, 125.4, 125.2, 124.9, 124.5, 123.1, 121.9, 32.7, 31.4, 28.4, 22.8, 20.3, 14.3 ppm. **HR-MS** (EI): calculated  $m/z$  for C<sub>20</sub>H<sub>22</sub><sup>+</sup> ([M+H]<sup>+</sup>): 262.1716; found 262.1717. **FTIR** (ATR, neat):  $\tilde{\nu}$  = 3051, 2952, 2924, 2857, 1621, 1530, 1489, 1454, 1424, 1408, 1375, 1343, 1321, 1263, 1200, 1151, 1111, 1071, 1032, 1018, 962, 949, 872, 838, 804, 773, 727, 698, 684, 644, 622, 553, 529, 517 cm<sup>-1</sup>.

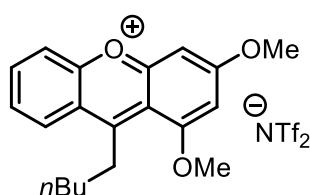
### 9-benzyl-1,3-dimethoxyanthracene (**199d**)



Following general procedure **J**, **199d** (14.5 mg, 44.2  $\mu$ mol, 44%) was prepared from **150d** (32.8 mg, 100  $\mu$ mol, 1.0 eq) and HNTf<sub>2</sub> (0.05 M in DCE, 1 mL, 50.0  $\mu$ mol, 50 mol%) in DCE (1 mL). Purification by column chromatography (SiO<sub>2</sub>, hexane/EtOAc,

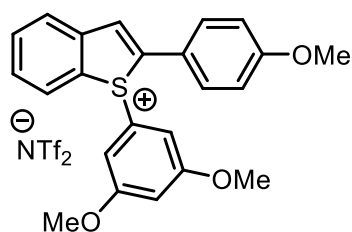
50:1,  $R_f$  = 0.22 (hexane/EtOAc, 30:1)) afforded **199d** as a yellow solid.

**<sup>1</sup>H-NMR** (300 MHz, CDCl<sub>3</sub>):  $\delta$  = 8.25 – 8.11 (m, 2H), 7.97 – 7.87 (m, 1H), 7.46 – 7.39 (m, 1H), 7.39 – 7.32 (m, 1H), 7.25 – 7.17 (m, 2H), 7.16 – 7.08 (m, 3H), 6.85 (d,  $J$  = 2.4 Hz, 1H), 6.44 (d,  $J$  = 2.4 Hz, 1H), 5.27 (s, 2H), 3.96 (s, 3H), 3.73 (s, 3H) ppm. **<sup>13</sup>C{<sup>1</sup>H}-NMR** (101 MHz, CDCl<sub>3</sub>):  $\delta$  = 159.1, 156.8, 143.2, 134.5, 133.0, 132.5, 130.7, 128.2, 125.5, 125.2, 124.9, 124.8, 121.8, 99.3, 97.7, 55.6, 55.4, 36.5 ppm. **HR-MS** (ESI): calculated  $m/z$  for C<sub>23</sub>H<sub>21</sub>O<sub>2</sub><sup>+</sup> ([M+H]<sup>+</sup>): 329.1536; found 329.1528. **FTIR** (ATR, neat):  $\tilde{\nu}$  = 3074, 3027, 2998, 2961, 2939, 2923, 2834, 1625, 1603, 1564, 1528, 1486, 1450, 1428, 1406, 1353, 1334, 1314, 1290, 1251, 1200, 1167, 1144, 1097, 1056, 1039, 991, 966, 940, 876, 843, 827, 780, 746, 735, 719, 693, 653, 628, 597, 569, 538, 504 cm<sup>-1</sup>.

**1,3-dimethoxy-9-pentylxanthylum bis((trifluoromethyl)sulfonyl)amide (200a)**

HNTf<sub>2</sub> (0.05 M in DCE, 2 mL, 100 μmol, 1.0 eq) was added to a solution of **151a** (31.0 mg, 100 μmol, 1.0 eq) in DCE (1 mL) in a dried Schlenk equipped with a stirring bar at room temperature under nitrogen atmosphere. The reaction mixture was heated to 80 °C for 5 h. After cooling down to room temperature, the solvent was removed to yield the desired product **200a** (51.8 mg, 87.6 μmol, 88%) as a dark orange oil. Single crystals suitable for X-ray analysis were obtained by crystallization from DCM and Et<sub>2</sub>O. Mp: 115–118 °C.

**<sup>1</sup>H-NMR** (400 MHz, CDCl<sub>3</sub>): δ = 8.40 (dd, *J* = 8.6, 1.4 Hz, 1H), 8.18 (ddd, *J* = 8.5, 7.1, 1.4 Hz, 1H), 8.01 (dd, *J* = 8.6, 1.2 Hz, 1H), 7.82 (ddd, *J* = 8.4, 7.0, 1.2 Hz, 1H), 7.20 (d, *J* = 2.3 Hz, 1H), 6.78 (d, *J* = 2.3 Hz, 1H), 4.22 (s, 3H), 4.21 (s, 3H), 3.97 – 3.82 (m, 2H), 1.88 – 1.76 (m, 2H), 1.70 – 1.60 (m, 2H), 1.47 (h, *J* = 7.3 Hz, 2H), 0.98 (t, *J* = 7.3 Hz, 3H) ppm. **<sup>19</sup>F-NMR** (376 MHz, CDCl<sub>3</sub>): δ = –78.4 ppm. **<sup>13</sup>C{<sup>1</sup>H}-NMR** (101 MHz, CDCl<sub>3</sub>): δ = 175.7, 175.0, 163.5, 160.6, 154.4, 140.3, 128.1, 127.8, 121.7, 119.8 (q, *J* = 323 Hz), 119.1, 114.6, 100.1, 95.1, 58.4, 58.1, 33.0, 32.9, 32.0, 22.4, 14.0 ppm. **HR-MS** (ESI): calculated *m/z* for C<sub>20</sub>H<sub>23</sub>O<sub>3</sub><sup>+</sup> ([M-NTf<sub>2</sub>]<sup>+</sup>): 311.1636; found 311.3642. **FTIR** (ATR, neat):  $\tilde{\nu}$  = 3098, 2963, 2936, 2876, 1633, 1604, 1578, 1516, 1476, 1431, 1347, 1316, 1228, 1171, 1136, 1119, 1093, 1054, 983, 933, 853, 793, 768, 739, 668, 611, 588, 567, 540, 508 cm<sup>-1</sup>.

**1-(3,5-dimethoxyphenyl)-2-(4-methoxyphenyl)-1*H*-benzo[*b*]thiophen-1-ium bis((trifluoromethyl)sulfonyl)amide (201a)**

HNTf<sub>2</sub> (0.05 M in DCE, 2 mL, 100 μmol, 1.0 eq) was added to a solution of **152a** (37.7 mg, 100 μmol, 1.0 eq) in DCE (1 mL) in a dried Schlenk equipped with a stirring bar at room temperature under nitrogen atmosphere. The reaction mixture was heated to 80 °C for 5 h. After cooling down to room temperature, the solvent was removed to yield the desired product **201a** (63.3 mg, 96.2 μmol, 96%) as a dark red oil. Single crystals suitable for X-ray analysis were obtained by crystallization from DCM and Et<sub>2</sub>O. Mp: 115–120 °C.

**<sup>1</sup>H-NMR** (400 MHz, CDCl<sub>3</sub>): δ = 7.99 (d, *J* = 7.9 Hz, 1H), 7.88 (dd, *J* = 7.8, 1.1 Hz, 1H), 7.82 (s, 1H), 7.71 (td, *J* = 7.7, 1.1 Hz, 1H), 7.62 – 7.55 (m, 2H), 7.51 (td, *J* = 7.8, 1.2 Hz, 1H), 6.94 – 6.87 (m, 2H), 6.78 (d, *J* = 2.2 Hz, 2H), 6.59 (t, *J* = 2.2 Hz, 1H), 3.76 (s, 3H), 3.75 (s, 6H) ppm. **<sup>19</sup>F-NMR** (376 MHz, CDCl<sub>3</sub>): δ = –78.6 ppm. **<sup>13</sup>C-NMR** (101 MHz, CDCl<sub>3</sub>): δ = 162.7, 162.3, 142.2, 141.0, 134.4, 132.5, 131.0, 130.4, 129.3, 127.6, 127.3, 124.1, 120.1 (q, *J* = 322 Hz) 119.4, 115.7, 107.6, 107.5, 56.3, 55.7 ppm. **HR-MS** (ESI): calculated *m/z* for C<sub>23</sub>H<sub>21</sub>O<sub>3</sub>S<sup>+</sup> ([M-NTf<sub>2</sub>]<sup>+</sup>): 377.1206; found 377.1206. **FTIR** (ATR, neat):  $\tilde{\nu}$  = 3086, 3006, 2979, 2947, 2843, 1601, 1572, 1507, 1461, 1425, 1350, 1332, 1306, 1285, 1260,

## 5. Experimental

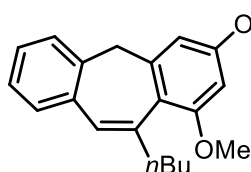
1242, 1177, 1160, 1137, 1049, 1027, 984, 948, 925, 889, 849, 830, 805, 787, 757, 740, 702, 669, 612, 568, 539, 511  $\text{cm}^{-1}$ .

### 5.2.7 Intramolecular cyclization of precursors **150**, **151**, **152** and **153** employing gold catalysis

#### General procedure **K**

A dried Schlenk equipped with a stirring bar was charged with the respective alkyne (100  $\mu\text{mol}$ , 1.0 eq) and precatalyst **C** (2 or 5 mol%) and was evacuated for 30 min. Under argon atmosphere DCM (0.05 M) was added and the reaction was pre-stirred for 2 min. A solution of  $\text{AgSbF}_6$  (0.05 M in DCM, 2 or 5 mol%) was added dropwise. After stirring at room temperature for 15 h, the reaction mixture was filtered through a silica pad eluting with DCM. The solvent was removed under reduced pressure and the crude product was purified by column chromatography ( $\text{SiO}_2$ , EtOAc in hexane) or crystallization.

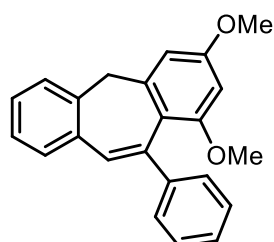
#### 11-butyl-1,3-dimethoxy-5*H*-dibenzo[*a,d*][7]annulene (**146b**)



Prepared from **150b** (30.8 mg, 100  $\mu\text{mol}$ , 1.0 eq), precatalyst **C** (4.25 mg, 5.00  $\mu\text{mol}$ , 5 mol%) and  $\text{AgSbF}_6$  (0.05 M in DCM, 100  $\mu\text{L}$ , 5.00  $\mu\text{mol}$ , 5 mol%) in DCM (2.0 mL) according to general procedure **K**. Purification by column chromatography ( $\text{SiO}_2$ , hexane/EtOAc, 50:1,  $R_f$  = 0.19 (hexane/EtOAc, 30:1)) afforded **146b** (26.6 mg, 86.2  $\mu\text{mol}$ , 86%) as a white solid.

**$^1\text{H-NMR}$**  (300 MHz,  $\text{CDCl}_3$ ):  $\delta$  = 7.25 – 7.09 (m, 4H), 6.95 (s, 1H), 6.46 (d,  $J$  = 2.5 Hz, 1H), 6.32 (d,  $J$  = 2.4 Hz, 1H), 3.81 (s, 3H), 3.77 (s, 3H), 3.64 – 3.51 (m, 2H), 3.35 – 3.21 (m, 1H), 2.54 – 2.41 (m, 1H), 1.45 – 1.23 (m, 4H), 0.88 (t,  $J$  = 7.0 Hz, 3H) ppm.  **$^{13}\text{C}\{^1\text{H}\}\text{-NMR}$**  (101 MHz,  $\text{CDCl}_3$ ):  $\delta$  = 160.4, 158.2, 144.6, 143.4, 140.0, 135.9, 128.3, 127.9, 127.1, 126.7, 126.0, 117.9, 103.4, 97.0, 55.5, 55.4, 42.1, 38.0, 32.6, 22.8, 14.1 ppm. **HR-MS** (ESI): calculated  $m/z$  for  $\text{C}_{21}\text{H}_{25}\text{O}_2^+$  ( $[\text{M}+\text{H}]^+$ ): 309.1849; found 309.1848. **FTIR** (ATR, neat):  $\tilde{\nu}$  = 3064, 2997, 2954, 2930, 2870, 2856, 2836, 1602, 1575, 1486, 1463, 1418, 1332, 111, 1284, 1203, 1156, 1088, 1065, 953, 831, 749  $\text{cm}^{-1}$ .

#### 1,3-dimethoxy-11-phenyl-5*H*-dibenzo[*a,d*][7]annulene (**146d**)

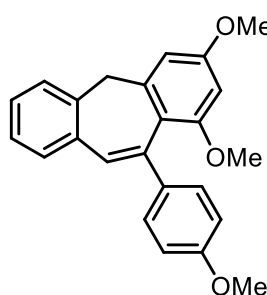


Prepared from **150d** (32.8 mg, 100  $\mu\text{mol}$ , 1.0 eq), precatalyst **C** (1.70 mg, 2.00  $\mu\text{mol}$ , 2 mol%) and  $\text{AgSbF}_6$  (0.05 M in DCM, 40  $\mu\text{L}$ , 2.00  $\mu\text{mol}$ , 2 mol%) in DCM (2.0 mL) according to general procedure **K**. Purification by column chromatography ( $\text{SiO}_2$ , hexane/EtOAc, 30:1,  $R_f$  = 0.15 (hexane/EtOAc, 30:1)) afforded **146d** (32.1 mg, 97.7  $\mu\text{mol}$ , 98%) as a white solid.

## 5.2 Synthesis and characterization of new compounds

**<sup>1</sup>H-NMR** (600 MHz, CDCl<sub>3</sub>): δ = 7.43 – 7.40 (m, 2H), 7.38 – 7.35 (m, 1H), 7.35 – 7.31 (m, 2H), 7.29 (s, 1H), 7.28 – 7.19 (m, 4H), 6.54 (d, *J* = 2.4 Hz, 1H), 6.28 (d, *J* = 2.4 Hz, 1H), 3.84 (s, 3H), 3.71 (s, 2H), 3.32 (s, 3H) ppm. **<sup>13</sup>C{<sup>1</sup>H}-NMR** (151 MHz, CDCl<sub>3</sub>): δ = 161.1, 158.8, 145.2, 145.0, 141.4, 140.2, 135.8, 130.1, 128.3, 128.0, 127.7, 127.0, 126.5, 126.5, 126.1, 117.9, 103.6, 97.7, 55.5, 55.4, 41.9 ppm. **HR-MS** (ESI): calculated *m/z* for C<sub>23</sub>H<sub>21</sub>O<sub>2</sub><sup>+</sup> ([M+H]<sup>+</sup>): 329.1536; found 329.1532. **FTIR** (ATR, neat):  $\tilde{\nu}$  = 3062, 3006, 2954, 2894, 2851, 1594, 1575, 1479, 1448, 1414, 1332, 1287, 1230, 1195, 1162, 1128, 1105, 1073, 1050, 950, 913, 884, 850, 832, 820, 773, 751, 708, 696, 680, 655, 628, 602, 581, 538, 526 cm<sup>-1</sup>.

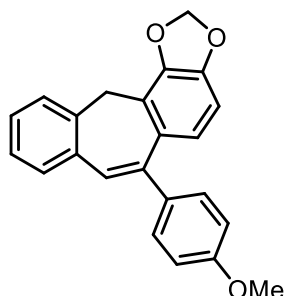
### 1,3-dimethoxy-11-(4-methoxyphenyl)-5H-dibenzo[a,d][7]annulene (146e)



Prepared from **150e** (35.8 mg, 100 μmol, 1.0 eq), precatalyst **C** (1.70 mg, 2.00 μmol, 2 mol%) and AgSbF<sub>6</sub> (0.05 M in DCM, 40 μL, 2.00 μmol, 2 mol%) in DCM (2.0 mL) according to general procedure **K**. Purification by column chromatography (SiO<sub>2</sub>, hexane/EtOAc, 30:1, *R<sub>f</sub>* = 0.22 (hexane/EtOAc, 9:1)) afforded **146e** (35.0 mg, 97.6 μmol, 98%) as a white solid.

**<sup>1</sup>H-NMR** (400 MHz, CDCl<sub>3</sub>): δ = 7.39 – 7.29 (m, 3H), 7.27 – 7.22 (m, 2H), 7.22 – 7.16 (m, 2H), 6.91 – 6.83 (m, 2H), 6.53 (d, *J* = 2.4 Hz, 1H), 6.28 (d, *J* = 2.4 Hz, 1H), 3.84 (s, 3H), 3.83 (s, 3H), 3.68 (s, 2H), 3.36 (s, 3H) ppm. **<sup>13</sup>C{<sup>1</sup>H}-NMR** (101 MHz, CDCl<sub>3</sub>): δ = 161.1, 158.8, 158.5, 145.0, 140.8, 140.2, 137.7, 135.9, 128.9, 128.2, 127.5, 127.5, 127.0, 126.1, 117.9, 113.4, 103.5, 97.7, 55.7, 55.5, 55.4, 42.0 ppm. **HR-MS** (ESI): calculated *m/z* for C<sub>24</sub>H<sub>22</sub>O<sub>3</sub><sup>+</sup> ([M+H]<sup>+</sup>): 359.1642; found 359.1644. **FTIR** (ATR, neat):  $\tilde{\nu}$  = 3065, 3000, 2952, 2935, 2904, 2835, 1603, 1575, 1509, 1488, 1461, 1419, 1332, 1312, 1290, 1244, 1201, 1177, 1163, 1130, 1107, 1052, 1039, 1036, 828, 798, 770, 755, 728 cm<sup>-1</sup>.

### 6-(4-methoxyphenyl)-12H-benzo[5',6']cyclohepta[1',2':3,4]benzo[1,2-d][1,3]dioxole (146f)



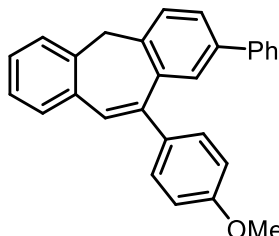
Prepared from **150f** (34.2 mg, 100 μmol, 1.0 eq), precatalyst **C** (1.70 mg, 2.00 μmol, 2 mol%) and AgSbF<sub>6</sub> (0.05 M in DCM, 40 μL, 2.00 μmol, 2 mol%) in DCM (2.0 mL) according to general procedure **K**. Purification by column chromatography (SiO<sub>2</sub>, hexane/EtOAc, 50:1, *R<sub>f</sub>* = 0.15 (hexane/EtOAc, 30:1)) afforded **146f** (34.0 mg, 99.3 μmol, 99%) as a pale yellow solid.

**<sup>1</sup>H-NMR** (400 MHz, CDCl<sub>3</sub>): δ = 7.46 – 7.38 (m, 2H), 7.35 (dd, *J* = 6.5, 2.3 Hz, 2H), 7.29 – 7.18 (m, 2H), 7.10 (s, 1H), 6.98 – 6.89 (m, 2H), 6.59-6.52 (m, 2H), 6.02 (s, 2H), 3.86 (s, 3H), 3.80 (br s, 2H) ppm. **<sup>13</sup>C{<sup>1</sup>H}-NMR** (101 MHz, CDCl<sub>3</sub>): δ = 159.3, 147.4, 144.3, 142.9, 138.4, 137.0, 136.4, 132.2, 130.5, 128.5, 127.9, 127.7, 127.6, 126.3, 123.4, 122.3, 113.7, 105.9, 101.2, 55.5, 32.8 ppm. **HR-MS** (ESI): calculated *m/z* for C<sub>23</sub>H<sub>19</sub>O<sub>3</sub><sup>+</sup> ([M+H]<sup>+</sup>):

## 5. Experimental

343.1329; found 343.1322. **FTIR** (ATR, neat):  $\tilde{\nu}$  = 3001, 2952, 2898, 2834, 2783, 1635, 1604, 1574, 1507, 1494, 1455, 1448, 1424, 1357, 1299, 1243, 1188, 1174, 1124, 1107, 1055, 1035, 1020, 985, 954, 930, 894, 868, 855, 829, 807, 758, 748, 741, 726, 678, 664, 635, 609  $\text{cm}^{-1}$ .

### 11-(4-methoxyphenyl)-2-phenyl-5H-dibenzo[a,d][7]annulene (**146g**)



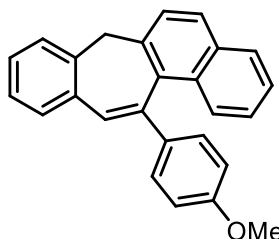
Prepared from **150g** (37.5 mg, 100  $\mu\text{mol}$ , 1.0 eq), precatalyst **C** (1.70 mg, 2.00  $\mu\text{mol}$ , 2 mol%) and  $\text{AgSbF}_6$  (0.05 M in DCM, 40  $\mu\text{L}$ , 2.00  $\mu\text{mol}$ , 2 mol%) in DCM (2.0 mL) according to general procedure **K**. Purification *via* crystallization (hexane/EtOAc, 50:1) afforded **146g** (36.4 mg, 97.2  $\mu\text{mol}$ , 97%) as colorless crystals and

single crystals suitable for X-ray analysis were obtained. Mp: 207-209  $^{\circ}\text{C}$ .

**$^1\text{H-NMR}$**  (400 MHz,  $\text{CDCl}_3$ ):  $\delta$  = 7.52 (dd,  $J$  = 7.9, 1.9 Hz, 1H), 7.50 – 7.45 (m, 2H), 7.45 – 7.37 (m, 4H), 7.37 – 7.19 (m, 8H), 6.99 – 6.92 (m, 2H), 3.87 (s, 3H), 3.84 (br s, 2H) ppm.

**$^{13}\text{C}\{^1\text{H}\}\text{-NMR}$**  (101 MHz,  $\text{CDCl}_3$ ):  $\delta$  = 159.3, 143.3, 141.1, 139.5, 139.3, 138.8, 137.0, 136.6, 135.6, 130.4, 129.3, 128.7, 128.4, 128.1, 127.9, 127.6, 127.22, 127.20, 127.1, 126.1, 113.9, 55.5, 41.3 ppm. **HR-MS** (ESI): calculated  $m/z$  for  $\text{C}_{28}\text{H}_{23}\text{O}^+$  ( $[\text{M}+\text{H}]^+$ ): 375.1743; found 375.1733. **FTIR** (ATR, neat):  $\tilde{\nu}$  = 3060, 3027, 2950, 2894, 2832, 1605, 1508, 1485, 1450, 1287, 1247, 1177, 1111, 1034, 905, 831, 796, 758, 732, 699, 667  $\text{cm}^{-1}$ .

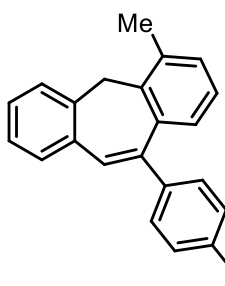
### 13-(4-methoxyphenyl)-7H-benzo[4,5]cyclohepta[1,2-a]naphthalene (**146h**)



Prepared from **150h** (34.8 mg, 100  $\mu\text{mol}$ , 1.0 eq), precatalyst **C** (1.70 mg, 2.00  $\mu\text{mol}$ , 2 mol%) and  $\text{AgSbF}_6$  (0.05 M in DCM, 40  $\mu\text{L}$ , 2.00  $\mu\text{mol}$ , 2 mol%) in DCM (2.0 mL) according to general procedure **K**. Purification by column chromatography ( $\text{SiO}_2$ , hexane/EtOAc, 50:1,  $R_f$  = 0.17 (hexane/EtOAc, 30:1)) afforded

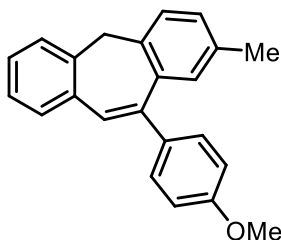
**146h** (32.0 mg, 91.8  $\mu\text{mol}$ , 92%) as a white solid. Single crystals suitable for X-ray analysis were obtained from DCM and hexane by diffusion crystallization. Mp: 200-203  $^{\circ}\text{C}$ .

**$^1\text{H-NMR}$**  (400 MHz,  $\text{CDCl}_3$ ):  $\delta$  = 7.79 (d,  $J$  = 8.4 Hz, 1H), 7.72 (d,  $J$  = 8.1 Hz, 1H), 7.64 (s, 1H), 7.55 – 7.45 (m, 2H), 7.39 (dd,  $J$  = 6.7, 2.2 Hz, 1H), 7.37 – 7.32 (m, 2H), 7.30 (dd,  $J$  = 6.7, 2.1 Hz, 1H), 7.26 – 7.15 (m, 3H), 7.10 (ddd,  $J$  = 8.4, 6.8, 1.4 Hz, 1H), 6.89 – 6.83 (m, 2H), 3.87 (s, 2H), 3.81 (s, 3H) ppm.  **$^{13}\text{C}\{^1\text{H}\}\text{-NMR}$**  (101 MHz,  $\text{CDCl}_3$ ):  $\delta$  = 159.0, 142.2, 141.3, 140.7, 137.2, 135.6, 133.1, 131.7, 130.8, 130.5, 129.4, 128.4, 128.2, 128.1, 127.9, 127.8, 126.7, 126.1, 126.0, 125.3, 124.5, 114.2, 55.4, 41.8 ppm. **HR-MS** (ESI): calculated  $m/z$  for  $\text{C}_{26}\text{H}_{21}\text{O}^+$  ( $[\text{M}+\text{H}]^+$ ): 349.1587; found 349.1584. **FTIR** (ATR, neat):  $\tilde{\nu}$  = 3050, 3014, 2953, 2927, 2895, 2834, 1604, 1571, 1505, 1481, 1459, 1438, 1342, 1284, 1247, 1211, 1174, 1108, 1027, 965, 952, 891, 867, 827, 813, 783, 760, 747, 712, 699, 645  $\text{cm}^{-1}$ .

**11-(4-methoxyphenyl)-4-methyl-5H-dibenzo[a,d][7]annulene (146i)**

Prepared from **150i** (31.2 mg, 100  $\mu\text{mol}$ , 1.0 eq), precatalyst **C** (1.70 mg, 2.00  $\mu\text{mol}$ , 2 mol%) and  $\text{AgSbF}_6$  (0.05 M in DCM, 40  $\mu\text{L}$ , 2.00  $\mu\text{mol}$ , 2 mol%) in DCM (2.0 mL) according to general procedure **K**. Purification by column chromatography ( $\text{SiO}_2$ , hexane/EtOAc, 50:1,  $R_f$  = 0.19 (hexane/EtOAc, 30:1)) afforded **146i** (30.7 mg, 98.2  $\mu\text{mol}$ , 98%) as a white solid.

**$^1\text{H-NMR}$**  (400 MHz,  $\text{CDCl}_3$ ):  $\delta$  = 7.47 – 7.40 (m, 2H), 7.38 (dd,  $J$  = 7.3, 1.4 Hz, 2H), 7.29 – 7.24 (m, 2H), 7.21 (td,  $J$  = 7.4, 1.4 Hz, 1H), 7.18 – 7.14 (m, 1H), 6.99 – 6.88 (m, 4H), 4.20 (br s, 1H), 3.86 (s, 3H), 3.34 (br s, 1H), 2.61 (s, 3H) ppm.  **$^{13}\text{C}\{^1\text{H}\}\text{-NMR}$**  (101 MHz,  $\text{CDCl}_3$ ):  $\delta$  = 159.2, 143.9, 139.3, 138.2, 137.2, 137.0, 136.0, 133.8, 130.42, 130.40, 128.7, 128.2, 127.8, 127.5, 127.0, 125.9, 125.0, 113.8, 55.5, 35.9, 20.8 ppm. **HR-MS** (ESI): calculated  $m/z$  for  $\text{C}_{23}\text{H}_{21}\text{O}^+$  ( $[\text{M}+\text{H}]^+$ ): 313.1587; found 313.1576. **FTIR** (ATR, neat):  $\tilde{\nu}$  = 3066, 3045, 2997, 2955, 2933, 2903, 2835, 1604, 1574, 1505, 1483, 1444, 1358, 1299, 1286, 1241, 1185, 1174, 1106, 1084, 1035, 948, 890, 871, 829, 795, 779, 754, 740, 733, 676, 656, 624, 614  $\text{cm}^{-1}$ .

**11-(4-methoxyphenyl)-2-methyl-5H-dibenzo[a,d][7]annulene (146j)**

Prepared from **150j** (31.2 mg, 100  $\mu\text{mol}$ , 1.0 eq), precatalyst **C** (1.70 mg, 2.00  $\mu\text{mol}$ , 2 mol%) and  $\text{AgSbF}_6$  (0.05 M in DCM, 40  $\mu\text{L}$ , 2.00  $\mu\text{mol}$ , 2 mol%) in DCM (2.0 mL) according to general procedure **K**. Purification by column chromatography ( $\text{SiO}_2$ , hexane/EtOAc, 50:1,  $R_f$  = 0.23 (hexane/EtOAc, 30:1)) afforded **146j**

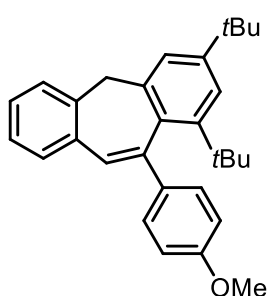
(30.0 mg, 96.0  $\mu\text{mol}$ , 96%) as a white solid.

**$^1\text{H-NMR}$**  (400 MHz,  $\text{CDCl}_3$ ):  $\delta$  = 7.49 – 7.42 (m, 2H), 7.38 (dd,  $J$  = 7.5, 1.5 Hz, 1H), 7.35 – 7.30 (m, 1H), 7.30 – 7.25 (m, 3H), 7.22 (td,  $J$  = 7.4, 1.6 Hz, 1H), 7.13 (dd,  $J$  = 7.7, 1.8 Hz, 1H), 7.01 – 6.95 (m, 2H), 6.89 (d,  $J$  = 1.9 Hz, 1H), 3.90 (s, 3H), 3.78 (br s, 2H), 2.21 (s, 3H) ppm.  **$^{13}\text{C}\{^1\text{H}\}\text{-NMR}$**  (101 MHz,  $\text{CDCl}_3$ ):  $\delta$  = 159.2, 143.3, 139.7, 137.6, 136.8, 136.5, 135.6, 135.1, 130.4, 130.0, 129.6, 129.1, 128.3, 128.0, 127.3, 127.1, 125.9, 113.8, 55.5, 41.3, 21.2 ppm. **HR-MS** (ESI): calculated  $m/z$  for  $\text{C}_{23}\text{H}_{21}\text{O}^+$  ( $[\text{M}+\text{H}]^+$ ): 313.1587; found 313.1582. **FTIR** (ATR, neat):  $\tilde{\nu}$  = 3018, 2955, 2917, 2891, 2832, 1507, 1462, 1451, 1421, 1355, 1299, 1246, 1173, 1144, 1108, 1030, 948, 898, 887, 860, 831, 821, 796, 768, 753, 733, 695, 656, 629, 612  $\text{cm}^{-1}$ .

**1,3-di-tert-butyl-11-(4-methoxyphenyl)-5H-dibenzo[a,d][7]annulene (146k)**

Prepared from **150k** (41.1 mg, 100  $\mu\text{mol}$ , 1.0 eq), precatalyst **C** (1.70 mg, 2.00  $\mu\text{mol}$ , 2 mol%) and  $\text{AgSbF}_6$  (0.05 M in DCM, 40  $\mu\text{L}$ , 2.00  $\mu\text{mol}$ , 2 mol%) in DCM (2.0 mL) according to general procedure **K**. Purification by column chromatography ( $\text{SiO}_2$ ,

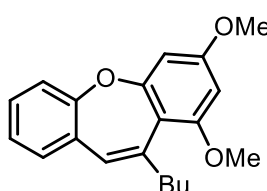
## 5. Experimental



hexane/EtOAc, 50:1,  $R_f$  = 0.25 (hexane/EtOAc, 30:1)) afforded **146k** (31.6 mg, 77.0  $\mu$ mol, 77%) as a white solid. Single crystals suitable for X-ray analysis were obtained from slow evaporation of chloroform. Mp: 150-155  $^{\circ}$ C.

**$^1\text{H-NMR}$**  (400 MHz,  $\text{CDCl}_3$ ):  $\delta$  = 7.34 (d,  $J$  = 2.0 Hz, 1H), 7.30 (dd,  $J$  = 6.9, 1.9 Hz, 1H), 7.28 – 7.22 (m, 2H), 7.20 – 7.06 (m, 4H), 6.84 (d,  $J$  = 8.4 Hz, 2H), 3.81 (s, 3H), 3.76 (d,  $J$  = 12.9 Hz, 1H), 3.58 (d,  $J$  = 12.9 Hz, 1H), 1.33 (s, 9H), 1.01 (s, 9H) ppm.  **$^{13}\text{C}\{^1\text{H}\}\text{-NMR}$**  (101 MHz,  $\text{CDCl}_3$ ):  $\delta$  = 158.6, 149.2, 148.8, 145.7, 145.71, 142.66, 138.1, 136.3, 130.8, 128.3, 127.5, 127.0, 126.8, 126.7, 125.7, 124.0, 120.7, 113.4, 55.1, 42.1, 36.8, 34.3, 32.0, 31.2 ppm. **HR-MS** (ESI): calculated  $m/z$  for  $\text{C}_{30}\text{H}_{35}\text{O}^+$  ( $[\text{M}+\text{H}]^+$ ): 411.2682; found 411.2668. **FTIR** (ATR, neat):  $\tilde{\nu}$  = 3067, 3013, 2959, 2949, 2898, 2864, 2840, 1602, 1508, 1478, 1461, 1440, 1360, 1285, 1248, 1178, 1156, 1111, 1030, 958, 900, 884, 873, 824, 798, 770, 745, 723, 676, 644, 627  $\text{cm}^{-1}$ .

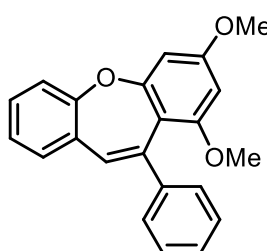
### 11-butyl-1,3-dimethoxydibenzo[*b,f*]oxepine (147a)



Prepared from **151a** (31.0 mg, 100  $\mu$ mol, 1.0 eq), precatalyst **C** (1.70 mg, 2.00  $\mu$ mol, 2 mol%) and  $\text{AgSbF}_6$  (0.05 M in DCM, 40  $\mu$ L, 2.00  $\mu$ mol, 2 mol%) in DCM (2.0 mL) according to general procedure **K**. Purification by column chromatography ( $\text{SiO}_2$ , hexane/EtOAc, 50:1,  $R_f$  = 0.19 (hexane/EtOAc, 30:1)) afforded **147a** (26.6 mg, 86.2  $\mu$ mol, 86%) as a colorless oil.

**$^1\text{H-NMR}$**  (300 MHz,  $\text{CDCl}_3$ ):  $\delta$  = 7.24 – 7.03 (m, 4H), 6.66 (s, 1H), 6.44 (d,  $J$  = 2.5 Hz, 1H), 6.28 (d,  $J$  = 2.5 Hz, 1H), 3.81 (s, 3H), 3.78 (s, 3H), 2.80 (s, 2H), 1.49 – 1.26 (m, 4H), 0.88 (t,  $J$  = 7.1 Hz, 3H) ppm.  **$^{13}\text{C}\{^1\text{H}\}\text{-NMR}$**  (101 MHz,  $\text{CDCl}_3$ ):  $\delta$  = 162.3, 161.1, 158.6, 158.5, 142.0, 131.4, 128.9, 128.4, 126.0, 124.9, 120.5, 113.6, 98.2, 96.2, 55.7, 55.6, 37.2, 31.7, 22.5, 14.1 ppm. **HR-MS** (ESI): calculated  $m/z$  for  $\text{C}_{20}\text{H}_{23}\text{O}_3^+$  ( $[\text{M}+\text{H}]^+$ ): 311.1642; found 311.1645. **FTIR** (ATR, neat):  $\tilde{\nu}$  = 3070, 3001, 2954, 2928, 2869, 2838, 1606, 1568, 1484, 1454, 1435, 1415, 1376, 1326, 1285, 1262, 1214, 1198, 1146, 1091, 1064, 1027, 980, 939, 863, 827, 758, 738, 682, 628, 605  $\text{cm}^{-1}$ .

### 1,3-dimethoxy-11-phenyldibenzo[*b,f*]oxepine (147b)



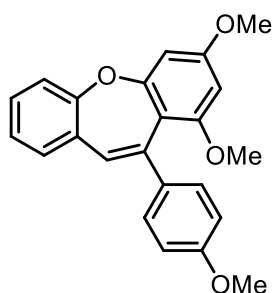
Prepared from **151b** (33.0 mg, 100  $\mu$ mol, 1.0 eq), precatalyst **C** (1.70 mg, 2.00  $\mu$ mol, 2 mol%) and  $\text{AgSbF}_6$  (0.05 M in DCM, 40  $\mu$ L, 2.00  $\mu$ mol, 2 mol%) in DCM (2.0 mL) according to general procedure **K**. Purification by column chromatography ( $\text{SiO}_2$ , hexane/EtOAc, 30:1,  $R_f$  = 0.16) afforded **147b** (32.5 mg, 98.4  $\mu$ mol, 98%) as a white solid. Single crystals suitable for X-ray analysis were obtained from hot EtOH. Mp: 134-137  $^{\circ}$ C.



## 5.2 Synthesis and characterization of new compounds

**<sup>1</sup>H-NMR** (400 MHz, CDCl<sub>3</sub>):  $\delta$  = 7.40 – 7.36 (m, 2H), 7.35 – 7.22 (m, 5H), 7.18 (dd,  $J$  = 8.1, 1.3 Hz, 1H), 7.14 (td,  $J$  = 7.3, 1.4 Hz, 1H), 6.96 (s, 1H), 6.52 (d,  $J$  = 2.4 Hz, 1H), 6.24 (d,  $J$  = 2.5 Hz, 1H), 3.84 (s, 3H), 3.32 (s, 3H) ppm. **<sup>13</sup>C{<sup>1</sup>H}-NMR** (101 MHz, CDCl<sub>3</sub>):  $\delta$  = 162.8, 162.0, 158.9, 158.6, 144.1, 140.4, 131.3, 129.4, 129.1, 128.0 (2C), 126.8, 126.4, 125.1, 120.9, 113.4, 98.3, 96.9, 55.7, 55.6 ppm. **HR-MS** (ESI): calculated  $m/z$  for C<sub>22</sub>H<sub>19</sub>O<sub>3</sub><sup>+</sup> ([M+H]<sup>+</sup>): 331.1329; found 331.1332. **FTIR** (ATR, neat):  $\tilde{\nu}$  = 3056, 3021, 2959, 2936, 2839, 1608, 1568, 1485, 1449, 1437, 1416, 1355, 1329, 1292, 1244, 1214, 1198, 1156, 1134, 1090, 1050, 985, 941, 910, 862, 827, 765, 737, 697 cm<sup>-1</sup>.

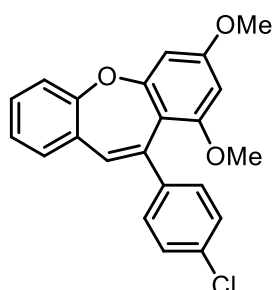
### 1,3-dimethoxy-11-(4-methoxyphenyl)dibenzo[*b,f*]oxepine (**147c**)



Prepared from **151c** (36.0 mg, 100  $\mu$ mol, 1.0 eq), precatalyst **C** (1.70 mg, 2.00  $\mu$ mol, 2 mol%) and AgSbF<sub>6</sub> (0.05 M in DCM, 40  $\mu$ L, 2.00  $\mu$ mol, 2 mol%) in DCM (2.0 mL) according to general procedure **K**. Purification by column chromatography (SiO<sub>2</sub>, hexane/EtOAc, 30:1,  $R_f$  = 0.15 (hexane/EtOAc, 10:1)) afforded **147c** (35.8 mg, 99.3  $\mu$ mol, 99%) as a white solid. Single crystals suitable for X-ray analysis were obtained from hot EtOH. Mp: 184-185 °C.

**<sup>1</sup>H-NMR** (400 MHz, CDCl<sub>3</sub>):  $\delta$  = 7.34 – 7.28 (m, 2H), 7.28 – 7.21 (m, 2H), 7.19 – 7.15 (m, 1H), 7.13 (td,  $J$  = 7.4, 1.4 Hz, 1H), 6.91 (s, 1H), 6.89 – 6.82 (m, 2H), 6.51 (d,  $J$  = 2.4 Hz, 1H), 6.24 (d,  $J$  = 2.5 Hz, 1H), 3.84 (s, 3H), 3.83 (s, 3H), 3.36 (s, 3H) ppm. **<sup>13</sup>C{<sup>1</sup>H}-NMR** (101 MHz, CDCl<sub>3</sub>):  $\delta$  = 162.7, 161.9, 158.9, 158.7, 158.6, 139.8, 136.6, 131.5, 129.3, 128.9, 127.5, 126.8, 125.0, 120.8, 113.4, 98.3, 96.9, 55.8, 55.6, 55.4 ppm. **HR-MS** (ESI): calculated  $m/z$  for C<sub>20</sub>H<sub>23</sub>O<sub>3</sub><sup>+</sup> ([M]<sup>+</sup>): 361.1434; found 361.1438. **FTIR** (ATR, neat):  $\tilde{\nu}$  = 3004, 2962, 2901, 2829, 1605, 1572, 1509, 1482, 1460, 1439, 1417, 1361, 1335, 1251, 1216, 1189, 1174, 1159, 1134, 1083, 1018, 938, 863, 794, 774, 758, 728, 681, 660, 628, 579, 553, 533, 516 cm<sup>-1</sup>.

### 11-(4-chlorophenyl)-1,3-dimethoxydibenzo[*b,f*]oxepine (**147d**)



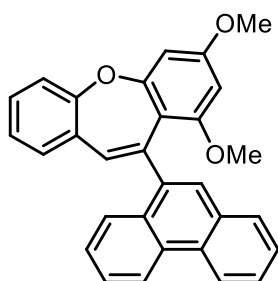
Prepared from **151d** (36.5 mg, 100  $\mu$ mol, 1.0 eq), precatalyst **C** (1.70 mg, 2.00  $\mu$ mol, 2 mol%) and AgSbF<sub>6</sub> (0.05 M in DCM, 40  $\mu$ L, 2.00  $\mu$ mol, 2 mol%) in DCM (2.0 mL) according to general procedure **K**. Purification by column chromatography (SiO<sub>2</sub>, hexane/EtOAc, 30:1,  $R_f$  = 0.17) afforded **147d** (35.6 mg, 97.7  $\mu$ mol, 98%) as a white solid.

**<sup>1</sup>H-NMR** (400 MHz, CDCl<sub>3</sub>):  $\delta$  = 7.35 – 7.23 (m, 6H), 7.22 – 7.10 (m, 2H), 6.93 (s, 1H), 6.51 (d,  $J$  = 2.4 Hz, 1H), 6.23 (d,  $J$  = 2.3 Hz, 1H), 3.84 (s, 3H), 3.35 (s, 3H) ppm. **<sup>13</sup>C{<sup>1</sup>H}-NMR** (101 MHz, CDCl<sub>3</sub>):  $\delta$  = 162.8, 162.1, 158.7, 158.6, 142.6, 139.2, 132.3, 131.0, 129.4, 129.3, 128.3, 128.1, 127.7, 125.1, 120.9, 112.8, 98.4, 96.8, 55.7, 55.6 ppm. **HR-MS** (EI):

## 5. Experimental

calculated  $m/z$  for  $C_{22}H_{18}ClO_3^+$  ( $[M]^+$ ): 364.0861; found 364.0862. **FTIR** (ATR, neat):  $\tilde{\nu} = 2998, 2963, 2933, 2840, 1604, 1568, 1487, 1461, 1434, 1415, 1357, 1336, 1290, 1248, 1215, 1196, 1158, 1134, 1090, 1047, 1014, 985, 954, 932, 884, 861, 822, 771, 759, 742, 720, 675, 630\text{ cm}^{-1}$ .

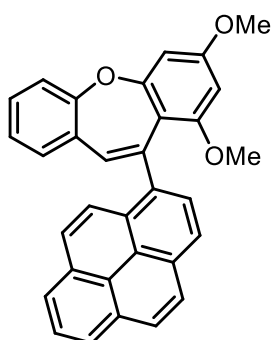
### 1,3-dimethoxy-11-(phenanthren-9-yl)dibenzo[*b,f*]oxepine (147e)



Prepared from **151e** (43.1 mg, 100  $\mu\text{mol}$ , 1.0 eq), precatalyst **C** (1.70 mg, 2.00  $\mu\text{mol}$ , 2 mol%) and  $\text{AgSbF}_6$  (0.05 M in DCM, 40  $\mu\text{L}$ , 2.00  $\mu\text{mol}$ , 2 mol%) in DCM (2.0 mL) according to general procedure **K**. Purification by column chromatography ( $\text{SiO}_2$ , hexane/EtOAc, 30:1,  $R_f = 0.14$ ) afforded **147e** (42.2 mg, 98.0  $\mu\text{mol}$ , 98%) as a white solid.

**$^1\text{H-NMR}$**  (400 MHz,  $\text{CDCl}_3$ ):  $\delta = 8.75 - 8.68$  (m, 2H), 8.15 (d,  $J = 8.2$  Hz, 1H), 7.91 (dd,  $J = 7.5, 1.7$  Hz, 1H), 7.80 (s, 1H), 7.68 – 7.56 (m, 2H), 7.52 – 7.47 (m, 1H), 7.37 – 7.30 (m, 2H), 7.29 – 7.25 (m, 2H), 7.19 (td,  $J = 7.3, 1.4$  Hz, 1H), 7.02 (s, 1H), 6.58 (d,  $J = 2.5$  Hz, 1H), 6.08 (d,  $J = 2.4$  Hz, 1H), 3.82 (s, 3H), 2.90 (s, 3H) ppm.  **$^{13}\text{C}\{^1\text{H}\}\text{-NMR}$**  (101 MHz,  $\text{CDCl}_3$ ):  $\delta = 162.0, 161.5, 159.0, 158.4, 141.7, 139.1, 132.1, 131.3, 131.2, 130.7, 130.4, 129.9, 129.44, 129.40, 128.7, 126.8, 126.6, 126.3, 126.2, 126.1, 125.5, 125.2, 122.8, 122.6, 120.9, 115.4, 98.7, 97.0, 55.7, 55.6$  ppm. **HR-MS** (ESI): calculated  $m/z$  for  $C_{30}H_{23}O_3^+$  ( $[M+H]^+$ ): 431.1642; found 431.1641. **FTIR** (ATR, neat):  $\tilde{\nu} = 3067, 3004, 2933, 2838, 1607, 1567, 1483, 1450, 1434, 1415, 1328, 1214, 1196, 1141, 1109, 1089, 1065, 1044, 982, 939, 884, 850, 838, 758, 740, 724, 673, 627, 570, 517\text{ cm}^{-1}$ .

### 1,3-dimethoxy-11-(pyren-1-yl)dibenzo[*b,f*]oxepine (147f)



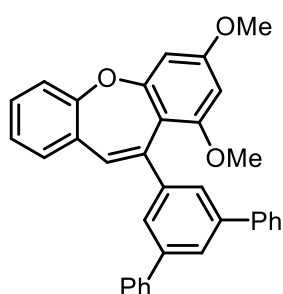
Prepared from **151f** (45.5 mg, 100  $\mu\text{mol}$ , 1.0 eq), precatalyst **C** (1.70 mg, 2.00  $\mu\text{mol}$ , 2 mol%) and  $\text{AgSbF}_6$  (0.05 M in DCM, 40  $\mu\text{L}$ , 2.00  $\mu\text{mol}$ , 2 mol%) in DCM (2.0 mL) according to general procedure **K**. Purification by column chromatography ( $\text{SiO}_2$ , hexane/EtOAc, 50:1,  $R_f = 0.08$ ) afforded **147f** (44.4 mg, 97.6  $\mu\text{mol}$ , 98%) as a yellow solid.

**$^1\text{H-NMR}$**  (400 MHz,  $\text{CDCl}_3$ ):  $\delta = 8.32$  (d,  $J = 9.2$  Hz, 1H), 8.19 – 8.14 (m, 2H), 8.14 – 8.02 (m, 4H), 8.01 – 7.94 (m, 2H), 7.38 (dd,  $J = 7.5, 1.6$  Hz, 1H), 7.34 (ddd,  $J = 8.8, 7.1, 1.7$  Hz, 1H), 7.29 (dd,  $J = 8.1, 1.5$  Hz, 1H), 7.21 (td,  $J = 7.3, 1.5$  Hz, 1H), 7.01 (s, 1H), 6.61 (d,  $J = 2.4$  Hz, 1H), 6.07 (d,  $J = 2.5$  Hz, 1H), 3.83 (s, 3H), 2.81 (s, 3H) ppm.  **$^{13}\text{C}\{^1\text{H}\}\text{-NMR}$**  (101 MHz,  $\text{CDCl}_3$ ):  $\delta = 162.1, 161.6, 159.0, 158.4, 140.9, 139.7, 131.7, 131.6, 131.3, 131.2, 130.2, 129.5, 129.4, 128.2, 127.7, 126.9, 126.7, 125.9, 125.6, 125.23, 125.16, 124.9, 124.8, 124.7, 124.5, 121.0, 115.7, 98.6, 97.0, 55.63, 55.58$  ppm. **HR-MS** (ESI): calculated  $m/z$  for  $C_{32}H_{23}O_3^+$  ( $[M+H]^+$ ): 455.1642; found 455.1641. **FTIR** (ATR, neat):

## 5.2 Synthesis and characterization of new compounds

$\tilde{\nu}$  = 3038, 3006, 2934, 2836, 1605, 1567, 1484, 1454, 1435, 1415, 1327, 1289, 1245, 1213, 1196, 1153, 1141, 1087, 1045, 938, 905, 843, 752, 681, 634, 546, 506  $\text{cm}^{-1}$ .

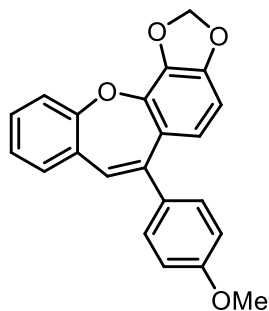
### 11-([1,1':3',1''-terphenyl]-5'-yl)-1,3-dimethoxydibenzo[*b,f*]oxepine (**147g**)



Prepared from **151g** (48.3 mg, 100  $\mu\text{mol}$ , 1.0 eq), precatalyst **C** (1.70 mg, 2.00  $\mu\text{mol}$ , 2 mol%) and  $\text{AgSbF}_6$  (0.05 M in DCM, 40  $\mu\text{L}$ , 2.00  $\mu\text{mol}$ , 2 mol%) in DCM (2.0 mL) according to general procedure **K**. Purification by column chromatography ( $\text{SiO}_2$ , hexane/EtOAc, 30:1,  $R_f$  = 0.22 (hexane/EtOAc, 10:1)) afforded **147g** (45.0 mg, 93.2  $\mu\text{mol}$ , 93%) as a white solid.

**$^1\text{H-NMR}$**  (400 MHz,  $\text{CDCl}_3$ ):  $\delta$  = 7.72 (t,  $J$  = 1.7 Hz, 1H), 7.70 – 7.65 (m, 4H), 7.60 (d,  $J$  = 1.7 Hz, 2H), 7.50 – 7.44 (m, 4H), 7.41 – 7.34 (m, 2H), 7.34 – 7.26 (m, 2H), 7.21 (dd,  $J$  = 8.1, 1.3 Hz, 1H), 7.16 (td,  $J$  = 7.4, 1.4 Hz, 1H), 7.09 (s, 1H), 6.54 (d,  $J$  = 2.4 Hz, 1H), 6.25 (d,  $J$  = 2.5 Hz, 1H), 3.85 (s, 3H), 3.35 (s, 3H) ppm.  **$^{13}\text{C}\{^1\text{H}\}\text{-NMR}$**  (101 MHz,  $\text{CDCl}_3$ ):  $\delta$  = 162.9, 162.1, 158.9, 158.7, 145.2, 141.54, 141.51, 140.2, 131.2, 129.5, 129.2, 128.9, 128.3, 127.5, 127.4, 125.1, 124.7, 124.4 (2C), 120.9, 113.3, 98.4, 97.0, 55.8, 55.7 ppm. **HR-MS** (ESI): calculated  $m/z$  for  $\text{C}_{34}\text{H}_{27}\text{O}_3^+$  ( $[\text{M}+\text{H}]^+$ ): 483.1955; found 483.1963. **FTIR** (ATR, neat):  $\tilde{\nu}$  = 3057, 3029, 3008, 2958, 2934, 2838, 1607, 1565, 1485, 1453, 1434, 1415, 1353, 1326, 1287, 1263, 1234, 1212, 1193, 1151, 1131, 1107, 1087, 1046, 1027, 986, 936, 876, 848, 827, 757, 715, 695, 670, 644, 611, 563, 521  $\text{cm}^{-1}$ .

### 6-(4-methoxyphenyl)-[1,3]dioxolo[4',5':5,6]benzo[1,2-*b*]benzo[*f*]oxepine (**147h**)

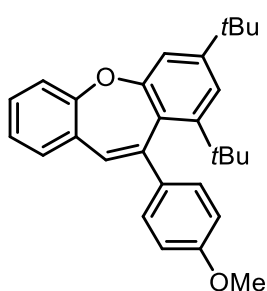


Prepared from **151h** (34.4 mg, 100  $\mu\text{mol}$ , 1.0 eq), precatalyst **C** (1.70 mg, 2.00  $\mu\text{mol}$ , 2 mol%) and  $\text{AgSbF}_6$  (0.05 M in DCM, 40  $\mu\text{L}$ , 2.00  $\mu\text{mol}$ , 2 mol%) in DCM (2.0 mL) according to general procedure **K**. Purification by column chromatography ( $\text{SiO}_2$ , hexane/EtOAc, 30:1,  $R_f$  = 0.13) afforded **147h** (25.5 mg, 74.0  $\mu\text{mol}$ , 74%) as a colorless oil.

**$^1\text{H-NMR}$**  (400 MHz,  $\text{CDCl}_3$ ):  $\delta$  = 7.42 – 7.35 (m, 2H), 7.31 – 7.24 (m, 3H), 7.19 – 7.13 (m, 1H), 6.97 – 6.90 (m, 2H), 6.77 (s, 1H), 6.53 (d,  $J$  = 8.3 Hz, 1H), 6.46 (d,  $J$  = 8.4 Hz, 1H), 6.07 (s, 2H), 3.86 (s, 3H) ppm.  **$^{13}\text{C}\{^1\text{H}\}\text{-NMR}$**  (101 MHz,  $\text{CDCl}_3$ ):  $\delta$  = 159.5, 157.5, 150.2, 141.9, 141.8, 139.2, 135.4, 131.1, 130.3, 129.7, 129.1, 128.0, 125.8, 125.2, 123.5, 121.1, 113.8, 104.9, 102.3, 55.5 ppm. **HR-MS** (ESI): calculated  $m/z$  for  $\text{C}_{22}\text{H}_{17}\text{O}_4^+$  ( $[\text{M}+\text{H}]^+$ ): 345.1121; found 345.1120. **FTIR** (ATR, neat):  $\tilde{\nu}$  = 3062, 3003, 2955, 2930, 2896, 2835, 2781, 1627, 1605, 1574, 1509, 1478, 1462, 1443, 1360, 1335, 1288, 1242, 1194, 1175, 1125, 1106, 1055, 1036, 985, 926, 907, 874, 853, 828, 809, 795, 782, 773, 749, 728, 680, 664, 649, 635, 624, 614, 564, 532, 512  $\text{cm}^{-1}$ .

## 5. Experimental

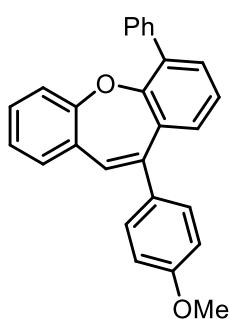
### 1,3-di-*tert*-butyl-11-(4-methoxyphenyl)dibenzo[*b,f*]oxepine (**147i**)



Prepared from **151i** (41.3 mg, 100  $\mu\text{mol}$ , 1.0 eq), precatalyst **C** (1.70 mg, 2.00  $\mu\text{mol}$ , 2 mol%) and  $\text{AgSbF}_6$  (0.05 M in DCM, 40  $\mu\text{L}$ , 2.00  $\mu\text{mol}$ , 2 mol%) in DCM (2.0 mL) according to general procedure **K**. Purification by column chromatography ( $\text{SiO}_2$ , hexane/EtOAc, 50:1,  $R_f = 0.26$  (hexane/EtOAc, 30:1)) afforded **146i** (27.0 mg, 65.4  $\mu\text{mol}$ , 65%) as a white solid. Single crystals suitable for X-ray analysis were obtained from hot EtOH. Mp: 205-207  $^\circ\text{C}$ .

**$^1\text{H-NMR}$**  (400 MHz,  $\text{CDCl}_3$ ):  $\delta = 7.32 - 7.26$  (m, 2H), 7.24 – 7.08 (m, 6H), 7.00 (s, 1H), 6.86 – 6.81 (m, 2H), 3.80 (s, 3H), 1.34 (s, 9H), 1.01 (s, 9H) ppm.  **$^{13}\text{C}\{^1\text{H}\}\text{-NMR}$**  (101 MHz,  $\text{CDCl}_3$ ):  $\delta = 164.8, 160.5, 159.1, 151.5, 150.9, 145.1, 137.9, 132.3, 128.6, 128.5, 126.3, 126.1, 124.8, 122.9, 120.8, 114.6, 113.7, 55.4, 37.2, 34.8, 32.2, 31.4$  ppm. **FTIR** (ATR, neat):  $\tilde{\nu} = 646, 680, 729, 753, 772, 826, 869, 906, 973, 1032, 1105, 1150, 1176, 1192, 1223, 1246, 1285, 1362, 1396, 1444, 1462, 1480, 1509, 1542, 1575, 1604, 2835, 2866, 2903, 2954, 3068$ . **HR-MS** (ESI): calculated  $m/z$  for  $\text{C}_{29}\text{H}_{33}\text{O}_2^+$  ( $[\text{M}+\text{H}]^+$ ): 413.2475; found 413.2476. **FTIR** (ATR, neat):  $\tilde{\nu} = 3068, 2954, 2903, 2866, 2835, 1604, 1575, 1542, 1509, 1480, 1444, 1396, 1362, 1285, 1246, 1223, 1192, 1176, 1150, 1105, 1032, 973, 906, 869, 851, 826, 772, 753, 729, 680, 646, 590, 577, 563, 533$   $\text{cm}^{-1}$ .

### 11-(4-methoxyphenyl)-4-phenyldibenzo[*b,f*]oxepine (**147j**)



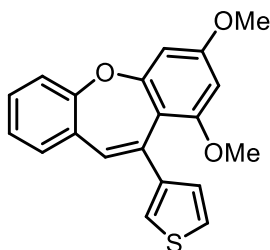
Prepared from **151j** (37.7 mg, 100  $\mu\text{mol}$ , 1.0 eq), precatalyst **C** (1.70 mg, 2.00  $\mu\text{mol}$ , 2 mol%) and  $\text{AgSbF}_6$  (0.05 M in DCM, 40  $\mu\text{L}$ , 2.00  $\mu\text{mol}$ , 2 mol%) in DCM (2.0 mL) according to general procedure **K**. Purification by column chromatography ( $\text{SiO}_2$ , hexane/EtOAc, 30:1,  $R_f = 0.20$ ) afforded **147j** (37.0 mg, 98.3  $\mu\text{mol}$ , 98%) as a white solid.

**$^1\text{H-NMR}$**  (400 MHz,  $\text{CDCl}_3$ ):  $\delta = 7.70 - 7.65$  (m, 2H), 7.56 – 7.49 (m, 2H), 7.49 – 7.42 (m, 3H), 7.38 (dd,  $J = 7.4, 1.8$  Hz, 1H), 7.23 (dd,  $J = 7.1, 2.2$  Hz, 1H), 7.09 (t,  $J = 7.7$  Hz, 1H), 7.06 – 6.89 (m, 6H), 6.25 (dd,  $J = 7.4, 1.9$  Hz, 1H), 3.88 (s, 3H) ppm.  **$^{13}\text{C}\{^1\text{H}\}\text{-NMR}$**  (101 MHz,  $\text{CDCl}_3$ ):  $\delta = 159.5, 157.7, 155.0, 142.1, 138.3, 135.5, 135.3, 133.0, 131.3, 131.2, 130.4, 130.3, 129.9, 129.2, 129.1, 128.1, 127.5, 127.1, 124.8, 124.4, 121.1, 113.9, 55.5$  ppm. **HR-MS** (ESI): calculated  $m/z$  for  $\text{C}_{27}\text{H}_{21}\text{O}_2^+$  ( $[\text{M}+\text{H}]^+$ ): 377.1536; found 377.1535. **FTIR** (ATR, neat):  $\tilde{\nu} = 3032, 3000, 2954, 2930, 2906, 2834, 1603, 1573, 1506, 1483, 1446, 1425, 1362, 1285, 1241, 1198, 1174, 1108, 1091, 1071, 1025, 957, 943, 878, 859, 837, 808, 783, 761, 754, 751, 727, 700, 674$   $\text{cm}^{-1}$ .

### 1,3-dimethoxy-11-(thiophen-3-yl)dibenzo[*b,f*]oxepine (**147k**)

Prepared from **151k** (33.6 mg, 100  $\mu\text{mol}$ , 1.0 eq), precatalyst **C** (1.70 mg, 2.00  $\mu\text{mol}$ , 2 mol%) and  $\text{AgSbF}_6$  (0.05 M in DCM, 40  $\mu\text{L}$ , 2.00  $\mu\text{mol}$ , 2 mol%) in DCM (2.0 mL)

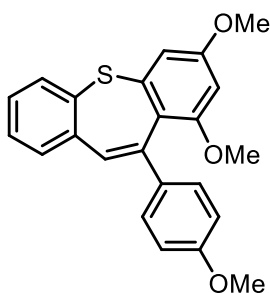
## 5.2 Synthesis and characterization of new compounds



according to general procedure **K**. Purification by column chromatography (SiO<sub>2</sub>, hexane/EtOAc, 30:1, *R<sub>f</sub>* = 0.15) afforded **147k** (31.0 mg, 92.1 μmol, 92%) as a white solid. Single crystals suitable for X-ray analysis were obtained from hot EtOH. Mp: 140-142 °C.

**<sup>1</sup>H-NMR** (400 MHz, CDCl<sub>3</sub>): δ = 7.30 – 7.20 (m, 3H), 7.19 – 7.10 (m, 4H), 7.05 (s, 1H), 6.50 (d, *J* = 2.5 Hz, 1H), 6.27 (d, *J* = 2.5 Hz, 1H), 3.83 (s, 3H), 3.45 (s, 3H) ppm. **<sup>13</sup>C{<sup>1</sup>H}-NMR** (101 MHz, CDCl<sub>3</sub>): δ = 162.6, 161.9, 158.9, 158.7, 144.5, 134.9, 131.2, 129.4, 129.0, 127.0, 126.7, 125.1, 124.5, 120.8, 120.0, 113.1, 98.2, 96.8, 55.8, 55.7 ppm. **HR-MS** (ESI): calculated *m/z* for C<sub>20</sub>H<sub>17</sub>O<sub>3</sub>S<sup>+</sup> ([M+H]<sup>+</sup>): 337.0893; found 337.0897. **FTIR** (ATR, neat):  $\tilde{\nu}$  = 3008, 2957, 2939, 2910, 2838, 1603, 1567, 1485, 1463, 1445, 1434, 1411, 1373, 1333, 1287, 1239, 1215, 1197, 1152, 1126, 1108, 1089, 1073, 1051, 1034, 993, 975, 943, 901, 855, 843, 829, 712, 675, 649, 641, 523 cm<sup>-1</sup>.

### 1,3-dimethoxy-11-(4-methoxyphenyl)dibenzo[b,f]thiepine (**148a**)

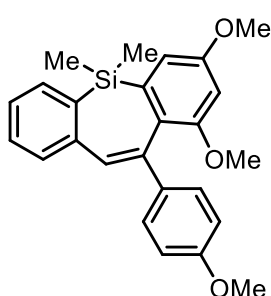


Prepared from **152a** (37.7 mg, 100 μmol, 1.0 eq), precatalyst **C** (1.70 mg, 2.00 μmol, 2 mol%) and AgSbF<sub>6</sub> (0.05 M in DCM, 40 μL, 2.00 μmol, 2 mol%) in DCM (2.0 mL) according to general procedure **K**. Purification by column chromatography (SiO<sub>2</sub>, hexane/EtOAc, 30:1, *R<sub>f</sub>* = 0.08) afforded **148a** (37.0 mg, 98.3 μmol, 98%) as an off-white solid. Single crystals suitable for X-ray analysis were obtained from hot EtOAc. Mp: 197-200 °C.

**<sup>1</sup>H-NMR** (400 MHz, CDCl<sub>3</sub>): δ = 7.50 (dd, *J* = 7.7, 1.3 Hz, 1H), 7.37 – 7.33 (m, 1H), 7.32 (s, 1H), 7.30 – 7.26 (m, 3H), 7.20 (td, *J* = 7.5, 1.6 Hz, 1H), 6.88 – 6.82 (m, 2H), 6.81 (d, *J* = 2.4 Hz, 1H), 6.35 (d, *J* = 2.4 Hz, 1H), 3.82 (s, 3H), 3.82 (s, 3H), 3.35 (s, 3H). **<sup>13</sup>C{<sup>1</sup>H}-NMR** (101 MHz, CDCl<sub>3</sub>): δ = 160.9, 159.1, 158.8, 143.8, 141.9, 140.8, 137.22, 137.17, 132.3, 130.7, 129.1, 128.2, 127.9, 127.4, 123.0, 113.5, 108.5, 100.5, 55.8, 55.6, 55.4 ppm. **HR-MS** (ESI): calculated *m/z* for C<sub>23</sub>H<sub>21</sub>O<sub>3</sub>S<sup>+</sup> ([M+H]<sup>+</sup>): 377.1206; found 377.1208. **FTIR** (ATR, neat):  $\tilde{\nu}$  = 2997, 2960, 2927, 2898, 2832, 1608, 1589, 1555, 1507, 1472, 1456, 1429, 1399, 1356, 1312, 1299, 1277, 1234, 1213, 1182, 960, 946, 933, 908, 887, 869, 857, 840, 821, 786, 769, 752, 740, 671, 637, 632, 620, 601, 535, 520 cm<sup>-1</sup>.

## 5. Experimental

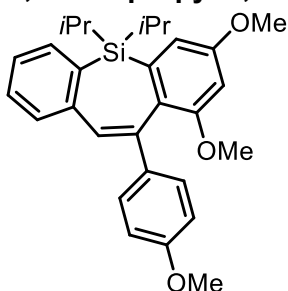
### 1,3-dimethoxy-11-(4-methoxyphenyl)-5,5-dimethyl-5H-dibenzo[*b,f*]silepine (**149a**)



Prepared from **153a** (40.3 mg, 100  $\mu\text{mol}$ , 1.0 eq), precatalyst **C** (1.70 mg, 2.00  $\mu\text{mol}$ , 2 mol%) and  $\text{AgSbF}_6$  (0.05 M in DCM, 40  $\mu\text{L}$ , 2.00  $\mu\text{mol}$ , 2 mol%) in DCM (2.0 mL) according to general procedure **K**. Purification by column chromatography ( $\text{SiO}_2$ , hexane/EtOAc, 30:1,  $R_f = 0.19$  (hexane/EtOAc, 10:1)) afforded **149a** (39.7 mg, 98.6  $\mu\text{mol}$ , 99%) as an off-white solid. Single crystals suitable for X-ray analysis were obtained from hot MeOH. Mp: 155-160  $^\circ\text{C}$ .

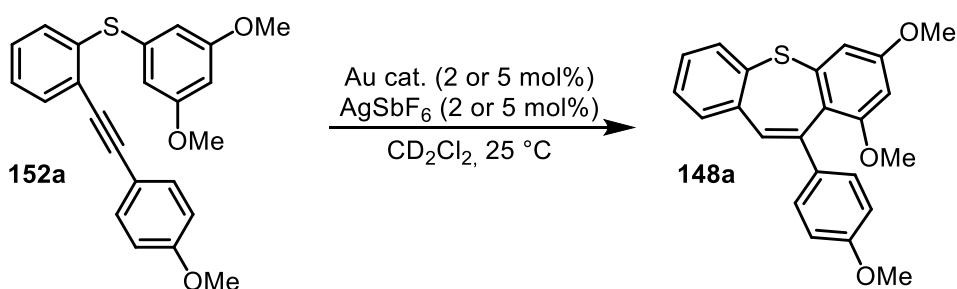
**$^1\text{H-NMR}$**  (400 MHz,  $\text{CDCl}_3$ ):  $\delta = 7.47$  (dd,  $J = 7.3, 1.4$  Hz, 1H), 7.40 (d,  $J = 7.6$  Hz, 1H), 7.33 (td,  $J = 7.5, 1.4$  Hz, 1H), 7.28 – 7.19 (m, 4H), 6.88-6.81 (m, 2H), 6.68 (d,  $J = 2.4$  Hz, 1H), 6.38 (d,  $J = 2.4$  Hz, 1H), 3.82 (s, 6H), 3.34 (s, 3H), 0.77 (s, 3H), 0.29 (s, 3H) ppm.  **$^{13}\text{C}\{^1\text{H}\}\text{-NMR}$**  (101 MHz,  $\text{CDCl}_3$ ):  $\delta = 160.5, 158.9, 158.5, 144.4, 142.6, 141.7, 139.6, 139.5, 132.0, 131.1, 128.9, 128.6, 127.3, 126.3, 125.1, 113.4, 107.6, 100.7, 55.8, 55.3, -4.0, -4.8$  ppm.  **$^{29}\text{Si-NMR}$**  (79 MHz,  $\text{CDCl}_3$ ):  $\delta = -11.9$  ppm. **HR-MS** (ESI): calculated  $m/z$  for  $\text{C}_{25}\text{H}_{27}\text{O}_3\text{Si}^+$  ( $[\text{M}+\text{H}]^+$ ): 403.1724; found 403.1727. **FTIR** (ATR, neat):  $\tilde{\nu} = 3048, 3001, 2953, 2934, 2903, 2834, 1603, 1586, 1559, 1508, 1245, 1215, 1190, 1177, 1161, 1125, 1078, 1037, 950, 909, 869, 830, 800, 780, 763, 733, 694, 652$   $\text{cm}^{-1}$ .

### 5,5-diisopropyl-1,3-dimethoxy-11-(4-methoxyphenyl)-5H-dibenzo[*b,f*]silepine (**149e**)



Prepared from **153e** (45.9 mg, 100  $\mu\text{mol}$ , 1.0 eq), precatalyst **C** (1.70 mg, 2.00  $\mu\text{mol}$ , 2 mol%) and  $\text{AgSbF}_6$  (0.05 M in DCM, 40  $\mu\text{L}$ , 2.00  $\mu\text{mol}$ , 2 mol%) in DCM (2.0 mL) according to general procedure **K**. Purification by column chromatography ( $\text{SiO}_2$ , hexane/EtOAc, 10:1,  $R_f = 0.25$ ) afforded **149e** (39.2 mg, 85.4  $\mu\text{mol}$ , 85%) as a colorless oil.

**$^1\text{H-NMR}$**  (300 MHz,  $\text{CDCl}_3$ ):  $\delta = 7.75$  (dt,  $J = 7.7, 0.9$  Hz, 1H), 7.62 – 7.56 (m, 1H), 7.41 (td,  $J = 7.6, 1.5$  Hz, 1H), 7.28 – 7.21 (m, 2H), 7.07 – 7.00 (m, 2H), 6.84 (d,  $J = 2.4$  Hz, 1H), 6.76 – 6.68 (m, 3H), 6.33 (d,  $J = 2.4$  Hz, 1H), 3.86 (s, 3H), 3.77 (s, 3H), 3.23 (s, 3H), 1.71 (hept,  $J = 7.6$  Hz, 1H), 1.33 (hept,  $J = 7.5$  Hz, 1H), 1.23 (dd,  $J = 7.5, 1.7$  Hz, 6H), 1.01 (t,  $J = 7.3$  Hz, 6H) ppm.  **$^{13}\text{C}\{^1\text{H}\}\text{-NMR}$**  (101 MHz,  $\text{CDCl}_3$ ):  $\delta = 159.5, 158.3, 157.0, 151.9, 136.7, 135.2, 133.1, 132.5, 131.6, 131.4, 129.4, 128.9, 127.1, 125.9, 125.3, 113.3, 109.8, 100.0, 55.4, 55.3, 54.9, 18.50, 18.45, 18.3$  (2C), 13.5, 10.5 ppm.  **$^{29}\text{Si-NMR}$**  (79 MHz,  $\text{CDCl}_3$ ):  $\delta = -11.5$  ppm. **HR-MS** (ESI): calculated  $m/z$  for  $\text{C}_{29}\text{H}_{35}\text{O}_3\text{Si}^+$  ( $[\text{M}+\text{H}]^+$ ): 459.2350; found 459.2351. **FTIR** (ATR, neat):  $\tilde{\nu} = 3046, 2998, 2939, 2890, 2862, 2834, 1604, 1585, 1556, 1508, 1455, 1432, 1408, 1362, 1296, 1263, 1246, 1213, 1190, 1175, 1161, 1134, 1052, 1034, 995, 951, 920, 880, 852, 823, 783, 766, 735, 681, 656, 621, 559, 534$   $\text{cm}^{-1}$ .

**5.3 Kinetic experiments via <sup>1</sup>H-NMR****Scheme S5:** Investigated reaction in kinetic experiments.

The starting material **152a** (9.4 mg, 25 μmol, 1.0 eq) and the respective amount of the precatalyst **A-F** (2 or 5 mol%) were weighted into a small vial, transferred into a glovebox and dissolved in CD<sub>2</sub>Cl<sub>2</sub> (0.40 mL). The solution was transferred into a Young-NMR tube and the vial was rinsed with CD<sub>2</sub>Cl<sub>2</sub> (0.15 mL). A solution of AgSbF<sub>6</sub> (0.05 M in CD<sub>2</sub>Cl<sub>2</sub>) was prepared and the respective amount (2 or 5 mol%) was added to the Young-NMR tube. The closed tube was shaken to ensure mixing and activation of the precatalyst. After removal from the glovebox, the Young NMR tube was placed in the NMR instrument, where automatic tuning and shimming was subsequently performed. The first <sup>1</sup>H-NMR spectrum was measured 10 min after addition of the AgSbF<sub>6</sub> solution. Afterwards, a spectrum (16 scans) was recorded every 5 min. One measurement (16 scans) lasted X s each. The evaluation was performed by integrating the signals of the methoxy groups in the product and reactant, respectively, in the range of 3.35-3.43 ppm (product, three protons) and 3.74-3.81 ppm (reactant, six protons). From this, the ratio of reactant to product and thus the reaction progress could be determined.

### 5.4 Enantioselective dynamic HPLC

Using the unified equation<sup>[140]</sup> (equations 1 and 2), developed by Oliver Trapp, interconversion barriers can be determined from the obtained chromatograms. This allows the calculation of reaction constants for first order reactions that take place during a chromatographic separation. The reaction constant  $k_1^{ue}$  can be derived directly from chromatographic parameters such as retention times ( $t_R^A$ ,  $t_R^B$ ) of the interconverting or reacting species A and B, the peak width at half maximum ( $w_A$ ,  $w_B$ ), and the relative plateau height ( $h_p$ ), independent of the initial concentrations of the converting analytes A and B and the equilibrium constant  $K_{A/B}$ . If the first eluted peak of the reaction profile is larger than the second eluted peak, equation 1 is valid. Accordingly, if the second peak is larger, equation 2 is applied.

$$k_1^{ue} = -\frac{1}{t_R^A} \left( \ln \left( B_0 e^{-\frac{A_0}{B_0} k_1^{ue} t_R^A} \left( \frac{100 e^{-\frac{(t_R^B - t_R^A)^2}{8\sigma_B^2}} - h_p e^{-\frac{(t_R^B - t_R^A)^2}{2\sigma_B^2}}}{\sigma_B \sqrt{2\pi}} - \frac{100}{t_R^B - t_R^A} \right) + \frac{100 B_0 + A_0 \left( 100 - h_p \left( 1 + \sqrt{\frac{2}{\pi N}} \right) \right)}{t_R^B - t_R^A} \right) - \ln \left( A_0 \left( \frac{h_p - 100 e^{-\frac{(t_R^A - t_R^B)^2}{8\sigma_A^2}}}{\sigma_A \sqrt{2\pi}} + \frac{100 - h_p \left( 1 + \sqrt{\frac{2}{\pi N}} \right)}{t_R^B - t_R^A} \right) \right) \right) \quad (1)$$

$$k_1^{ue} = -\frac{1}{t_R^A} \left( \ln \left( B_0 e^{-\frac{A_0}{B_0} k_1^{ue} t_R^A} \left( \frac{100 e^{-\frac{(t_R^B - t_R^A)^2}{8\sigma_B^2}} - h_p}{\sigma_B \sqrt{2\pi}} + \frac{h_p \left( 1 - \sqrt{\frac{2}{\pi N}} \right) - 100}{t_R^B - t_R^A} \right) + \frac{100 A_0 + B_0 \left( 100 - h_p \left( 1 + \sqrt{\frac{2}{\pi N}} \right) \right)}{t_R^B - t_R^A} \right) - \ln \left( A_0 \left( \frac{h_p e^{-\frac{(t_R^B - t_R^A)^2}{2\sigma_A^2}} - 100 e^{-\frac{(t_R^A - t_R^B)^2}{8\sigma_A^2}}}{\sigma_A \sqrt{2\pi}} + \frac{100}{t_R^B - t_R^A} \right) \right) \right) \quad (2)$$

where  $\sigma_i = \frac{w_i}{\sqrt{8 \ln 2}}$  with  $i = \{A, B\}$ ,  $k_1^{ue}$  represents the reaction rate,  $h_p$  is the height of the plateau between the individual peaks at the mean retention time,  $A_0$  and  $B_0$  denote the concentrations of the reactant and the product,  $t_R^A$  and  $t_R^B$  are the uncorrected retention times of the analytes A and B,  $w_A$  and  $w_B$  are the half widths and  $N$  is the theoretical plate number.

If the process being investigated is an enantiomerization, the unified equation can be solved analytically. For this purpose, Trapp and co-workers<sup>[140]</sup> implemented the analytical solution



## 5.4 Enantioselective dynamic HPLC

of the unified equation into the computer program DCXplorer, which calculates the required chromatographic parameters and also the rate constant  $k_1^{ue}$  directly from the elution profiles of the dynamic chromatography experiments. Subsequently, the Gibbs free activation energy  $\Delta G^\ddagger$  was determined using the Eyring equation (3) with  $R$  representing the gas constant ( $R = 8.31441 \text{ J} \cdot \text{K}^{-1} \cdot \text{mol}^{-1}$ ),  $h$  as the Planck constant ( $h = 6.62617 \cdot 10^{-34} \text{ J} \cdot \text{s}$ ),  $k_B$  as the Boltzmann constant ( $k_B = 1.380662 \cdot 10^{-23} \text{ J} \cdot \text{K}^{-1}$ ) and  $T$  as the measurement temperature in Kelvin.

$$\Delta G^\ddagger = -RT \ln \left( \frac{k_1^{ue} h}{k_B T} \right) \quad (3)$$

To obtain the activation enthalpy  $\Delta H^\ddagger$  and the activation entropy  $\Delta S^\ddagger$ , an Eyring plot ( $\ln(k_1^{ue}/T)$  as a function of  $T^{-1}$ ) was created where the activation enthalpy  $\Delta H^\ddagger$  can be calculated from the slope and the activation entropy  $\Delta S^\ddagger$  from the y-axis intercept or from the relation depicted in equation (4).

$$\Delta G^\ddagger = \Delta H^\ddagger - T\Delta S^\ddagger \quad (4)$$

All calculations were done using DCXplorer and Microsoft Excel 2019. The Eyring plots and the corresponding linear regression were performed using Origin 2020.

### Dibenzo[*a,e*]cycloheptatriene **146h**

Separation conditions: column: Chiralpak® IA-3; *n*-hexane/*iso*-propanol 99/1 (V/V); flow: 1.0 mL/min; temperature range between 13 °C and 20 °C. Chromatograms present the UV absorption at 254 nm. The elution profiles are displayed in **Figure S1**.

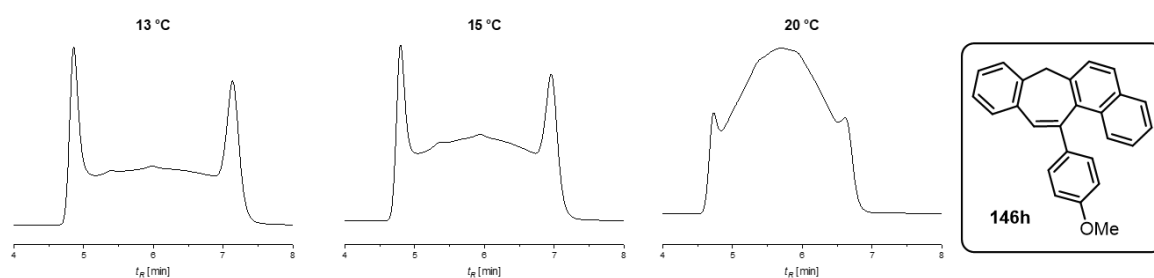


**Figure S1:** Elution profiles obtained for **146h** at different temperatures.

Experimental data of all temperature-dependent measurements are reported at 13 °C and 15 °C (**Table S1**). Elution profiles above 15 °C were not considered because of plateau heights higher than 50%, which makes the determination of peak widths and efficiencies with high precision impossible.

## 5. Experimental

**Table S1:** Parameters for the chiral separation of **146h** obtained from the corresponding chromatograms.

$T$ [°C]	$t_1$ [min]	$t_2$ [min]	Half width [s]		Height [%]		
			$w_1$	$w_2$	Peak 1	Plateau	Peak 2
13.0	4.864	7.136	9.0	12.8	100.0	33.02	81.25
15.0	4.800	6.955	9.0	12.8	100.0	48.69	83.40

**Table S2:** Parameters calculated for **146h** based on the experimental data in **Table S1**.

Plate Number			Forward Reaction			
N 1	N 2	$\alpha$	$k_1^{ue}$ [s <sup>-1</sup> ]	$\Delta G^\ddagger$ [kJ mol <sup>-1</sup> ]	$1/T$ [10 <sup>-3</sup> K <sup>-1</sup> ]	$\ln(k/T)$
5831	6204	1.47	4.51E-03	82.84	3.495	-11.059
5678	5894	1.45	5.75E-03	82.85	3.470	-10.822

### Dibenzo[a,e]cycloheptatriene **146k**

Separation conditions: column: Chiralpak® IA-3; *n*-hexane/*iso*-propanol 99/1 (V/V); flow: 1.0 mL/min; temperature range between 15 °C and 30 °C. Chromatograms present the UV absorption at 254 nm. The elution profiles are displayed in **Figure S2**.

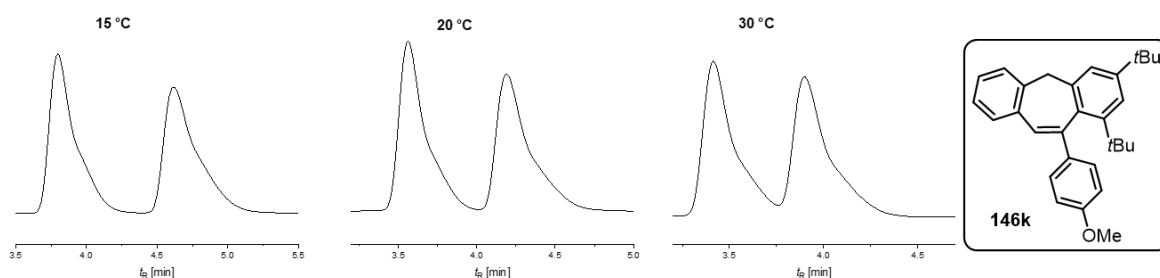


**Figure S2:** Elution profiles obtained for **146k** at different temperatures.

Since it was not possible to obtain a baseline separation of the enantiomers, it was not possible to reliably determine the height of the plateau and consequently any parameters related to it.

### Dibenzo[b,f]oxepine **147i**

Separation conditions: column: Chiralpak® IA-3; *n*-hexane/*iso*-propanol 98/2 (V/V); flow: 1.0 mL/min; temperature range between 15 °C and 35 °C. Chromatograms present the UV absorption at 254 nm. The elution profiles are displayed in **Figure S3**.

## 5.4 Enantioselective dynamic HPLC

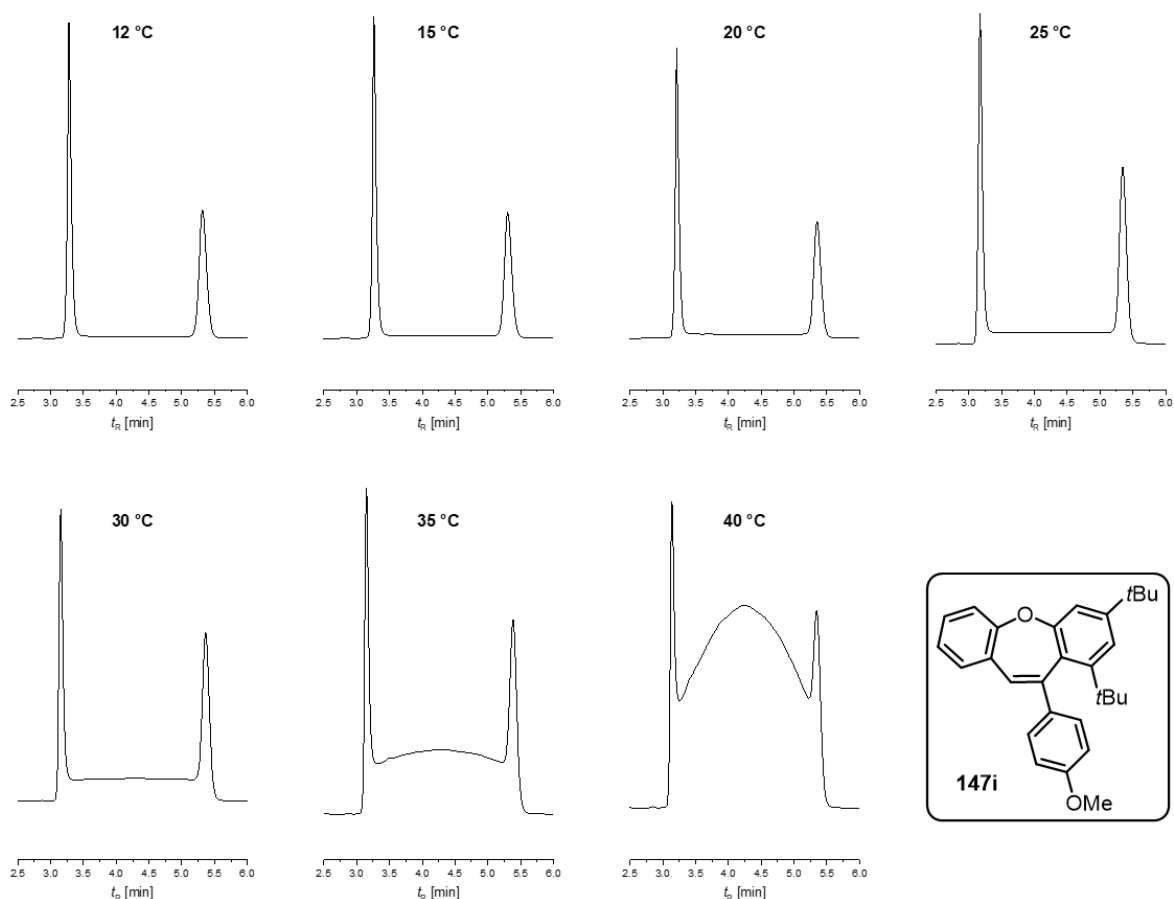


**Figure S3:** Elution profiles obtained for **147i** at different temperatures.

Experimental data of all temperature-dependent measurements are reported between 15 °C and 35 °C (**Table S3**). Below a temperature of 15 °C a plateau is hardly detectable and at 40 °C a plateau height of 50% is exceeded, thus peak width at half height and efficiencies cannot be reliably determined.

**Table S3:** Parameters for the chiral separation of **147i** obtained from the corresponding chromatograms.

<i>T</i> [°C]	<i>t</i> <sub>1</sub> [min]	<i>t</i> <sub>2</sub> [min]	Half width [s]		Height [%]		
			<i>w</i> <sub>1</sub>	<i>w</i> <sub>2</sub>	Peak 1	Plateau	Peak 2
15.0	3.264	5.301	3.8	9.0	100.0	0.75	3.264
20.0	3.211	5.355	3.8	7.7	100.0	1.70	3.211
25.0	3.168	5.344	3.8	7.7	100.0	3.48	3.168
30.0	3.157	5.365	3.8	7.7	100.0	7.87	3.157
35.0	3.157	5.387	5.1	7.7	100.0	20.4	3.157

**Table S4:** Parameters calculated for **147i** based on the experimental data in **Table S3**.

Plate Number			Forward Reaction			
N 1	N 2	$\alpha$	$k_1^{ue}$ [s <sup>-1</sup> ]	$\Delta G^\ddagger$ [kJ mol <sup>-1</sup> ]	$1/T$ [10 <sup>-3</sup> K <sup>-1</sup> ]	ln( <i>k</i> / <i>T</i> )
14728	6925	1.62	6.08E-04	88.23	3.47	-13.068
14253	9655	1.67	1.10E-03	88.36	3.41	-12.490
13874	9615	1.69	2.39E-03	87.99	3.35	-11.736
13778	9691	1.70	4.46E-03	87.93	3.30	-11.127
7649	9770	1.71	7.04E-03	88.26	3.25	-10.687

## 5. Experimental

The Eyring plot for **147i** is shown and the values obtained from the linear regression are shown in **Figure S4**.

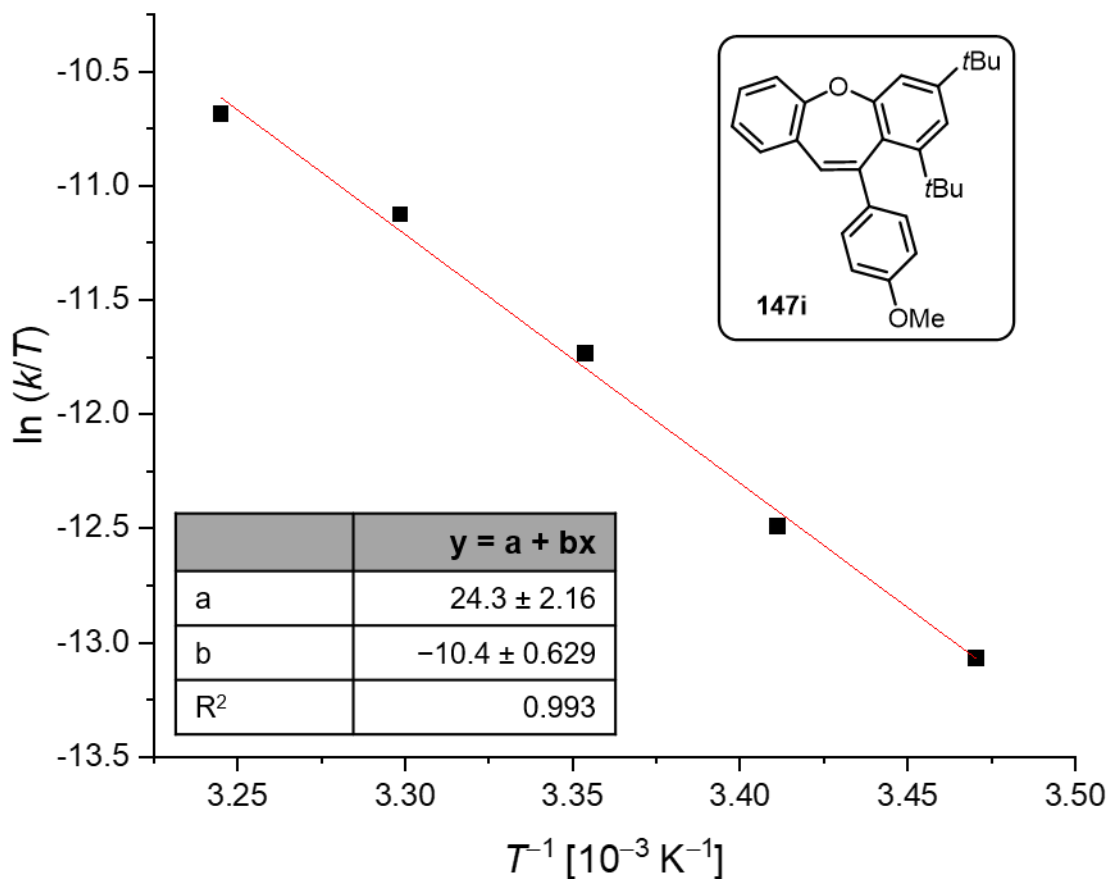


**Figure S4:** Eyring plot for **147i**.

### Dibenzo[b,f]silepine **149e**

Separation conditions: column: Chiralpak<sup>®</sup> IC-3; *n*-hexane/ethyl acetate 97/3 (V/V) (0-10 °C), *n*-hexane/ethyl acetate 96/4 (V/V) (12-35 °C); flow: 1.0 mL/min; temperature range between 0 °C and 35 °C. Chromatograms present the UV absorption at 254 nm. The elution profiles are shown in **Figure S5**.

## 5.4 Enantioselective dynamic HPLC

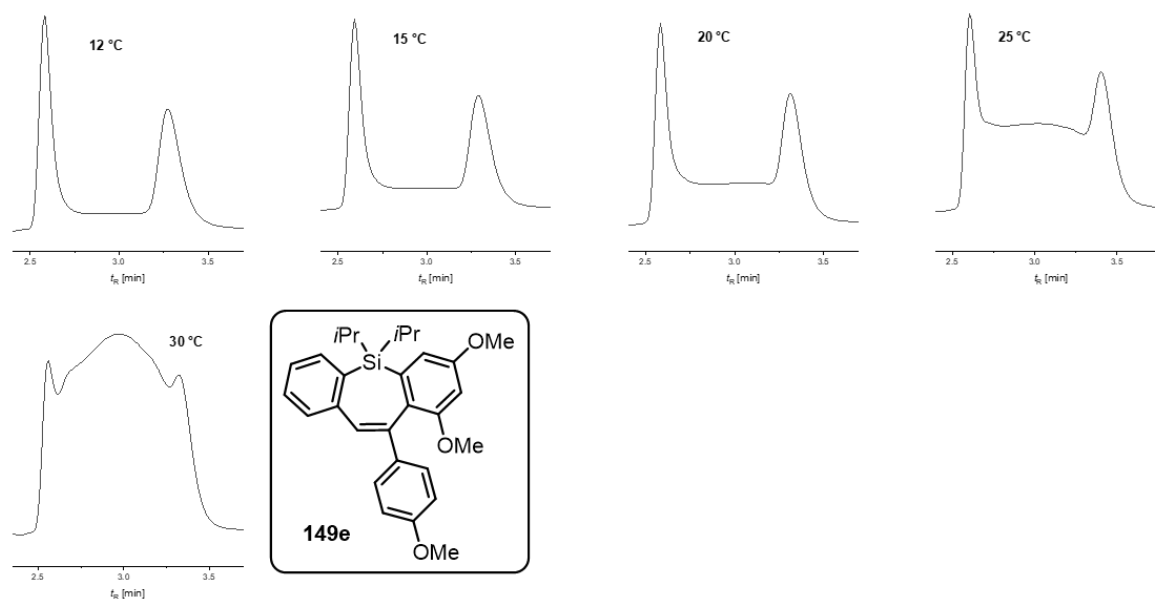


**Figure S5:** Elution profiles obtained for **149e** at different temperatures.

Experimental data of all temperature-dependent measurements are reported between 12 °C and 20 °C (**Table S5**). Below a temperature of 12 °C the peak shape and the retention times were affected by the external cooling of the column outside the column oven, which required system modification with additional capillary length. Above 25 °C peak coalescence was observed, thus peak width at half height and efficiencies cannot be reliably determined.

**Table S5:** Parameters for the chiral separation of **149e** obtained from the corresponding chromatograms.

T [°C]	t <sub>1</sub> [min]	t <sub>2</sub> [min]	Half width [s]		Height [%]		
			w <sub>1</sub>	w <sub>2</sub>	Peak 1	Plateau	Peak 2
12.0	2.581	3.275	5.1	10.2	100.0	7.35	56.43
15.0	2.592	3.296	5.1	9.0	100.0	10.8	59.53
20.0	2.581	3.317	5.1	9.0	100.0	19.8	65.06
25.0	2.613	3.403	5.1	10.2	100.0	44.6	71.85

**Table S6:** Parameters calculated for **149e** based on the experimental data in **Table S5**.

Plate Number			Forward Reaction			
N 1	N 2	$\alpha$	k <sub>1</sub> <sup>ue</sup> [s <sup>-1</sup> ]	$\Delta G^\ddagger$ [kJ mol <sup>-1</sup> ]	1/T [10 <sup>-3</sup> K <sup>-1</sup> ]	ln(k/T)
5113	2058	1.27	1.57E-03	85.04	3.51E-03	-12.111
5156	2677	1.27	2.28E-03	85.06	3.47E-03	-11.745
5113	2712	1.29	3.90E-03	85.28	3.41E-03	-11.228
5240	2222	1.30	8.23E-03	84.92	3.35E-03	-10.497

The Eyring plot for **149e** and the values obtained from the linear regression are shown in **Figure S6**.

## 5. Experimental

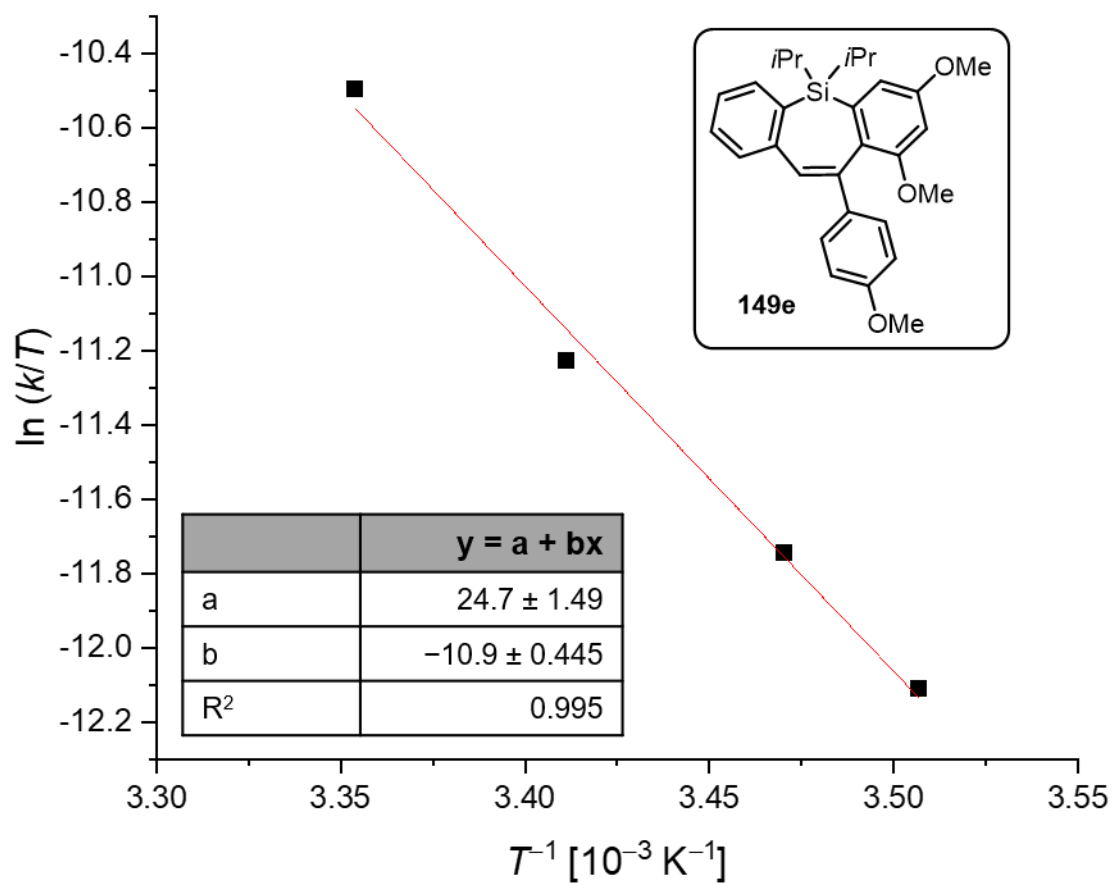


**Figure S6:** Eyring plot for **149e**.

## 5.5 Dynamic NMR experiments

For the evaluation of the EXSY experiments the free program EXSYCALC was used, which calculates the magnetization exchange rates  $k'$  of the exchange equilibrium through a quantitative analysis of the obtained NMR peaks. The program allows the calculation of systems with an arbitrary number of exchange sites, spins, populations and longitudinal relaxation rates. The calculations are performed based on a full relaxation matrix analysis of the peak intensities (**Figure S7**).

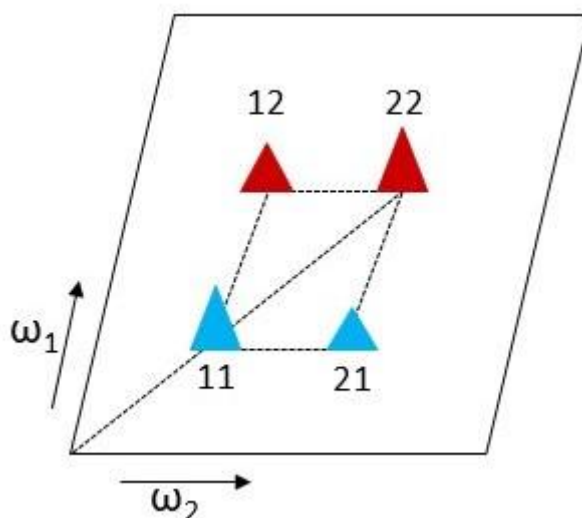


**Figure S7:** Schematic example for the determination of peak intensities in 2D-EXSY spectra required for A.

It was shown for a system with two exchange sites that the peak amplitude in 2D-EXSY spectra with the exchange rate constant  $k'$ , the relaxation rate and the mixing time  $\tau_m$  are given by the expression (5).<sup>[142]</sup>

$$A = \exp(-R\tau_m) \quad (5)$$

A and R are described by the matrices (6) and (7).

$$A = \begin{vmatrix} I_{11}/M_1 & I_{12}/M_2 \\ I_{21}/M_1 & I_{22}/M_2 \end{vmatrix} \quad (6)$$

$$R = \begin{vmatrix} -R_1 - k'_1 & k'_{-1} \\ k'_1 & -R_2 - k'_{-1} \end{vmatrix} \quad (7)$$

A contains the peak amplitudes  $I_{11}$ ,  $I_{12}$ ,  $I_{21}$  and  $I_{22}$  measured in an experiment with mixing and the equilibrium magnetization values  $M_1$  and  $M_2$  obtained from an experiment without mixing ( $\tau_m = 0$ ). R includes the kinetic parameters to be determined, which are chemical exchange and longitudinal relaxation rates. It can be obtained directly by first diagonalizing A and then calculating the eigenvector matrix X and its inverse  $X^{-1}$  so that  $XD X^{-1} = A$ , where

## 5. Experimental

$D$  is the diagonal eigenvalue matrix. Equation 5 can be rearranged and provides expression 8, where  $\ln D = \text{diag}(\ln \lambda_i)$ . Therefore,  $R$  can be calculated directly from  $A$ .<sup>[142]</sup>

$$R = -\frac{\ln A}{\tau_m} = -\frac{X(\ln D)X^{-1}}{\tau_m} \quad (8)$$

The applicability of this approach assumes that the signal from each species in the exchange process is conveniently separated from the others in the NMR spectrum (i.e., slow chemical exchange in the time scale of the chemical shift). For the calculation of the rate constants, the EXSYCALC program requires the experimental amplitudes of certain NMR peaks obtained in two different EXSY experiments. One is an EXSY experiment recorded at a specific mixing time, and the other is one recorded at  $\tau_m = 0$  or a very short mixing time and serves as a reference experiment. In the first experiment, the mixing time must be large enough to allow the magnetization exchange process to take place and to determine the intensity of the signals involved in the exchange, both for diagonal and cross peaks. Whereas in the reference experiment a thermal equilibrium should be present, so that no magnetization exchange and therefore no cross peaks can be observed. It is only used to determine the intensities of the diagonal peaks. Both EXSY experiments should be acquired and processed under identical conditions (temperature, number of scans, etc.). Since the process studied here is an enantiomerization, it can be assumed in a reasonable approximation that the sum of the amplitudes of the respective cross and diagonal peaks corresponds to the amplitudes of the diagonal peaks without mixing. Therefore, an EXSY experiment at  $\tau_m = 0$  was not performed. The peak amplitudes/intensities were obtained by integrating the cross and diagonal peaks. Moreover, the calculated magnetization exchange rates  $k'$  are equal to the exchange rate constants  $k$ . With the obtained rate constants, the Gibbs free energy  $\Delta G^\ddagger$  could be calculated accordingly using equation 3. The other activation parameters were estimated through creation of an Eyring plot followed by a linear regression. The activation enthalpy  $\Delta H^\ddagger$  could be obtained from the slope of the regression curve. The activation entropy  $\Delta S^\ddagger$  could be calculated dependent on the temperature using equation 4.

For silepine **149a**, 2D-EXSY spectra were recorded at  $-25^\circ\text{C}$  (**Figure S 8**),  $0^\circ\text{C}$  (**Figure S9**),  $25^\circ\text{C}$  (**Figure S10**), and  $50^\circ\text{C}$  (**Figure S11**). From the obtained spectra, the required intensities of the cross and diagonal peaks for the exchanging methyl groups were determined by integration and at the respective temperatures, the rate constants were calculated using the program EXSYCALC. The 2D-EXSY spectrum at  $-25^\circ\text{C}$  showed no exchange peaks and was used to estimate the interfering NOE to  $0.014\text{ s}^{-1}$  (**Figure S 8**).



## 5.5 Dynamic NMR experiments

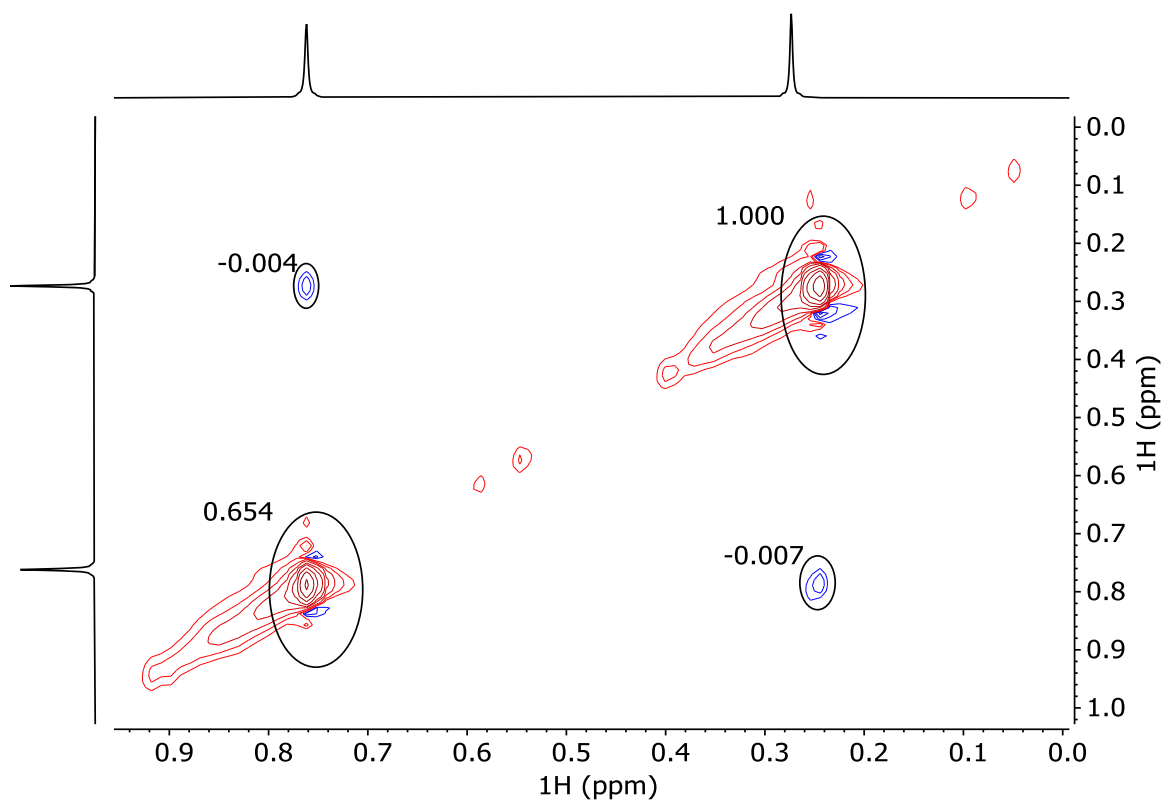


**Figure S 8:** Section from the 2D-EXSY spectrum of **149a** at  $-25\text{ }^{\circ}\text{C}$  and  $\tau_m = 0.5\text{ s}$ . No exchange of the methyl groups is observed.

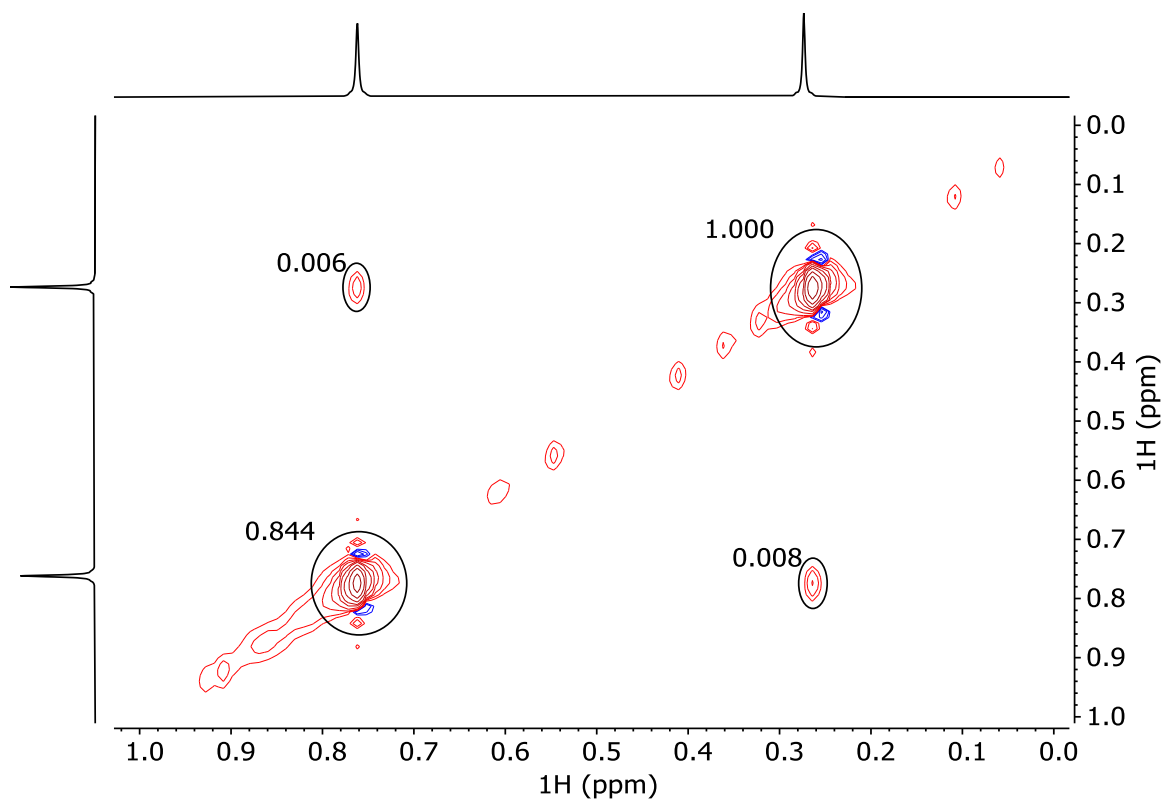


**Figure S9:** Section from the 2D-EXSY spectrum of **149a** at  $0\text{ }^{\circ}\text{C}$  and  $\tau_m = 0.5\text{ s}$ , showing the exchange of methyl groups. The exchange signals and diagonal peaks are used for integration.

## 5. Experimental

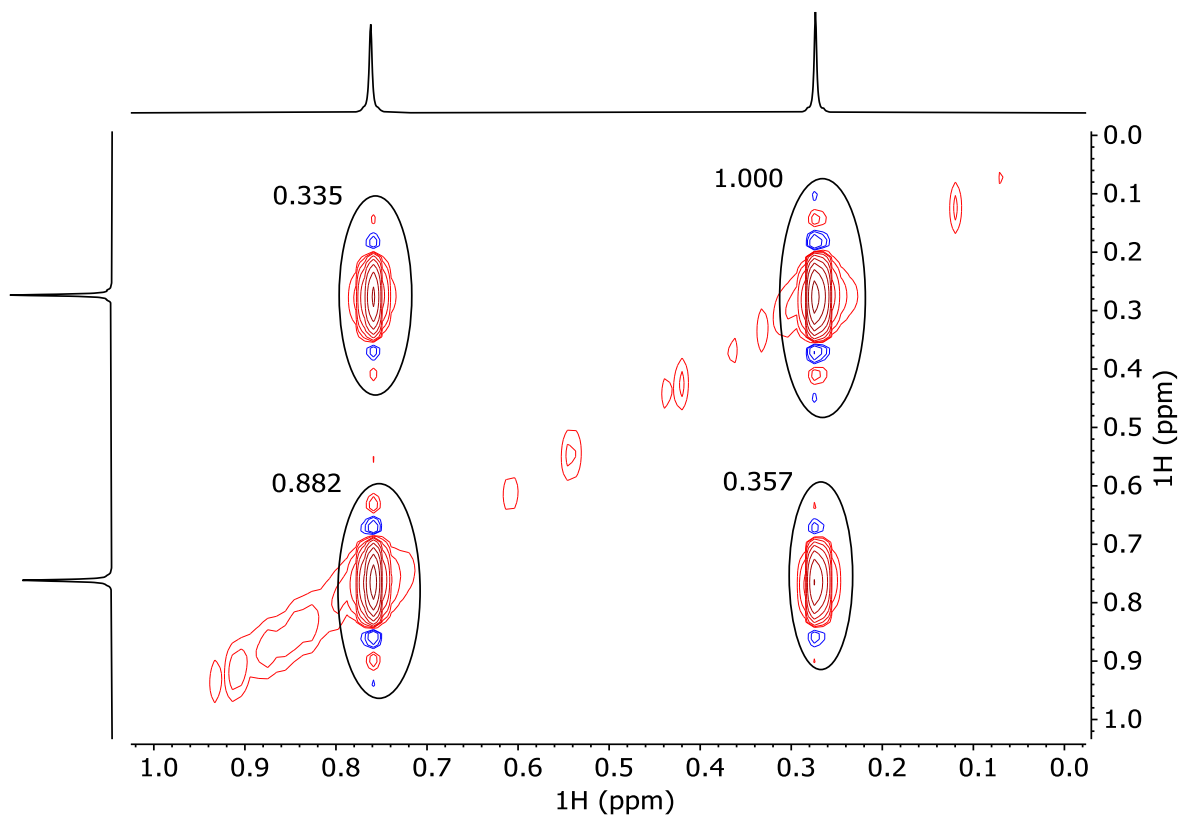


**Figure S10:** Section from the 2D-EXSY spectrum of **149a** at 25 °C and  $\tau_m = 0.5$  s, showing the exchange of methyl groups. The exchange signals and diagonal peaks are used for integration.

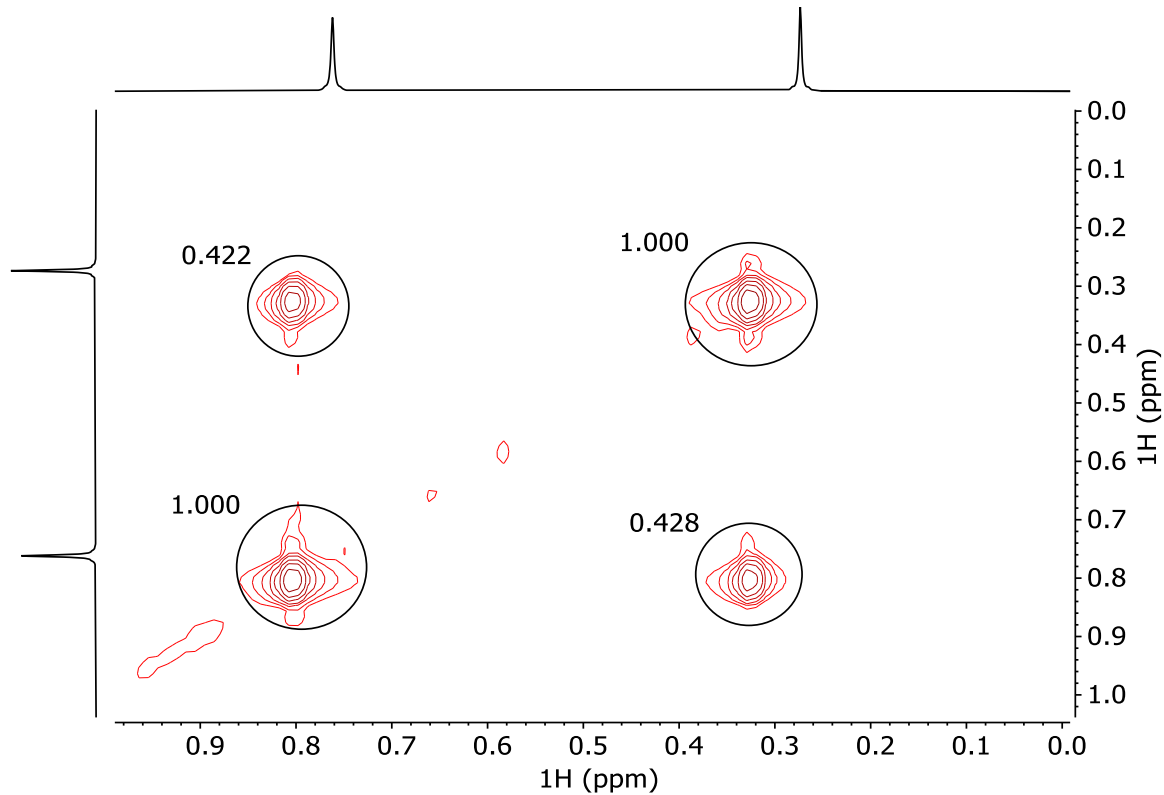


**Figure S11:** Section from the 2D-EXSY spectrum of **149a** at 50 °C and  $\tau_m = 0.05$  s, showing the exchange of methyl groups. The exchange signals and diagonal peaks are used for integration.

## 5.5 Dynamic NMR experiments

The Eyring plot for **149a** and the rate constants and activation parameters for the interconversion are shown in **Figure S12**.

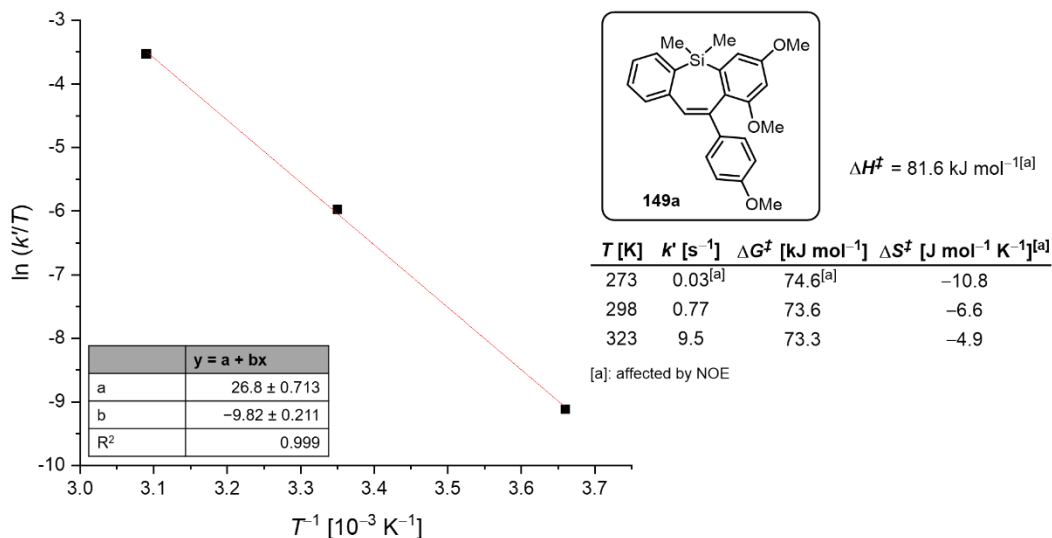


**Figure S12:** Eyring plot for **149a** (right) and the calculated activation parameters (left).

For silylene **149e**, 2D-EXSY spectra were recorded at 25 °C (**Figure S13**) and 50 °C (**Figure S14**). From the obtained spectra, the required intensities of the cross and diagonal peaks for the exchanging isopropyl groups were determined by integration and at the respective temperatures, the rate constants were calculated using the program EXSYCALC.

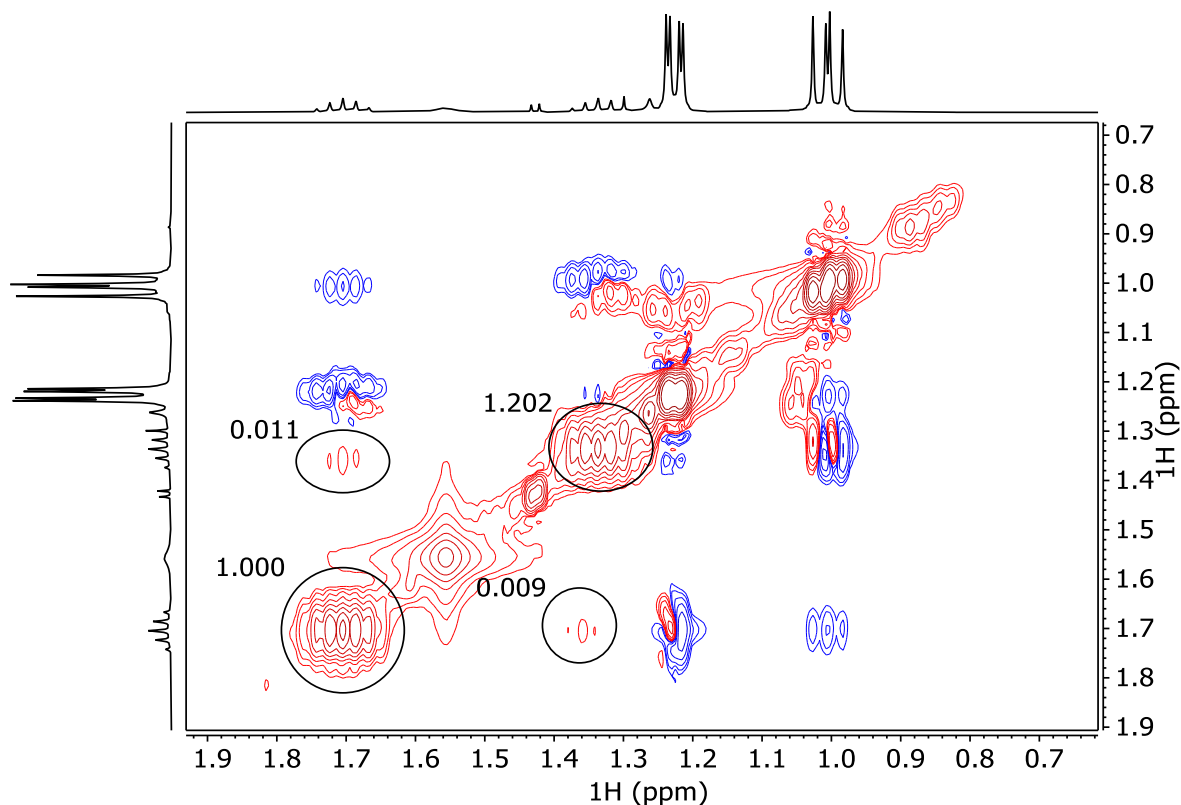


**Figure S13:** Section from the 2D-EXSY spectrum of **149e** at 25 °C and  $\tau_m = 0.5$  s, showing the exchange of isopropyl groups. The exchange signals and diagonal peaks are used for integration.

## 5. Experimental

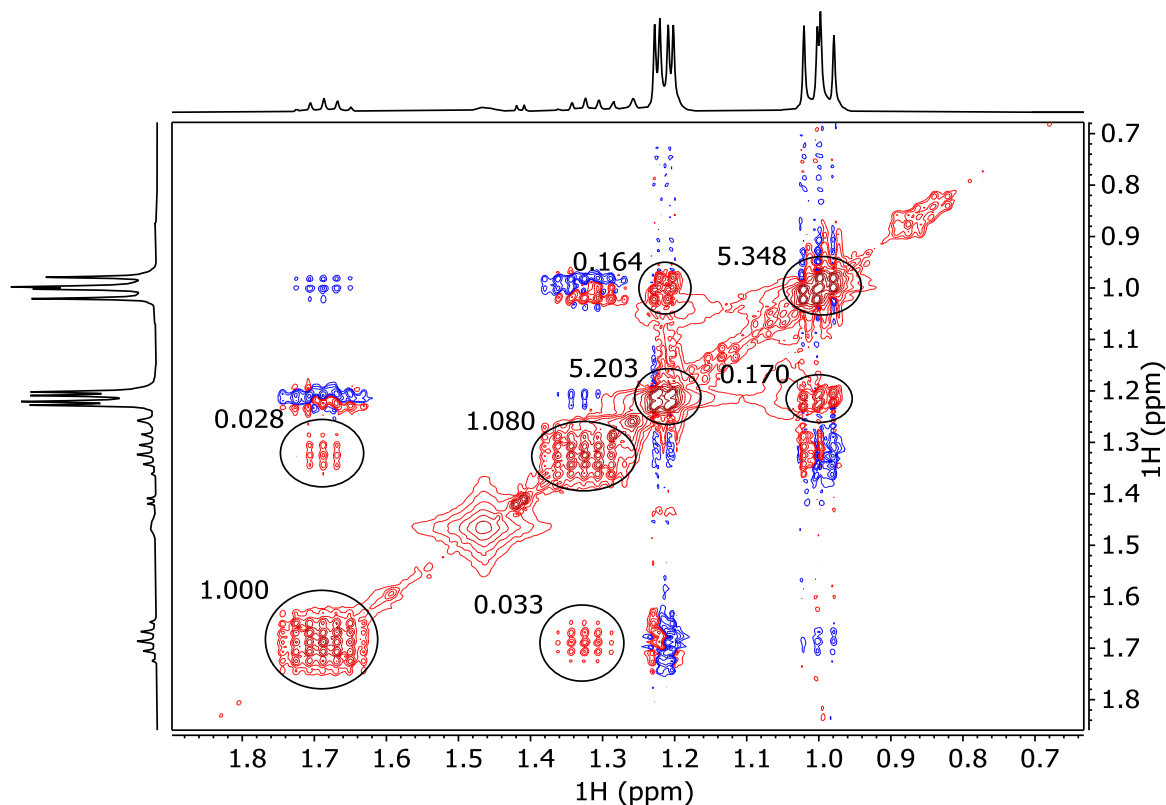
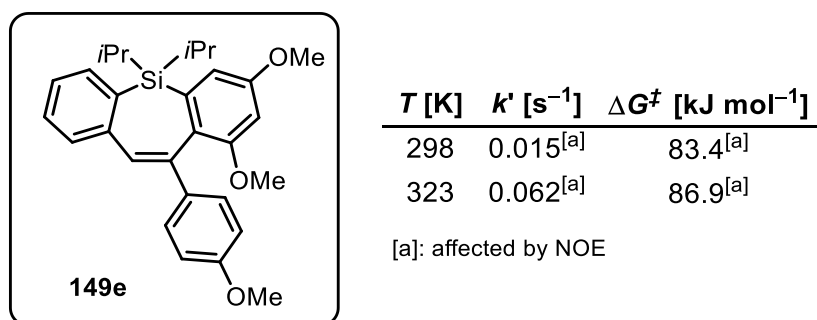


**Figure S14:** Section from the 2D-EXSY spectrum of **149e** at 50 °C and  $\tau_m = 0.5$  s, showing the exchange of isopropyl groups. The exchange signals and diagonal peaks are used for integration.

Since the exchange is slower for **149e** the interfering NOE distorts the correct determination of the peak intensities. The obtained rate constants and calculated Gibbs free energies  $\Delta G^\ddagger$  are summarized in **Scheme S6**.



**Scheme S6:** Rate constants and Gibbs free energies  $\Delta G^\ddagger$  for the interconversion of **149e**.

## 5.6 Computational details

The molecular structures and transition states were optimized with Gaussian 16, Rev A.03<sup>[160]</sup> and visualized with GausView 6.0.16.<sup>[161]</sup> Calculations were performed using the B3LYP functional<sup>[162]</sup> and either the 6-31+g(d) or def2-TZVP<sup>[163]</sup> basis set. The additional corrections applied, such as the D3 version of Grimme's dispersion with Becke-Johnson damping (GD3BJ)<sup>[164]</sup> or solvent corrections (CPCM) for chloroform, are stated separately for each molecular structure. Transition states and minima were confirmed by frequency calculations at the same level of theory; no imaginary frequencies were found for minima; one imaginary frequency was found for the transition states. The reaction paths were calculated using the internal reaction coordinate (IRC) approach applying the local quadratic approximation (LQA) algorithm from Gaussian at B3LYP/6-31+g(d) niveau to further confirm the found transition states. Due to low gradients and flat potential energy surfaces, only incomplete IRC profiles were obtained for compounds **146h** and **146k**. As soon as the change in energy per step was too small, the IRC scan stopped prematurely. Therefore, the last point of the IRC was taken and a geometry optimization was conducted to check the optimized geometry for consistency with the expected minimum.

The NICS were computed at the B3LYP/6-31+g\* level of theory. The magnetic shielding tensor was calculated for ghost atoms located at the geometrical ring centers. These values are denoted as NICS(0) according to the methodology described by Schleyer *et. al.*<sup>[145]</sup>

## 6. References

- [1] J. N. Brønsted, *Recl. Trav. Chim. Pays-Bas* **1923**, *42*, 718.
- [2] T. M. Lowry, *J. Chem. Technol. Biotechnol.* **1923**, *42*, 43.
- [3] G. N. Lewis, *Valence and the Structure of Atoms and Molecules*, Chemical Catalogue Company, New York, **1923**.
- [4] a) R. G. Pearson, *J. Am. Chem. Soc.* **1963**, *85*, 3533; b) R. G. Pearson, *J. Chem. Educ.* **1987**, *64*, 561.
- [5] Y. Ito, M. Sawamura, T. Hayashi, *J. Am. Chem. Soc.* **1986**, *108*, 6405.
- [6] A. Fürstner, P. W. Davies, *Angew. Chem. Int. Ed.* **2007**, *46*, 3410.
- [7] A. S. K. Hashmi, G. J. Hutchings, *Angew. Chem. Int. Ed.* **2006**, *45*, 7896.
- [8] P. Pyykkö, *Angew. Chem. Int. Ed.* **2004**, *43*, 4412.
- [9] P. Pyykkö, *Angew. Chem. Int. Ed.* **2002**, *41*, 3573.
- [10] D. J. Gorin, F. D. Toste, *Nature* **2007**, *446*, 395.
- [11] a) J. A. J. Jarvis, B. T. Kilbourn, P. G. Owston, *Acta Cryst. Sect. B* **1971**, *27*, 366; b) J. A. Wunderlich, D. P. Mellor, *Acta Cryst.* **1954**, *7*, 130.
- [12] S. Flügge, A. Anoop, R. Goddard, W. Thiel, A. Fürstner, *Chem. Eur. J.* **2009**, *15*, 8558.
- [13] R. Dorel, A. M. Echavarren, *Chem. Rev.* **2015**, *115*, 9028.
- [14] A. Fürstner, *Acc. Chem. Res.* **2014**, *47*, 925.
- [15] C. Nevado, A. M. Echavarren, *Synthesis* **2005**, *2005*, 167.
- [16] a) D. Wang, R. Cai, S. Sharma, J. Jirak, S. K. Thummanapelli, N. G. Akhmedov, H. Zhang, X. Liu, J. L. Petersen, X. Shi, *J. Am. Chem. Soc.* **2012**, *134*, 9012; b) M. Veguillas, G. M. Rosair, M. W. P. Bebbington, A.-L. Lee, *ACS Catal.* **2019**, *9*, 2552.
- [17] E. Jiménez-Núñez, C. K. Claverie, C. Nieto-Oberhuber, A. M. Echavarren, *Angew. Chem. Int. Ed.* **2006**, *45*, 5452.
- [18] a) N. Mézailles, L. Ricard, F. Gagosz, *Org. Lett.* **2005**, *7*, 4133; b) A. Buzas, F. Gagosz, *J. Am. Chem. Soc.* **2006**, *128*, 12614.
- [19] a) E. Mizushima, K. Sato, T. Hayashi, M. Tanaka, *Angew. Chem. Int. Ed.* **2002**, *41*, 4563; b) E. Mizushima, T. Hayashi, M. Tanaka, *Org. Lett.* **2003**, *5*, 3349; c) C. Nieto-Oberhuber, M. P. Muñoz, E. Buñuel, C. Nevado, D. J. Cárdenas, A. M. Echavarren, *Angew. Chem. Int. Ed.* **2004**, *43*, 2402.
- [20] a) W. Debrouwer, T. S. A. Heugebaert, B. I. Roman, C. V. Stevens, *Adv. Synth. Catal.* **2015**, *357*, 2975; b) D. B. Huple, S. Ghorpade, R.-S. Liu, *Adv. Synth. Catal.* **2016**, *358*, 1348; c) Z. Li, C. Brouwer, C. He, *Chem. Rev.* **2008**, *108*, 3239.
- [21] a) V. Mamane, P. Hannen, A. Fürstner, *Chem. Eur. J.* **2004**, *10*, 4556; b) A. Fürstner, V. Mamane, *J. Org. Chem.* **2002**, *67*, 6264.
- [22] A. W. Sromek, M. Rubina, V. Gevorgyan, *J. Am. Chem. Soc.* **2005**, *127*, 10500.

- [23] I. Alonso, B. Trillo, F. López, S. Montserrat, G. Ujaque, L. Castedo, A. Lledós, J. L. Mascareñas, *J. Am. Chem. Soc.* **2009**, *131*, 13020.
- [24] P. Mauleón, R. M. Zeldin, A. Z. González, F. D. Toste, *J. Am. Chem. Soc.* **2009**, *131*, 6348.
- [25] D. Benitez, E. Tkatchouk, A. Z. Gonzalez, W. A. Goddard, F. D. Toste, *Org. Lett.* **2009**, *11*, 4798.
- [26] C. Shu, C.-B. Chen, W.-X. Chen, L.-W. Ye, *Org. Lett.* **2013**, *15*, 5542.
- [27] W. Wang, G. B. Hammond, B. Xu, *J. Am. Chem. Soc.* **2012**, *134*, 5697.
- [28] Z. J. Wang, D. Benitez, E. Tkatchouk, W. A. Goddard, F. D. Toste, *J. Am. Chem. Soc.* **2010**, *132*, 13064.
- [29] M. Alcarazo, *Chem. Eur. J.* **2014**, *20*, 7868.
- [30] B. Cornils, E. G. Kuntz, *J. Organomet. Chem.* **1995**, *502*, 177.
- [31] D. M. Chisholm, J. S. McIndoe, *Dalton Trans.* **2008**, 3933.
- [32] T. Drews, D. Rusch, S. Seidel, S. Willemsen, K. Seppelt, *Chem. Eur. J.* **2008**, *14*, 4280.
- [33] A. G. Orpen, N. G. Connelly, *Organometallics* **1990**, *9*, 1206.
- [34] M. P. Mitoraj, A. Michalak, *Inorg. Chem.* **2010**, *49*, 578.
- [35] M. Alcarazo, *Acc. Chem. Res.* **2016**, *49*, 1797.
- [36] a) C. A. Tolman, *J. Am. Chem. Soc.* **1970**, *92*, 2956; b) C. A. Tolman, *J. Am. Chem. Soc.* **1970**, *92*, 2953.
- [37] C. A. Tolman, *Chem. Rev.* **1977**, *77*, 313.
- [38] D. G. Gusev, *Organometallics* **2009**, *28*, 763.
- [39] N. Kuhn, J. Fahl, D. Bläser, R. Boese, *Z. anorg. allg. Chem.* **1999**, *625*, 729.
- [40] L. Gu, Y. Zheng, E. Haldón, R. Goddard, E. Bill, W. Thiel, M. Alcarazo, *Angew. Chem. Int. Ed.* **2017**, *56*, 8790.
- [41] M. Azouri, J. Andrieu, M. Picquet, P. Richard, B. Hanquet, I. Tkatchenko, *Eur. J. Inorg. Chem.* **2007**, *2007*, 4877.
- [42] J. J. Weigand, K.-O. Feldmann, F. D. Henne, *J. Am. Chem. Soc.* **2010**, *132*, 16321.
- [43] A. A. Tolmachev, A. A. Yurchenko, E. S. Kozlov, A. S. Merkulov, M. G. Semenova, A. M. Pinchuk, *Heteroat. Chem.* **1995**, *6*, 419.
- [44] I. V. Komarov, M. Yu. Kornilov, A. A. Tolmachev, A. A. Yurchenko, E. B. Rusanov, A. N. Chernega, *Tetrahedron* **1995**, *51*, 11271.
- [45] E. González-Fernández, L. D. M. Nicholls, L. D. Schaaf, C. Farès, C. W. Lehmann, M. Alcarazo, *J. Am. Chem. Soc.* **2017**, *139*, 1428.
- [46] L. D. M. Nicholls, M. Marx, T. Hartung, E. González-Fernández, C. Golz, M. Alcarazo, *ACS Catal.* **2018**, *8*, 6079.
- [47] J. Petušková, H. Bruns, M. Alcarazo, *Angew. Chem. Int. Ed.* **2011**, *50*, 3799.

## 6. References

- [48] E. Haldón, Á. Kozma, H. Tinnermann, L. Gu, R. Goddard, M. Alcarazo, *Dalton Trans.* **2016**, 45, 1872.
- [49] H. Tinnermann, C. Wille, M. Alcarazo, *Angew. Chem. Int. Ed.* **2014**, 53, 8732.
- [50] T. Johannsen, C. Golz, M. Alcarazo, *Angew. Chem. Int. Ed.* **2020**, 59, 22779.
- [51] M. Azouri, J. Andrieu, M. Picquet, H. Cattey, *Inorg. Chem.* **2009**, 48, 1236.
- [52] F. D. Henne, A. T. Dickschat, F. Hennersdorf, K.-O. Feldmann, J. J. Weigand, *Inorg. Chem.* **2015**, 54, 6849.
- [53] C. Maaliki, Y. Canac, C. Lepetit, C. Duhayon, R. Chauvin, *RSC Adv.* **2013**, 3, 20391.
- [54] B. D. Ellis, C. A. Dyker, A. Decken, C. L. B. Macdonald, *Chem. Commun.* **2005**, 1965.
- [55] G. Mehler, P. Linowski, J. Carreras, A. Zanardi, J. W. Dube, M. Alcarazo, *Chem. Eur. J.* **2016**, 22, 15320.
- [56] J. Petušková, M. Patil, S. Holle, C. W. Lehmann, W. Thiel, M. Alcarazo, *J. Am. Chem. Soc.* **2011**, 133, 20758.
- [57] J. Carreras, G. Gopakumar, L. Gu, L. Gu, A. Gimeno, P. Linowski, J. Petušková, W. Thiel, M. Alcarazo, *J. Am. Chem. Soc.* **2013**, 135, 18815.
- [58] L. Gu, L. M. Wolf, A. Zieliński, W. Thiel, M. Alcarazo, *J. Am. Chem. Soc.* **2017**, 139, 4948.
- [59] L. Gu, L. M. Wolf, W. Thiel, C. W. Lehmann, M. Alcarazo, *Organometallics* **2018**, 37, 665.
- [60] J. Sirieix, M. Oßberger, B. Betzemeier, P. Knochel, *Synlett* **2000**, 2000, 1613.
- [61] S. Saleh, E. Fayad, M. Azouri, J.-C. Hierso, J. Andrieu, M. Picquet, *Adv. Synth. Catal.* **2009**, 351, 1621.
- [62] Q.-X. Wan, Y. Liu, Y. Lu, M. Li, H.-H. Wu, *Catal. Lett.* **2008**, 121, 331.
- [63] X. Marset, A. Khoshnood, L. Sotorriós, E. Gómez-Bengoa, D. A. Alonso, D. J. Ramón, *ChemCatChem* **2017**, 9, 1269.
- [64] a) C. C. Brasse, U. Englert, A. Salzer, H. Waffenschmidt, P. Wasserscheid, *Organometallics* **2000**, 19, 3818; b) D. J. Brauer, K. W. Kottsieper, C. Liek, O. Stelzer, H. Waffenschmidt, P. Wasserscheid, *J. Organomet. Chem.* **2001**, 630, 177.
- [65] J. Li, J. Peng, Y. Bai, G. Zhang, G. Lai, X. Li, *J. Organomet. Chem.* **2010**, 695, 431.
- [66] a) L. D. M. Nicholls, M. Alcarazo, *Chem. Lett.* **2019**, 48, 1; b) C. J. Rugen, M. Alcarazo, *Synlett* **2022**, 33, 16.
- [67] J. Carreras, M. Patil, W. Thiel, M. Alcarazo, *J. Am. Chem. Soc.* **2012**, 134, 16753.
- [68] A. Kozma, T. Deden, J. Carreras, C. Wille, J. Petušková, J. Rust, M. Alcarazo, *Chem. Eur. J.* **2014**, 20, 2208.
- [69] H. Tinnermann, L. D. M. Nicholls, T. Johannsen, C. Wille, C. Golz, R. Goddard, M. Alcarazo, *ACS Catal.* **2018**, 8, 10457.



- [70] X. Maset, M. Recort-Fornals, M. Kpante, A. Zieliński, C. Golz, L. M. Wolf, M. Alcarazo, *Adv. Synth. Catal.* **2021**, *363*, 3546.
- [71] T. Hartung, R. Machleid, M. Simon, C. Golz, M. Alcarazo, *Angew. Chem. Int. Ed.* **2020**, *59*, 5660.
- [72] V. Pelliccioli, T. Hartung, M. Simon, C. Golz, E. Licandro, S. Caeteruccio, M. Alcarazo, *Angew. Chem. Int. Ed.* **2022**, *61*, e202114577.
- [73] J. Zhang, M. Simon, C. Golz, M. Alcarazo, *Angew. Chem. Int. Ed.* **2020**, *59*, 5647.
- [74] G. R. Pettit, A. Numata, C. Iwamoto, Y. Usami, T. Yamada, H. Ohishi, G. M. Cragg, *J. Nat. Prod.* **2006**, *69*, 323.
- [75] P. Kittakoop, S. Nopichai, N. Thongon, P. Charoenchai, Y. Thebtaranonth, *Helv. Chim. Acta* **2004**, *87*, 175.
- [76] T. Spaulding, S. Fielding, M. Cornfeldt, J. Wilker, D. B. Ellis, W. J. Novick, H. H. Ong, *Drug Dev. Res.* **1985**, *5*, 207.
- [77] a) Y. Sagot, N. Toni, D. Perrelet, S. Lurot, B. King, H. Rixner, L. Mattenberger, P. C. Waldmeier, A. C. Kato, *Br. J. Pharmacol.* **2000**, *131*, 721; b) K. Zimmermann, P. C. Waldmeier, W. G. Tatton, *Pure Appl. Chem.* **1999**, *71*, 2039.
- [78] U. K. Tambar, D. C. Ebner, B. M. Stoltz, *J. Am. Chem. Soc.* **2006**, *128*, 11752.
- [79] T. Repiso Montero, S. López, C. Rodríguez, R. Del Rio, A. Badell, M. R. Gratacós, *International journal of dermatology* **2006**, *45*, 600.
- [80] J. Metysová, J. Metys, A. Dlabac, E. Kazdová, M. Valchár, *Acta Biol Med Ger.* **1980**, *39*, 723.
- [81] W. W. Fleischhacker, C. Barnas, C. H. Stuppäck, B. Unterweger, C. Miller, H. Hinterhuber, *Psychopharmacol. Bull.* **1989**, *25*, 97.
- [82] T. W. Harris, H. E. Smith, P. L. Mobley, D. H. Manier, F. Sulser, *J. Med. Chem.* **1982**, *25*, 855.
- [83] M. I. Ansari, M. K. Hussain, A. Arun, B. Chakravarti, R. Konwar, K. Hajela, *Eur. J. Med. Chem.* **2015**, *99*, 113.
- [84] S. Yadav, S. Suresh, *Asian J. Org. Chem.* **2021**, *10*, 1406.
- [85] T. Kitamura, T. Takachi, H. Kawasato, H. Taniguchi, *J. Chem. Soc., Perkin Trans. 1* **1992**, 1969.
- [86] N. Panda, I. Mattan, S. Ojha, C. S. Purohit, *Org. Biomol. Chem.* **2019**, *17*, 2824.
- [87] L. A. Arnold, W. Luo, R. K. Guy, *Org. Lett.* **2004**, *6*, 3005.
- [88] B. K. Villuri, S. S. Ichake, S. R. Reddy, V. Kavala, V. Bandi, C.-W. Kuo, C.-F. Yao, *J. Org. Chem.* **2018**, *83*, 10241.
- [89] D. R. R. Moreno, G. Giorgi, C. O. Salas, R. A. Tapia, *Molecules* **2013**, *18*, 14797.
- [90] Y. L. Choi, H. S. Lim, H. J. Lim, J.-N. Heo, *Org. Lett.* **2012**, *14*, 5102.

## 6. References

- [91] H. Krawczyk, M. Wrzesiński, D. Mielecki, P. Szczeciński, E. Grzesiuk, *Tetrahedron* **2016**, *72*, 3877.
- [92] Y. Bharath, B. Thirupathi, G. Ranjit, D. K. Mohapatra, *Asian J. Org. Chem.* **2013**, *2*, 848.
- [93] K. Bera, S. Jalal, S. Sarkar, U. Jana, *Org. Biomol. Chem.* **2014**, *12*, 57.
- [94] a) F. A. L. Anet, P. M. G. Bavin, *Can. J. Chem.* **1957**, *35*, 1084; b) B. A. Hess, A. S. Bailey, V. Boekelheide, *J. Am. Chem. Soc.* **1967**, *89*, 2746; c) T. Storz, E. Vangrevelinghe, P. Dittmar, *Synthesis* **2005**, *2005*, 2562.
- [95] T. Stopka, L. Marzo, M. Zurro, S. Janich, E.-U. Würthwein, C. G. Daniliuc, J. Alemán, O. G. Mancheño, *Angew. Chem. Int. Ed.* **2015**, *54*, 5049.
- [96] Z. Cong, T. Miki, O. Urakawa, H. Nishino, *J. Org. Chem.* **2009**, *74*, 3978.
- [97] A. Dorn, V. Schattel, S. Laufer, *Bioorg. Med. Chem. Lett.* **2010**, *20*, 3074.
- [98] C.-K. Chan, Y.-L. Chan, Y.-L. Tsai, M.-Y. Chang, *Tetrahedron* **2017**, *73*, 2074.
- [99] Y. Yu, P. Chakraborty, J. Song, L. Zhu, C. Li, X. Huang, *Nat. Commun.* **2020**, *11*, 461.
- [100] D. Arican, R. Brückner, *Org. Lett.* **2013**, *15*, 2582.
- [101] B. Rao, J. Tang, Y. Wei, X. Zeng, *Chem. Asian J.* **2016**, *11*, 991.
- [102] H. Shirani, T. Janosik, *J. Org. Chem.* **2007**, *72*, 8984.
- [103] T. Jepsen, M. Larsen, M. Jørgensen, M. Nielsen, *Synlett* **2012**, *23*, 418.
- [104] T. Matsuda, S. Sato, *J. Org. Chem.* **2013**, *78*, 3329.
- [105] a) W. Bains, R. Tacke, *Curr. Opin. Drug Discov. Devel.* **2003**, *6*, 526; b) P. K. Pooni, G. A. Showell, *Mini-Rev. Med. Chem.* **2006**, *6*, 1169.
- [106] L. G. Mercier, S. Furukawa, W. E. Piers, A. Wakamiya, S. Yamaguchi, M. Parvez, R. W. Harrington, W. Clegg, *Organometallics* **2011**, *30*, 1719.
- [107] G. Landek, I. Ozimec Landek, D. Pešić, M. Mesić, V. Šunjić, *Monatsh Chem* **2013**, *144*, 1825.
- [108] R. S. Cahn, C. K. Ingold, V. Prelog, *Angew. Chem. Int. Ed.* **1966**, *5*, 385.
- [109] M. Ōki in *Topics in Stereochemistry* (Eds.: N. L. Allinger, E. L. Eliel, S. H. Wilen), John Wiley & Sons, Inc, Hoboken, NJ, USA, **1983**, pp. 1–81.
- [110] a) J. Clayden, W. J. Moran, P. J. Edwards, S. R. LaPlante, *Angew. Chem. Int. Ed.* **2009**, *48*, 6398; b) S. R. LaPlante, L. D Fader, K. R. Fandrick, D. R. Fandrick, O. Hucke, R. Kemper, S. P. F. Miller, P. J. Edwards, *J. Med. Chem.* **2011**, *54*, 7005.
- [111] a) W. B. Jennings, M. Rutherford, S. K. Agarwal, D. R. Boyd, J. F. Malone, D. A. Kennedy, *J. Chem. Soc., Chem. Commun.* **1986**, 970; b) M. Nógrádi, W. D. Ollis, I. O. Sutherland, *J. Chem. Soc. D* **1970**, *0*, 158.
- [112] C.-X. Liu, Q. Gu, S.-L. You, *Trends Chem.* **2020**, *2*, 737.
- [113] a) N. Butt, D. Liu, W. Zhang, *Synlett* **2014**, *25*, 615; b) M. Drusan, R. Šebesta, *Tetrahedron* **2014**, *70*, 759.

- [114] Š. Toma, J. Csizmadiová, M. Mečiarová, R. Šebesta, *Dalton Trans.* **2014**, *43*, 16557.
- [115] T. Hayashi, K. Yamamoto, M. Kumada, *Tetrahedron Lett.* **1974**, *15*, 4405.
- [116] A. Togni, C. Breutel, A. Schnyder, F. Spindler, H. Landert, A. Tijani, *J. Am. Chem. Soc.* **1994**, *116*, 4062.
- [117] a) G. C. Fu, *Acc. Chem. Res.* **2000**, *33*, 412; b) G. C. Fu, *Acc. Chem. Res.* **2004**, *37*, 542.
- [118] F. Rebière, O. Riant, L. Ricard, H. B. Kagan, *Angew. Chem. Int. Ed.* **1993**, *32*, 568.
- [119] a) M. Tsukazaki, M. Tinkl, A. Roglans, B. J. Chapell, N. J. Taylor, V. Snieckus, *J. Am. Chem. Soc.* **1996**, *118*, 685; b) P. Steffen, C. Unkelbach, M. Christmann, W. Hiller, C. Strohmam, *Angew. Chem. Int. Ed.* **2013**, *52*, 9836.
- [120] M. Ogasawara, S. Watanabe, L. Fan, K. Nakajima, T. Takahashi, *Organometallics* **2006**, *25*, 5201.
- [121] S. Siegel, H.-G. Schmalz, *Angew. Chem. Int. Ed.* **1997**, *36*, 2456.
- [122] A. Urbano, G. Hernández-Torres, A. M. Del Hoyo, A. Martínez-Carrión, M. Carmen Carreño, *Chem. Commun.* **2016**, *52*, 6419.
- [123] T. Shibata, N. Uno, T. Sasaki, K. S. Kanyiva, *J. Org. Chem.* **2016**, *81*, 6266.
- [124] M. Ito, M. Okamura, K. S. Kanyiva, T. Shibata, *Organometallics* **2019**, *38*, 4029.
- [125] M. Zhao, A. G. Barrado, K. Sprenger, C. Golz, R. A. Mata, M. Alcarazo, *Org. Lett.* **2020**, *22*, 4932.
- [126] L. F. Tietze, T. Hungerland, A. Düfert, I. Objartel, D. Stalke, *Chem. Eur. J.* **2012**, *18*, 3286.
- [127] L. Rout, P. Saha, S. Jammi, T. Punniyamurthy, *Eur. J. Org. Chem.* **2008**, *2008*, 640.
- [128] R. Sanders, U. T. Mueller-Westerhoff, *J. Organomet. Chem.* **1996**, *512*, 219.
- [129] J. Feng, M. Lv, G. Lu, C. Cai, *Eur. J. Org. Chem.* **2014**, *2014*, 5312.
- [130] K. Hiroya, R. Jouka, M. Kameda, A. Yasuhara, T. Sakamoto, *Tetrahedron* **2001**, *57*, 9697.
- [131] P. M. Tadross, P. Bugga, B. M. Stoltz, *Org. Biomol. Chem.* **2011**, *9*, 5354.
- [132] Y. Ichikawa, T. Nishimura, T. Hayashi, *Organometallics* **2011**, *30*, 2342.
- [133] S.-B. Wang, Q. Gu, S.-L. You, *J. Org. Chem.* **2017**, *82*, 11829.
- [134] G. D. Frey, S. D. Hoffmann, *Z. Naturforsch.* **2015**, *70*, 65.
- [135] M. Roemer, C. A. Nijhuis, *Dalton Trans.* **2014**, *43*, 11815.
- [136] S. Akabori, M. Sato, S. Ebine, *Synthesis* **1981**, *1981*, 278.
- [137] M. Korb, D. Schaarschmidt, H. Lang, *Organometallics* **2014**, *33*, 2099.
- [138] F. H. Allen, O. Kennard, D. G. Watson, L. Brammer, A. G. Orpen, R. Taylor, *J. Chem. Soc., Perkin Trans. 2* **1987**, S1.

## 6. References

- [139] I. D'Acquarica, F. Gasparri, M. Pierini, C. Villani, G. Zappia, *J. Sep. Sci.* **2006**, 29, 1508.
- [140] O. Trapp, *Anal. Chem.* **2006**, 78, 189.
- [141] D. W. H. Rankin, C. A. Morrison, N. W. Mitzel, *Structural methods in molecular inorganic chemistry*, John Wiley & Sons Inc, Chichester, West Sussex, United Kingdom, **2013**.
- [142] J. Lu, D. Ma, J. Hu, W. Tang, D. Zhu, *J. Chem. Soc., Dalton Trans.* **1998**, 2267.
- [143] C. L. Perrin, T. J. Dwyer, *Chem. Rev.* **1990**, 90, 935.
- [144] T. Nishinaga, Y. Izukawa, K. Komatsu, *J. Phys. Org. Chem.* **1998**, 11, 475.
- [145] P. v. R. Schleyer, C. Maerker, A. Dransfeld, H. Jiao, N. J. R. van Eikema Hommes, *J. Am. Chem. Soc.* **1996**, 118, 6317.
- [146] L. Krause, R. Herbst-Irmer, G. M. Sheldrick, D. Stalke, *J. Appl. Cryst.* **2015**, 48, 3.
- [147] G. M. Sheldrick, *Acta Cryst.* **2008**, 64, 112.
- [148] O. V. Dolomanov, L. J. Bourhis, R. J. Gildea, J. A. K. Howard, H. Puschmann, *J. Appl. Cryst.* **2009**, 42, 339.
- [149] T. Kottke, D. Stalke, *J. Appl. Cryst.* **1993**, 26, 615.
- [150] A. C. Shaikh, D. S. Ranade, P. R. Rajamohanan, P. P. Kulkarni, N. T. Patil, *Angew. Chem. Int. Ed.* **2017**, 56, 757.
- [151] C. Körner, P. Starkov, T. D. Sheppard, *J. Am. Chem. Soc.* **2010**, 132, 5968.
- [152] M. Kuhn, F. C. Falk, J. Paradies, *Org. Lett.* **2011**, 13, 4100.
- [153] K. Hirano, Y. Inaba, K. Takasu, S. Oishi, Y. Takemoto, N. Fujii, H. Ohno, *J. Org. Chem.* **2011**, 76, 9068.
- [154] L. F. Tietze, B. Waldecker, D. Ganapathy, C. Eichhorst, T. Lenzer, K. Oum, S. O. Reichmann, D. Stalke, *Angew. Chem. Int. Ed.* **2015**, 54, 10317.
- [155] a) A. G. Brook, C. M. Warner, M. E. McGriskin, *J. Am. Chem. Soc.* **1959**, 81, 981;  
b) A. Deally, F. Hackenberg, G. Lally, H. Müller-Bunz, M. Tacke, *Organometallics* **2012**, 31, 5782.
- [156] Y. Zhang, H. Jiang, D. Chen, Y. Zhang, *Org. Biomol. Chem.* **2016**, 14, 4585.
- [157] T. Sanji, A. Fuchigami, M. Tanaka, *Heteroat. Chem.* **2016**, 27, 389.
- [158] O. N. Kadkin, H. Han, Y. G. Galyametdinov, *J. Organomet. Chem.* **2007**, 692, 5571.
- [159] M. Herberhold, A. Ayazi, W. Milius, B. Wrackmeyer, *J. Organomet. Chem.* **2002**, 656, 71.
- [160] M. J. Frisch, G. W. Trucks, H. B. Schlegel, G. E. Scuseria, M. A. Robb, J. R. Cheeseman, G. Scalmani, V. Barone, G. A. Petersson, H. Nakatsuji et al., *Gaussian 16, Revision A.03*, Gaussian, Inc., Wallingford CT, **2016**.

- [161] R. Dennington, T. A. Keith, J. M. Millam, *GaussView, Version 6*, Semichem Inc., Shawnee Mission, KS, **2016**.
- [162] a) A. D. Becke, *J. Chem. Phys.* **1993**, *98*, 5648; b) A. D. Becke, *Phys. Rev. A* **1988**, *38*, 3098.
- [163] a) F. Weigend, *Phys. Chem. Chem. Phys.* **2006**, *8*, 1057; b) F. Weigend, R. Ahlrichs, *Phys. Chem. Chem. Phys.* **2005**, *7*, 3297.
- [164] S. Grimme, S. Ehrlich, L. Goerigk, *J. Comp. Chem.* **2011**, *32*, 1456.

## 7. Appendix

### 7.1 Crystallographic details

#### Compound 199a

Single crystals suitable for X-ray analysis were obtained by evaporation of hexane/EtOAc.

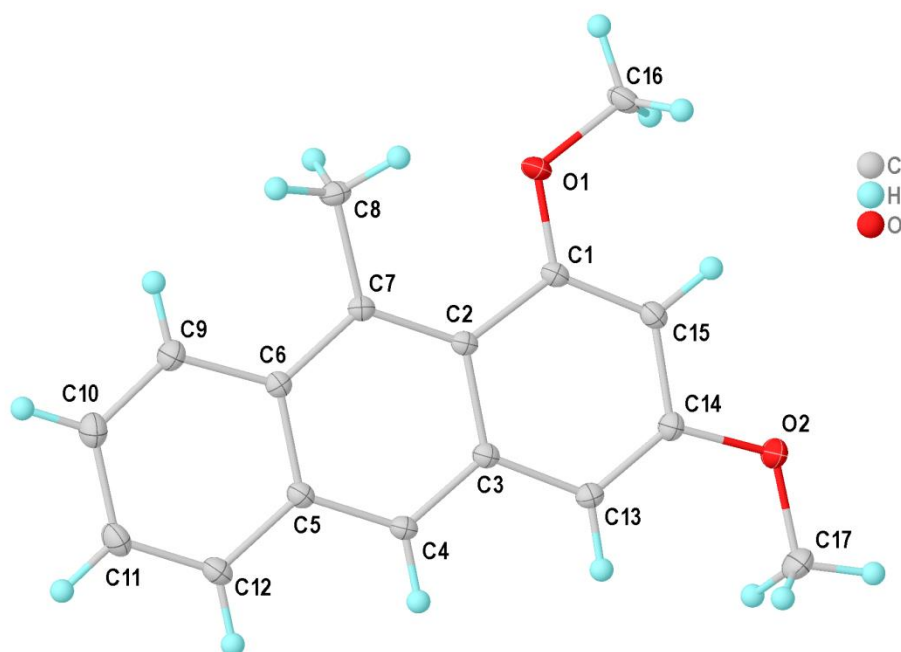


**Figure S15:** Full asymmetric unit and labeling scheme of **199a**. Displacement ellipsoids are drawn at 50% probability level. Final refinement as inversion twin (-1 0 0 / 0 -1 0 / 0 0 -1) as indicated by the Flack parameter of 0.4(10).

CCDC number	0989
Empirical formula	C <sub>17</sub> H <sub>16</sub> O <sub>2</sub>
Formula weight	252.30
Temperature/K	100
Crystal system	Orthorhombic
Space group	P2 <sub>1</sub> 2 <sub>1</sub> 2 <sub>1</sub>
a/Å	6.8034(3)
b/Å	11.7521(4)
c/Å	15.8912(6)
α/°	90
β/°	90
γ/°	90
Volume/Å <sup>3</sup>	1270.57(9)
Z	4
ρ <sub>calc</sub> /cm <sup>3</sup>	1.319
μ/mm <sup>-1</sup>	0.085
F(000)	536.0

## 7.1 Crystallographic details

Crystal size/mm <sup>3</sup>	0.2 × 0.15 × 0.15
Crystal color	colorless
Crystal shape	block
Radiation	MoK $\alpha$ ( $\lambda$ = 0.71073)
2 $\theta$ range for data collection/°	4.31 to 59.16
Index ranges	-9 ≤ h ≤ 9, -16 ≤ k ≤ 16, -22 ≤ l ≤ 22
Reflections collected	84229
Independent reflections	3561 [ $R_{\text{int}}$ = 0.0239, $R_{\text{sigma}}$ = 0.0087]
Data/restraints/parameters	3561/0/176
Goodness-of-fit on $F^2$	1.066
Final R indexes [ $I \geq 2\sigma(I)$ ]	$R_1$ = 0.0349, $wR_2$ = 0.1022
Final R indexes [all data]	$R_1$ = 0.0361, $wR_2$ = 0.1043
Largest diff. peak/hole / e $\text{\AA}^{-3}$	0.44/-0.17
Flack parameter	0.4(10)

### Compound 200

Single crystals suitable for X-ray analysis were obtained by crystallization from DCM and Et<sub>2</sub>O.

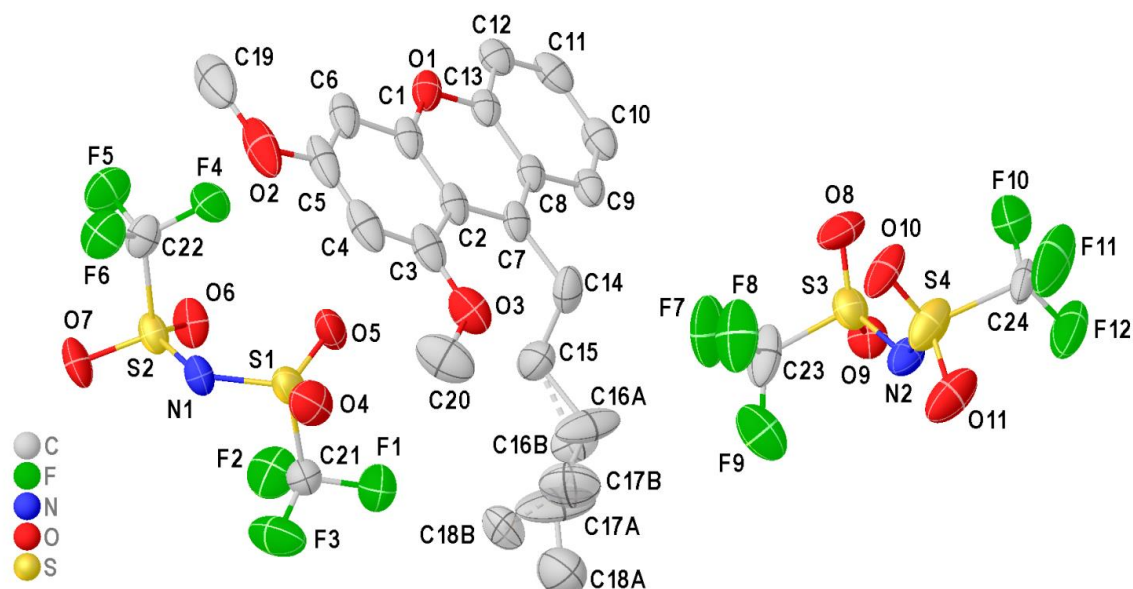


**Figure S16:** Full asymmetric unit and labeling scheme of **200**. Hydrogen atoms omitted for clarity; minor disorder part drawn partly translucent and with stippled cones. Both NTf<sub>2</sub> anions on special positions, refined in PART - 1 with occupancy fixed at 50%. Displacement ellipsoids are drawn at 50% probability level.

CCDC number	1061
Empirical formula	C <sub>22</sub> H <sub>23</sub> F <sub>6</sub> NO <sub>7</sub> S <sub>2</sub>
Formula weight	591.53

## 7. Appendix

Temperature/K	100
Crystal system	Triclinic
Space group	P-1
a/Å	8.6787(14)
b/Å	12.1633(17)
c/Å	12.669(2)
$\alpha$ /°	104.877(5)
$\beta$ /°	92.245(4)
$\gamma$ /°	97.275(5)
Volume/Å <sup>3</sup>	1278.5(3)
Z	2
$\rho_{\text{calc}}$ /cm <sup>3</sup>	1.537
$\mu$ /mm <sup>-1</sup>	0.295
F(000)	608.0
Crystal size/mm <sup>3</sup>	0.268 × 0.139 × 0.04
Crystal color	orange
Crystal shape	plate
Radiation	MoK $\alpha$ ( $\lambda$ = 0.71073)
2 $\theta$ range for data collection/°	4.148 to 55.852
Index ranges	-11 ≤ h ≤ 11, -16 ≤ k ≤ 16, -16 ≤ l ≤ 16
Reflections collected	105176
Independent reflections	6107 [ $R_{\text{int}}$ = 0.0412, $R_{\text{sigma}}$ = 0.0194]
Data/restraints/parameters	6107/30/508
Goodness-of-fit on $F^2$	1.058
Final R indexes [ $ I  \geq 2\sigma(I)$ ]	$R_1$ = 0.0507, $wR_2$ = 0.1359
Final R indexes [all data]	$R_1$ = 0.0624, $wR_2$ = 0.1451
Largest diff. peak/hole / e Å <sup>-3</sup>	0.32/-0.33



## 7.1 Crystallographic details

### Compound 201a

Single crystals suitable for X-ray analysis were obtained by crystallization from DCM and Et<sub>2</sub>O.

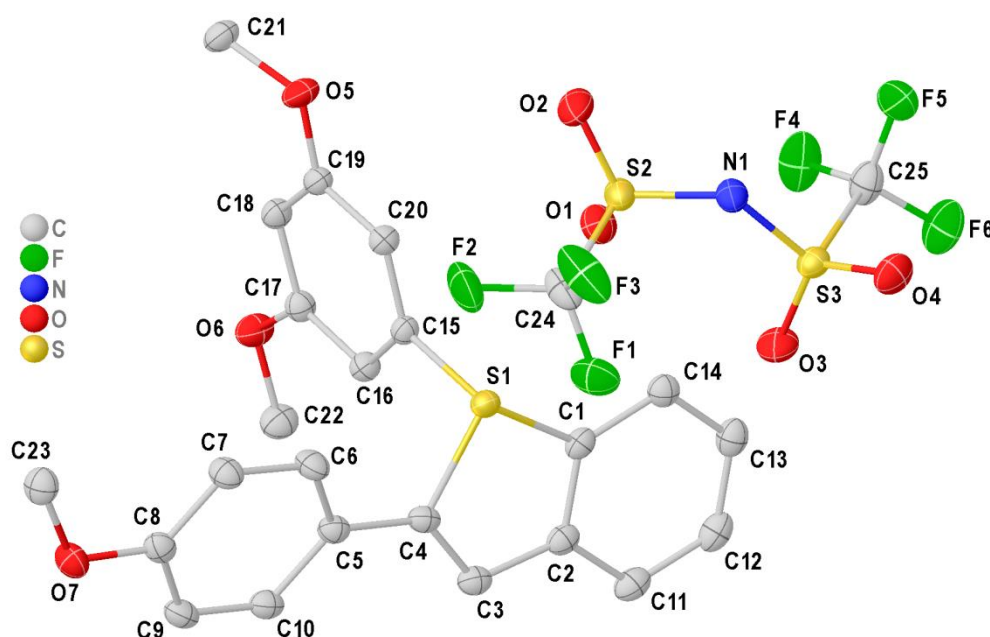


**Figure S17:** Full asymmetric unit and labeling scheme of **201a**. Hydrogen atoms omitted for clarity. Displacement ellipsoids are drawn at 50% probability level.

CCDC number	1059
Empirical formula	C <sub>25</sub> H <sub>21</sub> F <sub>6</sub> NO <sub>7</sub> S <sub>3</sub>
Formula weight	657.61
Temperature/K	100
Crystal system	Triclinic
Space group	P-1
a/Å	8.9226(8)
b/Å	10.8517(9)
c/Å	15.6903(14)
α/°	77.190(3)
β/°	76.055(3)
γ/°	70.312(2)
Volume/Å <sup>3</sup>	1371.7(2)
Z	2
ρ <sub>calc</sub> /cm <sup>3</sup>	1.592
μ/mm <sup>-1</sup>	0.358
F(000)	672.0
Crystal size/mm <sup>3</sup>	0.562 × 0.471 × 0.268
Crystal color	orange
Crystal shape	block

## 7. Appendix

Radiation	MoK $\alpha$ ( $\lambda = 0.71073$ )
2 $\theta$ range for data collection/ $^\circ$	4.034 to 59.342
Index ranges	$-12 \leq h \leq 12$ , $-15 \leq k \leq 14$ , $-21 \leq l \leq 21$
Reflections collected	38041
Independent reflections	7718 [ $R_{\text{int}} = 0.0235$ , $R_{\text{sigma}} = 0.0193$ ]
Data/restraints/parameters	7718/0/382
Goodness-of-fit on $F^2$	1.042
Final R indexes [ $I \geq 2\sigma(I)$ ]	$R_1 = 0.0328$ , $wR_2 = 0.0855$
Final R indexes [all data]	$R_1 = 0.0361$ , $wR_2 = 0.0878$
Largest diff. peak/hole / $e \text{ \AA}^{-3}$	0.46/-0.51

**Compound 146e**

Single crystals suitable for X-ray analysis were obtained by crystallization from EtOH.

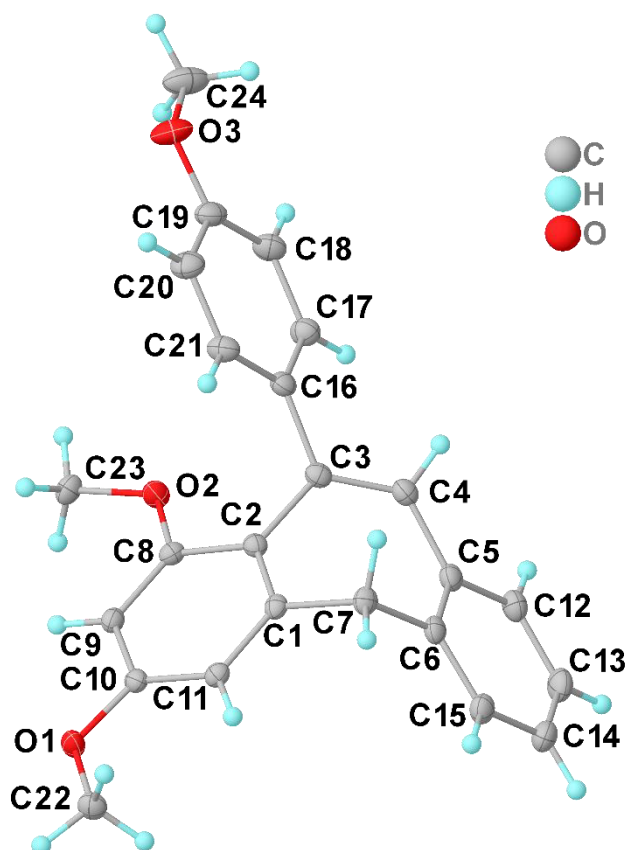


**Figure S18:** Full asymmetric unit and labeling scheme of **146e**. Displacement ellipsoids are drawn at 50% probability level.

CCDC number	-
Empirical formula	$C_{24}H_{22}O_3$
Formula weight	358.41
Temperature/K	100.00

## 7.1 Crystallographic details

Crystal system	monoclinic
Space group	$P2_1/c$ (14)
$a/\text{\AA}$	16.981(3)
$b/\text{\AA}$	5.5345(8)
$c/\text{\AA}$	20.671(3)
$\alpha/^\circ$	90
$\beta/^\circ$	109.041(5)
$\gamma/^\circ$	90
Volume/ $\text{\AA}^3$	1836.5(5)
Z	4
$\rho_{\text{calc}}/\text{cm}^3$	1.296
$\mu/\text{mm}^{-1}$	0.084
F(000)	760
Crystal size/ $\text{mm}^3$	0.882×0.052×0.05
Crystal color	colourless
Crystal shape	needle
Radiation	MoK $_{\alpha}$ ( $\lambda=0.71073 \text{\AA}$ )
2 $\theta$ range for data collection/ $^\circ$	5.08 to 61.06 (0.70 $\text{\AA}$ )
Index ranges	-24 $\leq h \leq$ 24 -7 $\leq k \leq$ 7 -28 $\leq l \leq$ 29
Reflections collected	52911
Independent reflections	5600 $R_{\text{int}} = 0.0417$ $R_{\text{sigma}} = 0.0226$
Data/restraints/parameters	5600/0/248
Goodness-of-fit on $F^2$	1.028
Final R indexes [ $I \geq 2\sigma(I)$ ]	$R_1 = 0.0416$ $wR_2 = 0.1017$
Final R indexes [all data]	$R_1 = 0.0531$ $wR_2 = 0.1099$
Largest diff. peak/hole / $e \text{\AA}^{-3}$	0.35/-0.21

**Compound 146g**

Single crystals suitable for X-ray analysis were obtained by crystallization from hexane and EtOAc (50:1).

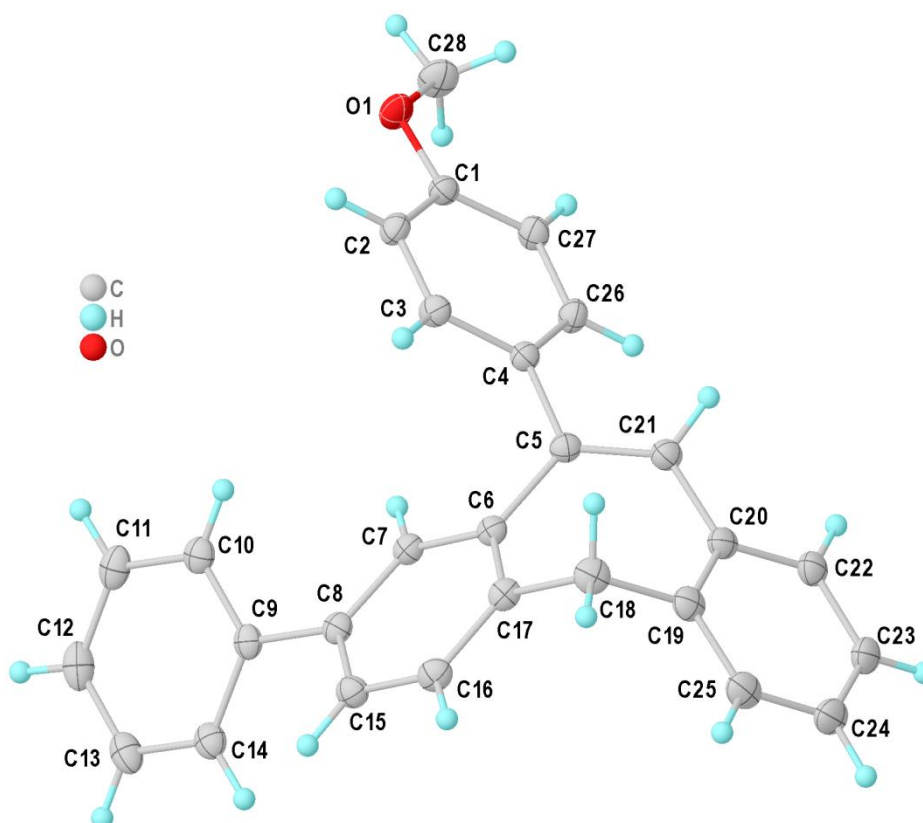


**Figure S19:** Full asymmetric unit and labeling scheme of **146g**. Displacement ellipsoids are drawn at 50% probability level.

CCDC number	0956
Empirical formula	$C_{28}H_{22}O$
Formula weight	374.45
Temperature/K	100
Crystal system	Monoclinic
Space group	$P2_1/n$
$a/\text{\AA}$	7.6568(6)
$b/\text{\AA}$	14.4160(11)
$c/\text{\AA}$	19.0021(13)
$\alpha/^\circ$	90
$\beta/^\circ$	97.365(2)
$\gamma/^\circ$	90
Volume/ $\text{\AA}^3$	2080.2(3)

## 7.1 Crystallographic details

Z	4
$\rho_{\text{calc}}/\text{cm}^3$	1.196
$\mu/\text{mm}^{-1}$	0.071
F(000)	792.0
Crystal size/ $\text{mm}^3$	0.264 × 0.205 × 0.187
Radiation	MoK $\alpha$ ( $\lambda = 0.71073$ )
2 $\theta$ range for data collection/ $^\circ$	4.322 to 59.408
Index ranges	-10 ≤ h ≤ 10, -18 ≤ k ≤ 18, -25 ≤ l ≤ 25
Reflections collected	97720
Independent reflections	5316 [ $R_{\text{int}} = 0.0297$ , $R_{\text{sigma}} = 0.0120$ ]
Data/restraints/parameters	5316/0/266
Goodness-of-fit on $F^2$	1.033
Final R indexes [ $I \geq 2\sigma(I)$ ]	$R_1 = 0.0397$ , $wR_2 = 0.1041$
Final R indexes [all data]	$R_1 = 0.0440$ , $wR_2 = 0.1083$
Largest diff. peak/hole / e $\text{\AA}^{-3}$	0.33/-0.20

**Compound 146h**

Single crystals suitable for X-ray analysis were obtained from DCM and hexane by diffusion crystallization.

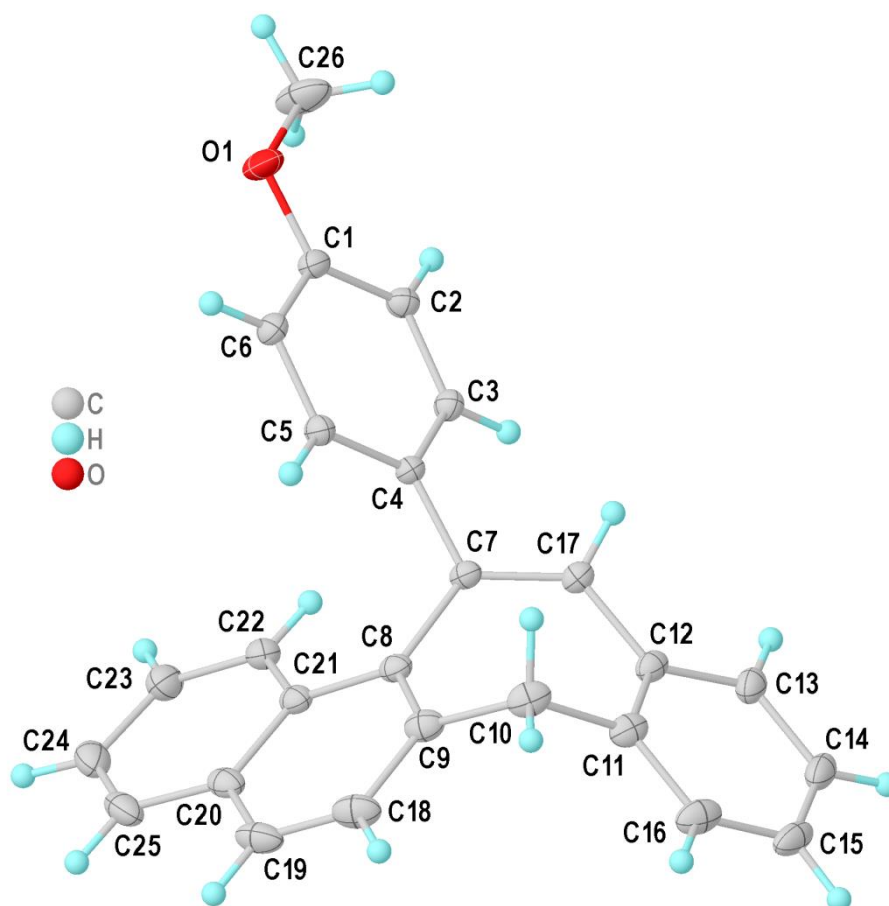


**Figure S20:** Full asymmetric unit and labeling scheme of **146h**. Displacement ellipsoids are drawn at 50% probability level.

CCDC number	0964
Empirical formula	C <sub>26</sub> H <sub>20</sub> O
Formula weight	348.42
Temperature/K	100
Crystal system	Orthorhombic
Space group	Pca2 <sub>1</sub>
a/Å	18.9268(14)
b/Å	6.2685(4)
c/Å	15.2686(11)
α/°	90
β/°	90
γ/°	90
Volume/Å <sup>3</sup>	1811.5(2)

## 7.1 Crystallographic details

Z	4
$\rho_{\text{calc}}/\text{cm}^3$	1.278
$\mu/\text{mm}^{-1}$	0.076
F(000)	736.0
Crystal size/ $\text{mm}^3$	0.488 × 0.384 × 0.297
Crystal color	colorless
Crystal shape	block
Radiation	MoK $\alpha$ ( $\lambda = 0.71073$ )
2 $\theta$ range for data collection/ $^\circ$	5.064 to 59.186
Index ranges	-26 ≤ h ≤ 26, -8 ≤ k ≤ 8, -21 ≤ l ≤ 21
Reflections collected	73519
Independent reflections	5089 [ $R_{\text{int}} = 0.0327$ , $R_{\text{sigma}} = 0.0138$ ]
Data/restraints/parameters	5089/1/245
Goodness-of-fit on $F^2$	1.058
Final R indexes [ $I \geq 2\sigma(I)$ ]	$R_1 = 0.0309$ , $wR_2 = 0.0835$
Final R indexes [all data]	$R_1 = 0.0317$ , $wR_2 = 0.0844$
Largest diff. peak/hole / $e \text{ \AA}^{-3}$	0.24/-0.18
Flack parameter	-0.1(2)

**Compound 146k**

Single crystals suitable for X-ray analysis were obtained from slow evaporation of chloroform.

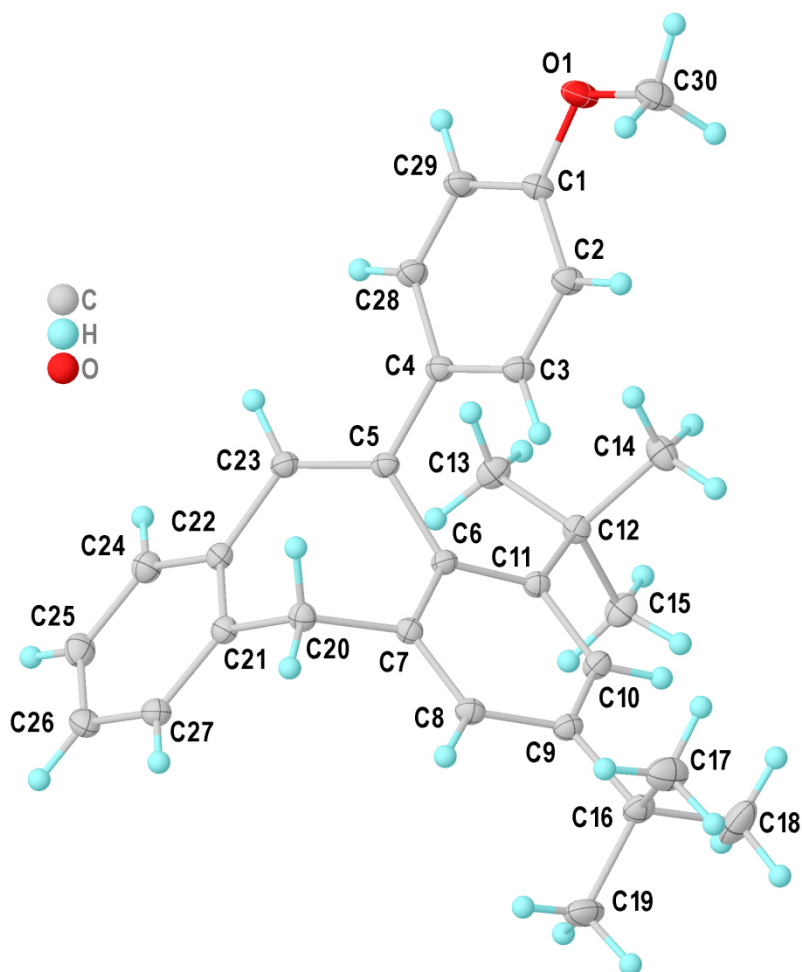


**Figure S21:** Full asymmetric unit and labeling scheme of **146k**. Displacement ellipsoids are drawn at 50% probability level.

CCDC number	0965
Empirical formula	C <sub>30</sub> H <sub>34</sub> O
Formula weight	410.57
Temperature/K	100
Crystal system	Monoclinic
Space group	P2 <sub>1</sub> /c
a/Å	10.4161(9)
b/Å	12.7468(10)
c/Å	17.8461(13)
α/°	90
β/°	97.953(3)
γ/°	90



## 7.1 Crystallographic details

Volume/Å <sup>3</sup>	2346.7(3)
Z	4
$\rho_{\text{calc}}/\text{cm}^3$	1.162
$\mu/\text{mm}^{-1}$	0.068
F(000)	888.0
Crystal size/mm <sup>3</sup>	0.296 × 0.189 × 0.18
Crystal color	colorless
Crystal shape	block
Radiation	MoK $\alpha$ ( $\lambda = 0.71073$ )
2 $\theta$ range for data collection/°	4.61 to 61.134
Index ranges	-14 ≤ h ≤ 14, -18 ≤ k ≤ 18, -25 ≤ l ≤ 25
Reflections collected	160611
Independent reflections	7190 [ $R_{\text{int}} = 0.0307$ , $R_{\text{sigma}} = 0.0119$ ]
Data/restraints/parameters	7190/0/287
Goodness-of-fit on F <sup>2</sup>	1.034
Final R indexes [ $l \geq 2\sigma(l)$ ]	$R_1 = 0.0395$ , $wR_2 = 0.1080$
Final R indexes [all data]	$R_1 = 0.0418$ , $wR_2 = 0.1100$
Largest diff. peak/hole / e Å <sup>-3</sup>	0.42/-0.19

**Compound 147b**

Single crystals suitable for X-ray analysis were obtained from hot EtOH.

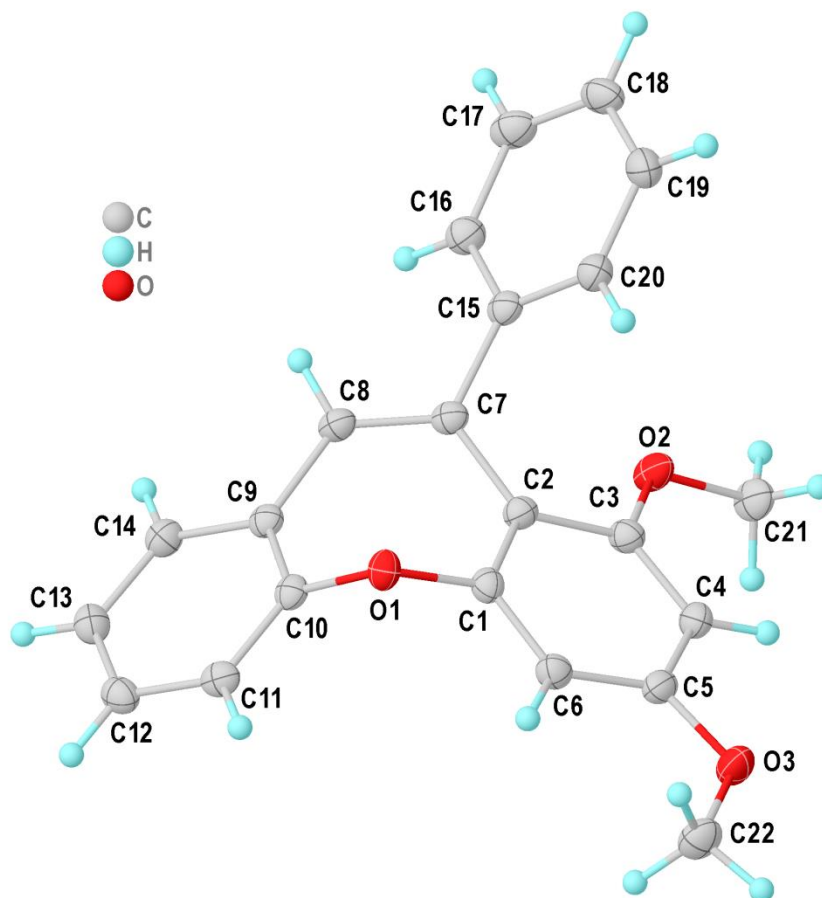


**Figure S22:** Full asymmetric unit and labeling scheme of **147b**. Displacement ellipsoids are drawn at 50% probability level.

CCDC number	0666
Empirical formula	$C_{22}H_{18}O_3$
Formula weight	330.36
Temperature/K	100
Crystal system	Orthorhombic
Space group	$P2_12_12_1$
$a/\text{\AA}$	6.2198(2)
$b/\text{\AA}$	14.9940(5)
$c/\text{\AA}$	17.7817(6)
$\alpha/^\circ$	90
$\beta/^\circ$	90
$\gamma/^\circ$	90
Volume/ $\text{\AA}^3$	1658.32(10)
Z	4

## 7.1 Crystallographic details

$\rho_{\text{calc}}/\text{cm}^3$	1.323
$\mu/\text{mm}^{-1}$	0.700
F(000)	696.0
Crystal size/ $\text{mm}^3$	$0.475 \times 0.27 \times 0.21$
Crystal color	colorless
Crystal shape	block
Radiation	CuK $\alpha$ ( $\lambda = 1.54178$ )
2 $\theta$ range for data collection/ $^\circ$	7.712 to 160.554
Index ranges	$-7 \leq h \leq 7, -19 \leq k \leq 18, -22 \leq l \leq 22$
Reflections collected	53975
Independent reflections	3568 [ $R_{\text{int}} = 0.0196, R_{\text{sigma}} = 0.0071$ ]
Data/restraints/parameters	3568/0/228
Goodness-of-fit on $F^2$	1.060
Final R indexes [ $I \geq 2\sigma(I)$ ]	$R_1 = 0.0257, wR_2 = 0.0658$
Final R indexes [all data]	$R_1 = 0.0257, wR_2 = 0.0659$
Largest diff. peak/hole / $e \text{ \AA}^{-3}$	0.19/-0.17
Flack parameter	0.011(16)

**Compound 147c**

Single crystals suitable for X-ray analysis were obtained from hot EtOH.

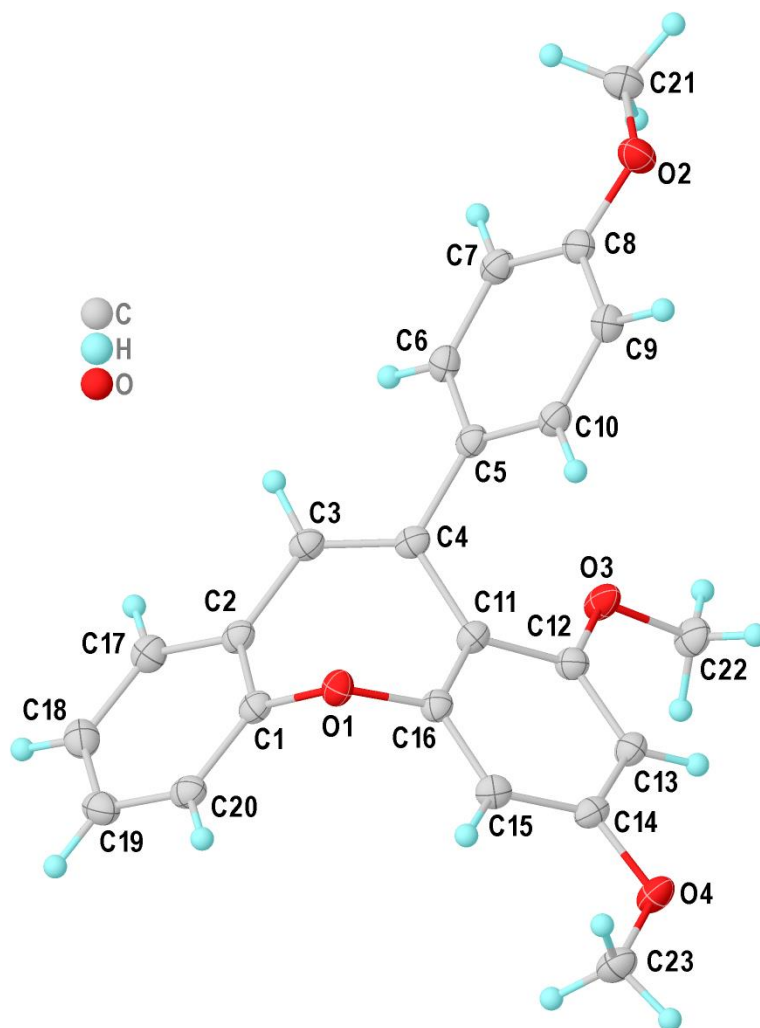


**Figure S23:** Full asymmetric unit and labeling scheme of **147c**. Displacement ellipsoids are drawn at 50% probability level.

CCDC number	0470
Empirical formula	C <sub>23</sub> H <sub>20</sub> O <sub>4</sub>
Formula weight	360.39
Temperature/K	100
Crystal system	Orthorhombic
Space group	Pna2 <sub>1</sub>
a/Å	15.0429(4)
b/Å	6.3692(2)
c/Å	18.6523(5)
α/°	90
β/°	90
γ/°	90
Volume/Å <sup>3</sup>	1787.10(9)

## 7.1 Crystallographic details

Z	4
$\rho_{\text{calc}}/\text{cm}^3$	1.339
$\mu/\text{mm}^{-1}$	0.738
F(000)	760.0
Crystal size/ $\text{mm}^3$	0.309 × 0.17 × 0.068
Crystal color	colorless
Crystal shape	plate
Radiation	CuK $\alpha$ ( $\lambda = 1.54178$ )
2 $\theta$ range for data collection/ $^\circ$	9.482 to 149.812
Index ranges	-18 ≤ h ≤ 18, -7 ≤ k ≤ 7, -20 ≤ l ≤ 23
Reflections collected	28648
Independent reflections	3591 [ $R_{\text{int}} = 0.0242$ , $R_{\text{sigma}} = 0.0133$ ]
Data/restraints/parameters	3591/1/247
Goodness-of-fit on $F^2$	1.061
Final R indexes [ $I \geq 2\sigma(I)$ ]	$R_1 = 0.0237$ , $wR_2 = 0.0592$
Final R indexes [all data]	$R_1 = 0.0241$ , $wR_2 = 0.0593$
Largest diff. peak/hole / $e \text{ \AA}^{-3}$	0.14/-0.15
Flack parameter	0.03(3)

**Compound 147i**

Single crystals suitable for X-ray analysis were obtained from hot EtOH.

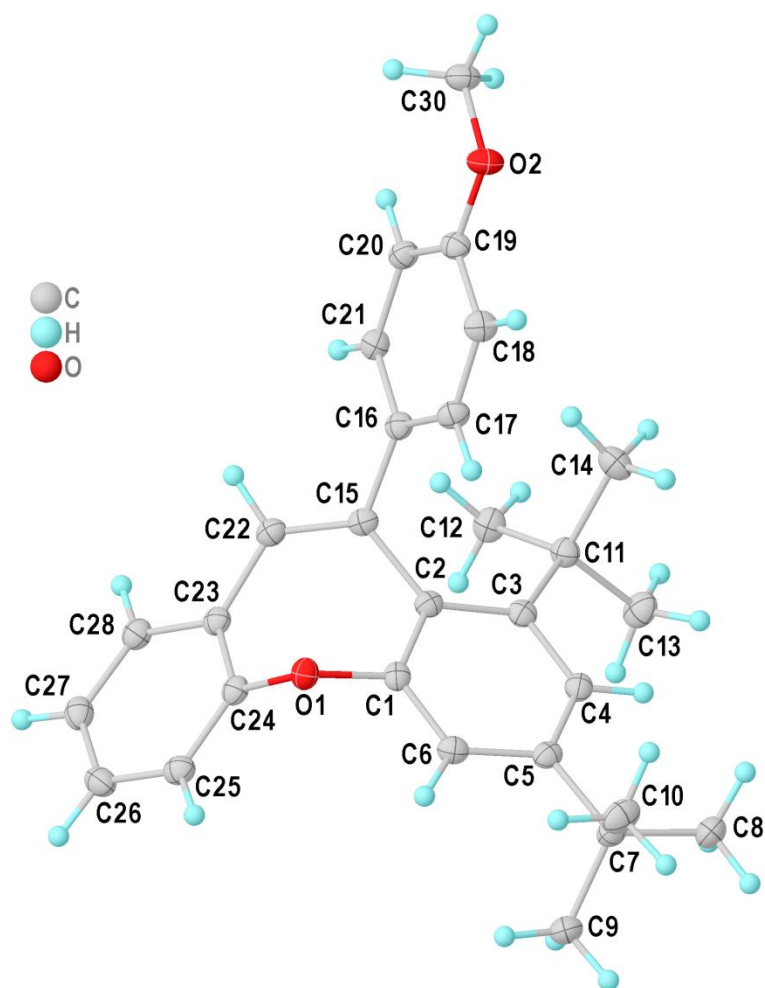


**Figure S24:** Full asymmetric unit and labeling scheme of **147i**. Displacement ellipsoids are drawn at 50% probability level. Non-merohedral twinning found for **147i**, twin domain transformation matrix is (1.009 0.018 0.021/ -0.010 1.000 -0.009/ -0.068 0.083 0.989). Detwinned hklf4 data worked better on this structure and was used for final refinement in favor of hklf5 data.

CCDC number	0541
Empirical formula	C <sub>29</sub> H <sub>32</sub> O <sub>2</sub>
Formula weight	412.54
Temperature/K	100
Crystal system	Monoclinic
Space group	P2 <sub>1</sub> /n
a/Å	13.2714(4)
b/Å	7.4122(2)
c/Å	24.0531(7)
α/°	90
β/°	104.9300(10)
γ/°	90

## 7.1 Crystallographic details

Volume/Å <sup>3</sup>	2286.23(11)
Z	4
$\rho_{\text{calc}}/\text{cm}^3$	1.199
$\mu/\text{mm}^{-1}$	0.566
F(000)	888.0
Crystal size/mm <sup>3</sup>	0.408 × 0.062 × 0.054
Crystal color	colorless
Crystal shape	needles
Radiation	CuK $\alpha$ ( $\lambda = 1.54178$ )
2 $\theta$ range for data collection/°	6.962 to 149.022
Index ranges	-16 ≤ h ≤ 16, 0 ≤ k ≤ 9, 0 ≤ l ≤ 30
Reflections collected	4658
Independent reflections	4658 [ $R_{\text{int}} = 0.0080$ , $R_{\text{sigma}} = 0.0078$ ]
Data/restraints/parameters	4658/0/408
Goodness-of-fit on F <sup>2</sup>	1.037
Final R indexes [ $l \geq 2\sigma(l)$ ]	$R_1 = 0.0348$ , $wR_2 = 0.0886$
Final R indexes [all data]	$R_1 = 0.0356$ , $wR_2 = 0.0892$
Largest diff. peak/hole / e Å <sup>-3</sup>	0.27/-0.18

**Compound 147k**

Single crystals suitable for X-ray analysis were obtained from hot EtOH.

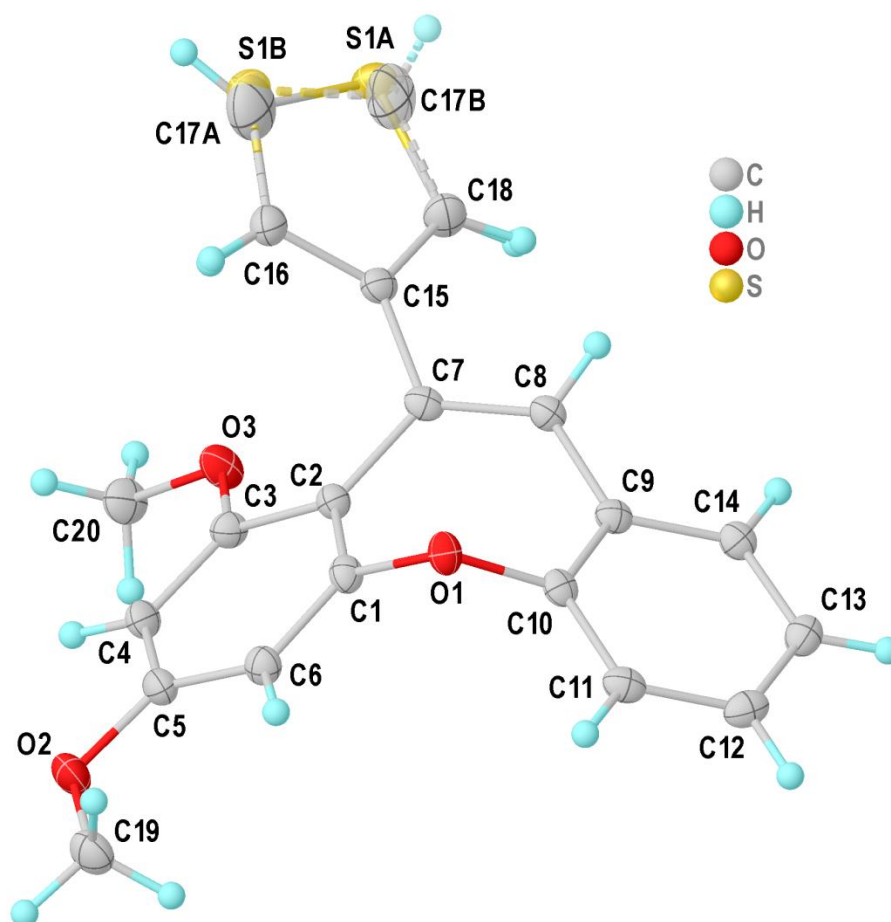


**Figure S25:** Full asymmetric unit and labeling scheme of **147k**. Minor disorder part is drawn partly translucent and with stippled cones. Displacement ellipsoids are drawn at 50% probability level.

CCDC number	0664
Empirical formula	C <sub>20</sub> H <sub>16</sub> O <sub>3</sub> S
Formula weight	336.39
Temperature/K	100
Crystal system	Orthorhombic
Space group	P2 <sub>1</sub> 2 <sub>1</sub> 2 <sub>1</sub>
a/Å	5.8533(7)
b/Å	16.375(3)
c/Å	16.635(3)
α/°	90
β/°	90
γ/°	90
Volume/Å <sup>3</sup>	1594.4(4)
Z	4



## 7.1 Crystallographic details

$\rho_{\text{calc}}/\text{cm}^3$	1.401
$\mu/\text{mm}^{-1}$	0.218
F(000)	704.0
Crystal size/ $\text{mm}^3$	$0.331 \times 0.147 \times 0.038$
Crystal color	colorless
Crystal shape	plates
Radiation	MoK $\alpha$ ( $\lambda = 0.71073$ )
2 $\theta$ range for data collection/ $^\circ$	4.898 to 57.53
Index ranges	$-7 \leq h \leq 7, -20 \leq k \leq 22, -22 \leq l \leq 22$
Reflections collected	19484
Independent reflections	4124 [ $R_{\text{int}} = 0.0307, R_{\text{sigma}} = 0.0234$ ]
Data/restraints/parameters	4124/42/238
Goodness-of-fit on $F^2$	1.044
Final R indexes [ $ I  \geq 2\sigma(I)$ ]	$R_1 = 0.0290, wR_2 = 0.0706$
Final R indexes [all data]	$R_1 = 0.0307, wR_2 = 0.0719$
Largest diff. peak/hole / $e \text{ \AA}^{-3}$	0.21/-0.19
Flack parameter	0.04(3)

**Compound 148a**

Single crystals suitable for X-ray analysis were obtained from hot EtOAc.

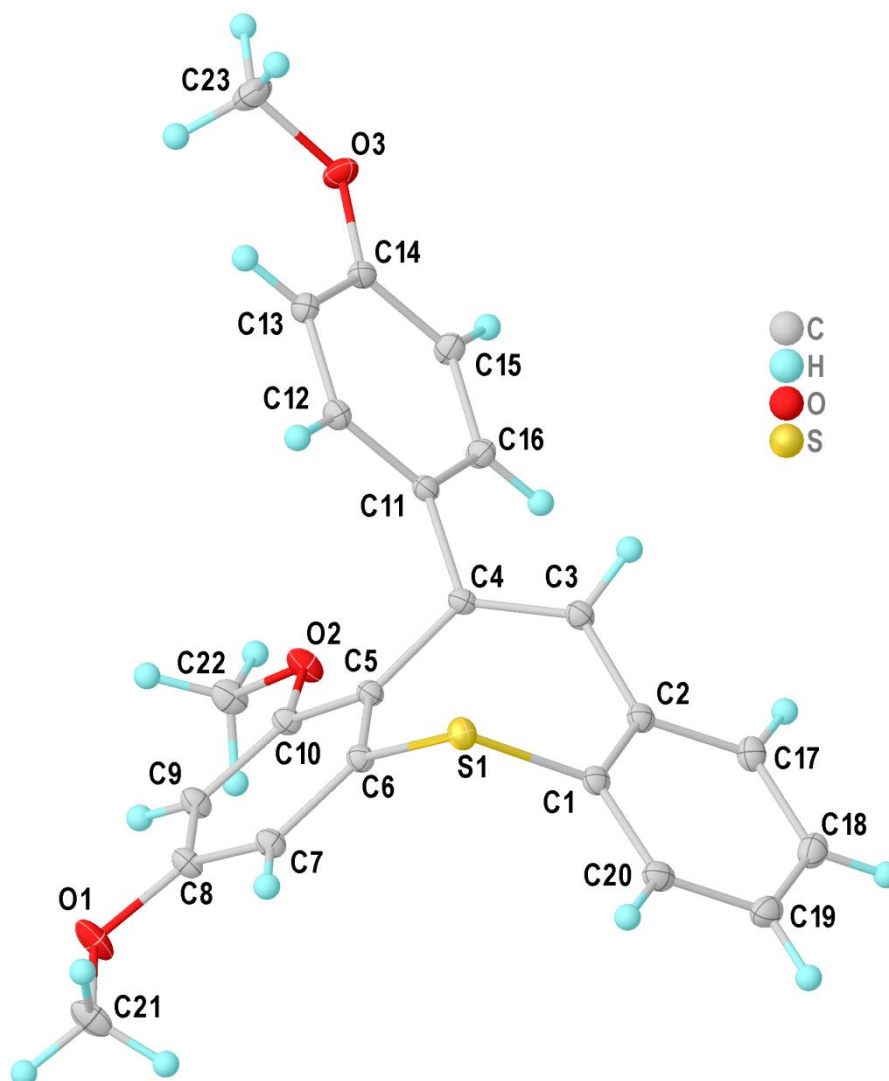


**Figure S26:** Full asymmetric unit and labeling scheme of **148a**. Displacement ellipsoids are drawn at 50% probability level.

CCDC number	0480
Empirical formula	$C_{23}H_{20}O_3S$
Formula weight	376.45
Temperature/K	100
Crystal system	Monoclinic
Space group	$P2_1/n$
$a/\text{\AA}$	9.7648(7)
$b/\text{\AA}$	13.2679(8)
$c/\text{\AA}$	14.7613(9)
$\alpha/^\circ$	90
$\beta/^\circ$	108.778(2)

## 7.1 Crystallographic details

$\gamma/^\circ$	90
Volume/ $\text{\AA}^3$	1810.7(2)
Z	4
$\rho_{\text{calc}}/\text{g/cm}^3$	1.381
$\mu/\text{mm}^{-1}$	0.200
F(000)	792.0
Crystal size/ $\text{mm}^3$	0.342 × 0.259 × 0.181
Crystal color	colorless
Crystal shape	plates
Radiation	MoK $\alpha$ ( $\lambda = 0.71073$ )
2 $\theta$ range for data collection/ $^\circ$	5.392 to 63.102
Index ranges	-14 ≤ h ≤ 14, -19 ≤ k ≤ 19, -21 ≤ l ≤ 21
Reflections collected	77791
Independent reflections	6049 [ $R_{\text{int}} = 0.0205$ , $R_{\text{sigma}} = 0.0120$ ]
Data/restraints/parameters	6049/0/247
Goodness-of-fit on $F^2$	1.043
Final R indexes [ $ I  \geq 2\sigma(I)$ ]	$R_1 = 0.0310$ , $wR_2 = 0.0858$
Final R indexes [all data]	$R_1 = 0.0317$ , $wR_2 = 0.0863$
Largest diff. peak/hole / $e \text{\AA}^{-3}$	0.83/-0.25

**Compound 149a**

Single crystals suitable for X-ray analysis were obtained from hot MeOH.

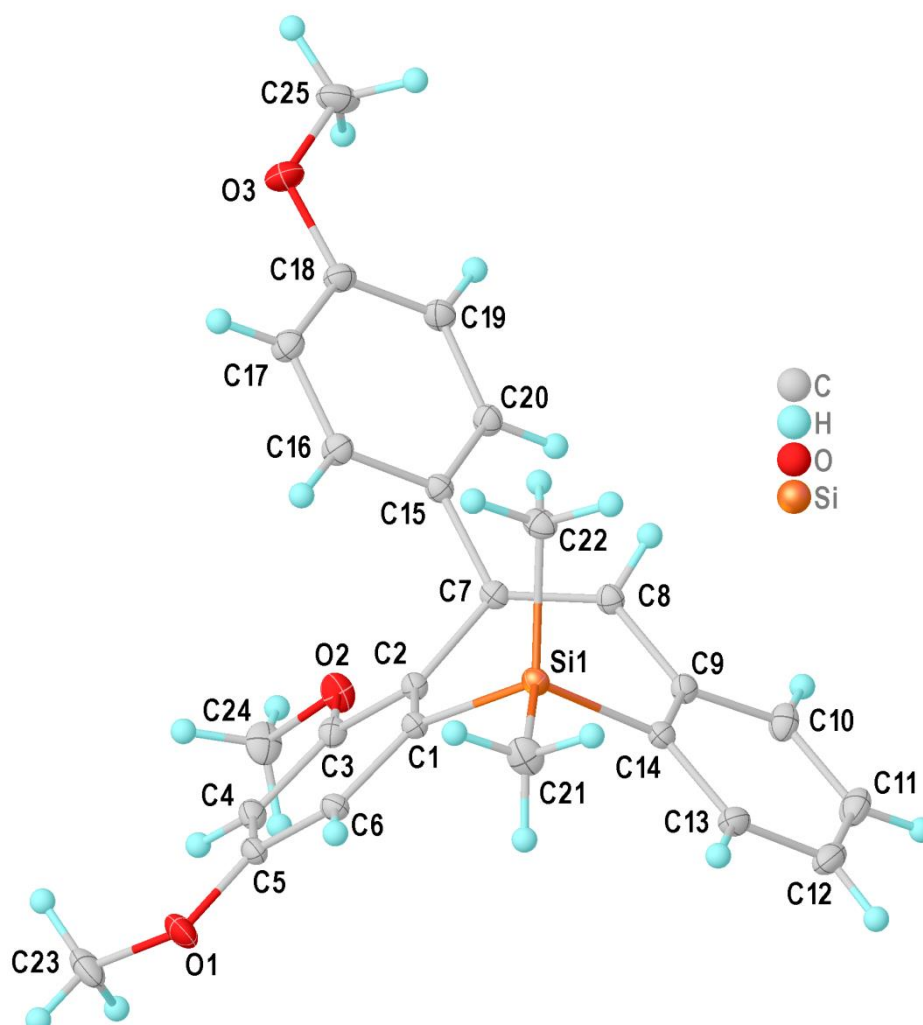


**Figure S27:** Full asymmetric unit and labeling scheme of **149a**. Displacement ellipsoids are drawn at 50% probability level.

CCDC number	0495
Empirical formula	C <sub>25</sub> H <sub>26</sub> O <sub>3</sub> Si
Formula weight	402.55
Temperature/K	100
Crystal system	Monoclinic
Space group	C2/c
a/Å	30.196(6)
b/Å	7.0088(15)
c/Å	24.092(4)
α/°	90
β/°	124.559(6)
γ/°	90

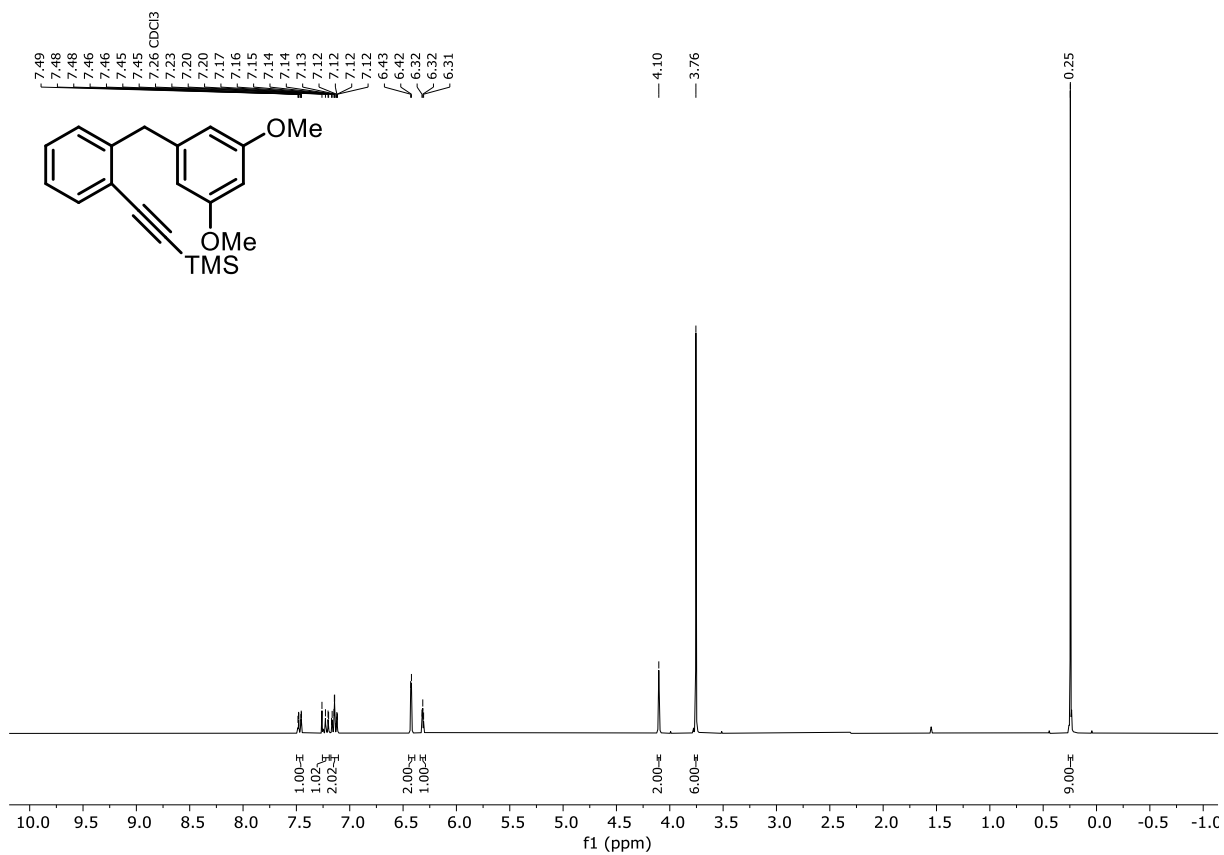
## 7.1 Crystallographic details

Volume/Å <sup>3</sup>	4199.1(14)
Z	8
$\rho_{\text{calc}}/\text{cm}^3$	1.273
$\mu/\text{mm}^{-1}$	0.135
F(000)	1712.0
Crystal size/mm <sup>3</sup>	0.297 × 0.136 × 0.057
Crystal color	colorless
Crystal shape	needles
Radiation	MoK $\alpha$ ( $\lambda = 0.71073$ )
2 $\theta$ range for data collection/°	5.41 to 63.222
Index ranges	-44 ≤ h ≤ 44, -10 ≤ k ≤ 10, -35 ≤ l ≤ 35
Reflections collected	86396
Independent reflections	7022 [ $R_{\text{int}} = 0.0331$ , $R_{\text{sigma}} = 0.0154$ ]
Data/restraints/parameters	7022/0/267
Goodness-of-fit on F <sup>2</sup>	1.079
Final R indexes [ $l \geq 2\sigma(l)$ ]	$R_1 = 0.0460$ , $wR_2 = 0.1264$
Final R indexes [all data]	$R_1 = 0.0499$ , $wR_2 = 0.1296$
Largest diff. peak/hole / e Å <sup>-3</sup>	1.12/-0.30

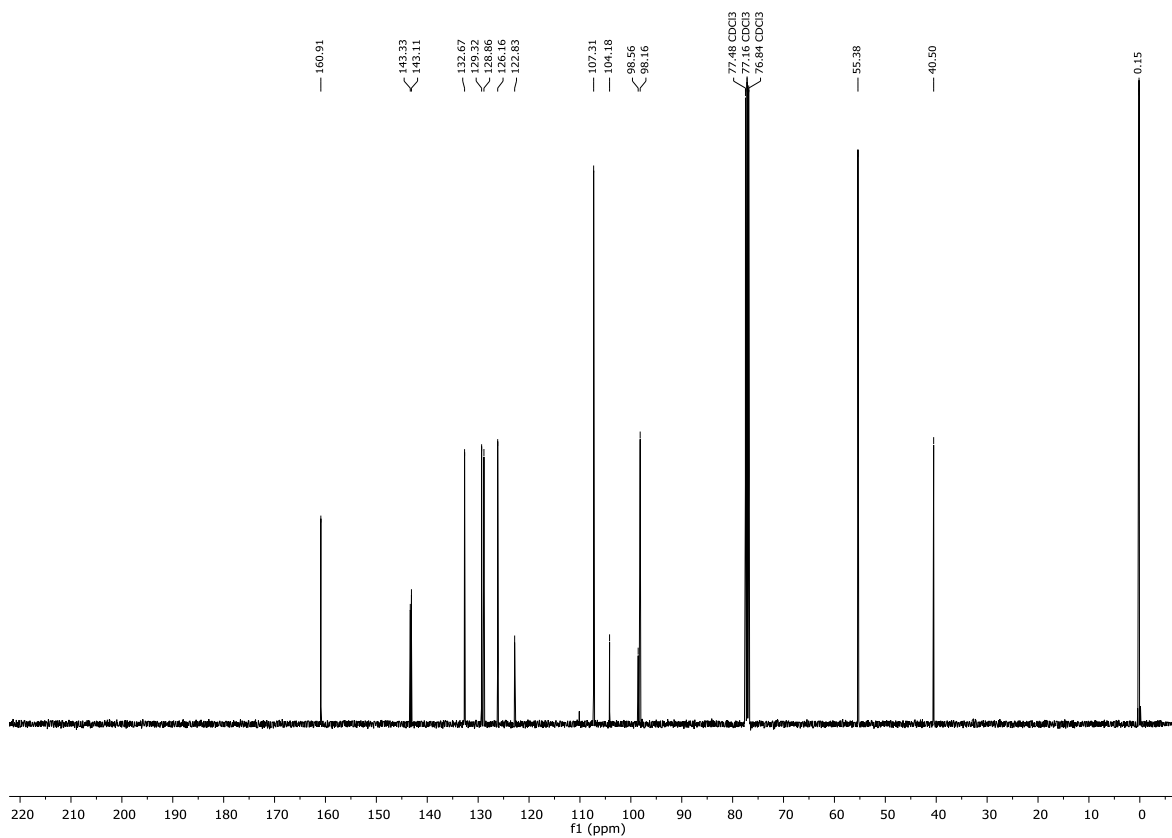
## 7. Appendix

### 7.2 NMR spectra

#### $^1\text{H-NMR}$ (300 MHz, $\text{CDCl}_3$ ) Compound **169**

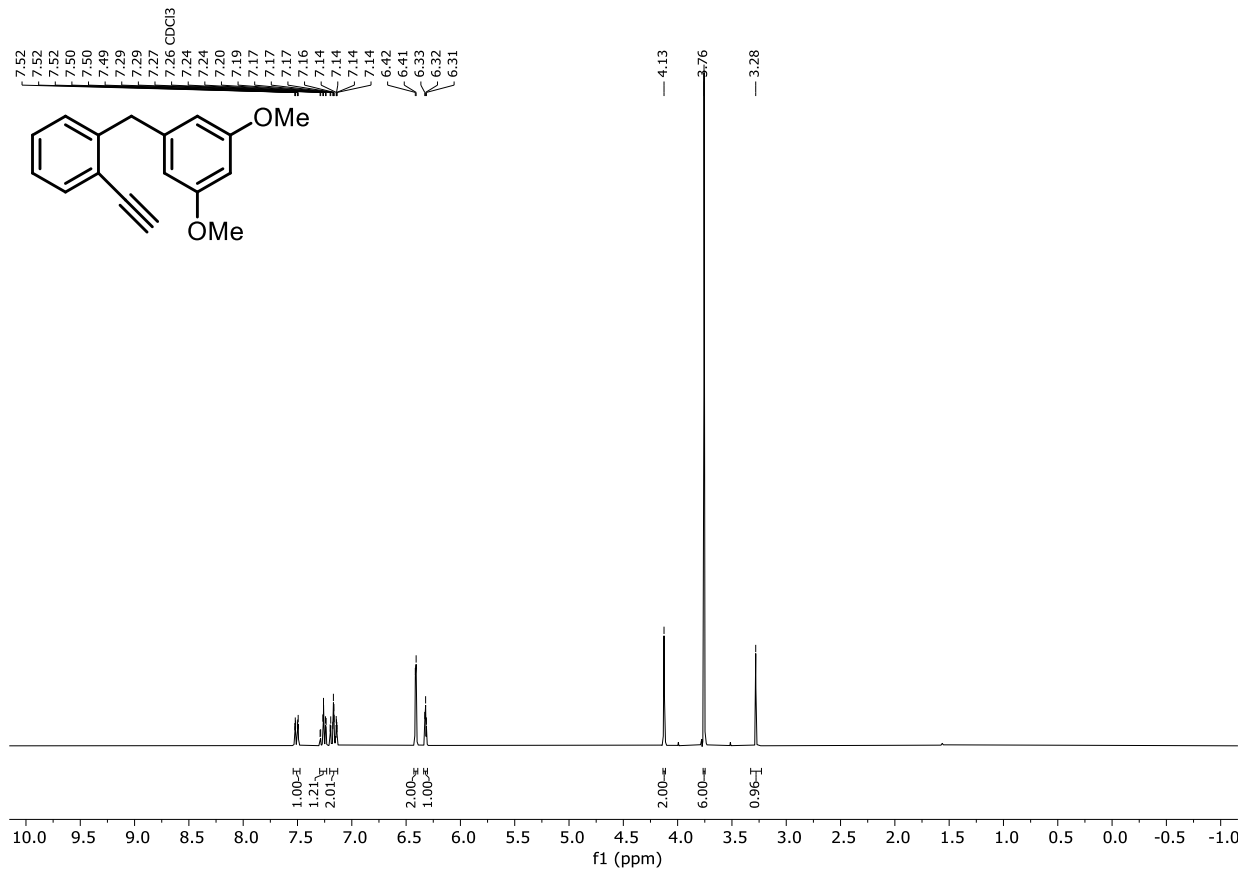


#### $^{13}\text{C}\{^1\text{H}\}\text{-NMR}$ (101 MHz, $\text{CDCl}_3$ ) Compound **169**

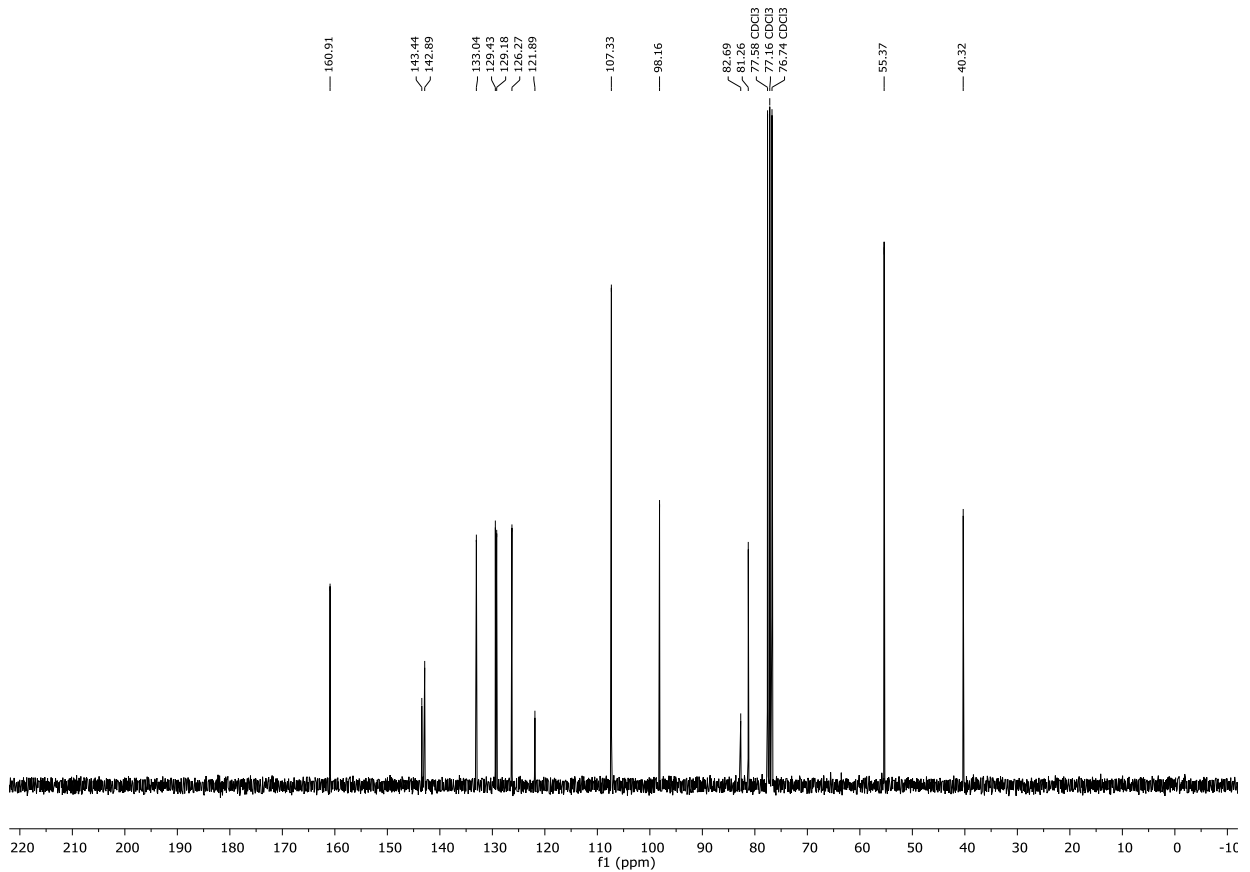


## 7.2 NMR spectra

### <sup>1</sup>H-NMR (300 MHz, CDCl<sub>3</sub>) Compound **150a**

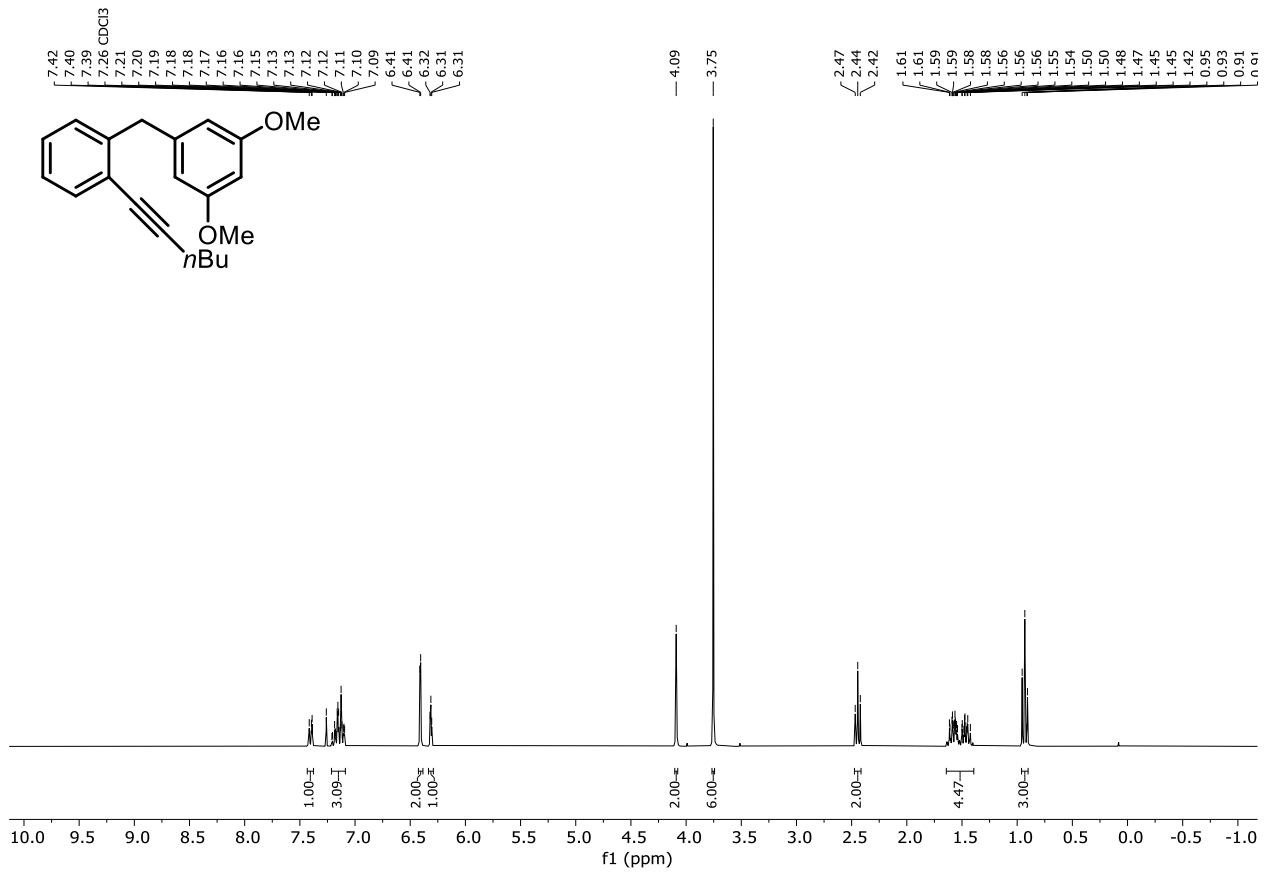


### <sup>13</sup>C{<sup>1</sup>H}-NMR (75 MHz, CDCl<sub>3</sub>) Compound **150a**

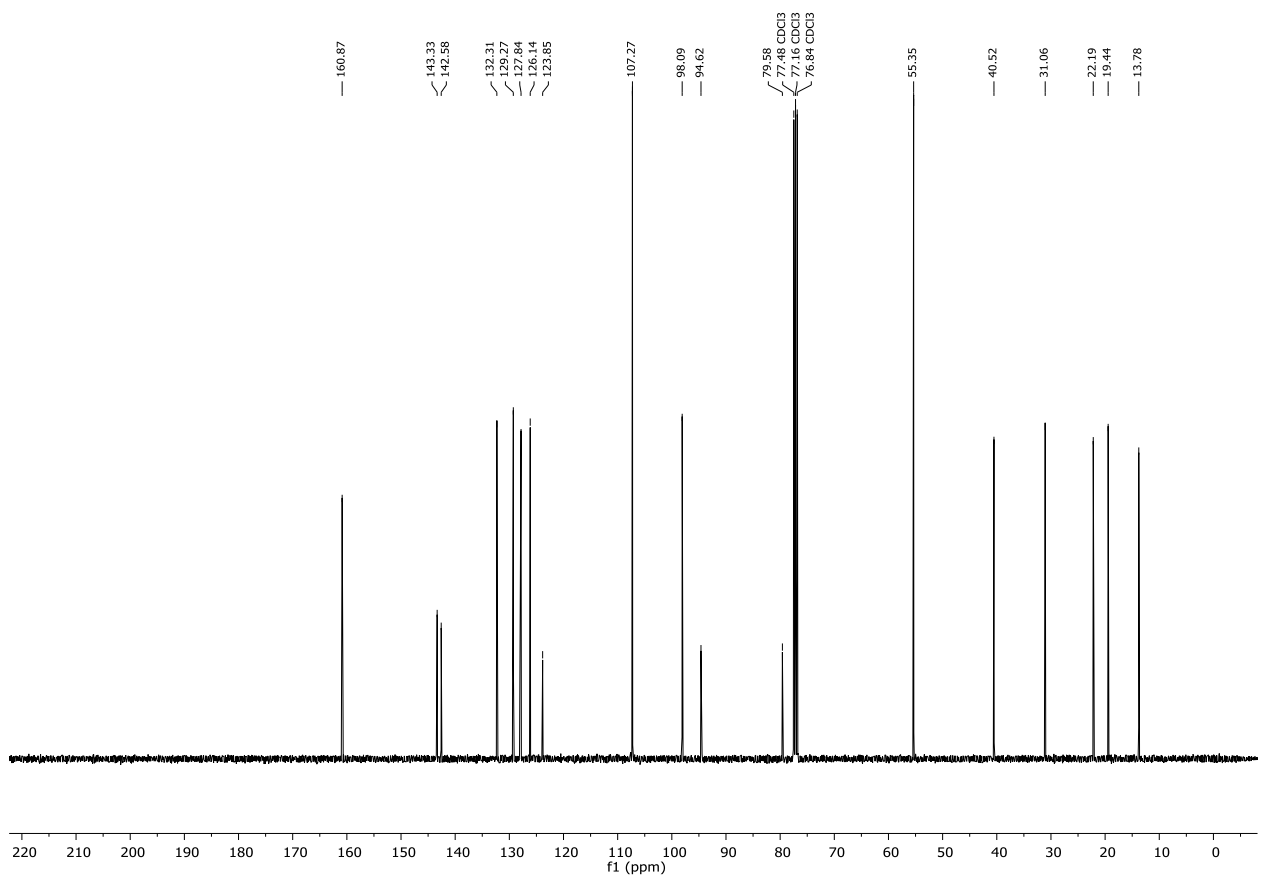


## 7. Appendix

### $^1\text{H-NMR}$ (300 MHz, $\text{CDCl}_3$ ) Compound **150b**



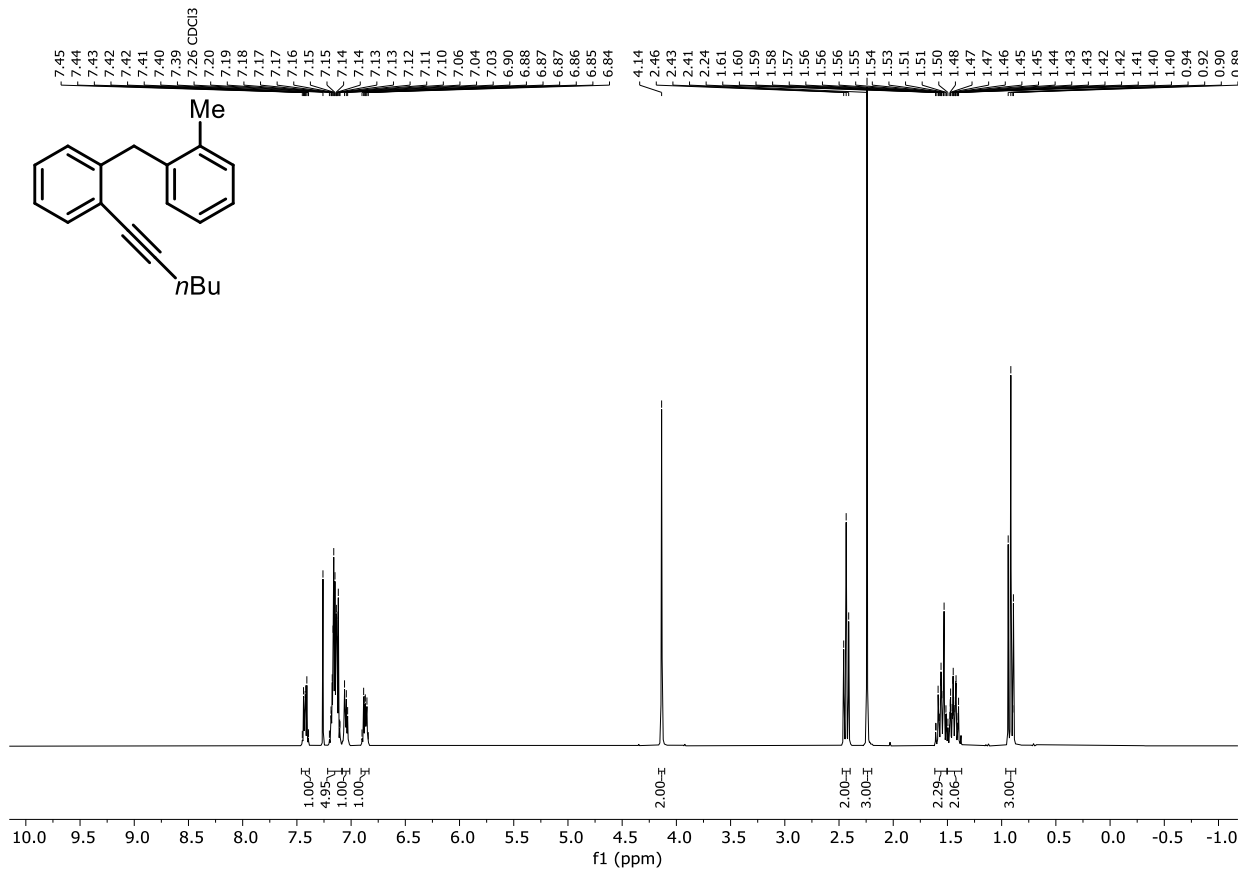
### $^{13}\text{C}\{^1\text{H}\}$ -NMR (101 MHz, $\text{CDCl}_3$ ) Compound **150b**



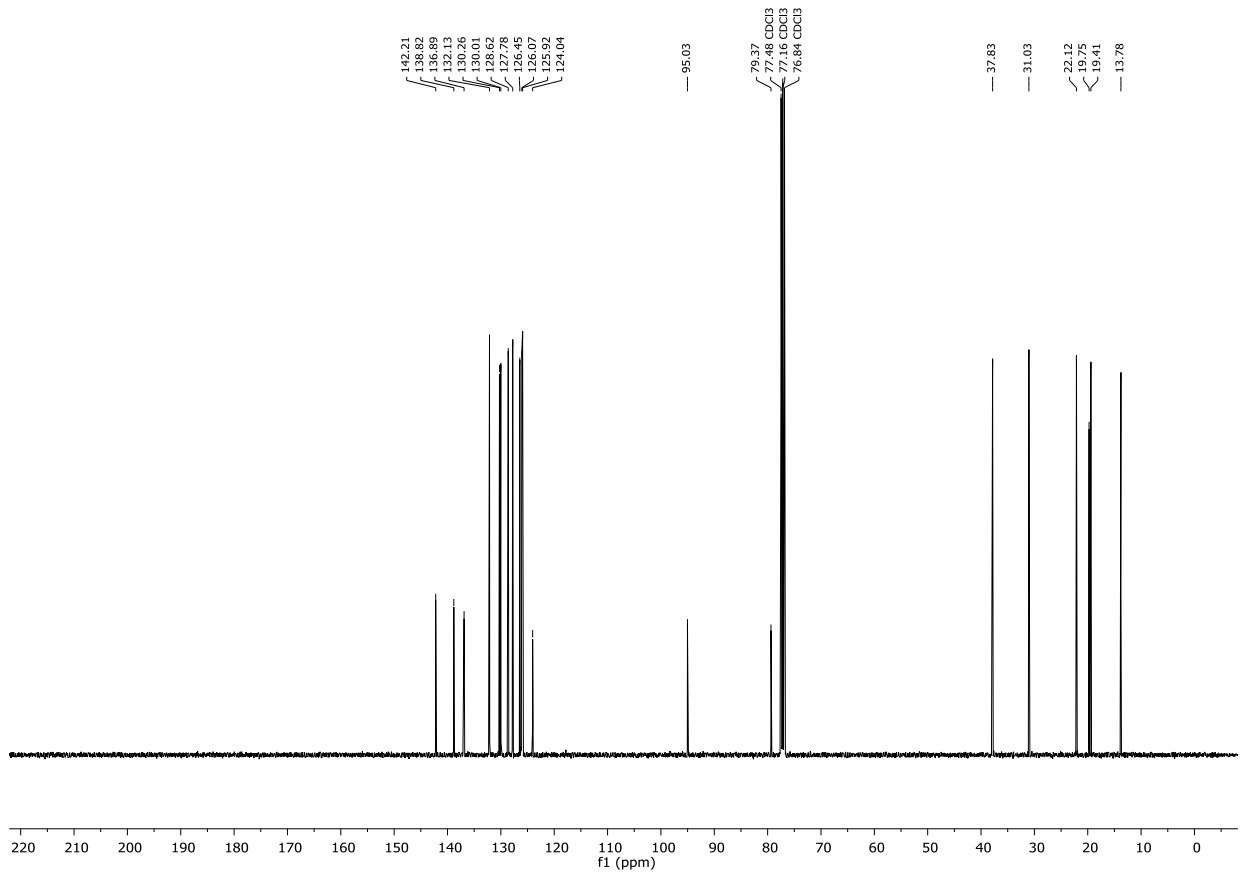


## 7.2 NMR spectra

### $^1\text{H-NMR}$ (300 MHz, $\text{CDCl}_3$ ) Compound **150c**

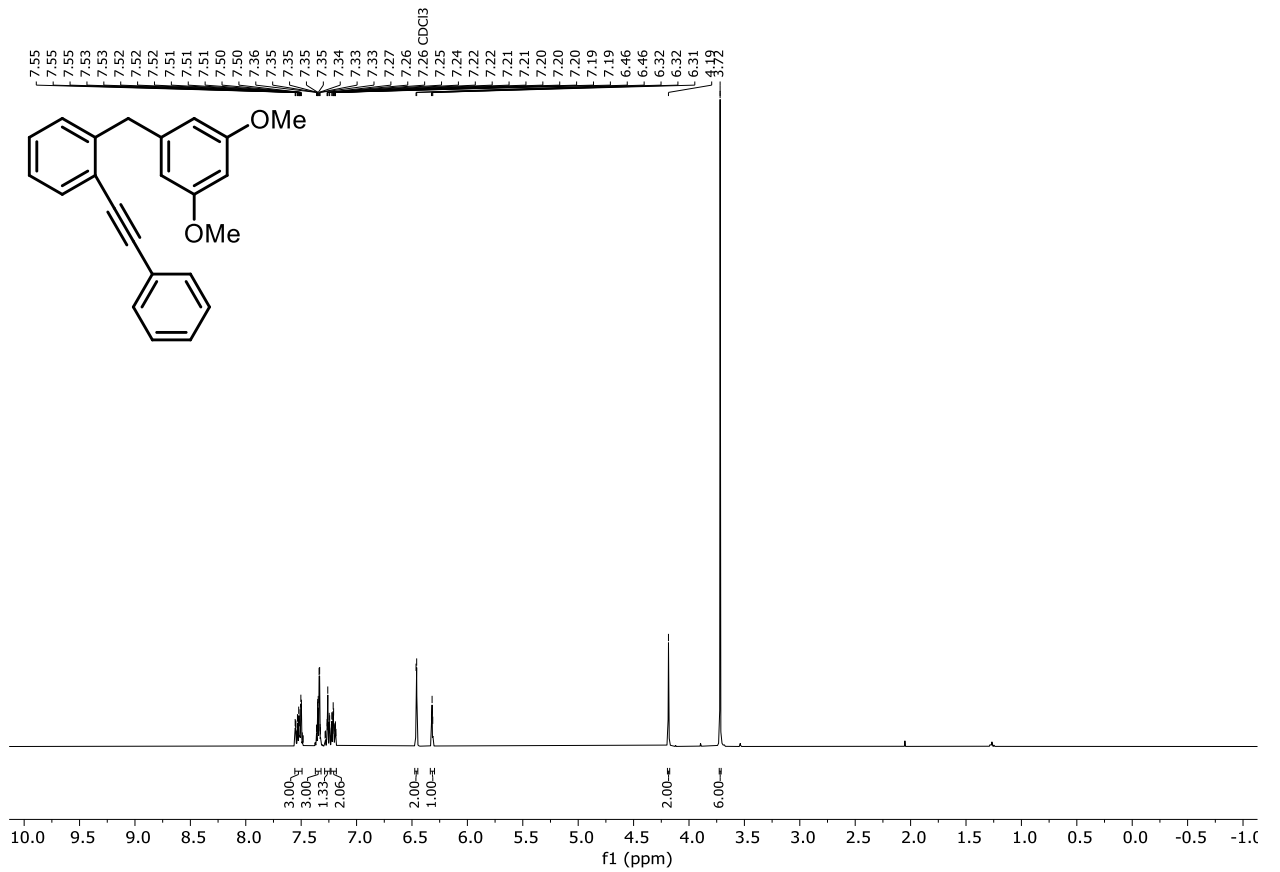


### $^{13}\text{C}\{^1\text{H}\}$ -NMR (101 MHz, $\text{CDCl}_3$ ) Compound **150c**

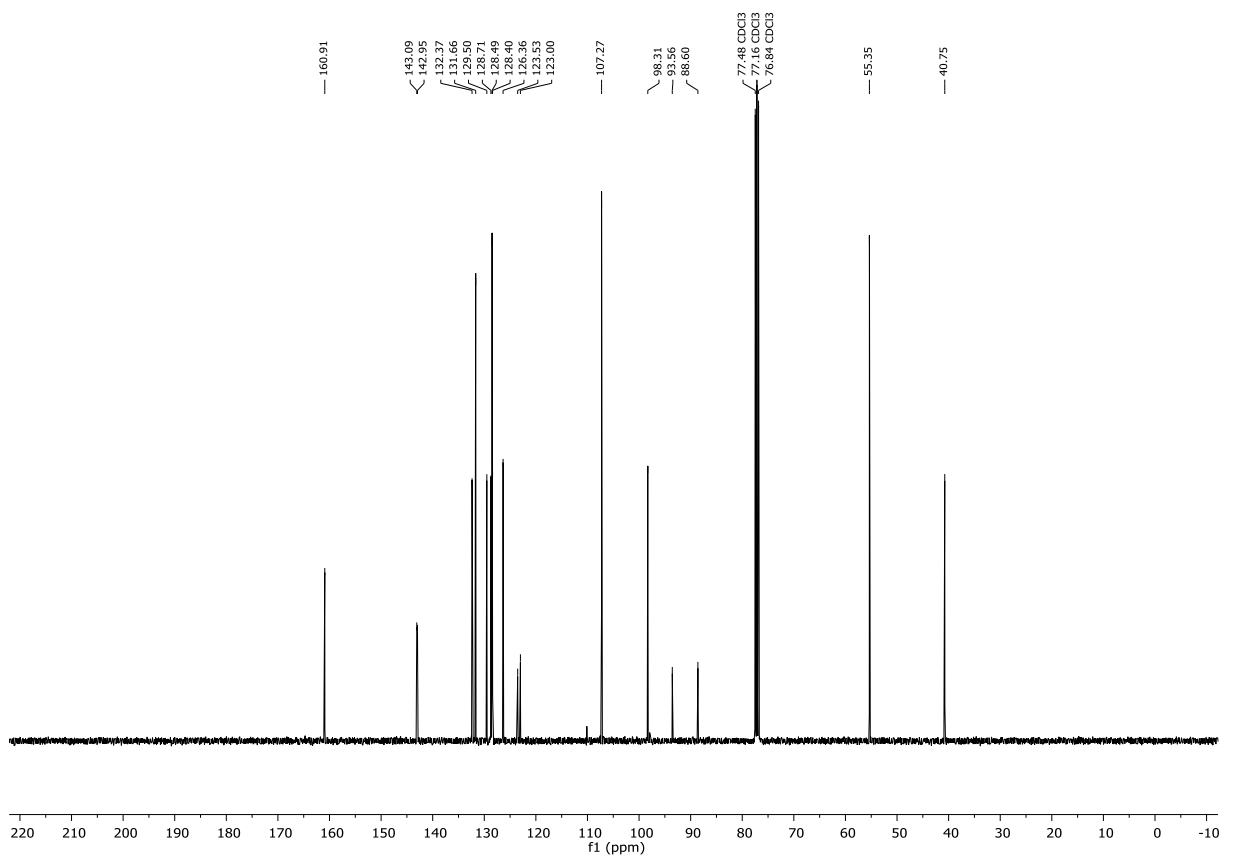


## 7. Appendix

### $^1\text{H-NMR}$ (300 MHz, $\text{CDCl}_3$ ) Compound **150d**

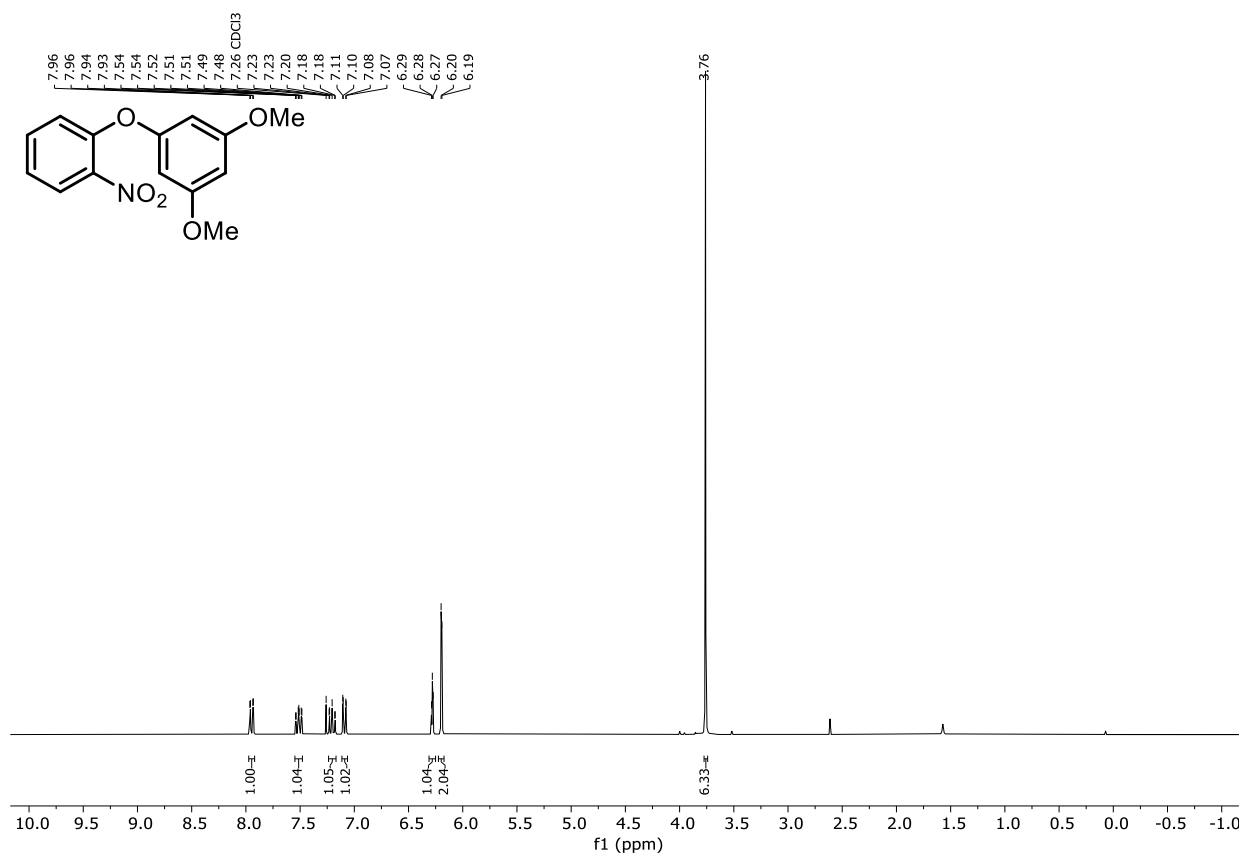


### $^{13}\text{C}\{^1\text{H}\}$ -NMR (101 MHz, $\text{CDCl}_3$ ) Compound **150d**

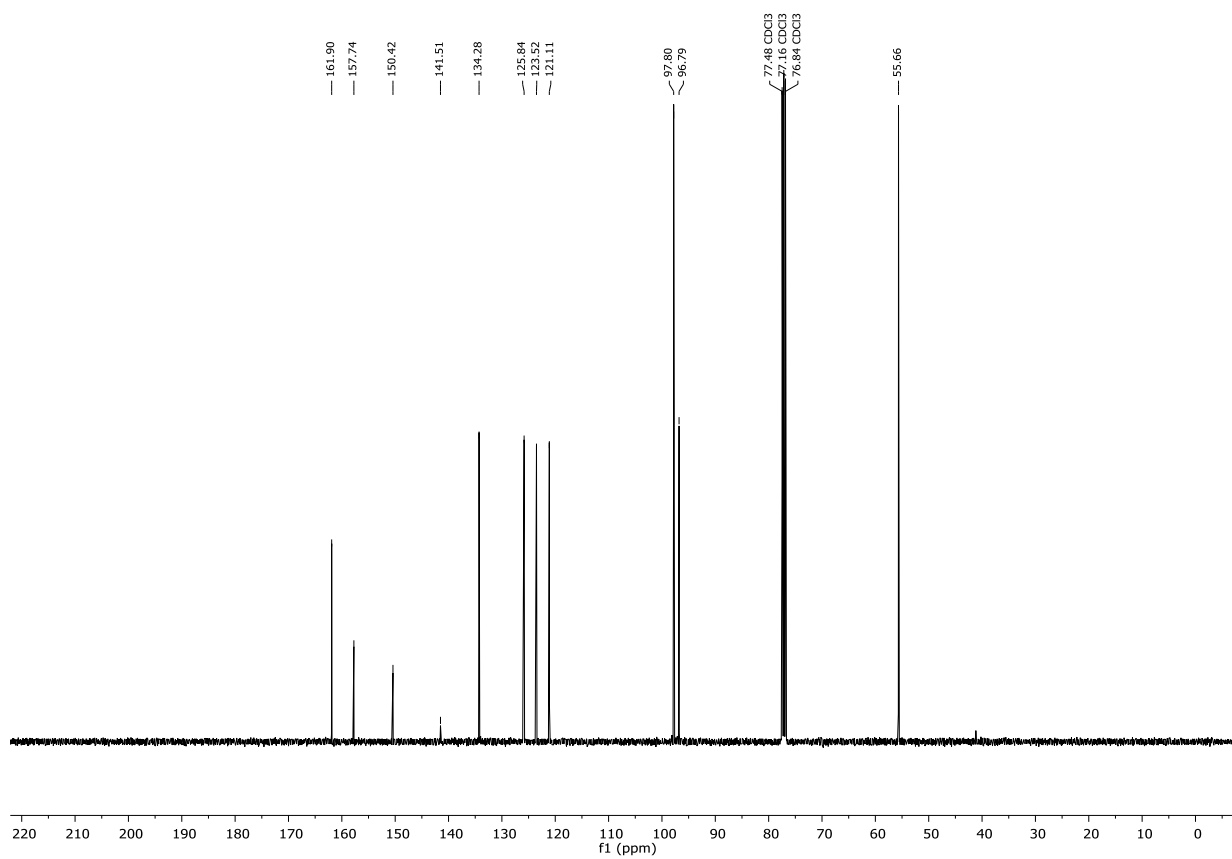


## 7.2 NMR spectra

### <sup>1</sup>H-NMR (300 MHz, CDCl<sub>3</sub>) Compound **171a**

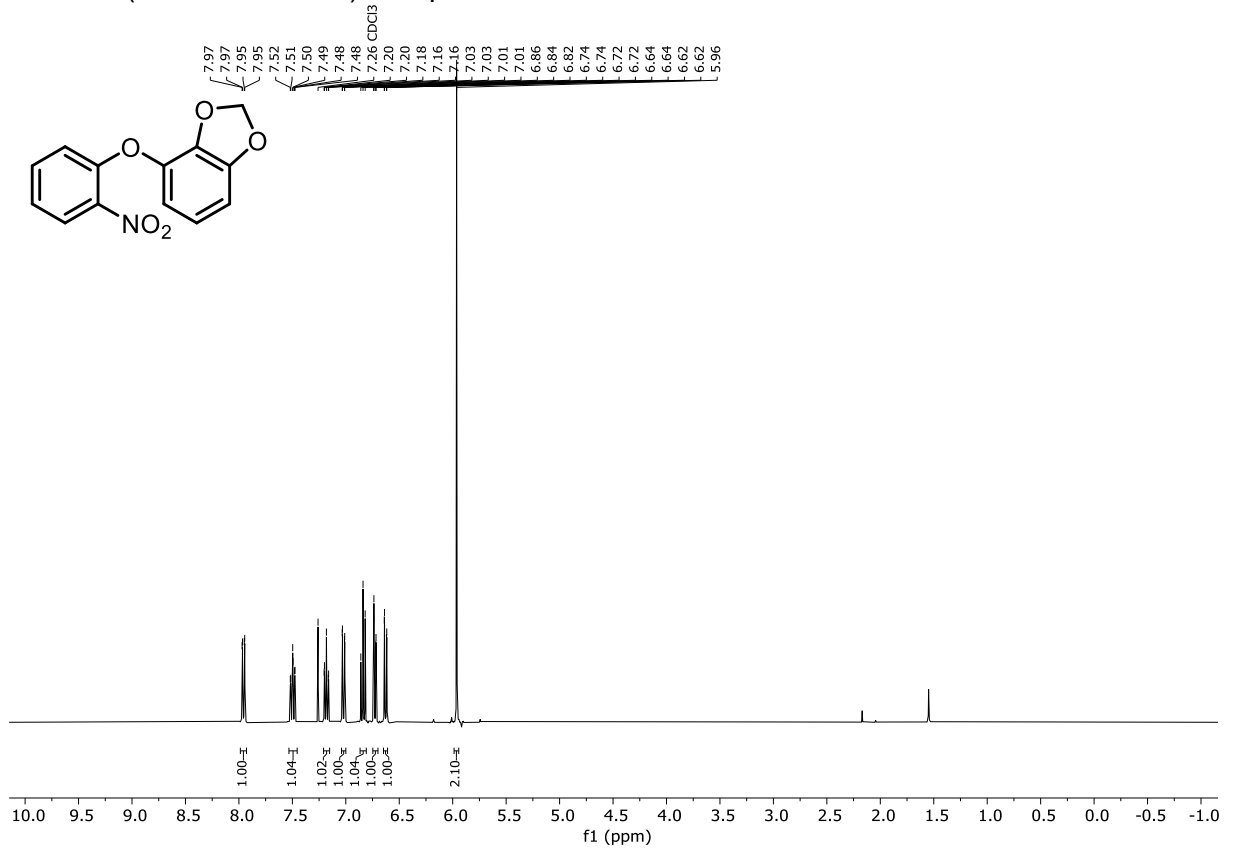


### <sup>13</sup>C{<sup>1</sup>H}-NMR (101 MHz, CDCl<sub>3</sub>) Compound **171a**

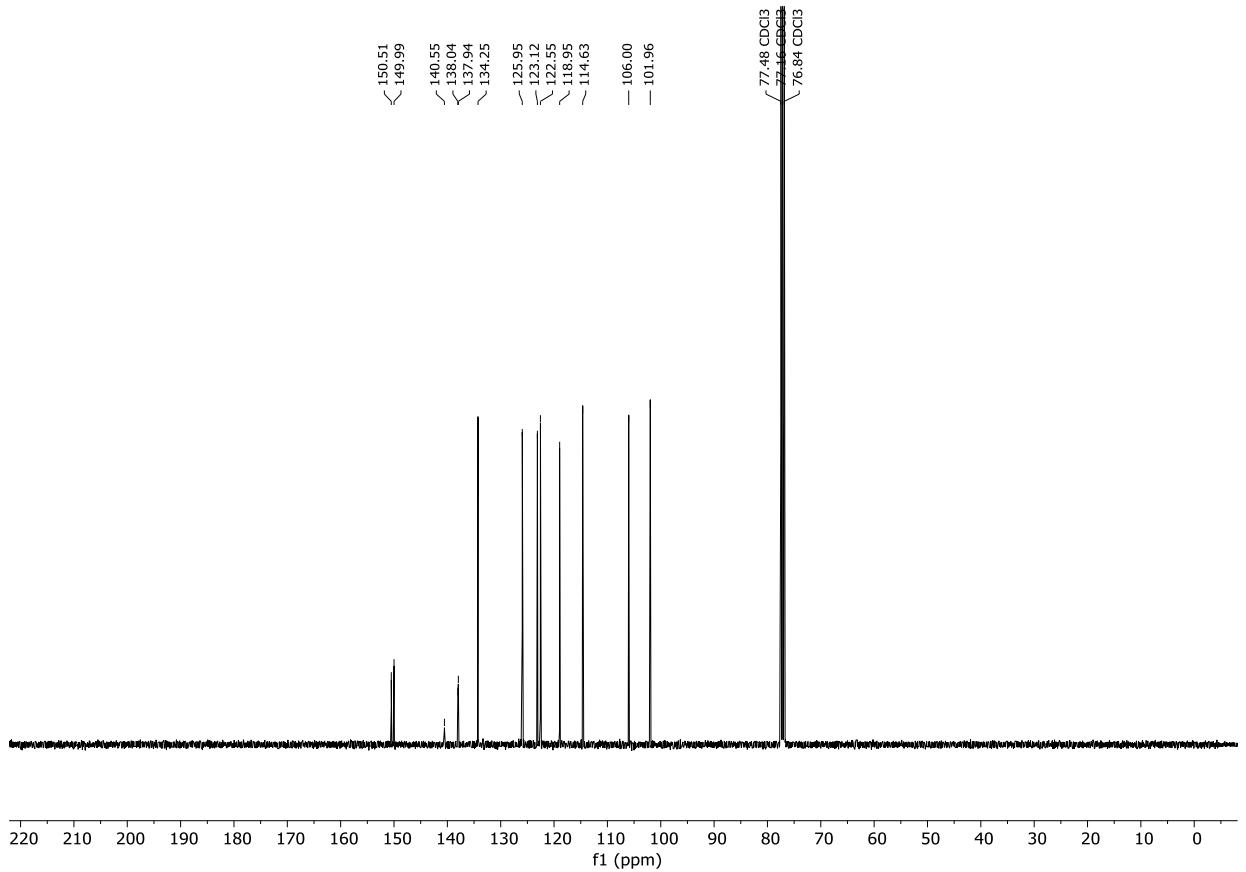


## 7. Appendix

### <sup>1</sup>H-NMR (300 MHz, CDCl<sub>3</sub>) Compound **171b**

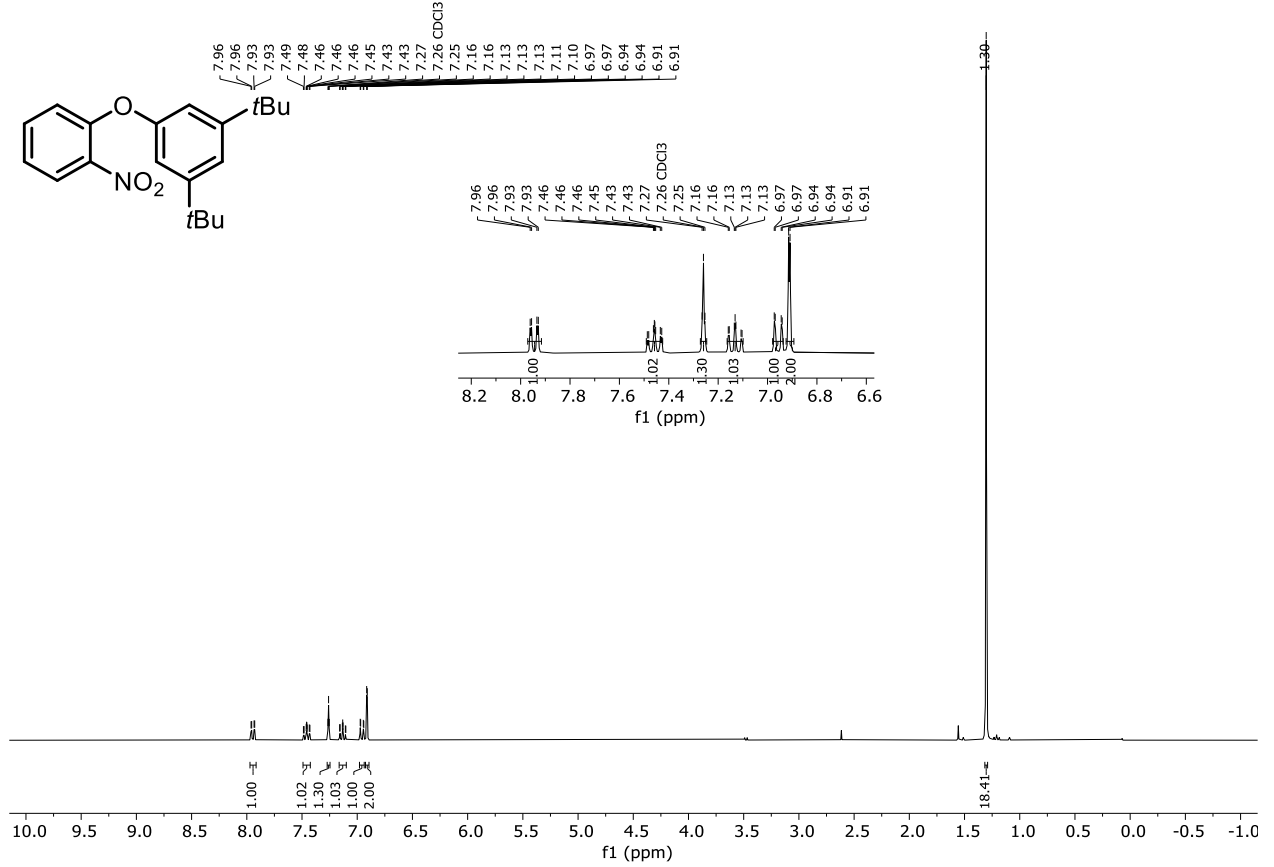


### <sup>13</sup>C{<sup>1</sup>H}-NMR (101 MHz, CDCl<sub>3</sub>) Compound **171b**

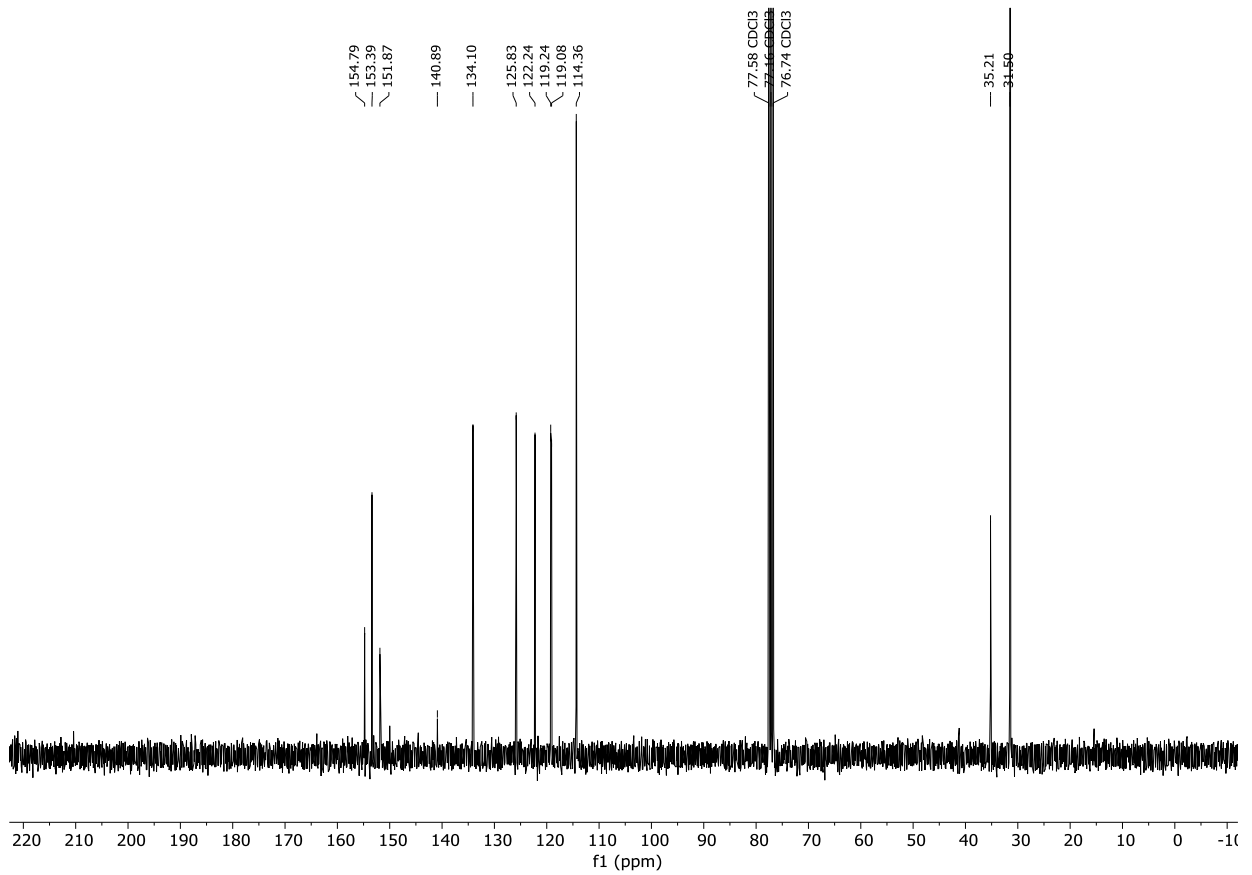


## 7.2 NMR spectra

### $^1\text{H-NMR}$ (300 MHz, $\text{CDCl}_3$ ) Compound **171c**

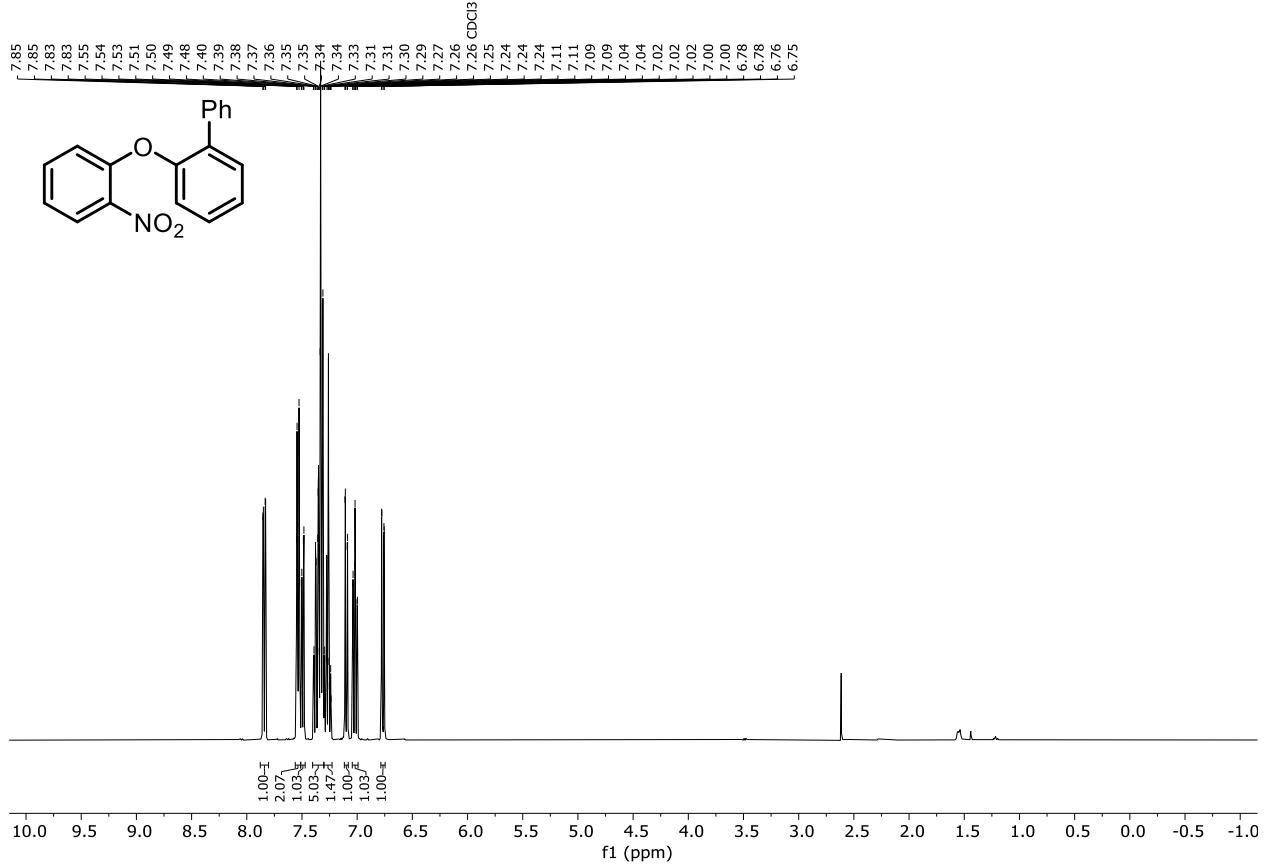


### $^{13}\text{C}\{^1\text{H}\}$ -NMR (101 MHz, $\text{CDCl}_3$ ) Compound **171c**

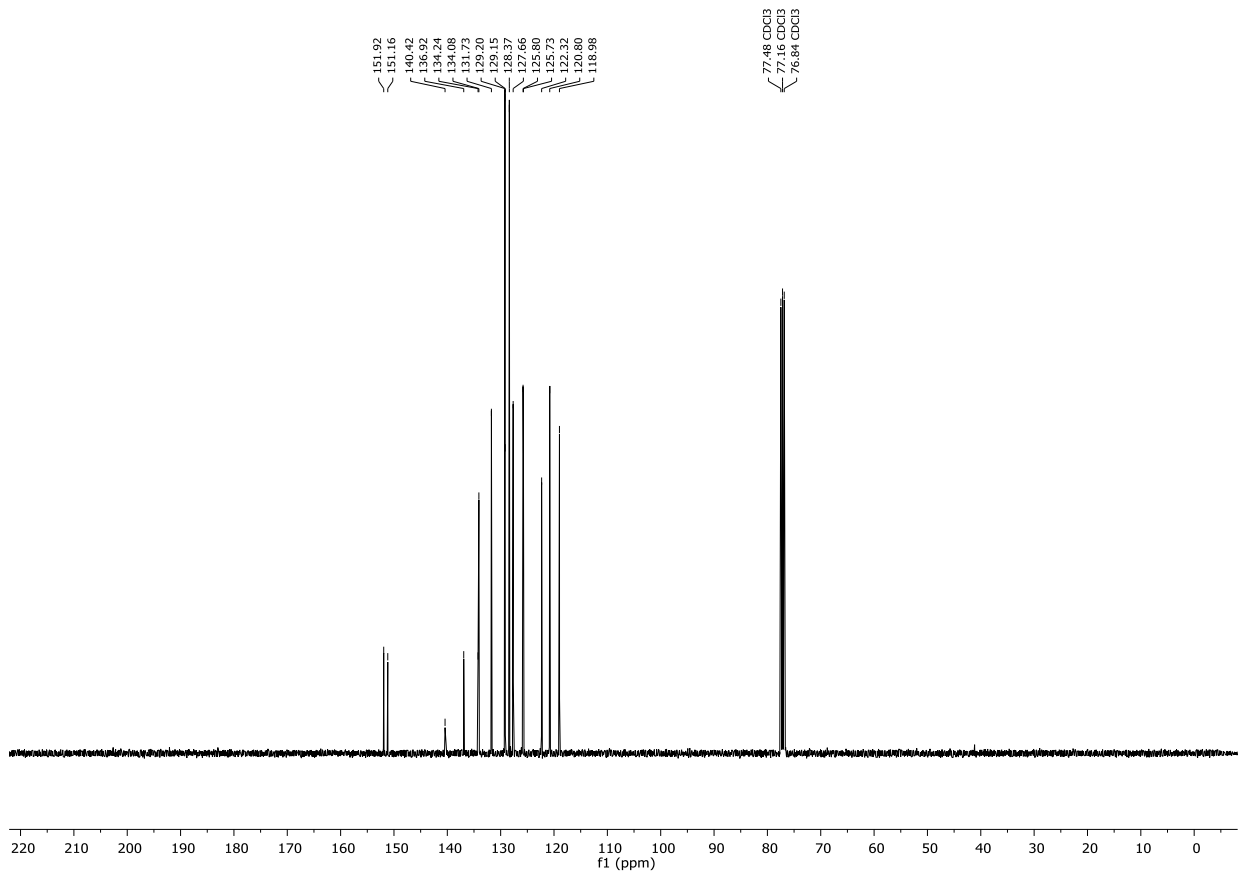


## 7. Appendix

### $^1\text{H-NMR}$ (300 MHz, $\text{CDCl}_3$ ) Compound **171d**



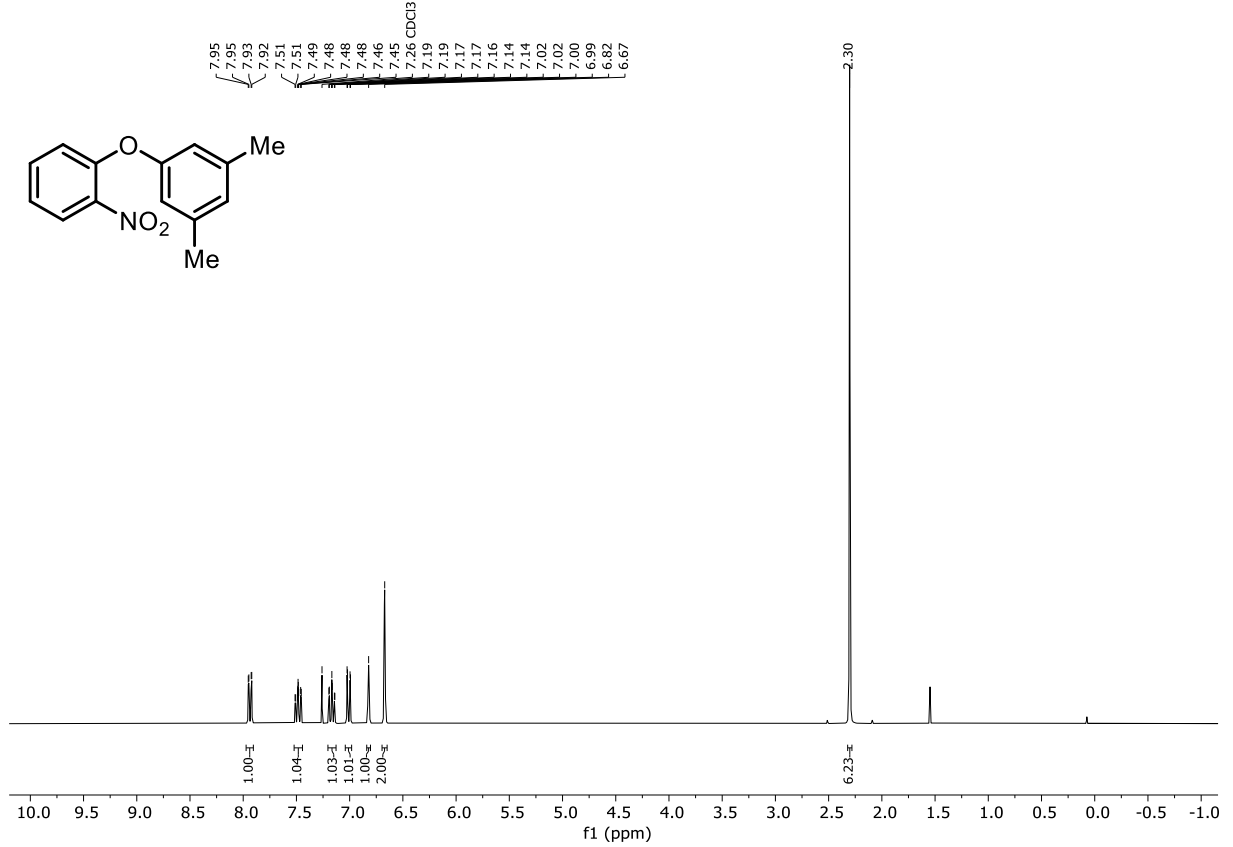
### $^{13}\text{C}\{^1\text{H}\}$ -NMR (101 MHz, $\text{CDCl}_3$ ) Compound **171d**



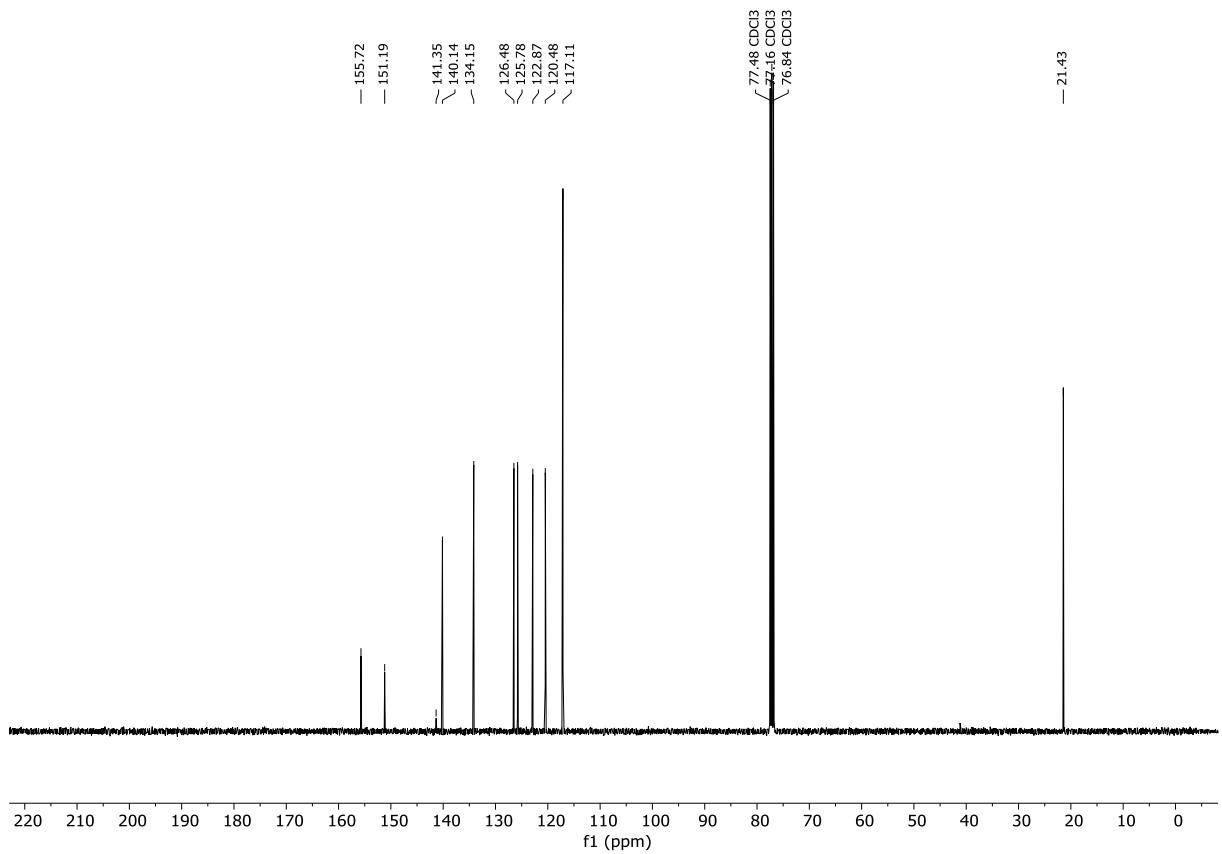


## 7. Appendix

### $^1\text{H-NMR}$ (300 MHz, $\text{CDCl}_3$ ) Compound **171f**



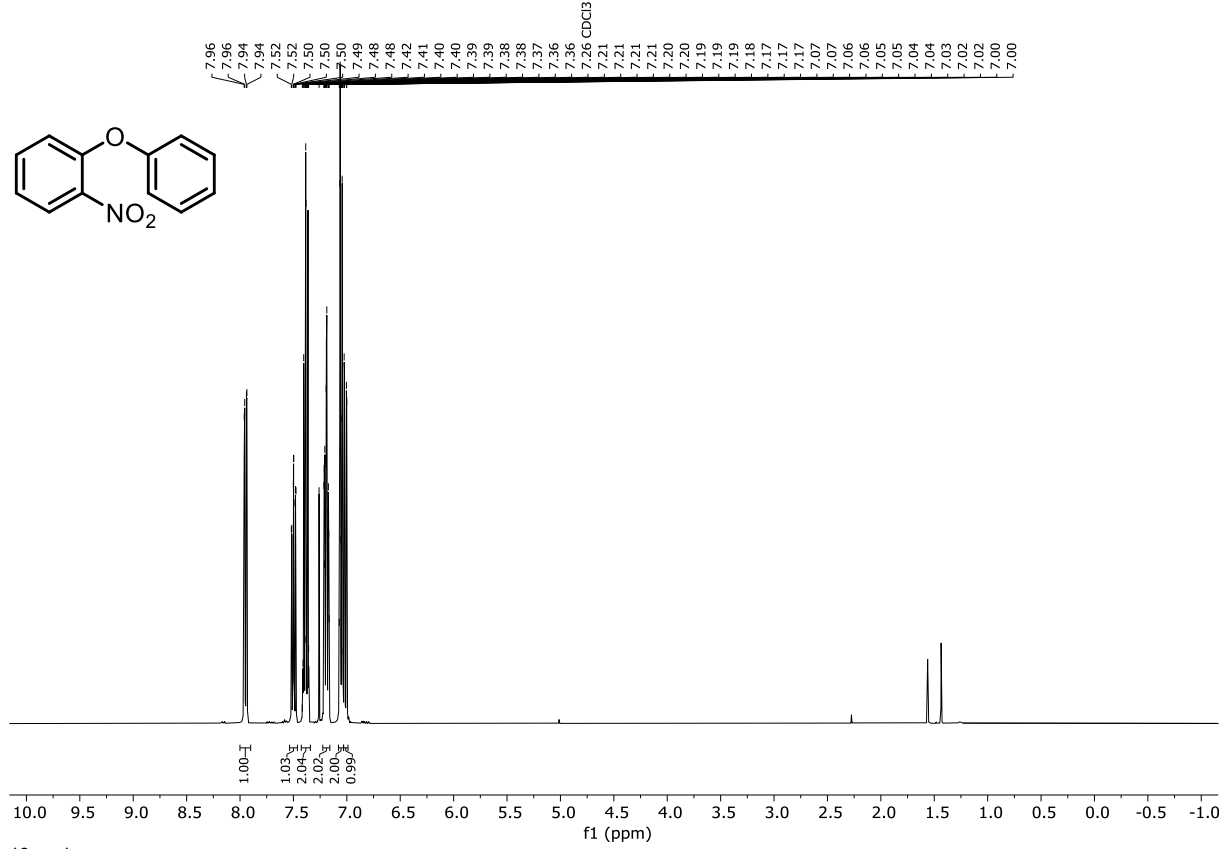
### $^{13}\text{C}\{^1\text{H}\}$ -NMR (101 MHz, $\text{CDCl}_3$ ) Compound **171f**



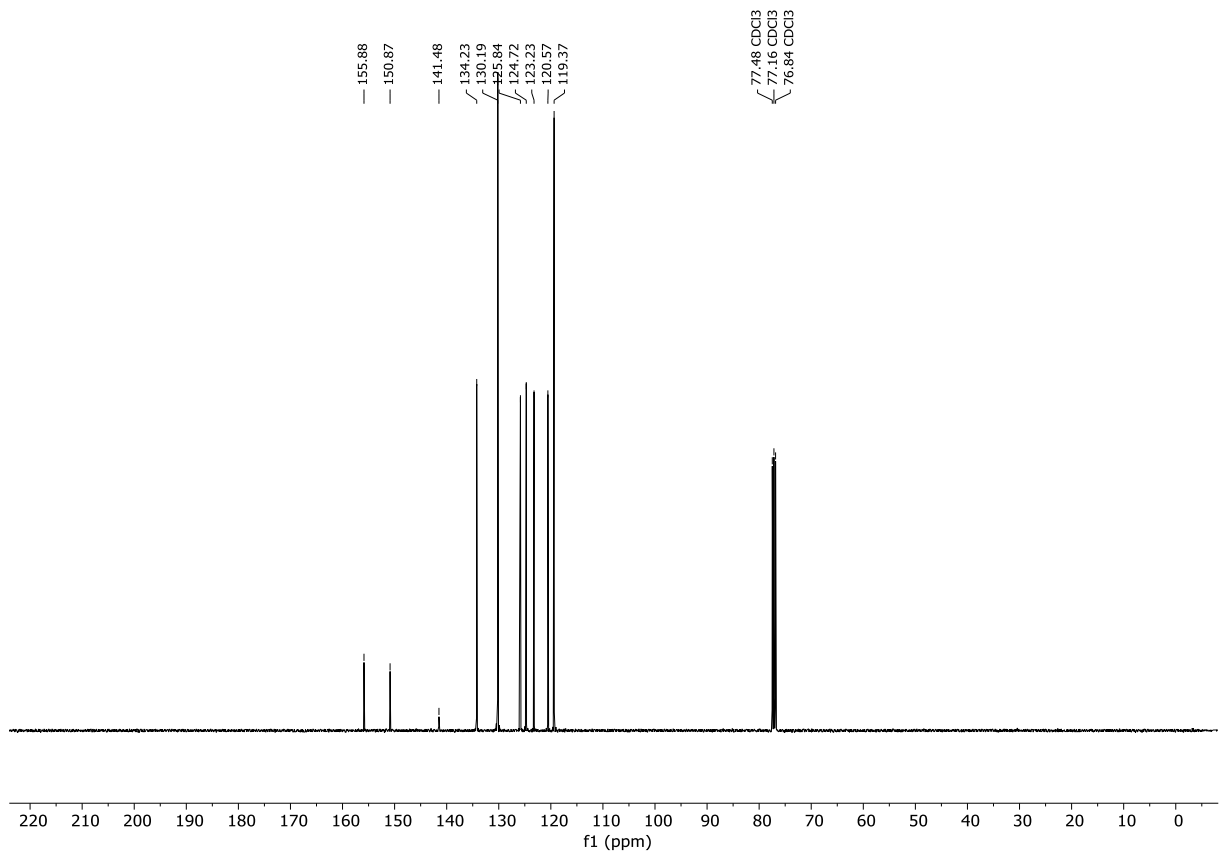


## 7.2 NMR spectra

### $^1\text{H-NMR}$ (400 MHz, $\text{CDCl}_3$ ) Compound **171g**

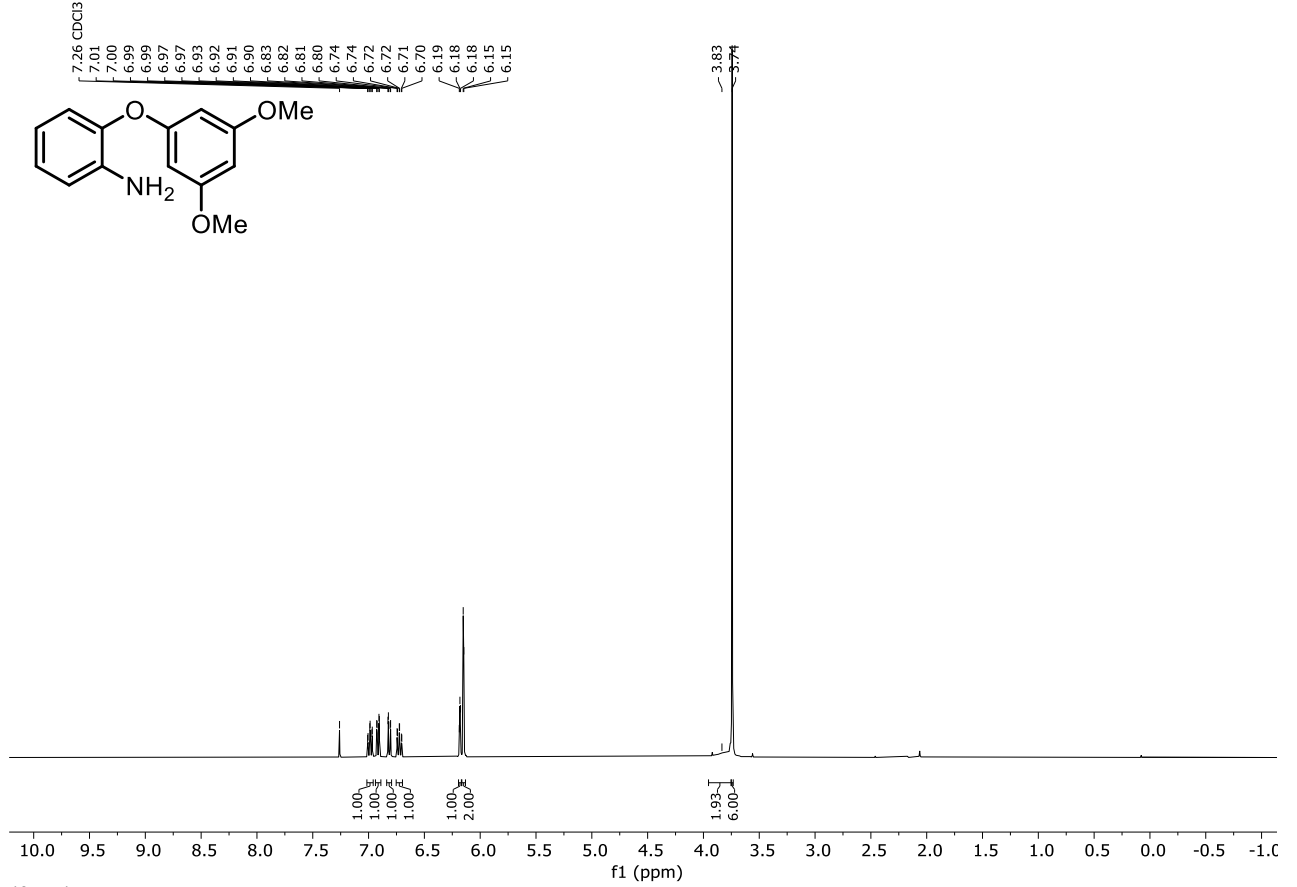


### $^{13}\text{C}\{^1\text{H}\}$ -NMR (101 MHz, $\text{CDCl}_3$ ) Compound **171g**

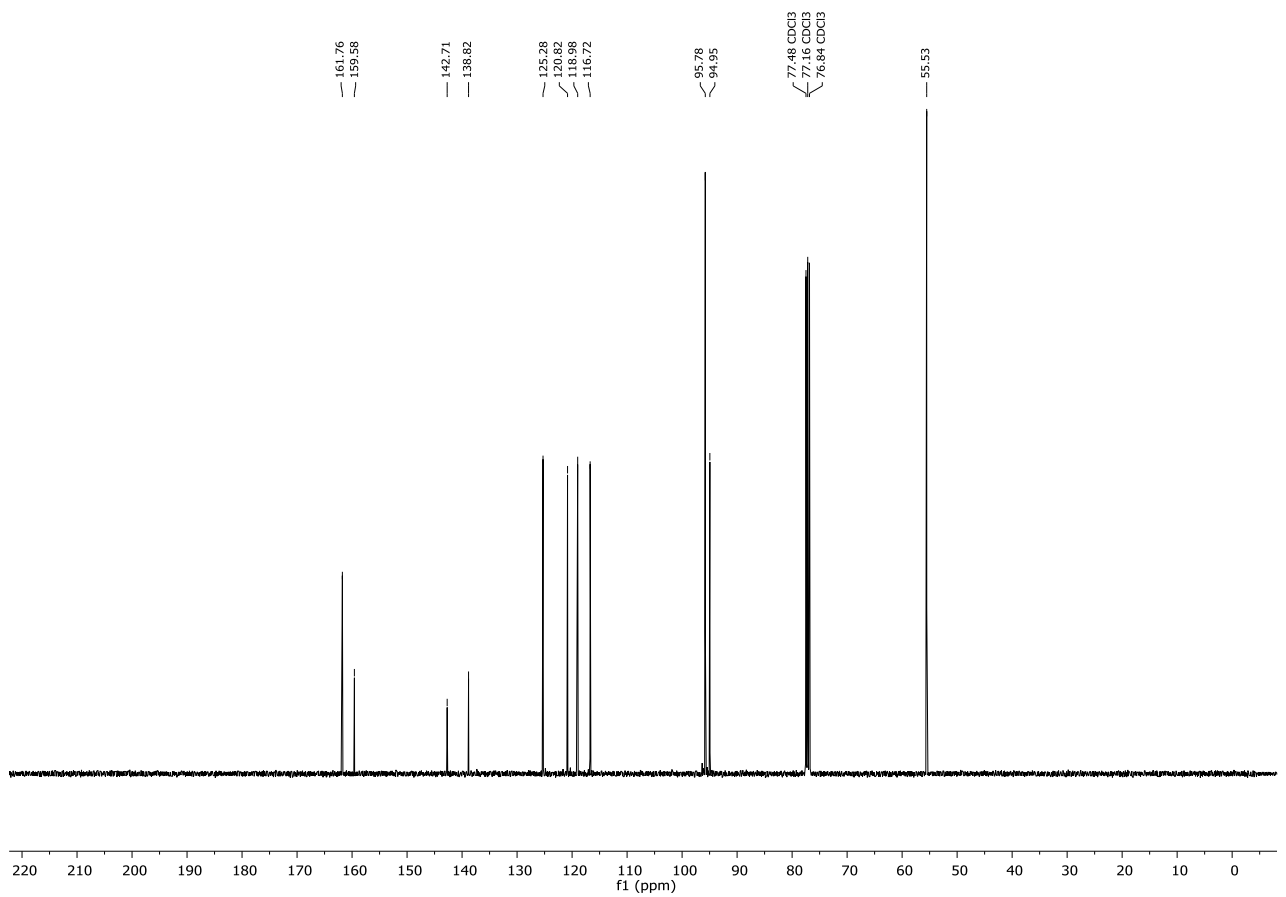


## 7. Appendix

### $^1\text{H-NMR}$ (400 MHz, $\text{CDCl}_3$ ) Compound **172a**

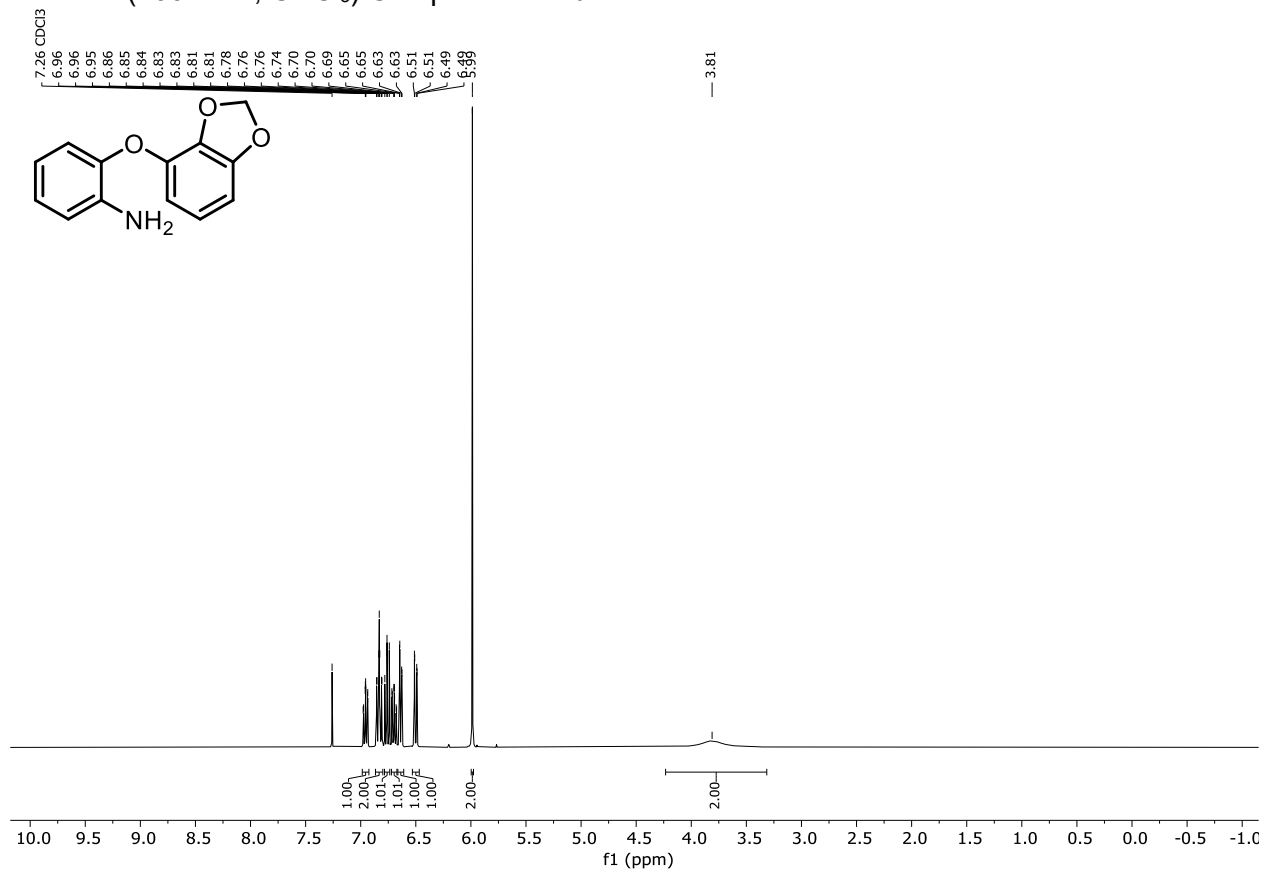


### $^{13}\text{C}\{^1\text{H}\}$ -NMR (101 MHz, $\text{CDCl}_3$ ) Compound **172a**

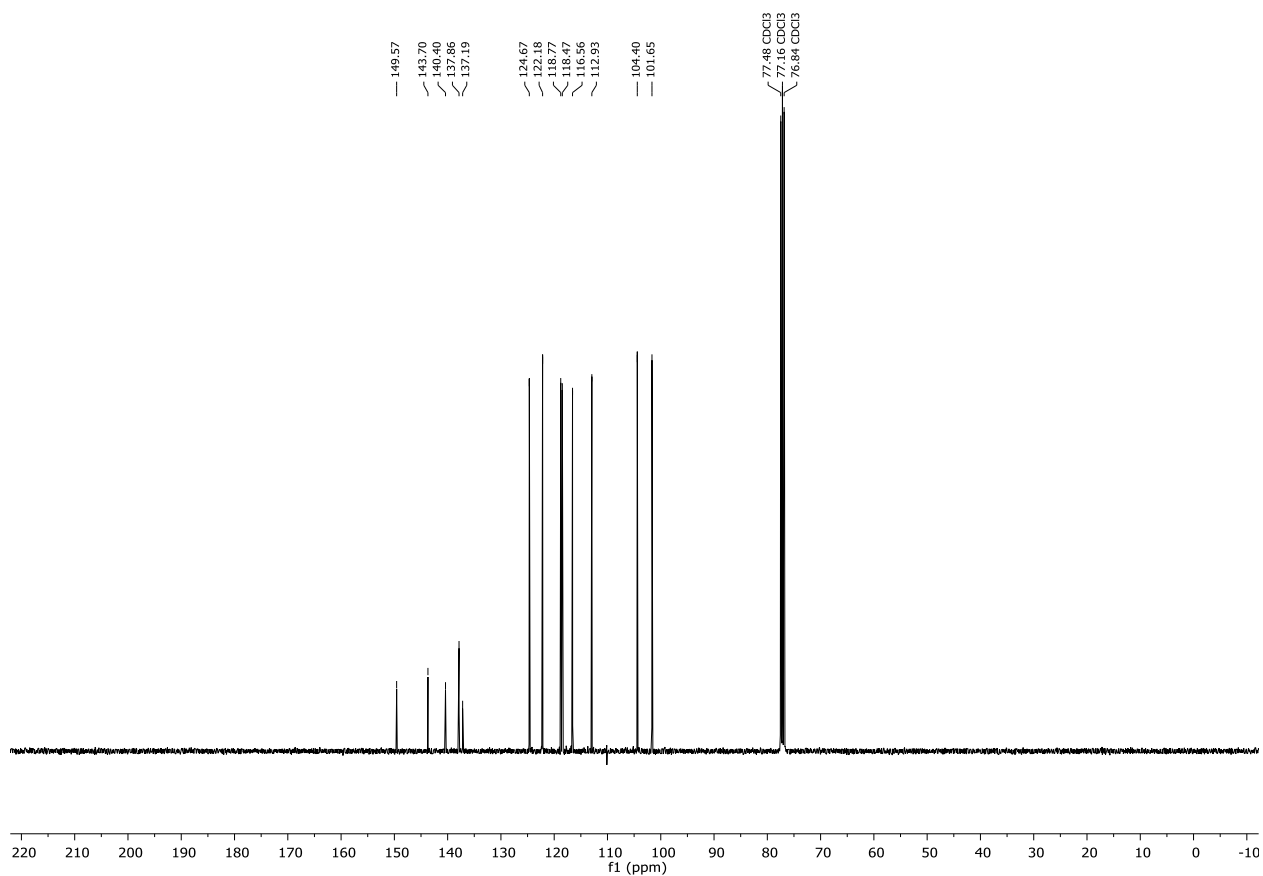


## 7.2 NMR spectra

$^1\text{H-NMR}$  (400 MHz,  $\text{CDCl}_3$ ) Compound **172b**

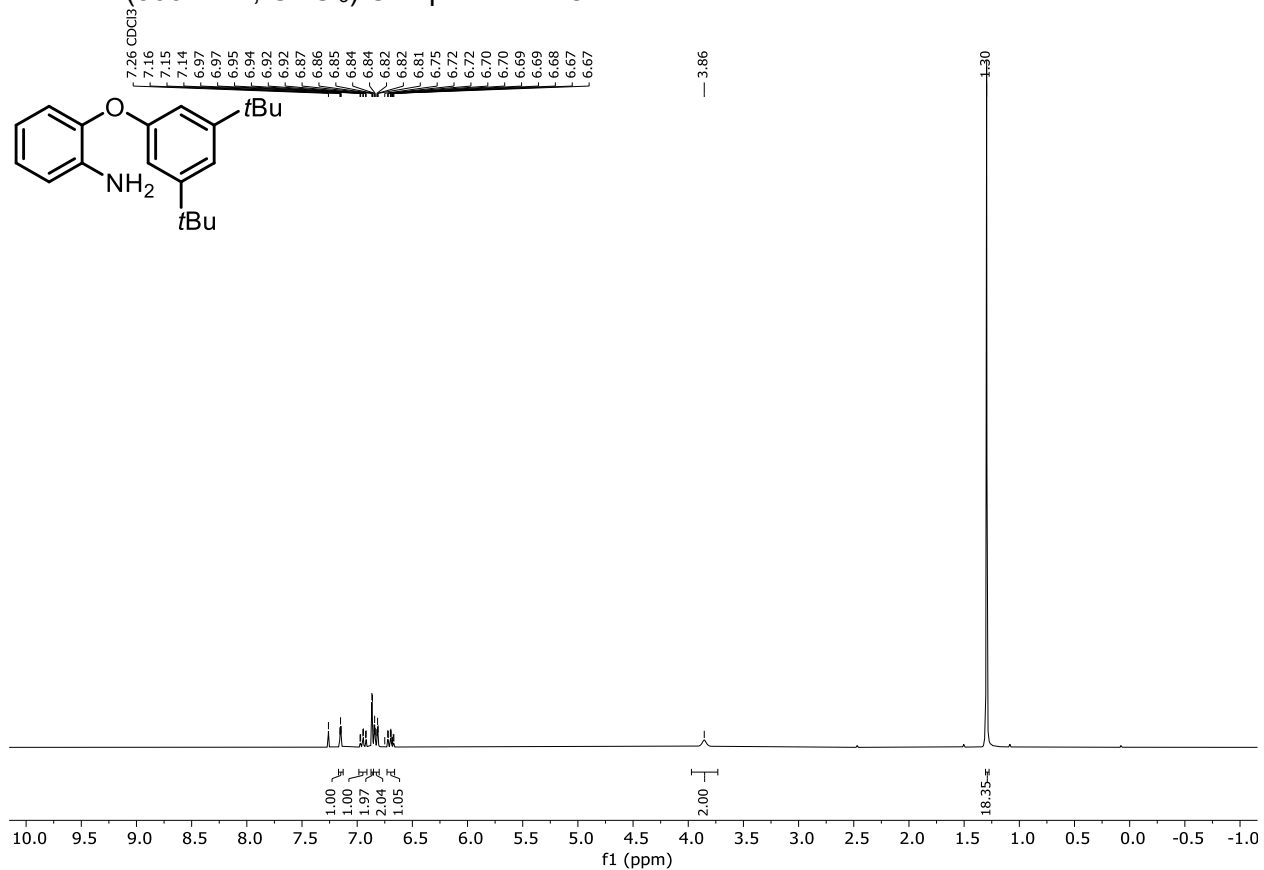


$^{13}\text{C}\{^1\text{H}\}$ -NMR (101 MHz,  $\text{CDCl}_3$ ) Compound **172b**

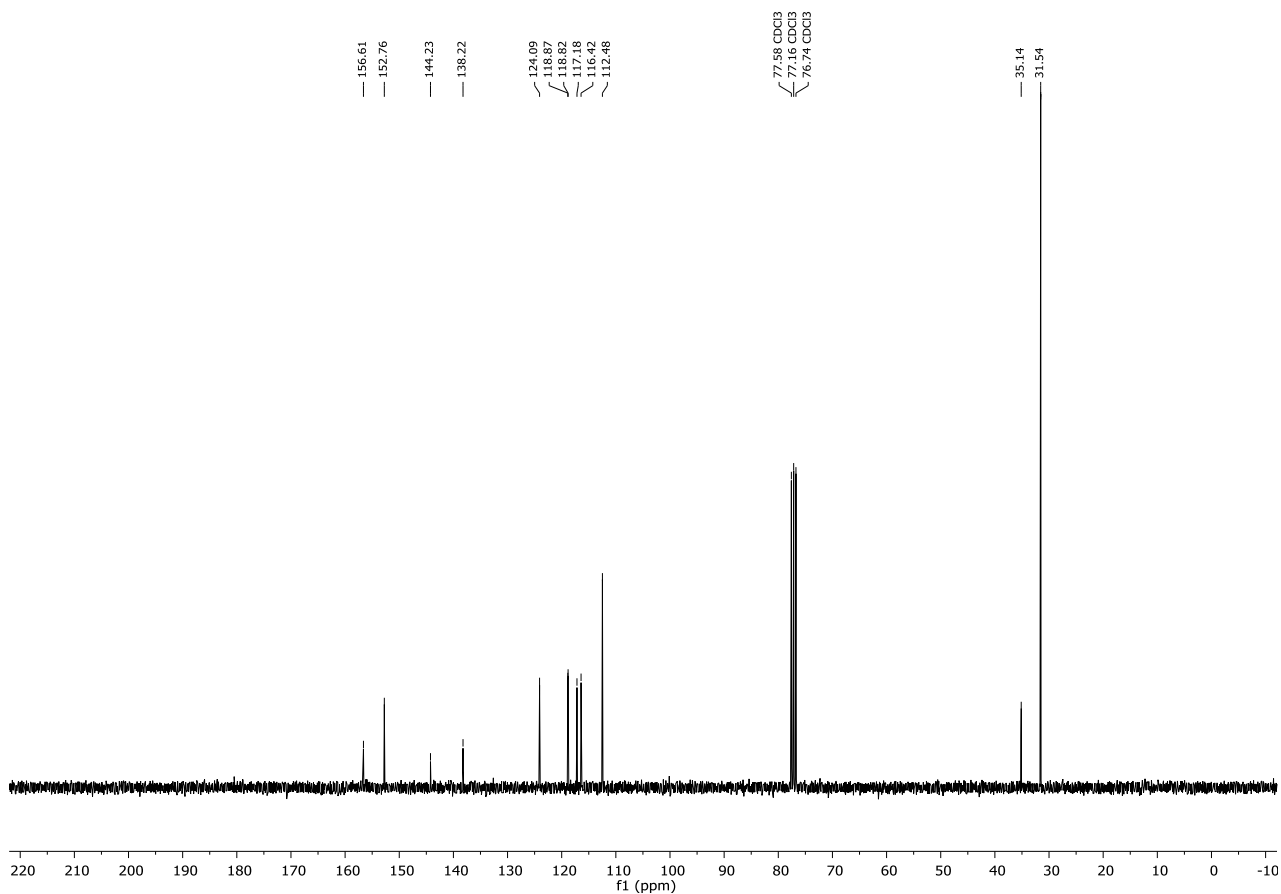


## 7. Appendix

### $^1\text{H-NMR}$ (300 MHz, $\text{CDCl}_3$ ) Compound **172c**

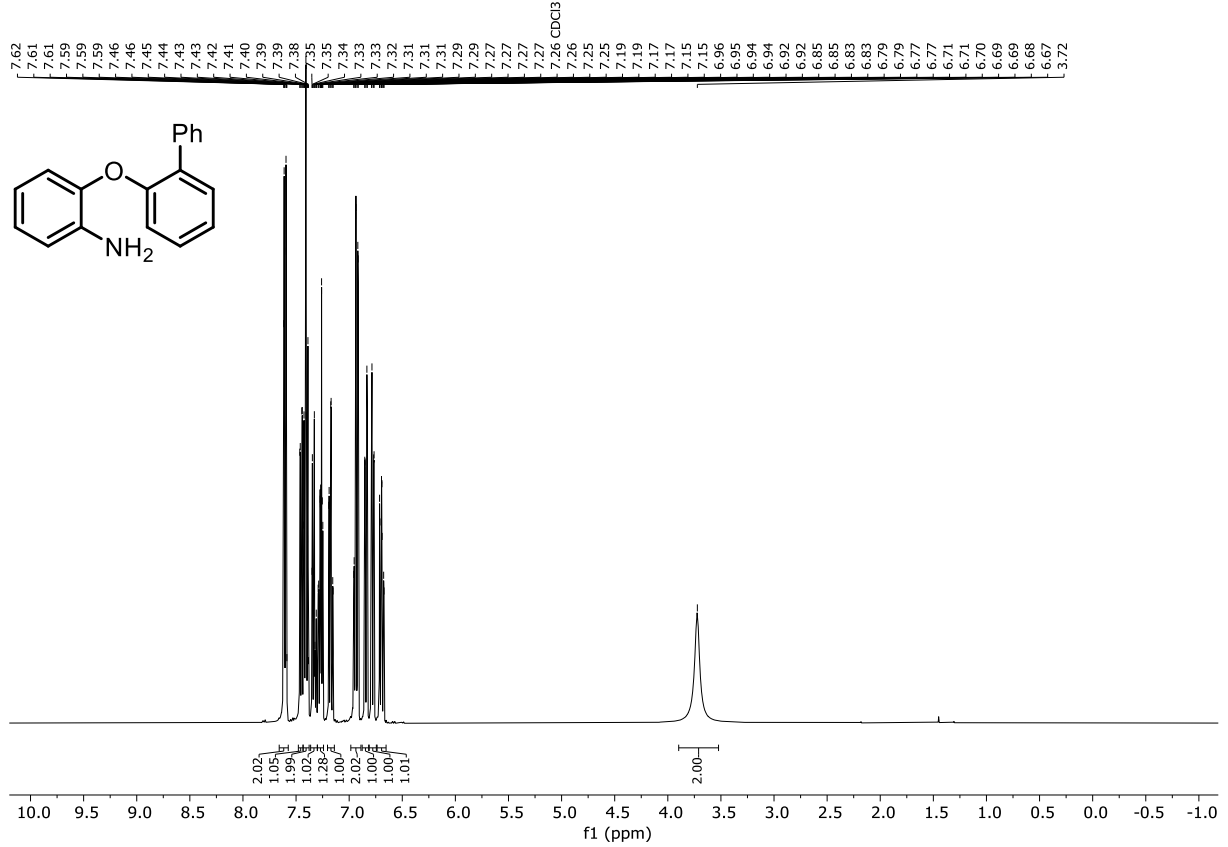


### $^{13}\text{C}\{^1\text{H}\}$ -NMR (75 MHz, $\text{CDCl}_3$ ) Compound **172c**

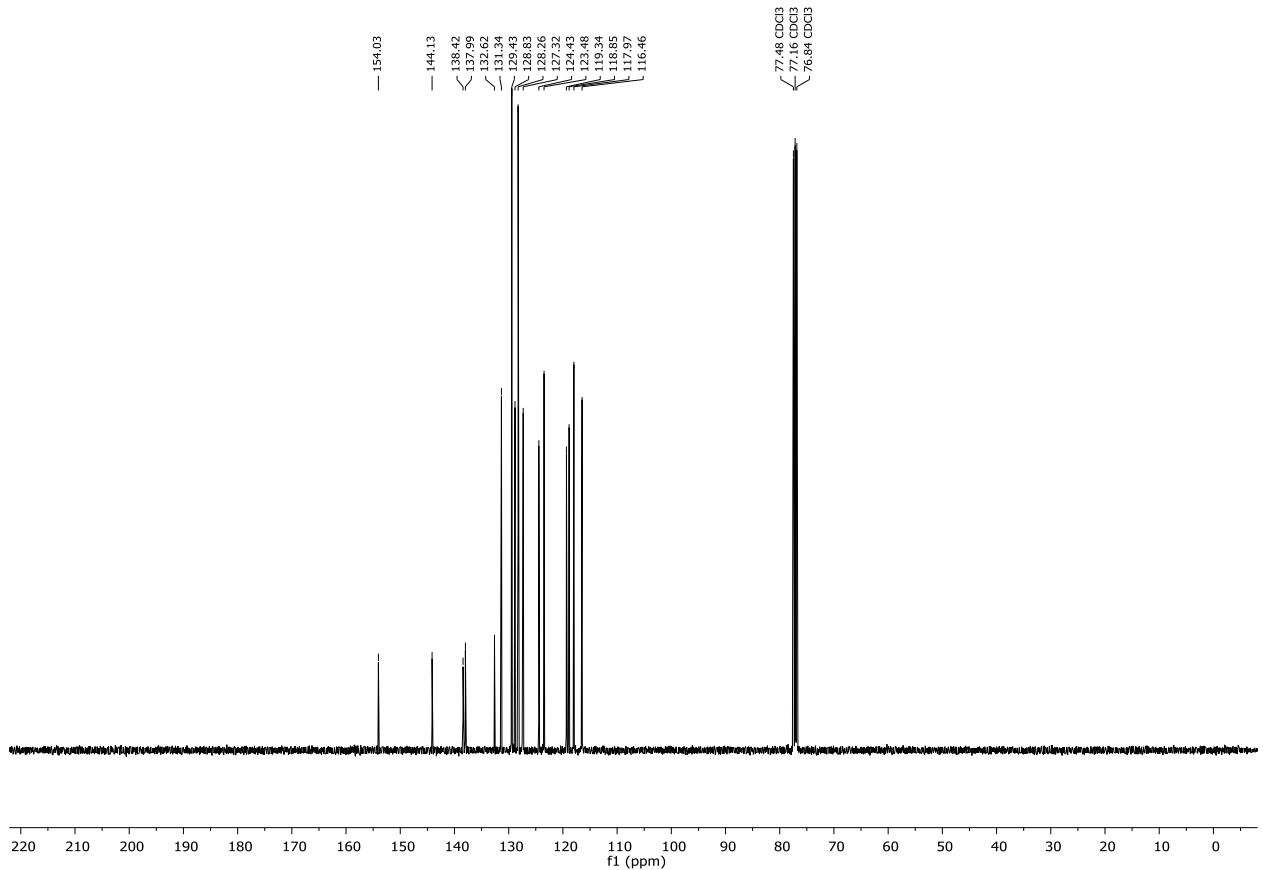


## 7.2 NMR spectra

### <sup>1</sup>H-NMR (400 MHz, CDCl<sub>3</sub>) Compound **172d**

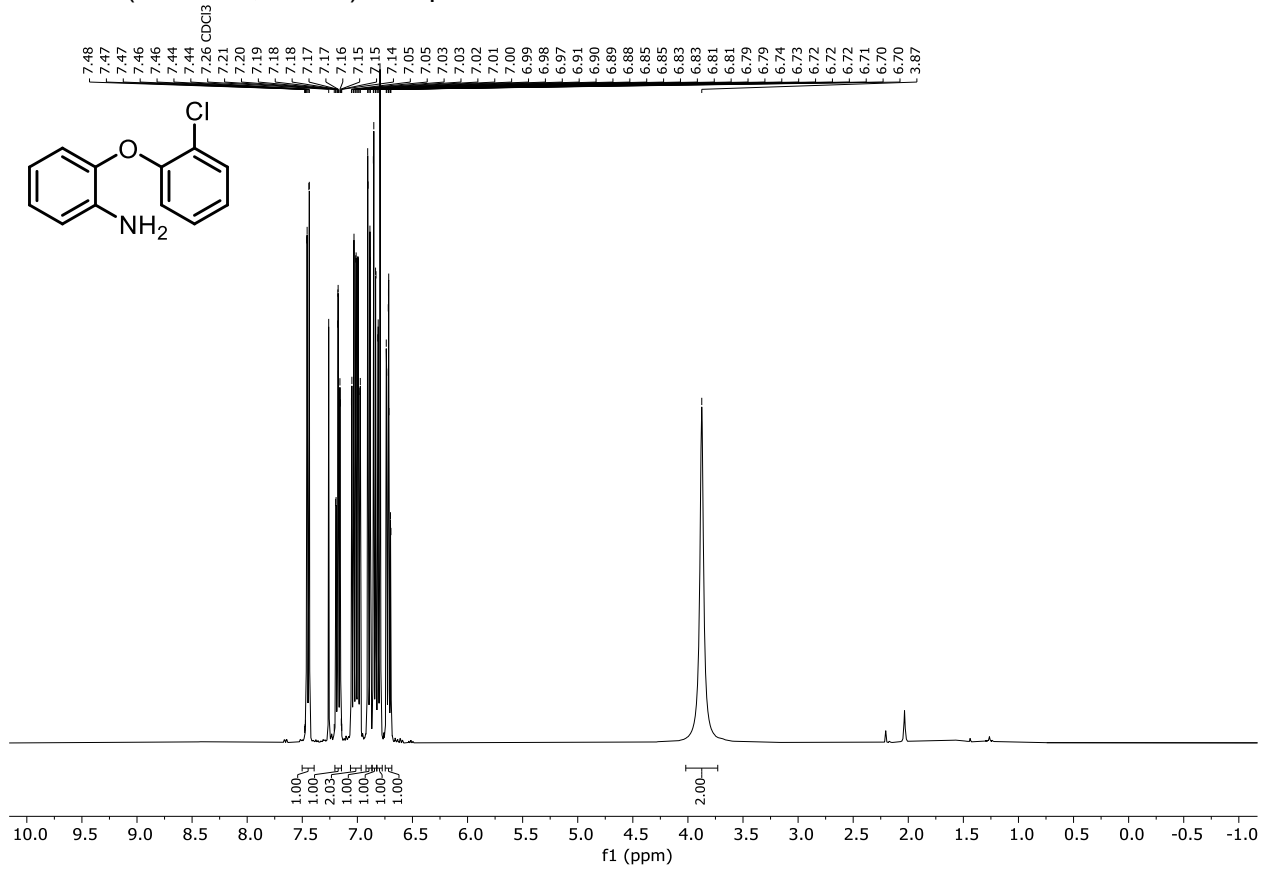


### <sup>13</sup>C{<sup>1</sup>H}-NMR (101 MHz, CDCl<sub>3</sub>) Compound **172d**

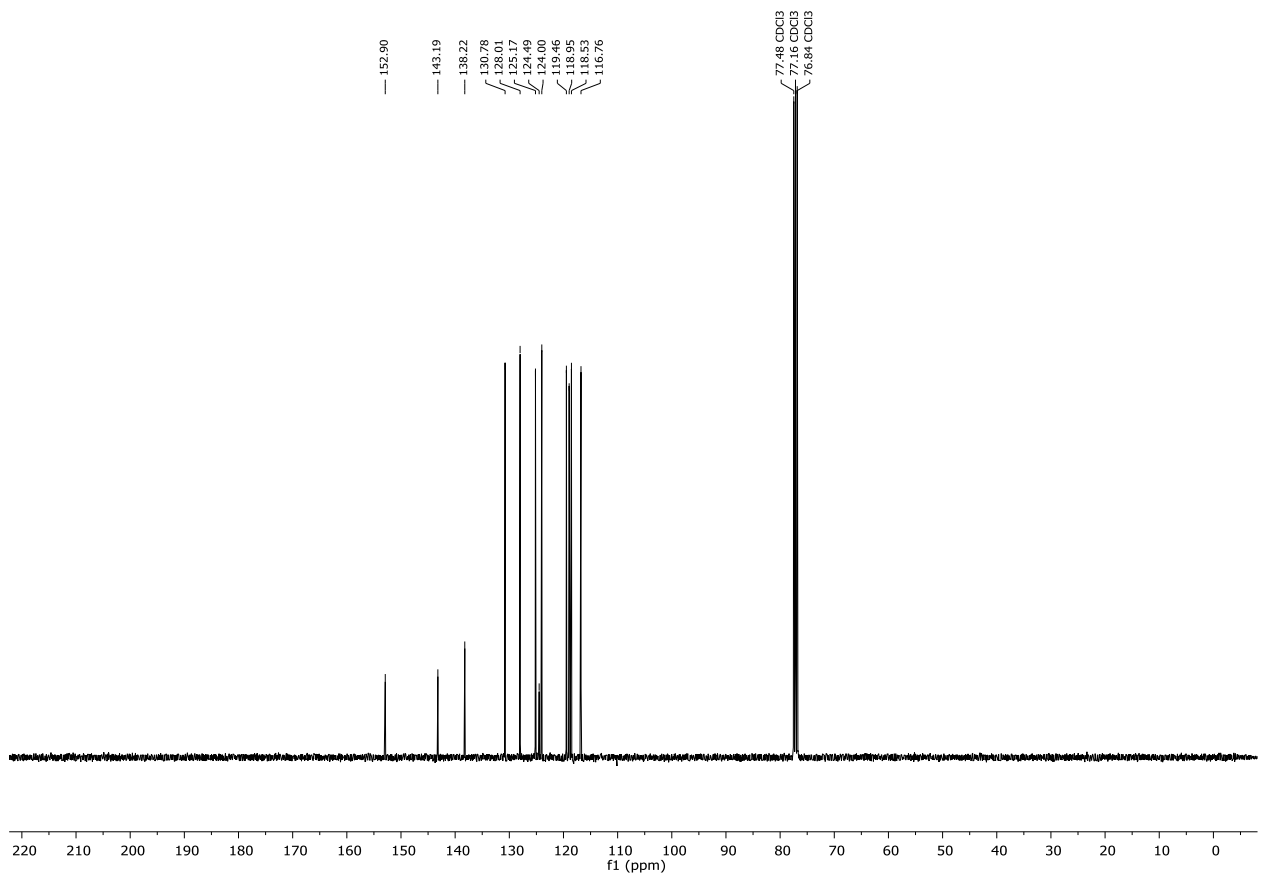


## 7. Appendix

### $^1\text{H-NMR}$ (400 MHz, $\text{CDCl}_3$ ) Compound **172e**

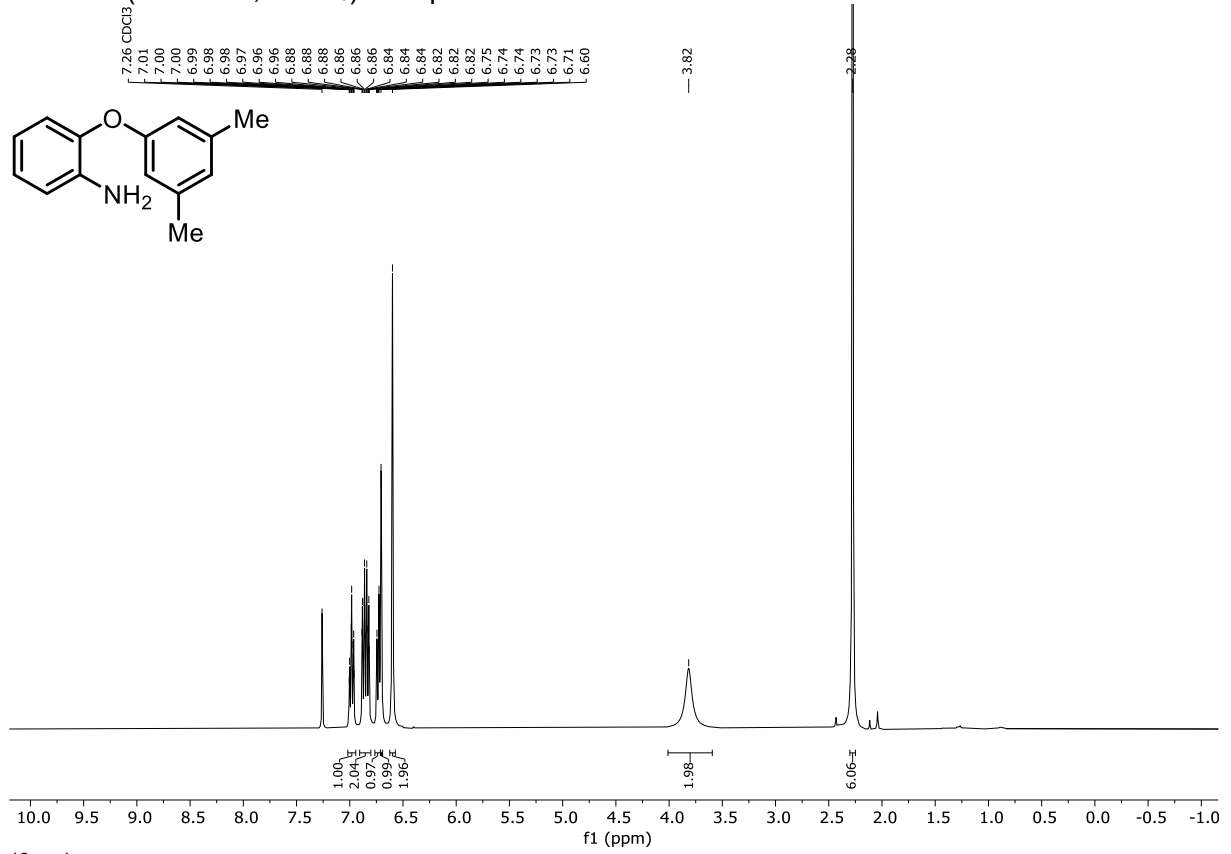


### $^{13}\text{C}\{^1\text{H}\}$ -NMR (101 MHz, $\text{CDCl}_3$ ) Compound **172e**

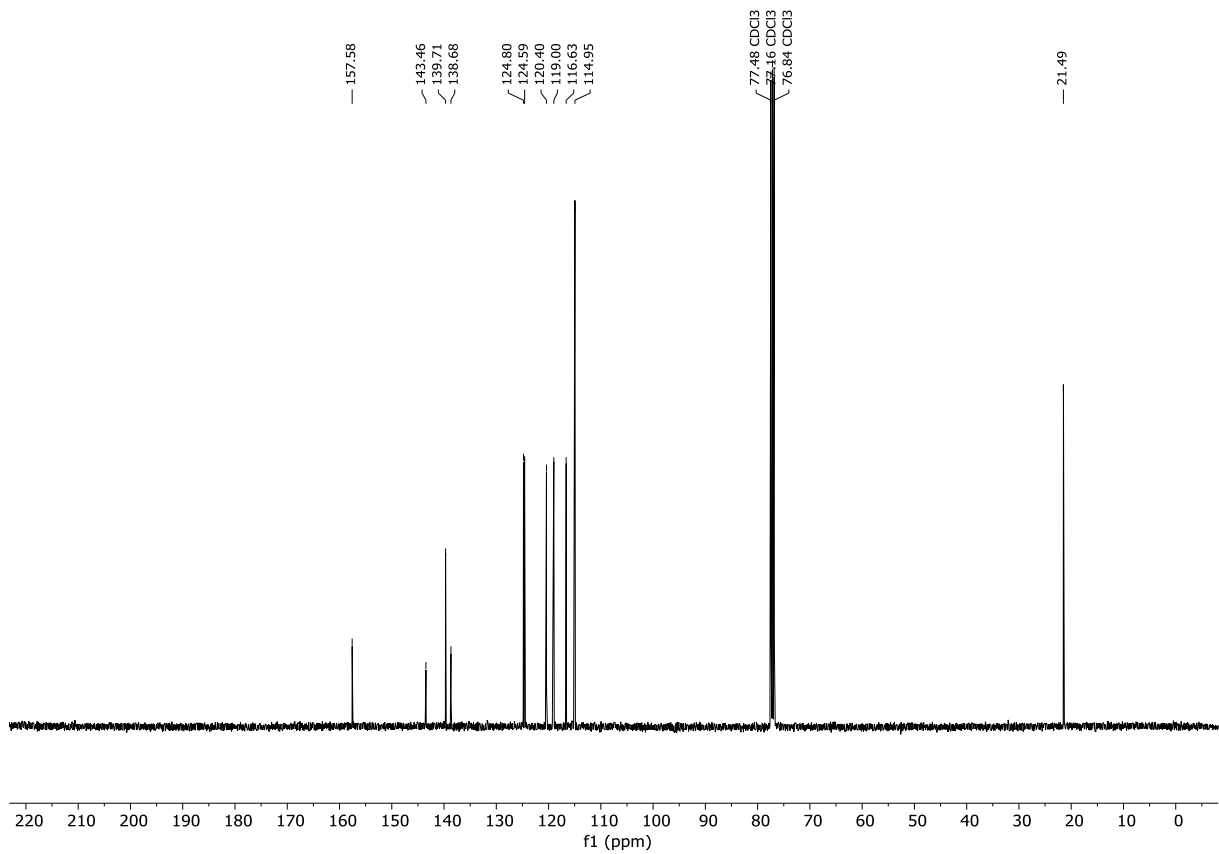


## 7.2 NMR spectra

$^1\text{H-NMR}$  (400 MHz,  $\text{CDCl}_3$ ) Compound **172f**

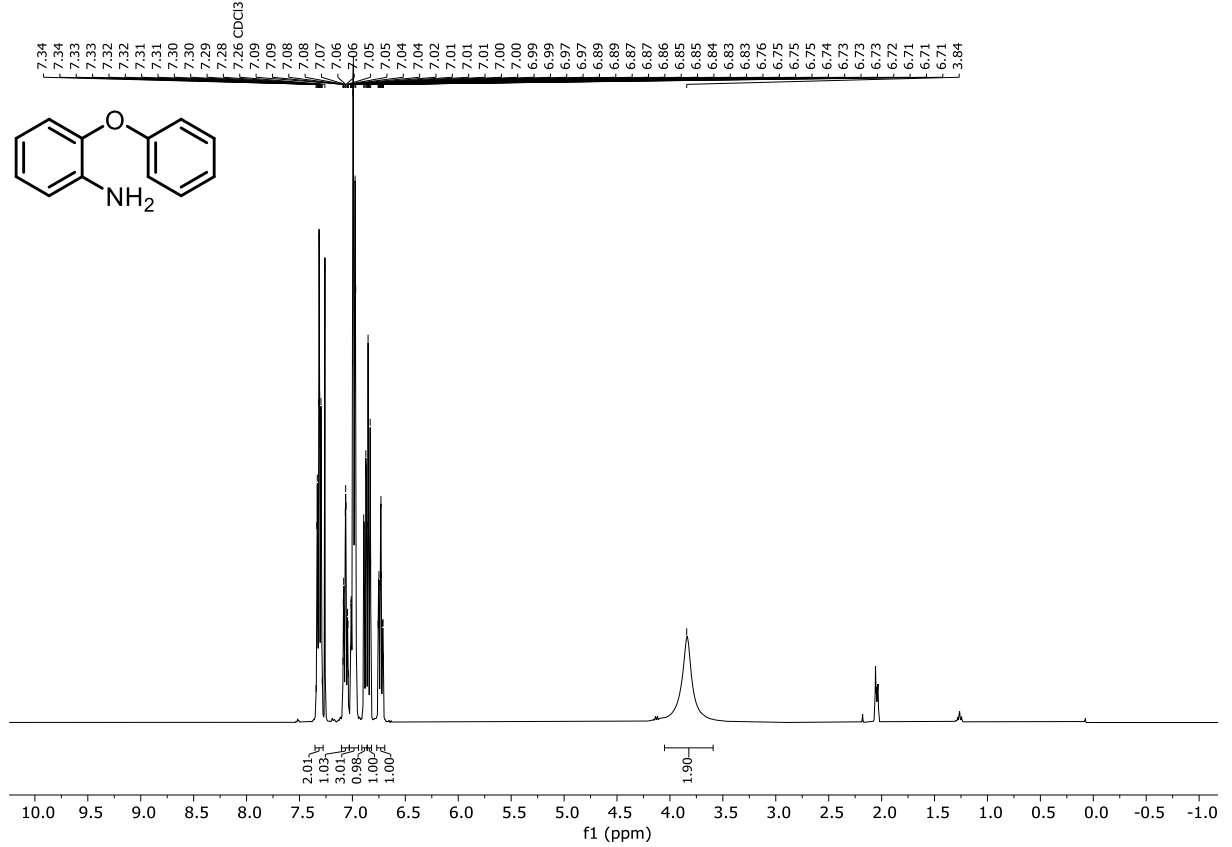


$^{13}\text{C}\{^1\text{H}\}$ -NMR (101 MHz,  $\text{CDCl}_3$ ) Compound **172f**

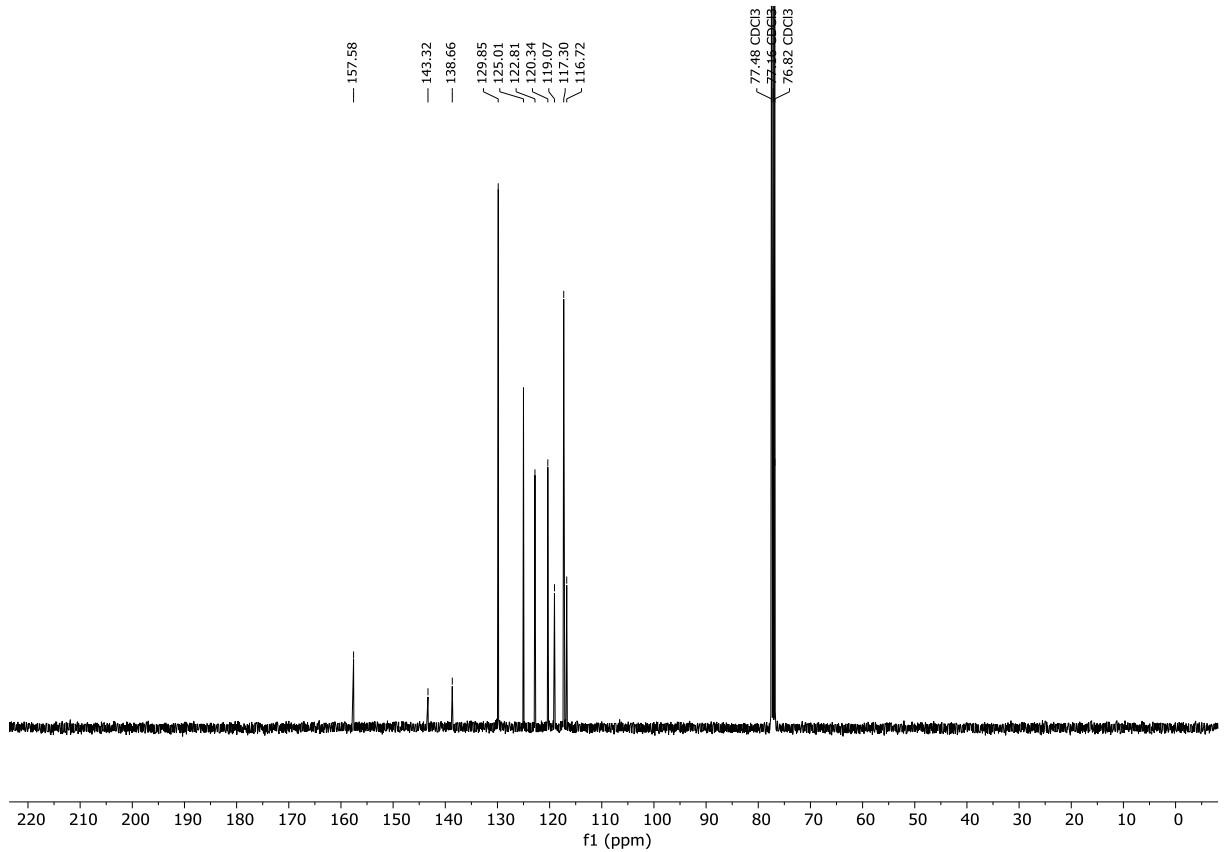


## 7. Appendix

### $^1\text{H-NMR}$ (400 MHz, $\text{CDCl}_3$ ) Compound **172g**



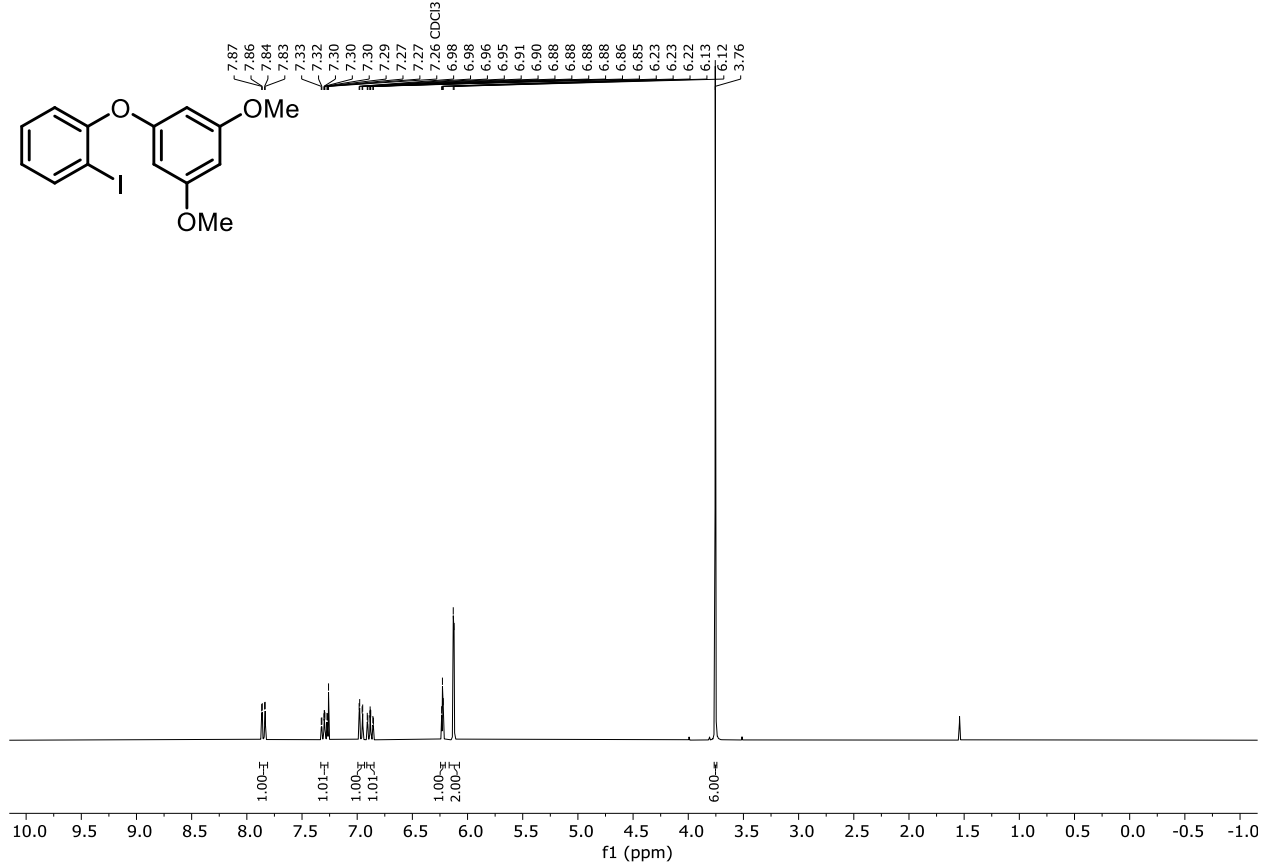
### $^{13}\text{C}\{^1\text{H}\}$ -NMR (101 MHz, $\text{CDCl}_3$ ) Compound **172g**



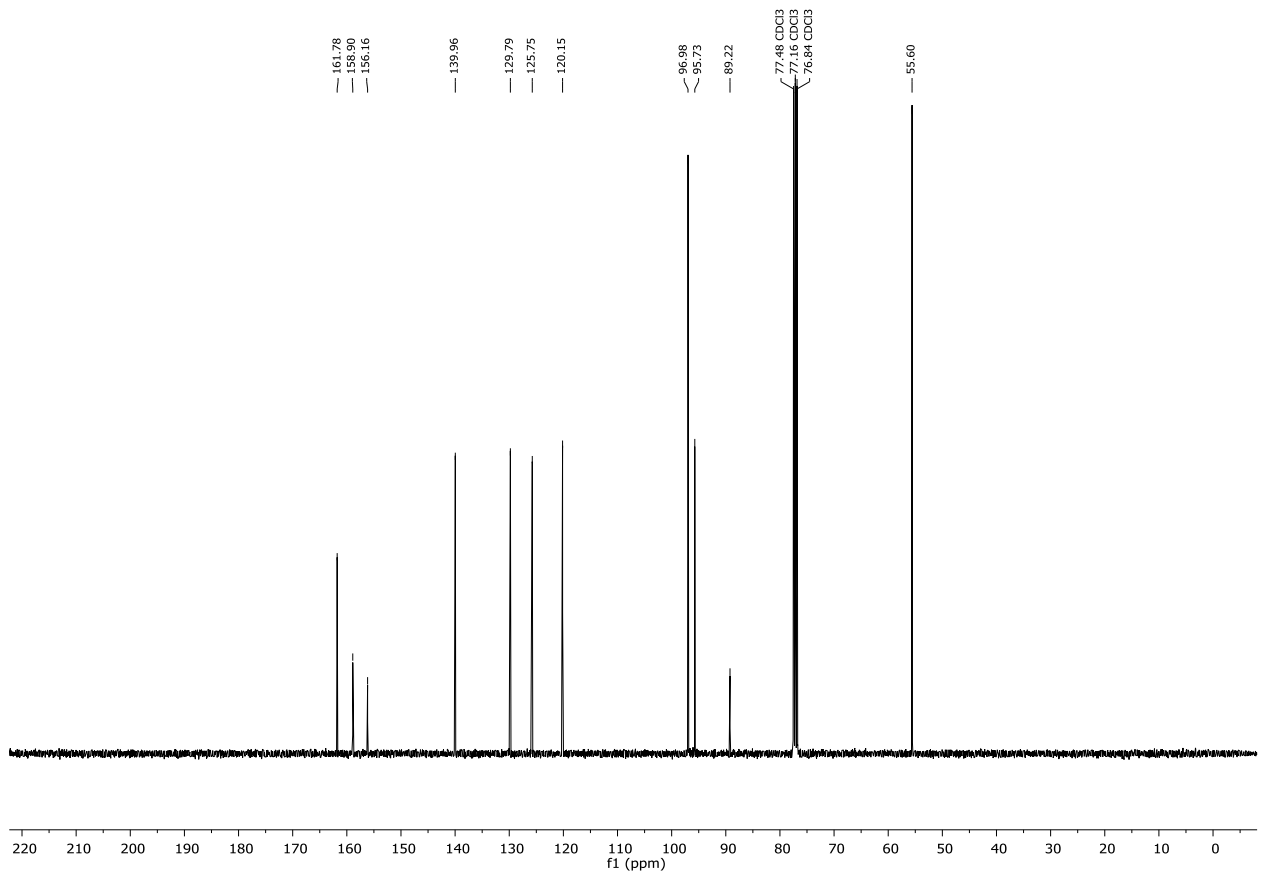


## 7.2 NMR spectra

### $^1\text{H-NMR}$ (300 MHz, $\text{CDCl}_3$ ) Compound **173a**

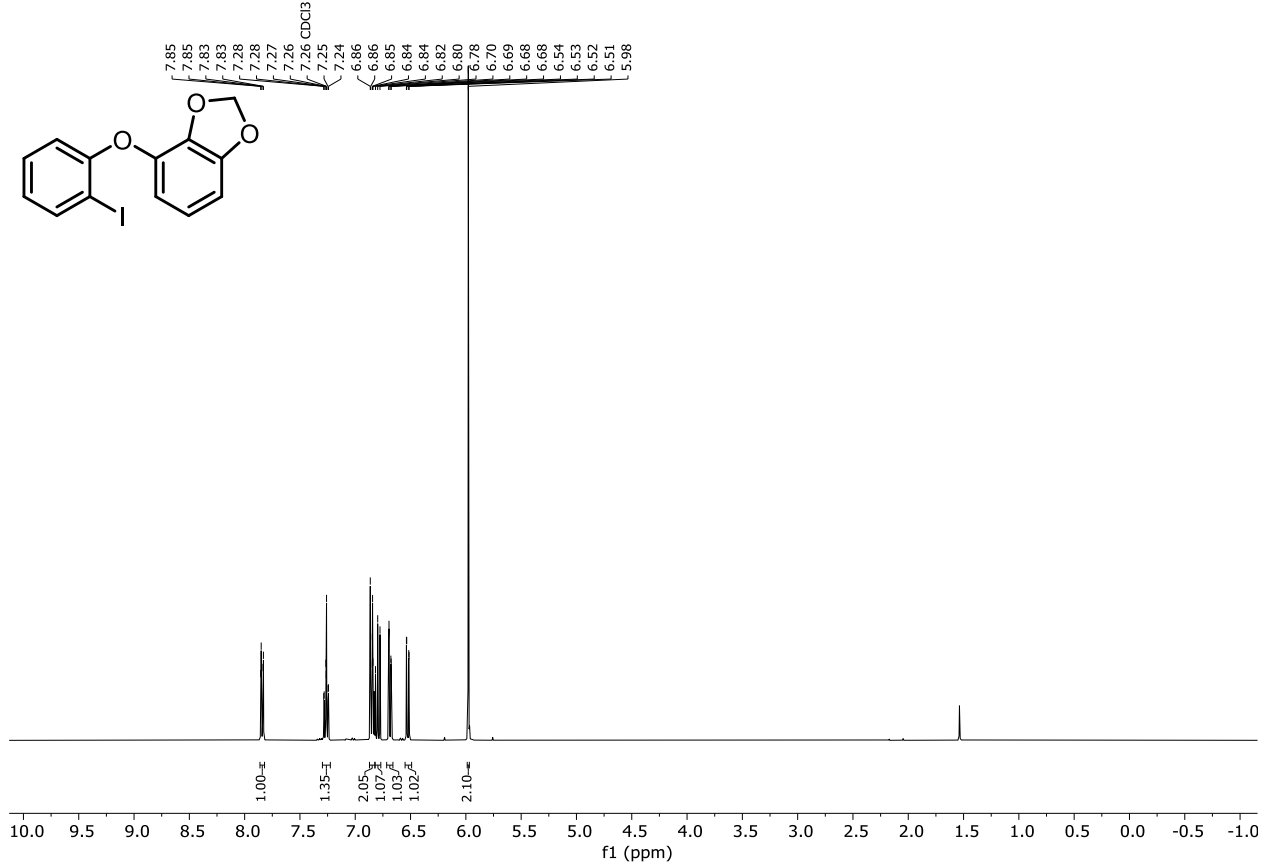


### $^{13}\text{C}\{^1\text{H}\}$ -NMR (101 MHz, $\text{CDCl}_3$ ) Compound **173a**

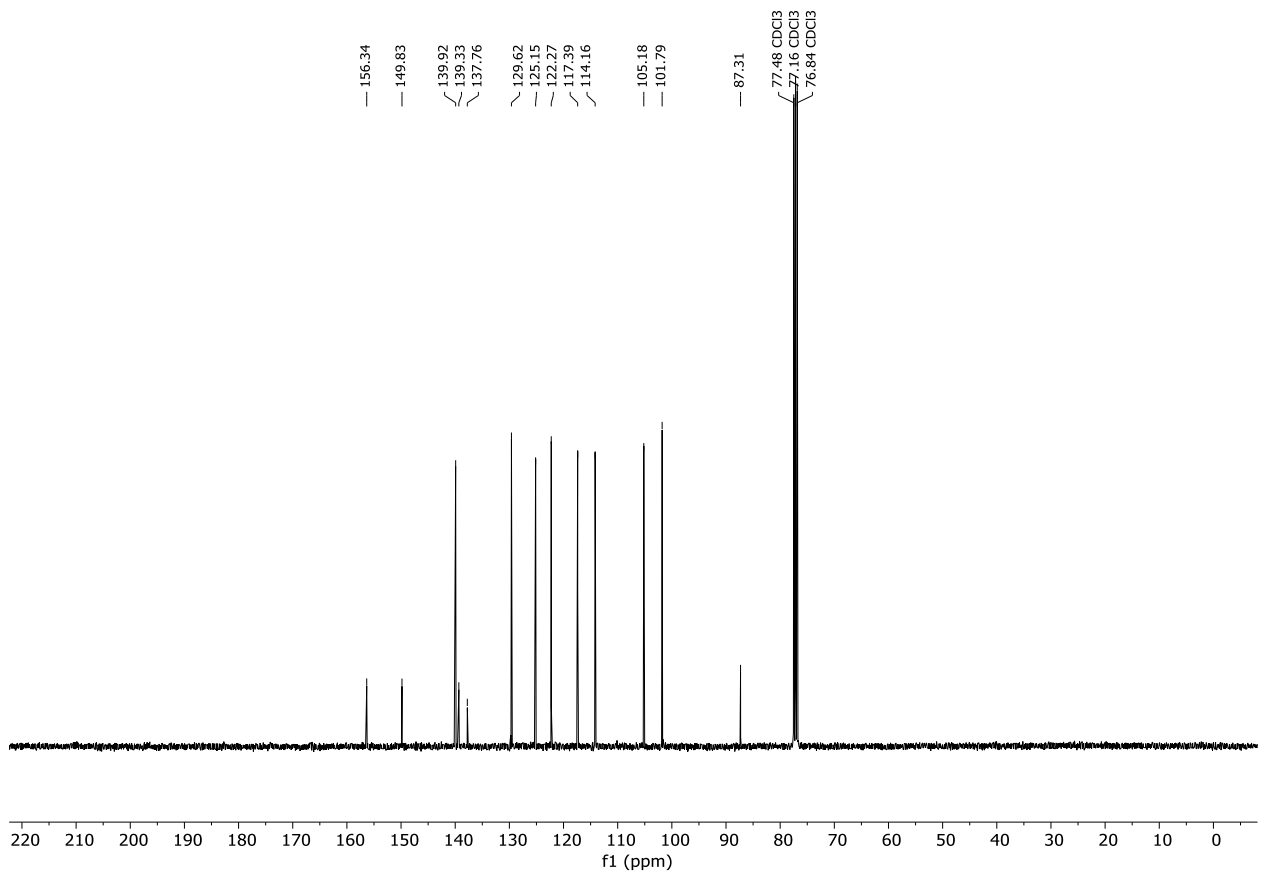


## 7. Appendix

### $^1\text{H-NMR}$ (400 MHz, $\text{CDCl}_3$ ) Compound **173b**

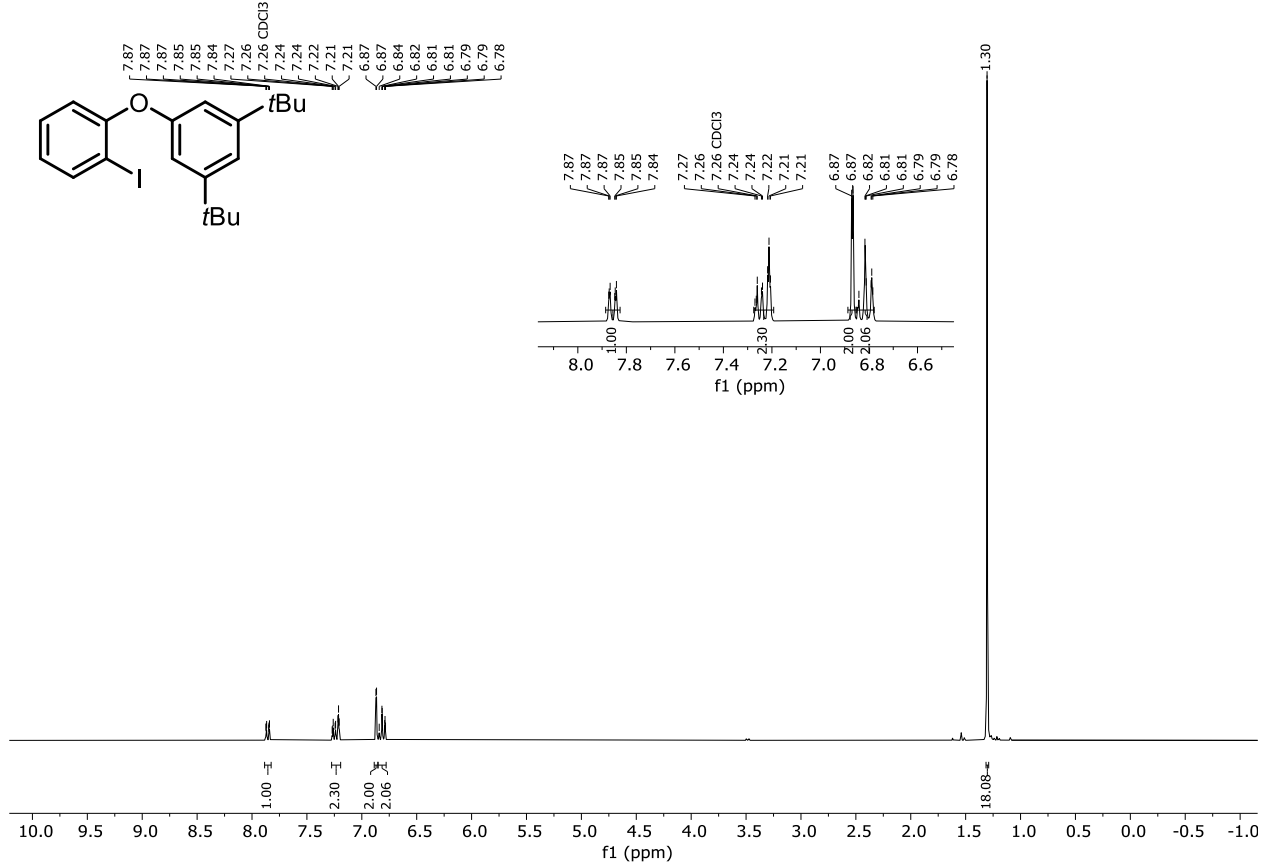


### $^{13}\text{C}\{^1\text{H}\}$ -NMR (101 MHz, $\text{CDCl}_3$ ) Compound **173b**

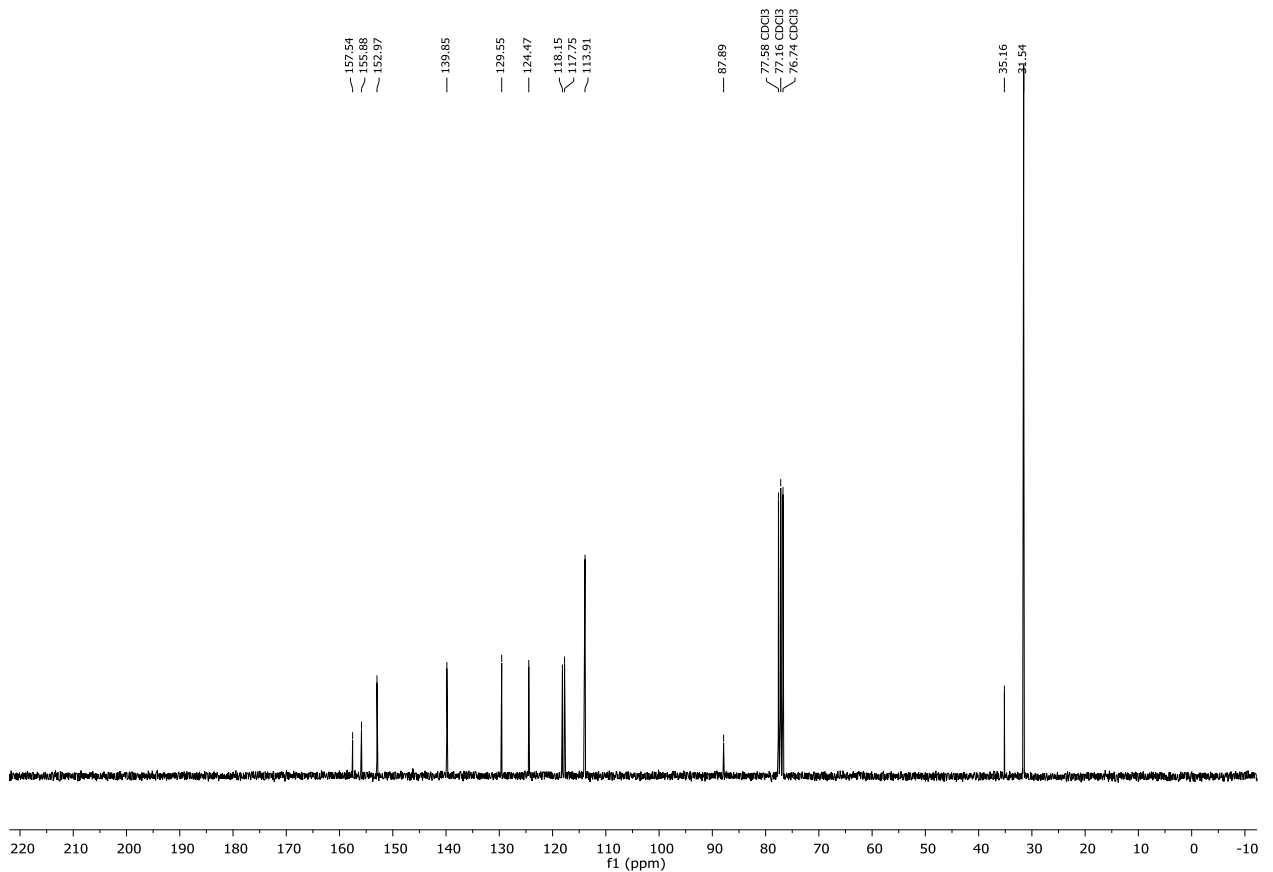


## 7.2 NMR spectra

### $^1\text{H-NMR}$ (300 MHz, $\text{CDCl}_3$ ) Compound **173c**

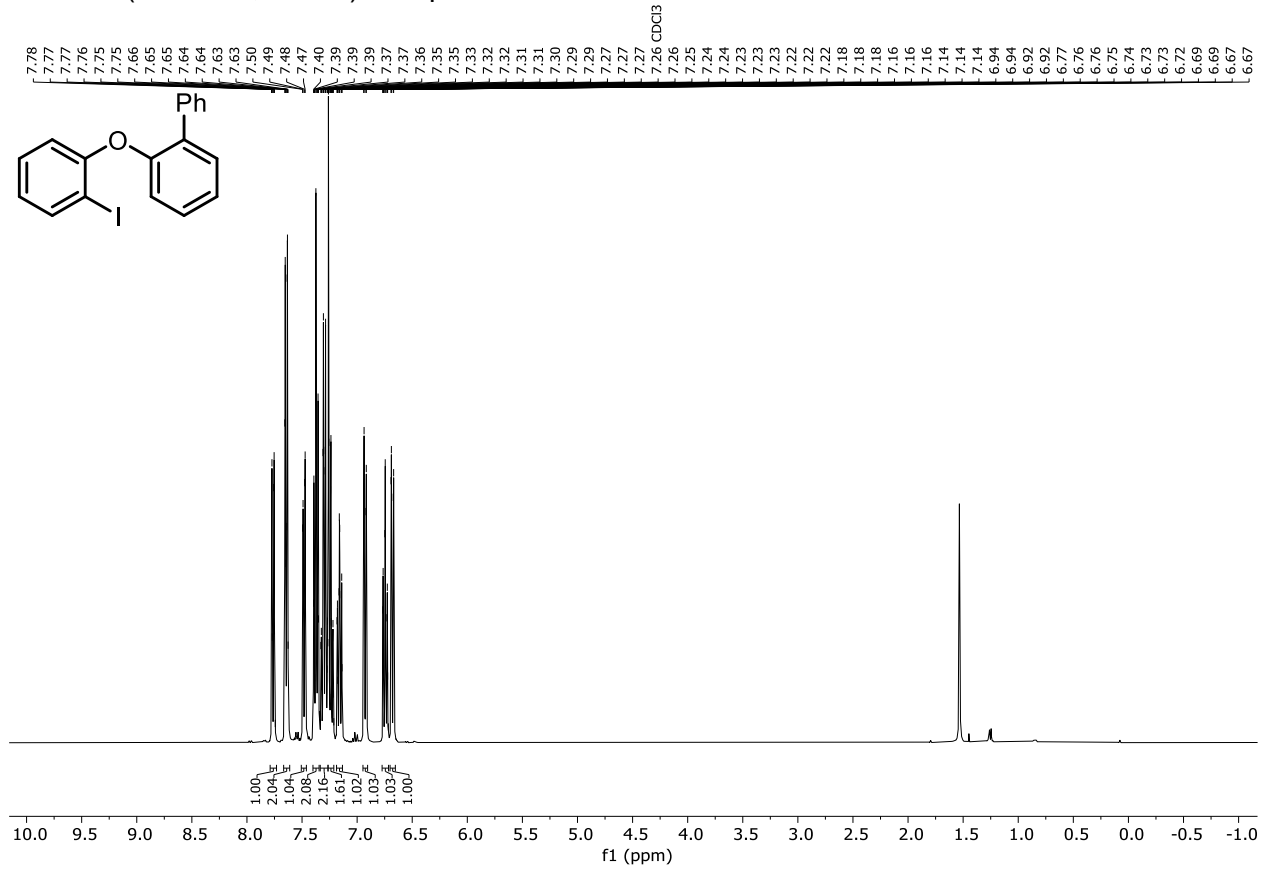


### $^{13}\text{C}\{^1\text{H}\}$ -NMR (75 MHz, $\text{CDCl}_3$ ) Compound **173c**

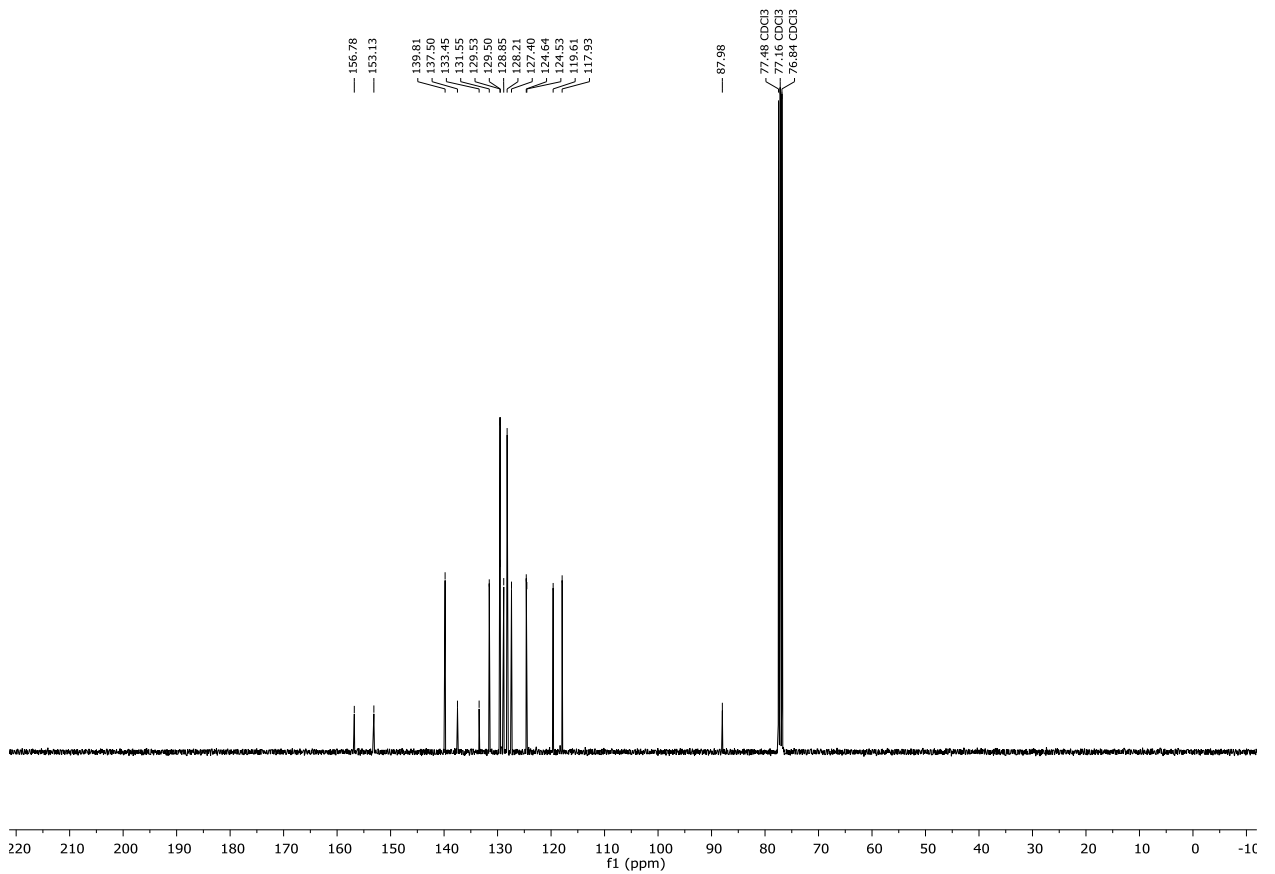


## 7. Appendix

### <sup>1</sup>H-NMR (400 MHz, CDCl<sub>3</sub>) Compound **173d**

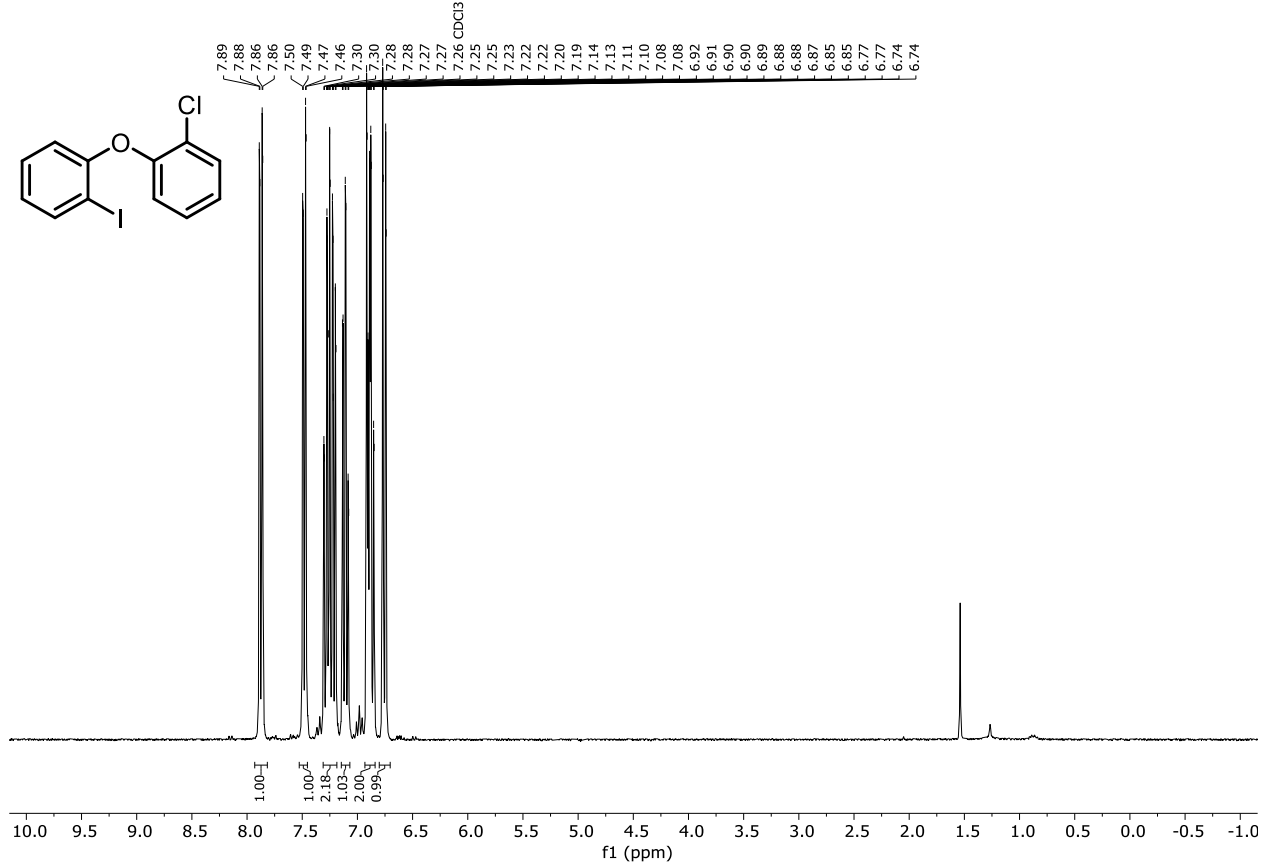


### <sup>13</sup>C{<sup>1</sup>H}-NMR (101 MHz, CDCl<sub>3</sub>) Compound **173d**

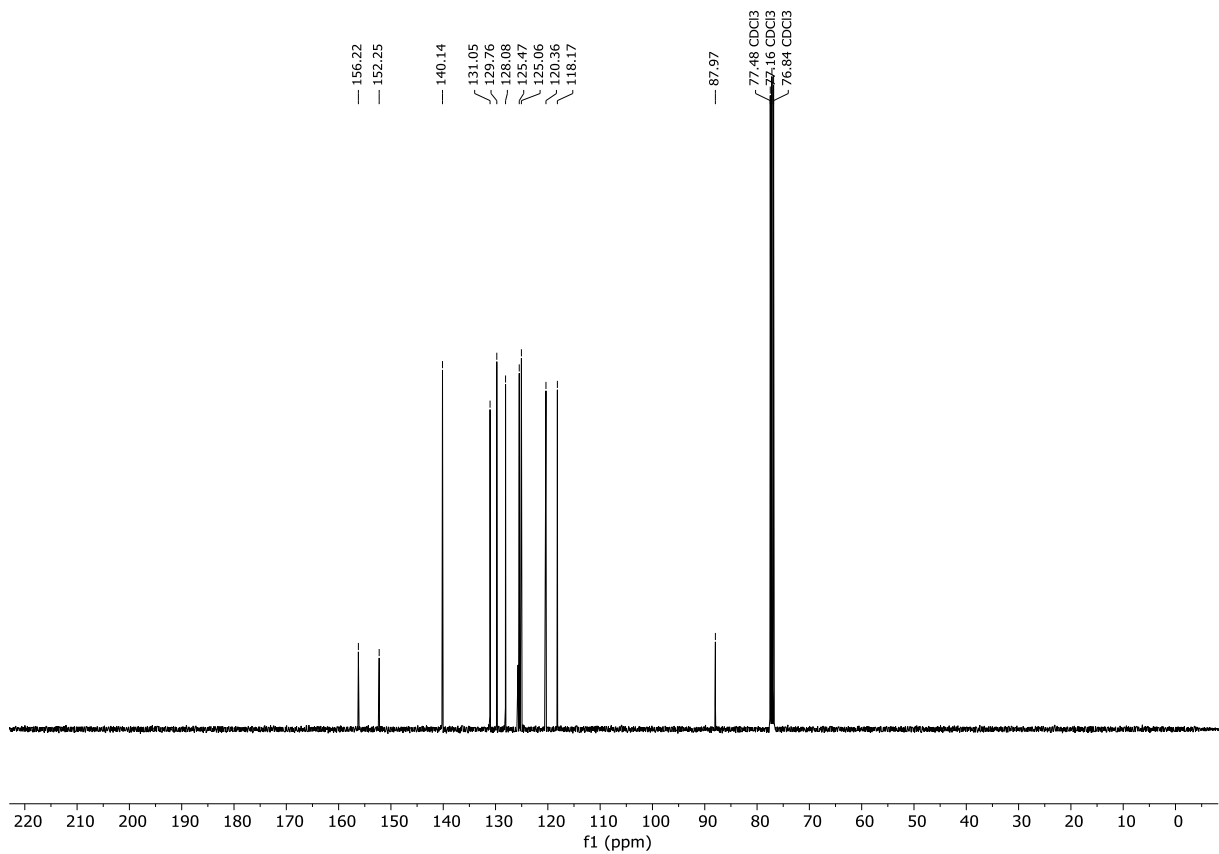


## 7.2 NMR spectra

### $^1\text{H-NMR}$ (400 MHz, $\text{CDCl}_3$ ) Compound **173e**

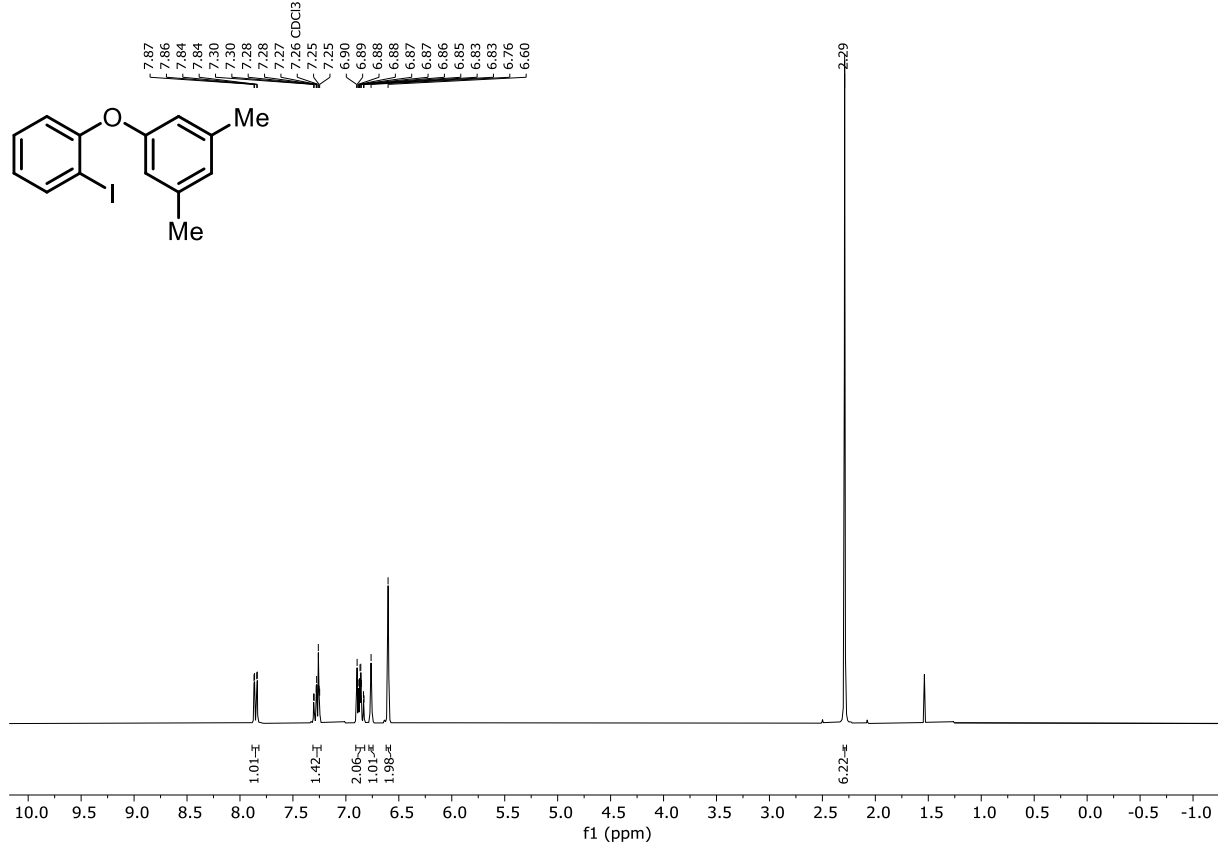


### $^{13}\text{C}\{^1\text{H}\}$ -NMR (101 MHz, $\text{CDCl}_3$ ) Compound **173e**

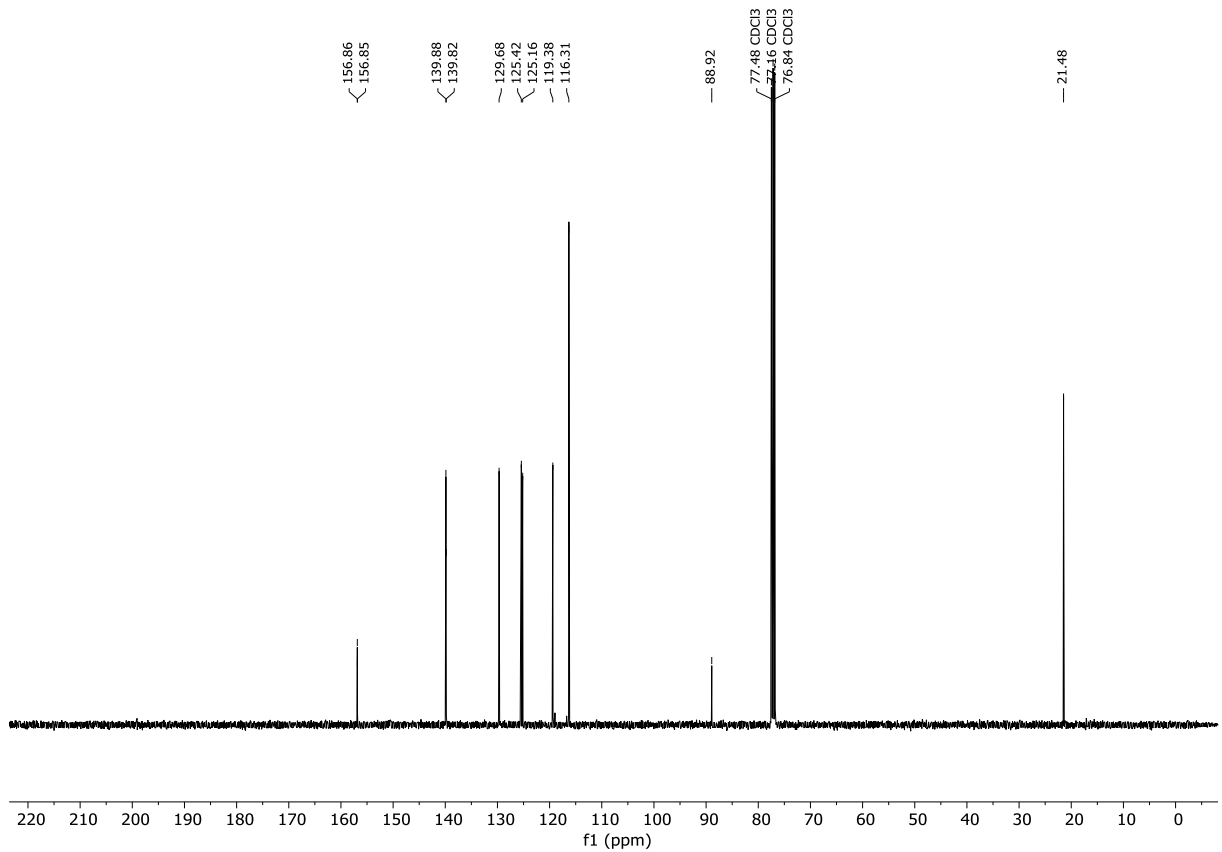


## 7. Appendix

### $^1\text{H-NMR}$ (300 MHz, $\text{CDCl}_3$ ) Compound **173f**

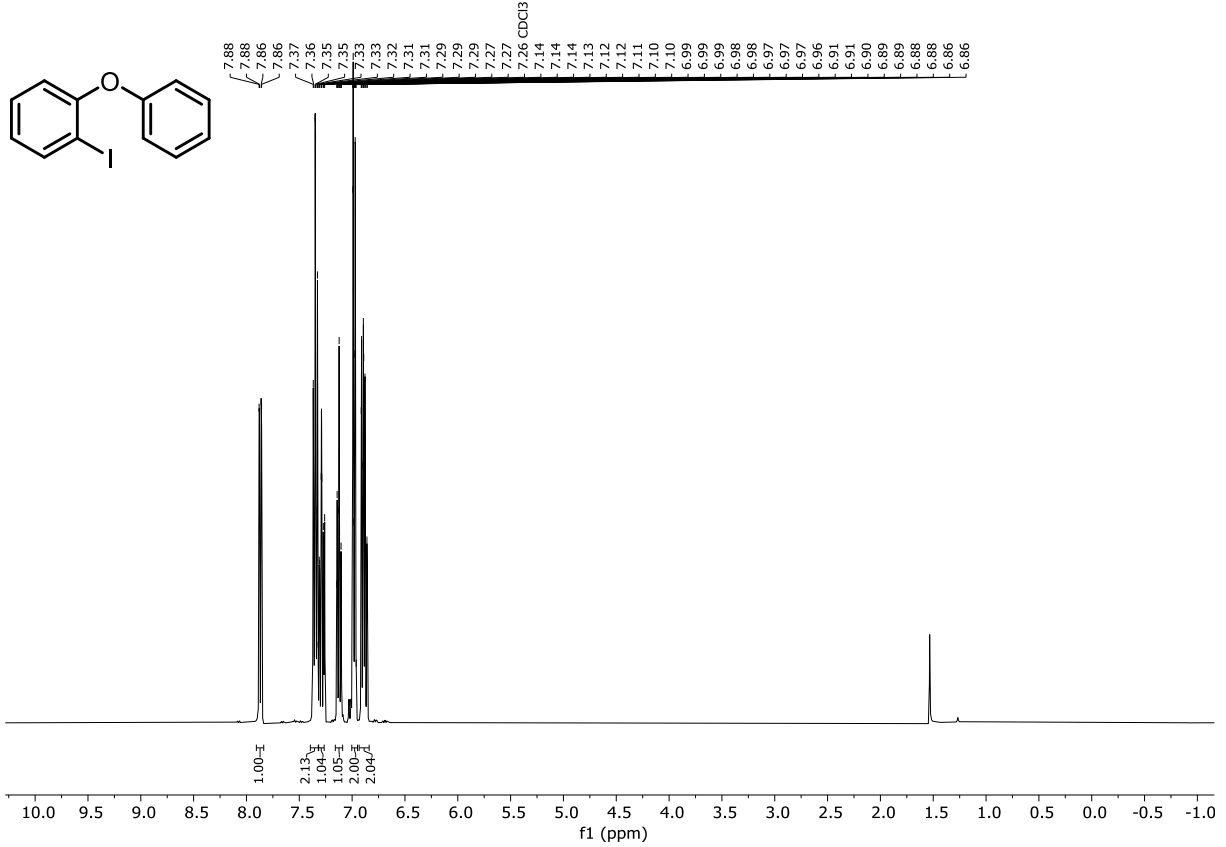


### $^{13}\text{C}\{^1\text{H}\}$ -NMR (101 MHz, $\text{CDCl}_3$ ) Compound **173f**

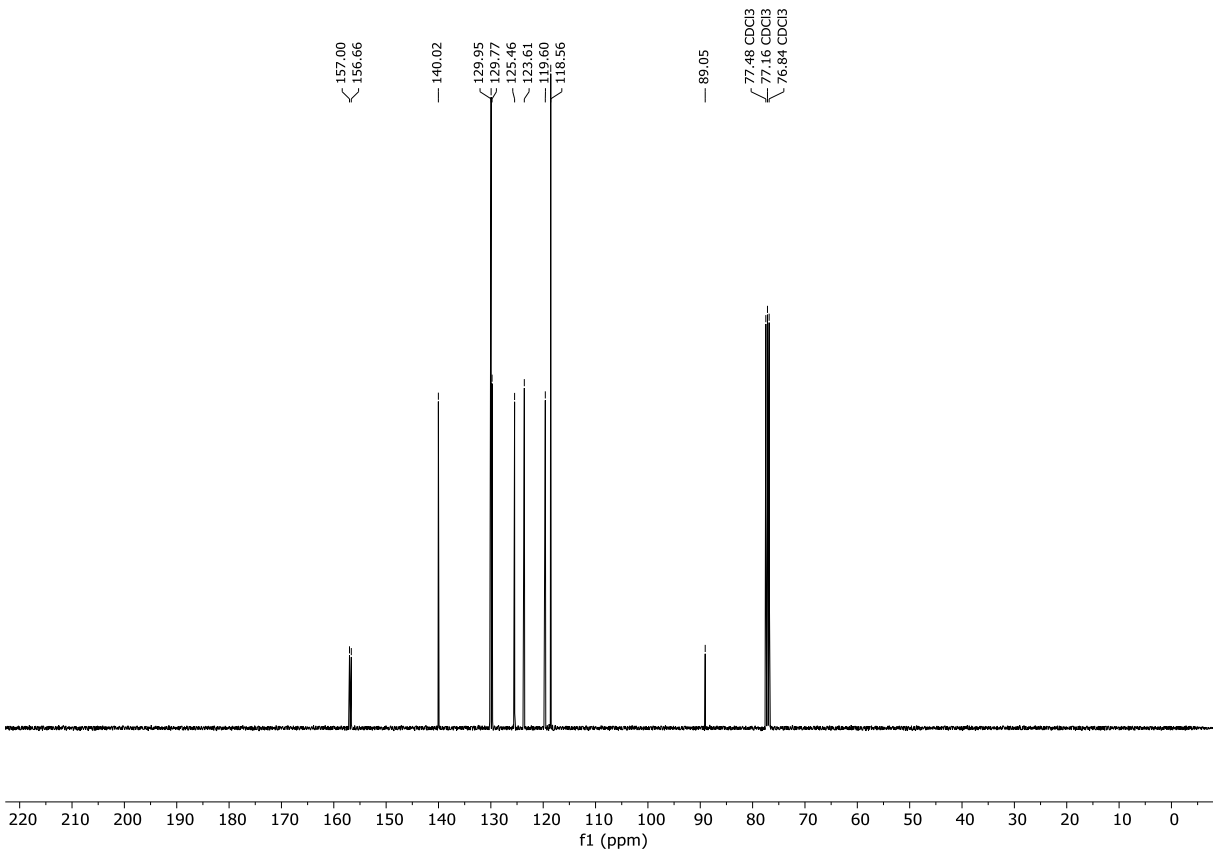


## 7.2 NMR spectra

### <sup>1</sup>H-NMR (400 MHz, CDCl<sub>3</sub>) Compound **173g**



### <sup>13</sup>C{<sup>1</sup>H}-NMR (101 MHz, CDCl<sub>3</sub>) Compound **173g**

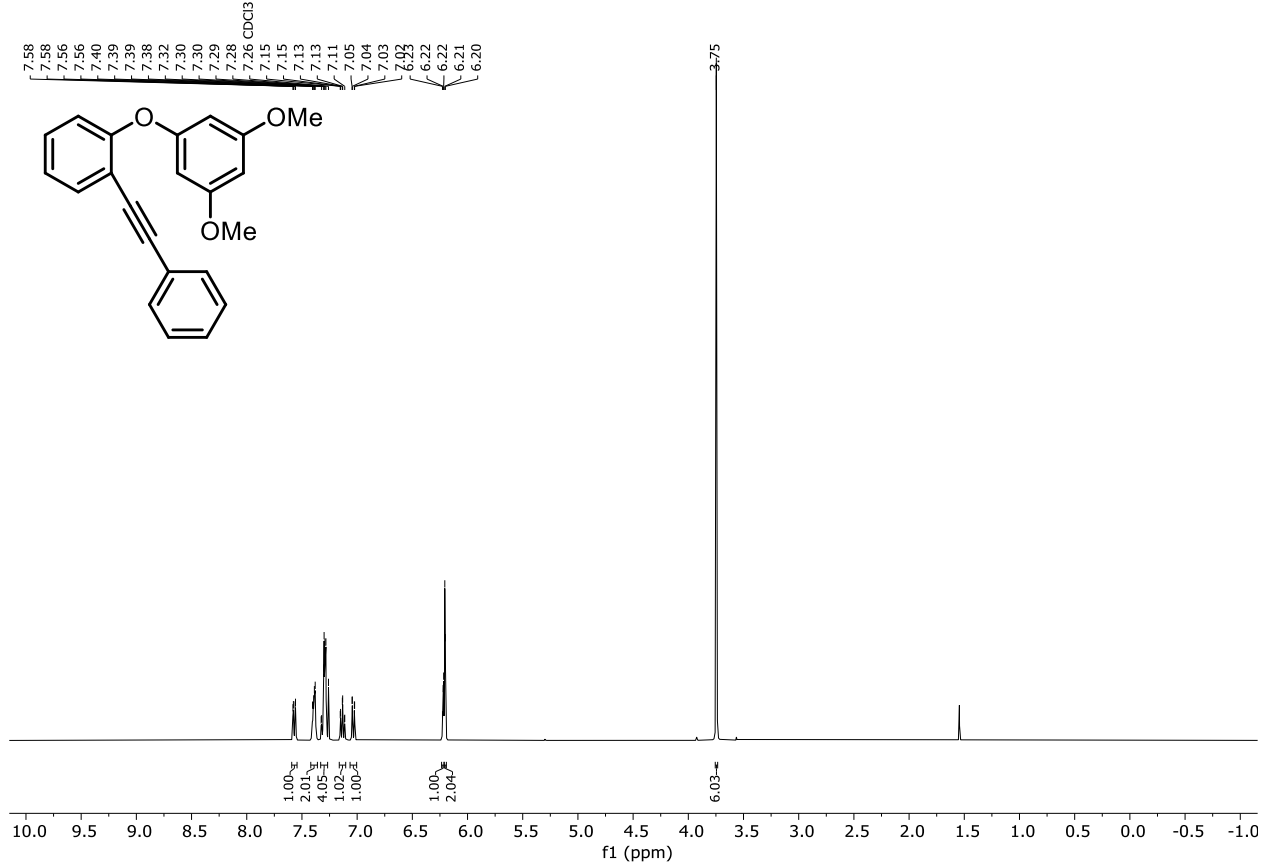




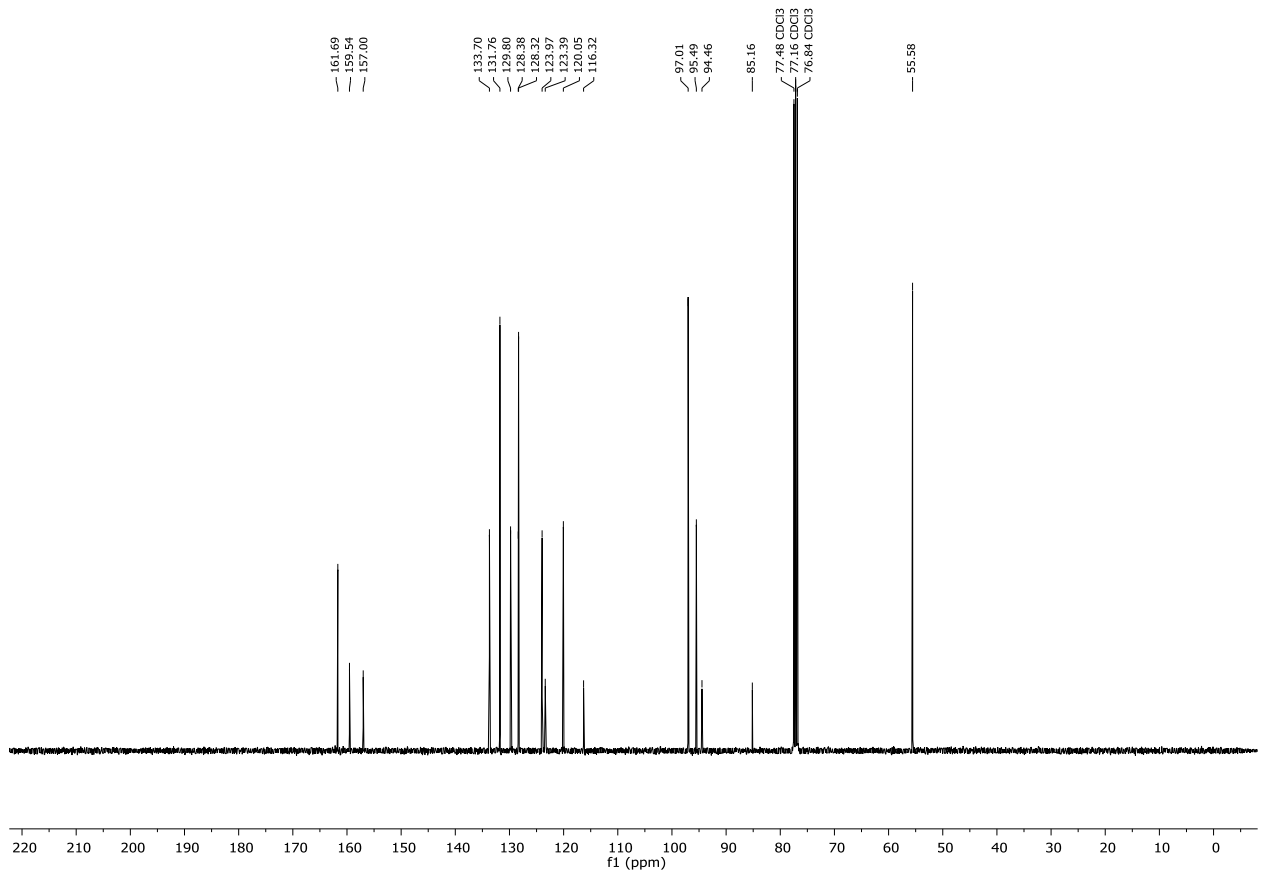


## 7.2 NMR spectra

### $^1\text{H-NMR}$ (400 MHz, $\text{CDCl}_3$ ) Compound **151b**

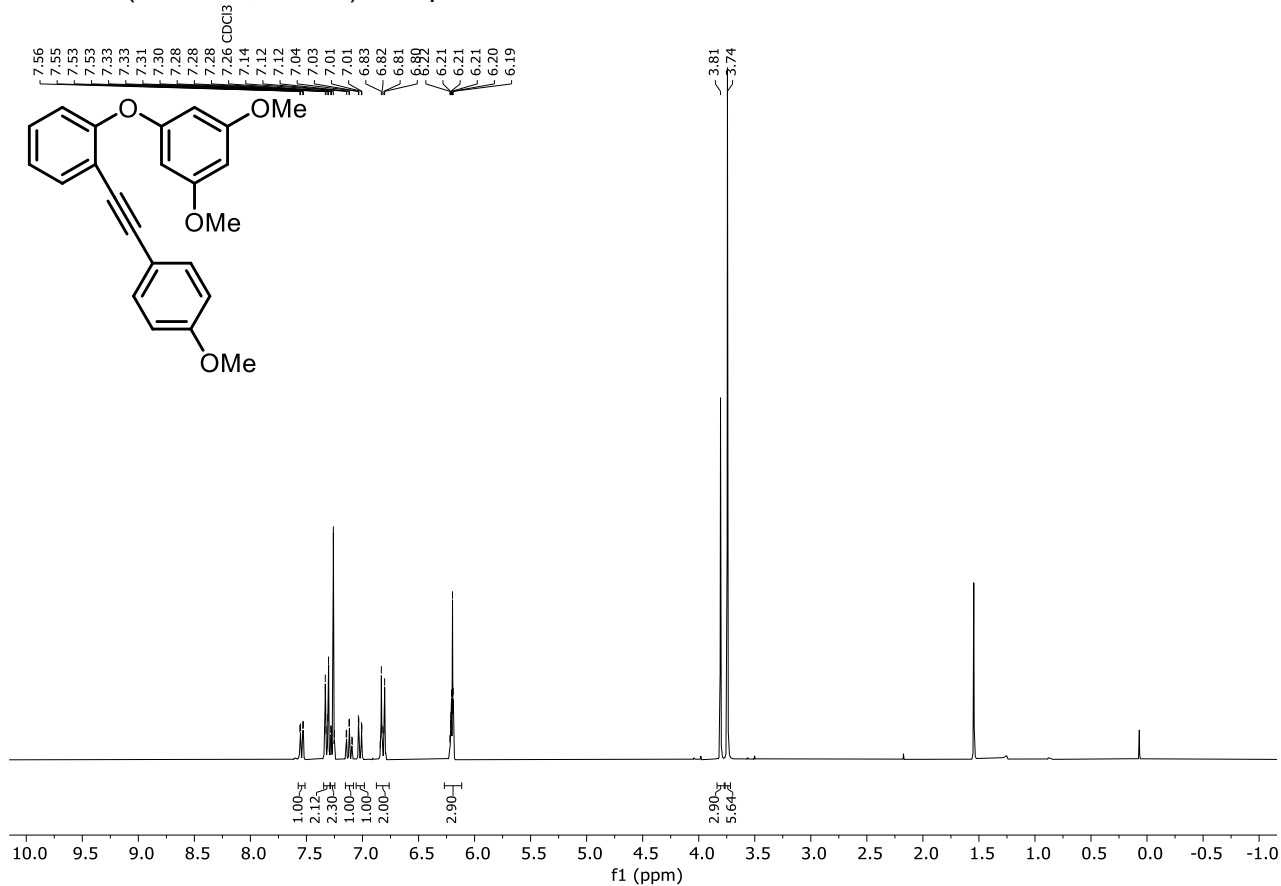


### $^{13}\text{C}\{^1\text{H}\}$ -NMR (101 MHz, $\text{CDCl}_3$ ) Compound **151b**

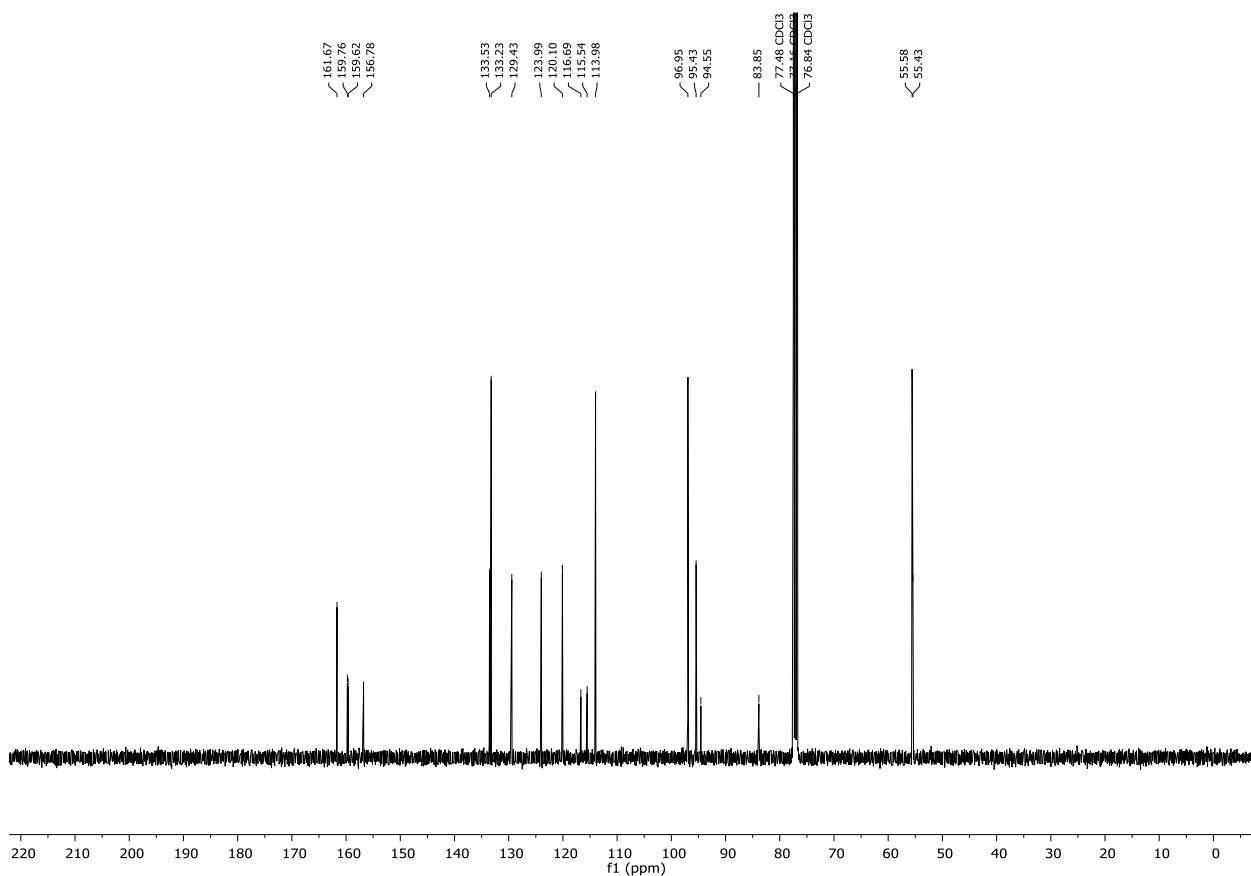


## 7. Appendix

### $^1\text{H-NMR}$ (300 MHz, $\text{CDCl}_3$ ) Compound **151c**

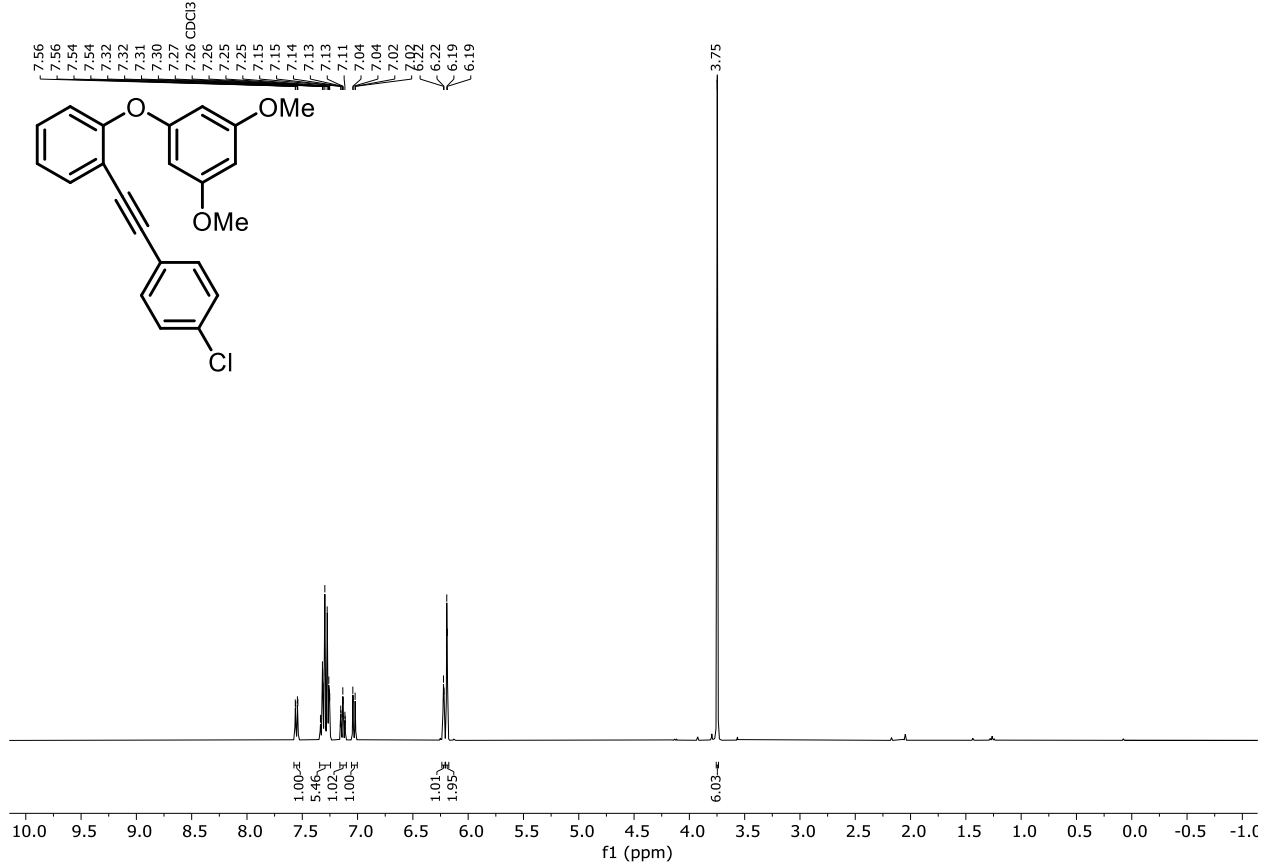


### $^{13}\text{C}\{^1\text{H}\}$ -NMR (101 MHz, $\text{CDCl}_3$ ) Compound **151c**

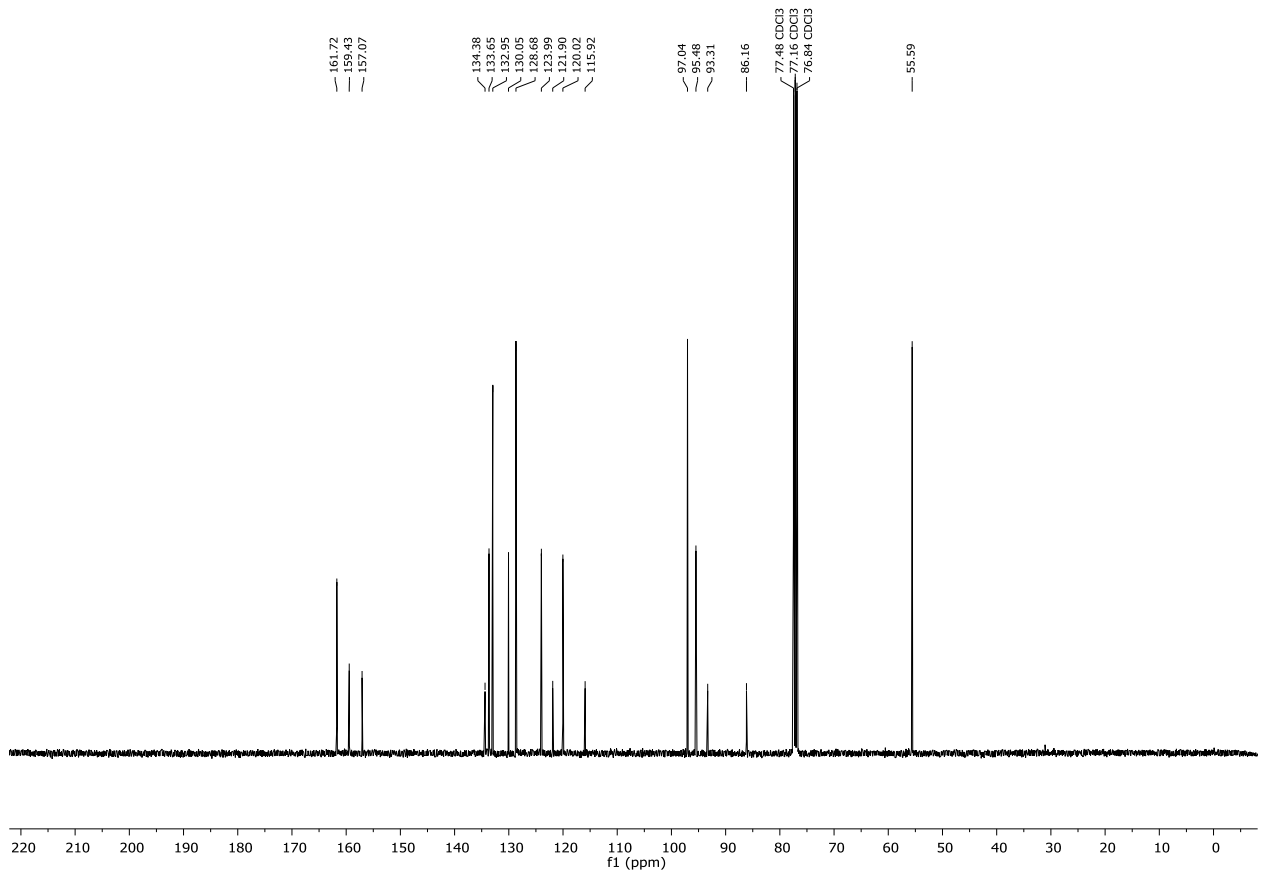


## 7.2 NMR spectra

### $^1\text{H-NMR}$ (400 MHz, $\text{CDCl}_3$ ) Compound **151d**

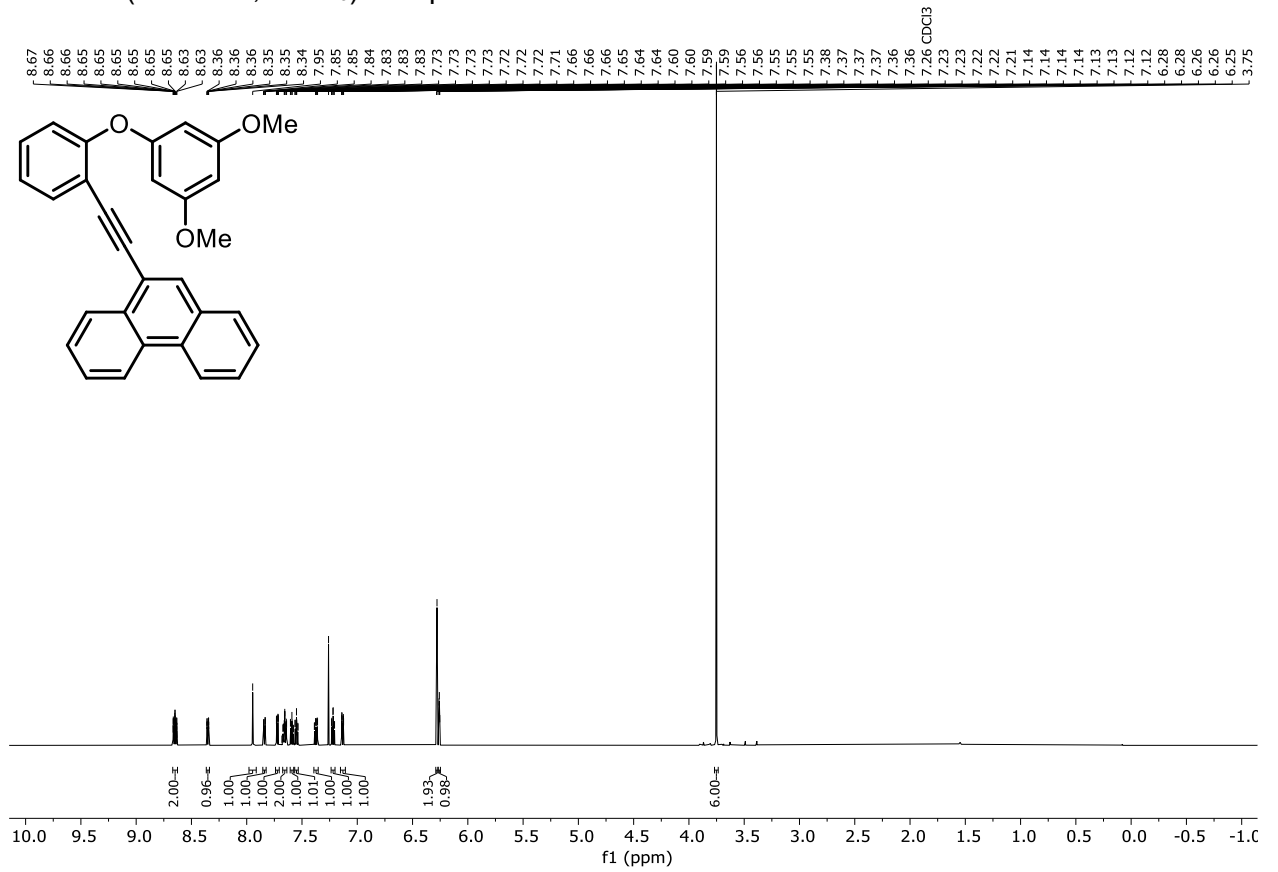


### $^{13}\text{C}\{^1\text{H}\}$ -NMR (101 MHz, $\text{CDCl}_3$ ) Compound **151d**

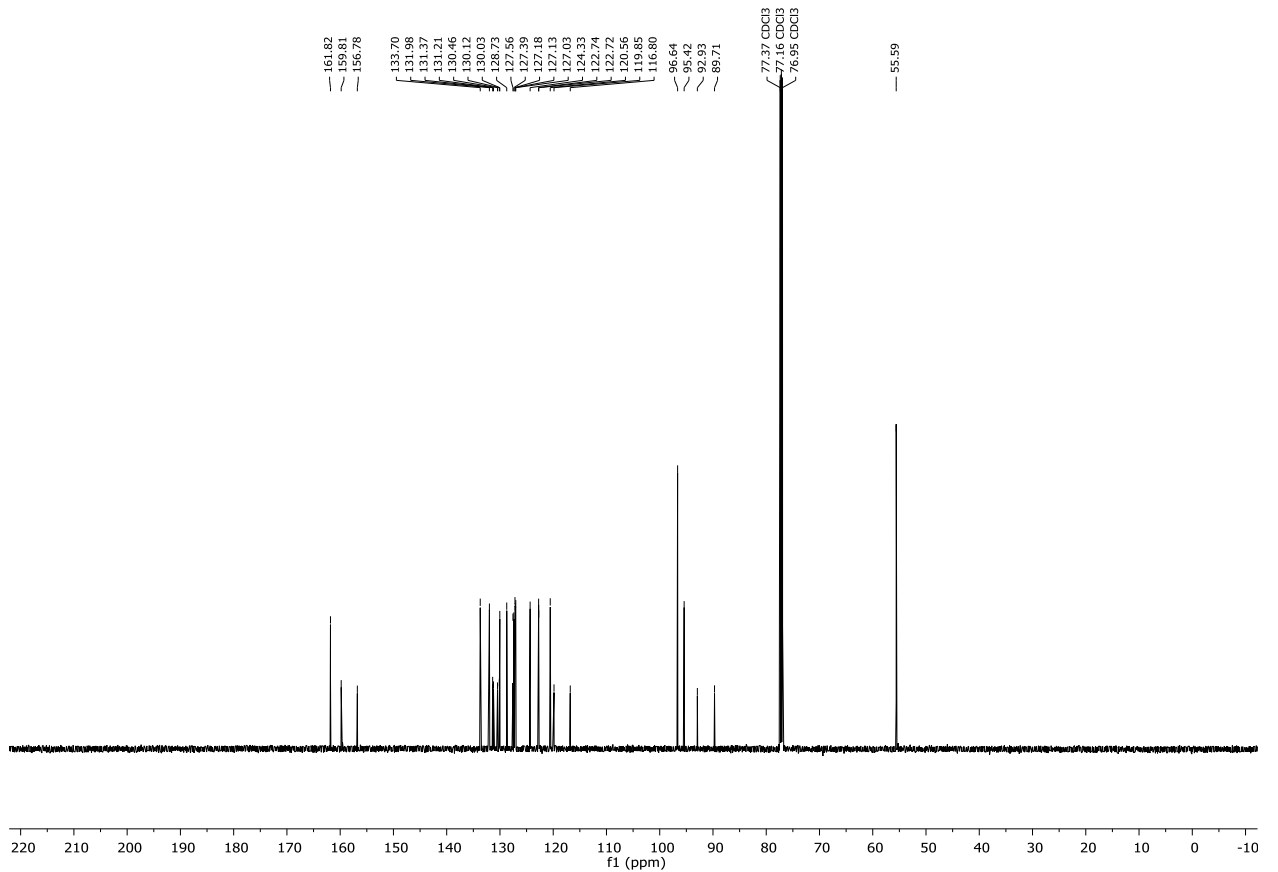


## 7. Appendix

### $^1\text{H-NMR}$ (600 MHz, $\text{CDCl}_3$ ) Compound **151e**

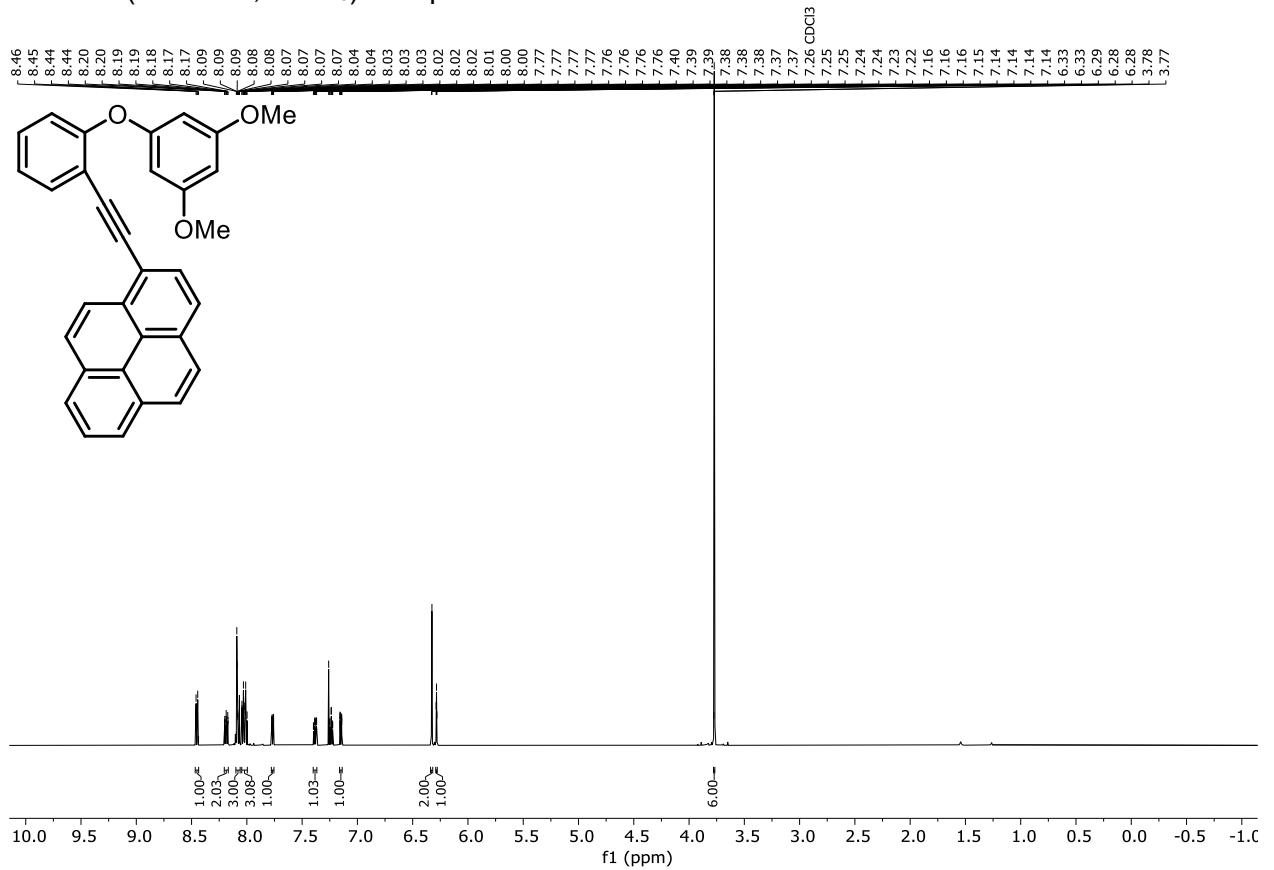


### $^{13}\text{C}\{^1\text{H}\}$ -NMR (151 MHz, $\text{CDCl}_3$ ) Compound **151e**

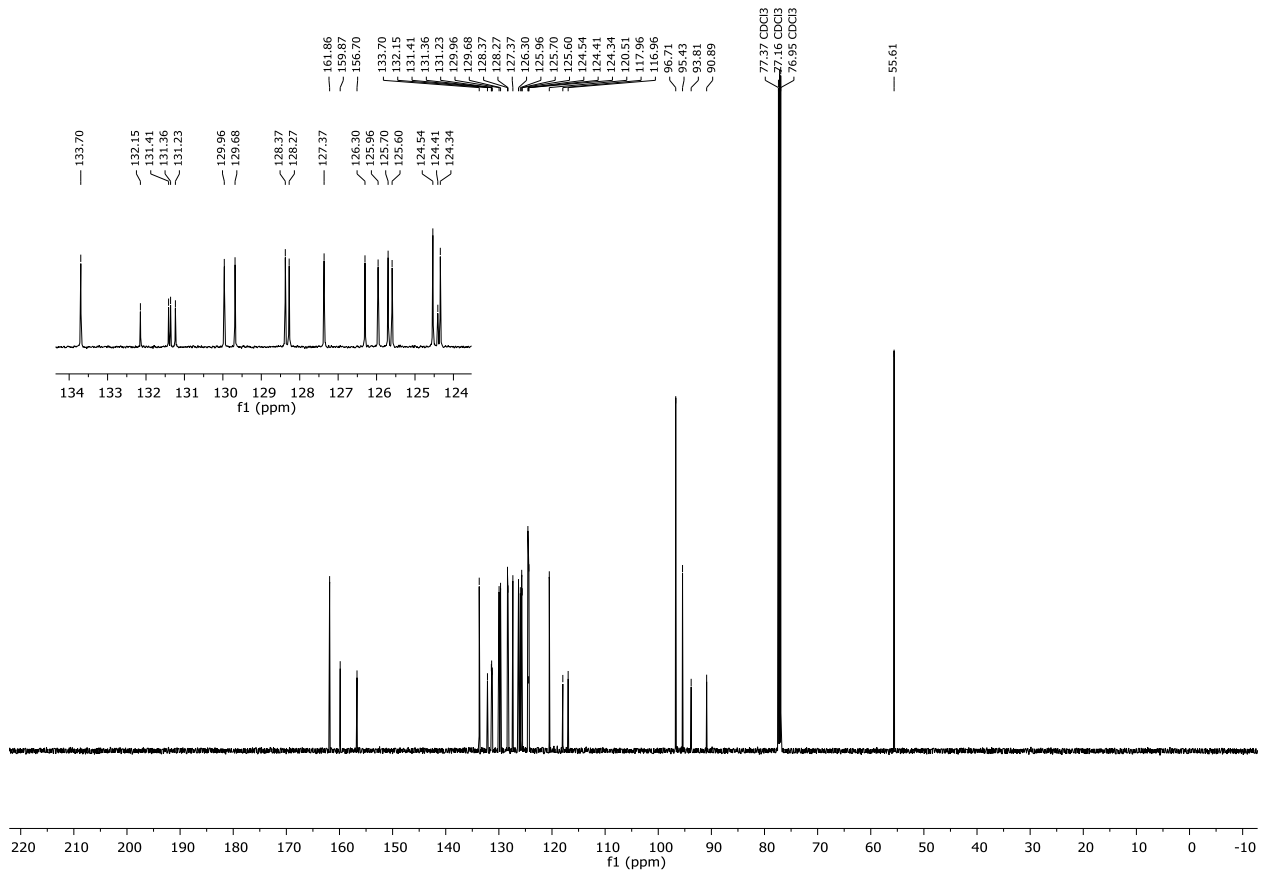


## 7.2 NMR spectra

### $^1\text{H-NMR}$ (600 MHz, $\text{CDCl}_3$ ) Compound **151f**

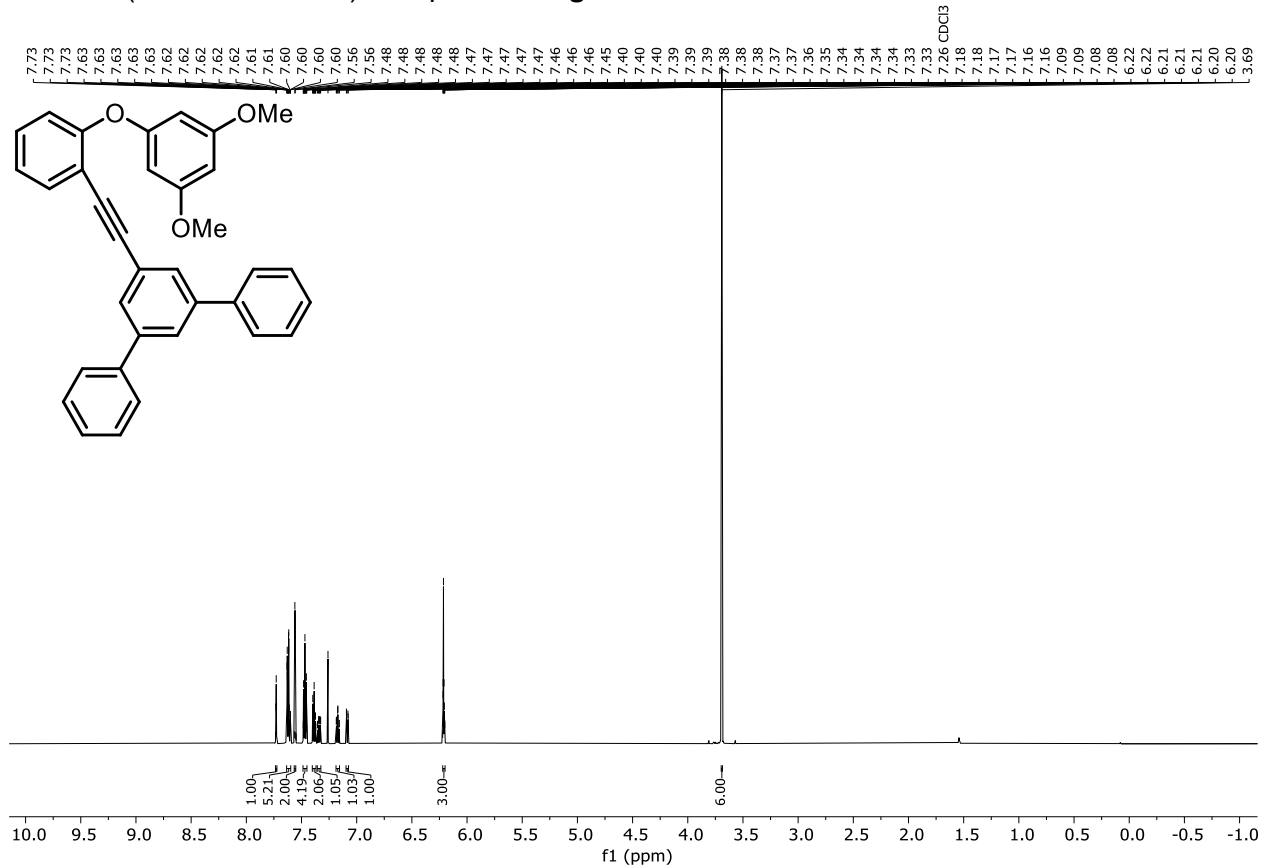


### $^{13}\text{C}\{^1\text{H}\}$ -NMR (151 MHz, $\text{CDCl}_3$ ) Compound **151f**

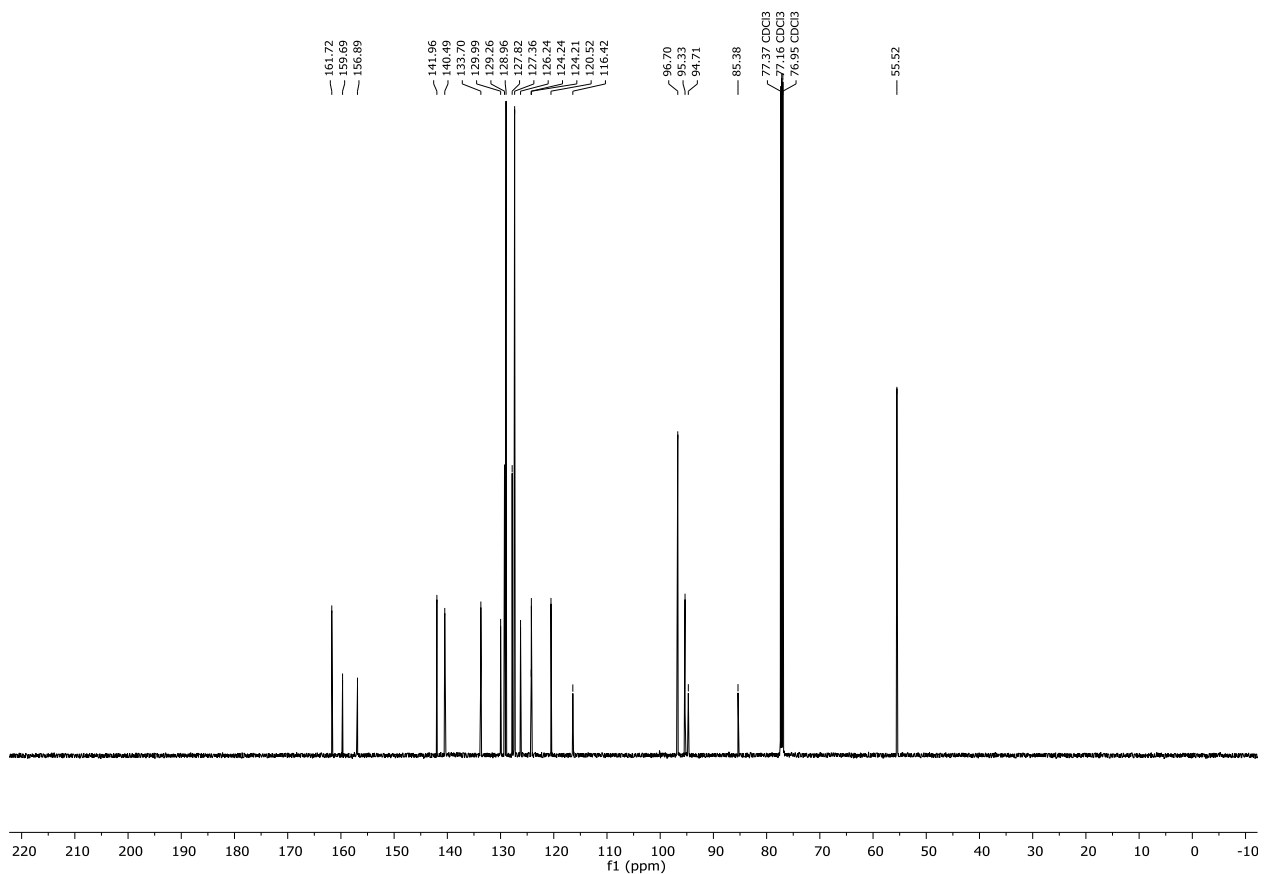


## 7. Appendix

### $^1\text{H-NMR}$ (600 MHz, $\text{CDCl}_3$ ) Compound **151g**

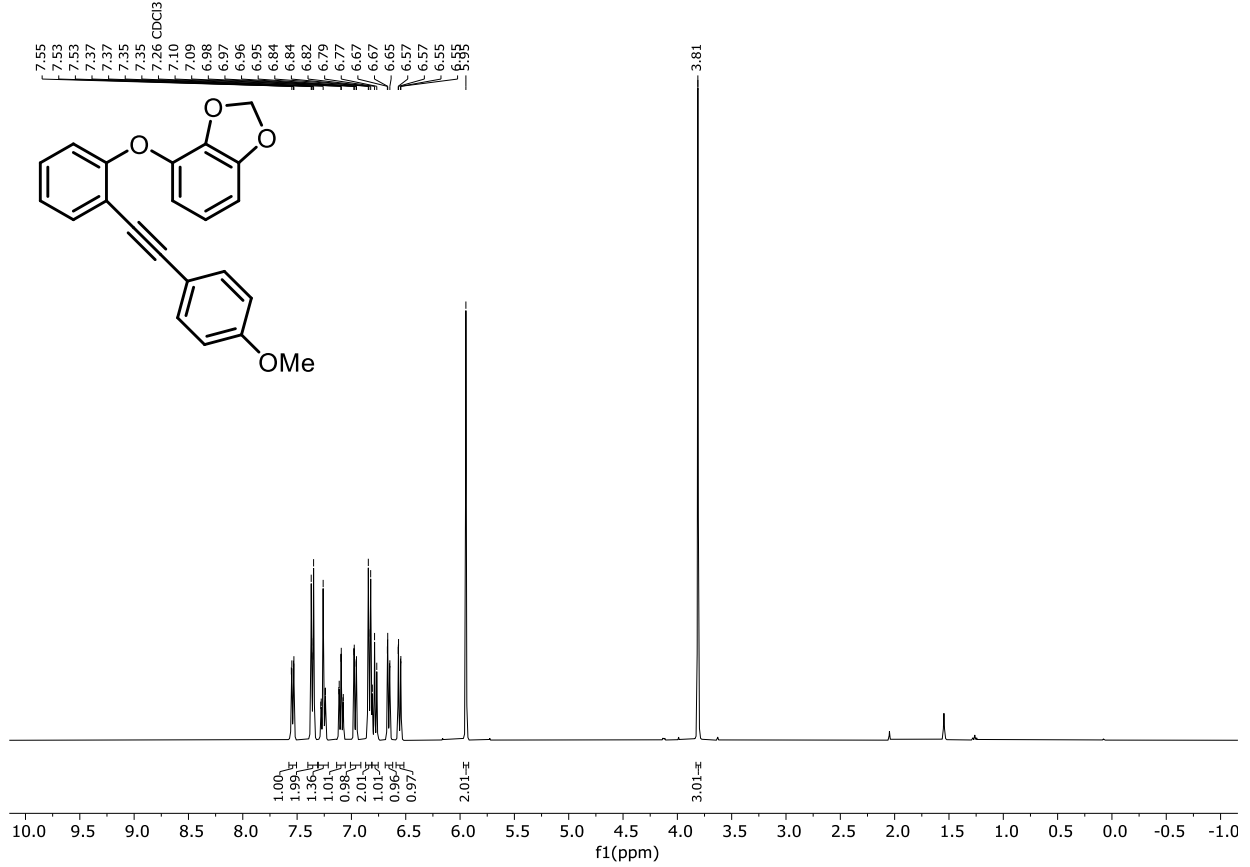


### $^{13}\text{C}\{^1\text{H}\}$ -NMR (151 MHz, $\text{CDCl}_3$ ) Compound **151g**

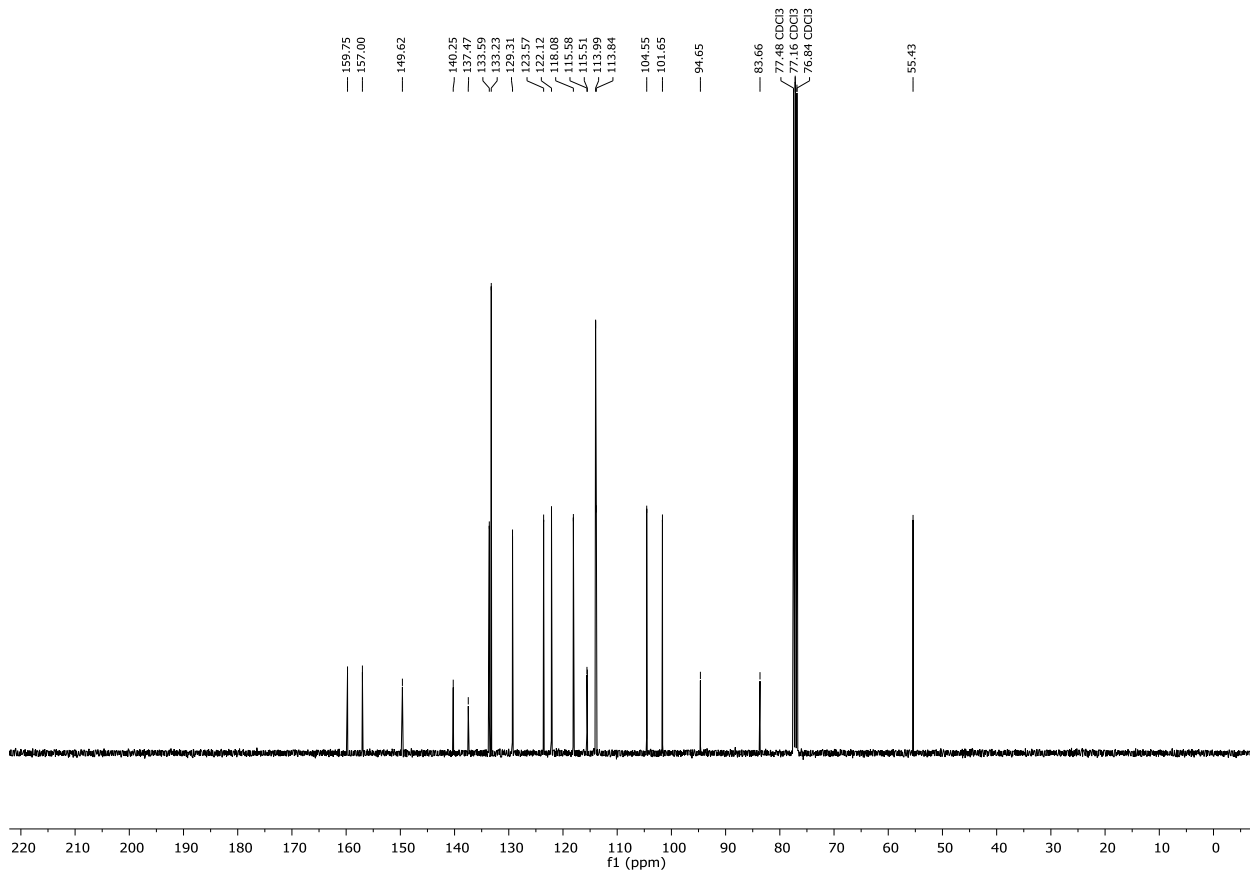


## 7.2 NMR spectra

### $^1\text{H-NMR}$ (400 MHz, $\text{CDCl}_3$ ) Compound **146h**

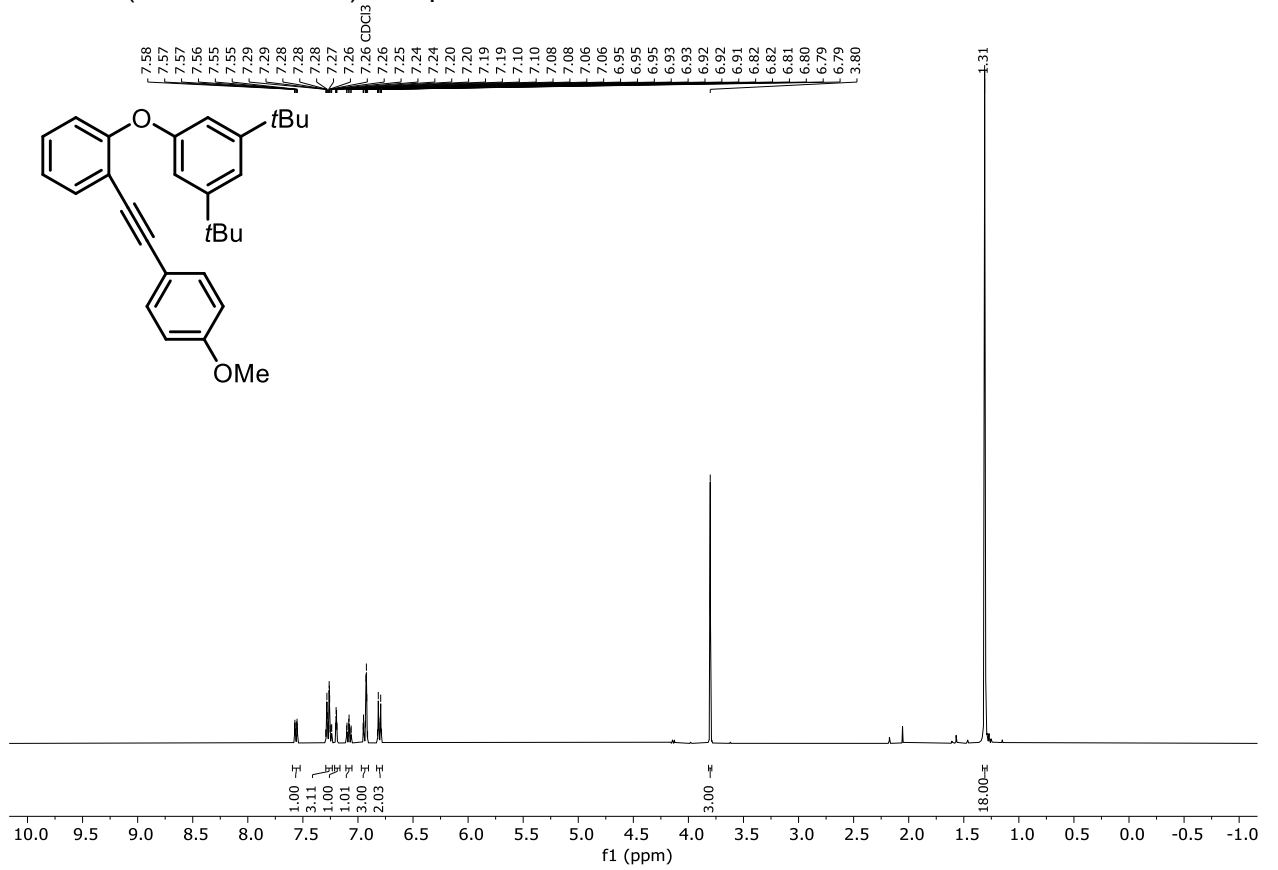


### $^{13}\text{C}\{^1\text{H}\}$ -NMR (101 MHz, $\text{CDCl}_3$ ) Compound **146h**

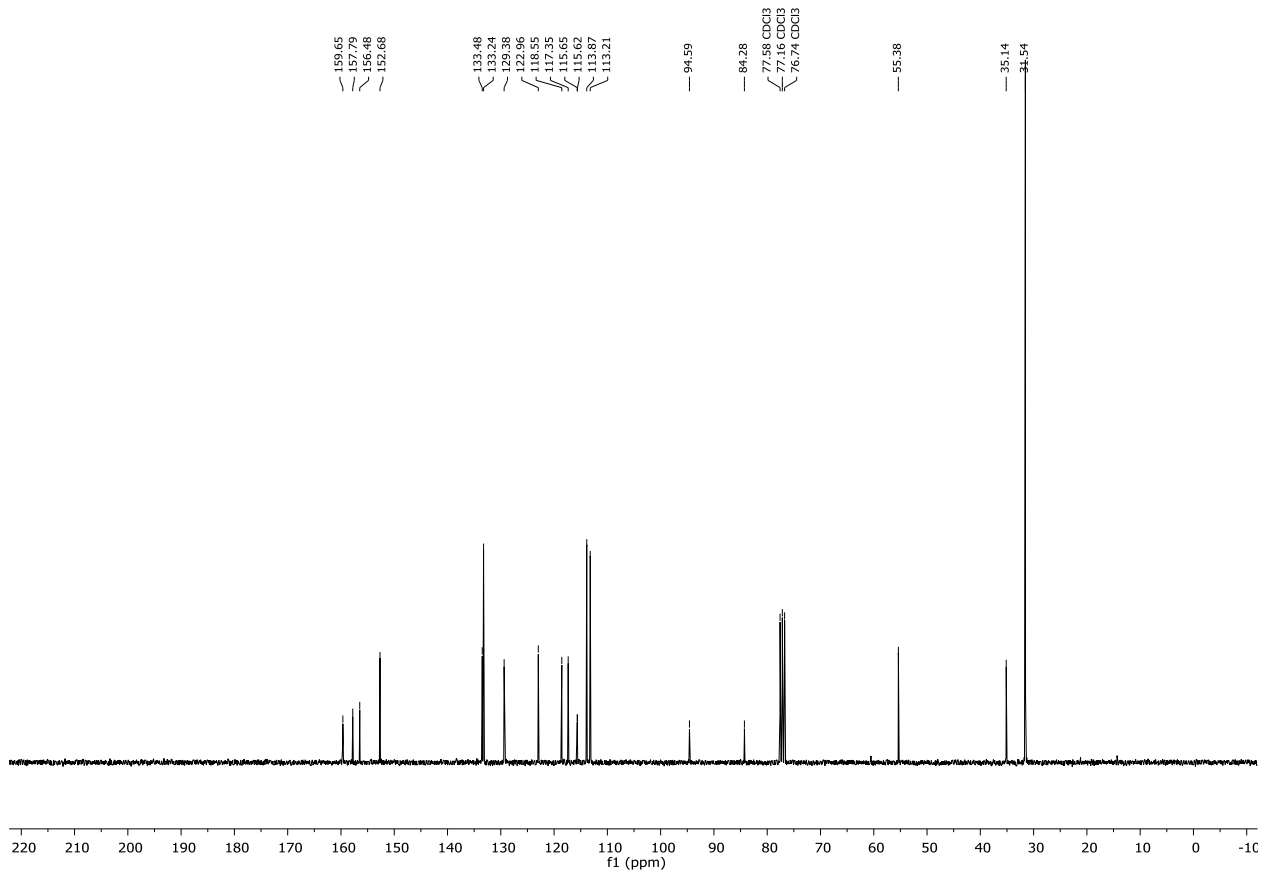


## 7. Appendix

### <sup>1</sup>H-NMR (400 MHz, CDCl<sub>3</sub>) Compound **146i**



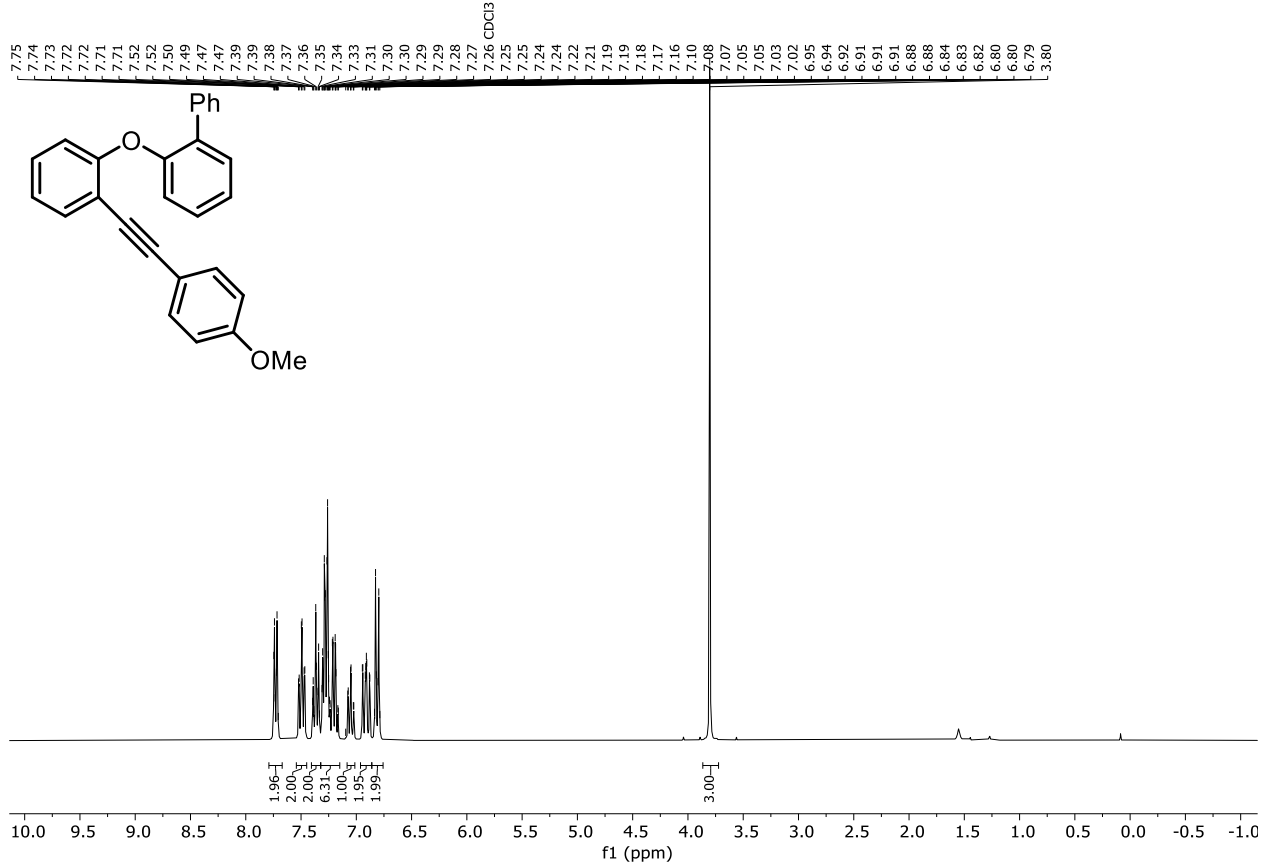
### <sup>13</sup>C{<sup>1</sup>H}-NMR (75 MHz, CDCl<sub>3</sub>) Compound **146i**



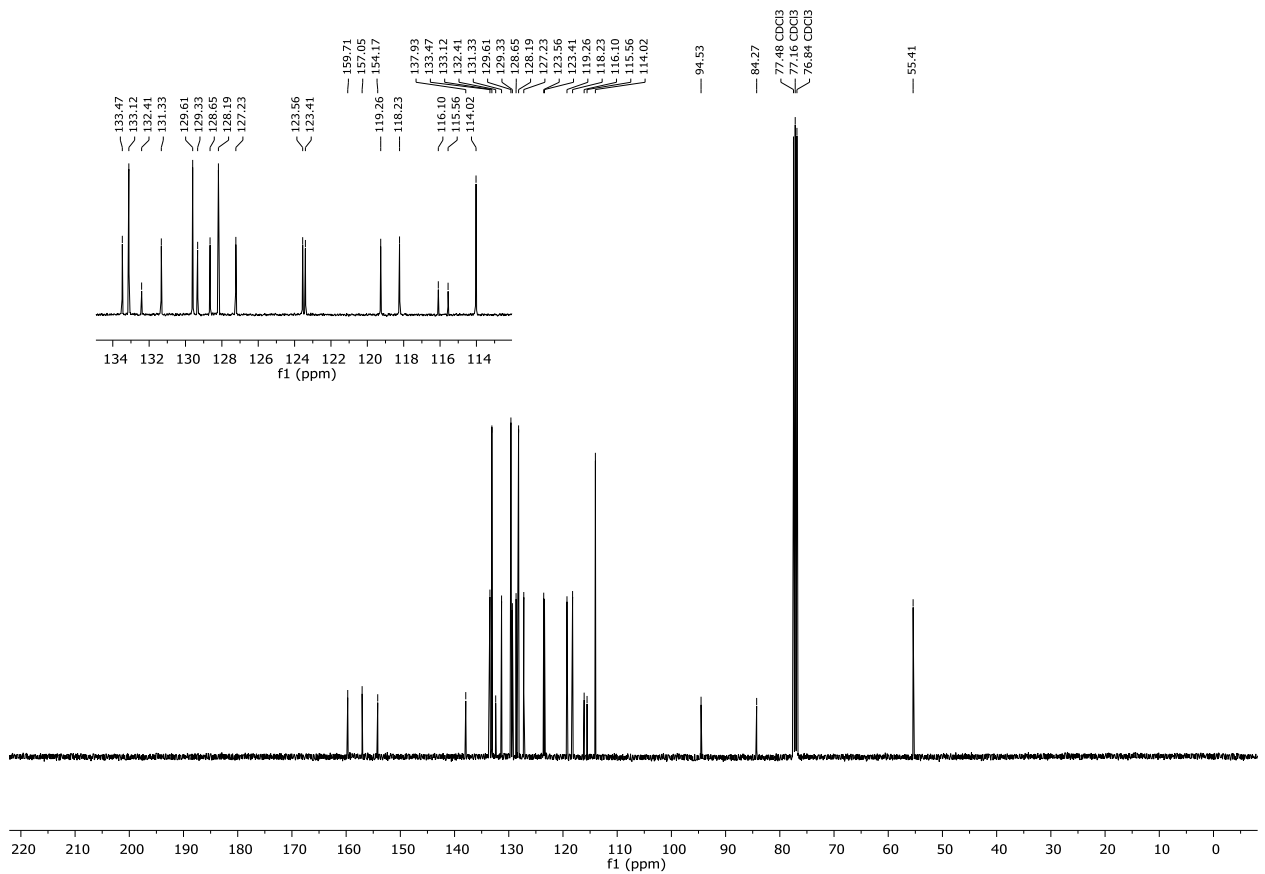


## 7.2 NMR spectra

### $^1\text{H-NMR}$ (300 MHz, $\text{CDCl}_3$ ) Compound **146j**

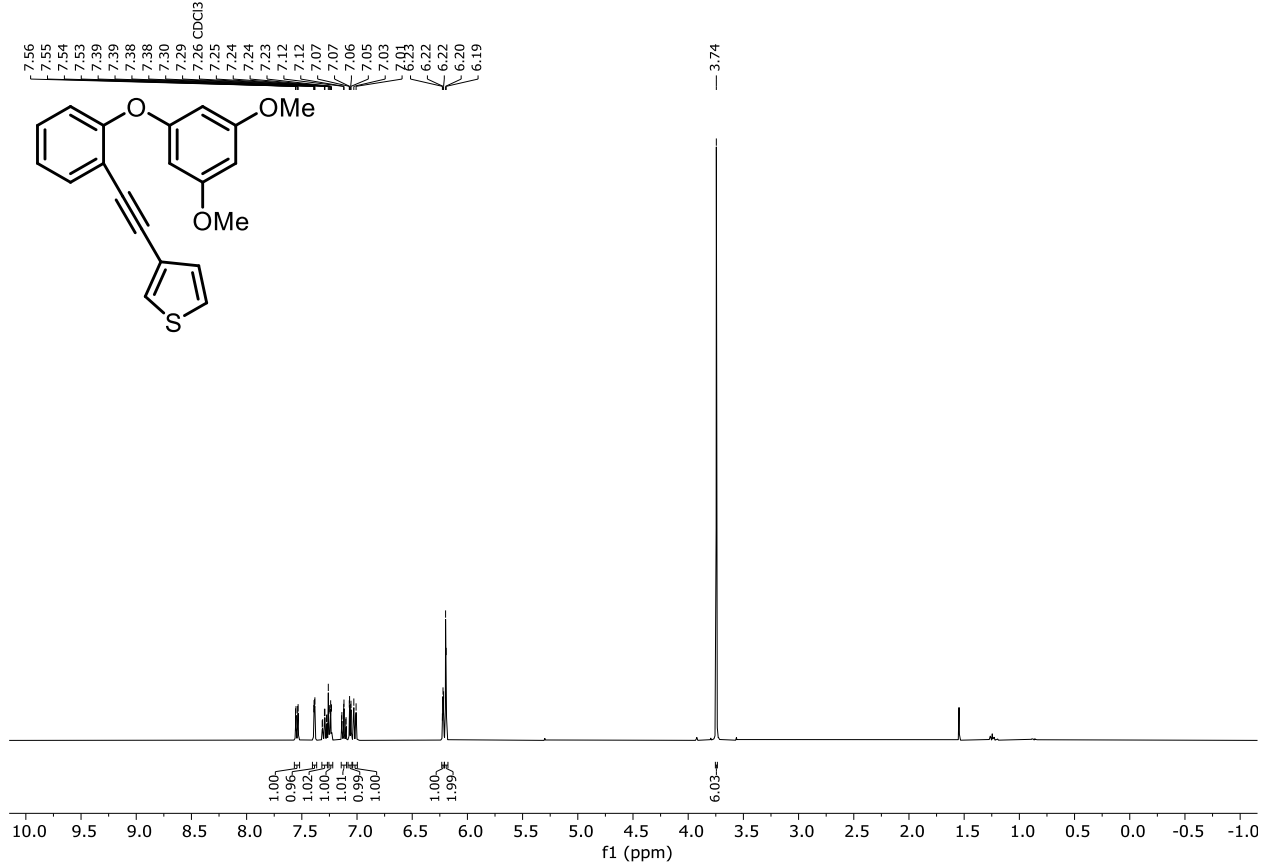


### $^{13}\text{C}\{^1\text{H}\}$ -NMR (101 MHz, $\text{CDCl}_3$ ) Compound **146j**

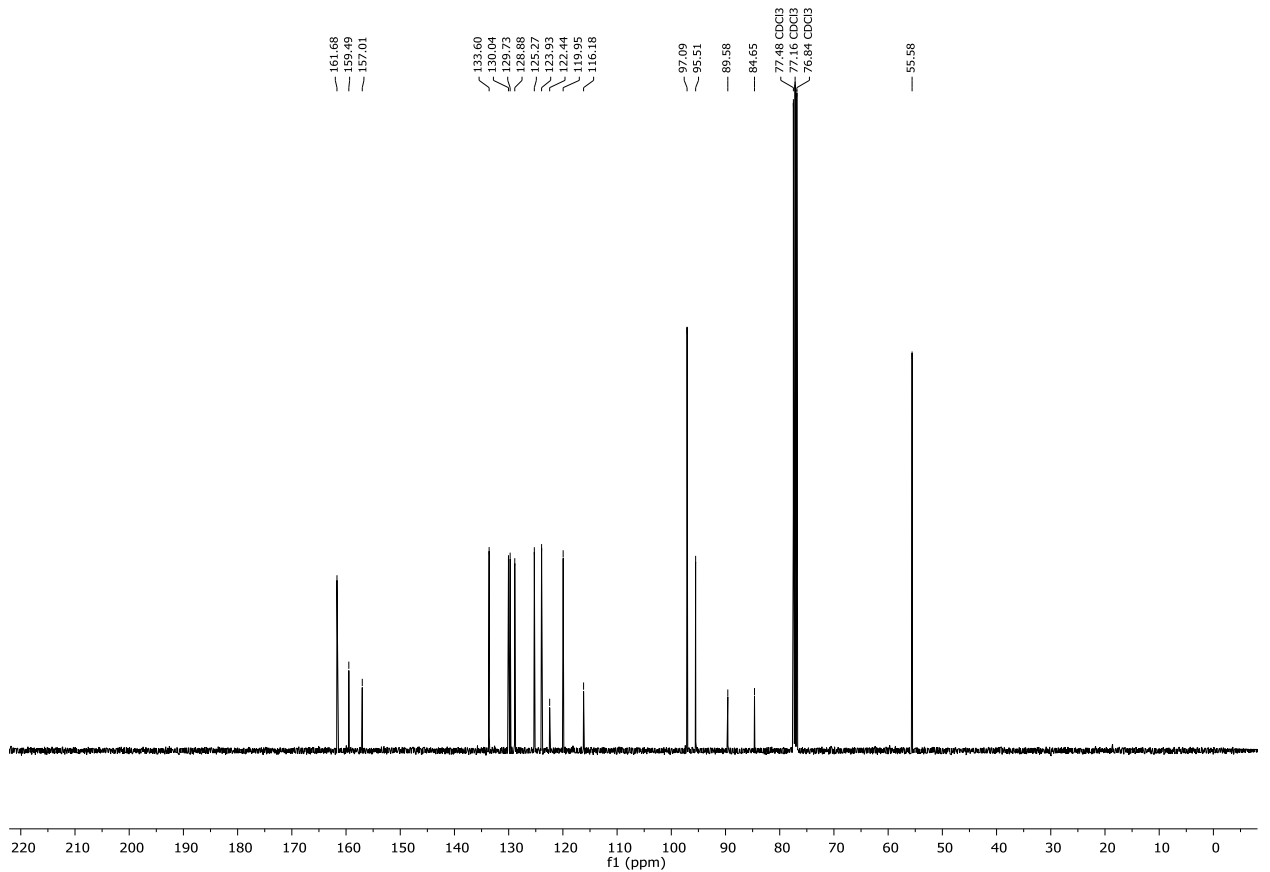


7. Appendix

<sup>1</sup>H-NMR (400 MHz, CDCl<sub>3</sub>) Compound **151k**

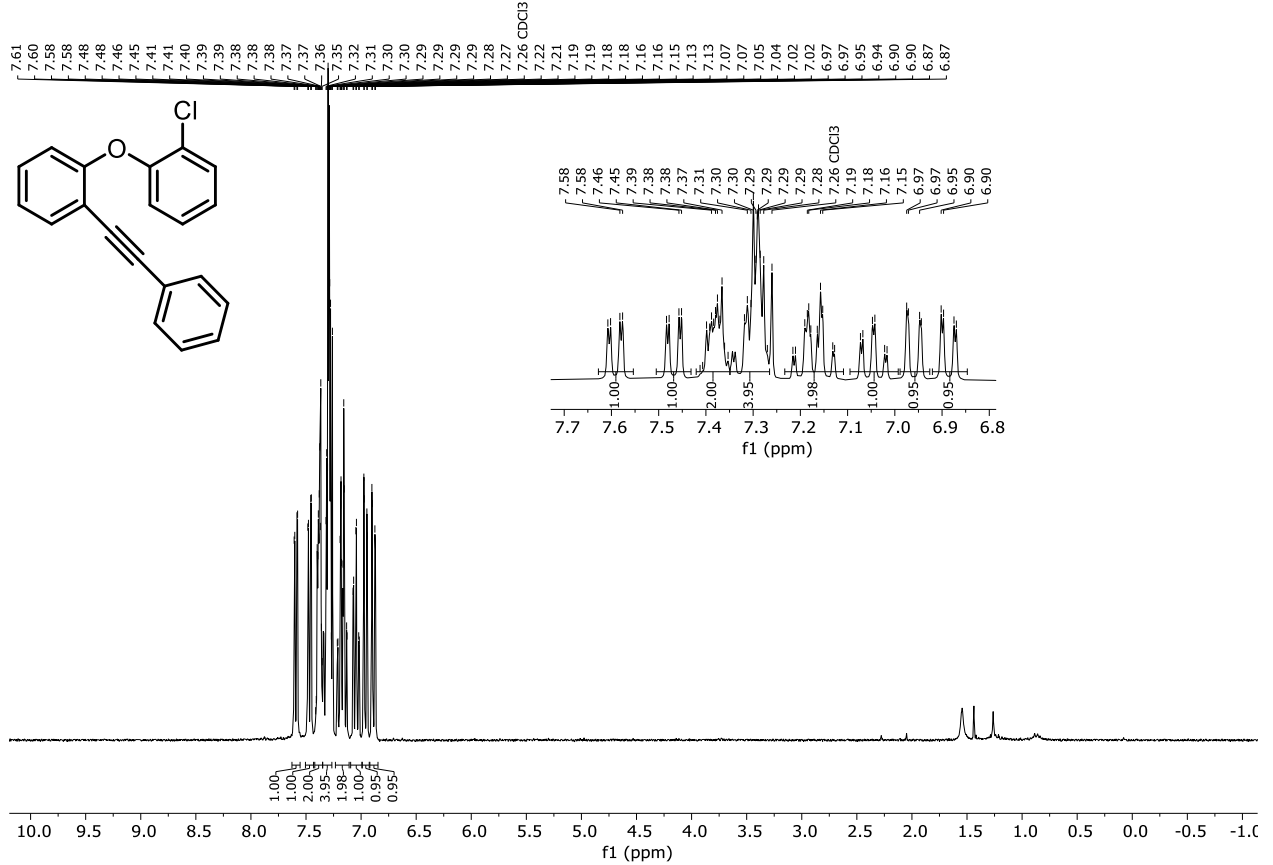


<sup>13</sup>C{<sup>1</sup>H}-NMR (101 MHz, CDCl<sub>3</sub>) Compound **151k**

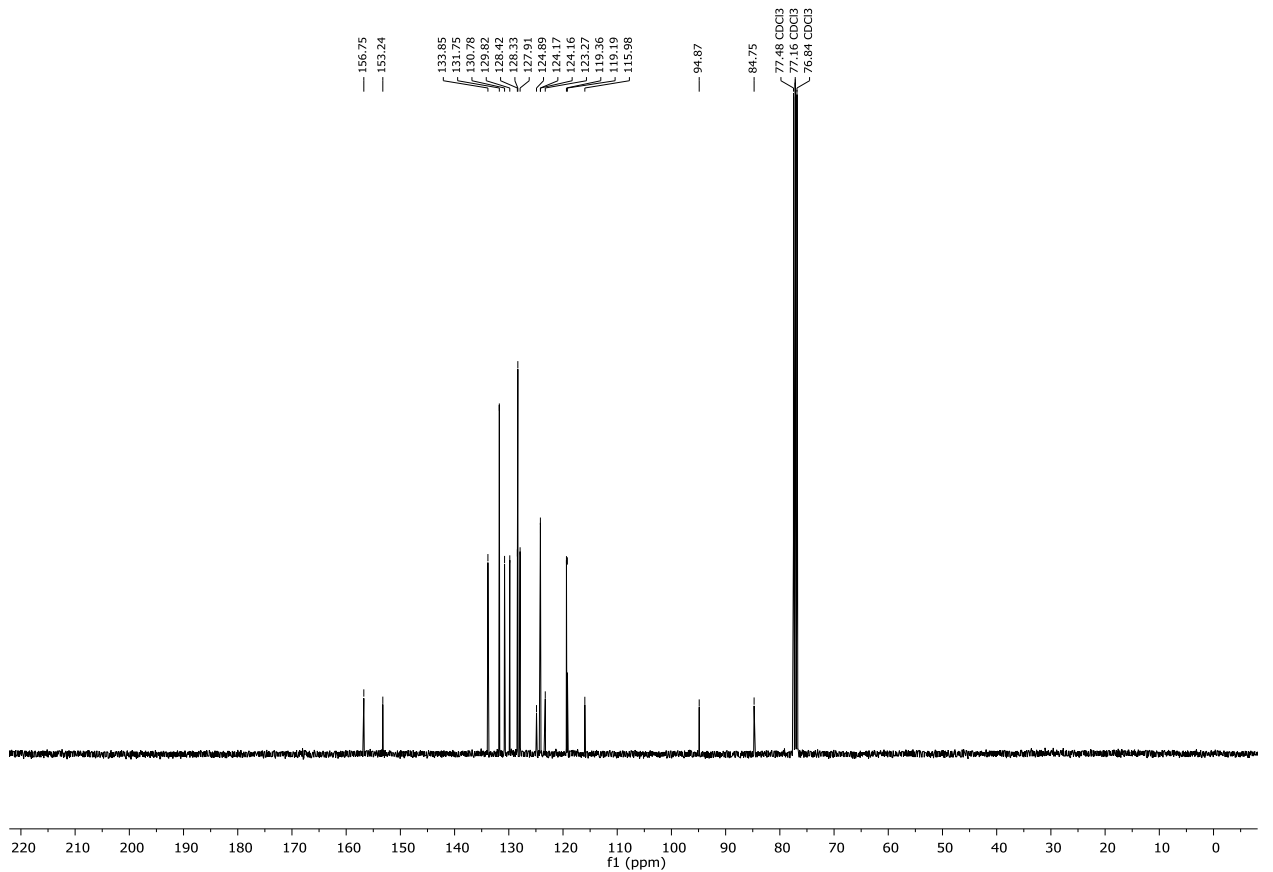


## 7.2 NMR spectra

### <sup>1</sup>H-NMR (400 MHz, CDCl<sub>3</sub>) Compound **151I**

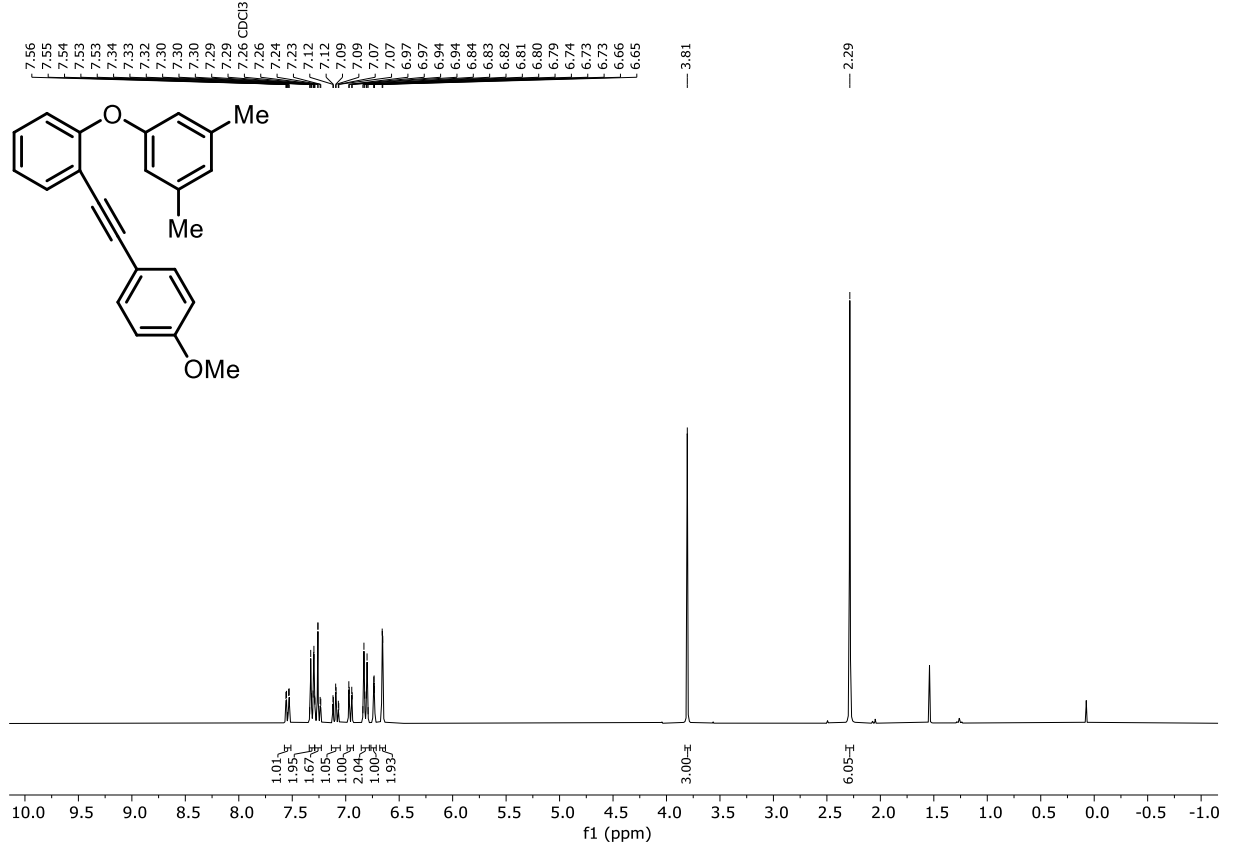


### <sup>13</sup>C{<sup>1</sup>H}-NMR (101 MHz, CDCl<sub>3</sub>) Compound **151I**

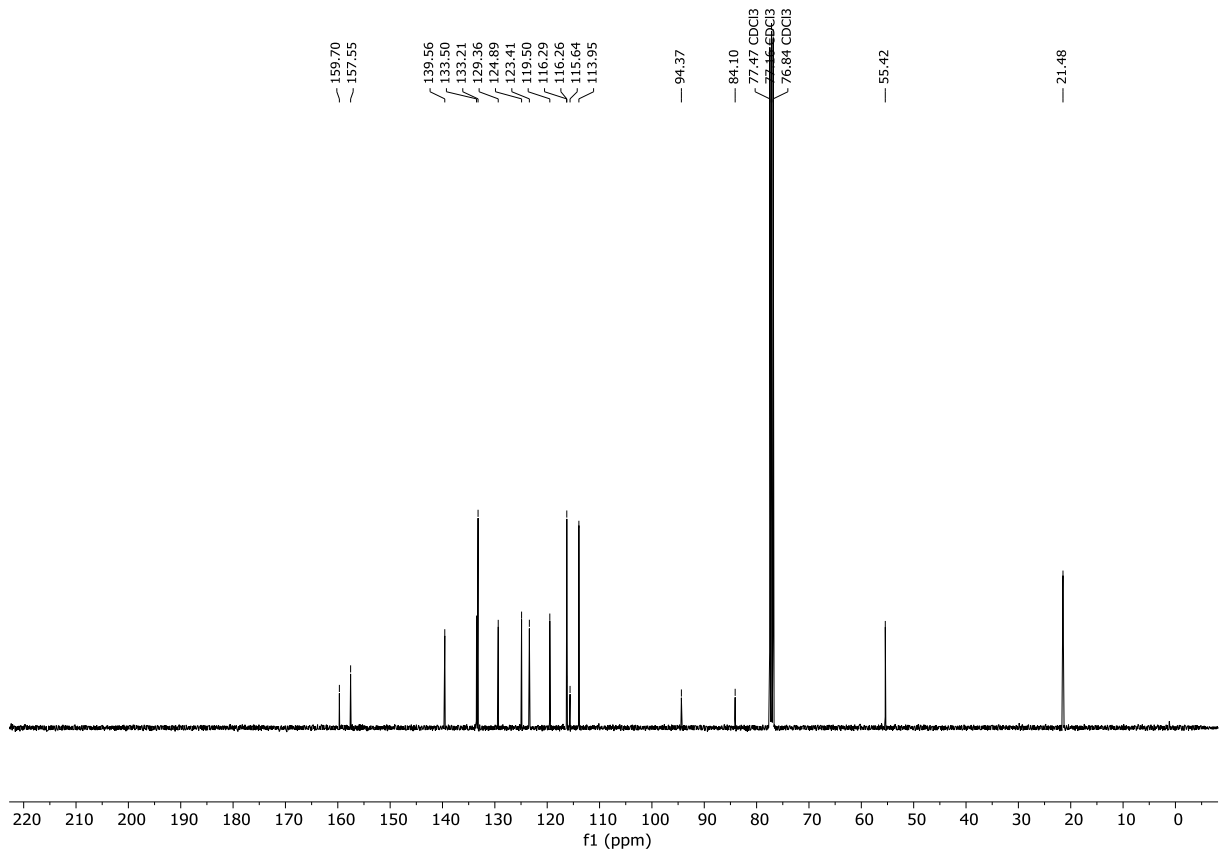


## 7. Appendix

### $^1\text{H-NMR}$ (300 MHz, $\text{CDCl}_3$ ) Compound **151m**

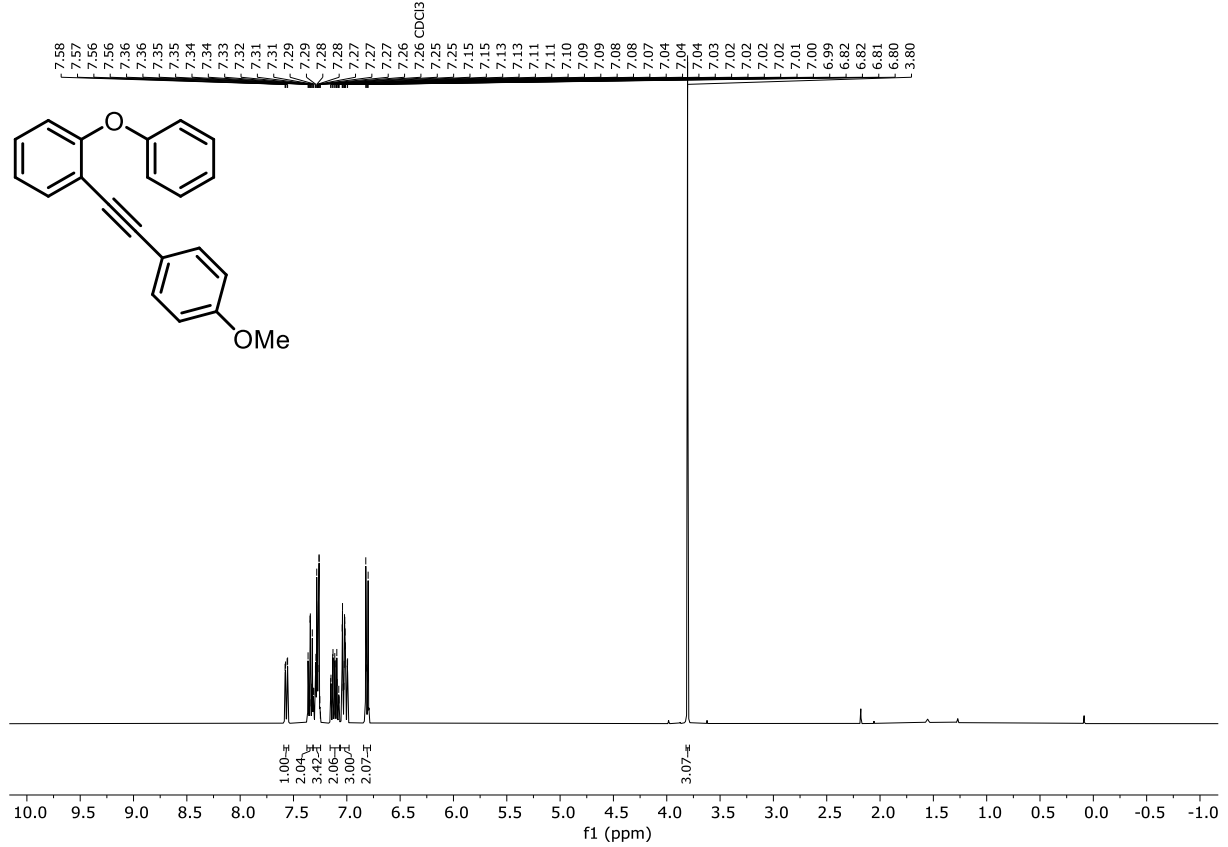


### $^{13}\text{C}\{^1\text{H}\}$ -NMR (101 MHz, $\text{CDCl}_3$ ) Compound **151m**

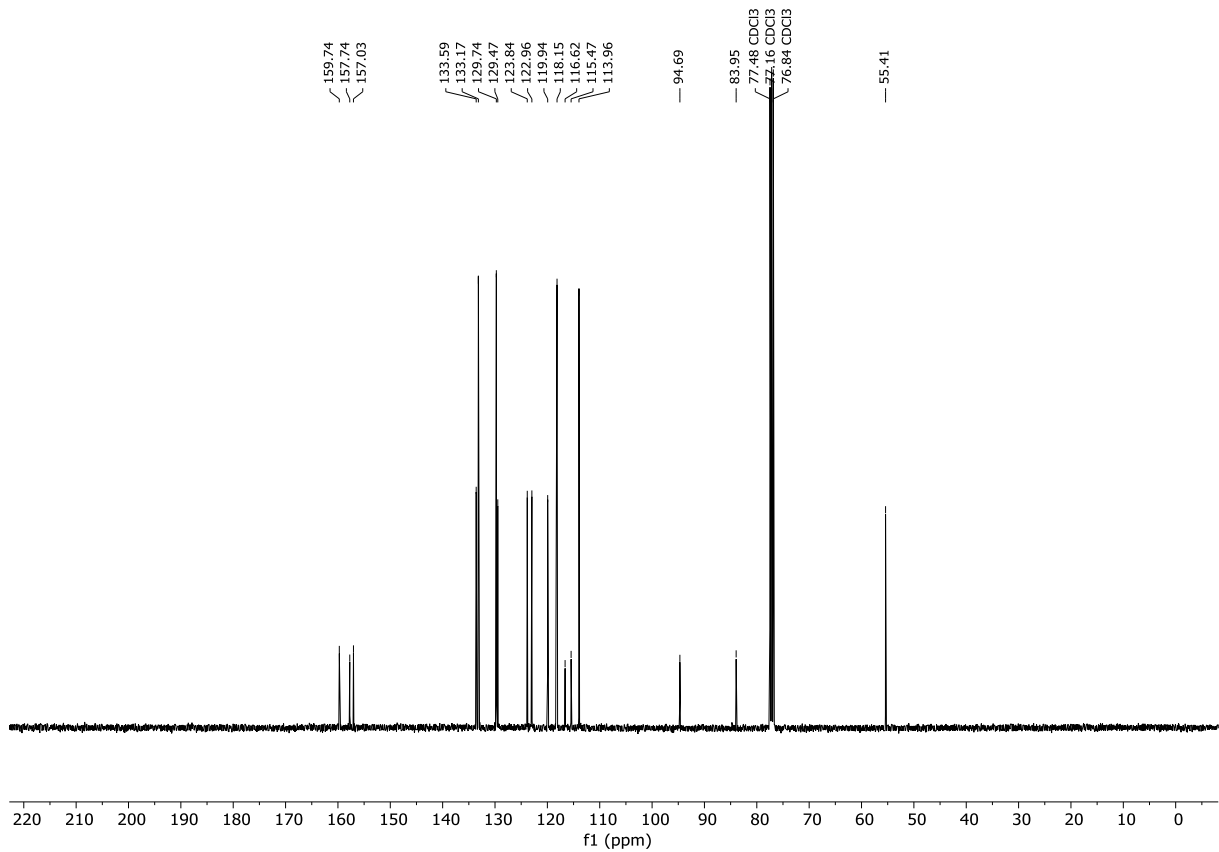


## 7.2 NMR spectra

### $^1\text{H-NMR}$ (400 MHz, $\text{CDCl}_3$ ) Compound **151n**

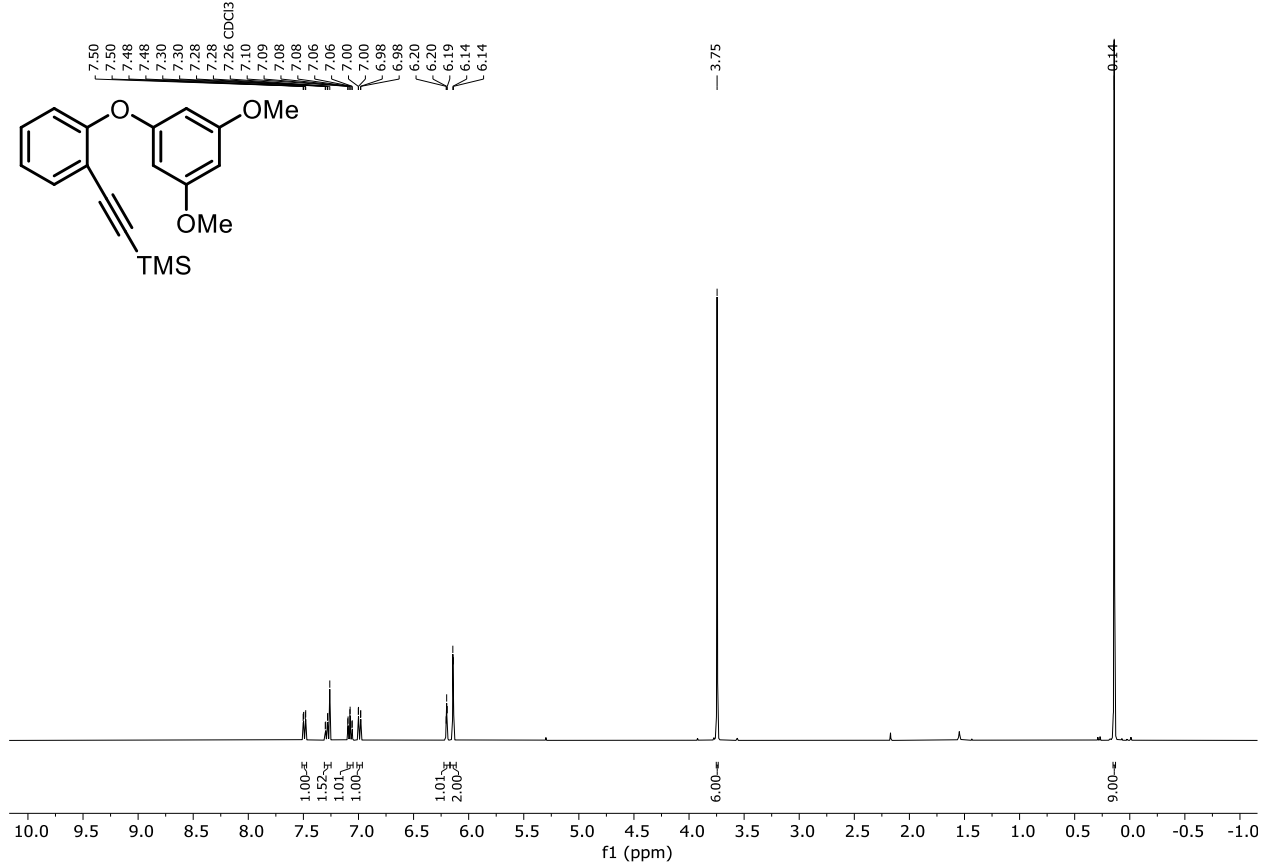


### $^{13}\text{C}\{^1\text{H}\}$ -NMR (101 MHz, $\text{CDCl}_3$ ) Compound **151n**

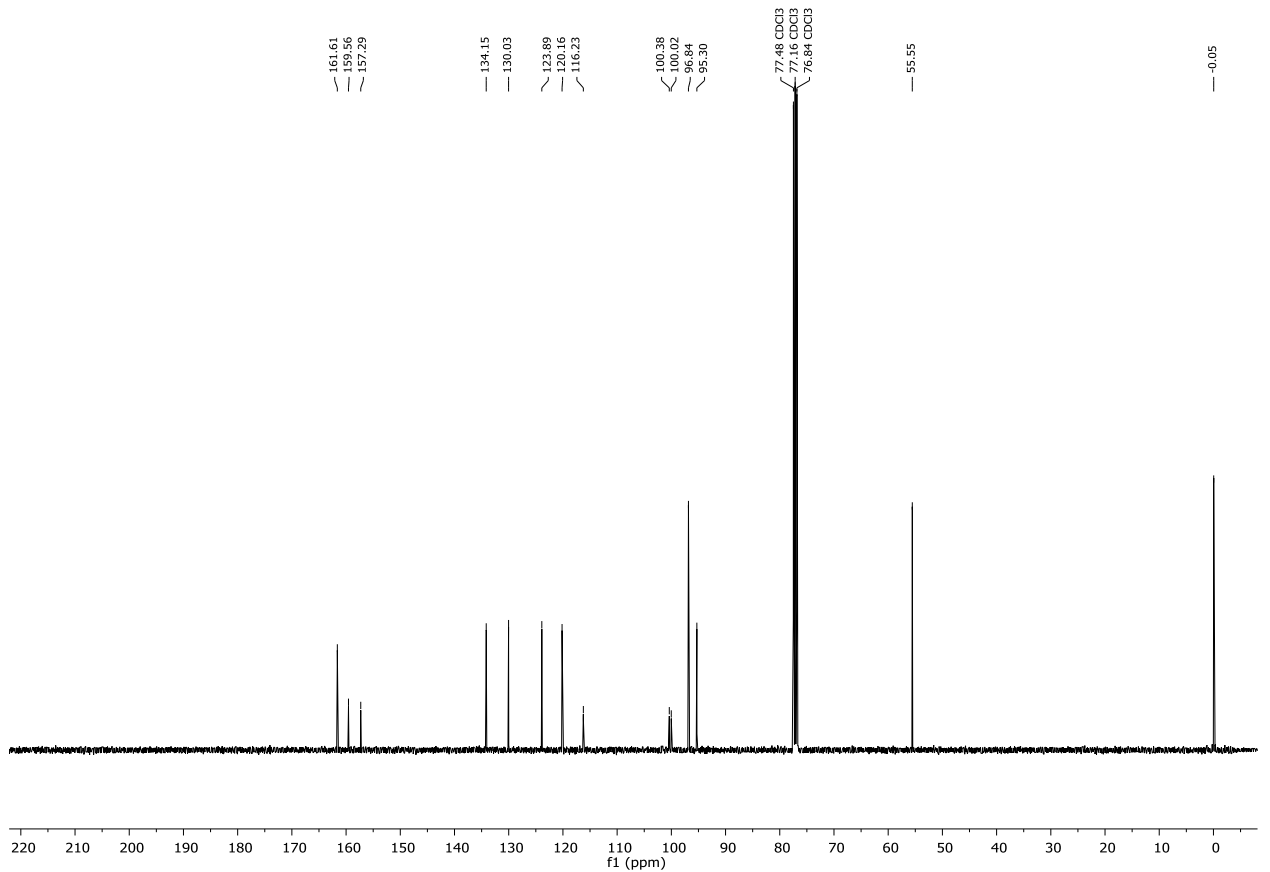


7. Appendix

$^1\text{H-NMR}$  (400 MHz,  $\text{CDCl}_3$ ) Compound **151o**

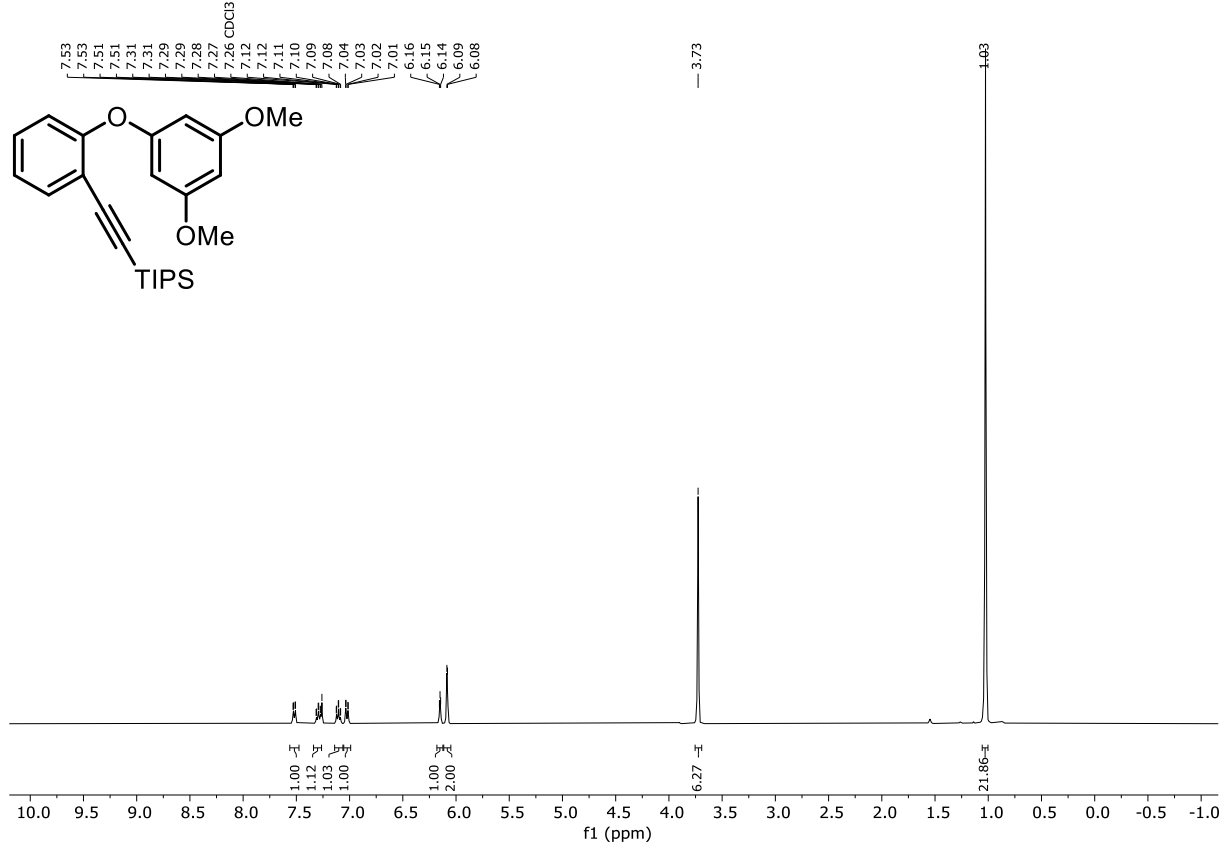


$^{13}\text{C}\{^1\text{H}\}$ -NMR (101 MHz,  $\text{CDCl}_3$ ) Compound **151o**

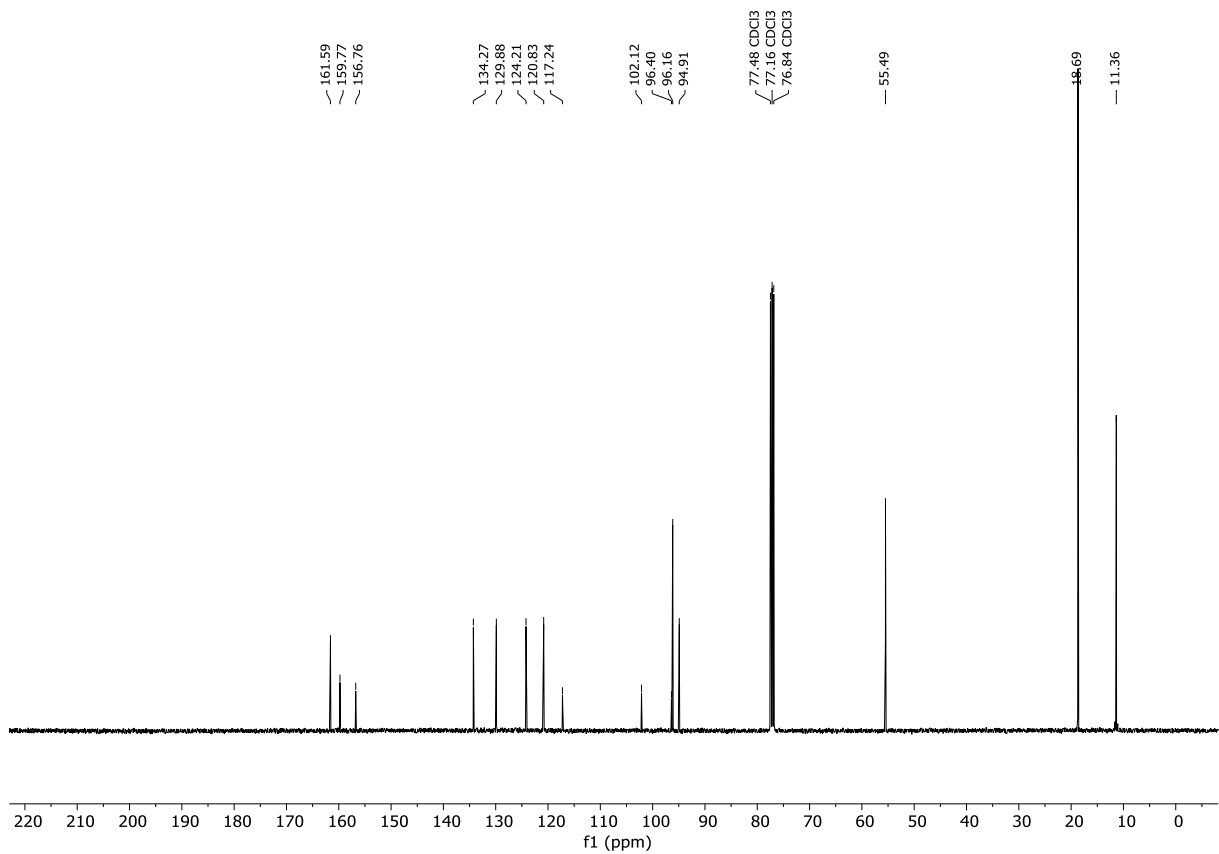


## 7.2 NMR spectra

### $^1\text{H-NMR}$ (400 MHz, $\text{CDCl}_3$ ) Compound **151p**

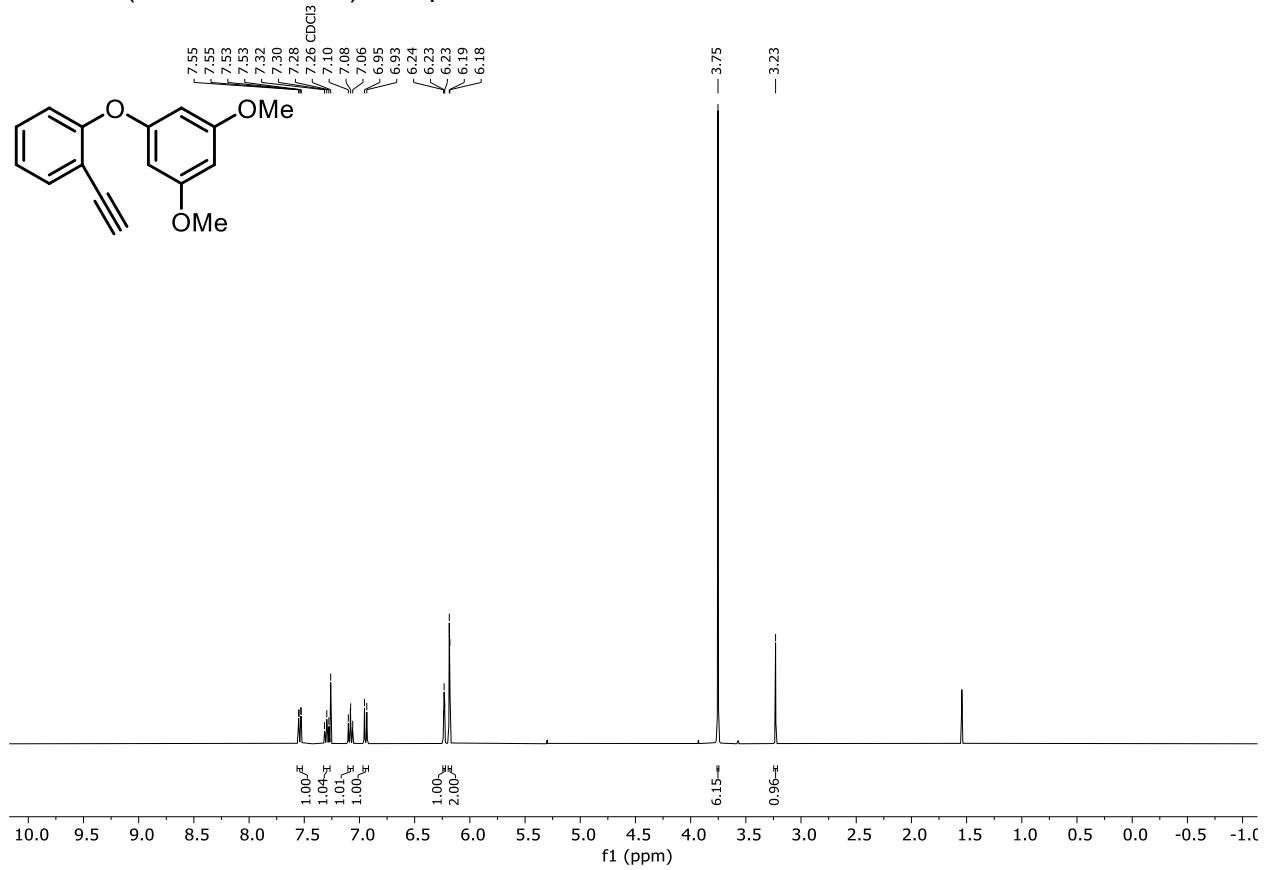


### $^{13}\text{C}\{^1\text{H}\}$ -NMR (101 MHz, $\text{CDCl}_3$ ) Compound **151p**

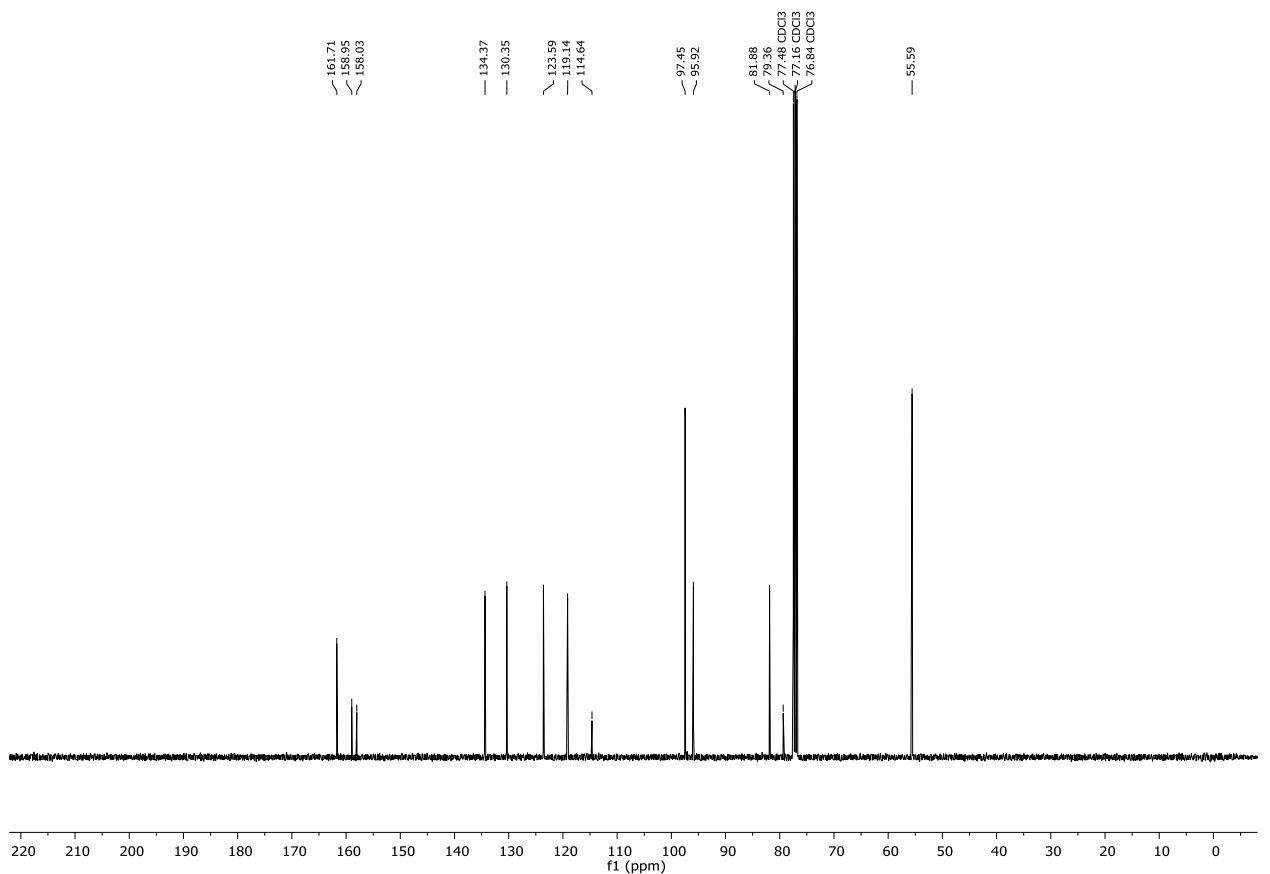


## 7. Appendix

### $^1\text{H-NMR}$ (400 MHz, $\text{CDCl}_3$ ) Compound **174**



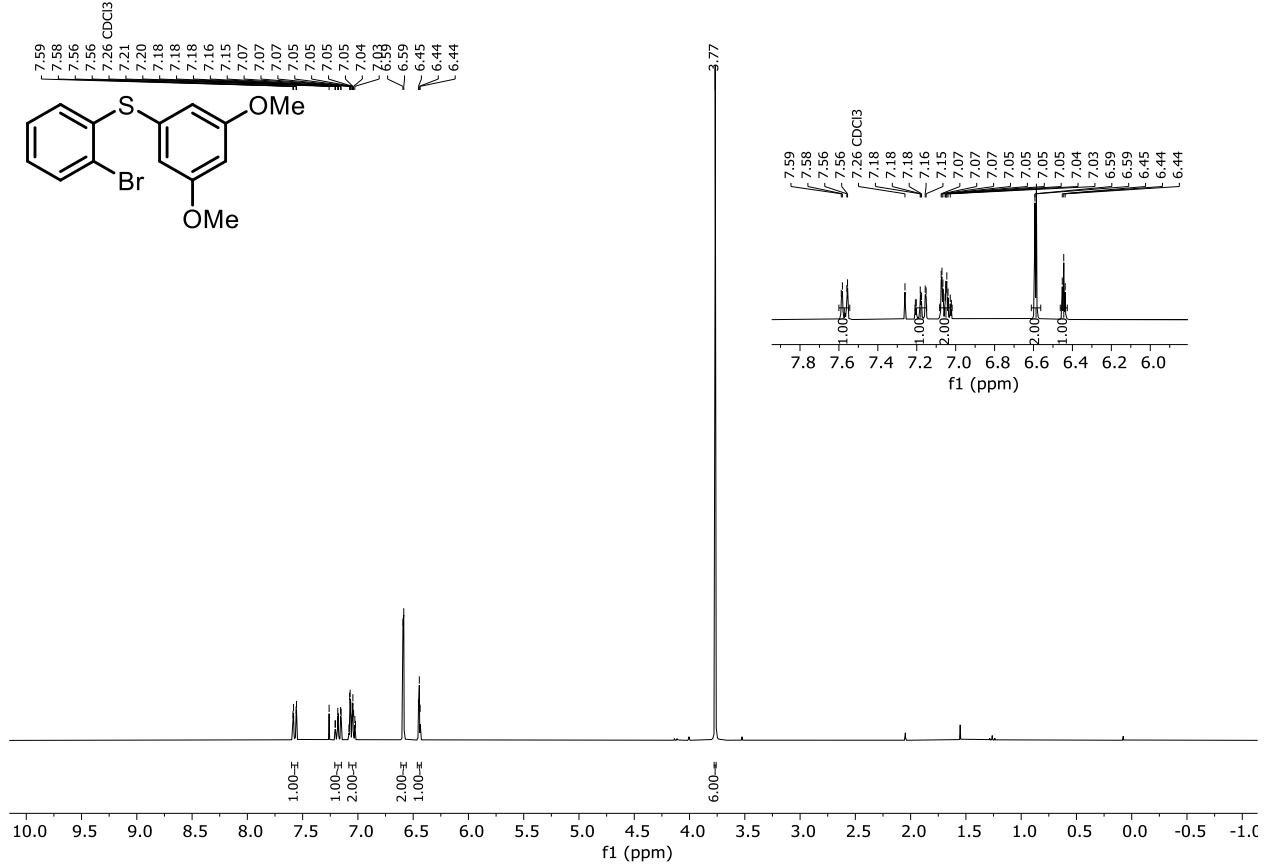
### $^{13}\text{C}\{^1\text{H}\}$ -NMR (101 MHz, $\text{CDCl}_3$ ) Compound **174**



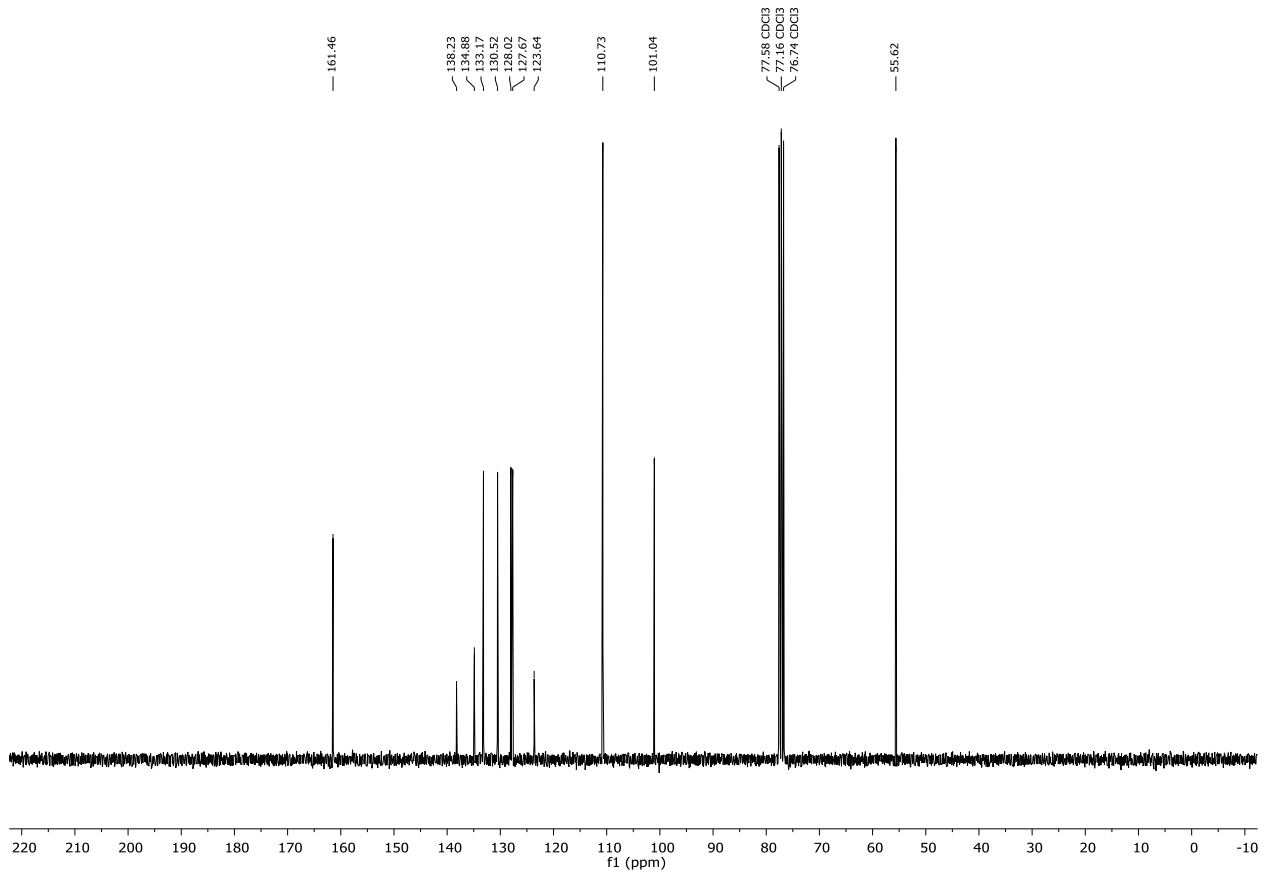


## 7.2 NMR spectra

$^1\text{H-NMR}$  (300 MHz,  $\text{CDCl}_3$ ) Compound **177a**

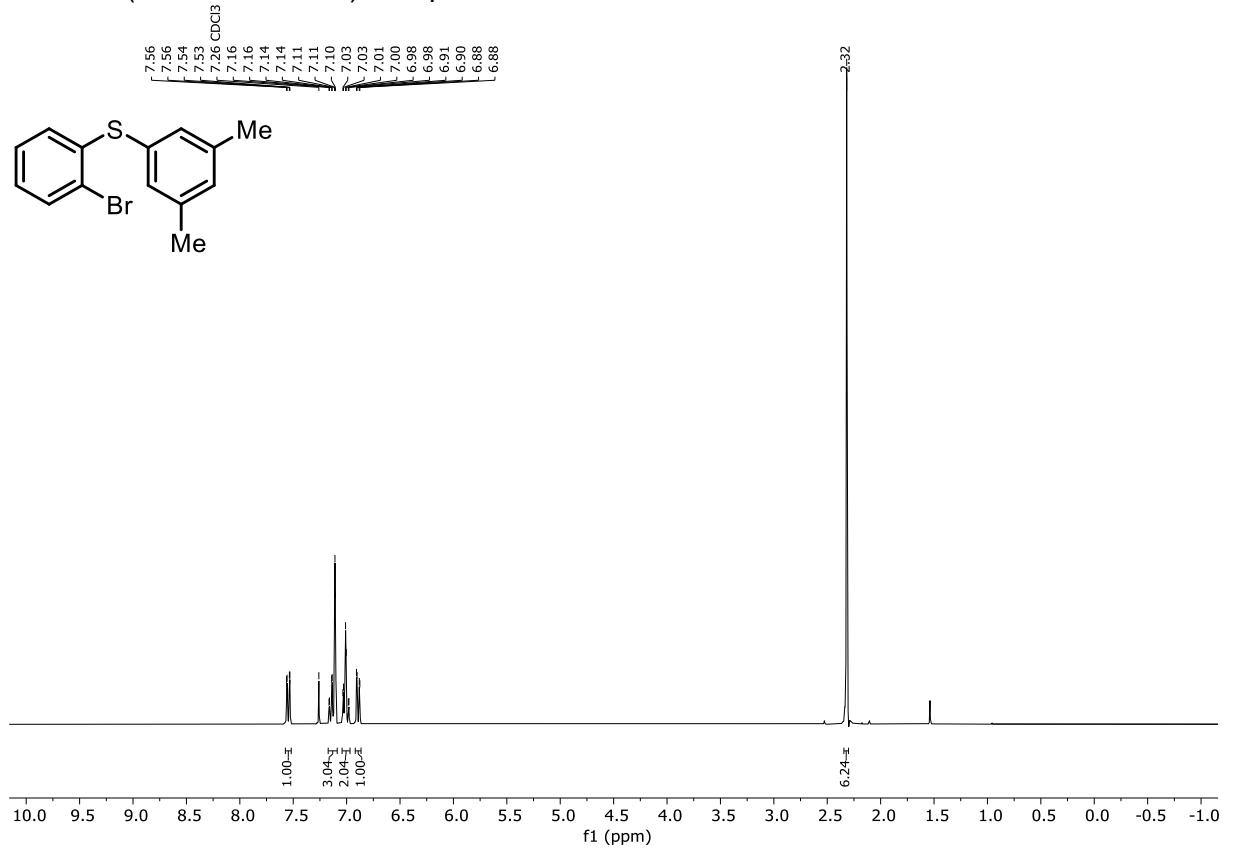


$^{13}\text{C}\{^1\text{H}\}$ -NMR (75 MHz,  $\text{CDCl}_3$ ) Compound **177a**

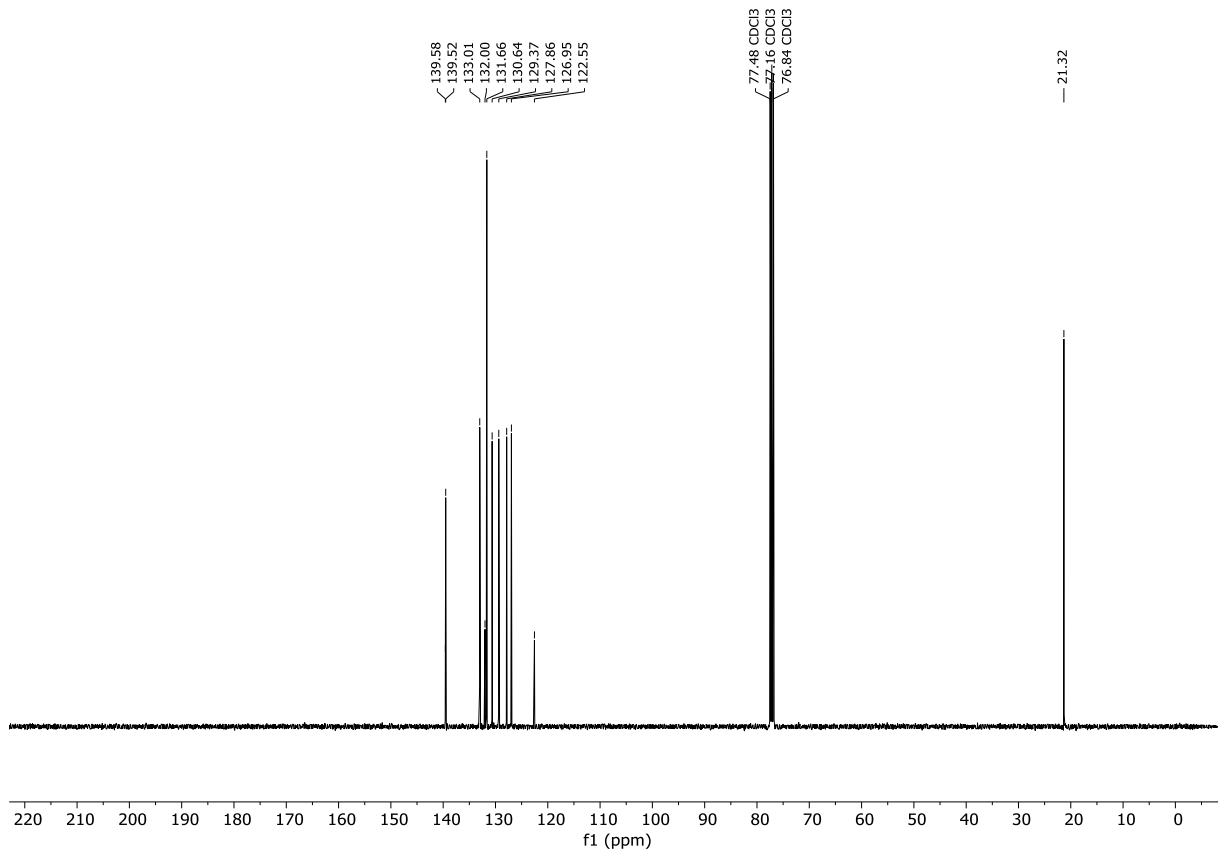


## 7. Appendix

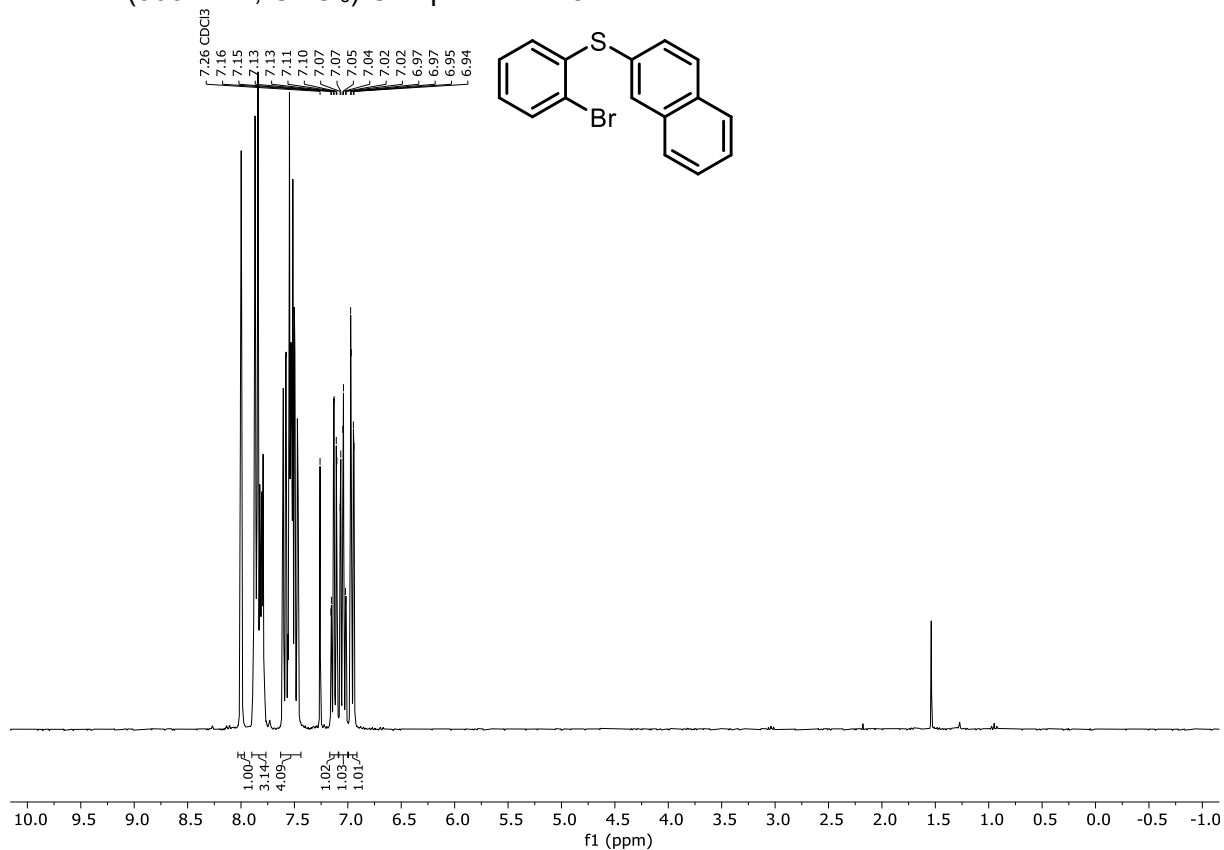
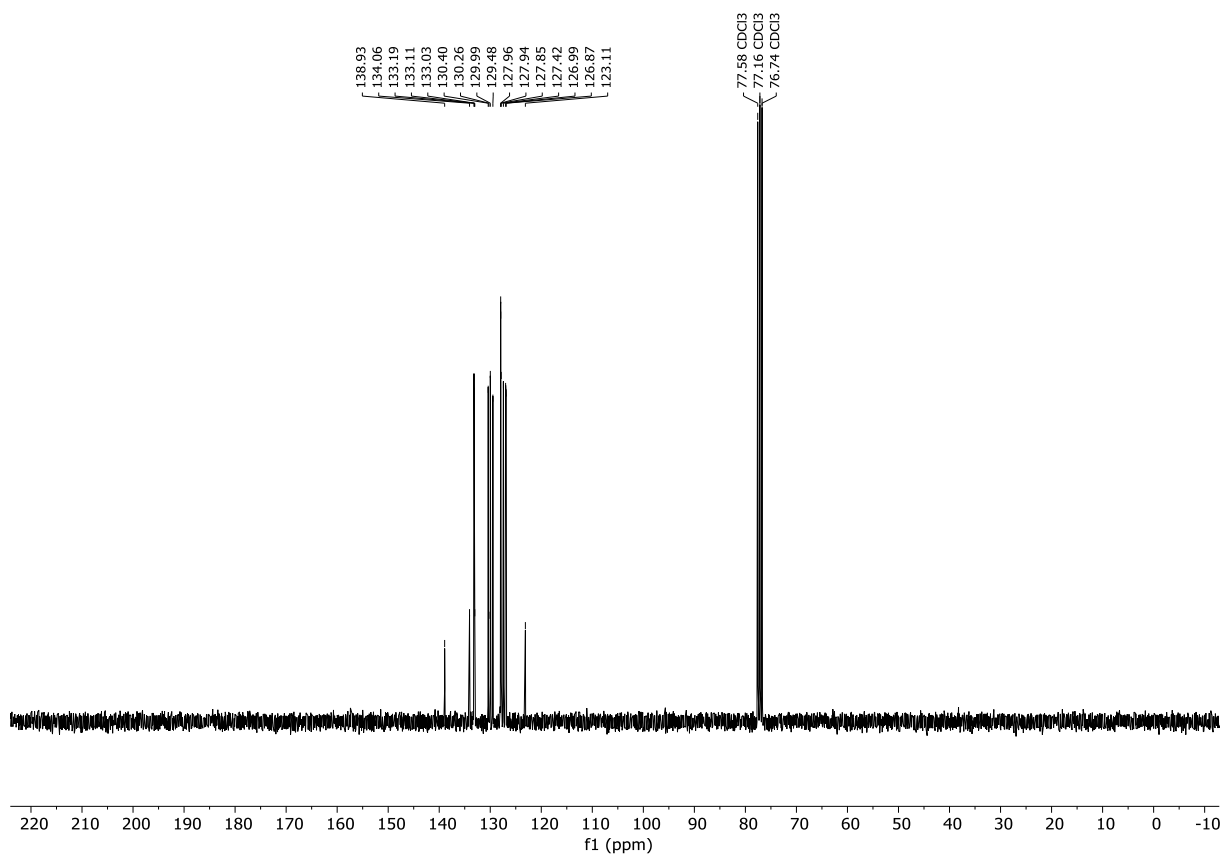
### $^1\text{H-NMR}$ (300 MHz, $\text{CDCl}_3$ ) Compound **177b**



### $^{13}\text{C}\{^1\text{H}\}\text{-NMR}$ (101 MHz, $\text{CDCl}_3$ ) Compound **177b**

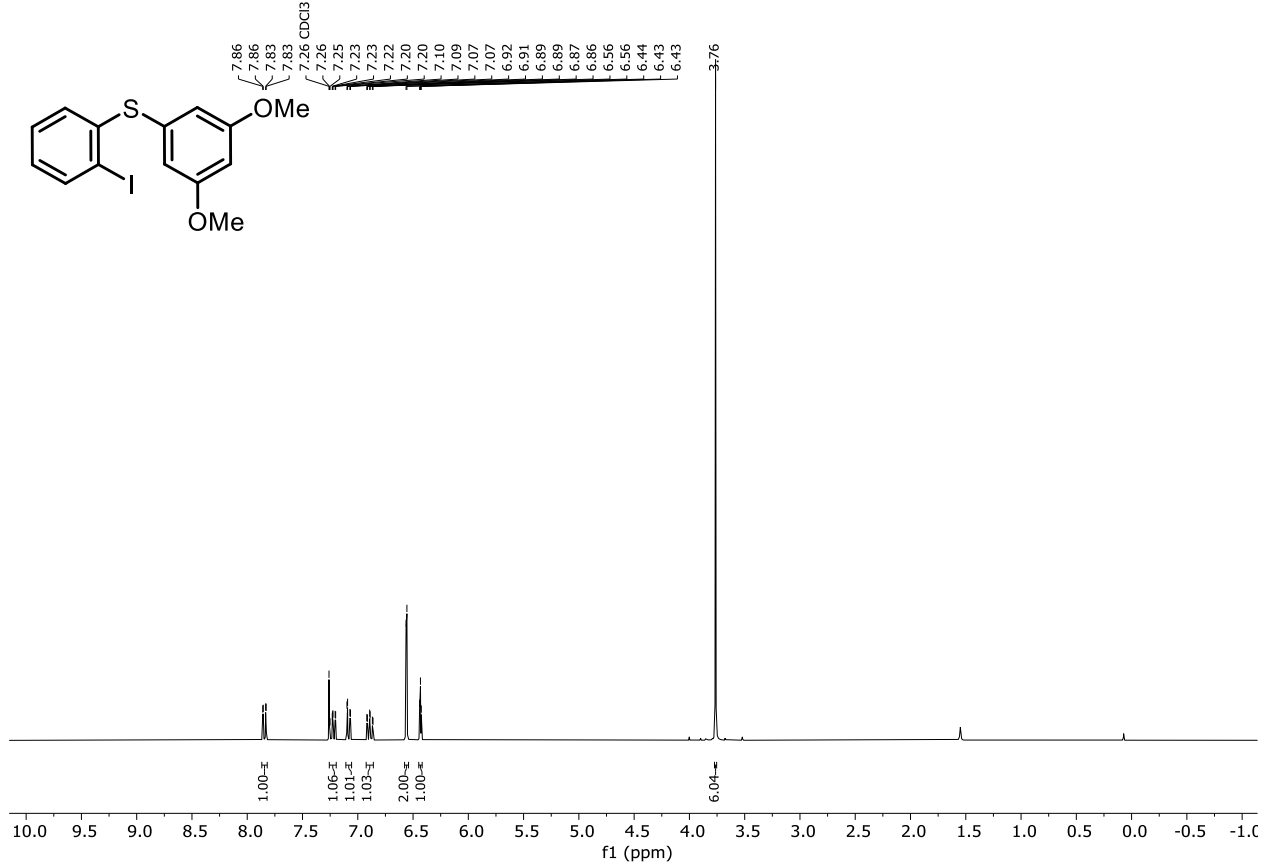


## 7.2 NMR spectra

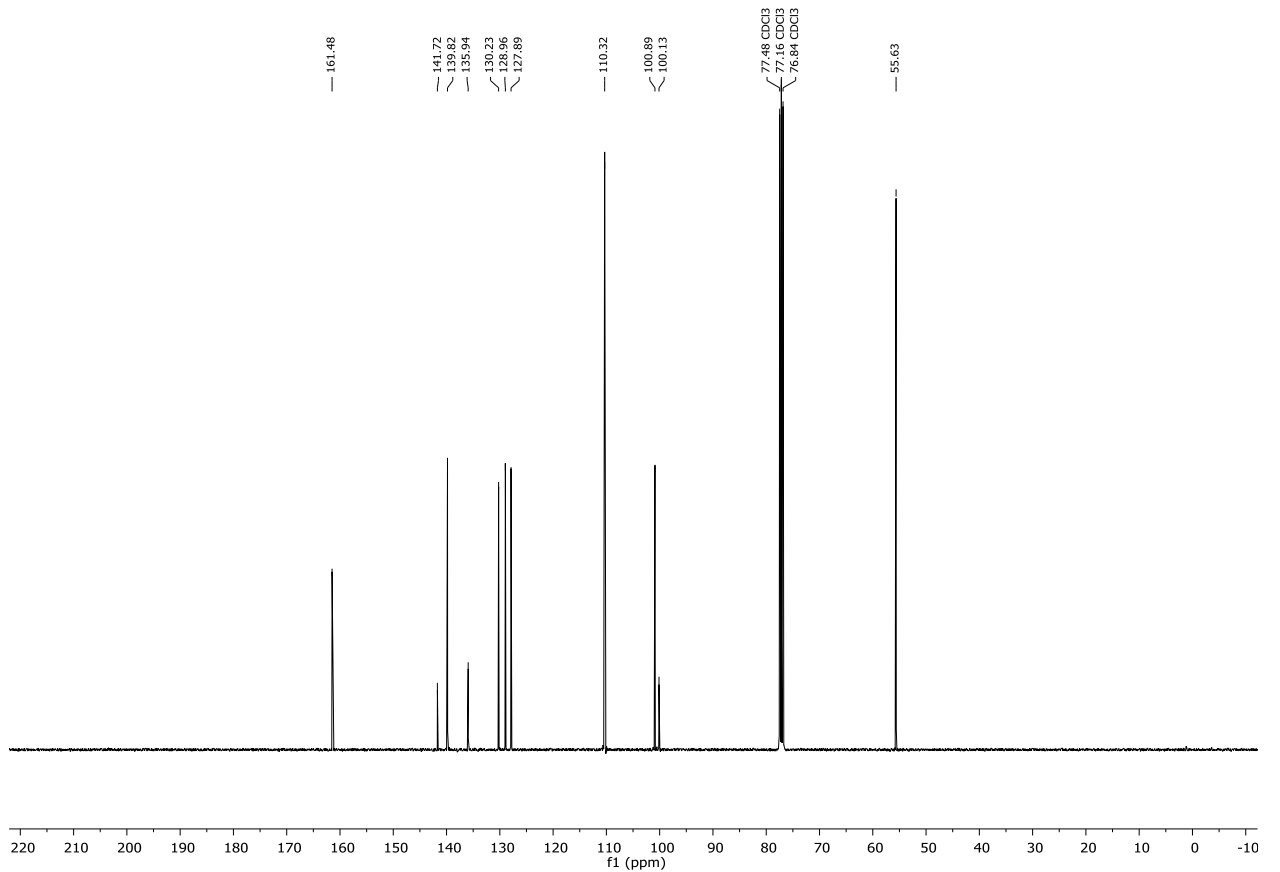
 $^1\text{H-NMR}$  (300 MHz,  $\text{CDCl}_3$ ) Compound **177c** $^{13}\text{C}\{^1\text{H}\}$ -NMR (75 MHz,  $\text{CDCl}_3$ ) Compound **177c**

## 7. Appendix

### <sup>1</sup>H-NMR (300 MHz, CDCl<sub>3</sub>) Compound **178a**

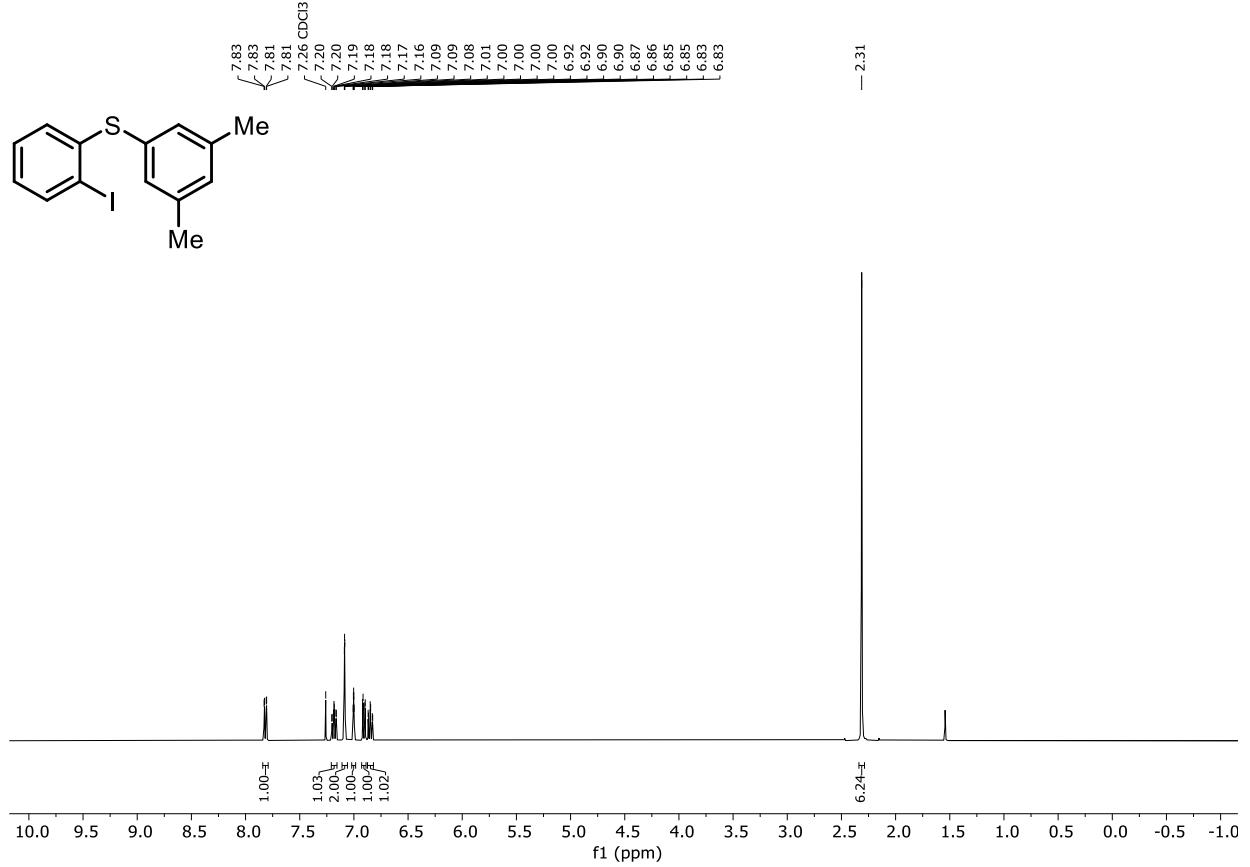


### <sup>13</sup>C{<sup>1</sup>H}-NMR (101 MHz, CDCl<sub>3</sub>) Compound **178a**

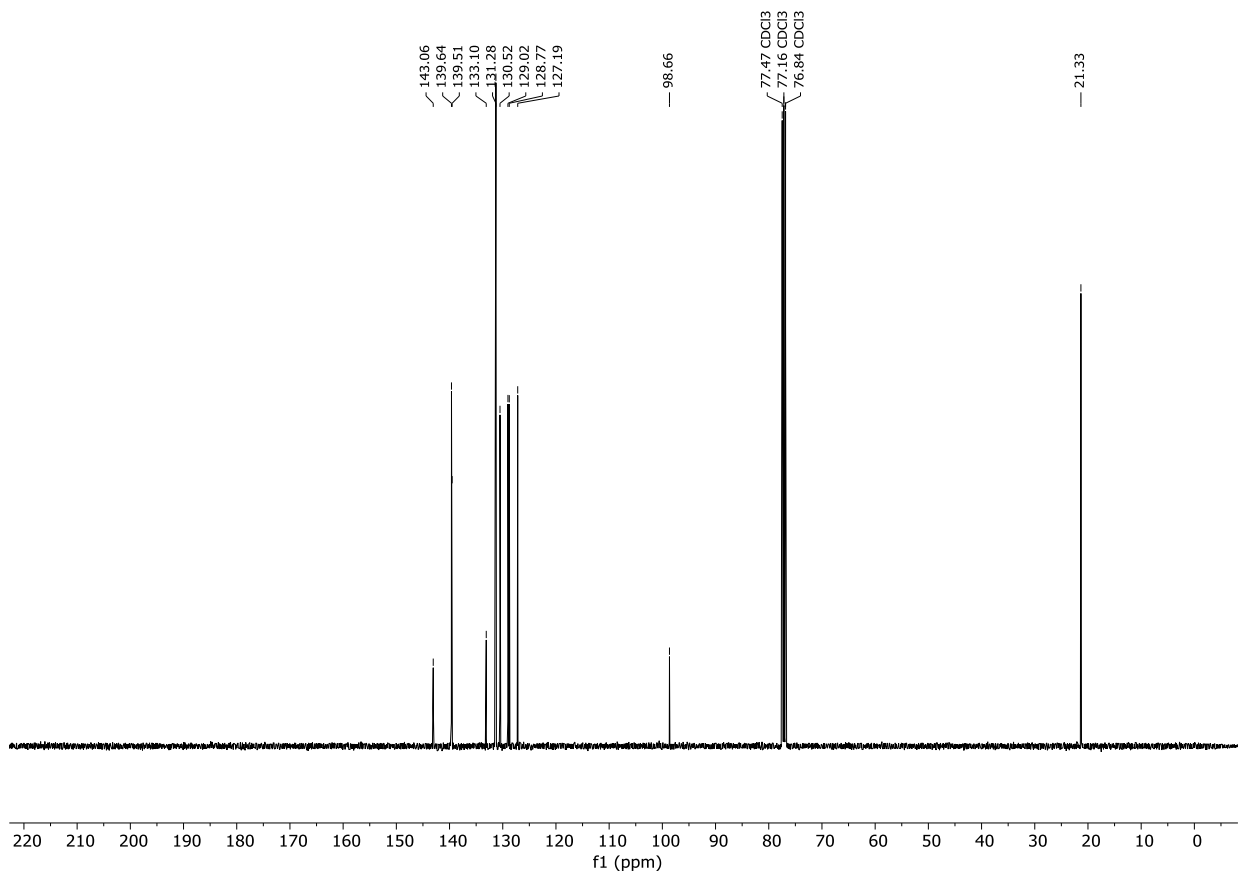


## 7.2 NMR spectra

### $^1\text{H-NMR}$ (400 MHz, $\text{CDCl}_3$ ) Compound **178b**

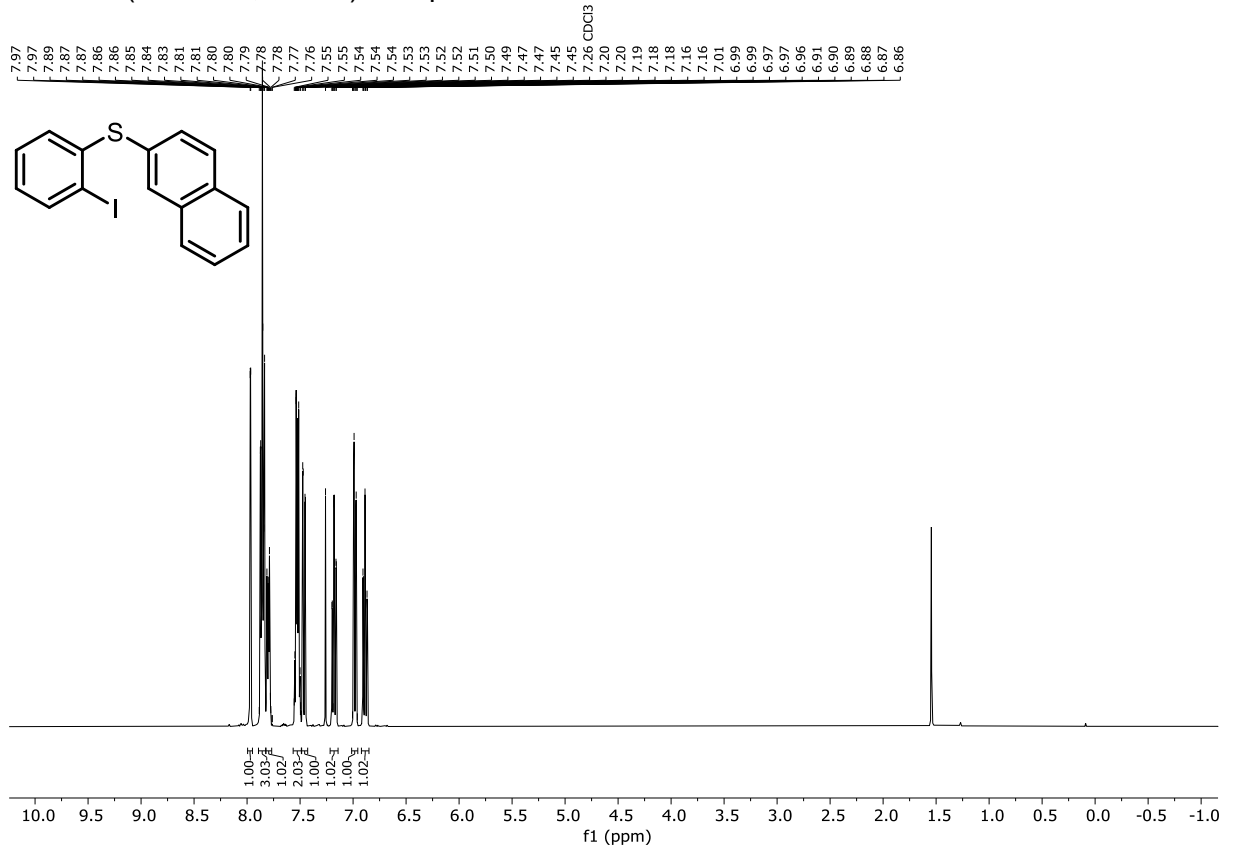


### $^{13}\text{C}\{^1\text{H}\}$ -NMR (101 MHz, $\text{CDCl}_3$ ) Compound **178b**

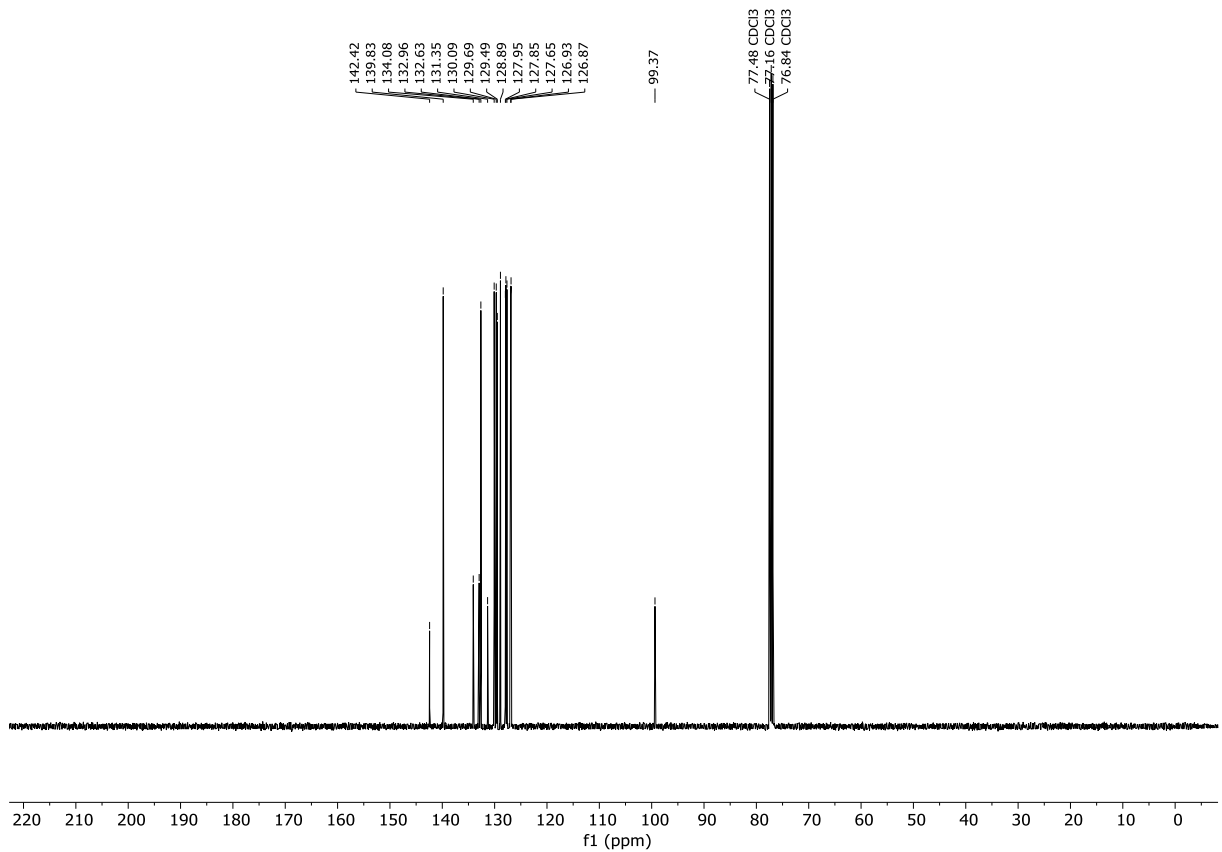


## 7. Appendix

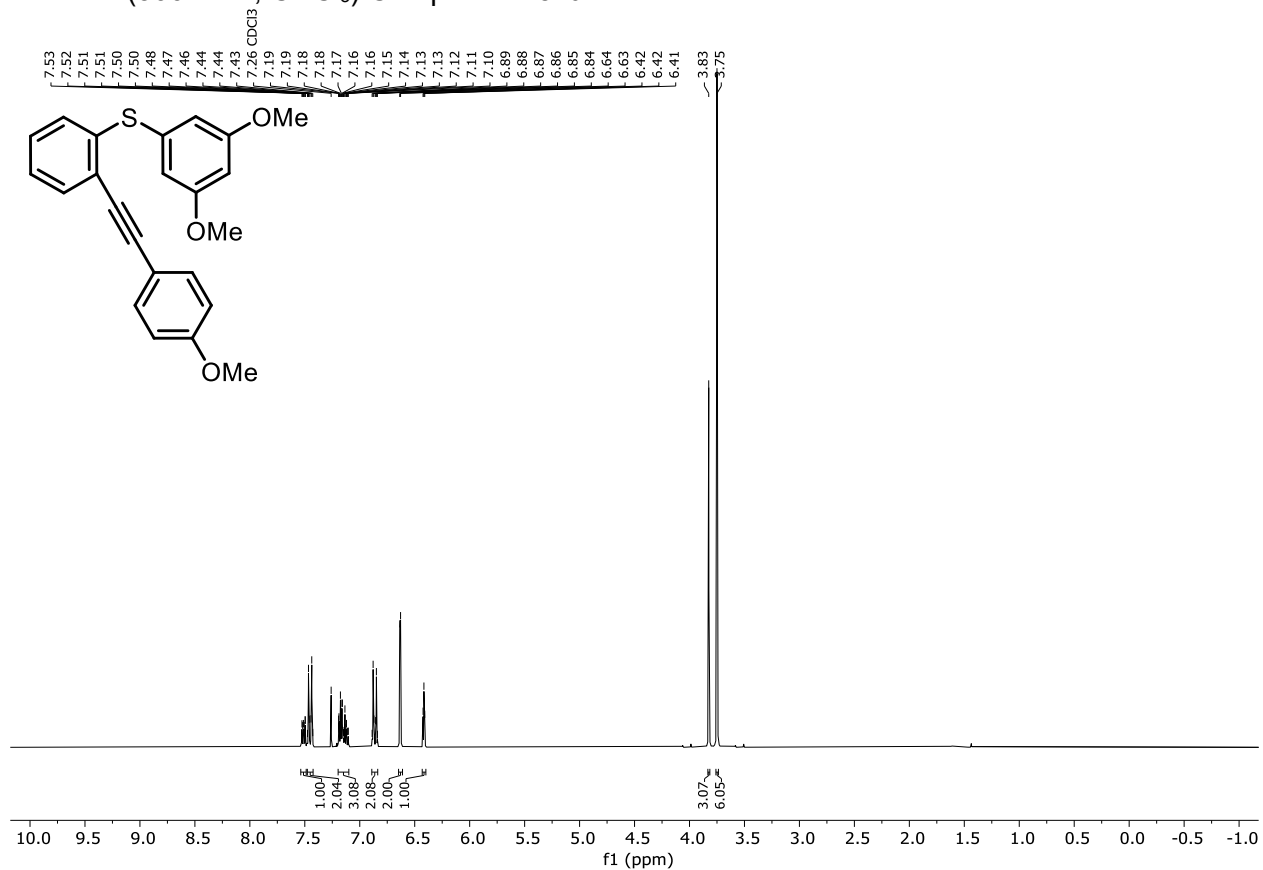
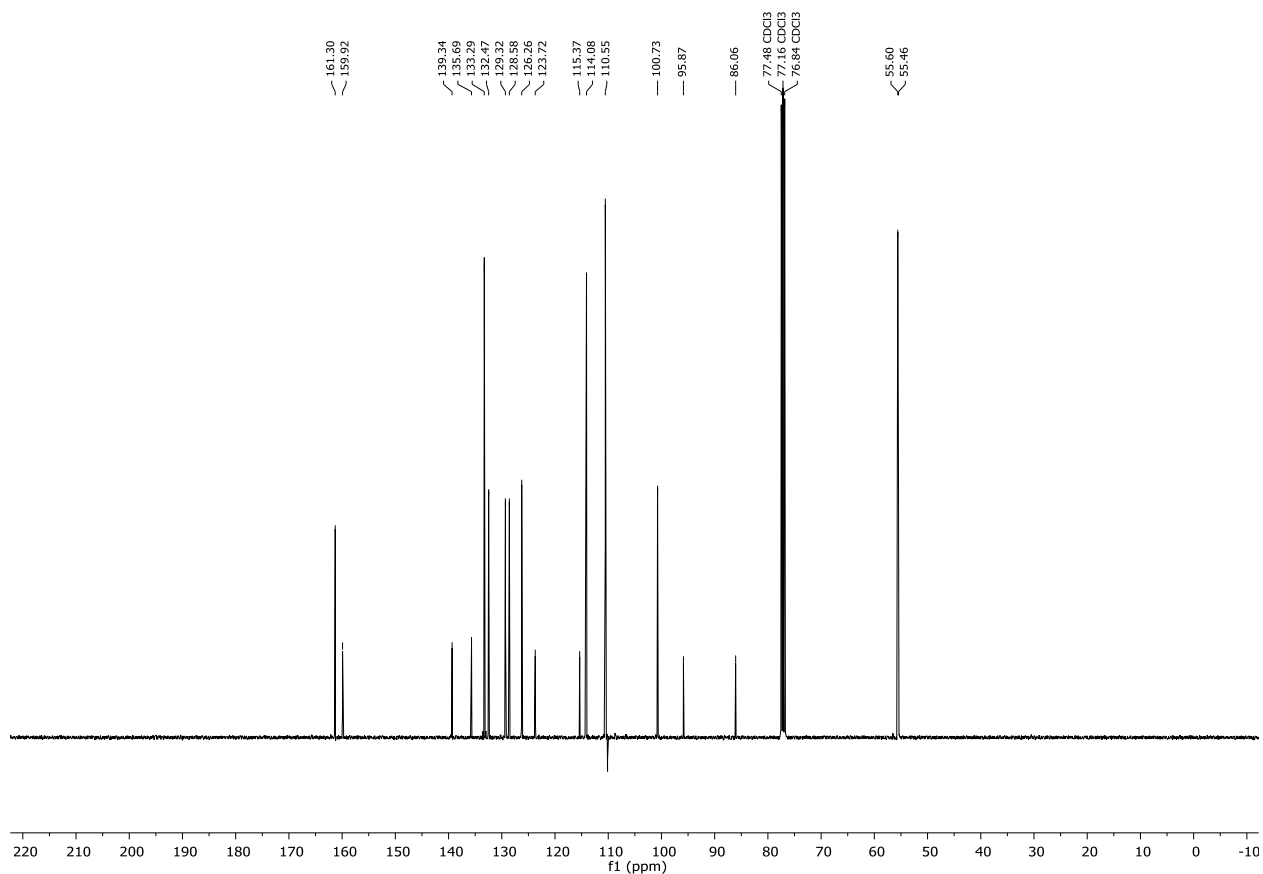
### $^1\text{H-NMR}$ (400 MHz, $\text{CDCl}_3$ ) Compound **178c**



### $^{13}\text{C}\{^1\text{H}\}$ -NMR (101 MHz, $\text{CDCl}_3$ ) Compound **178c**

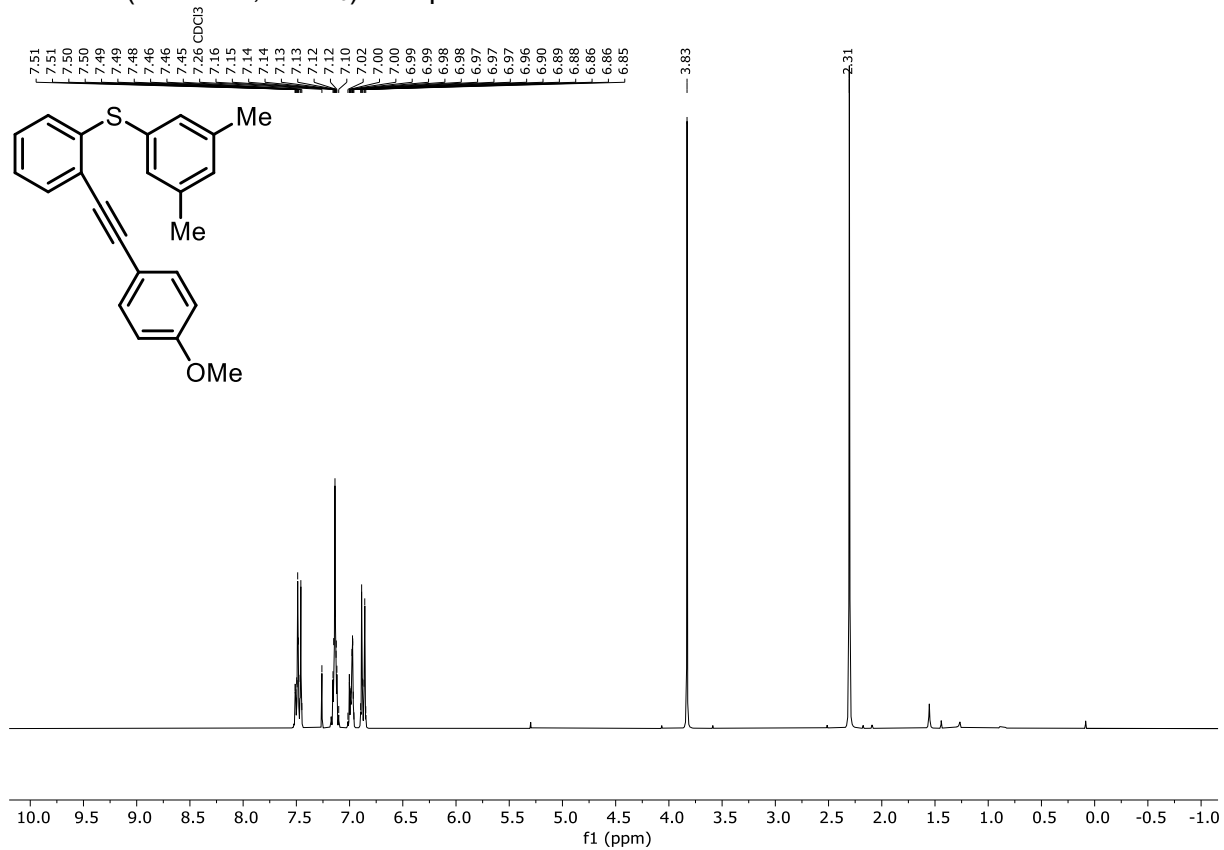


## 7.2 NMR spectra

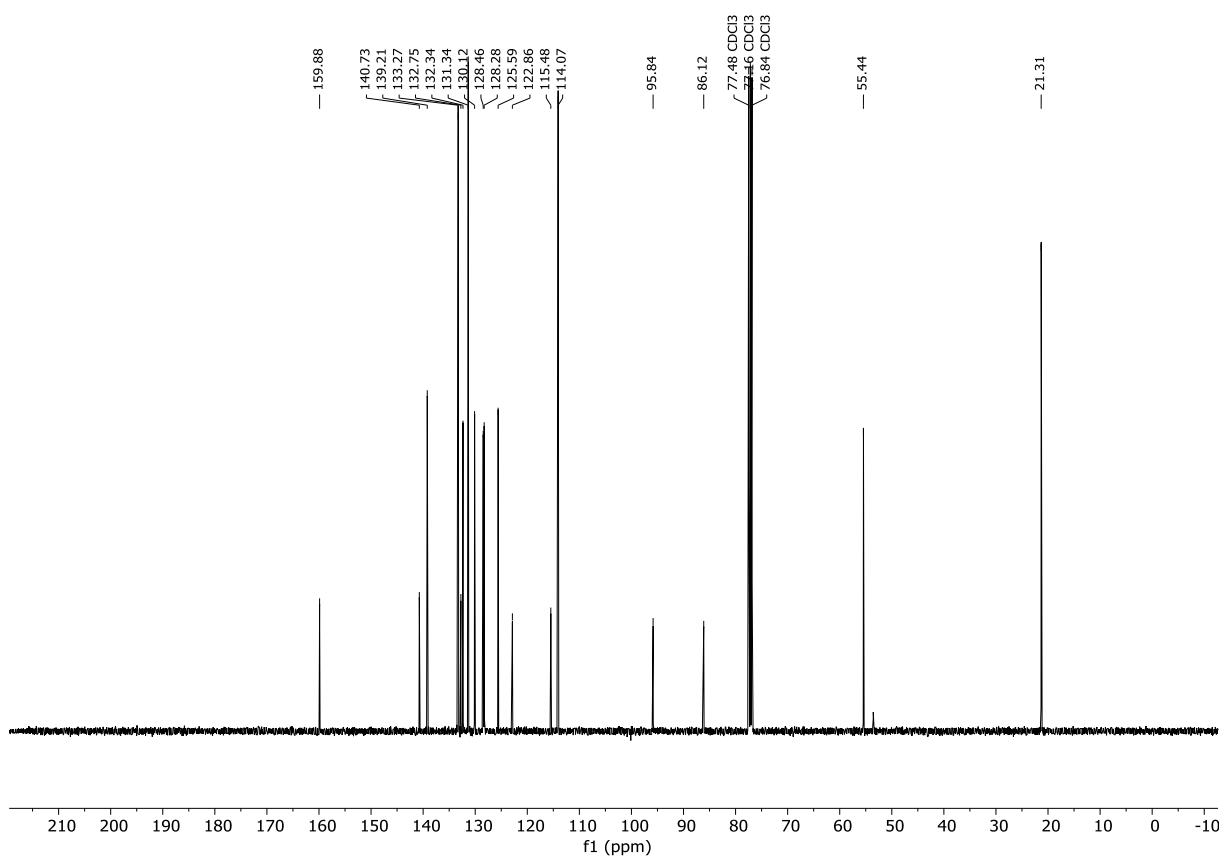
 $^1\text{H-NMR}$  (300 MHz,  $\text{CDCl}_3$ ) Compound **152a** $^{13}\text{C}\{^1\text{H}\}$ -NMR (101 MHz,  $\text{CDCl}_3$ ) Compound **152a**

## 7. Appendix

### $^1\text{H-NMR}$ (300 MHz, $\text{CDCl}_3$ ) Compound **152b**



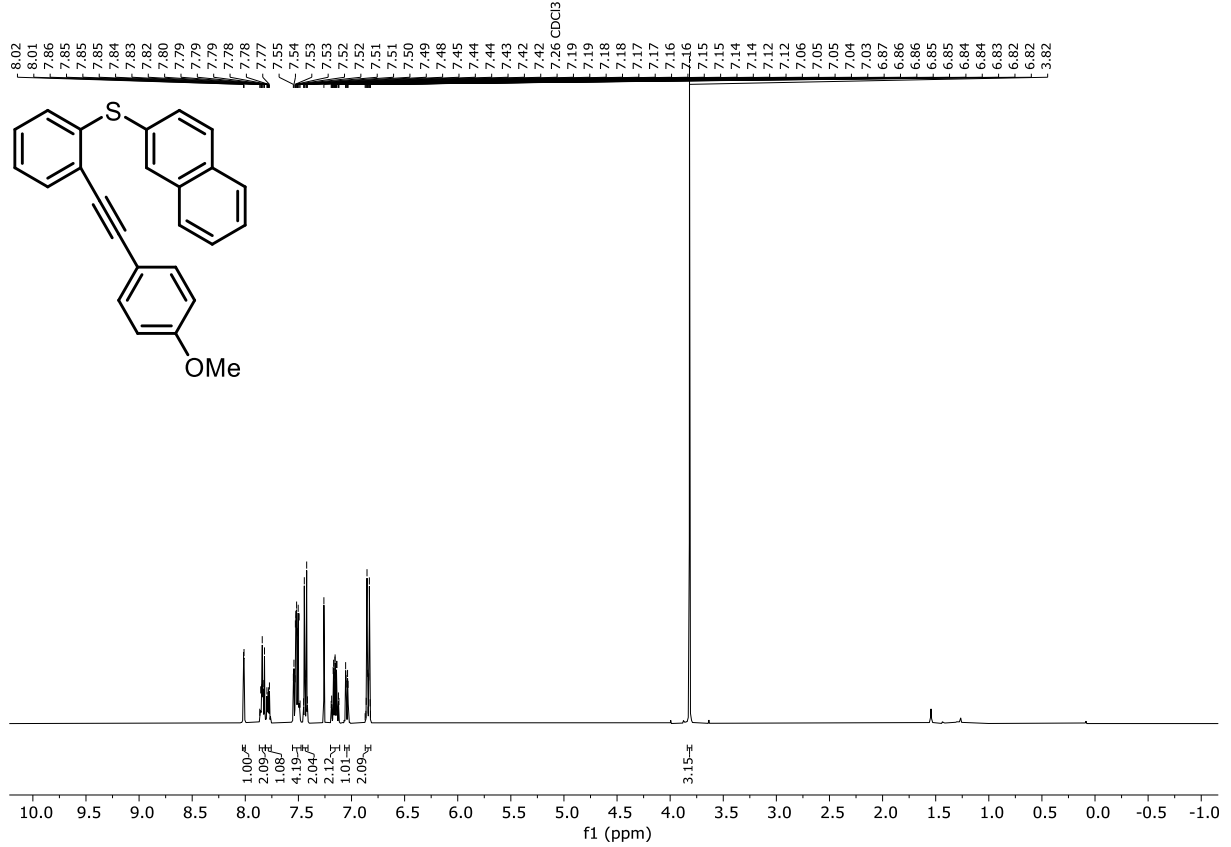
### $^{13}\text{C}\{^1\text{H}\}$ -NMR (101 MHz, $\text{CDCl}_3$ ) Compound **152b**



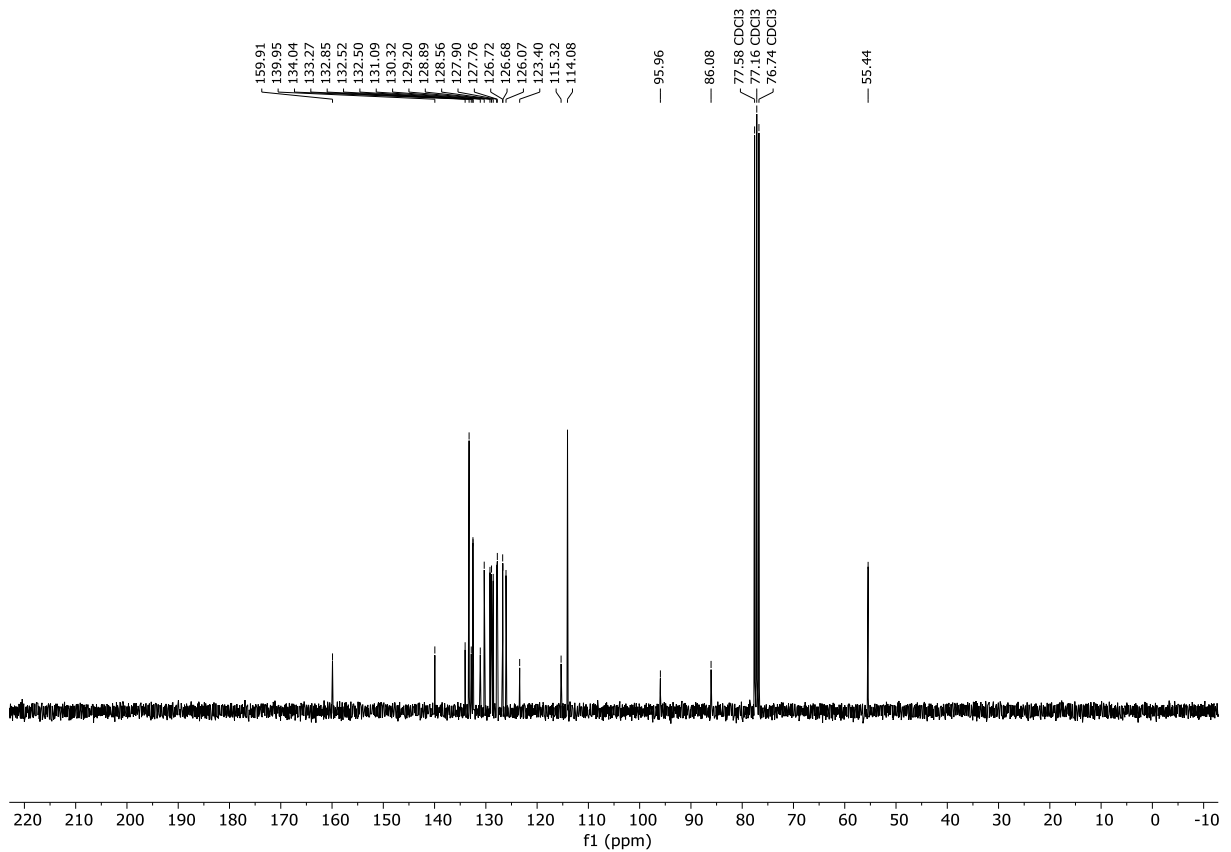


## 7.2 NMR spectra

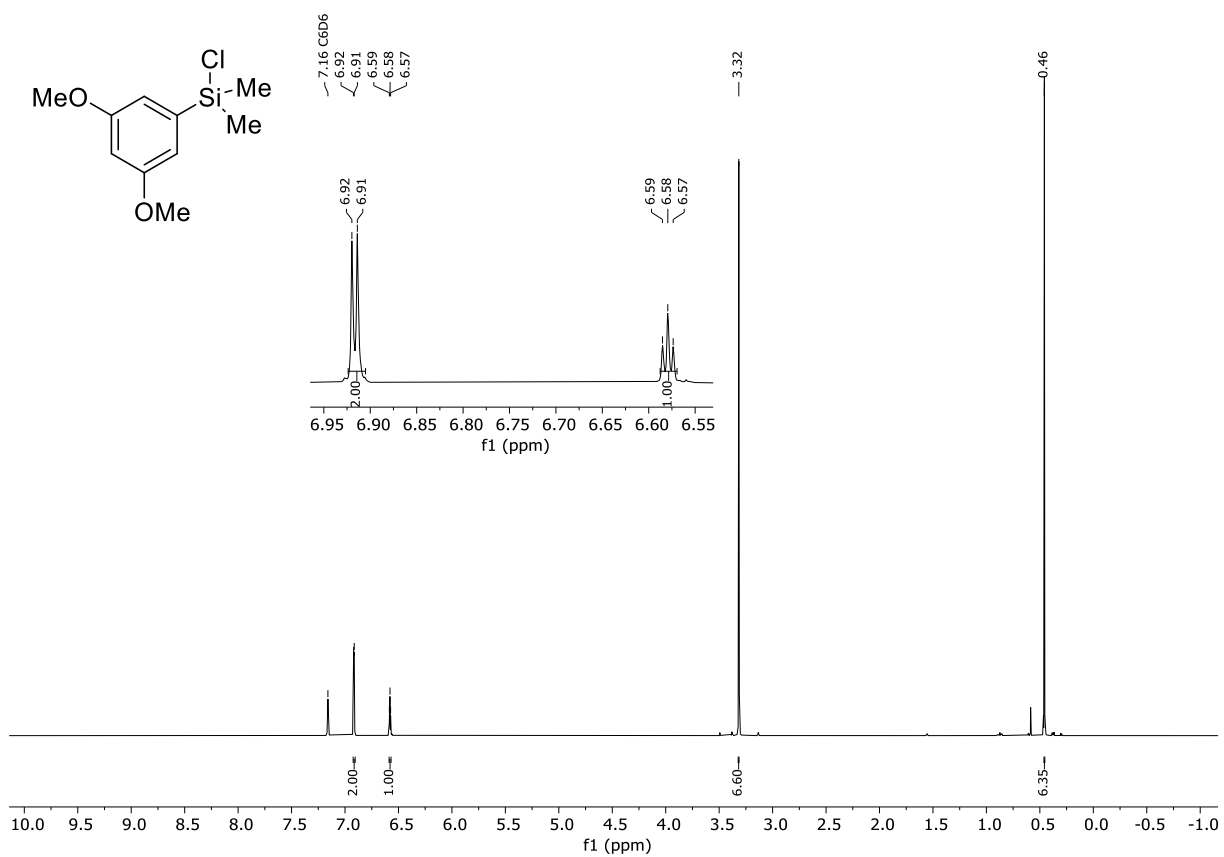
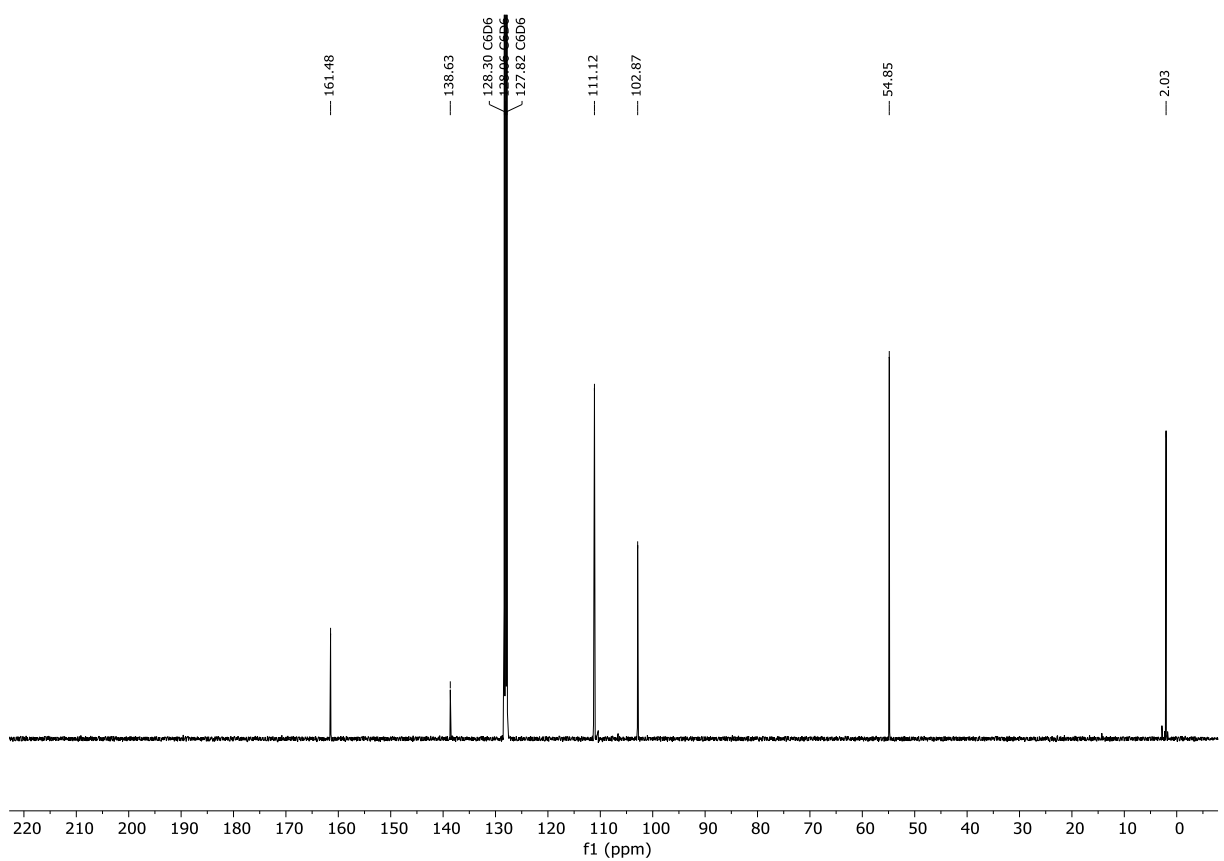
### <sup>1</sup>H-NMR (400 MHz, CDCl<sub>3</sub>) Compound **152c**



### <sup>13</sup>C{<sup>1</sup>H}-NMR (75 MHz, CDCl<sub>3</sub>) Compound **152c**

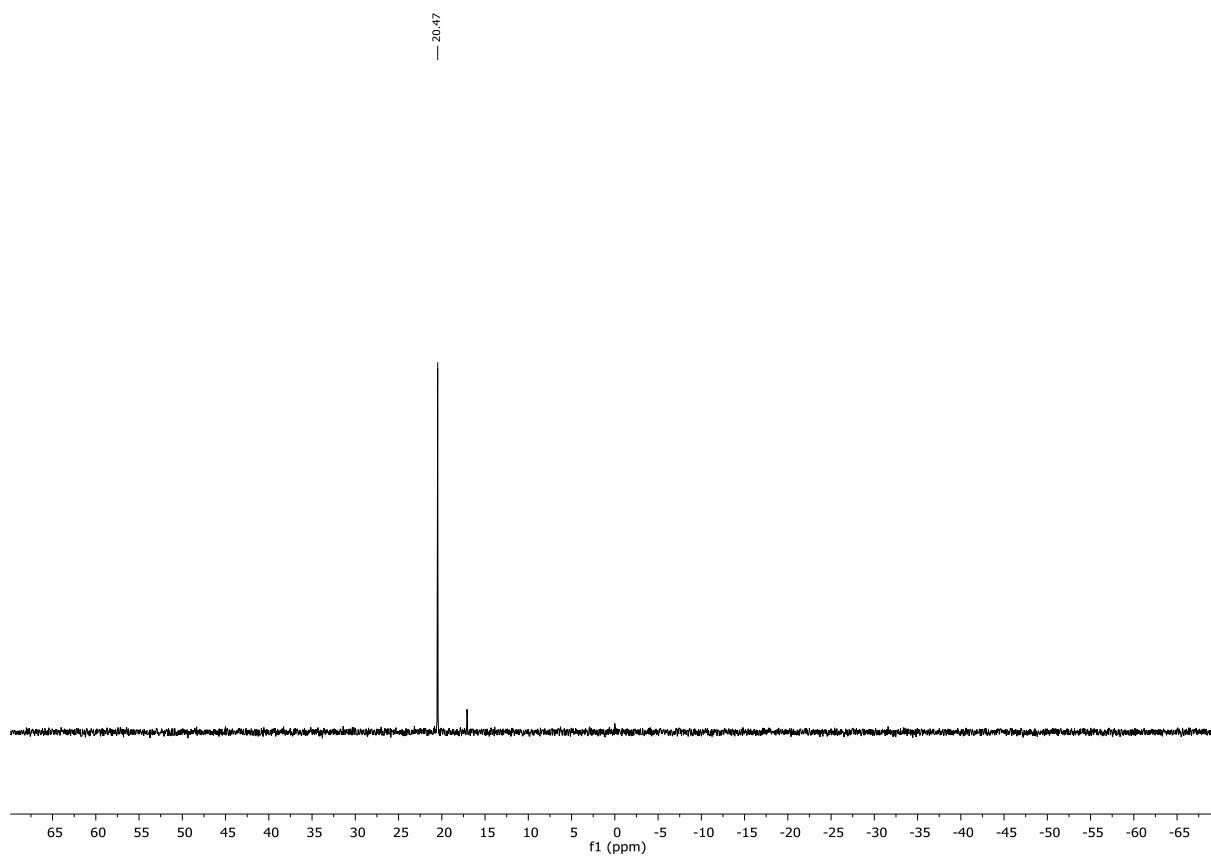


## 7. Appendix

 $^1\text{H}$  NMR (400 MHz,  $\text{C}_6\text{D}_6$ ) Compound **180a** $^{13}\text{C}$  NMR (126 MHz,  $\text{C}_6\text{D}_6$ ) Compound **180a**

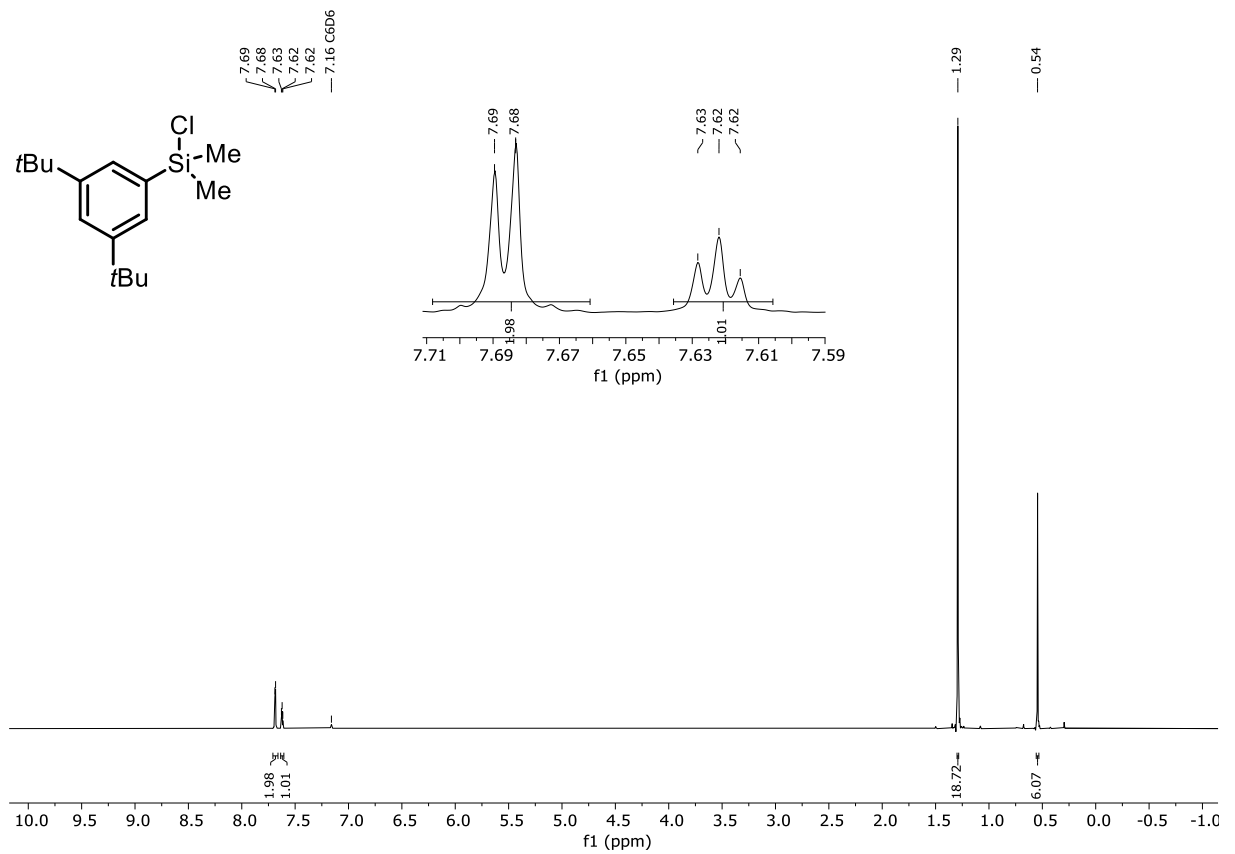
## 7.2 NMR spectra

$^{29}\text{Si}$  NMR (79 MHz,  $\text{C}_6\text{D}_6$ ) Compound **180a**

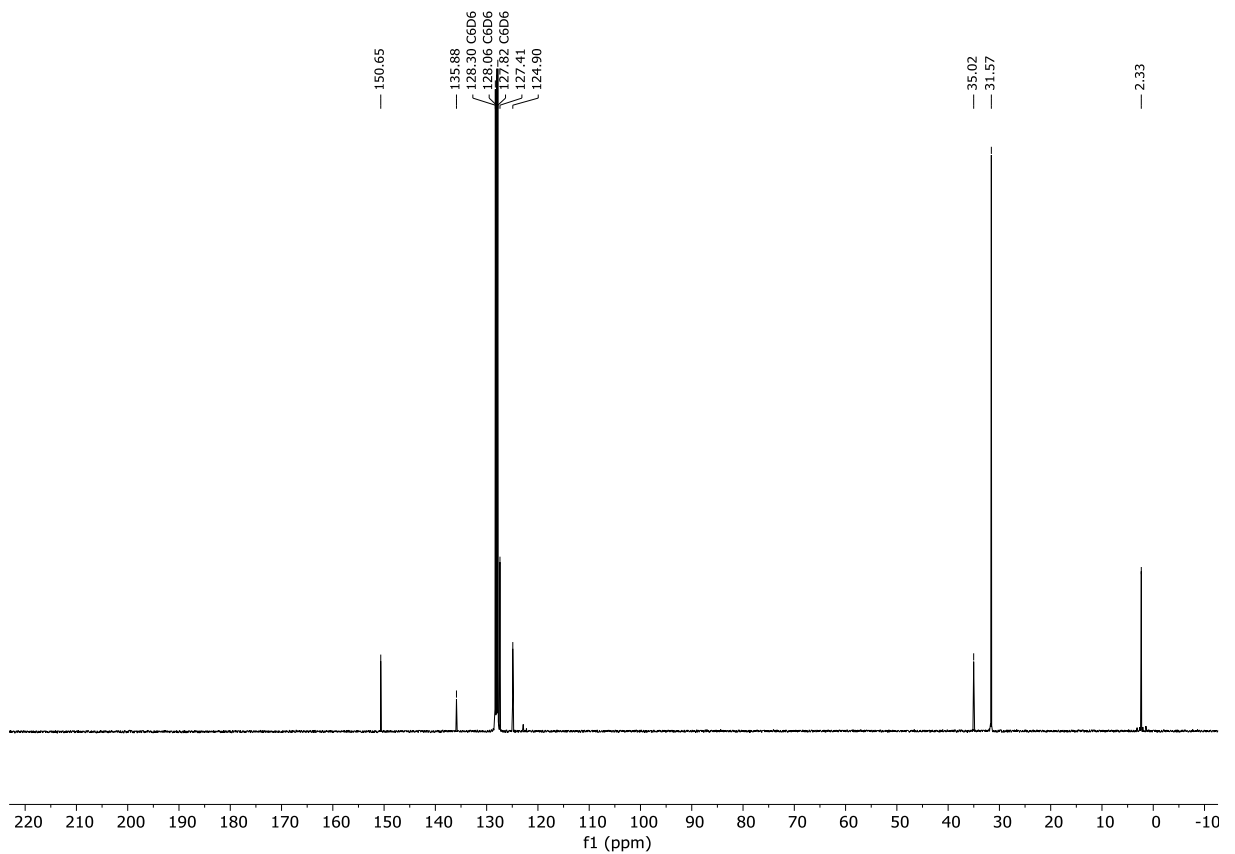


## 7. Appendix

### $^1\text{H}$ NMR (300 MHz, $\text{C}_6\text{D}_6$ ) Compound **180b**

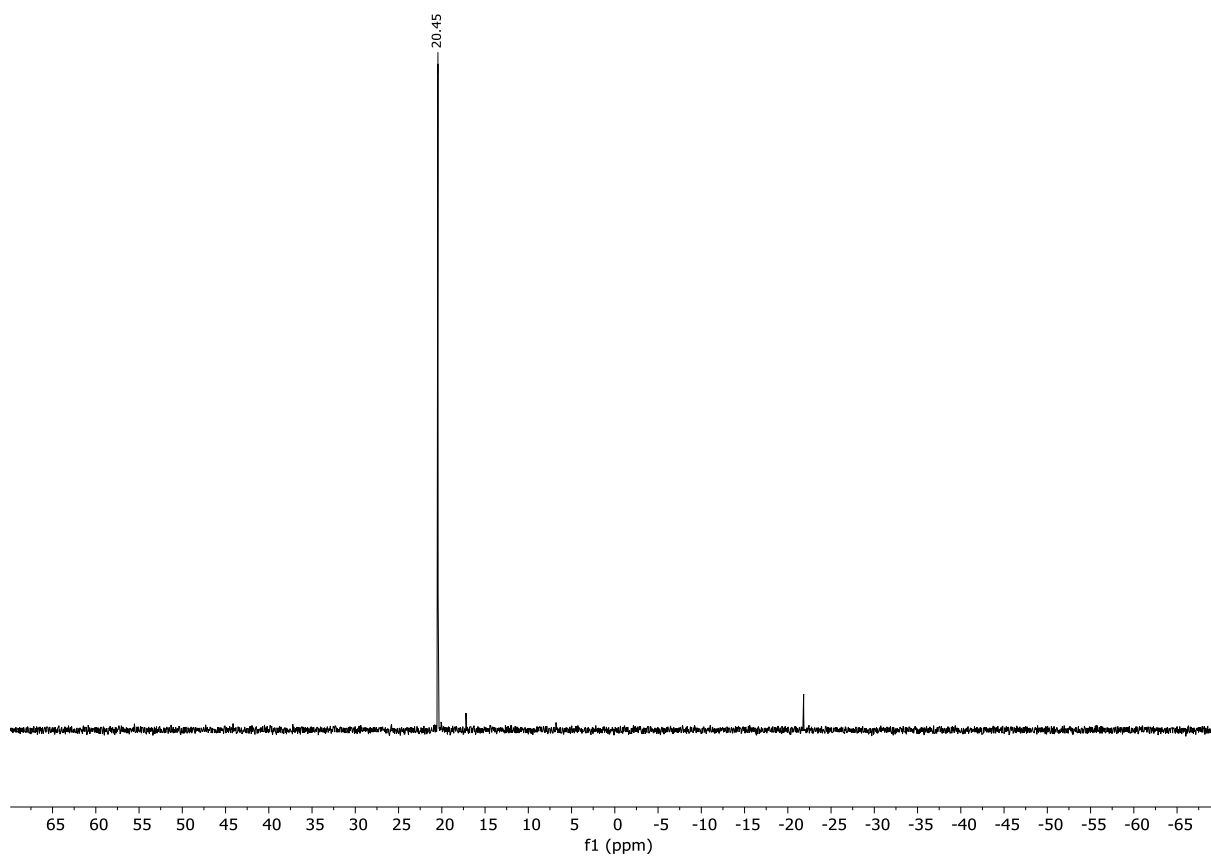


### $^{13}\text{C}\{^1\text{H}\}$ -NMR (101 MHz, $\text{C}_6\text{D}_6$ ) Compound **180b**



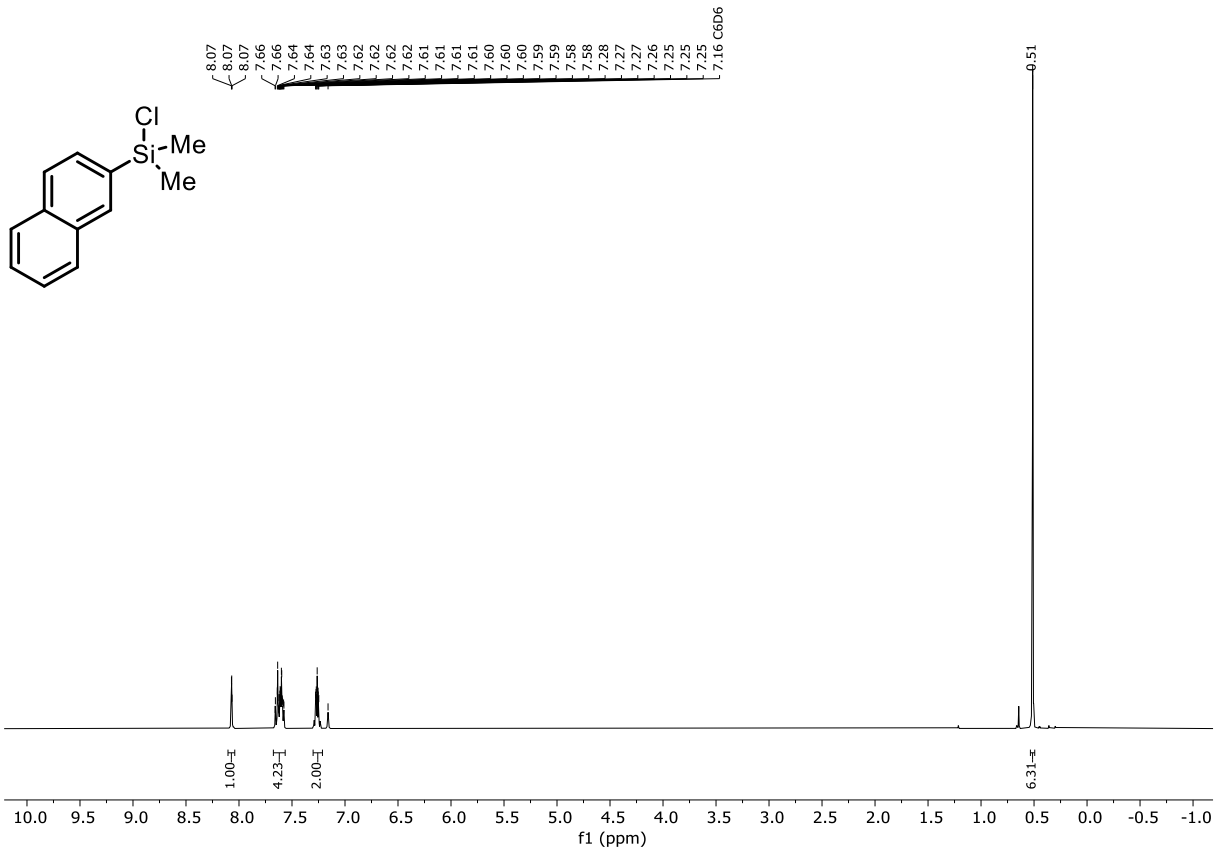
## 7.2 NMR spectra

$^{29}\text{Si}$ -NMR (79 MHz,  $\text{CDCl}_3$ ) **180b**

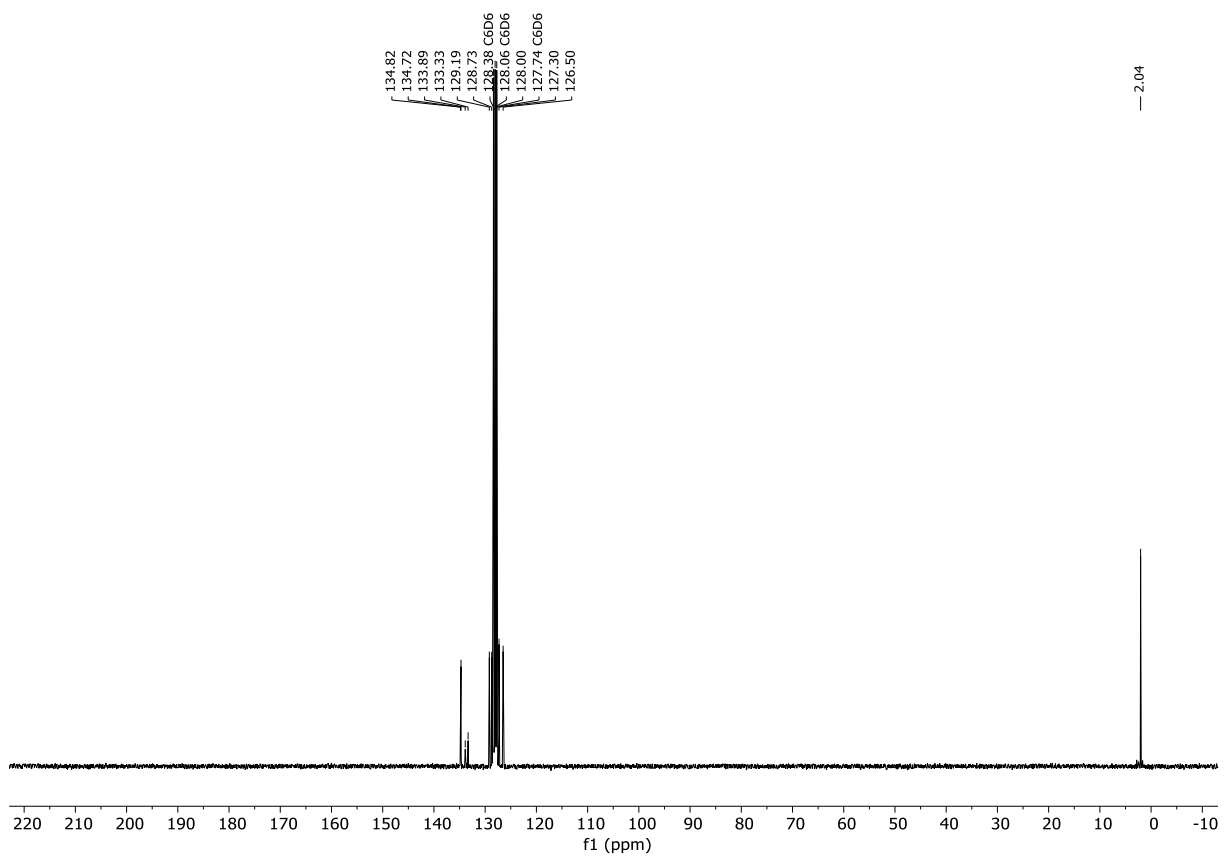


## 7. Appendix

### $^1\text{H}$ NMR (400 MHz, $\text{C}_6\text{D}_6$ ) Compound **180c**

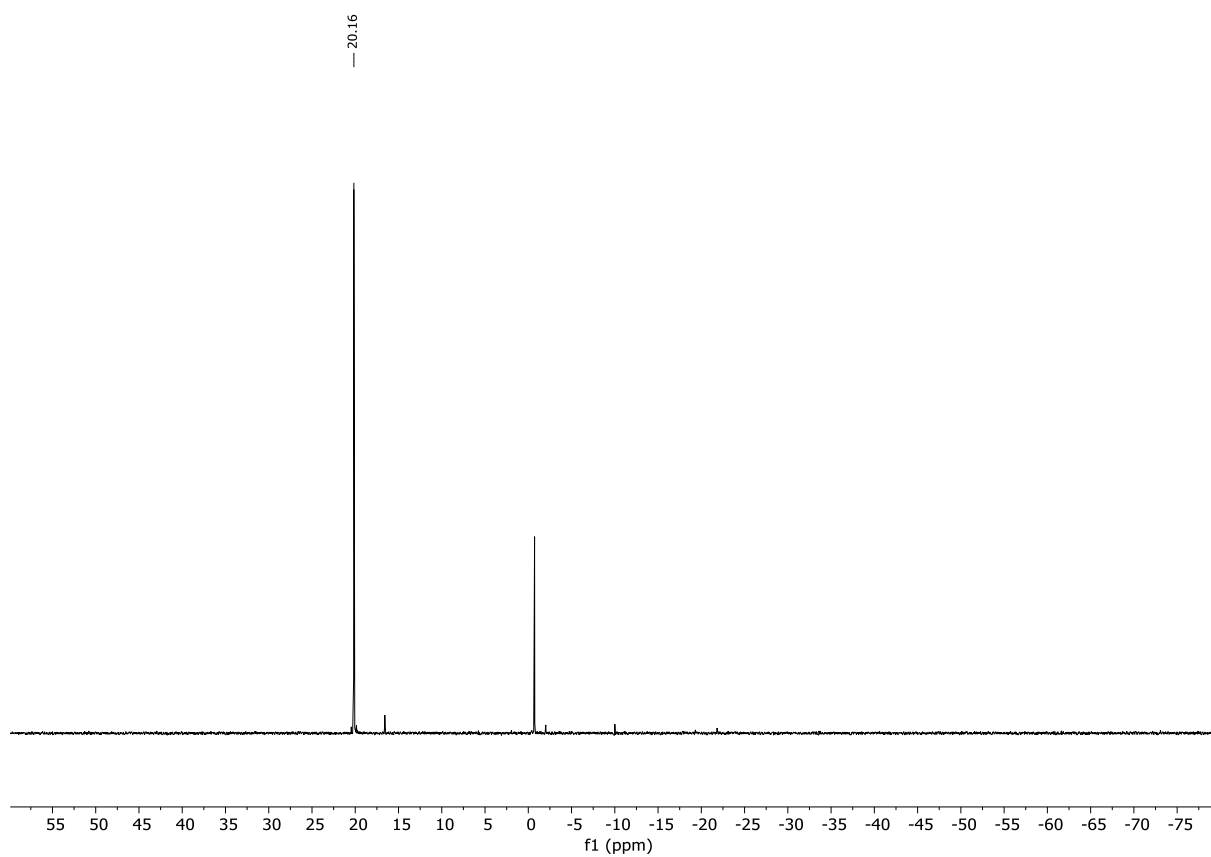


### $^{13}\text{C}\{^1\text{H}\}$ -NMR (75 MHz, $\text{C}_6\text{D}_6$ ) Compound **180c**



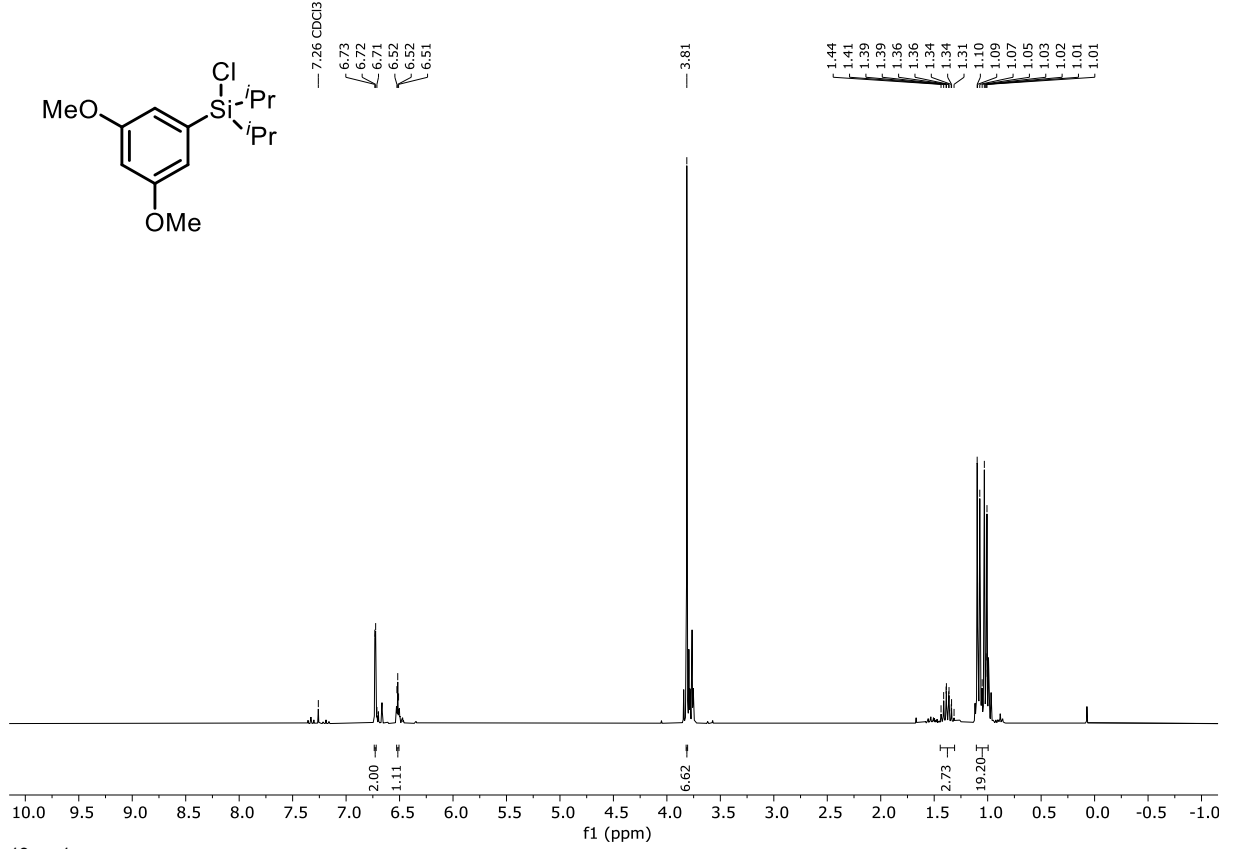
## 7.2 NMR spectra

$^{29}\text{Si}$ -NMR (99 MHz,  $\text{C}_6\text{D}_6$ ) **180c**

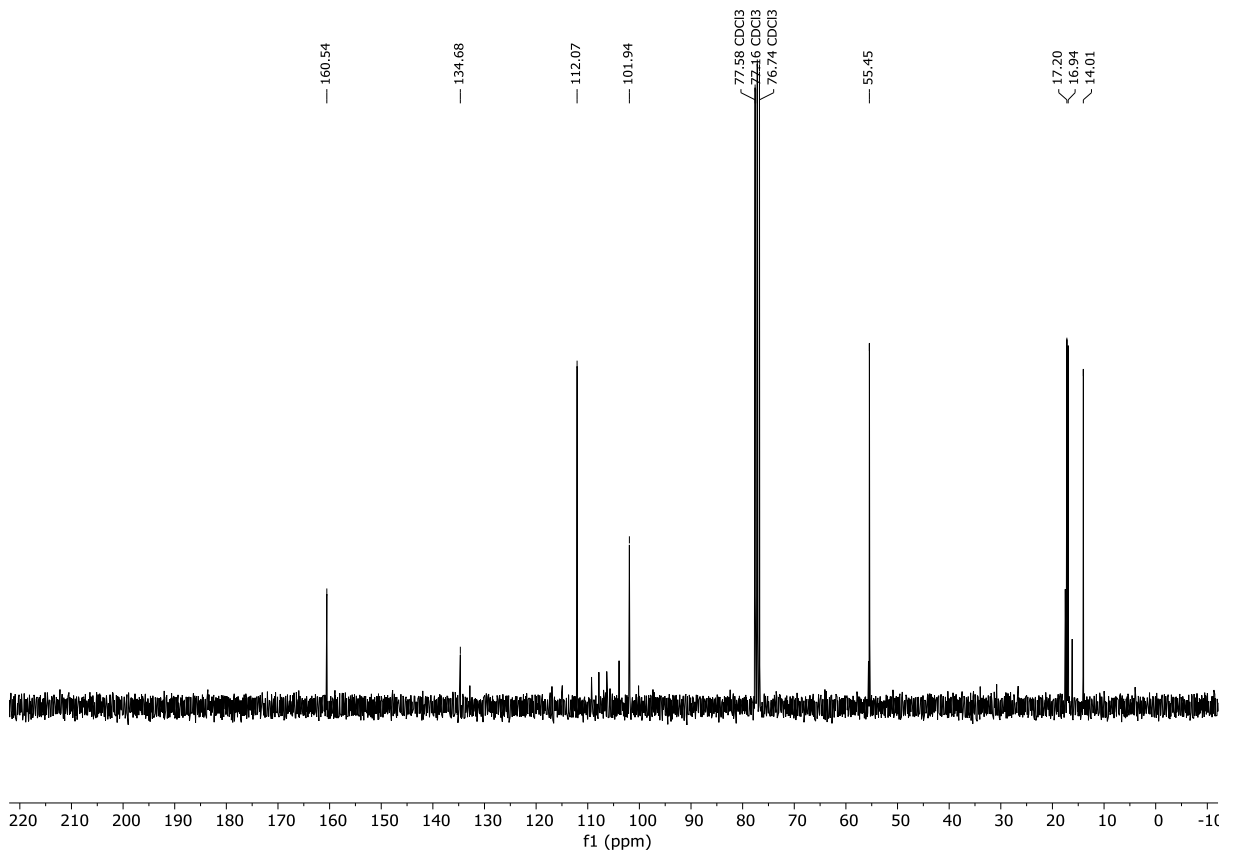


## 7. Appendix

### $^1\text{H-NMR}$ (300 MHz, $\text{CDCl}_3$ ) Compound **180d**



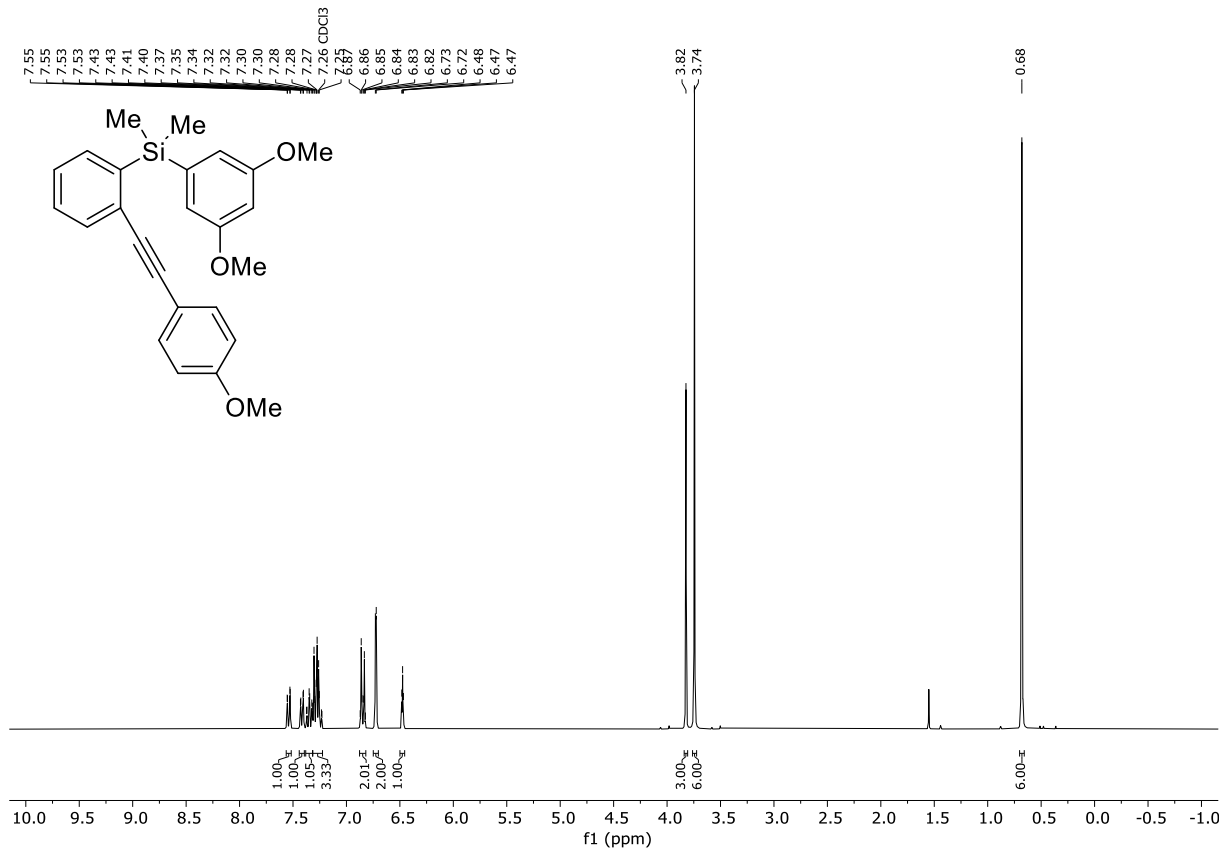
### $^{13}\text{C}\{^1\text{H}\}$ -NMR (75 MHz, $\text{CDCl}_3$ ) Compound **180d**



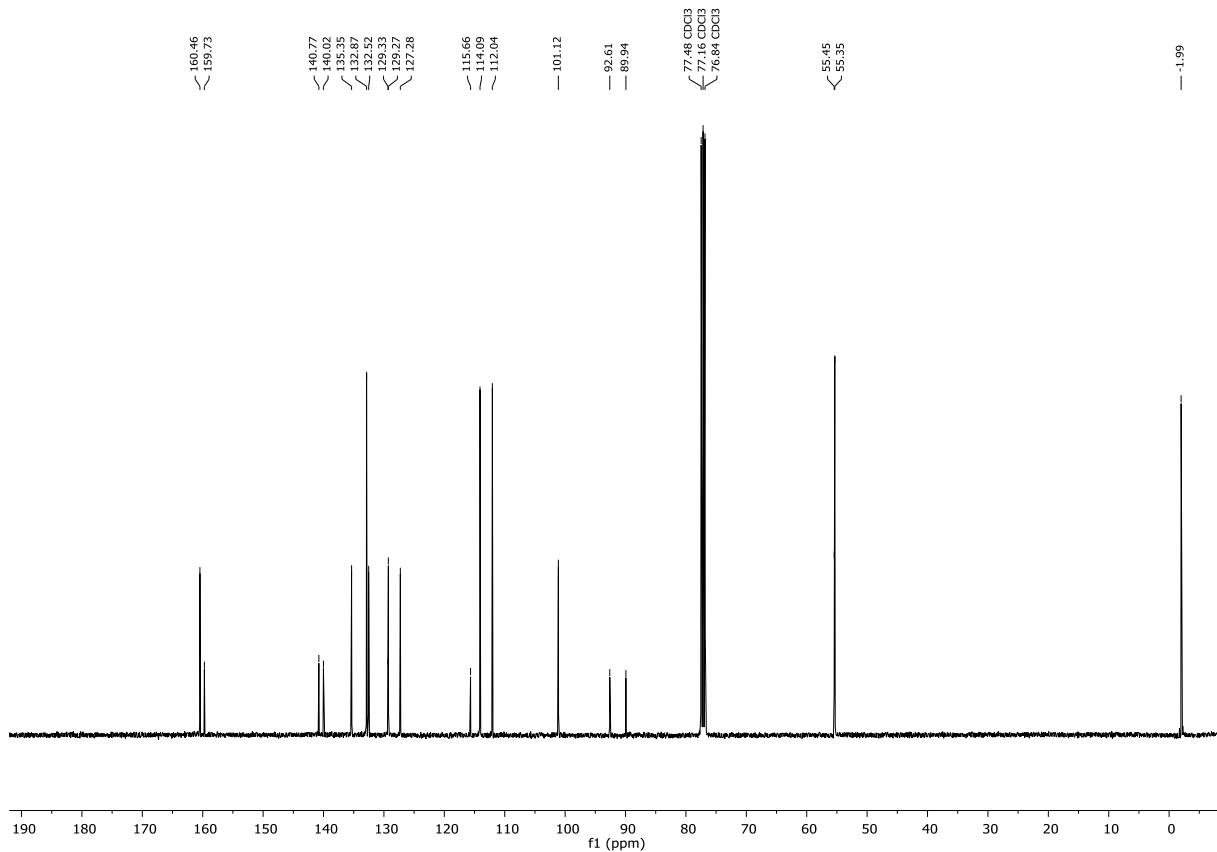


## 7.2 NMR spectra

### <sup>1</sup>H NMR (300 MHz, CDCl<sub>3</sub>) Compound **153a**

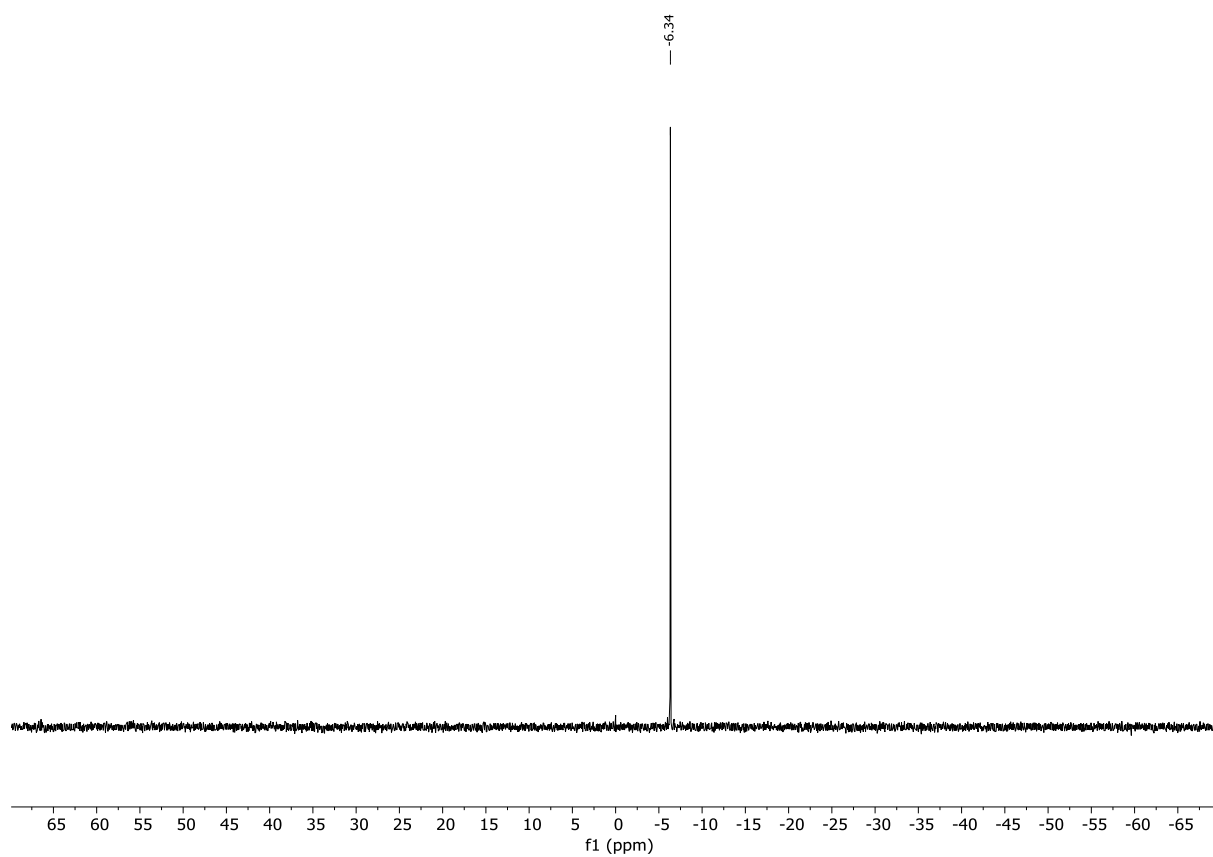


### <sup>13</sup>C NMR (101 MHz, CDCl<sub>3</sub>) Compound **153a**



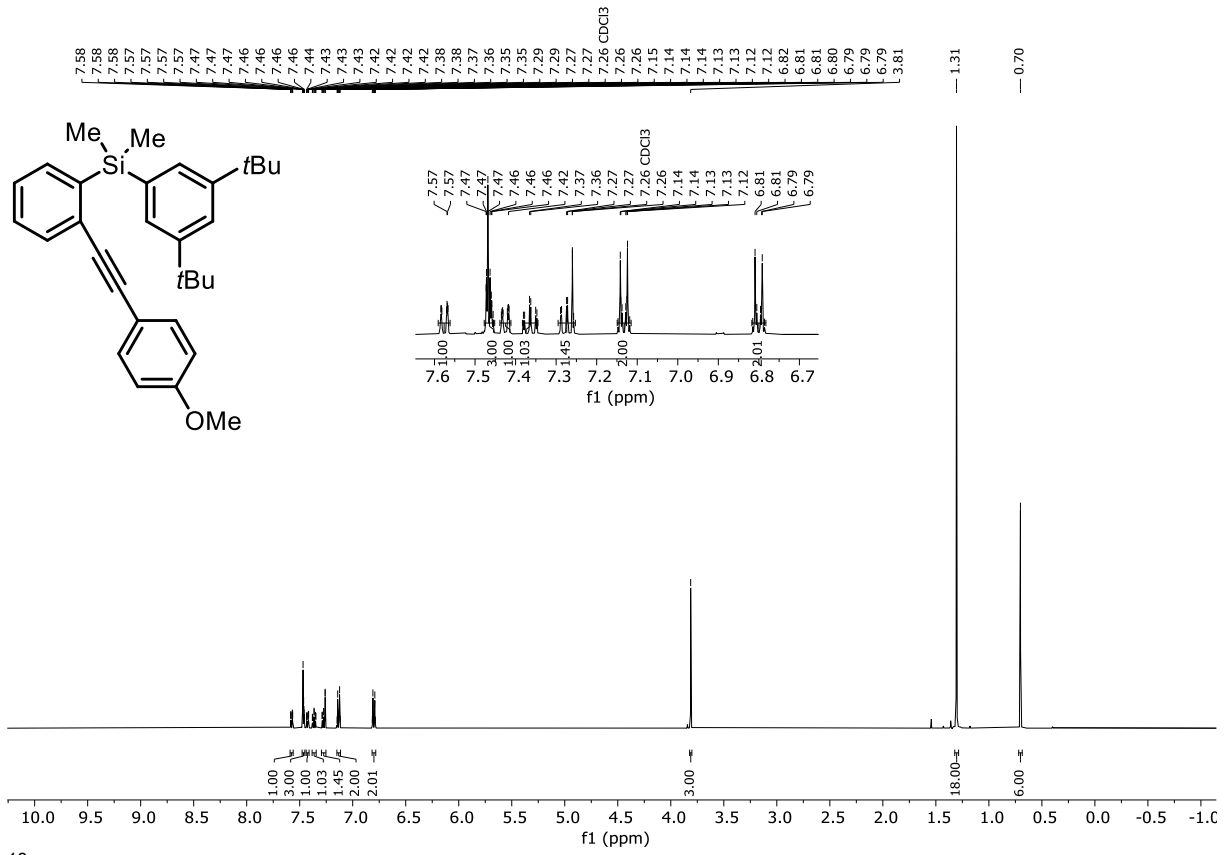
## 7. Appendix

$^{29}\text{Si}$  NMR (79 MHz,  $\text{CDCl}_3$ ) Compound **153a**



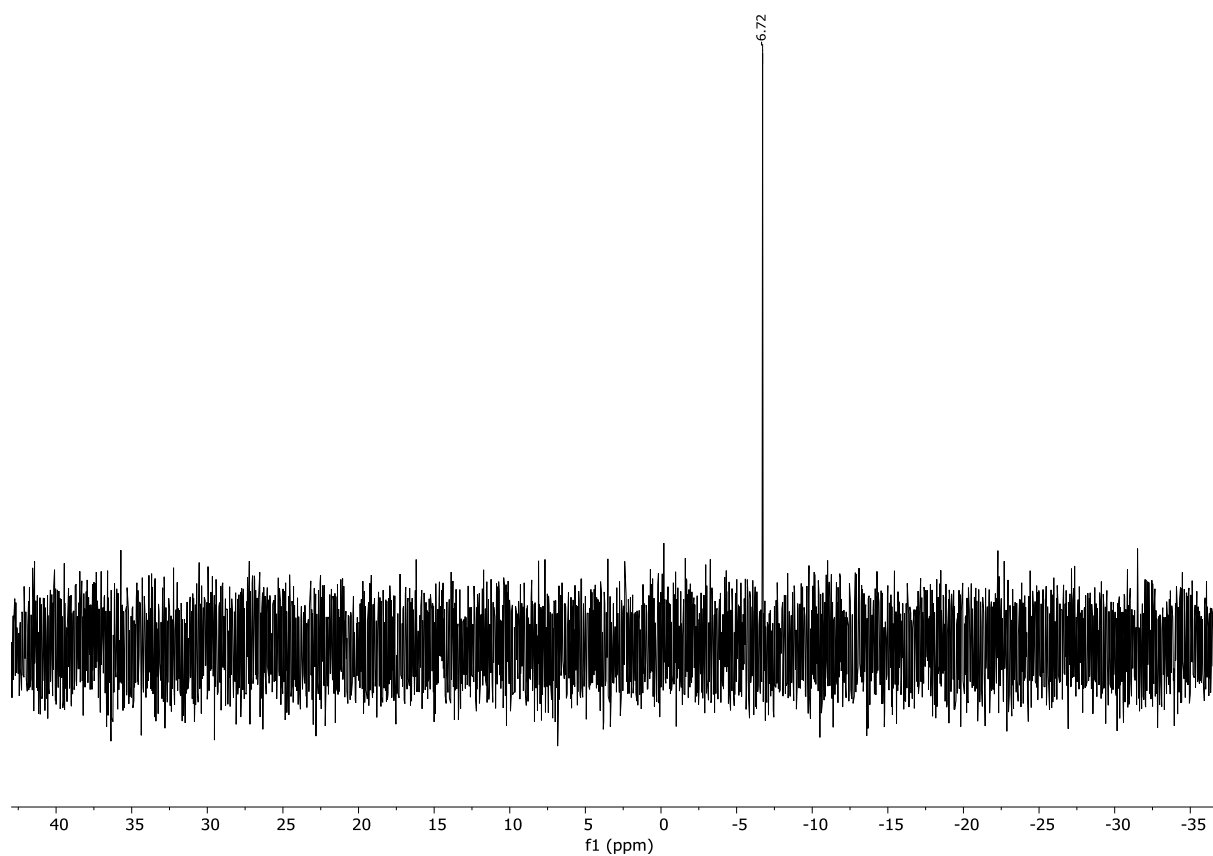
## 7.2 NMR spectra

### <sup>1</sup>H NMR (400 MHz, CDCl<sub>3</sub>) Compound **153b**



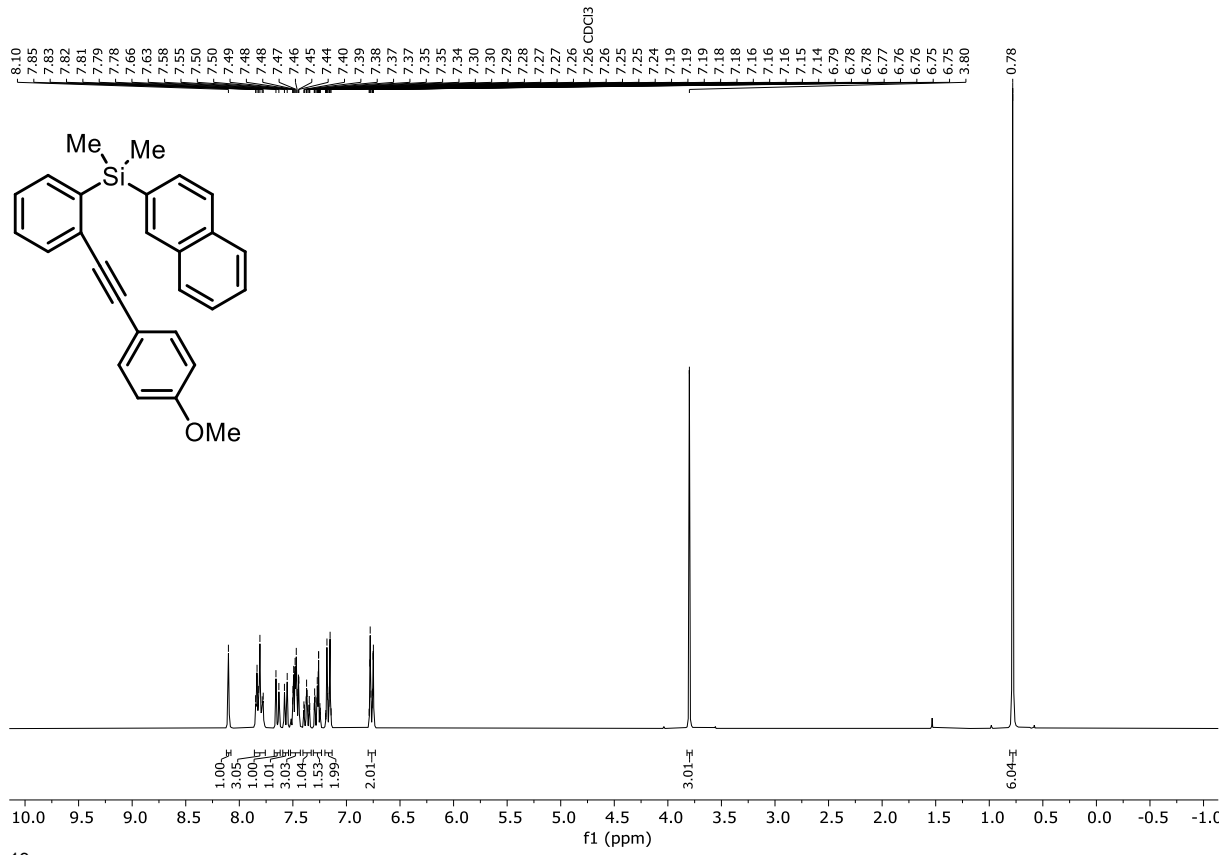
7. Appendix

$^{29}\text{Si}$  NMR (99 MHz,  $\text{CDCl}_3$ ) Compound **153b**

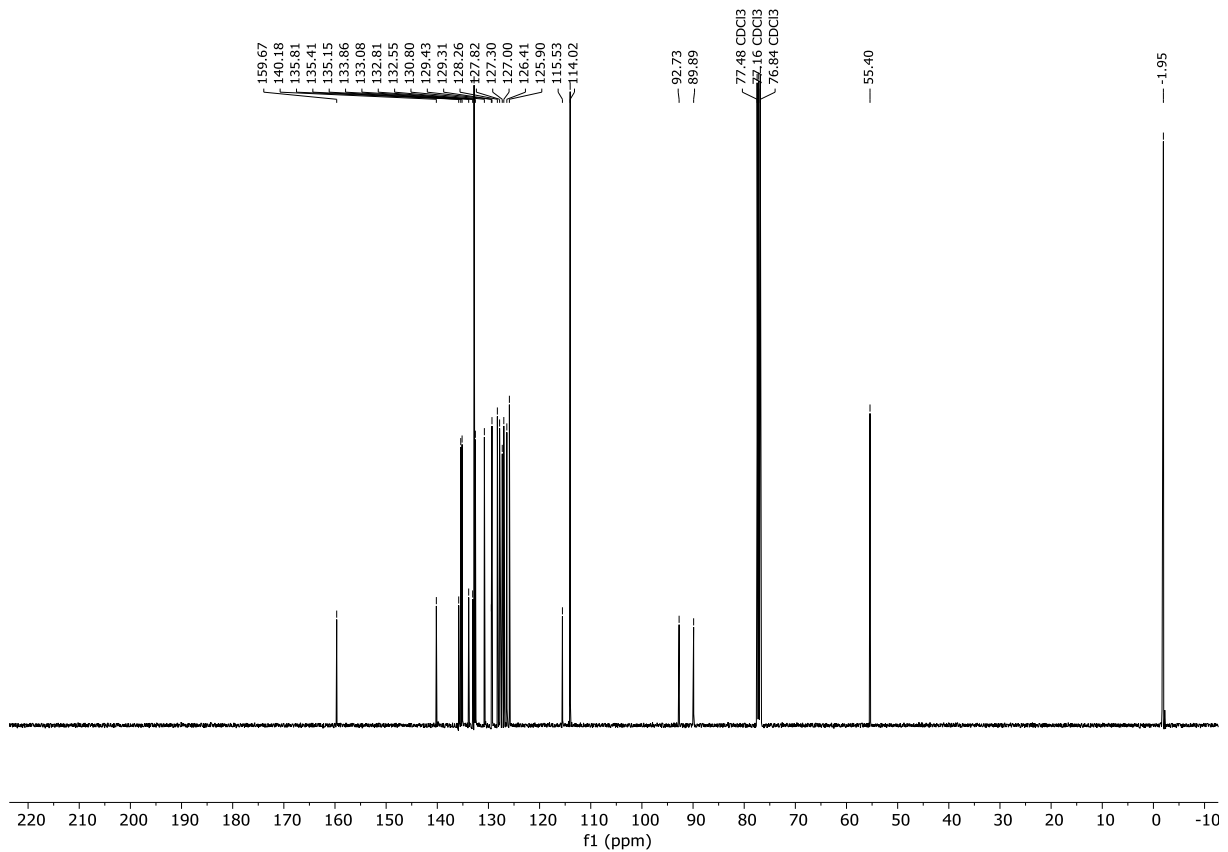


## 7.2 NMR spectra

### $^1\text{H}$ NMR (400 MHz, $\text{CDCl}_3$ ) Compound **153c**

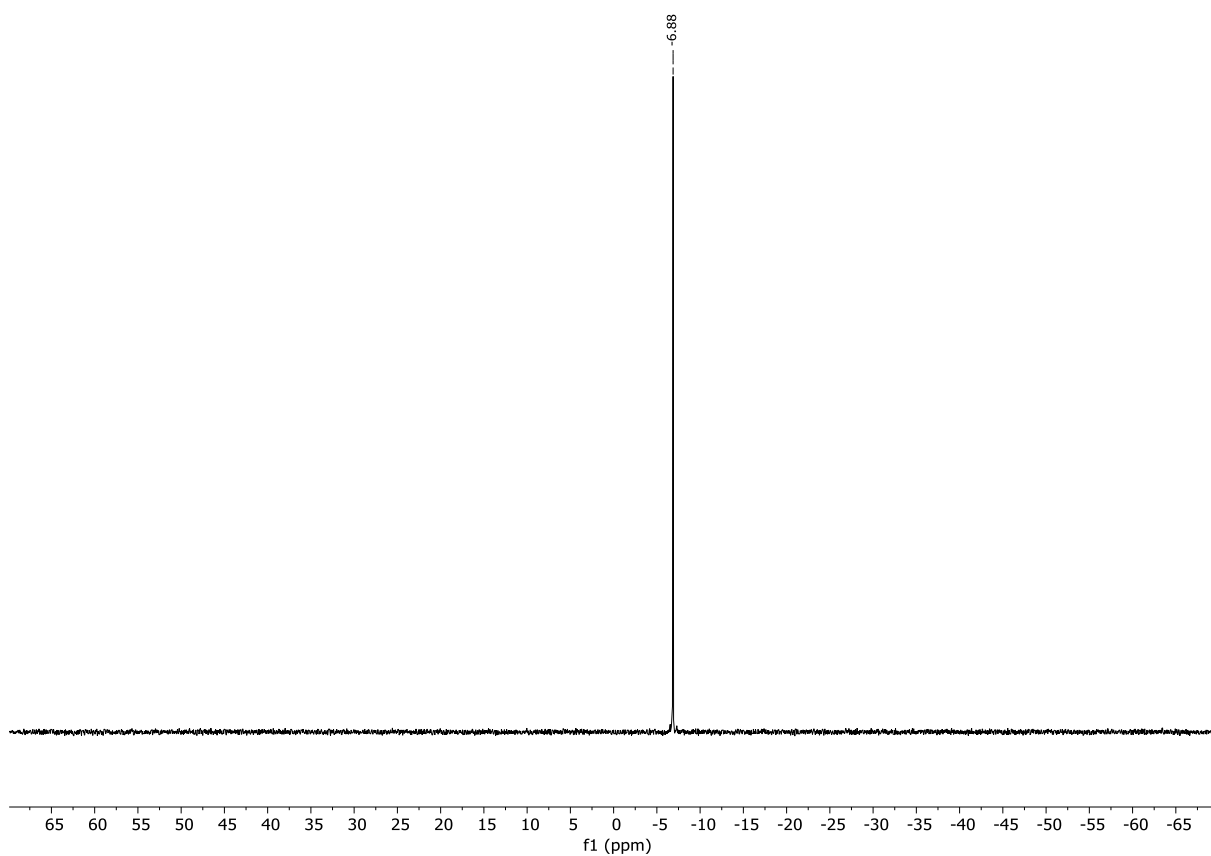


### $^{13}\text{C}$ NMR (75 MHz, $\text{CDCl}_3$ ) Compound **153c**

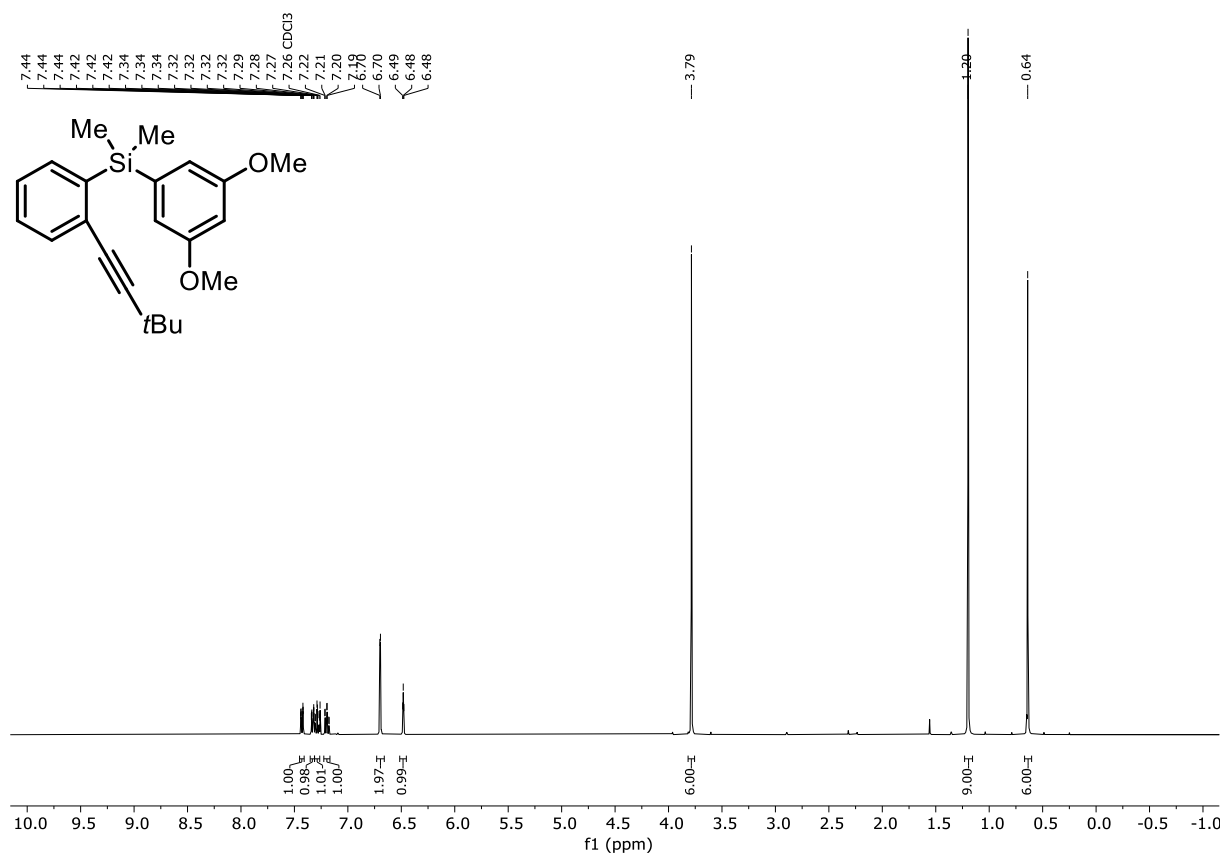
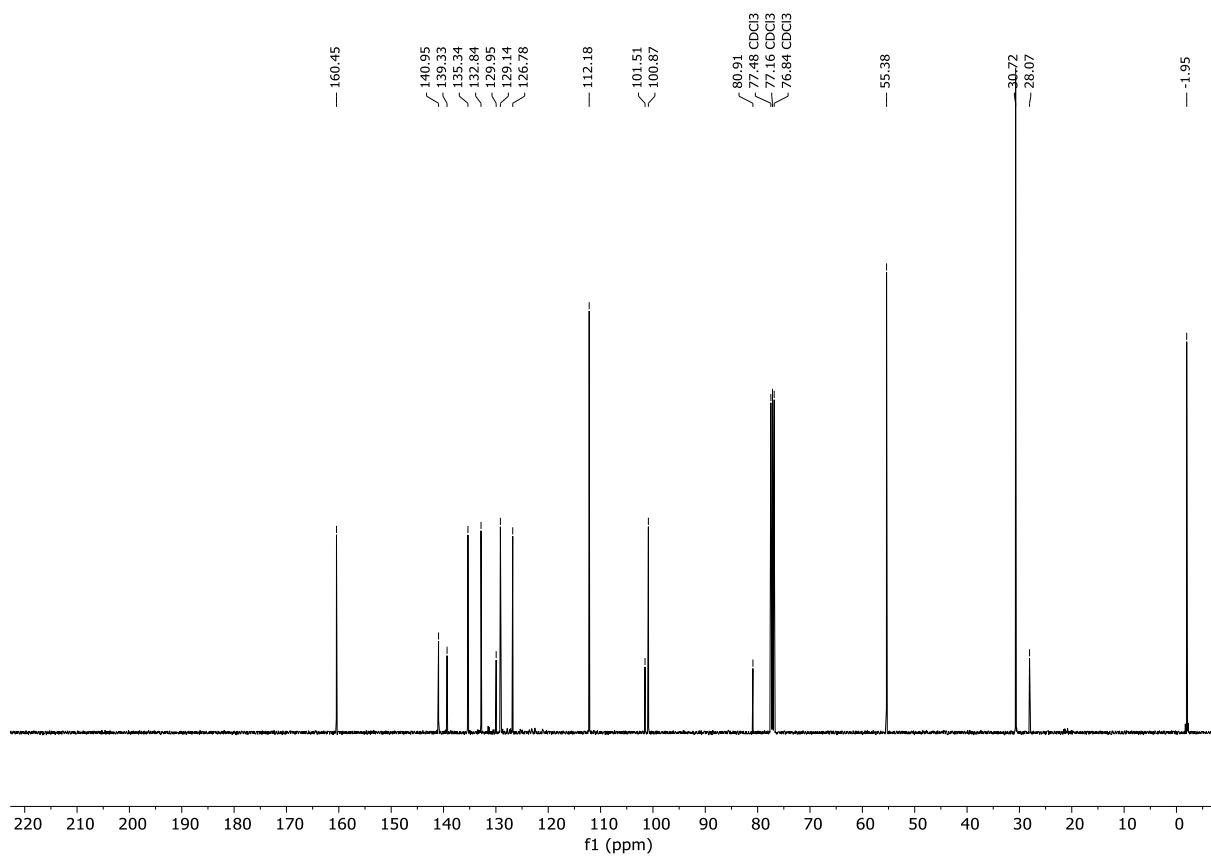


7. Appendix

$^{29}\text{Si}$  NMR (79 MHz,  $\text{CDCl}_3$ ) Compound **153c**

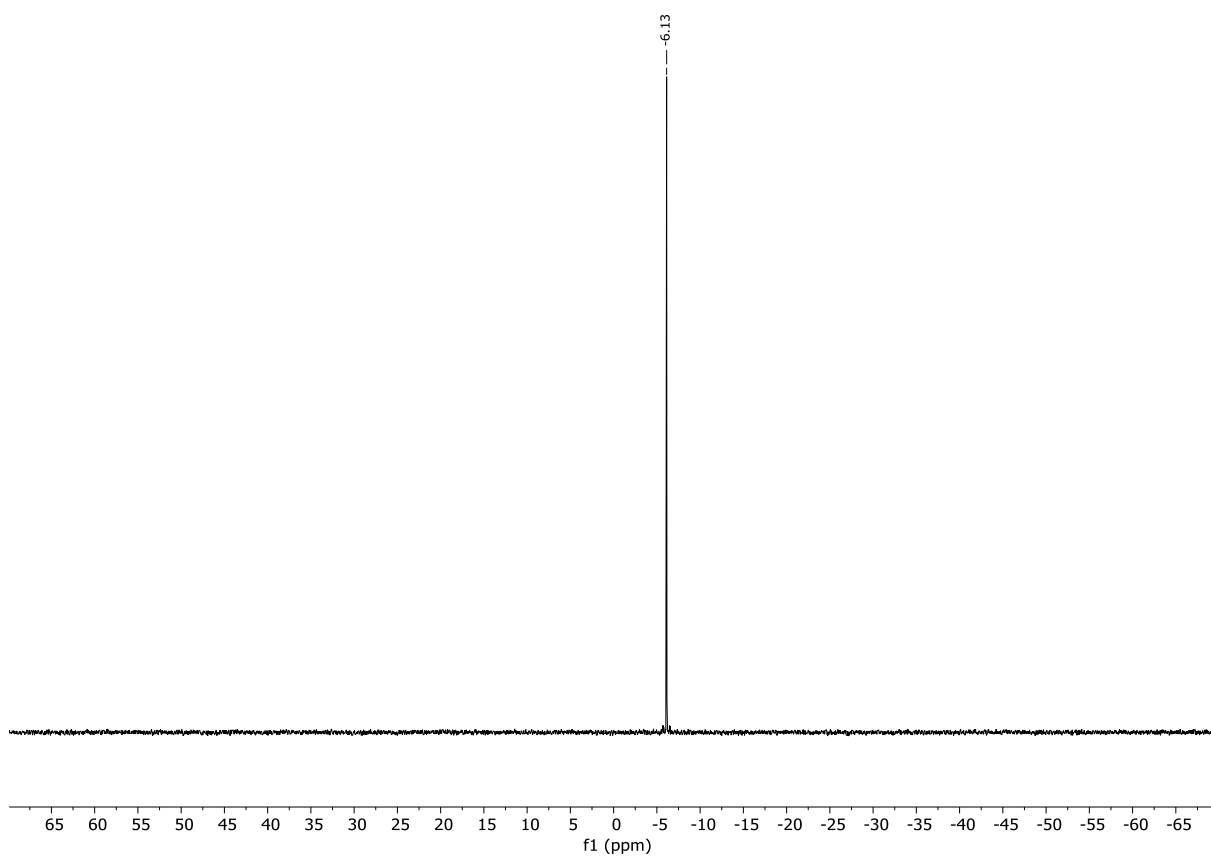


## 7.2 NMR spectra

 $^1\text{H}$  NMR (400 MHz,  $\text{CDCl}_3$ ) Compound **153d** $^{13}\text{C}$  NMR (101 MHz,  $\text{CDCl}_3$ ) Compound **153d**

7. Appendix

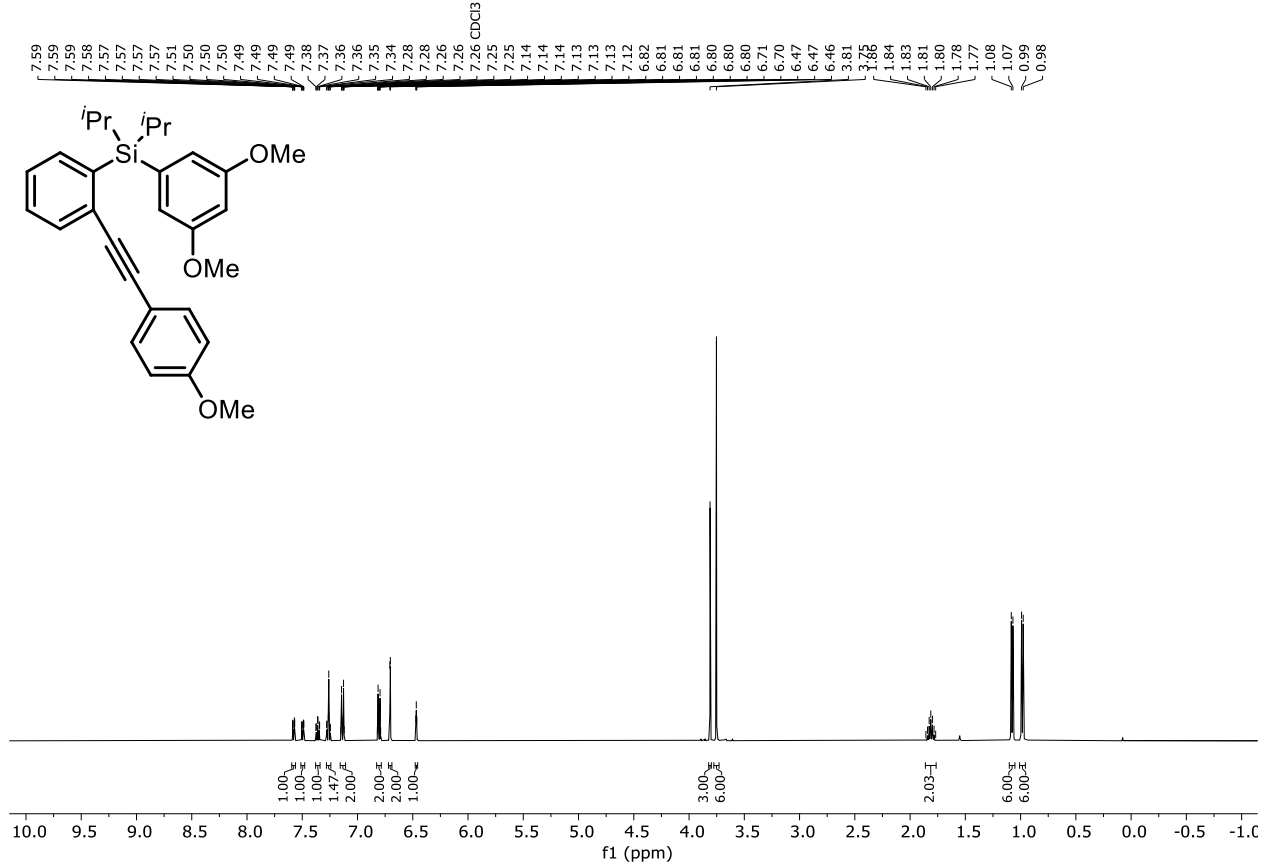
$^{29}\text{Si}$  NMR (79 MHz,  $\text{CDCl}_3$ ) Compound **153d**



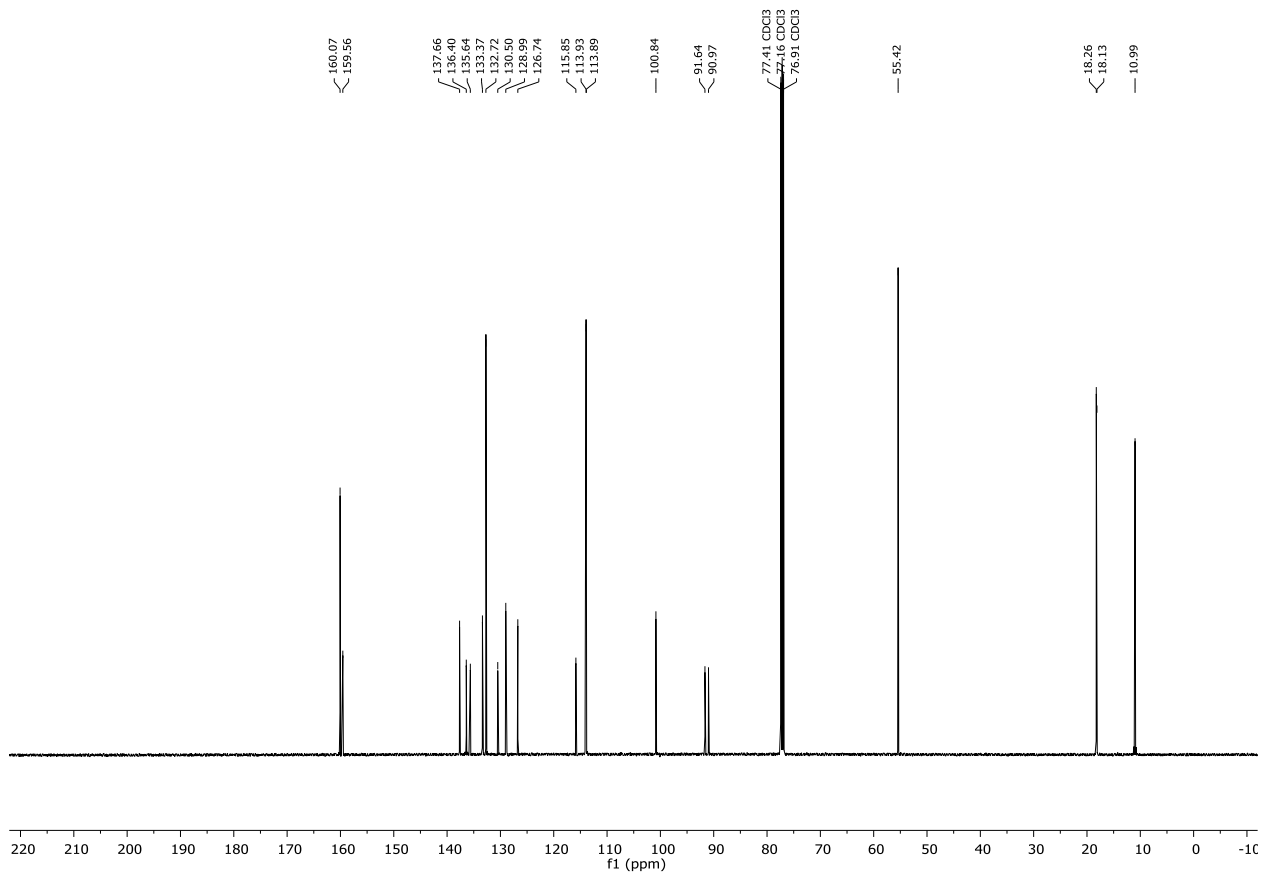


## 7.2 NMR spectra

### $^1\text{H-NMR}$ (500 MHz, $\text{CDCl}_3$ ) Compound **153e**

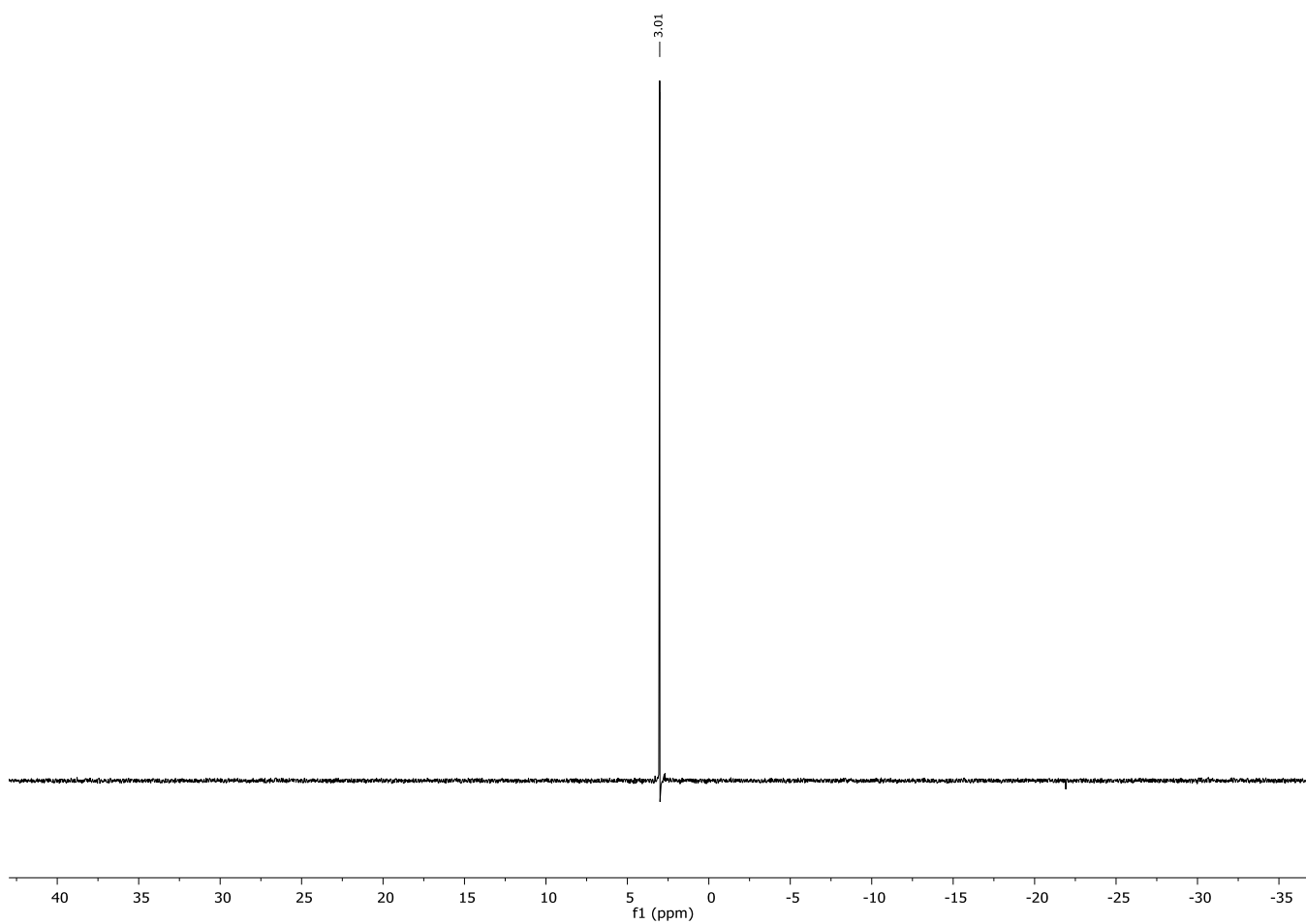


### $^{13}\text{C}\{^1\text{H}\}$ -NMR (126 MHz, $\text{CDCl}_3$ ) Compound **153e**



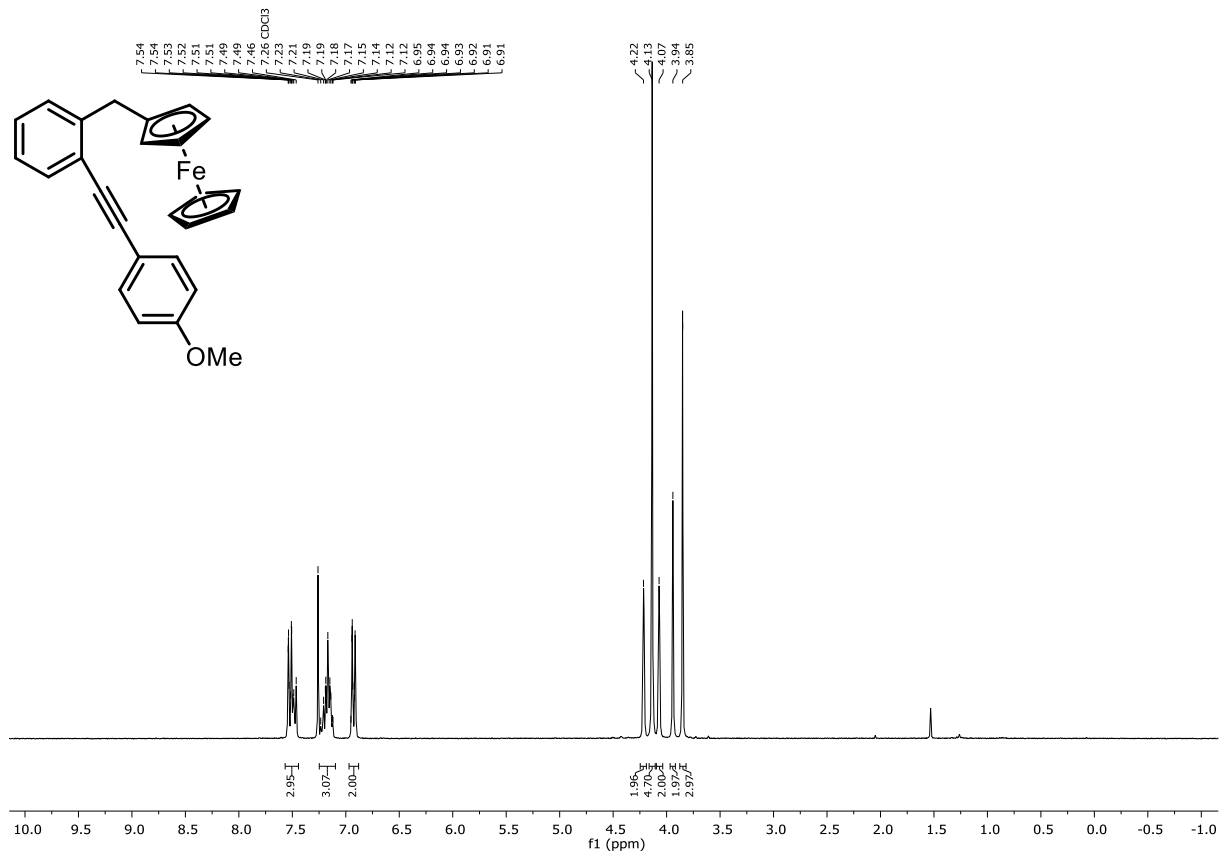
7. Appendix

$^{29}\text{Si-NMR}$  (99 MHz,  $\text{CDCl}_3$ ) Compound **153e**

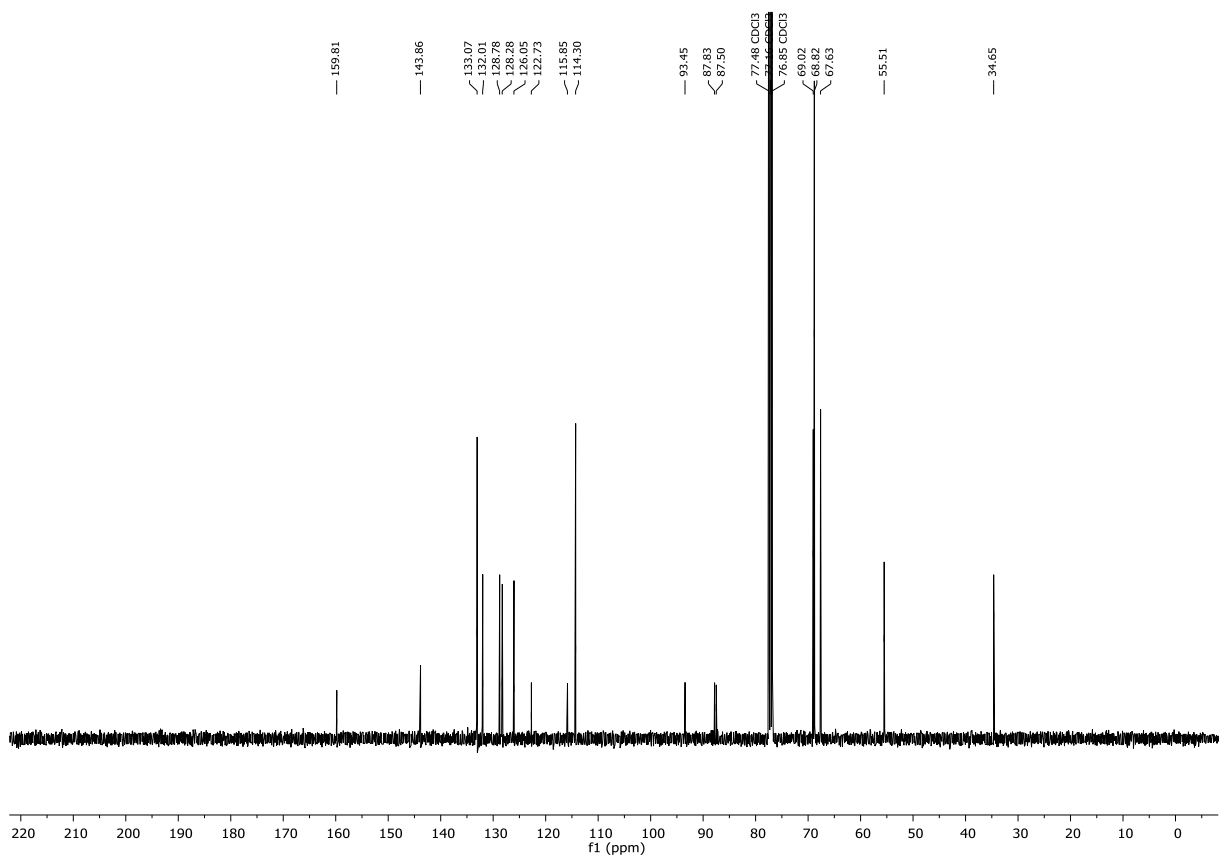


## 7.2 NMR spectra

### $^1\text{H}$ -NMR (300 MHz, $\text{CDCl}_3$ ) Compound **162a**

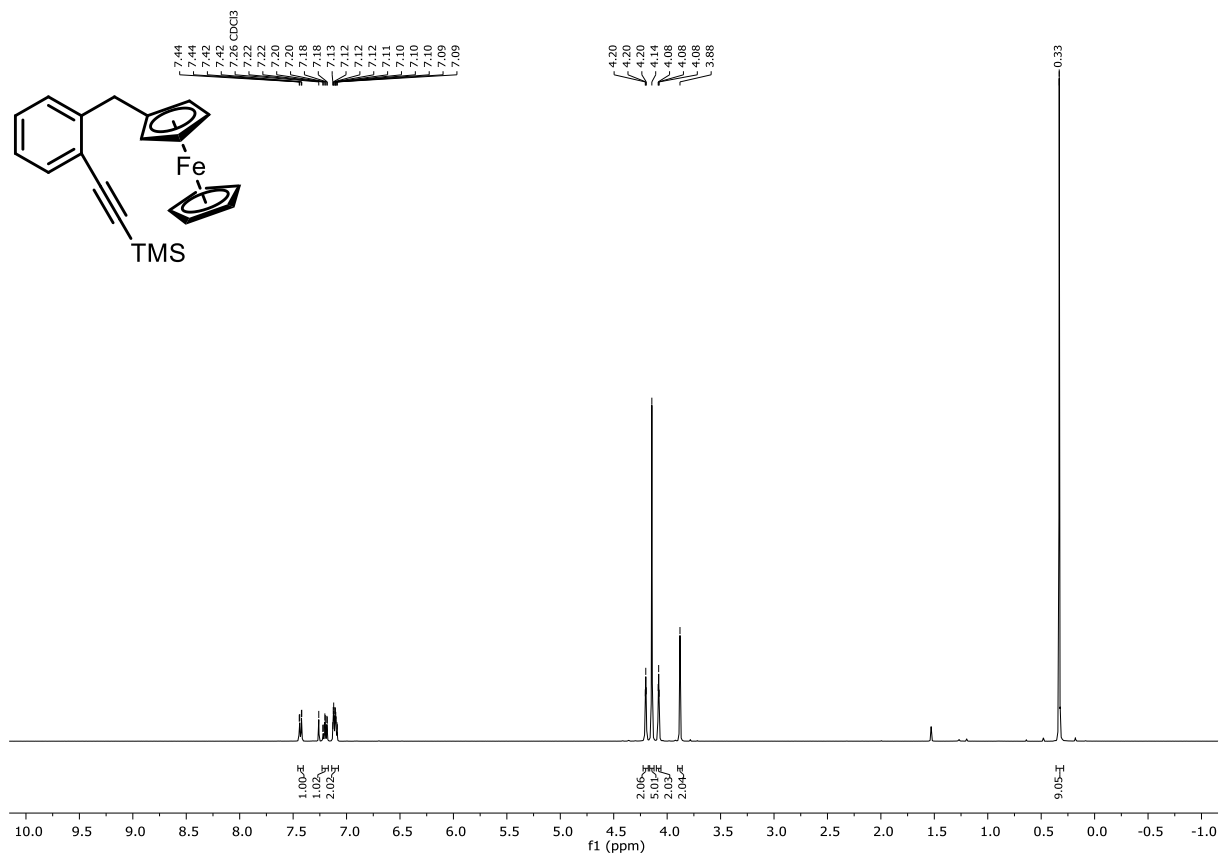


### $^{13}\text{C}\{^1\text{H}\}$ -NMR (101 MHz, $\text{CDCl}_3$ ) Compound **162a**

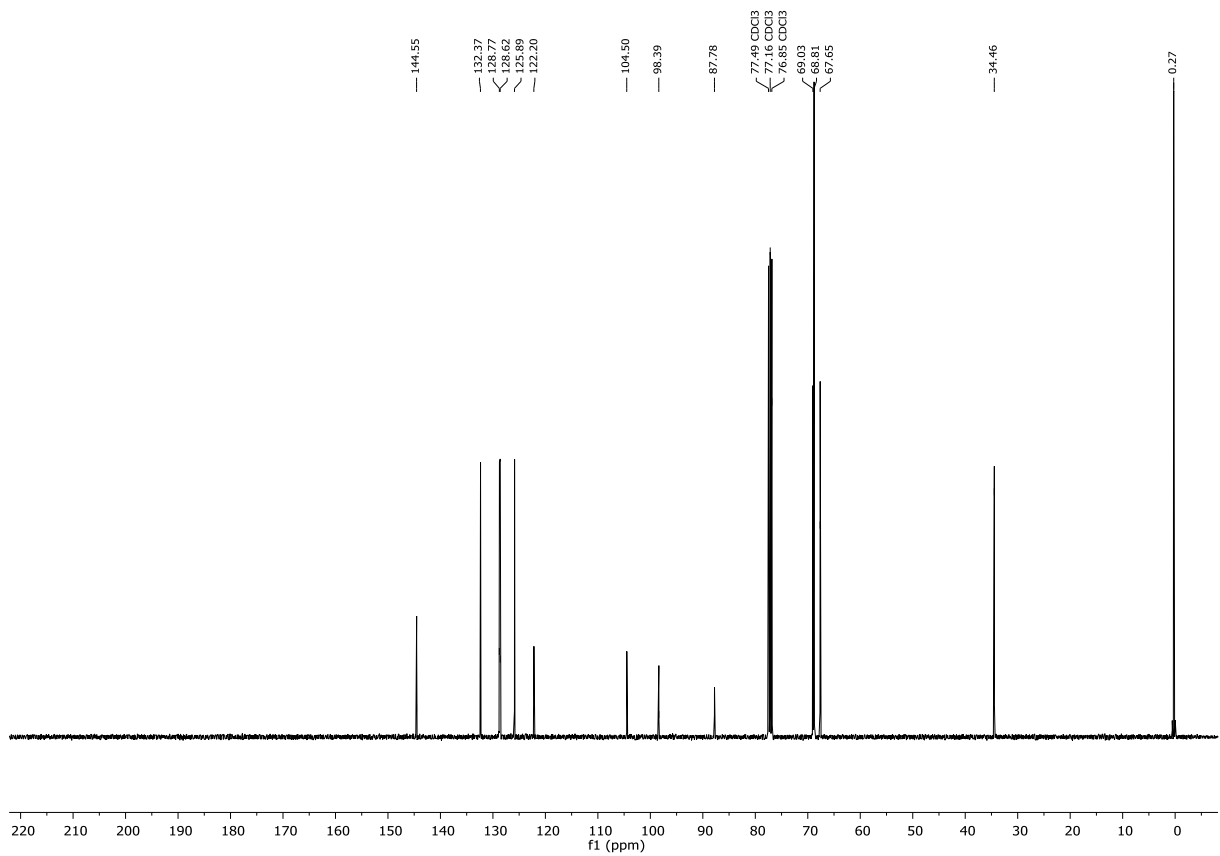


## 7. Appendix

### $^1\text{H-NMR}$ (400 MHz, $\text{CDCl}_3$ ) Compound **162b**

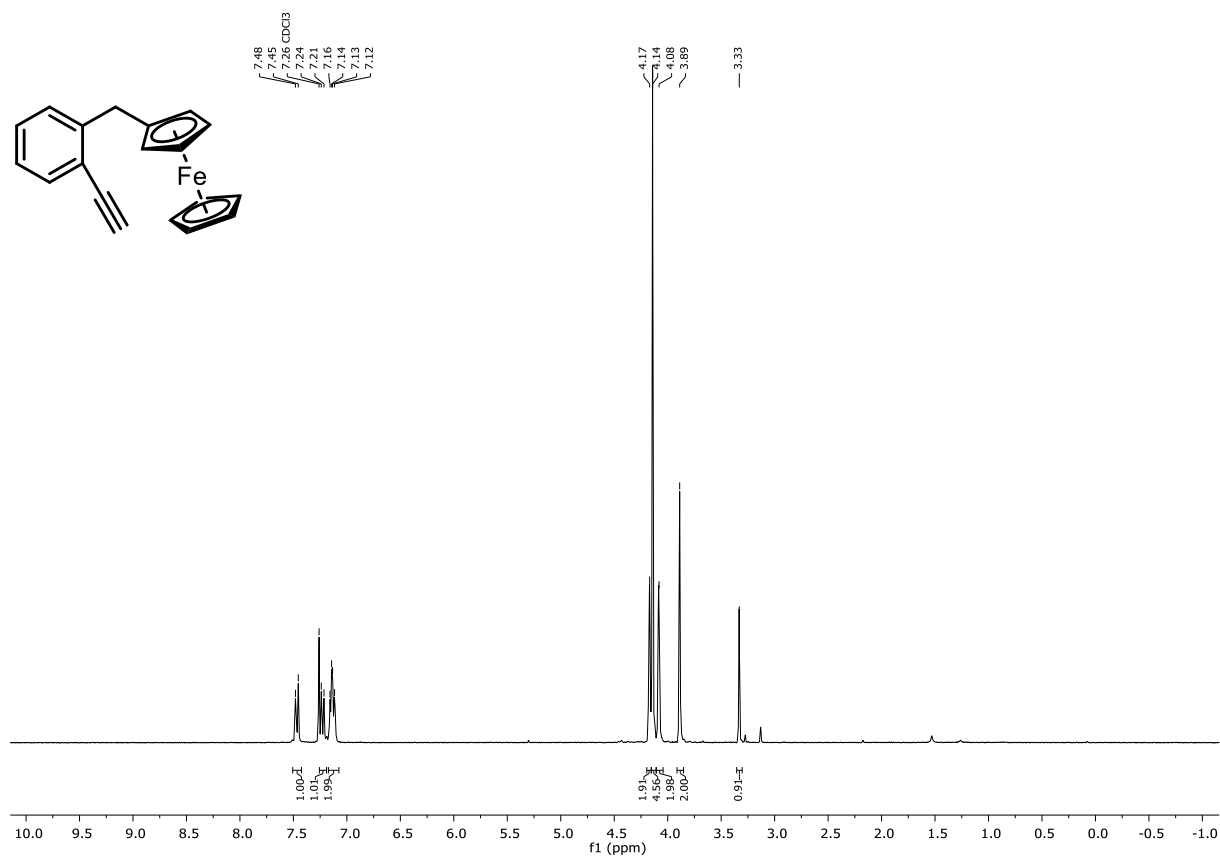


### $^{13}\text{C}\{^1\text{H}\}$ -NMR (101 MHz, $\text{CDCl}_3$ ) Compound **162b**

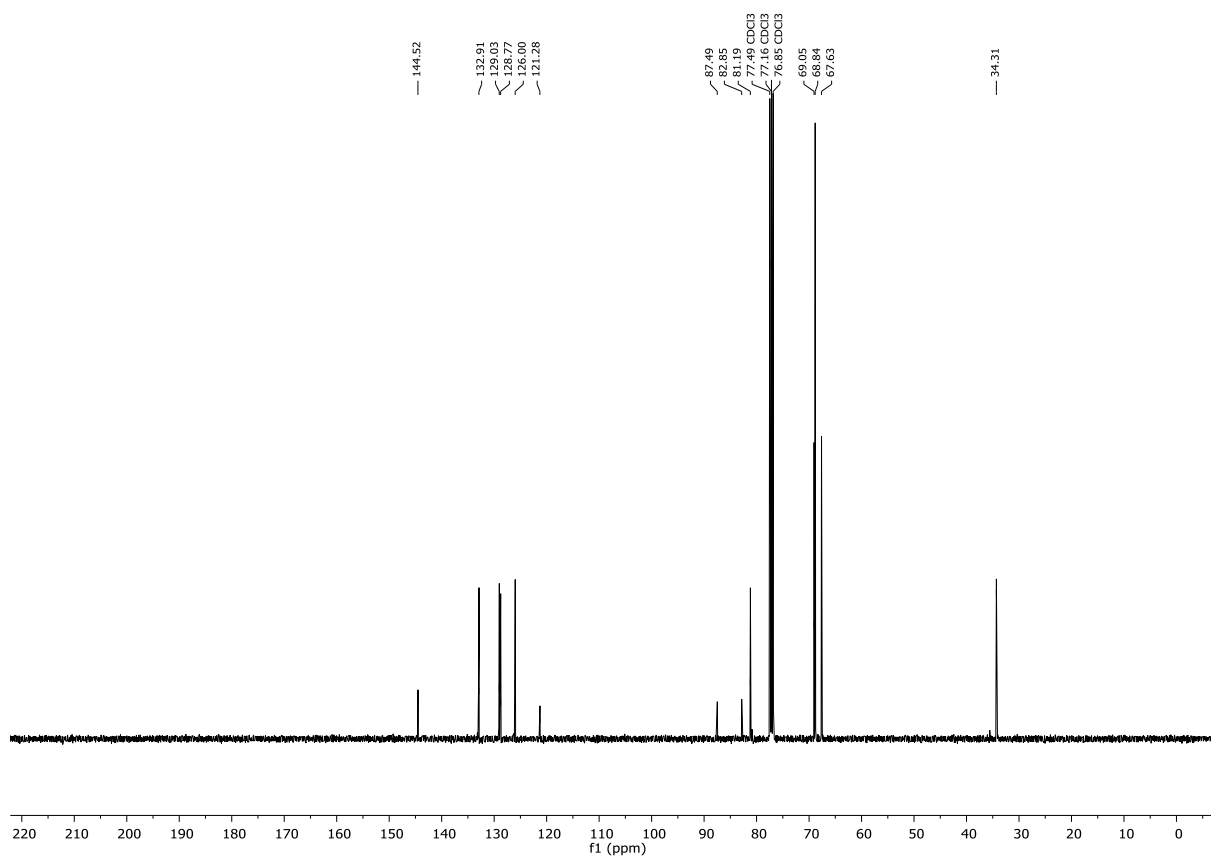


## 7.2 NMR spectra

### $^1\text{H-NMR}$ (300 MHz, $\text{CDCl}_3$ ) Compound **162c**

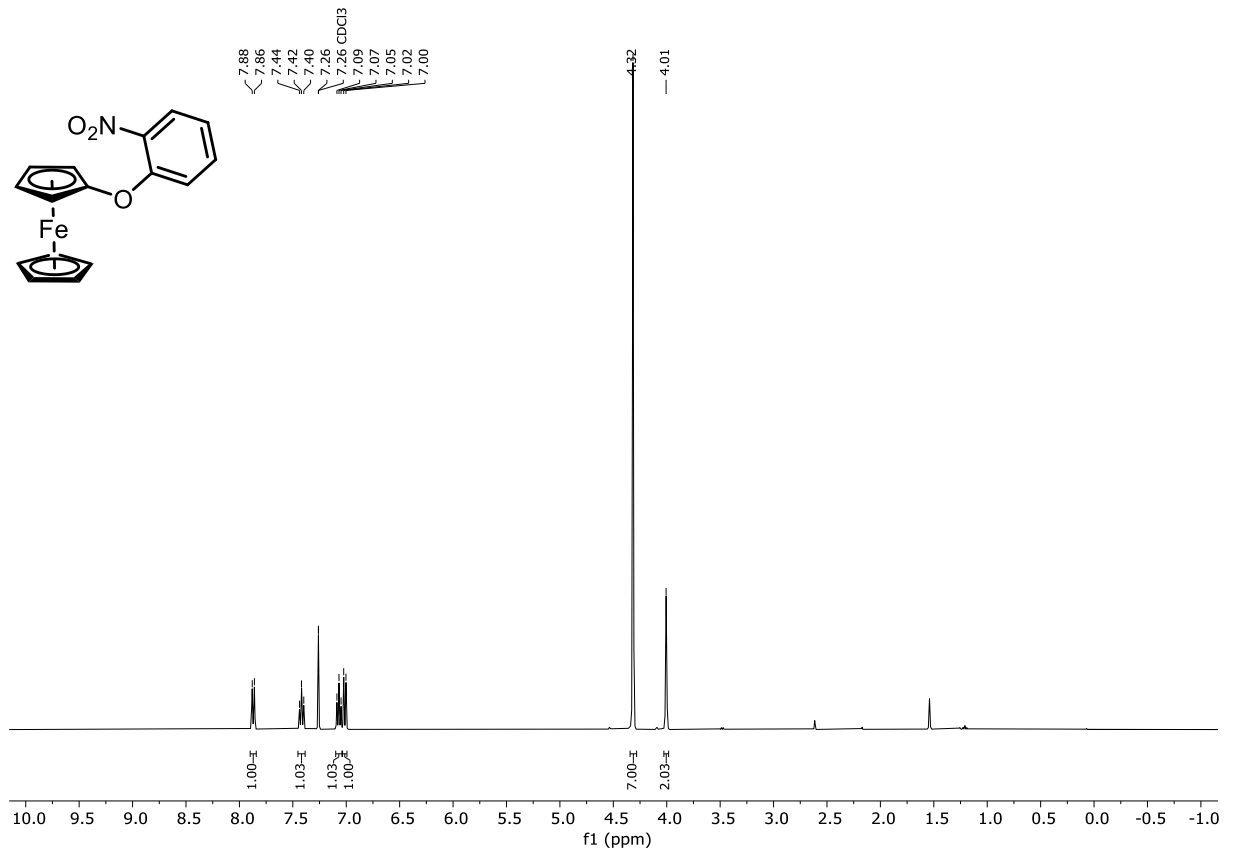


### $^{13}\text{C}\{^1\text{H}\}$ -NMR (101 MHz, $\text{CDCl}_3$ ) Compound **162c**

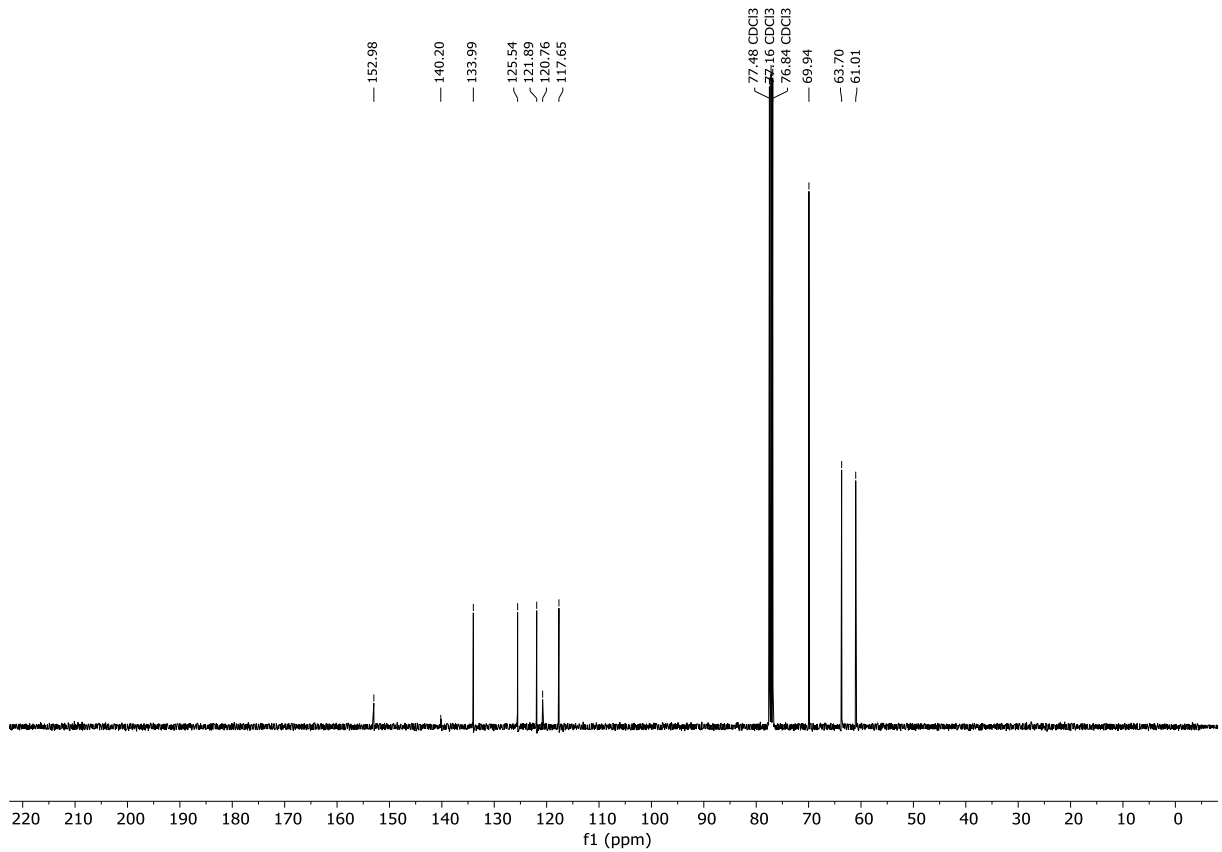


## 7. Appendix

### $^1\text{H-NMR}$ (400 MHz, $\text{CDCl}_3$ ) Compound **193**

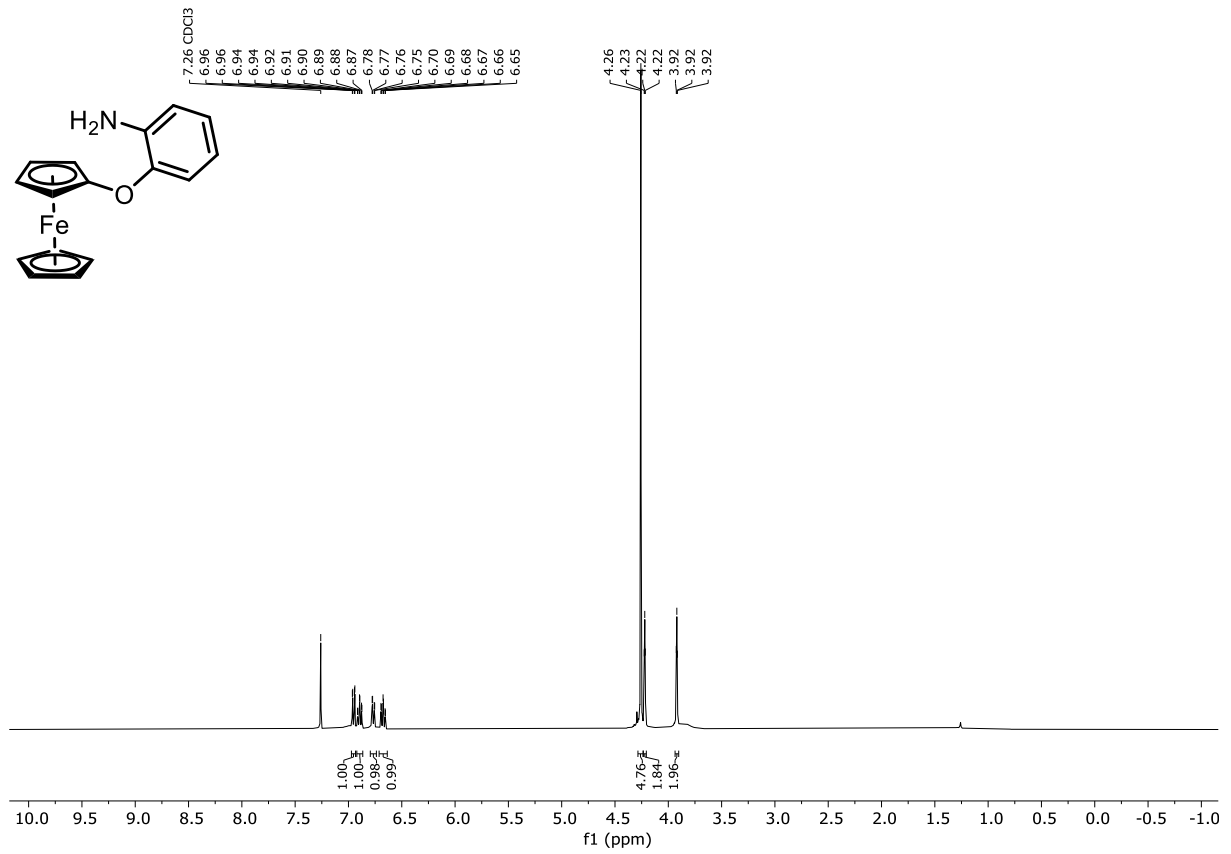


### $^{13}\text{C}\{^1\text{H}\}$ -NMR (101 MHz, $\text{CDCl}_3$ ) Compound **193**

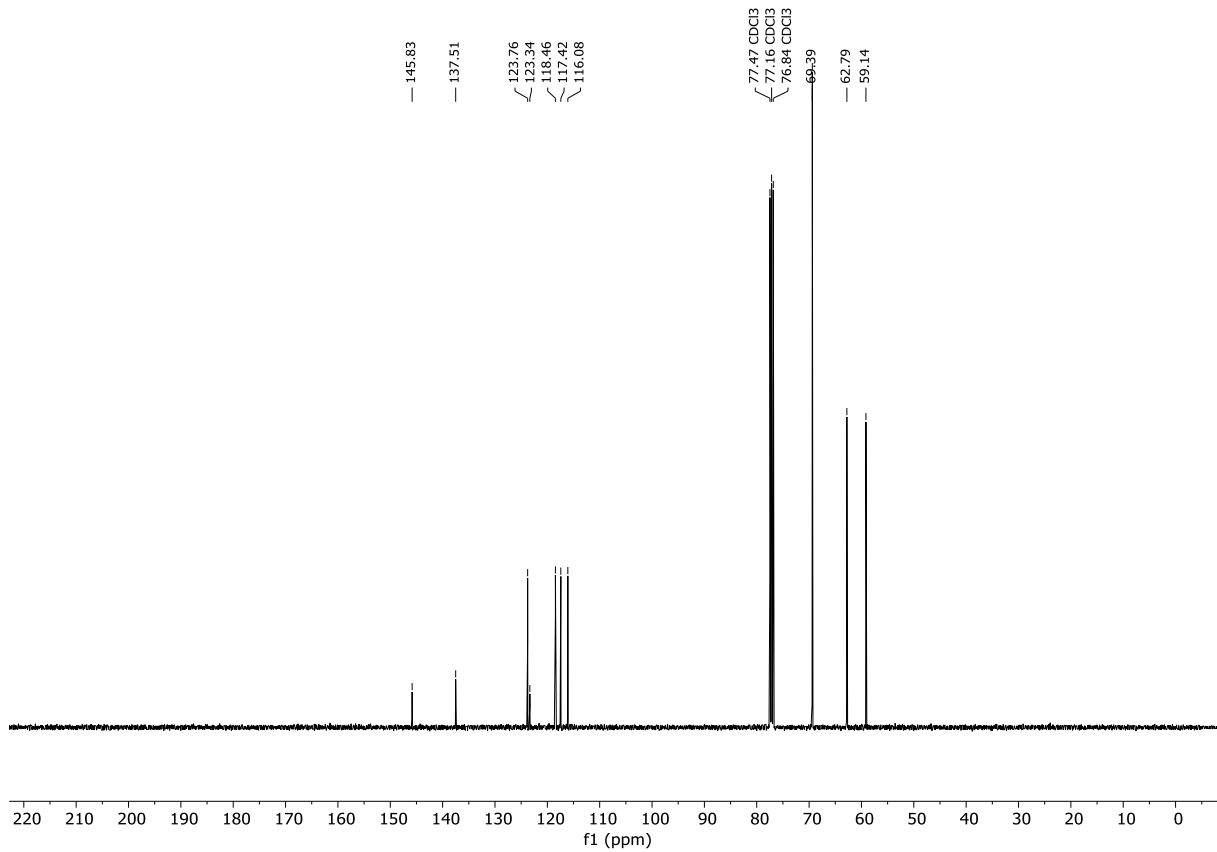


## 7.2 NMR spectra

### $^1\text{H-NMR}$ (400 MHz, $\text{CDCl}_3$ ) Compound **194**

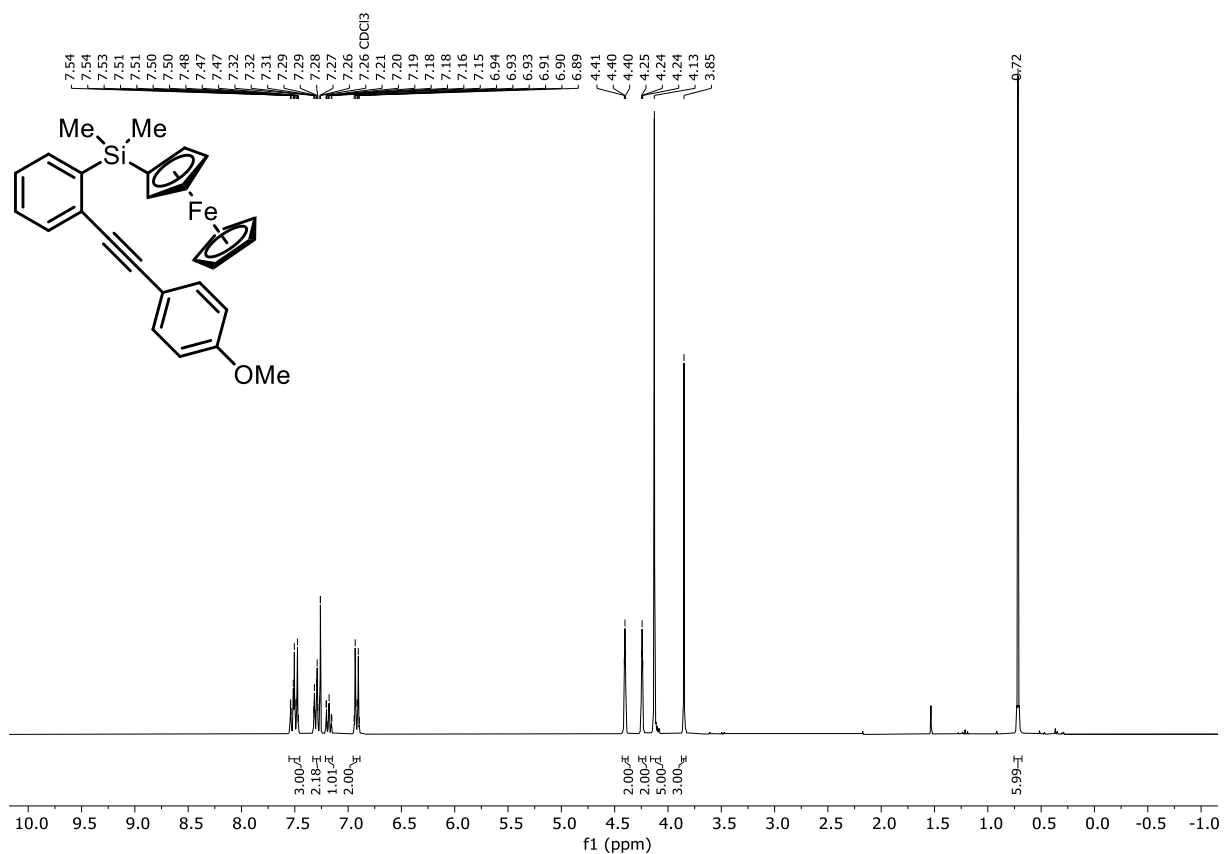


### $^{13}\text{C}\{^1\text{H}\}$ -NMR (101 MHz, $\text{CDCl}_3$ ) Compound **194**

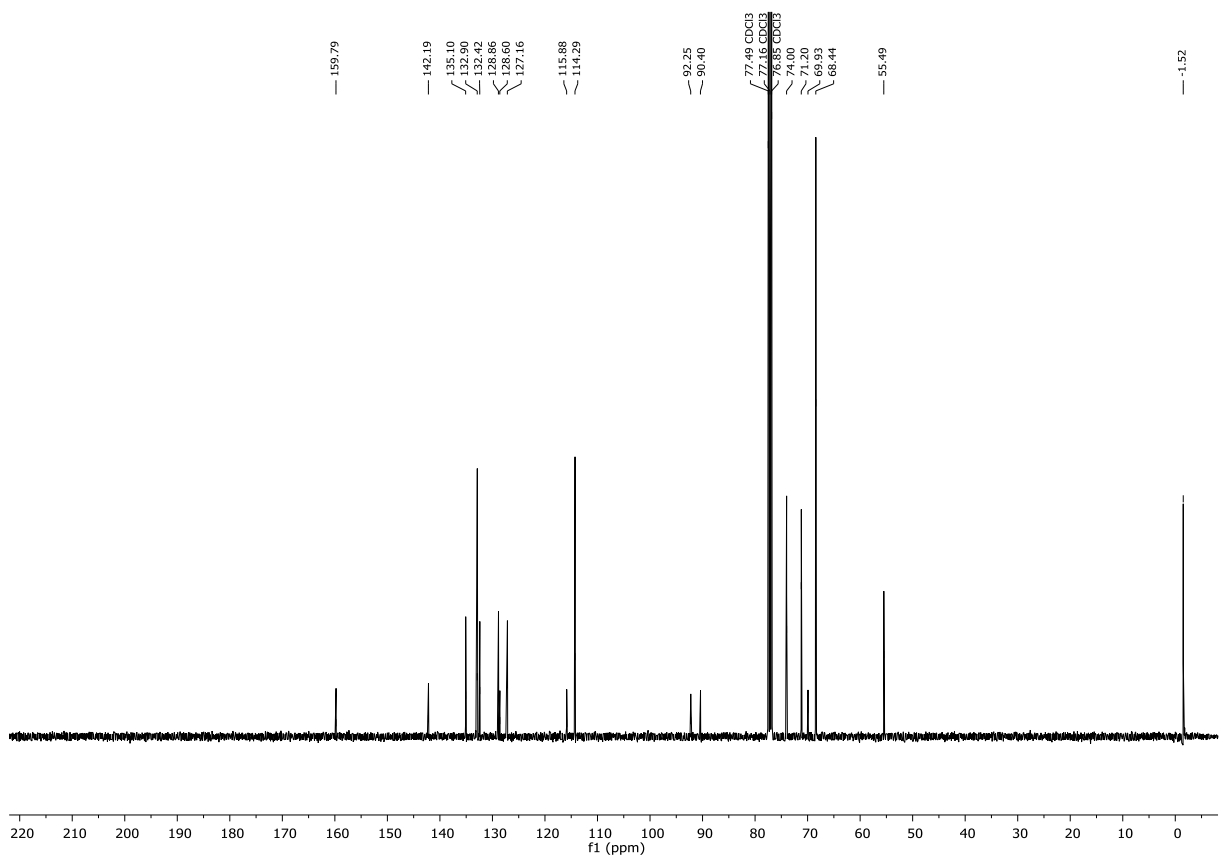


## 7. Appendix

### $^1\text{H-NMR}$ (300 MHz, $\text{CDCl}_3$ ) Compound **164**



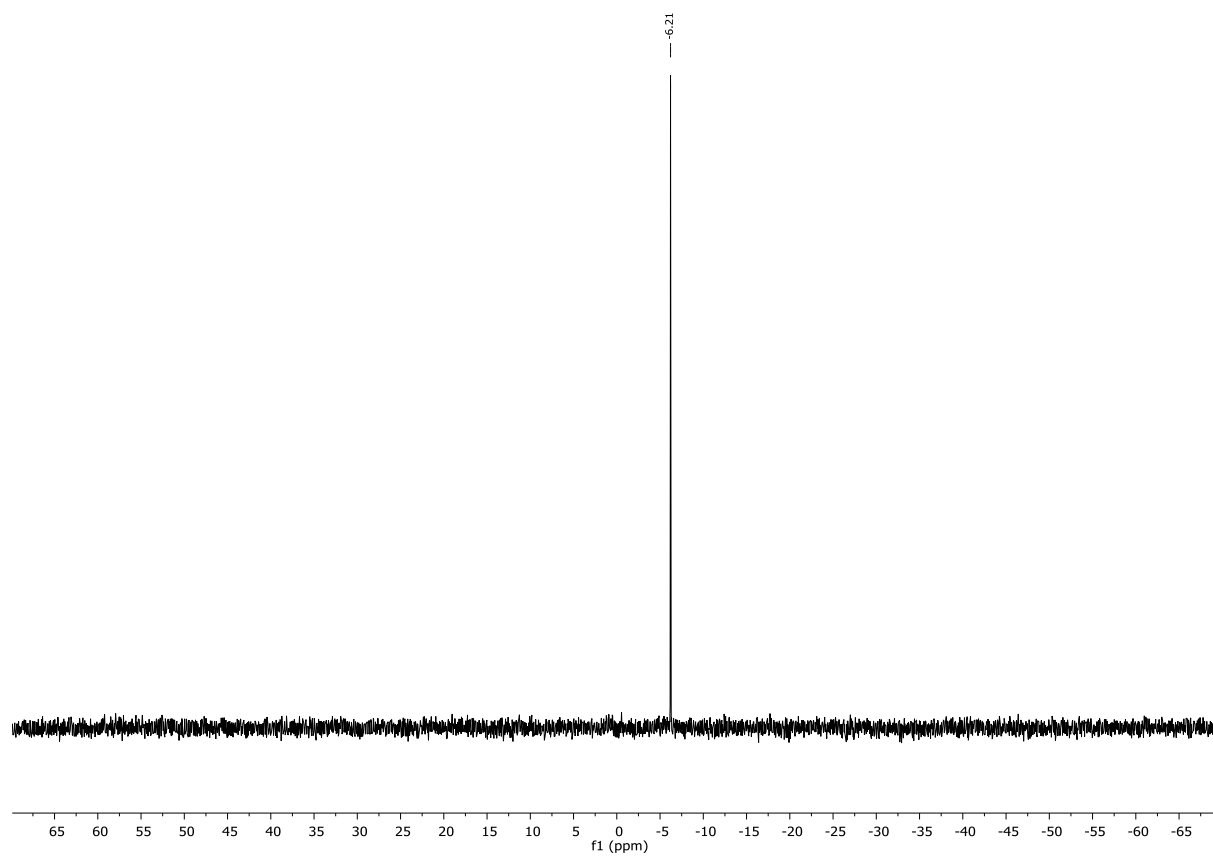
### $^{13}\text{C}\{^1\text{H}\}$ -NMR (101 MHz, $\text{CDCl}_3$ ) Compound **164**





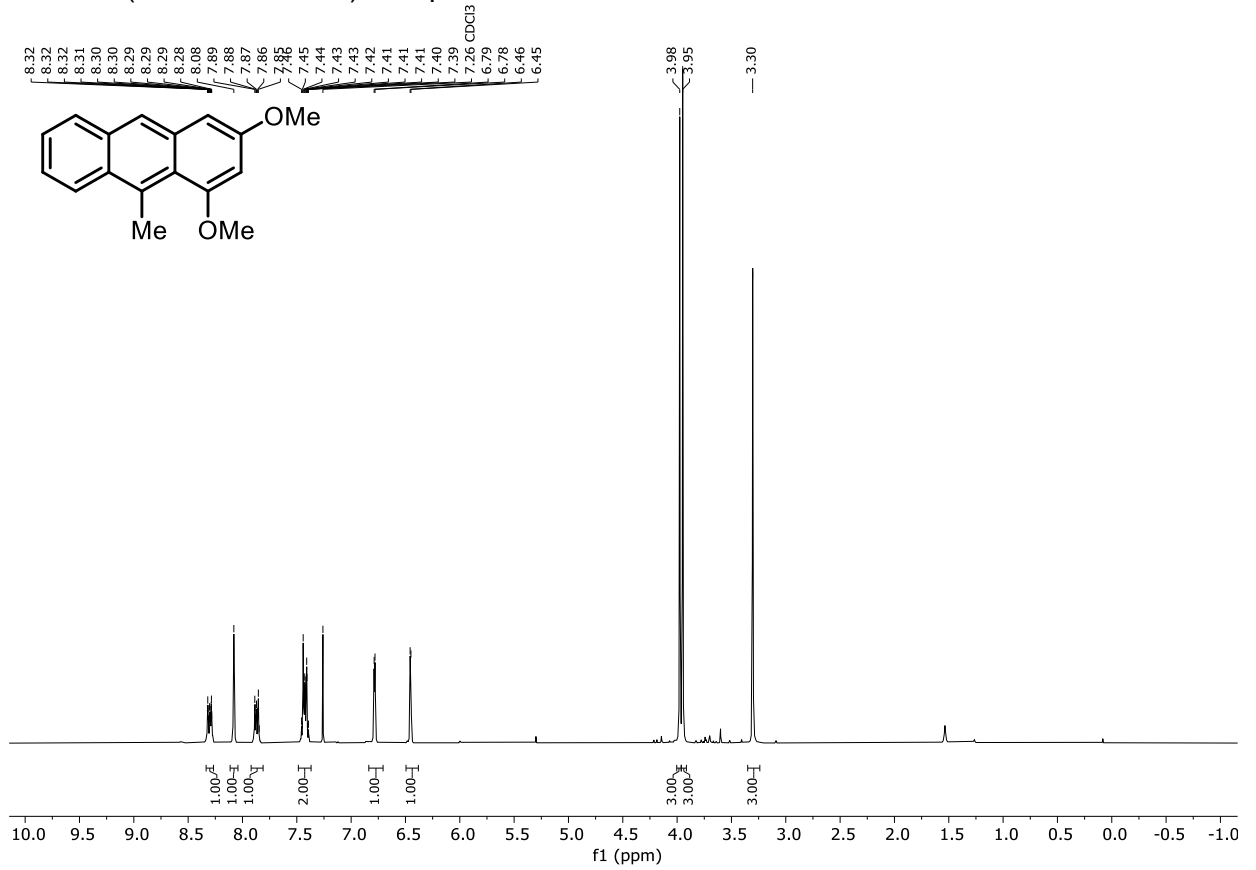
## 7.2 NMR spectra

$^{29}\text{Si}$ -NMR (79 MHz,  $\text{CDCl}_3$ ) Compound **164**

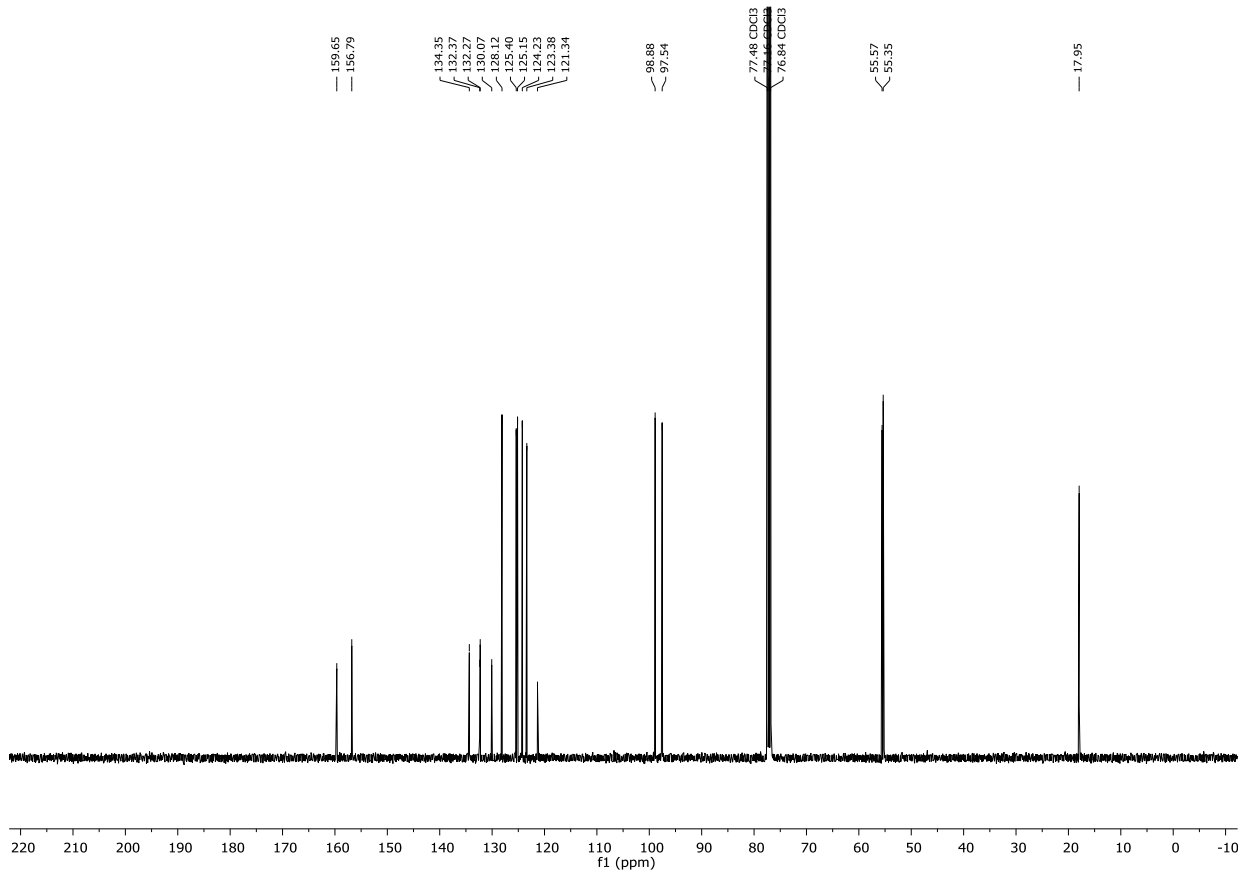


7. Appendix

<sup>1</sup>H-NMR (300 MHz, CDCl<sub>3</sub>) Compound **199a**

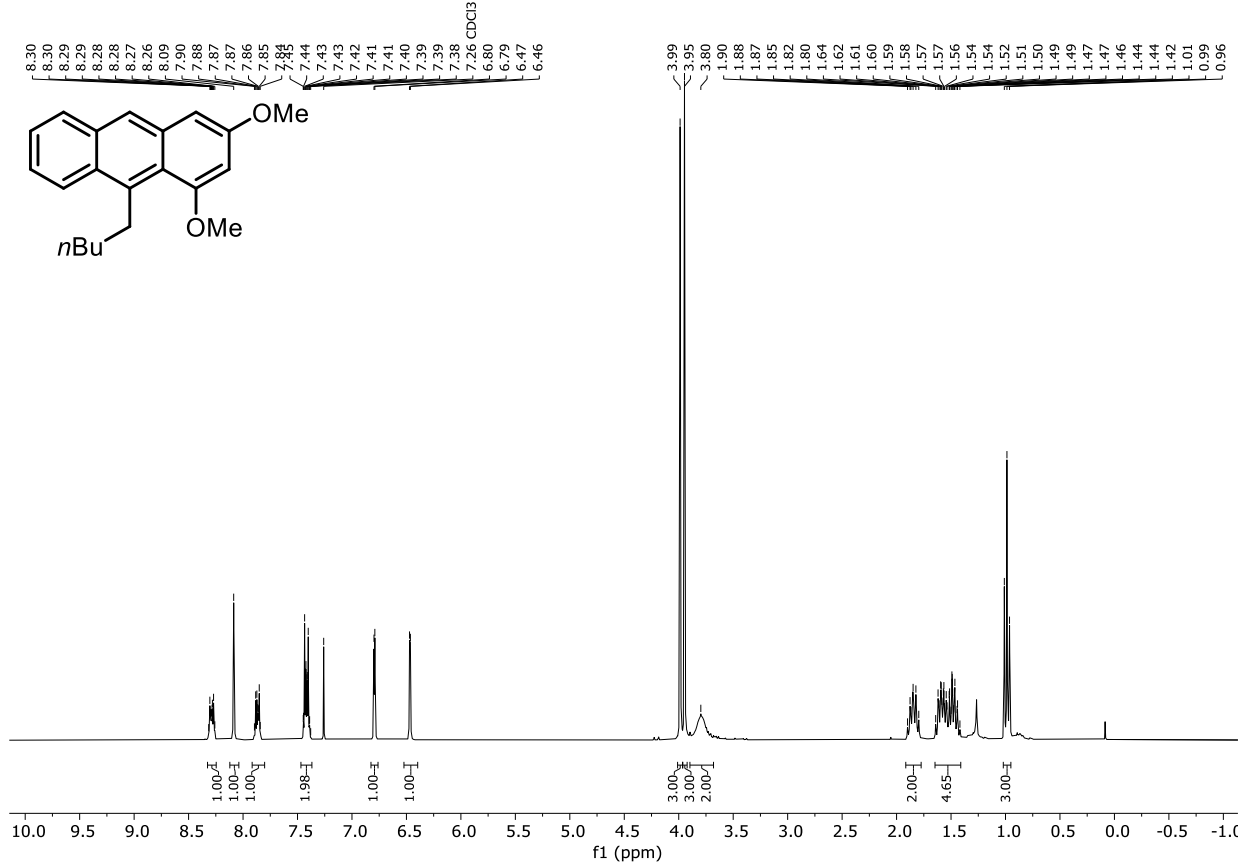


<sup>13</sup>C{<sup>1</sup>H}-NMR (101 MHz, CDCl<sub>3</sub>) Compound **199a**

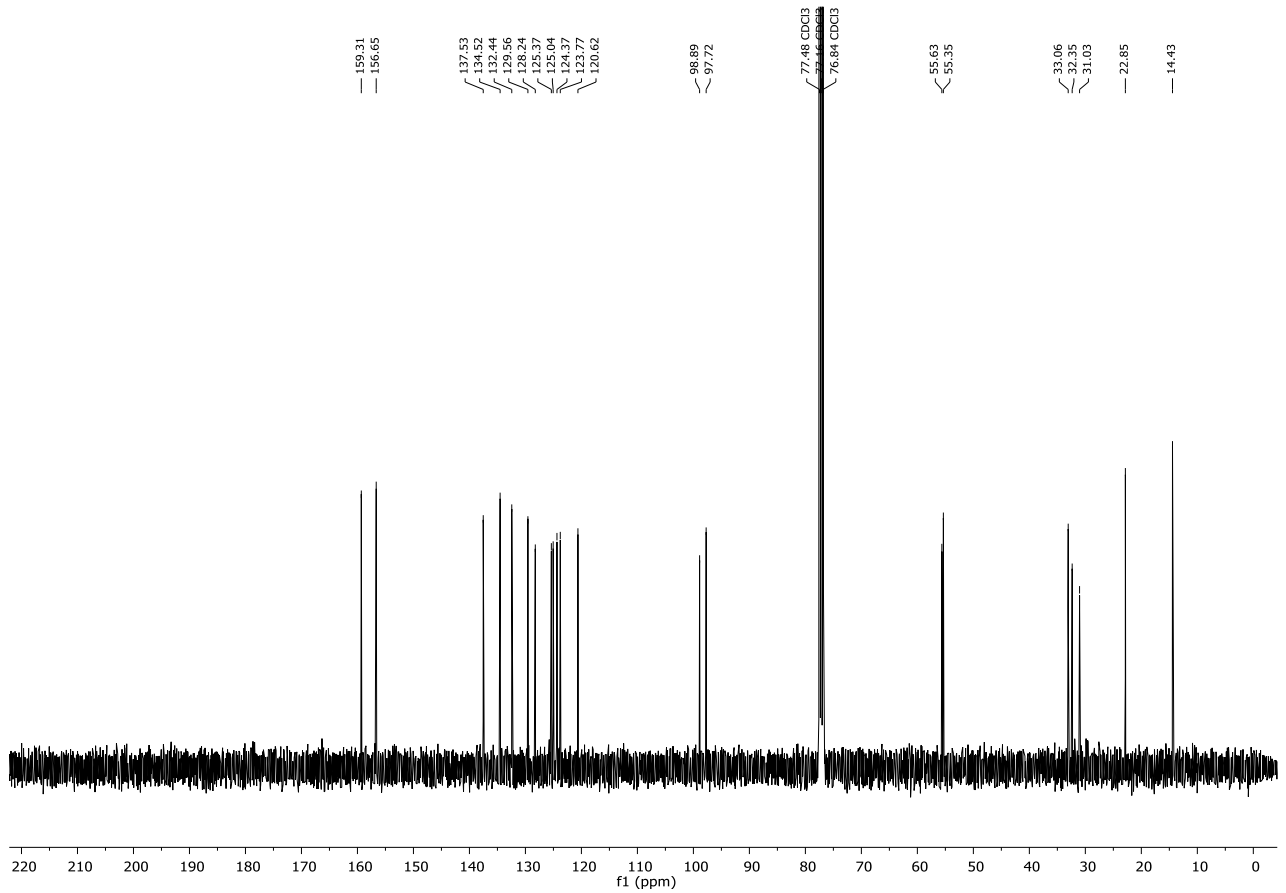


## 7.2 NMR spectra

### $^1\text{H-NMR}$ (300 MHz, $\text{CDCl}_3$ ) Compound **199b**

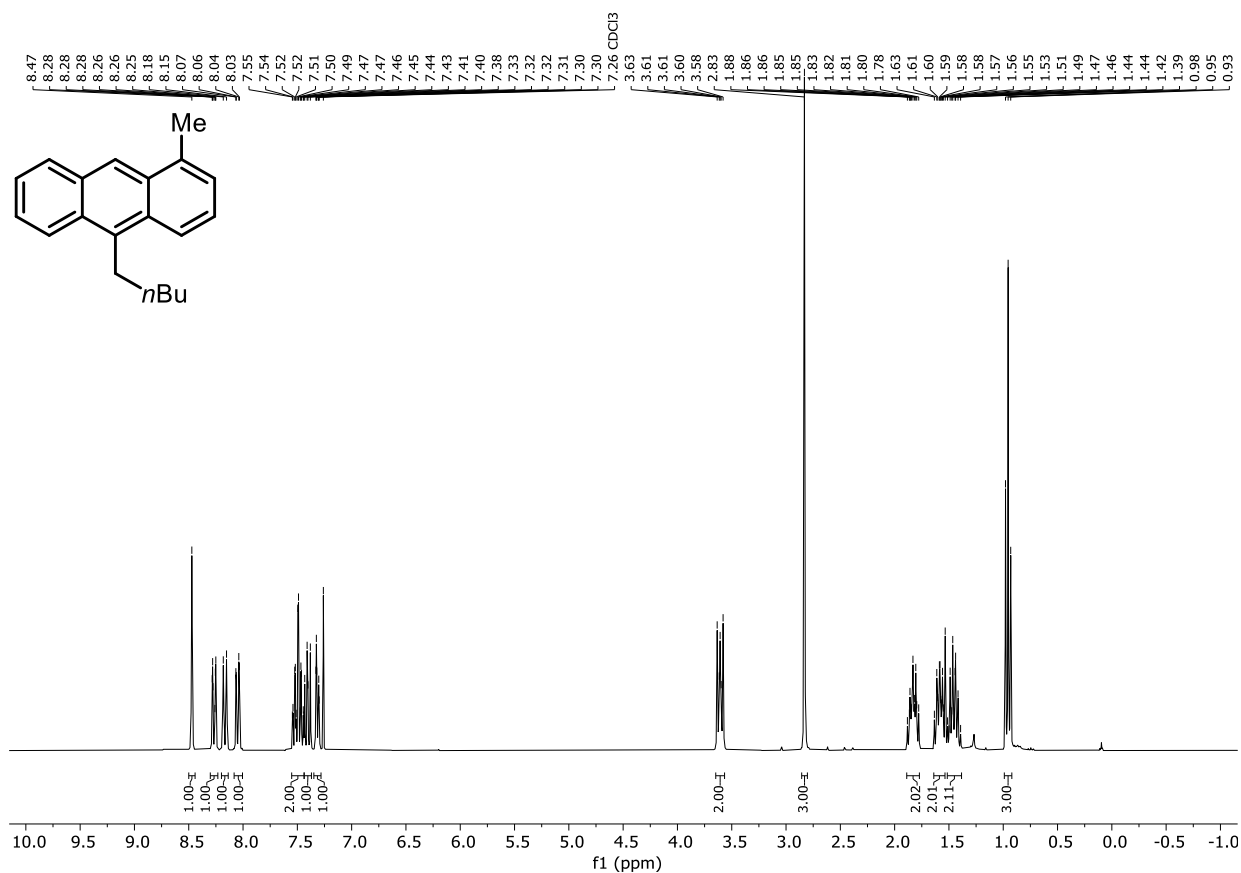


### $^{13}\text{C}\{^1\text{H}\}$ -NMR (101 MHz, $\text{CDCl}_3$ ) Compound **199b**

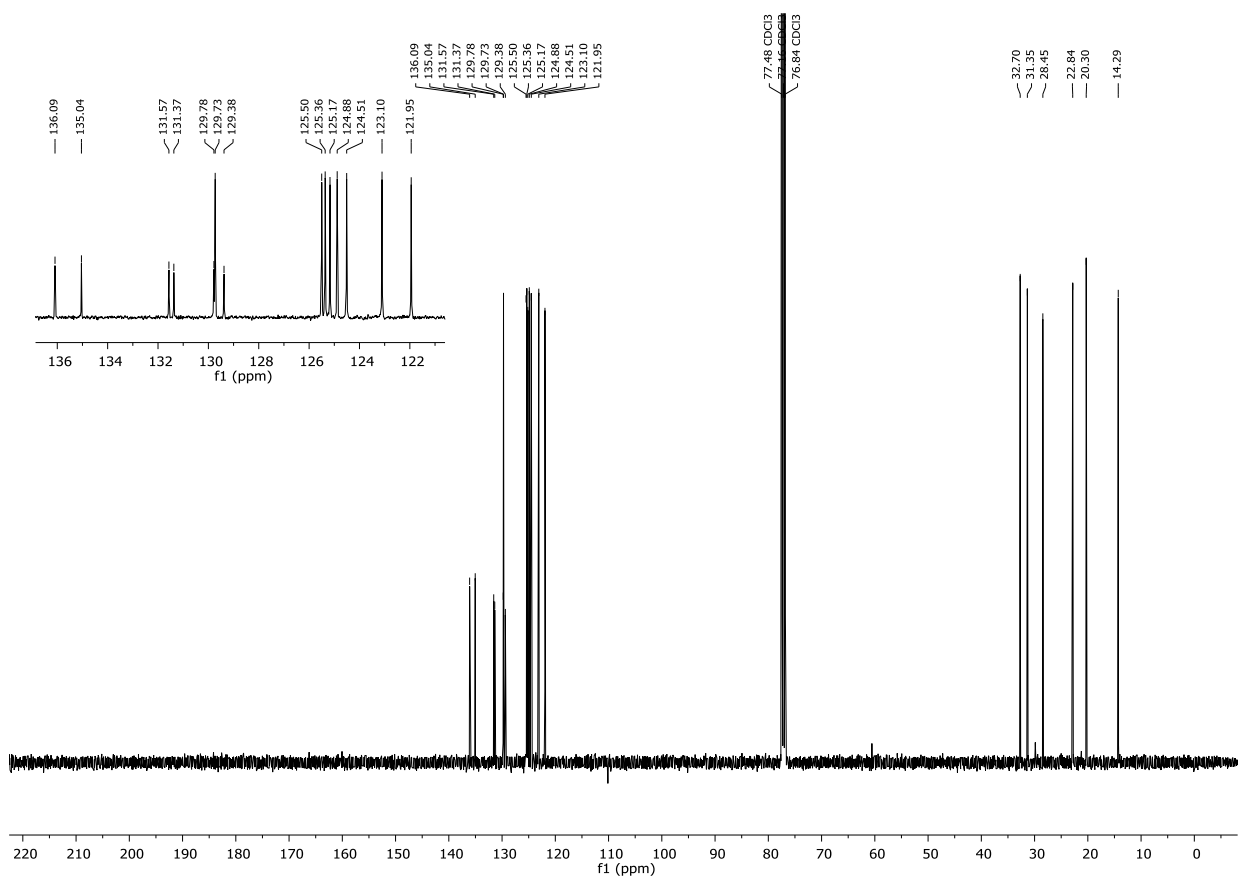


## 7. Appendix

### $^1\text{H-NMR}$ (300 MHz, $\text{CDCl}_3$ ) Compound **199c**

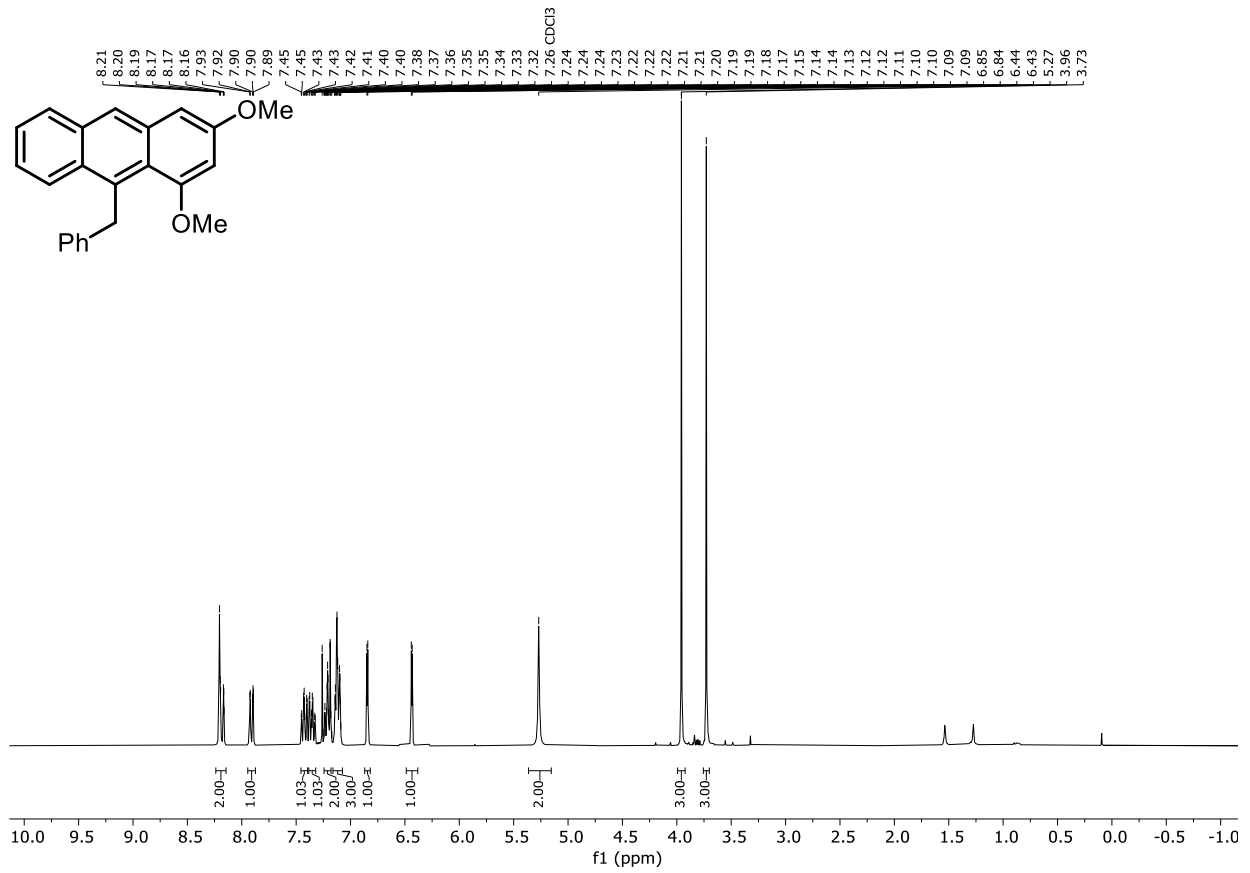


### $^{13}\text{C}\{^1\text{H}\}$ -NMR (101 MHz, $\text{CDCl}_3$ ) Compound **199c**

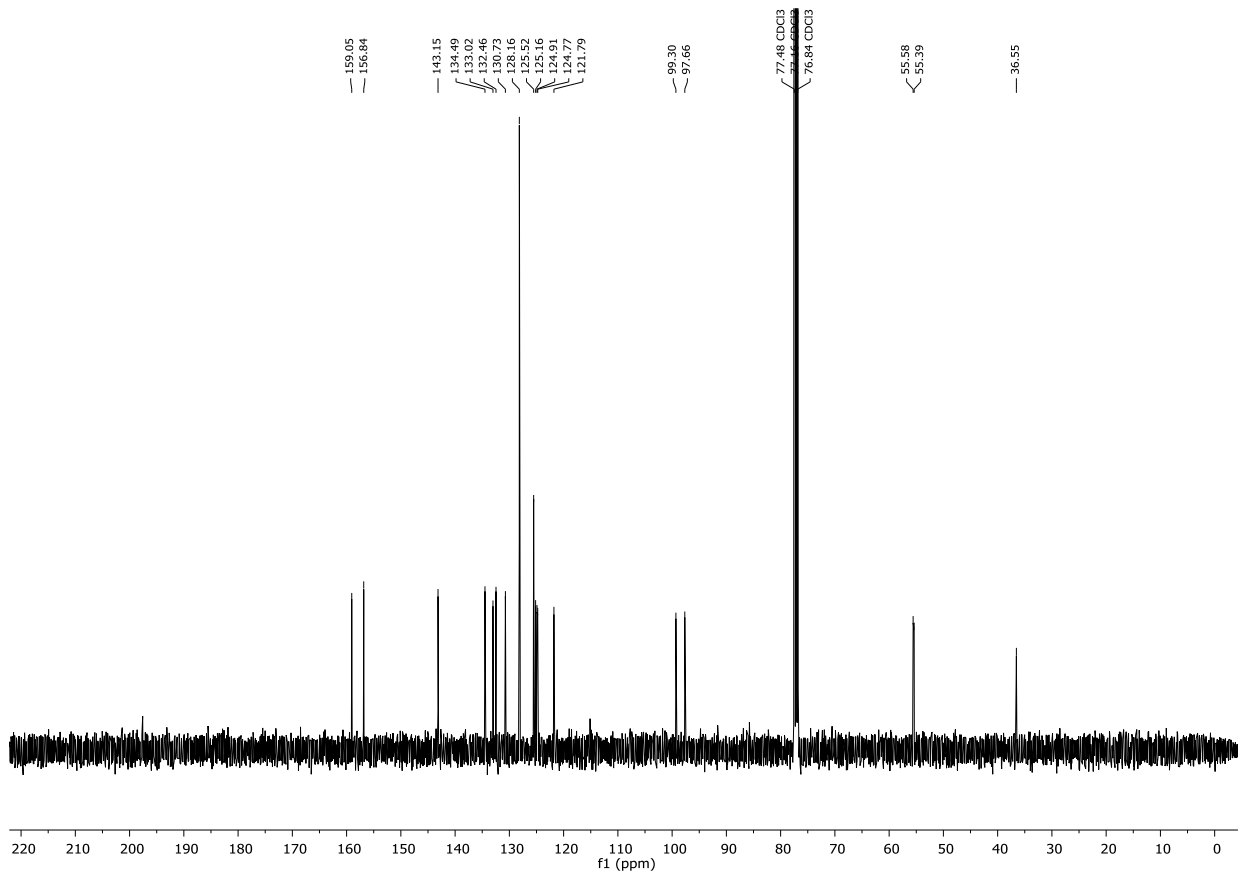


## 7.2 NMR spectra

### $^1\text{H-NMR}$ (300 MHz, $\text{CDCl}_3$ ) Compound **199d**

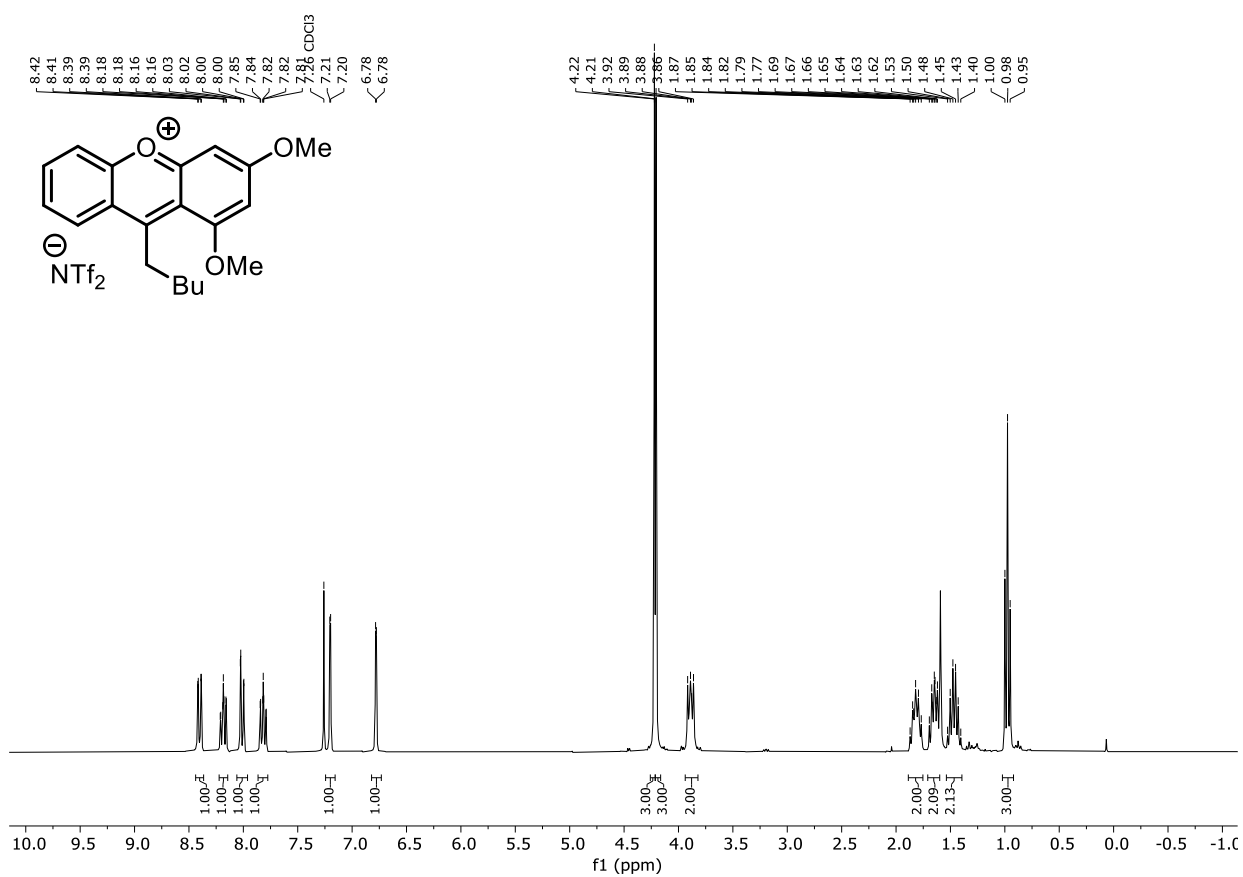


### $^{13}\text{C}\{^1\text{H}\}$ -NMR (101 MHz, $\text{CDCl}_3$ ) Compound **199d**

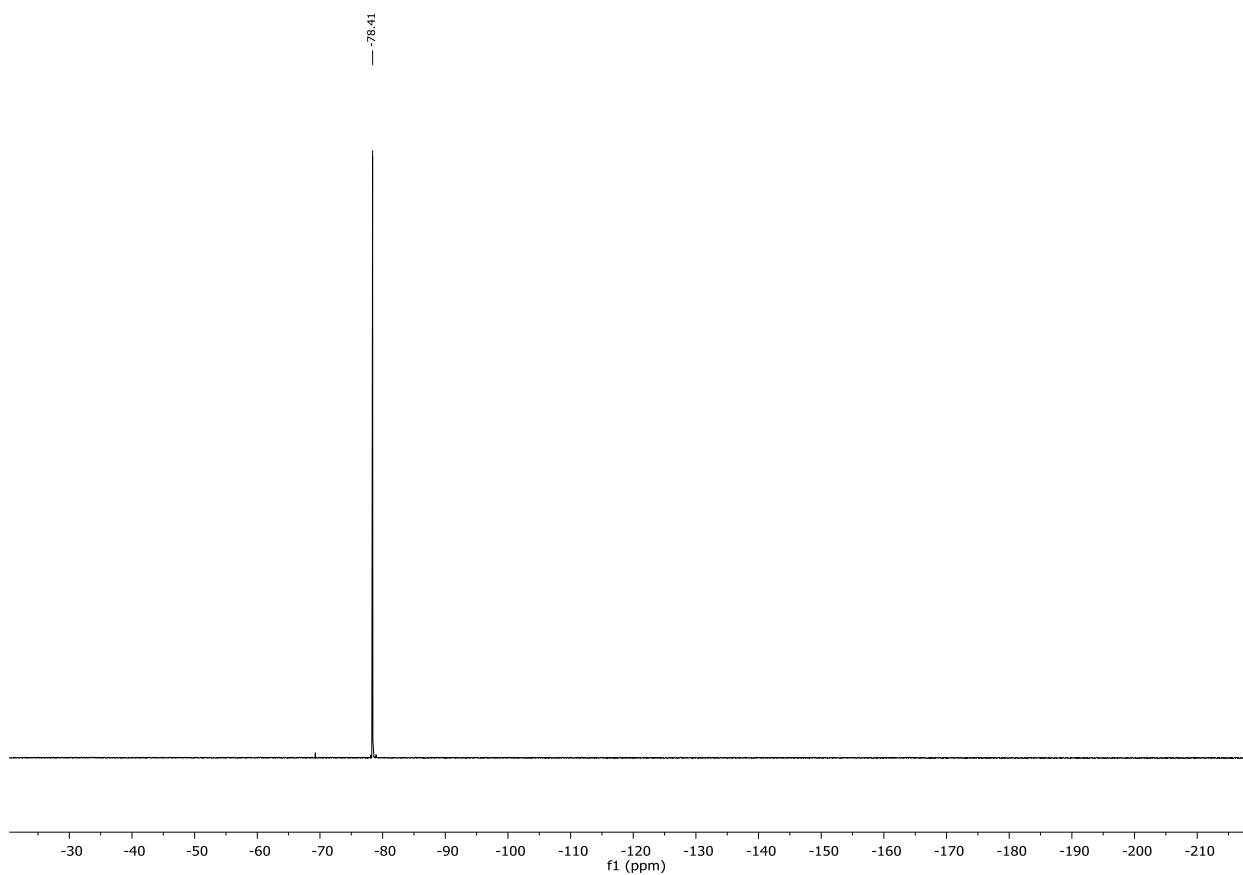


## 7. Appendix

### $^1\text{H-NMR}$ (300 MHz, $\text{CDCl}_3$ ) Compound **200a**

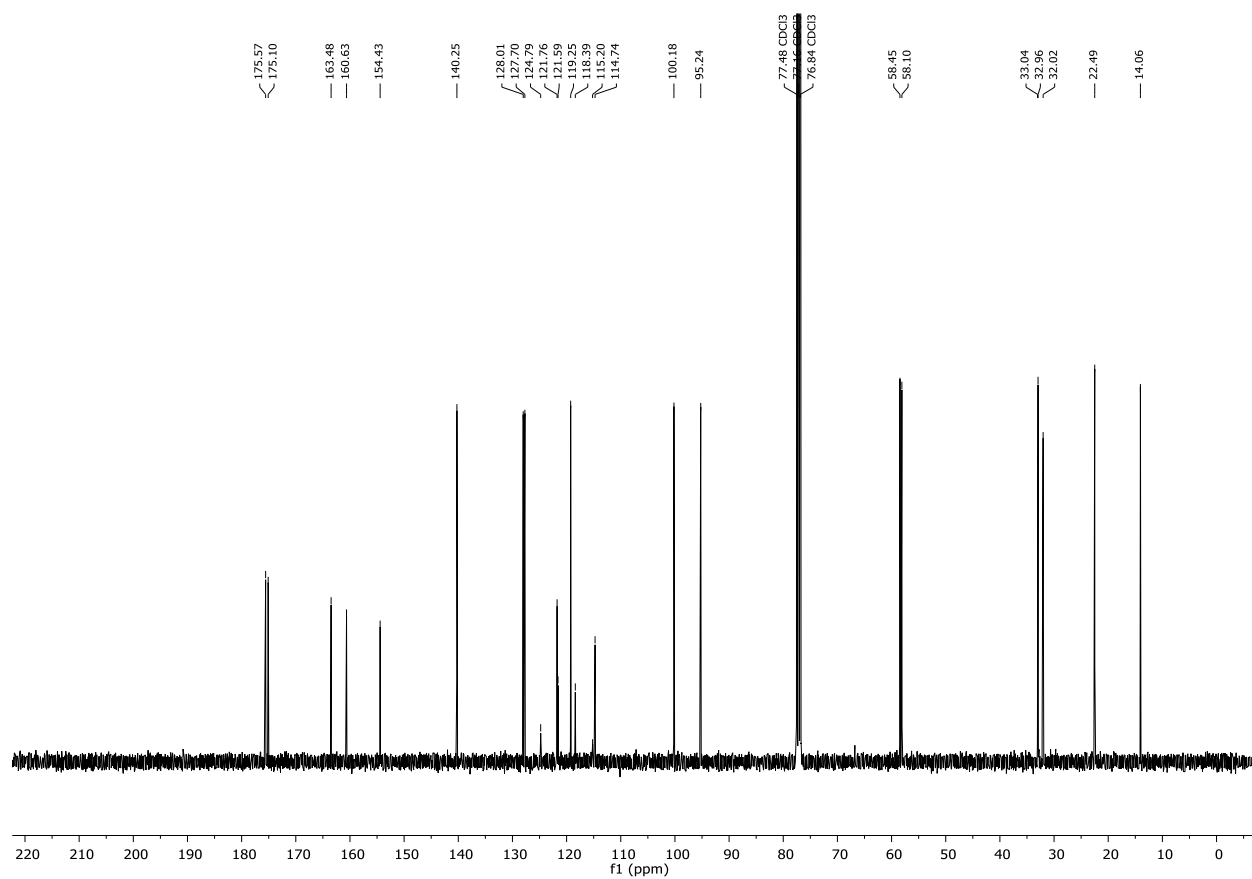


### $^{19}\text{F-NMR}$ (376 MHz, $\text{CDCl}_3$ ) Compound **200a**

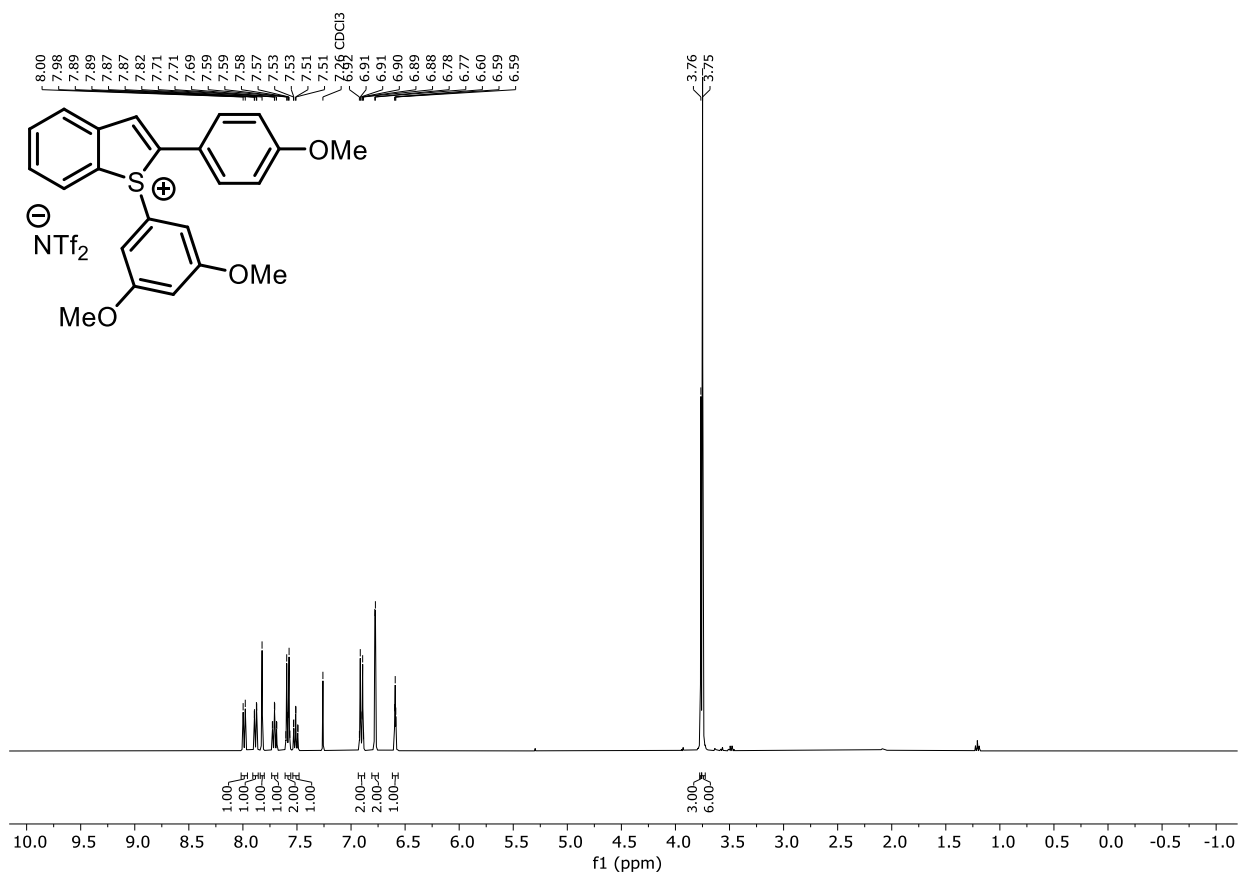
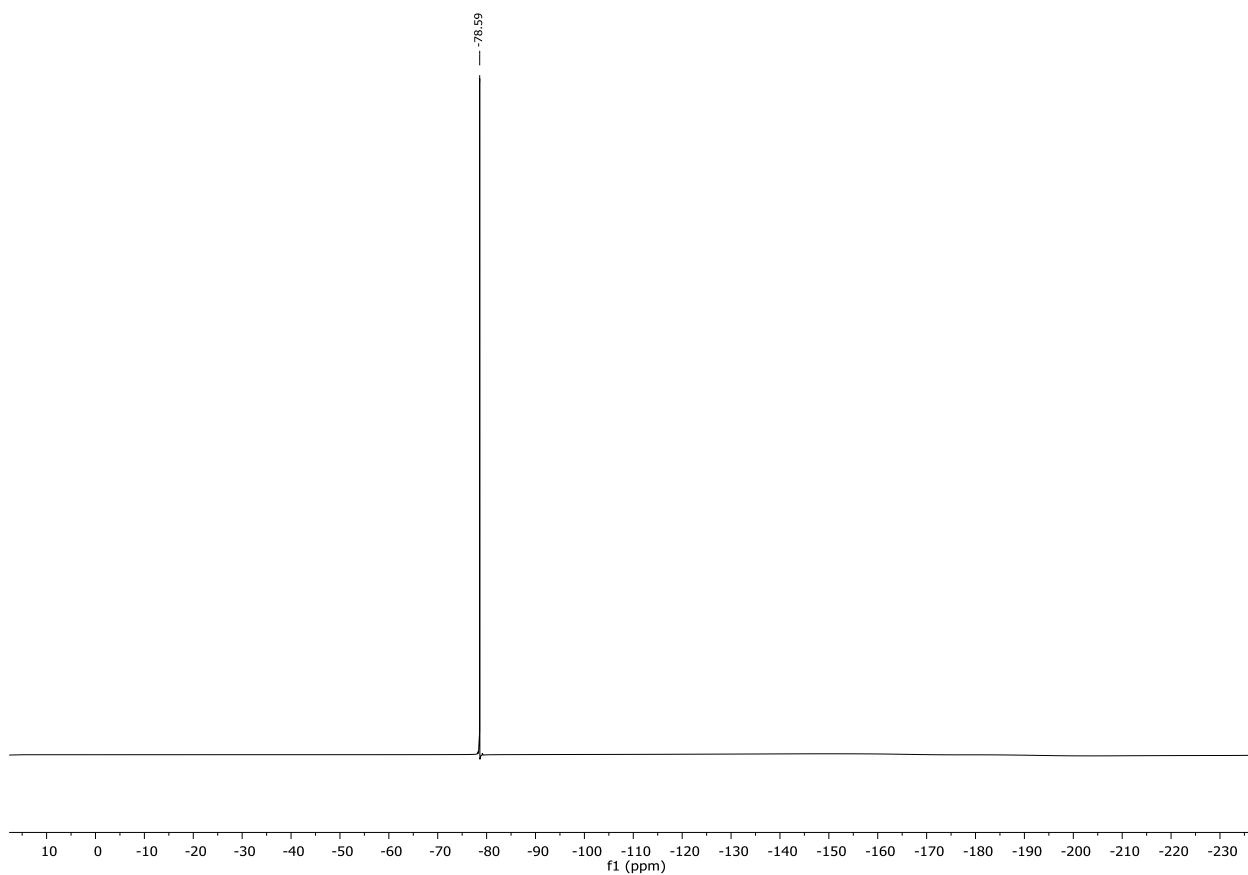


## 7.2 NMR spectra

$^{13}\text{C}\{^1\text{H}\}$ -NMR (101 MHz,  $\text{CDCl}_3$ ) Compound **200a**



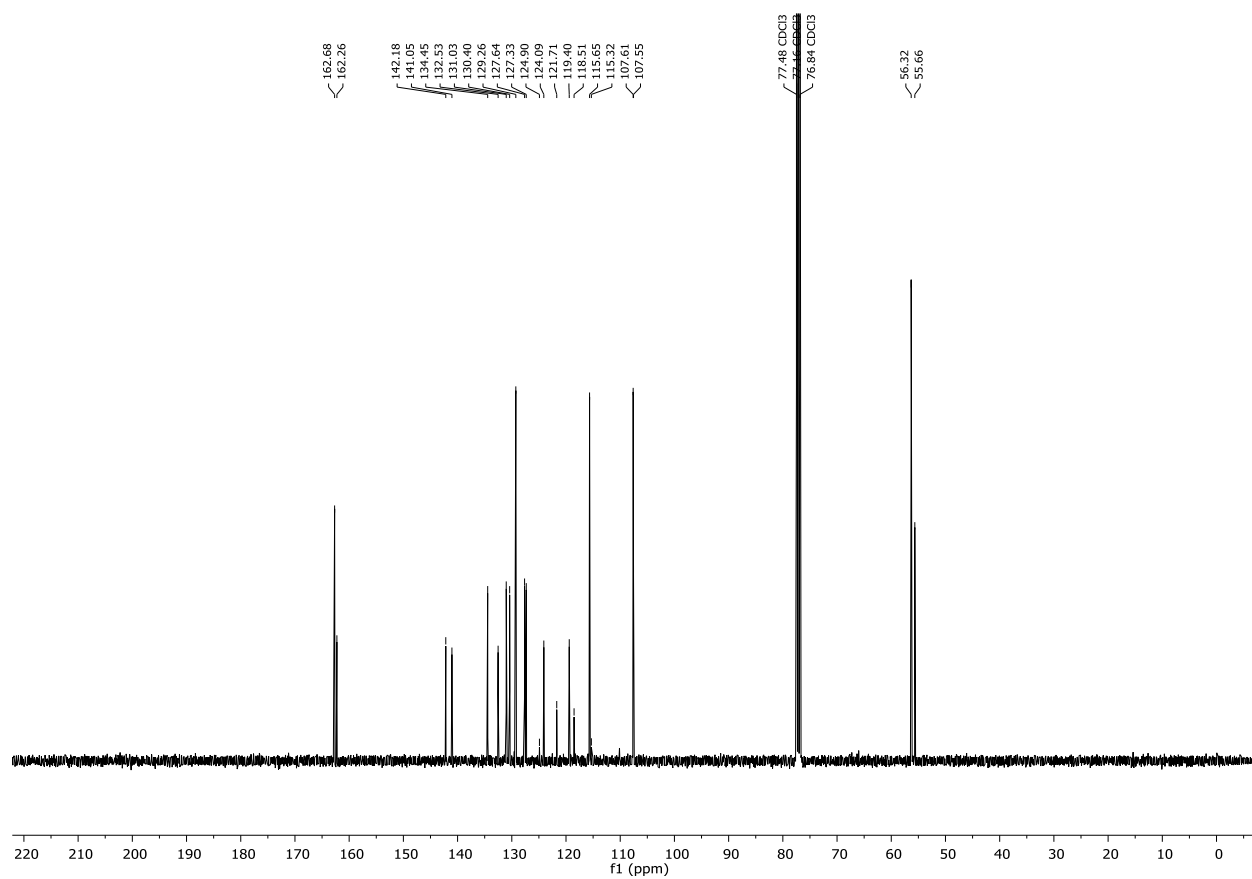
## 7. Appendix

 $^1\text{H-NMR}$  (400 MHz,  $\text{CDCl}_3$ ) Compound **201a** $^{19}\text{F-NMR}$  (376 MHz,  $\text{CDCl}_3$ ) Compound **201a**



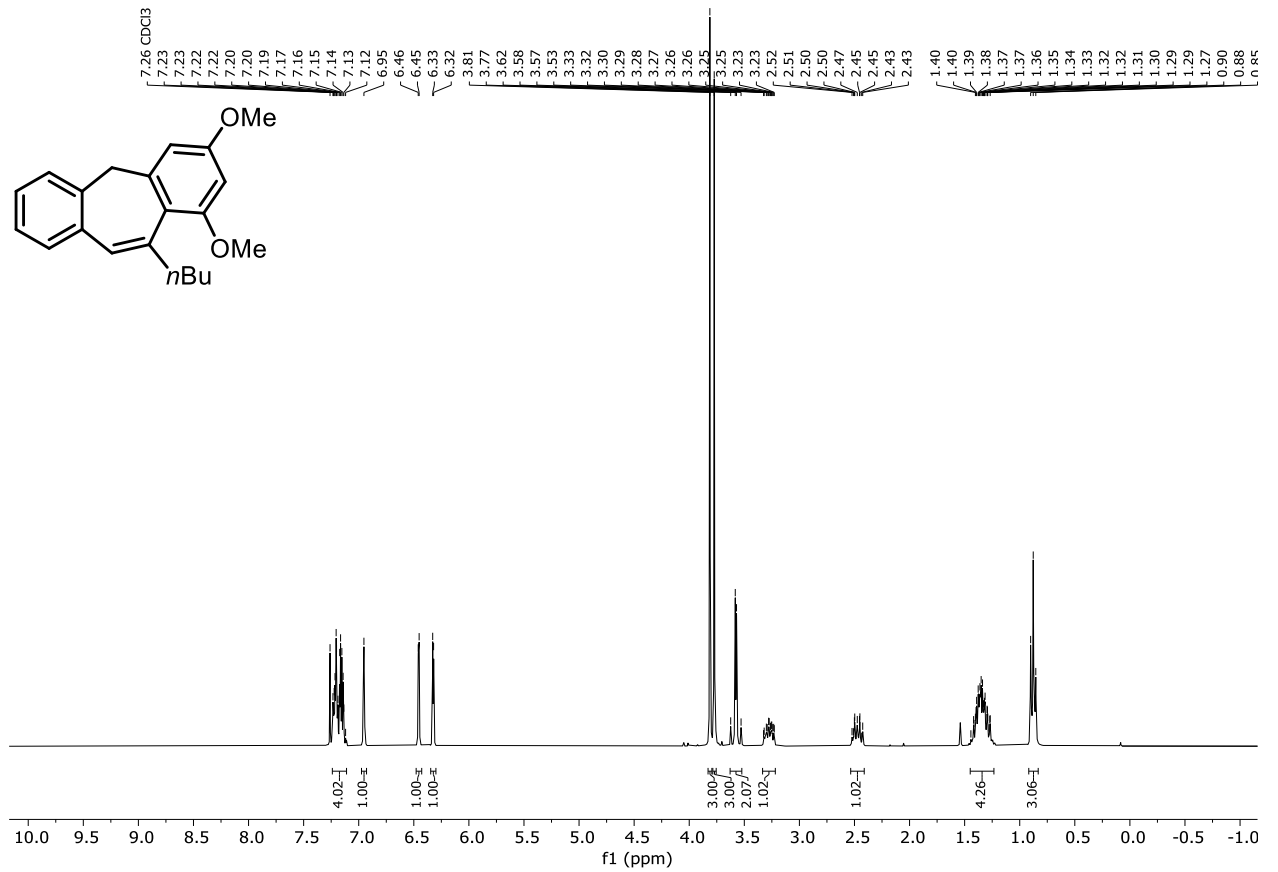
## 7.2 NMR spectra

$^{13}\text{C}\{^1\text{H}\}$ -NMR (101 MHz,  $\text{CDCl}_3$ ) Compound **201a**

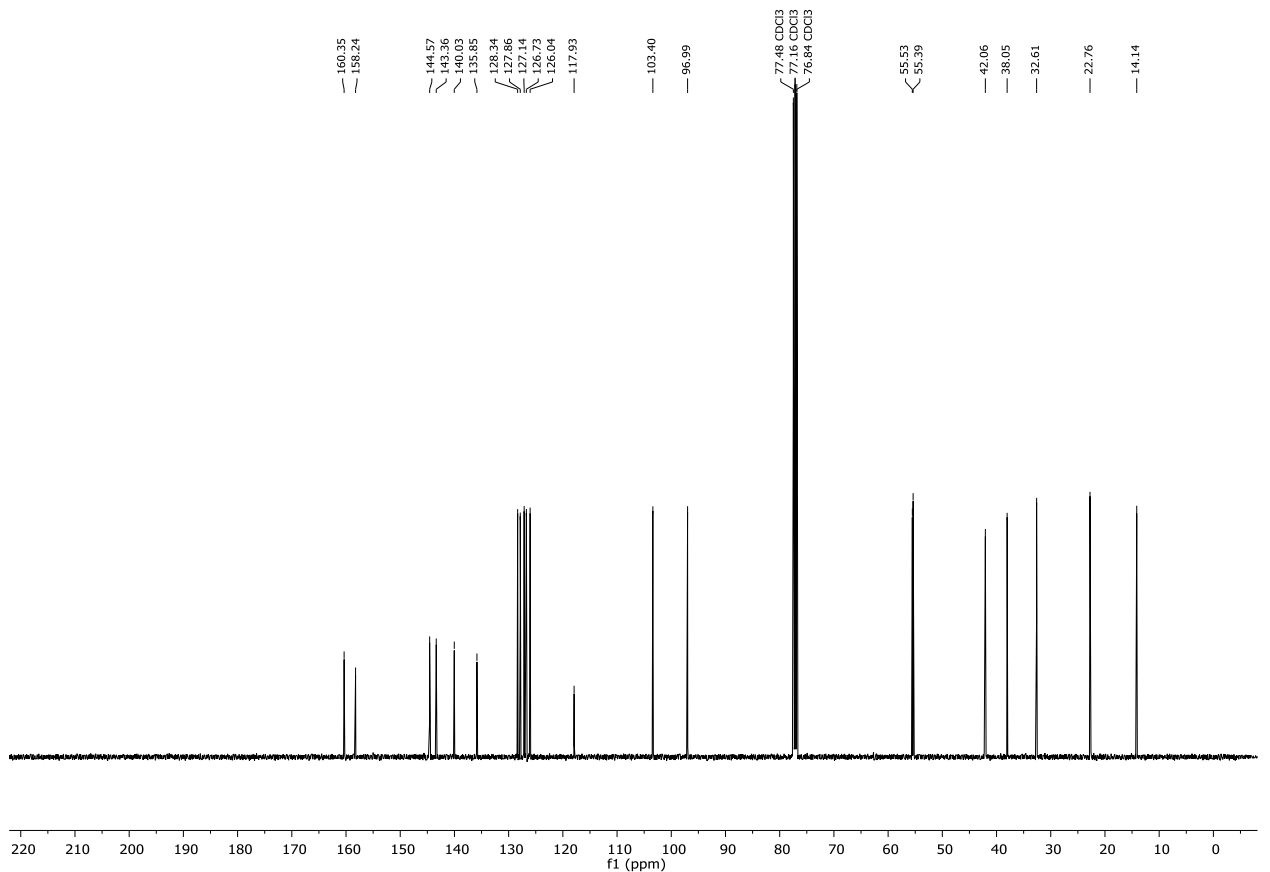


## 7. Appendix

### $^1\text{H-NMR}$ (300 MHz, $\text{CDCl}_3$ ) Compound **146b**

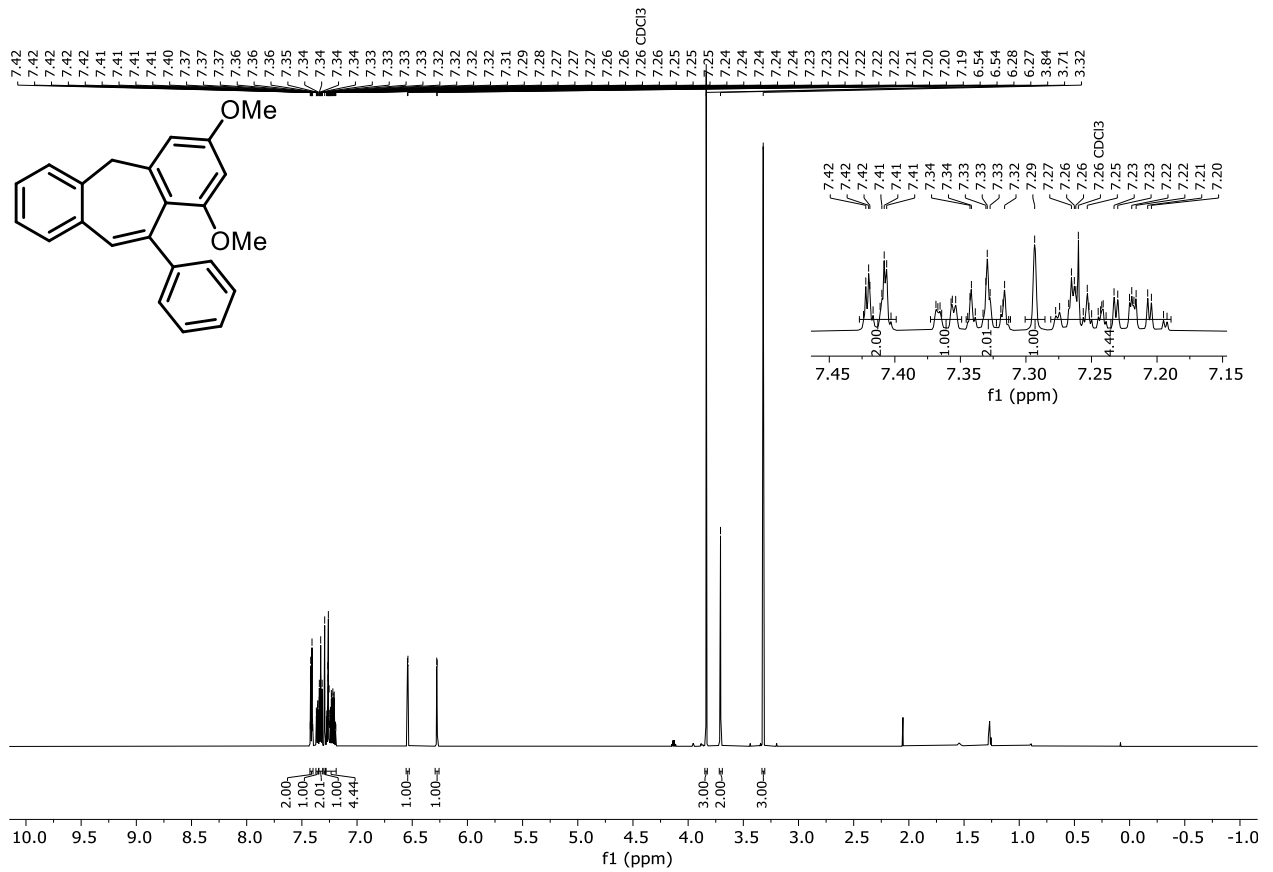


### $^{13}\text{C}\{^1\text{H}\}$ -NMR (101 MHz, $\text{CDCl}_3$ ) Compound **146b**

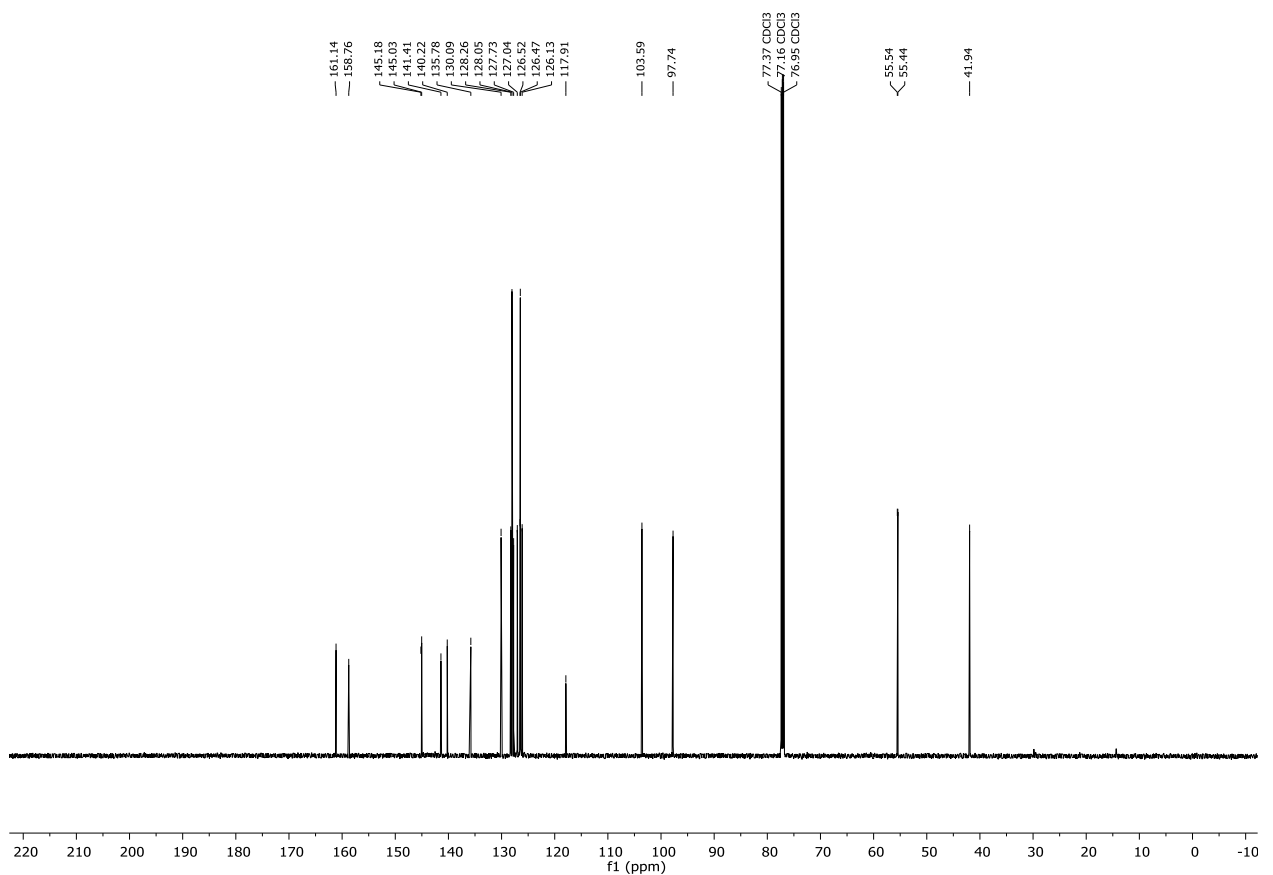


## 7.2 NMR spectra

### <sup>1</sup>H-NMR (600 MHz, CDCl<sub>3</sub>) Compound **146d**

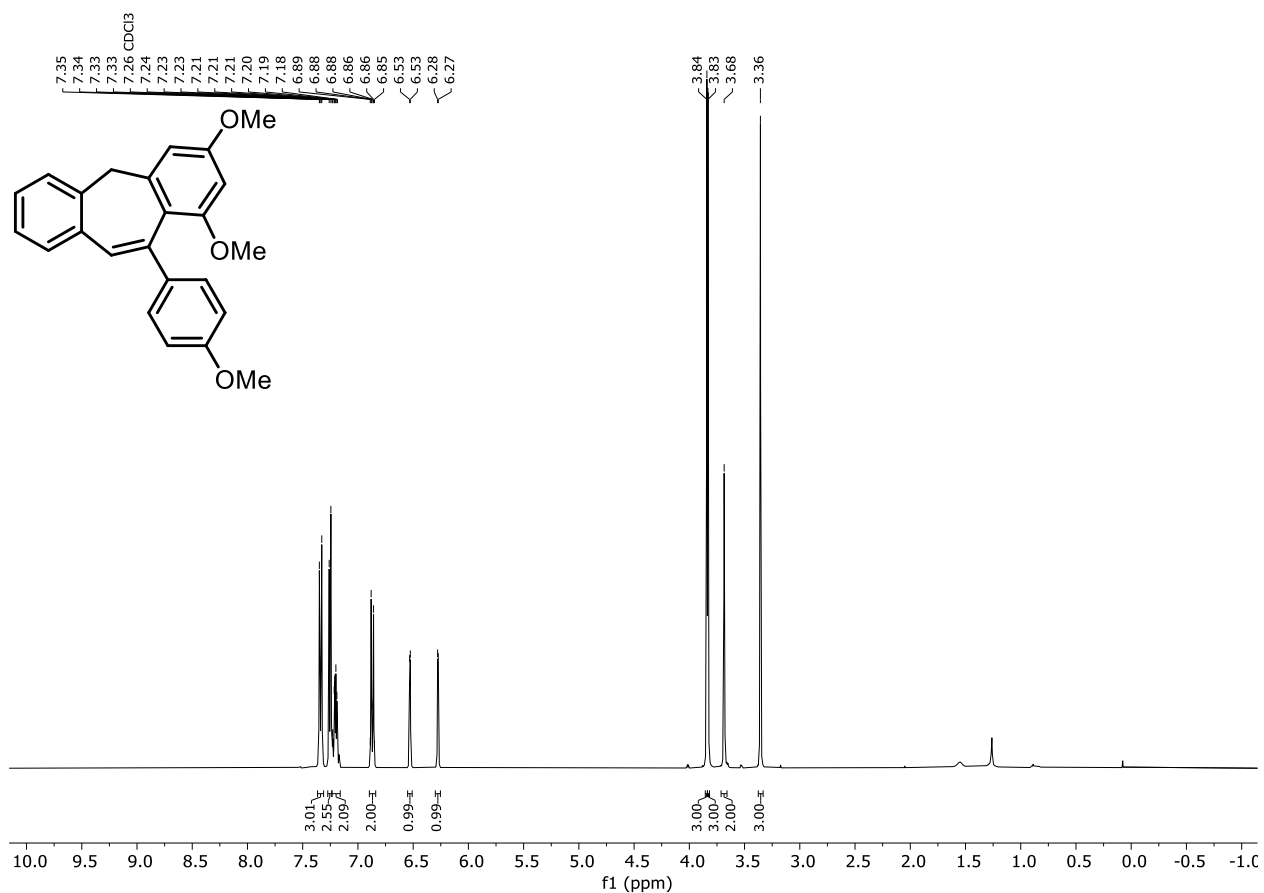


### <sup>13</sup>C{<sup>1</sup>H}-NMR (151 MHz, CDCl<sub>3</sub>) Compound **146d**

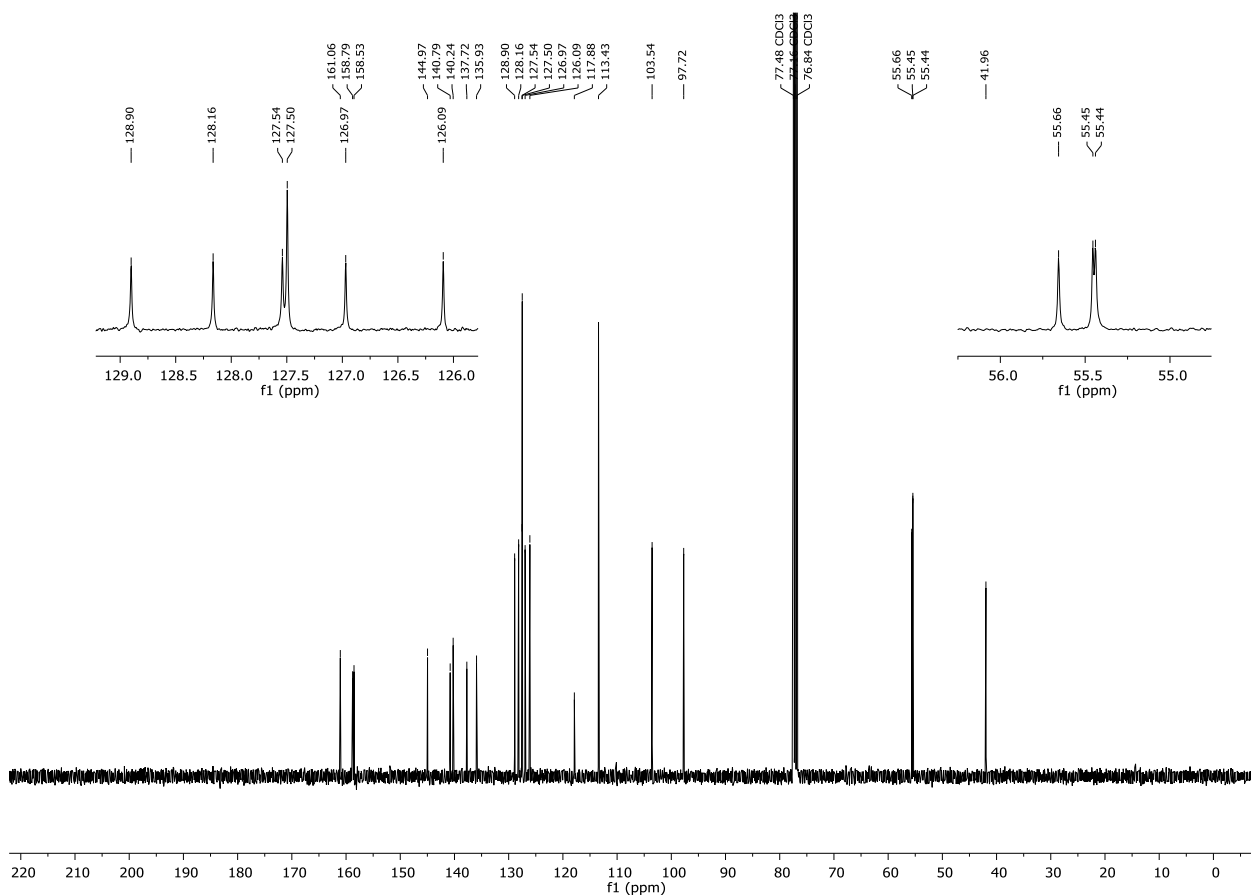


## 7. Appendix

### $^1\text{H-NMR}$ (400 MHz, $\text{CDCl}_3$ ) Compound **146e**

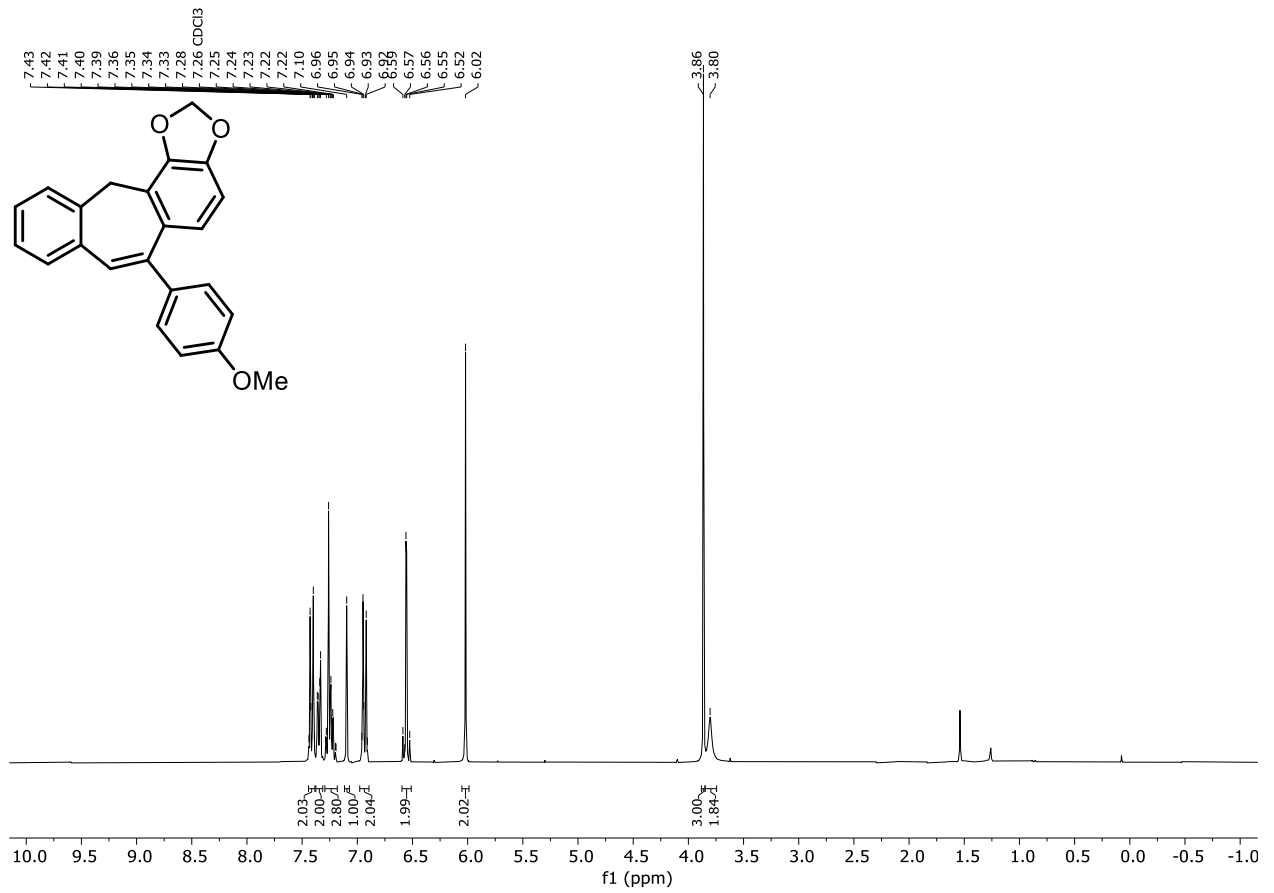


### $^{13}\text{C}\{^1\text{H}\}$ -NMR (101 MHz, $\text{CDCl}_3$ ) Compound **146e**

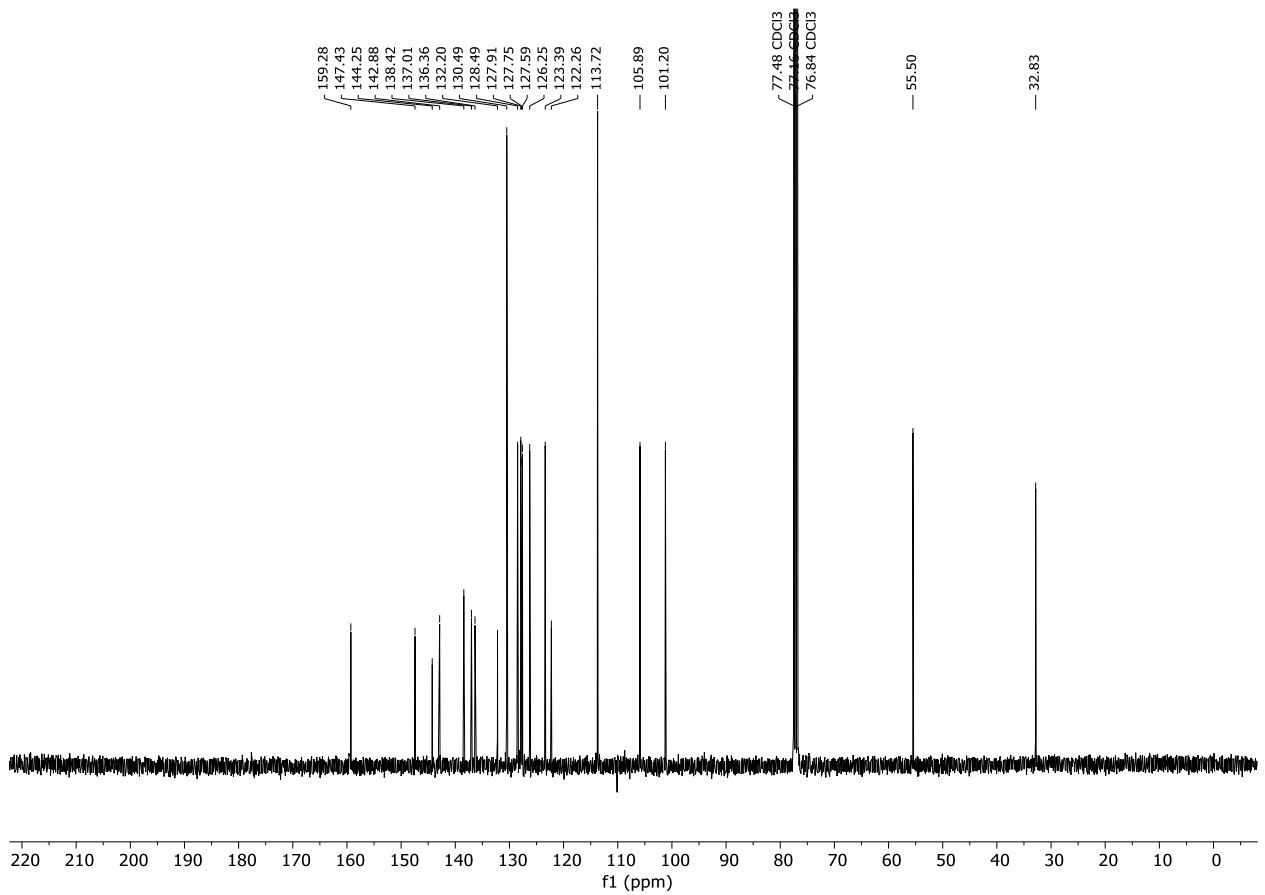


## 7.2 NMR spectra

### $^1\text{H-NMR}$ (400 MHz, $\text{CDCl}_3$ ) Compound **146f**

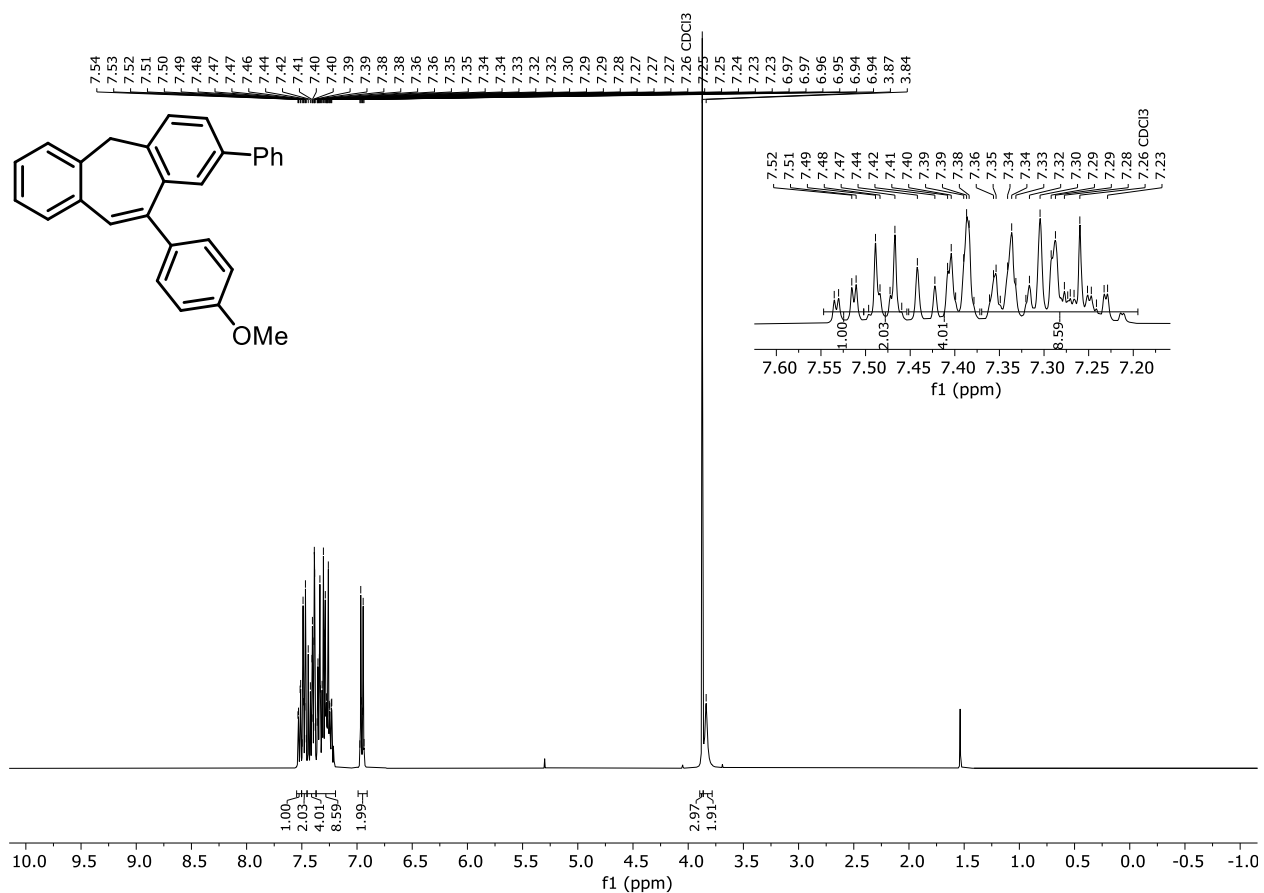


### $^{13}\text{C}\{^1\text{H}\}$ -NMR (101 MHz, $\text{CDCl}_3$ ) Compound **146f**

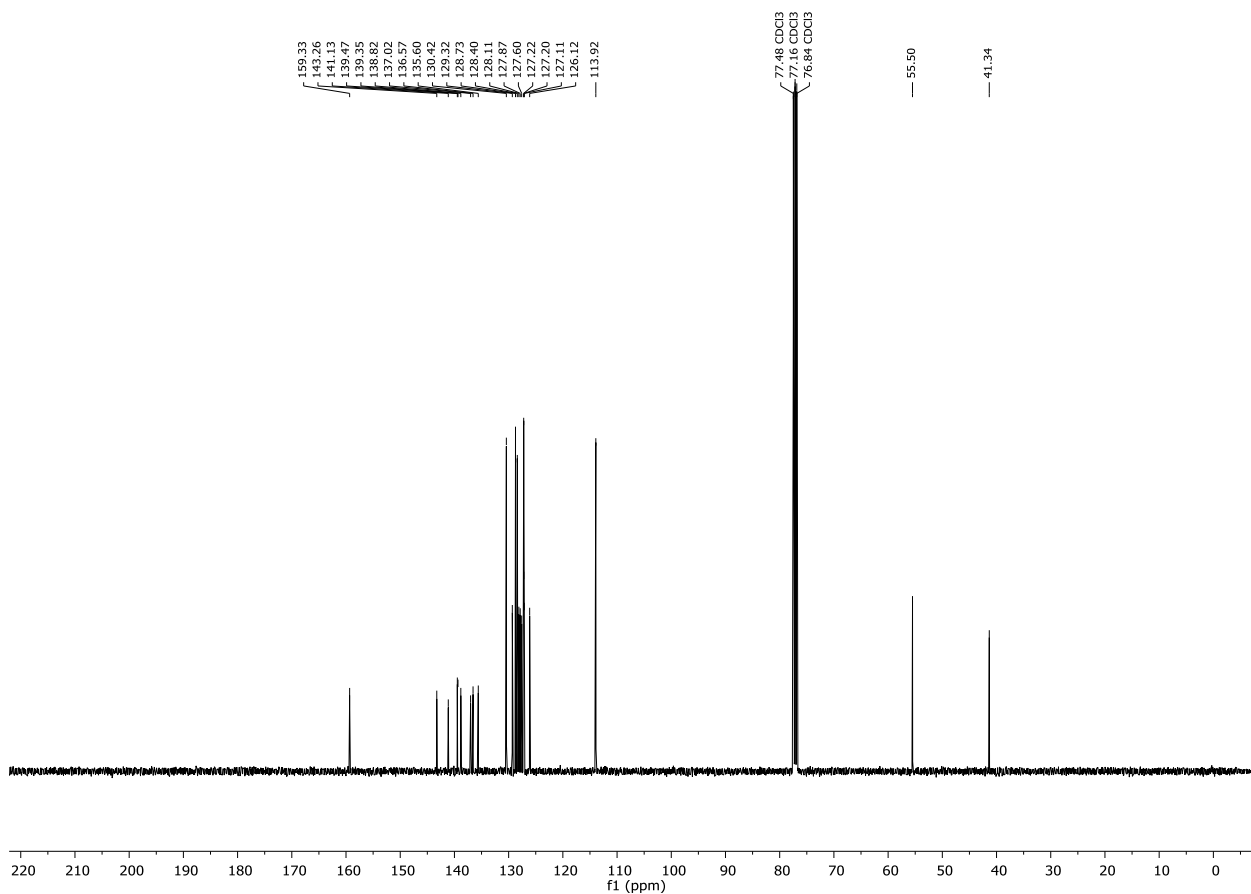


## 7. Appendix

### $^1\text{H-NMR}$ (400 MHz, $\text{CDCl}_3$ ) Compound **146g**

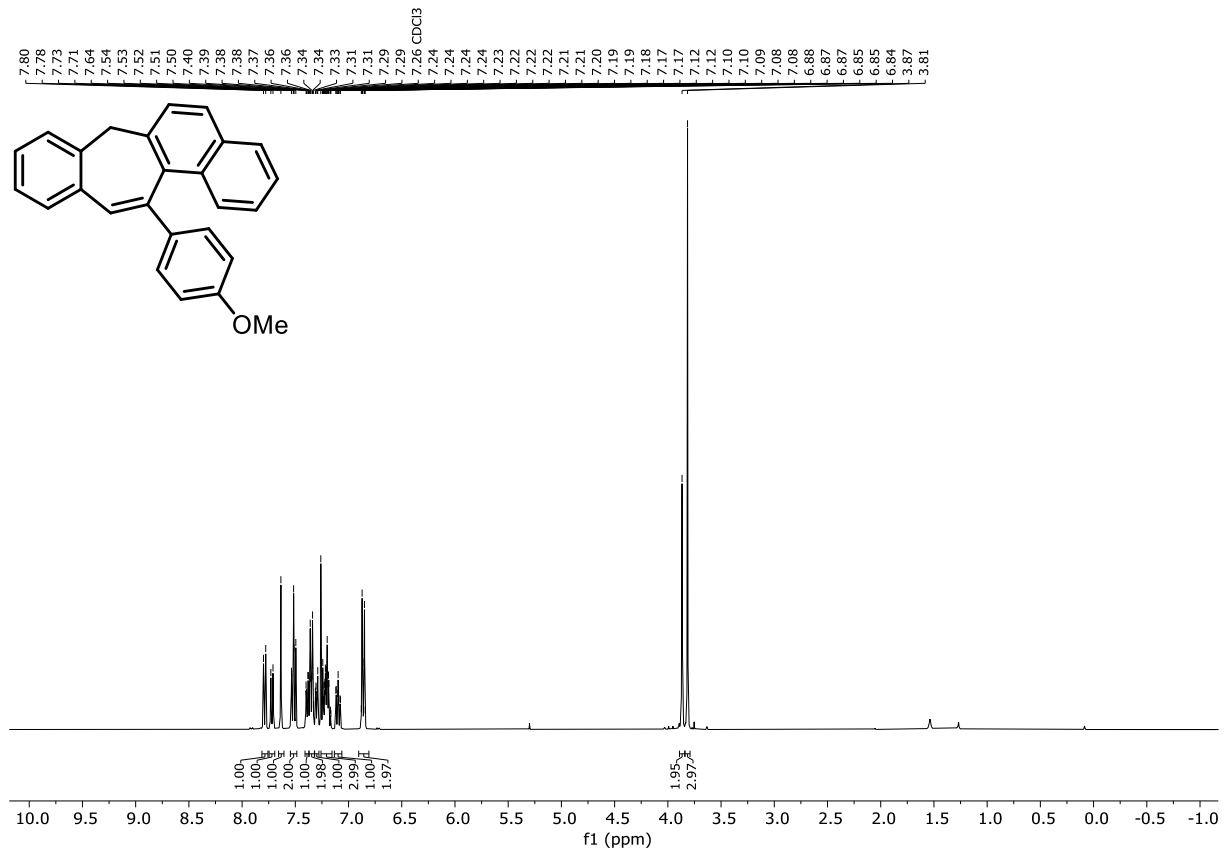


### $^{13}\text{C}\{^1\text{H}\}$ -NMR (101 MHz, $\text{CDCl}_3$ ) Compound **146g**

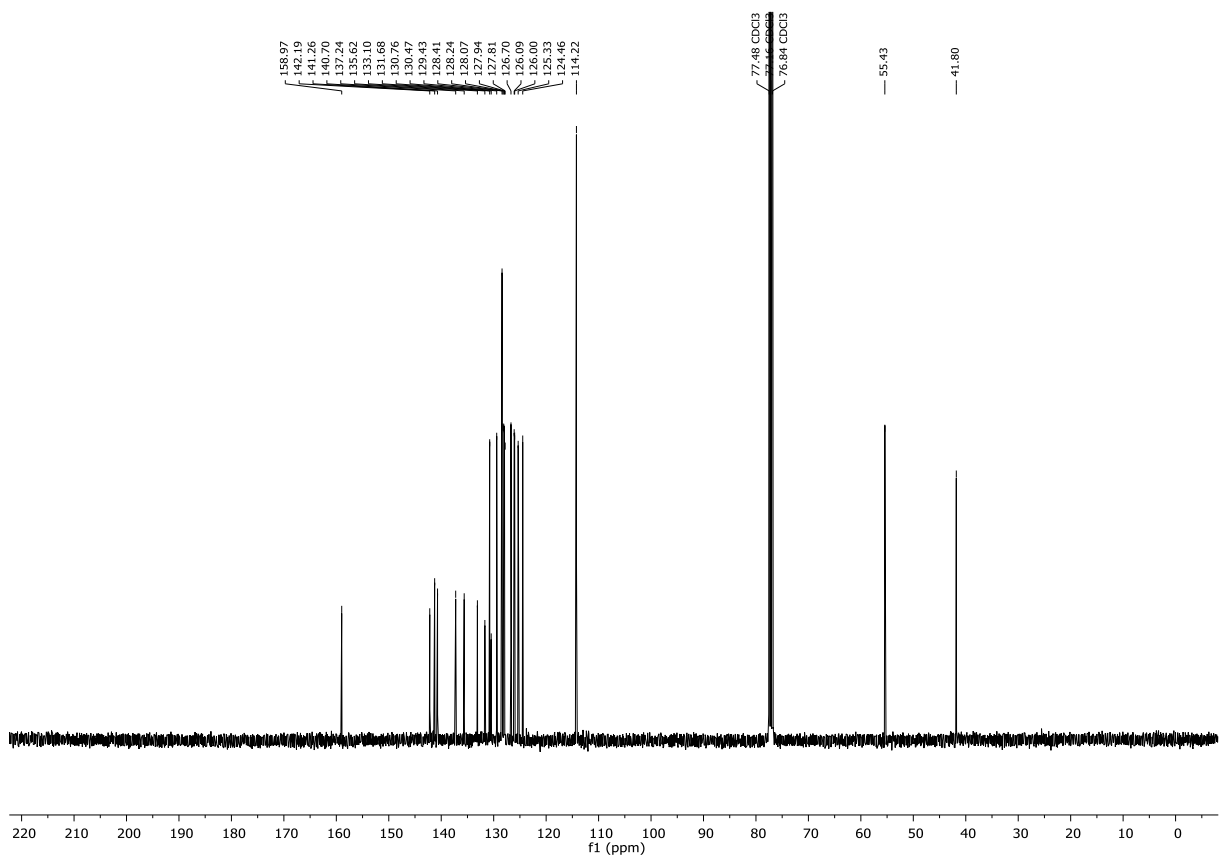


## 7.2 NMR spectra

### $^1\text{H-NMR}$ (400 MHz, $\text{CDCl}_3$ ) Compound **146h**

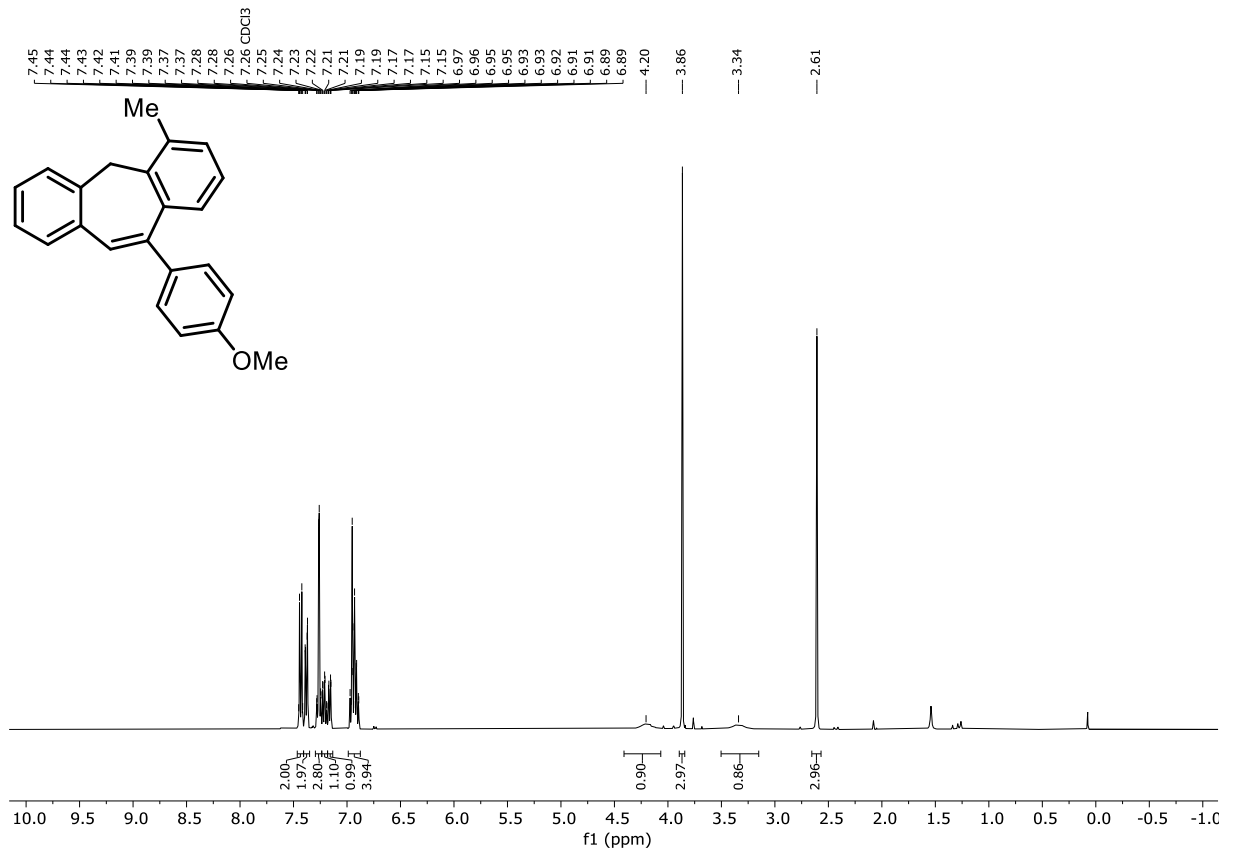


### $^{13}\text{C}\{^1\text{H}\}$ -NMR (101 MHz, $\text{CDCl}_3$ ) Compound **146h**

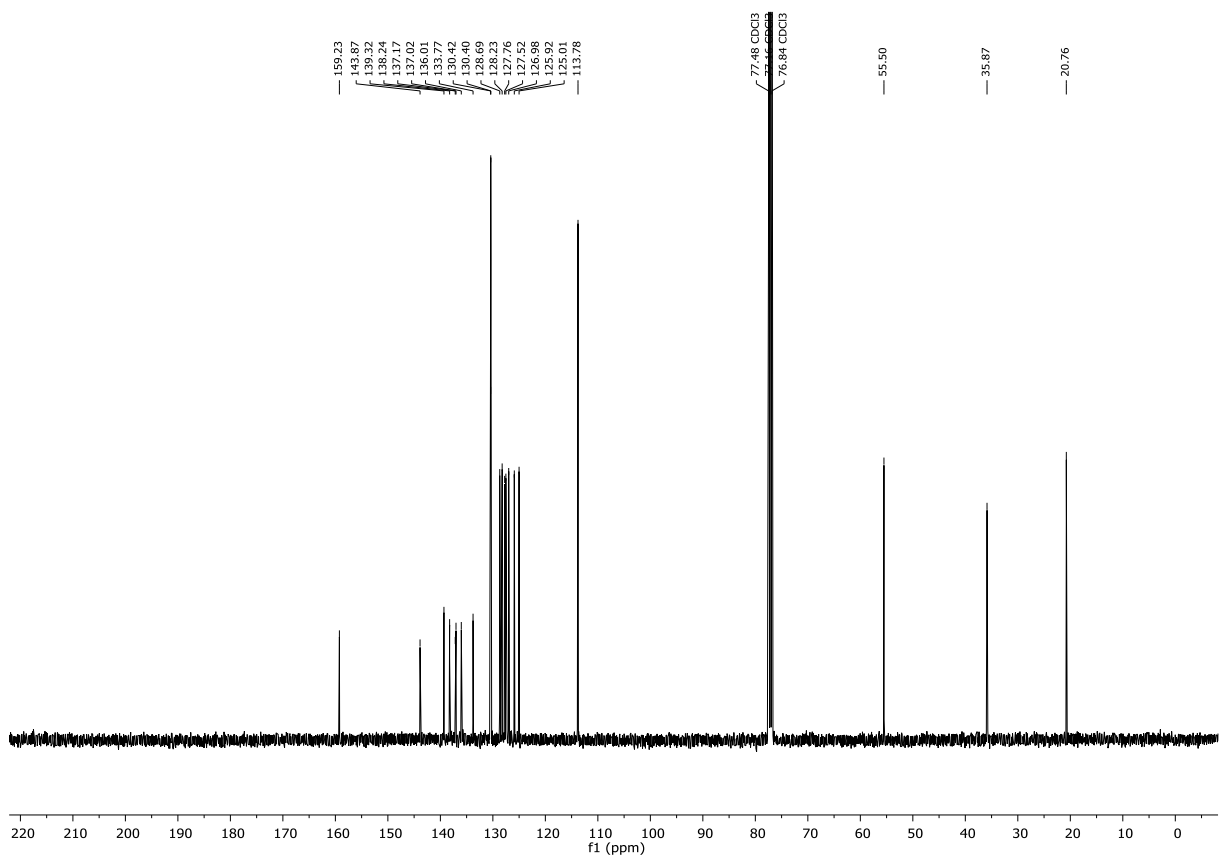


## 7. Appendix

### $^1\text{H-NMR}$ (400 MHz, $\text{CDCl}_3$ ) Compound **146i**



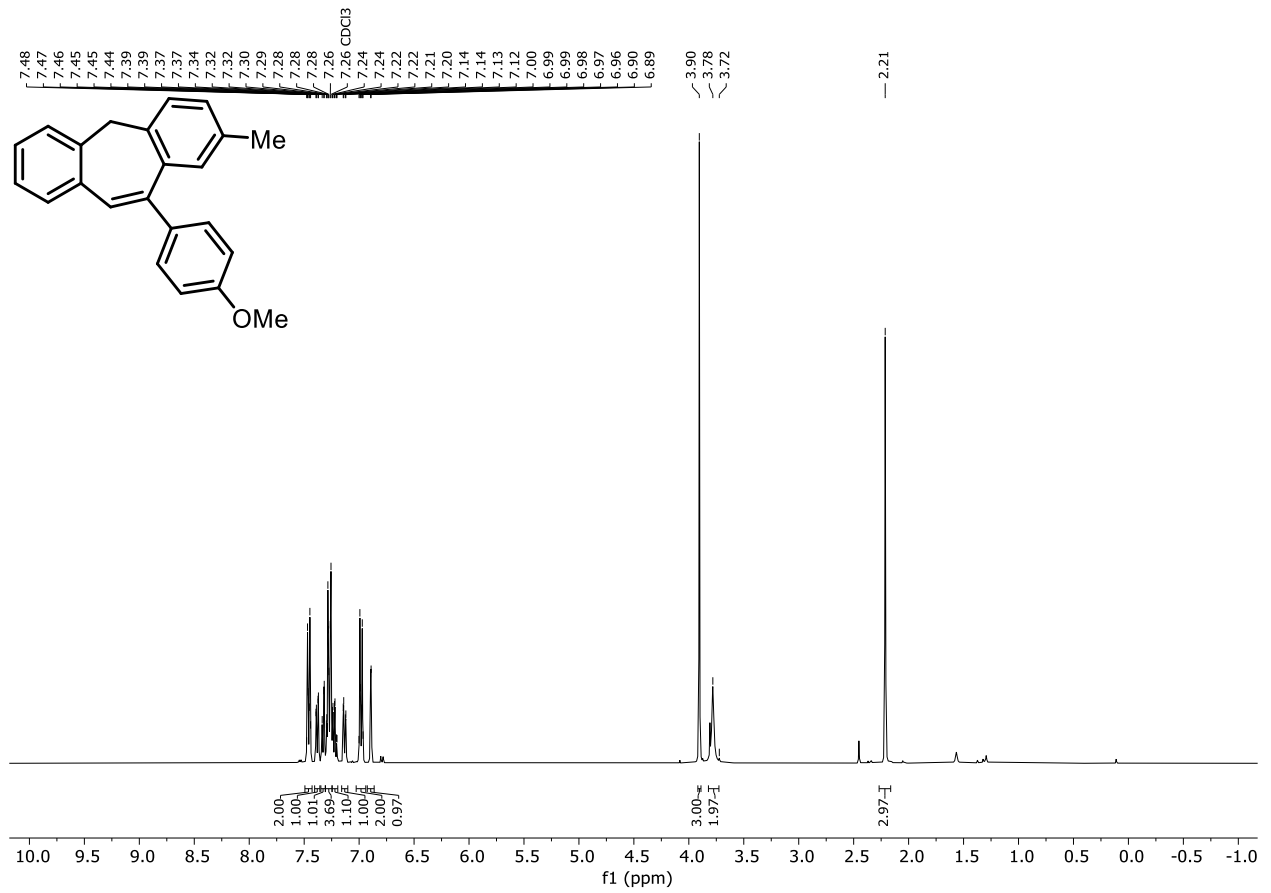
### $^{13}\text{C}\{^1\text{H}\}$ -NMR (101 MHz, $\text{CDCl}_3$ ) Compound **146i**



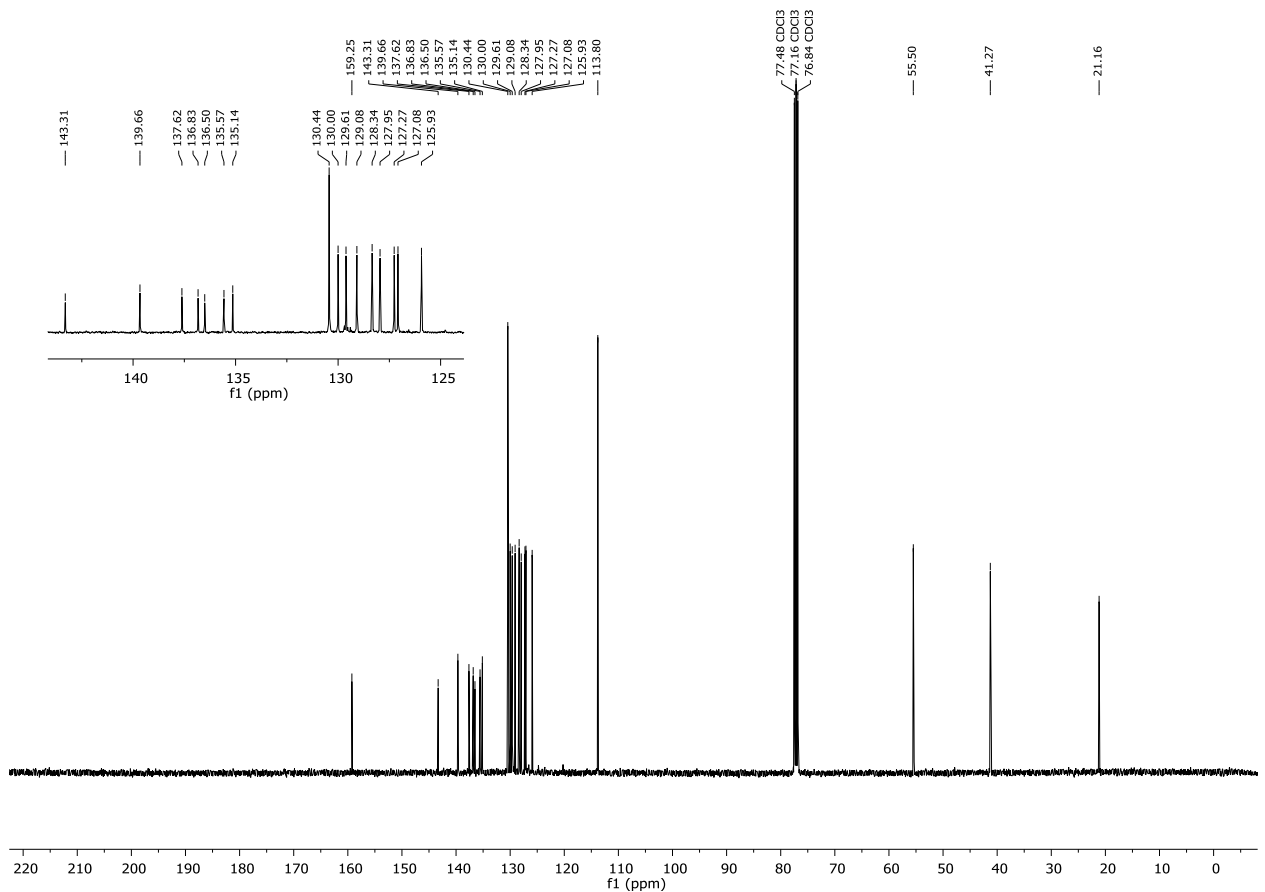


## 7.2 NMR spectra

### $^1\text{H-NMR}$ (400 MHz, $\text{CDCl}_3$ ) Compound **146j**

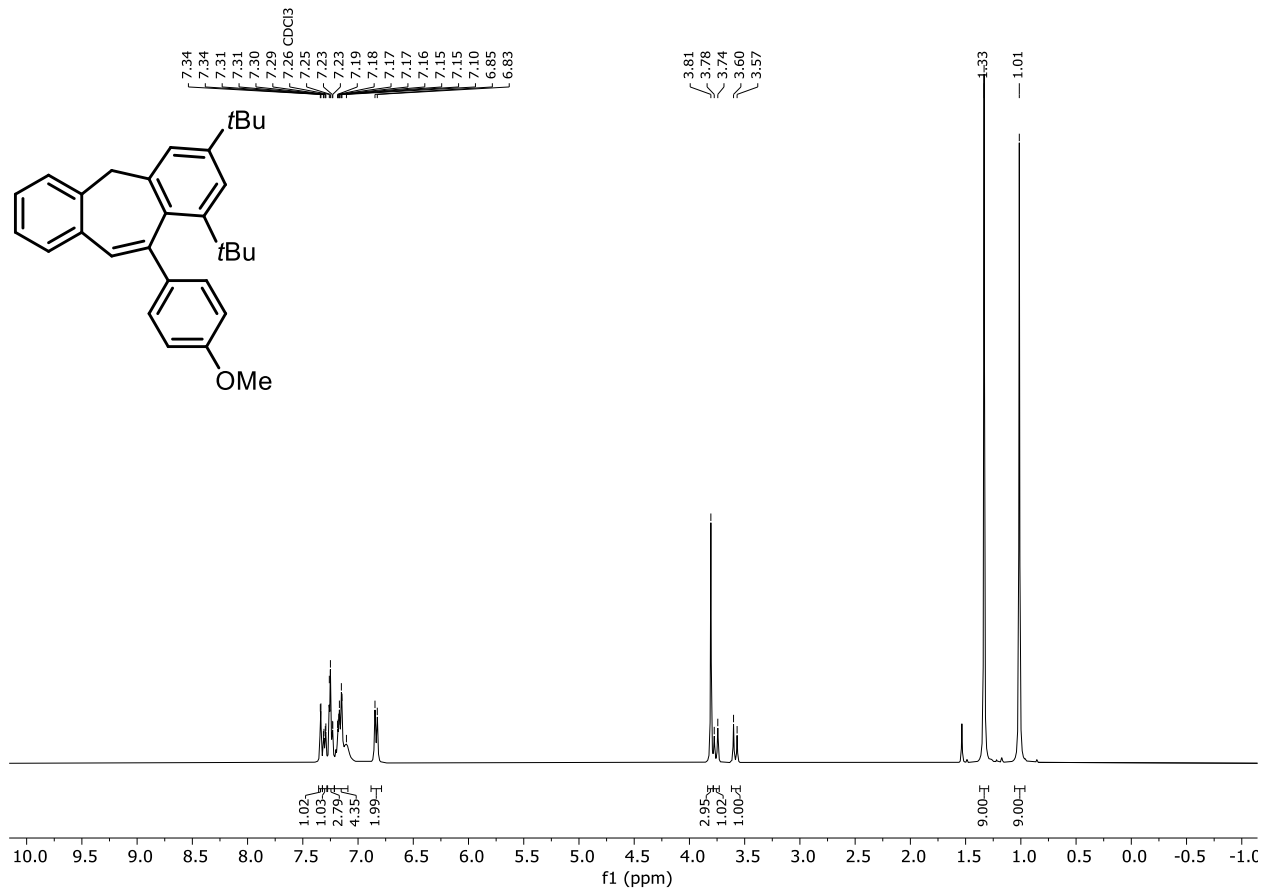


### $^{13}\text{C}\{^1\text{H}\}$ -NMR (101 MHz, $\text{CDCl}_3$ ) Compound **146j**

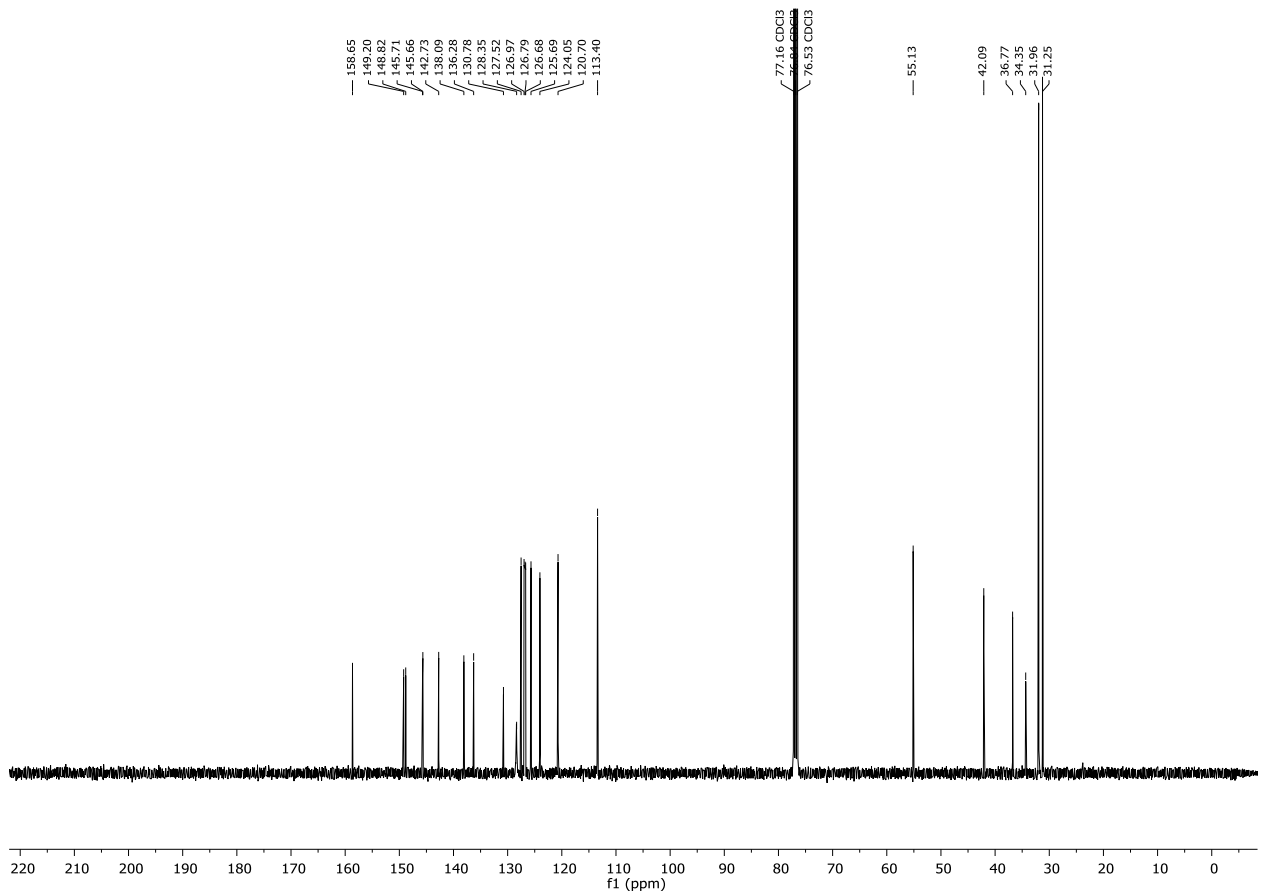


## 7. Appendix

### $^1\text{H-NMR}$ (400 MHz, $\text{CDCl}_3$ ) Compound **146k**

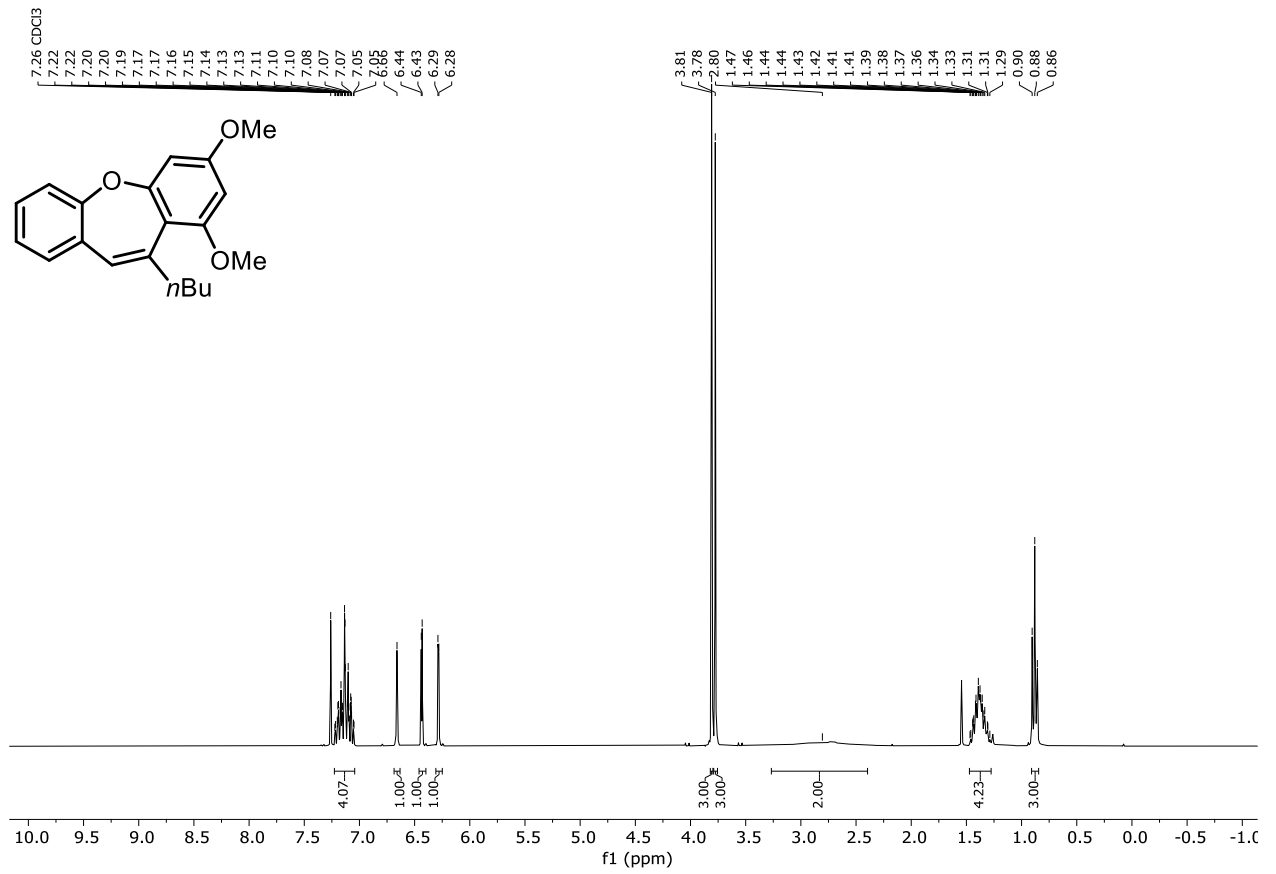


### $^{13}\text{C}\{^1\text{H}\}$ -NMR (101 MHz, $\text{CDCl}_3$ ) Compound **146k**

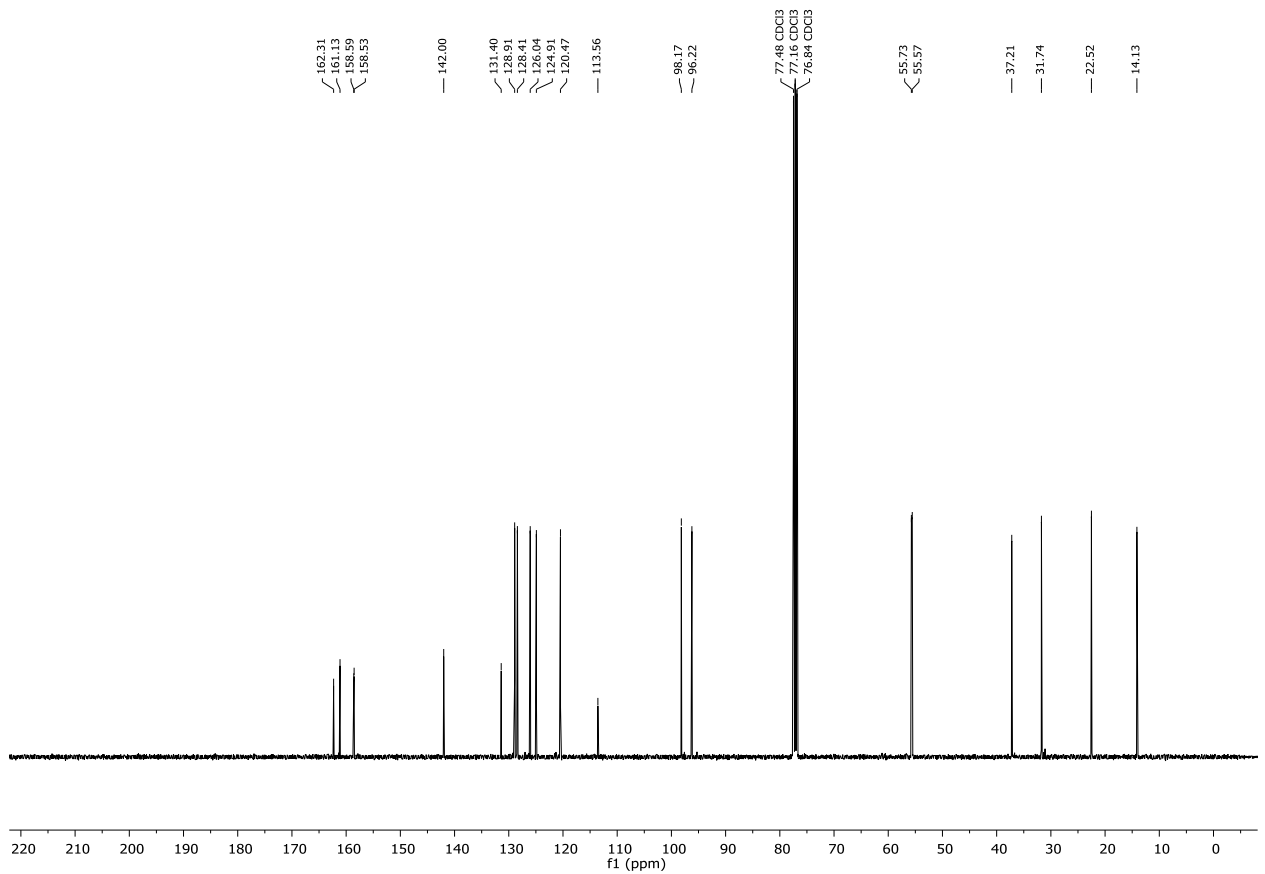


## 7.2 NMR spectra

### $^1\text{H-NMR}$ (300 MHz, $\text{CDCl}_3$ ) Compound **147a**

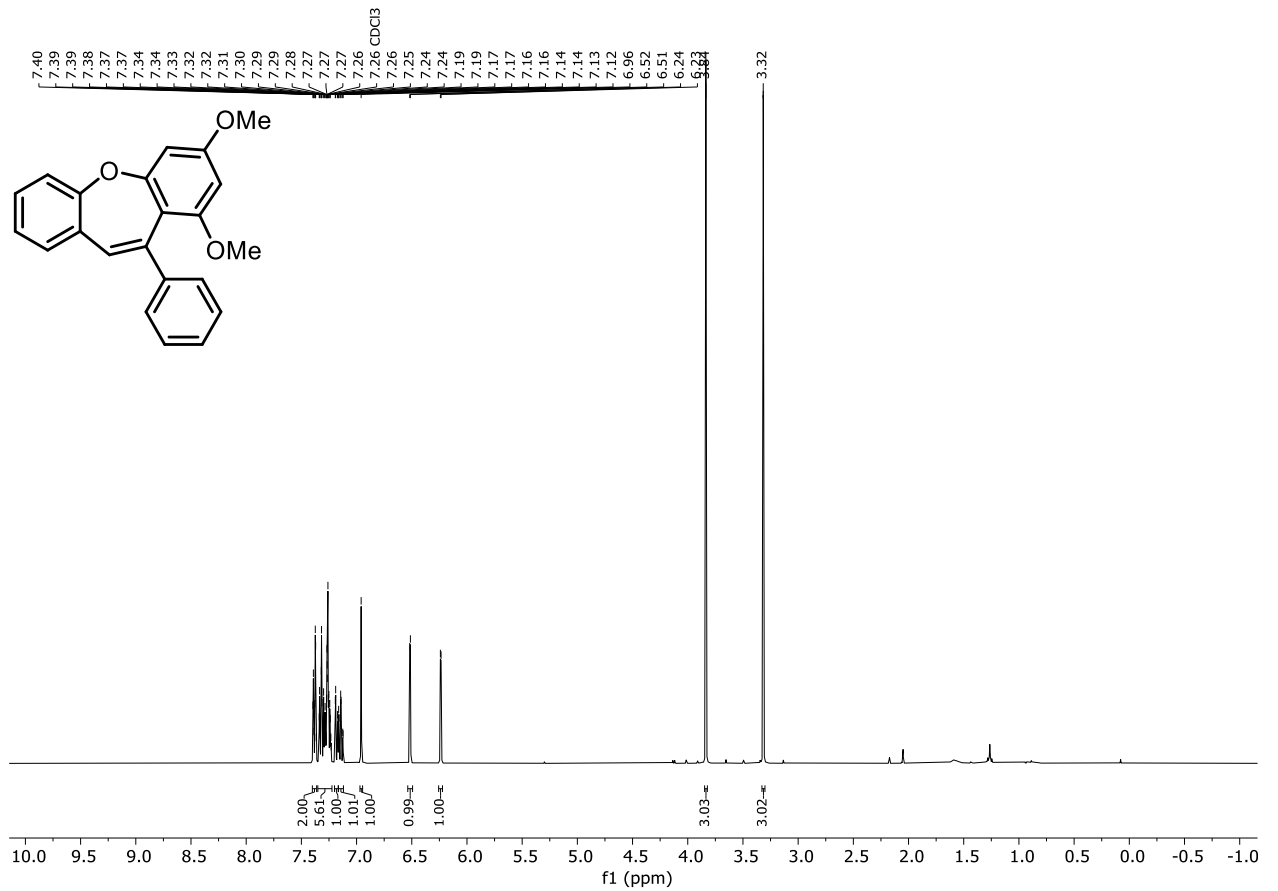


### $^{13}\text{C}\{^1\text{H}\}$ -NMR (101 MHz, $\text{CDCl}_3$ ) Compound **147a**

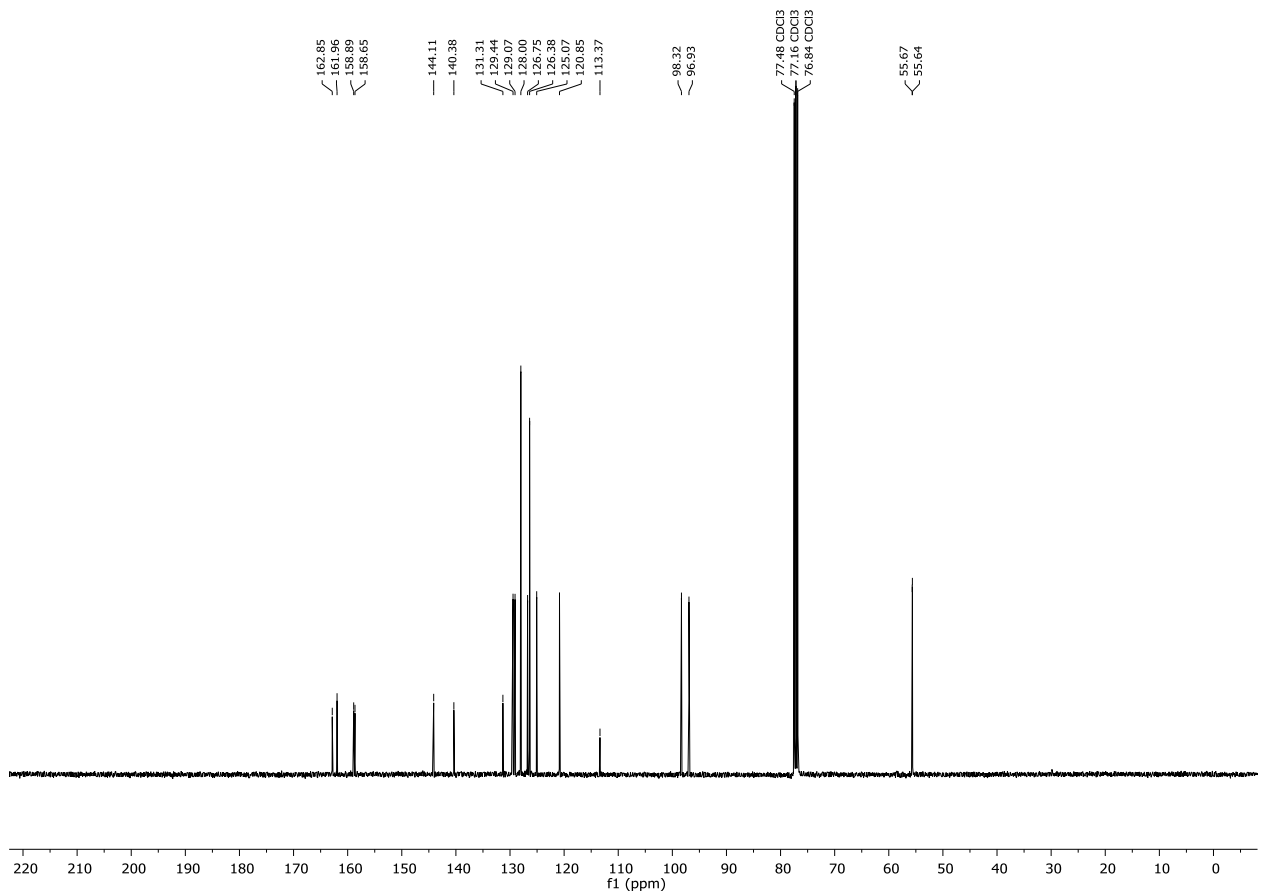


## 7. Appendix

### $^1\text{H-NMR}$ (400 MHz, $\text{CDCl}_3$ ) Compound **147b**

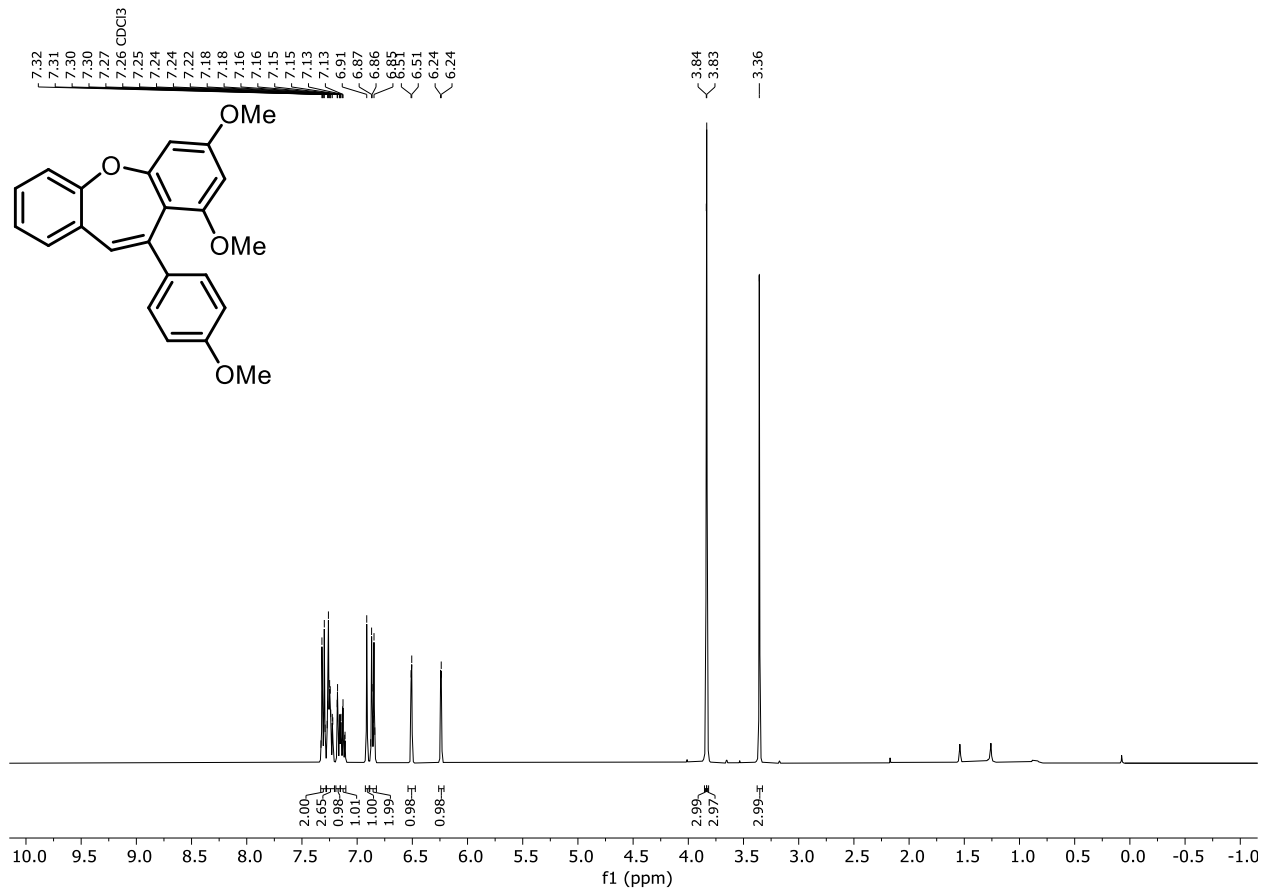


### $^{13}\text{C}\{^1\text{H}\}$ -NMR (101 MHz, $\text{CDCl}_3$ ) Compound **147b**

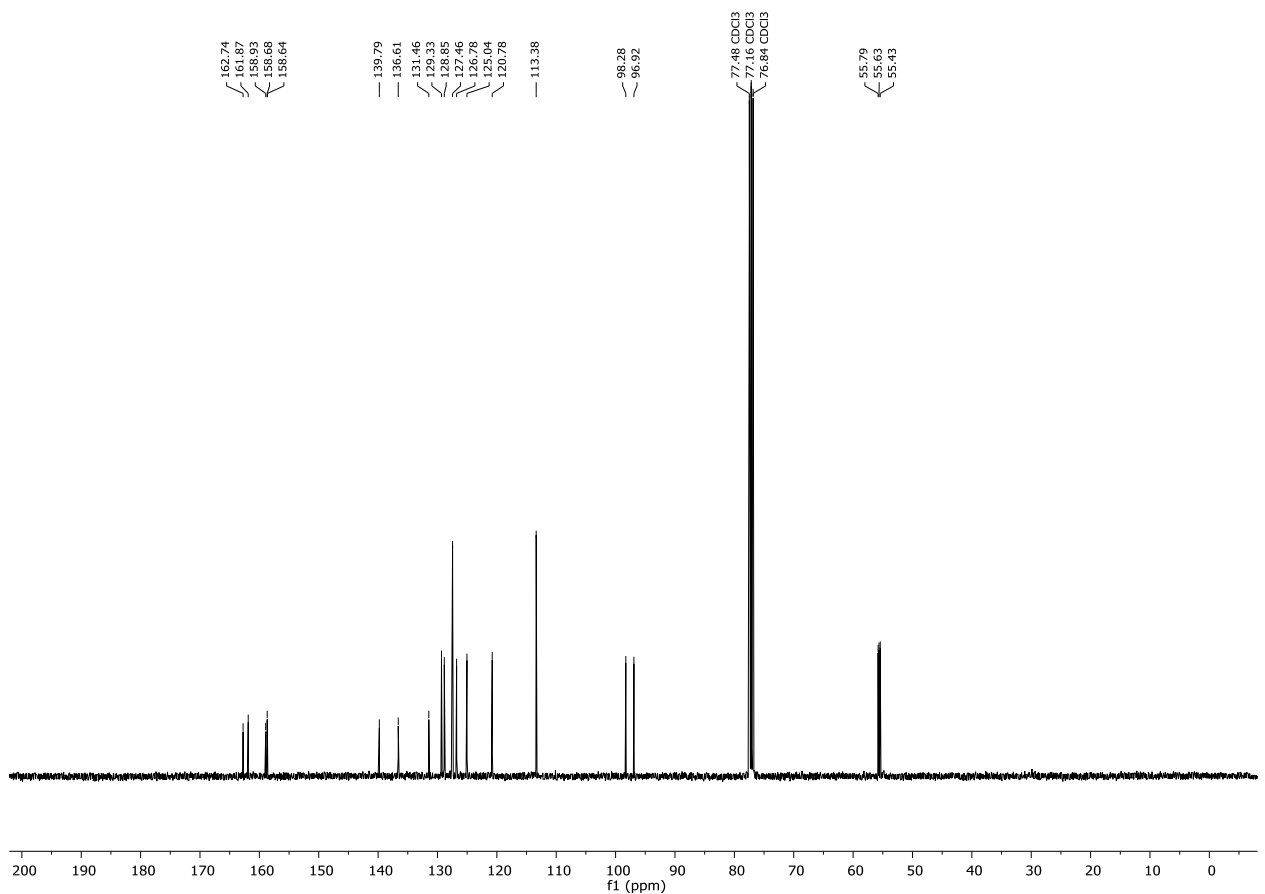


## 7.2 NMR spectra

### $^1\text{H-NMR}$ (400 MHz, $\text{CDCl}_3$ ) Compound **147c**

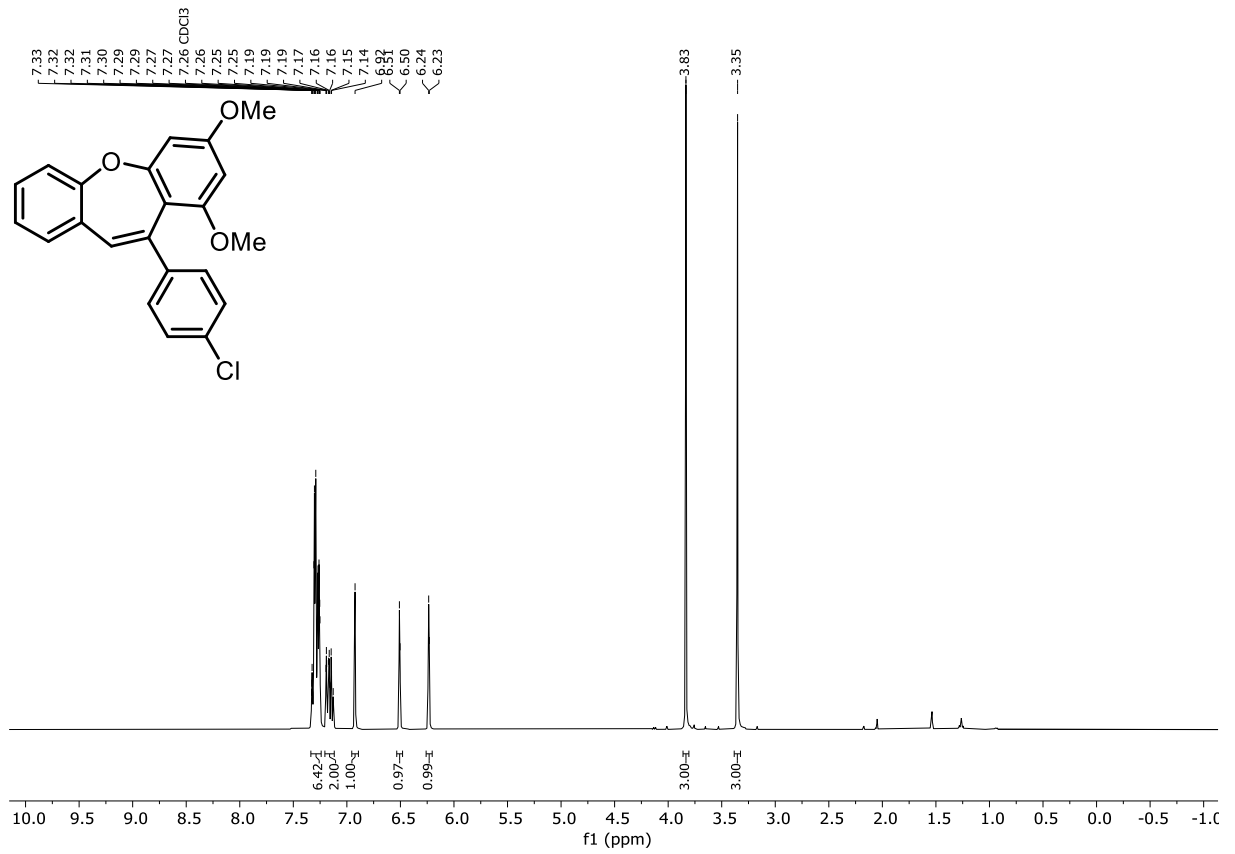


### $^{13}\text{C}\{^1\text{H}\}$ -NMR (101 MHz, $\text{CDCl}_3$ ) Compound **147c**

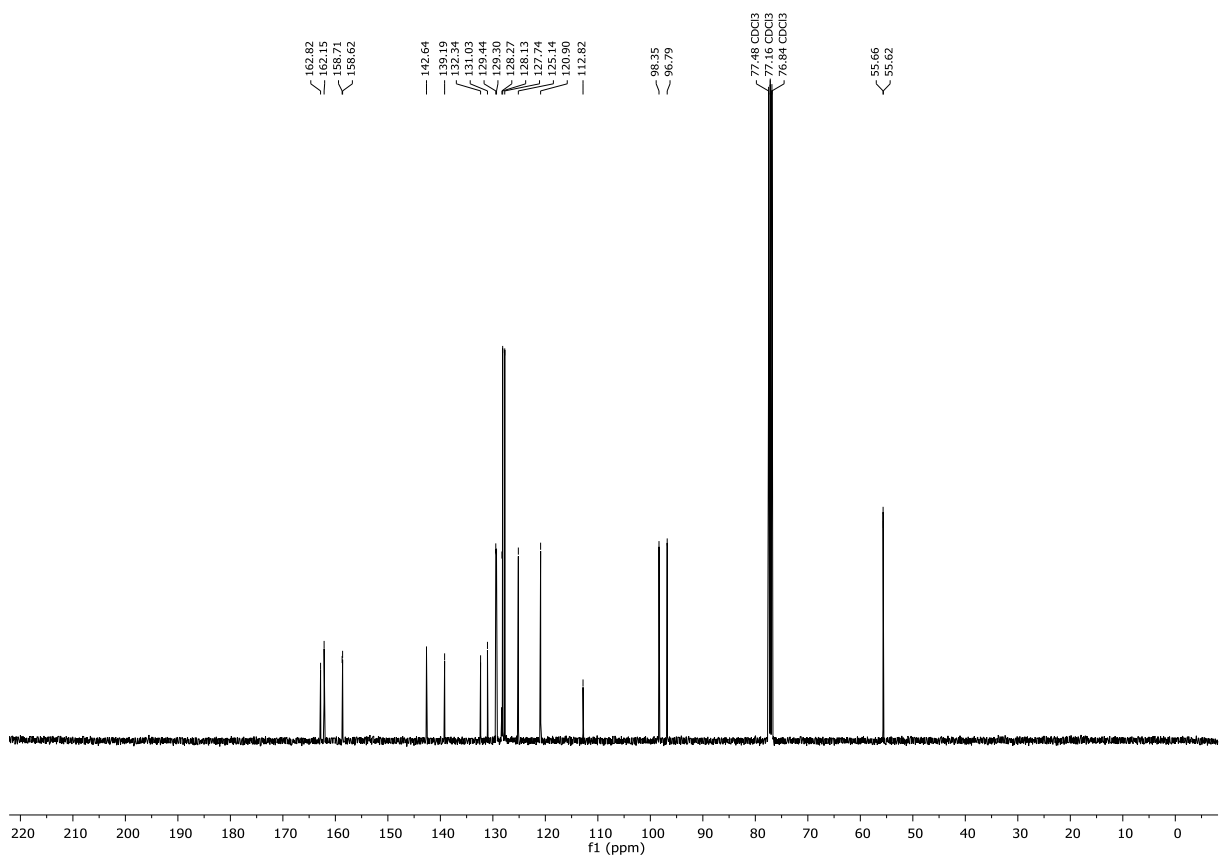


## 7. Appendix

### $^1\text{H-NMR}$ (400 MHz, $\text{CDCl}_3$ ) Compound **147d**

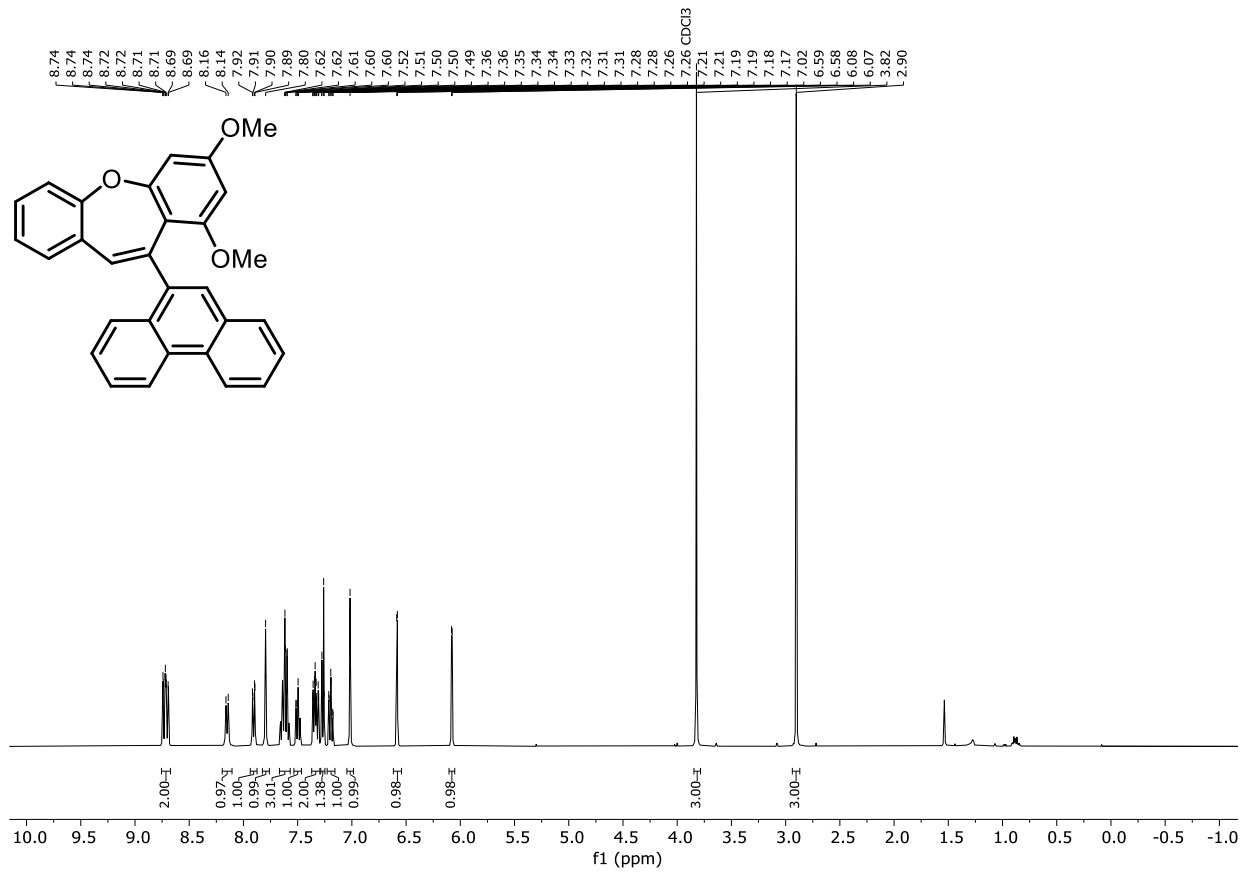


### $^{13}\text{C}\{^1\text{H}\}$ -NMR (101 MHz, $\text{CDCl}_3$ ) Compound **147d**

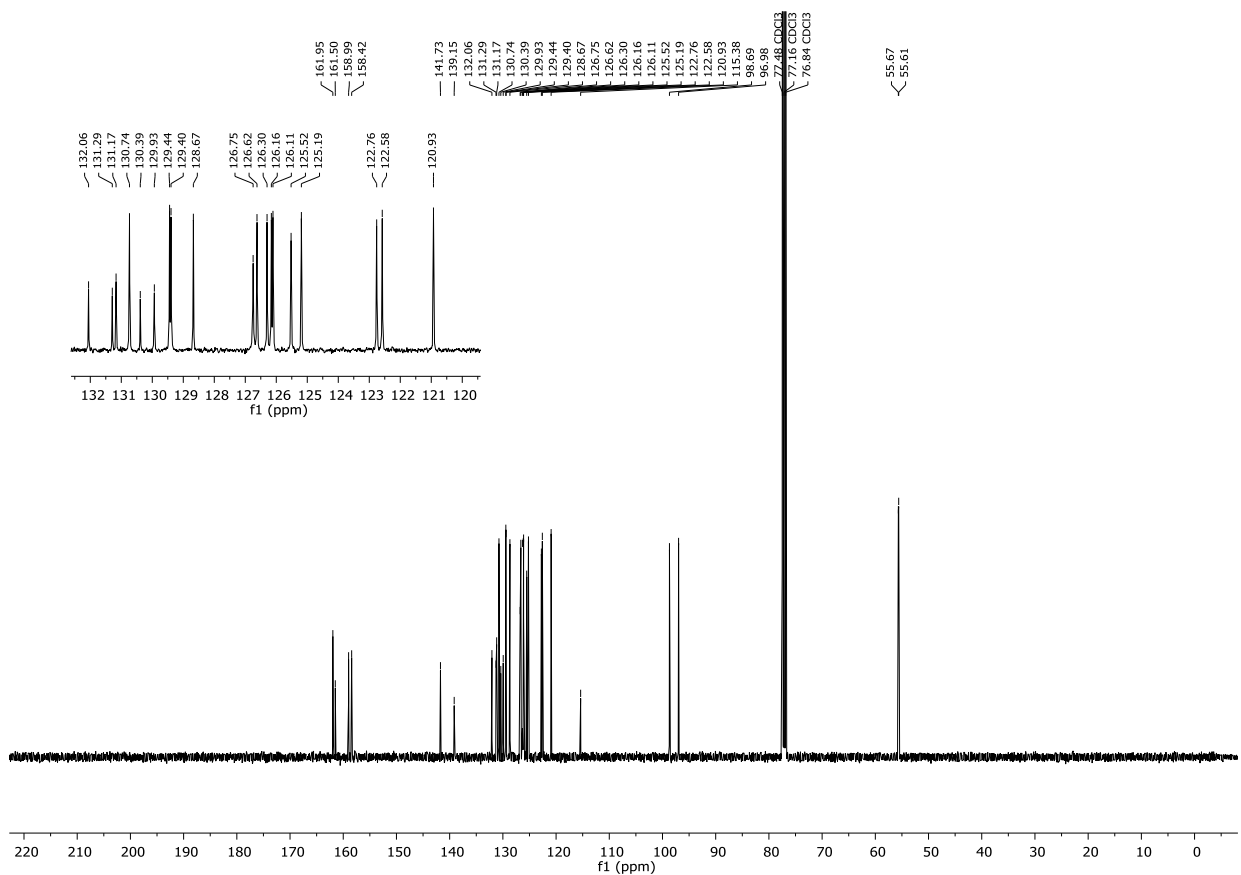


## 7.2 NMR spectra

### <sup>1</sup>H-NMR (400 MHz, CDCl<sub>3</sub>) Compound **147e**

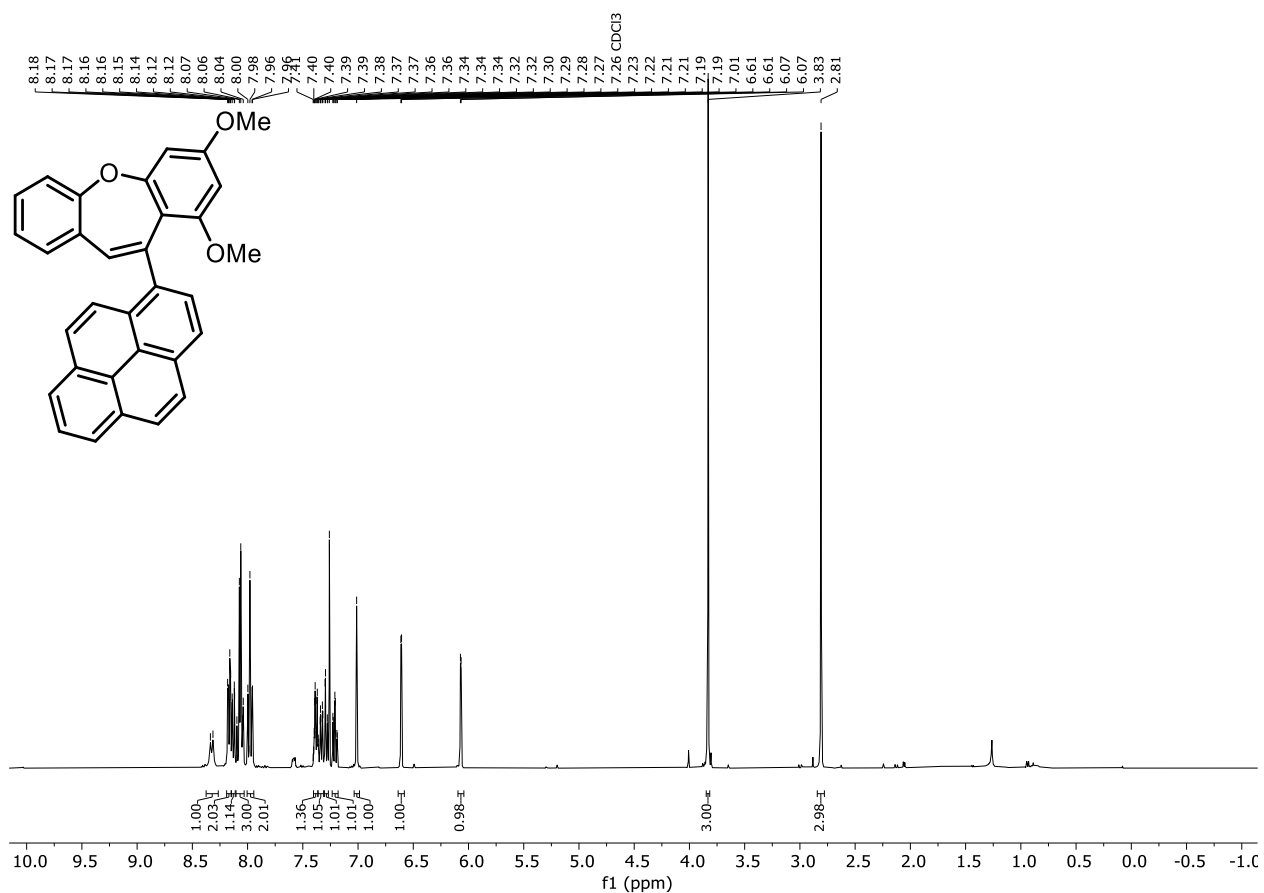


### <sup>13</sup>C{<sup>1</sup>H}-NMR (101 MHz, CDCl<sub>3</sub>) Compound **147e**

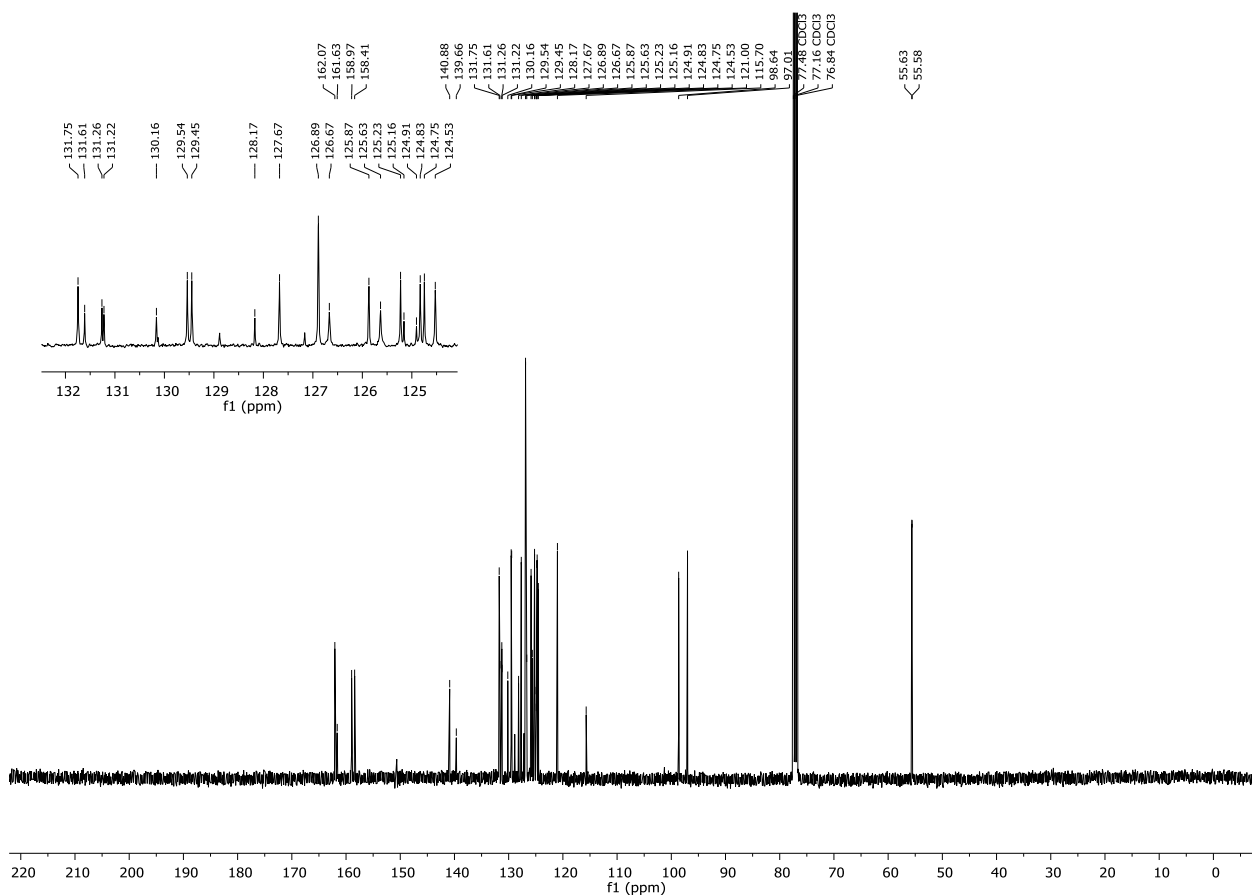


## 7. Appendix

### $^1\text{H-NMR}$ (400 MHz, $\text{CDCl}_3$ ) Compound **147f**



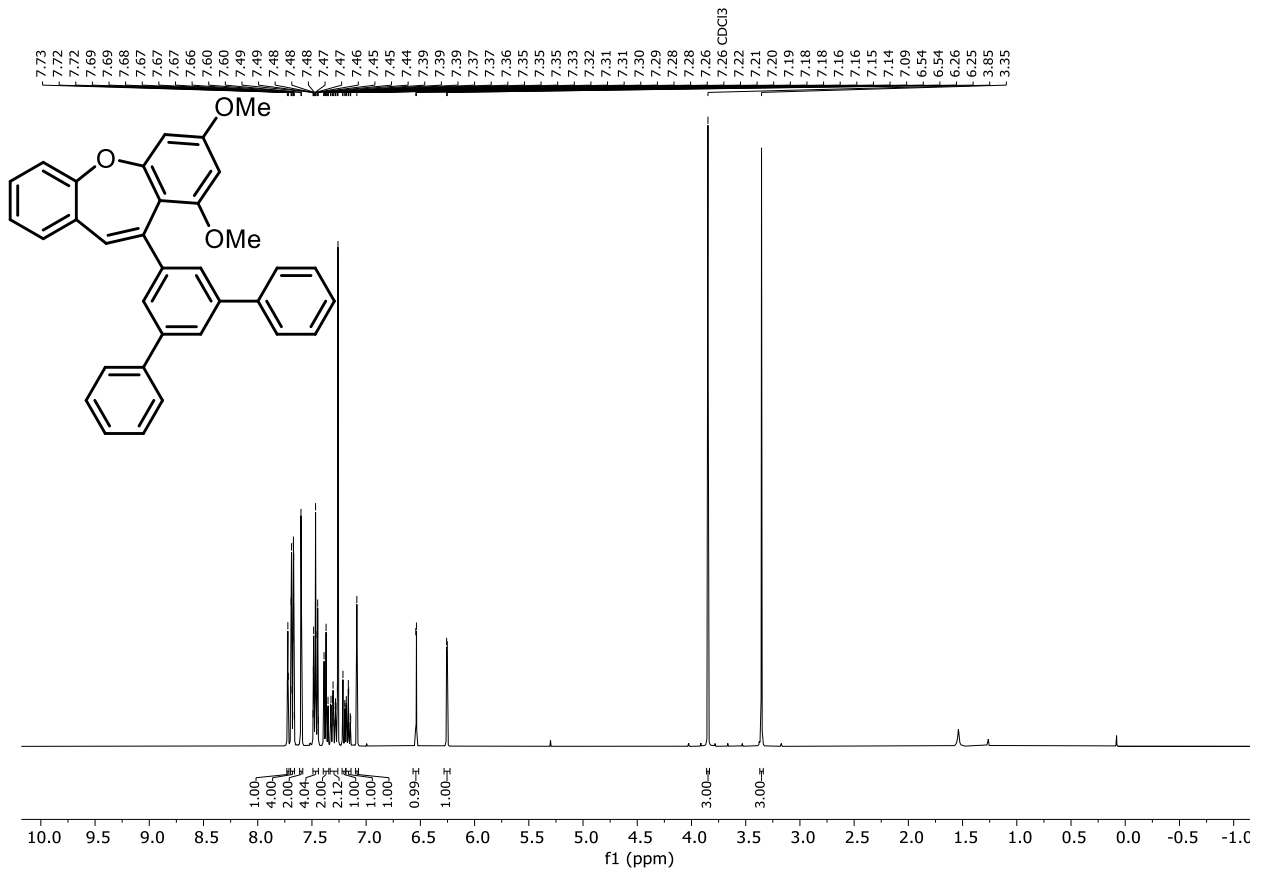
### $^{13}\text{C}\{^1\text{H}\}$ -NMR (101 MHz, $\text{CDCl}_3$ ) Compound **147f**



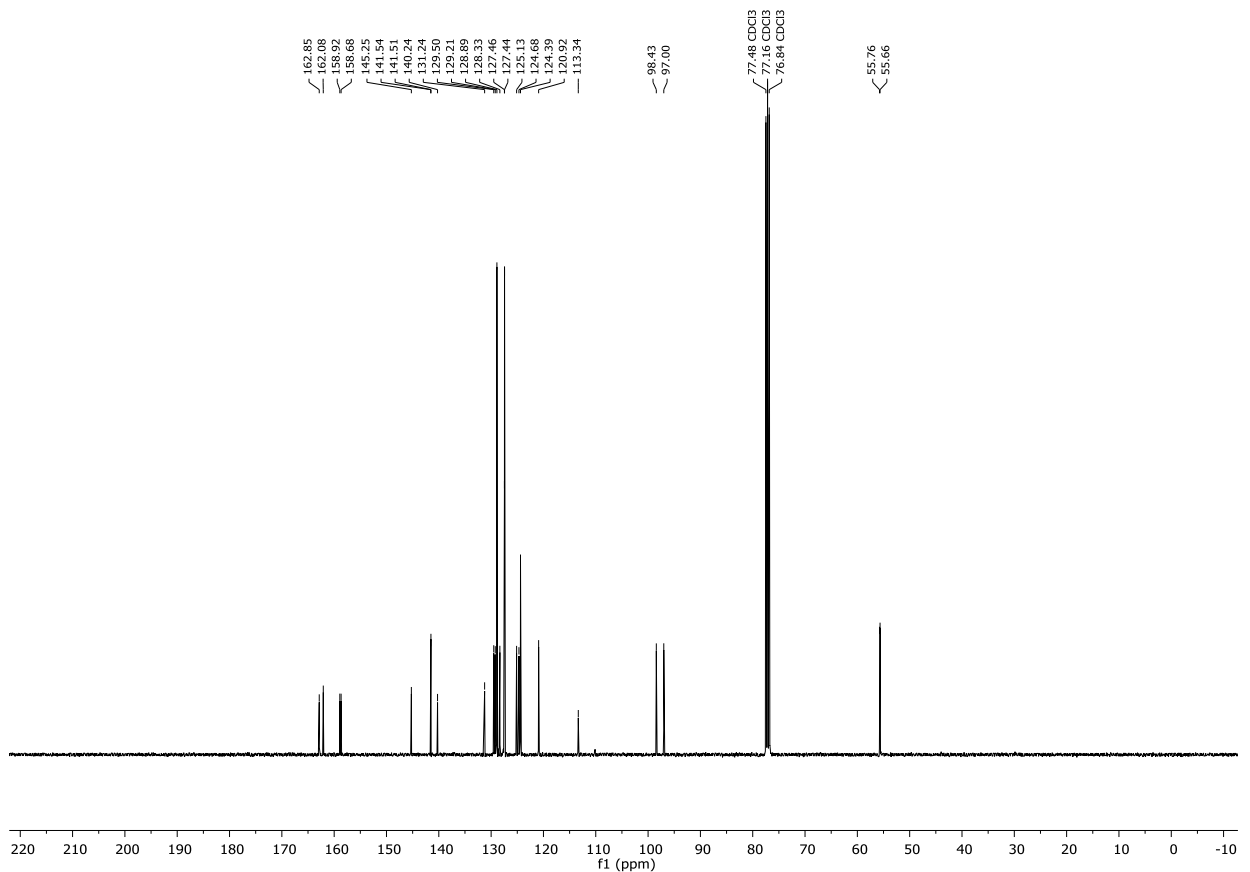


## 7.2 NMR spectra

### <sup>1</sup>H-NMR (400 MHz, CDCl<sub>3</sub>) Compound **147g**

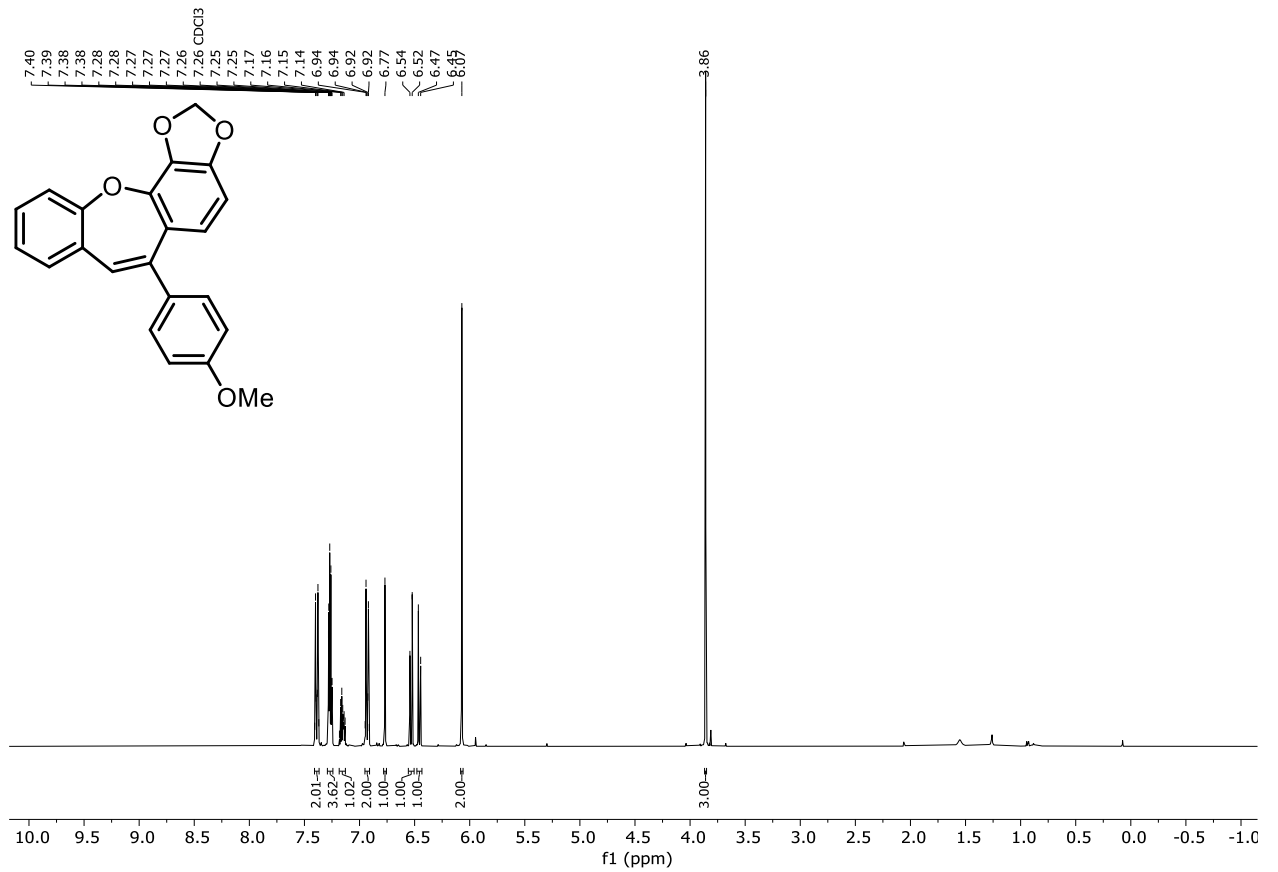


### <sup>13</sup>C{<sup>1</sup>H}-NMR (101 MHz, CDCl<sub>3</sub>) Compound **147g**

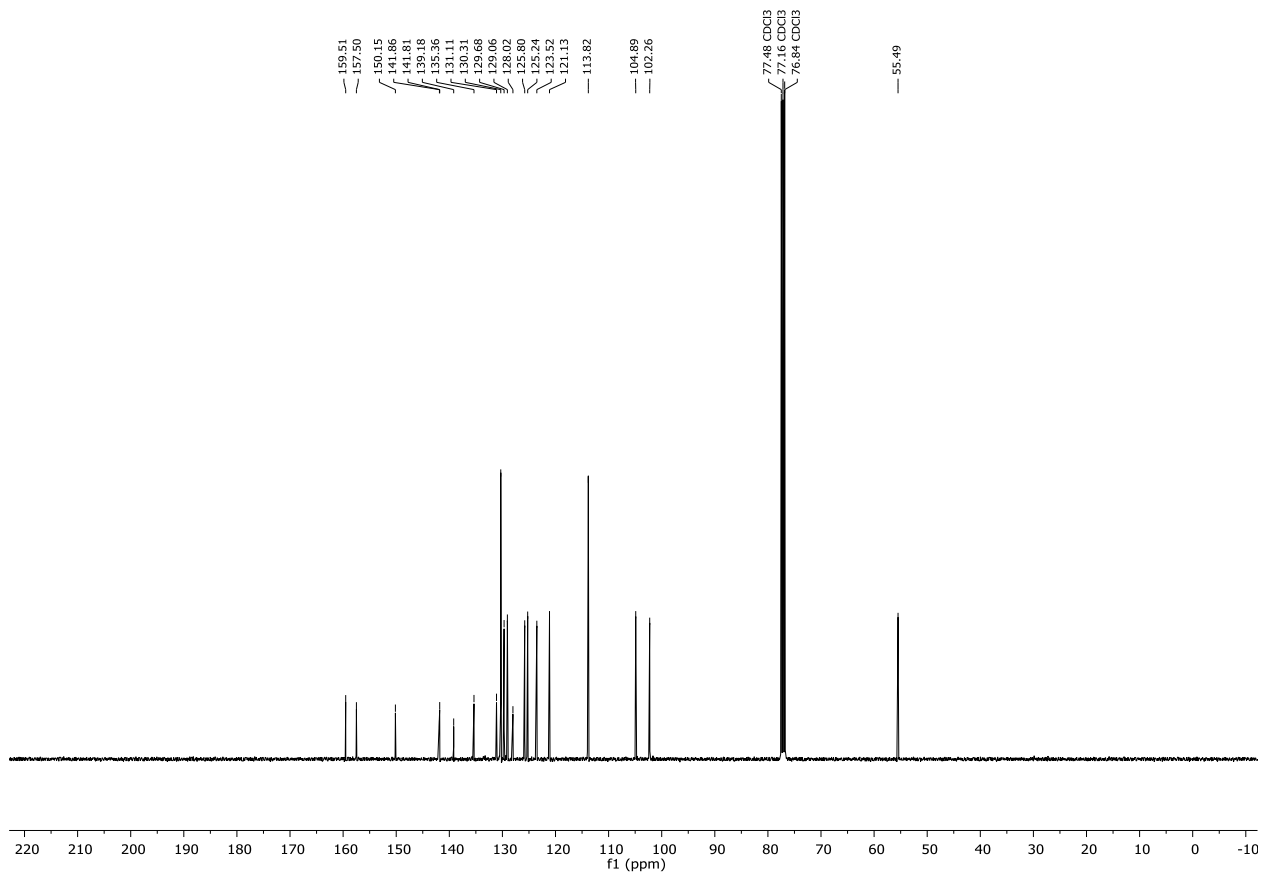


## 7. Appendix

### $^1\text{H-NMR}$ (400 MHz, $\text{CDCl}_3$ ) Compound **147h**

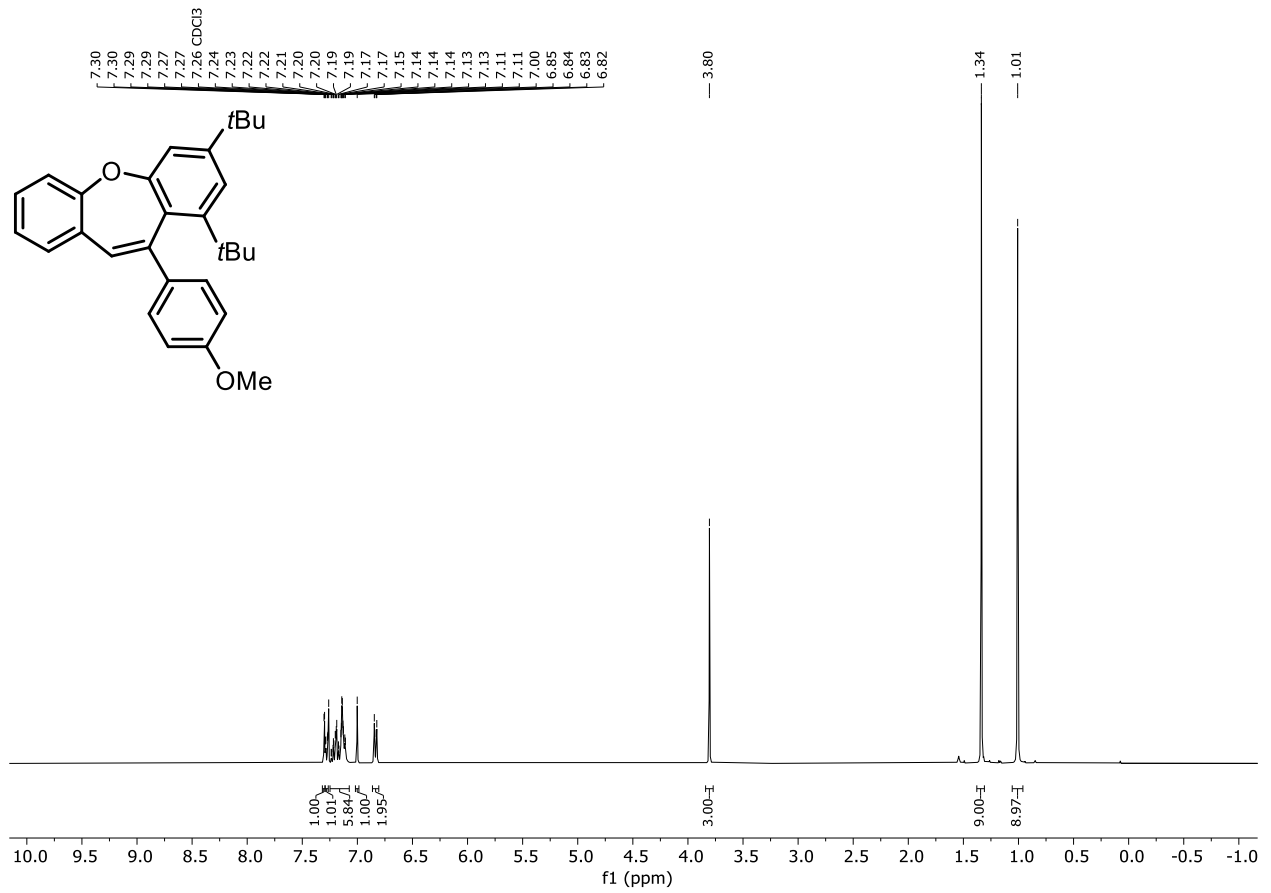


### $^{13}\text{C}\{^1\text{H}\}$ -NMR (101 MHz, $\text{CDCl}_3$ ) Compound **147h**

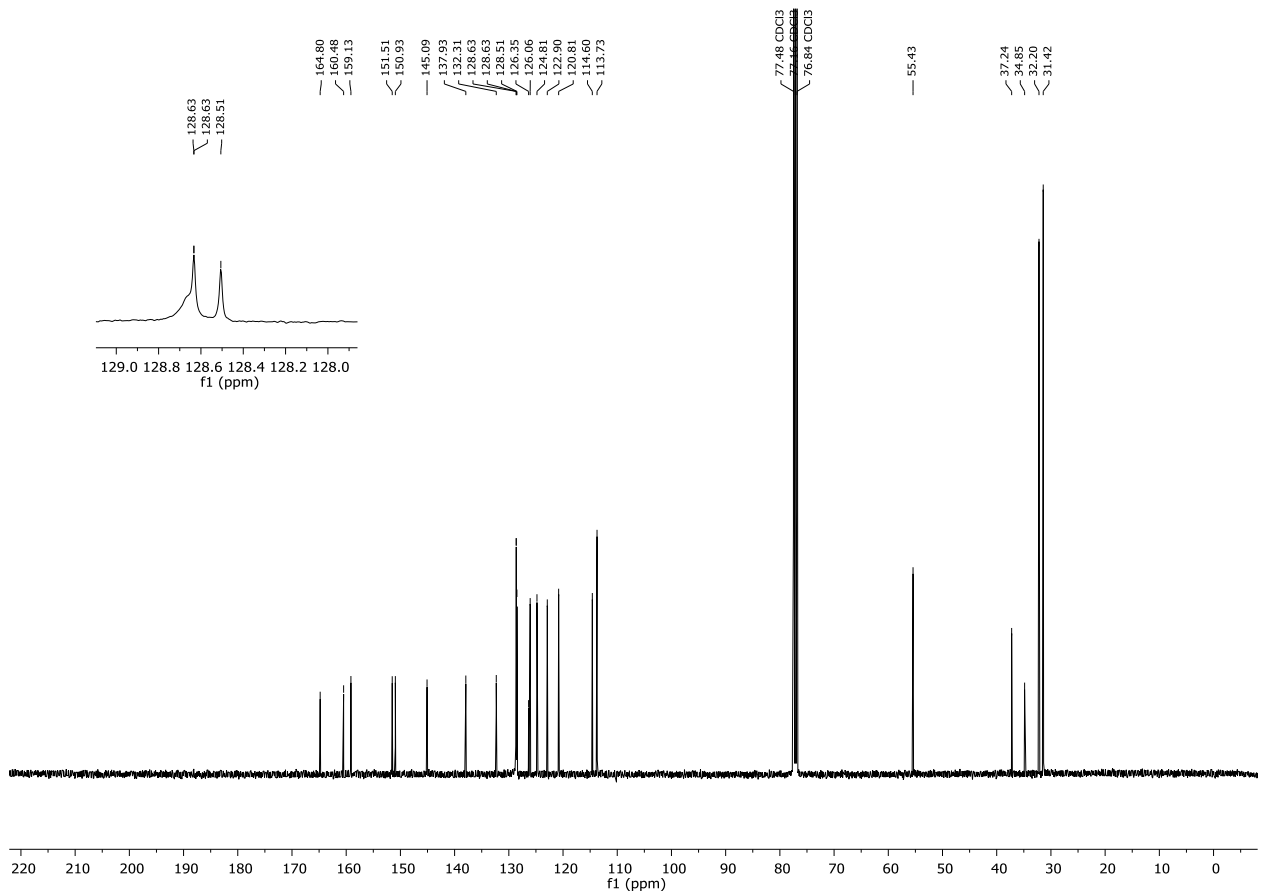


## 7.2 NMR spectra

### $^1\text{H-NMR}$ (400 MHz, $\text{CDCl}_3$ ) Compound **147i**

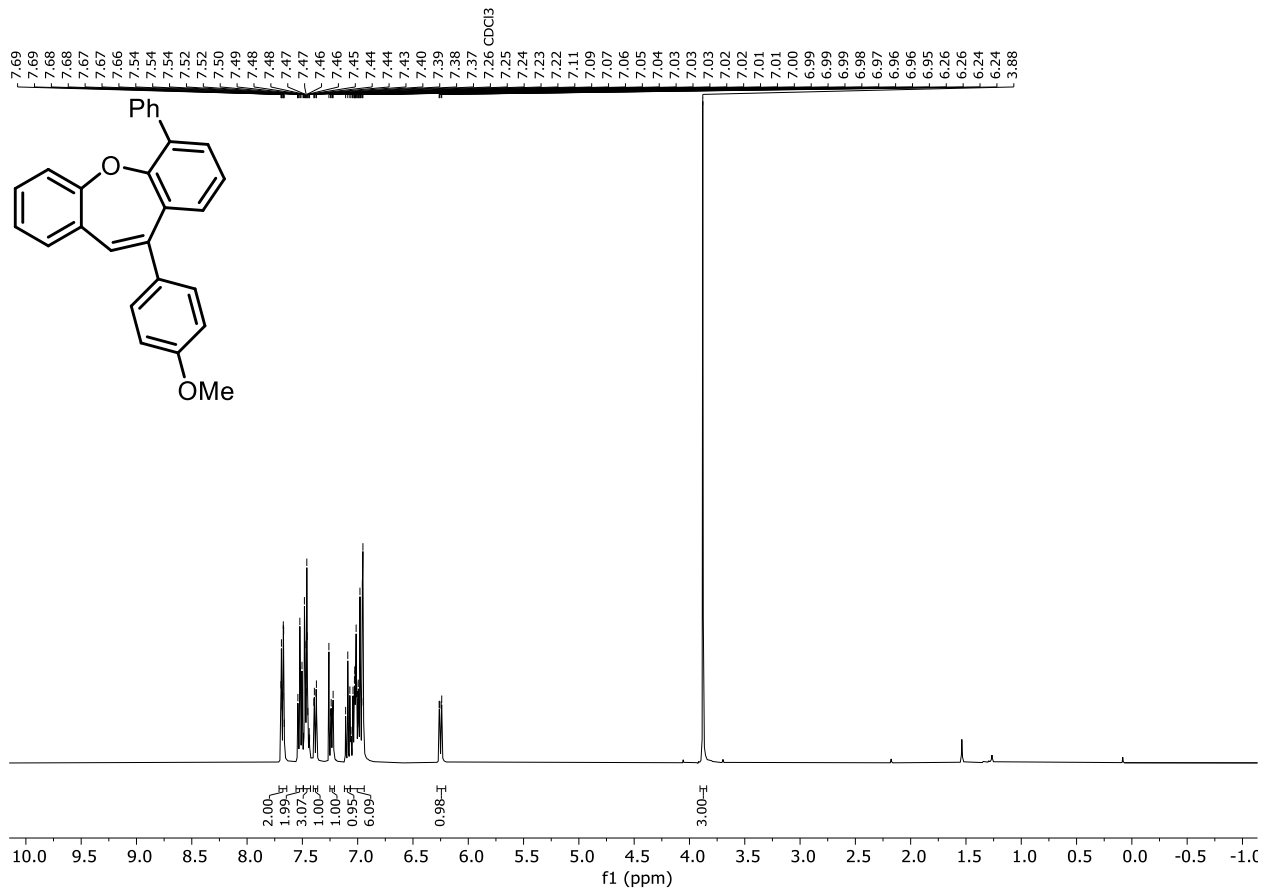


### $^{13}\text{C}\{^1\text{H}\}$ -NMR (101 MHz, $\text{CDCl}_3$ ) Compound **147i**

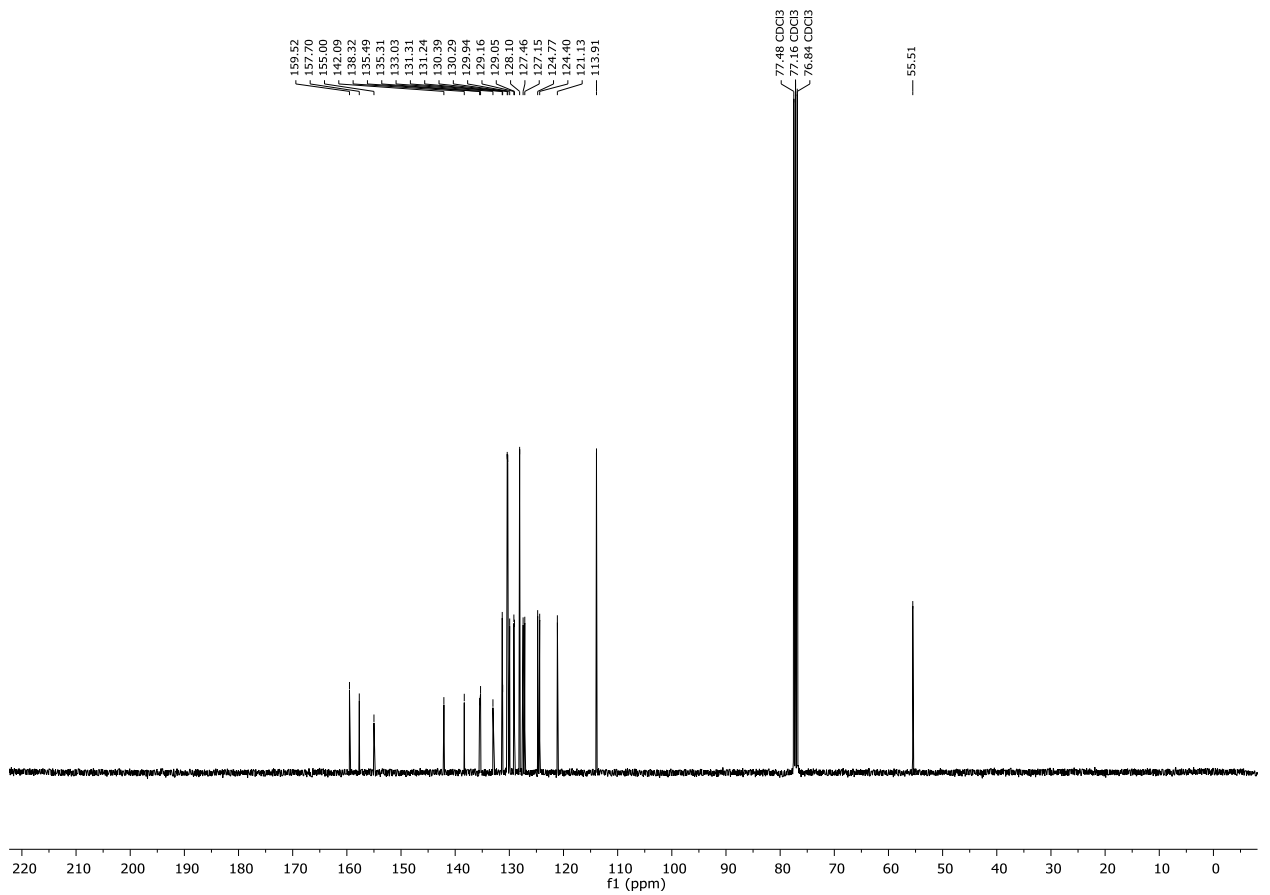


## 7. Appendix

### $^1\text{H-NMR}$ (400 MHz, $\text{CDCl}_3$ ) Compound **147j**

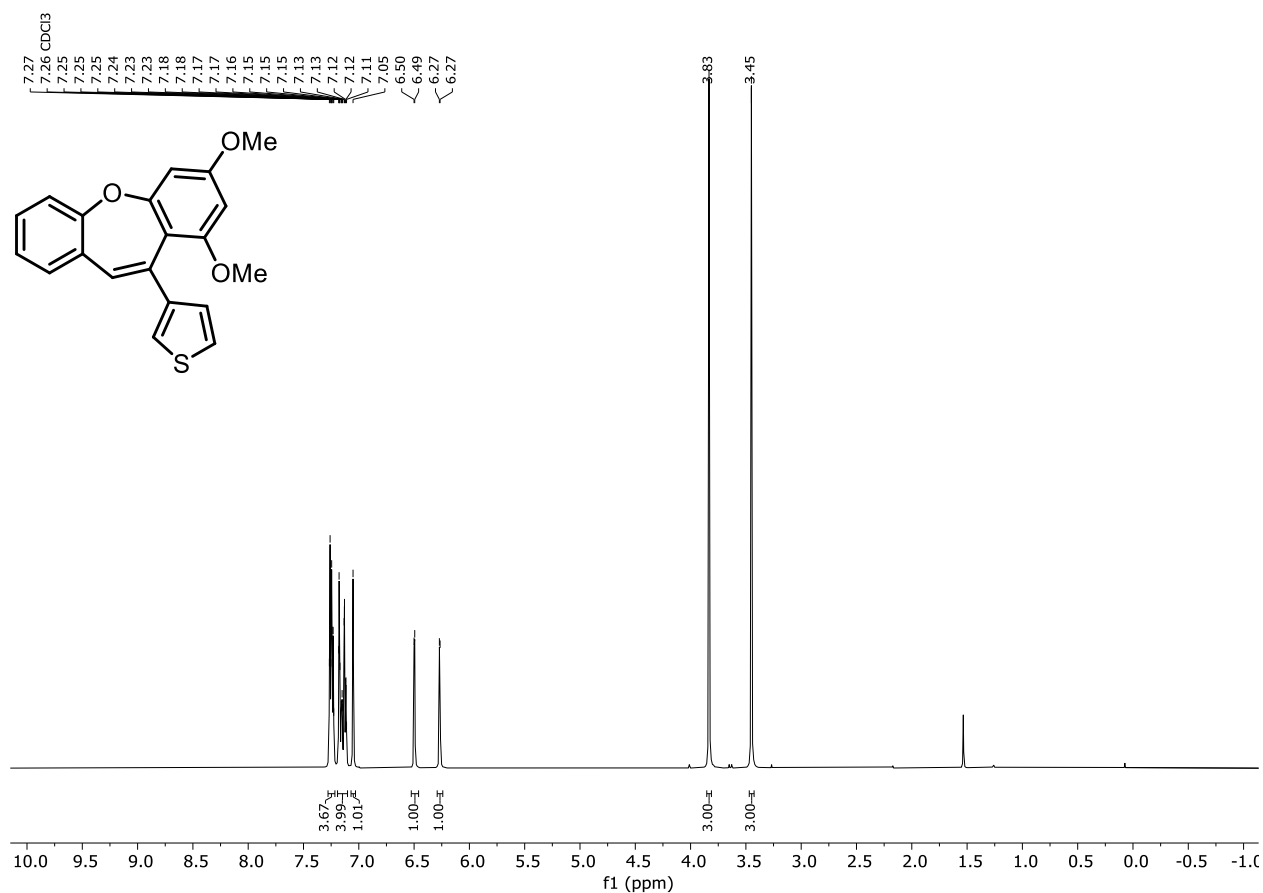


### $^{13}\text{C}\{^1\text{H}\}$ -NMR (101 MHz, $\text{CDCl}_3$ ) Compound **147j**

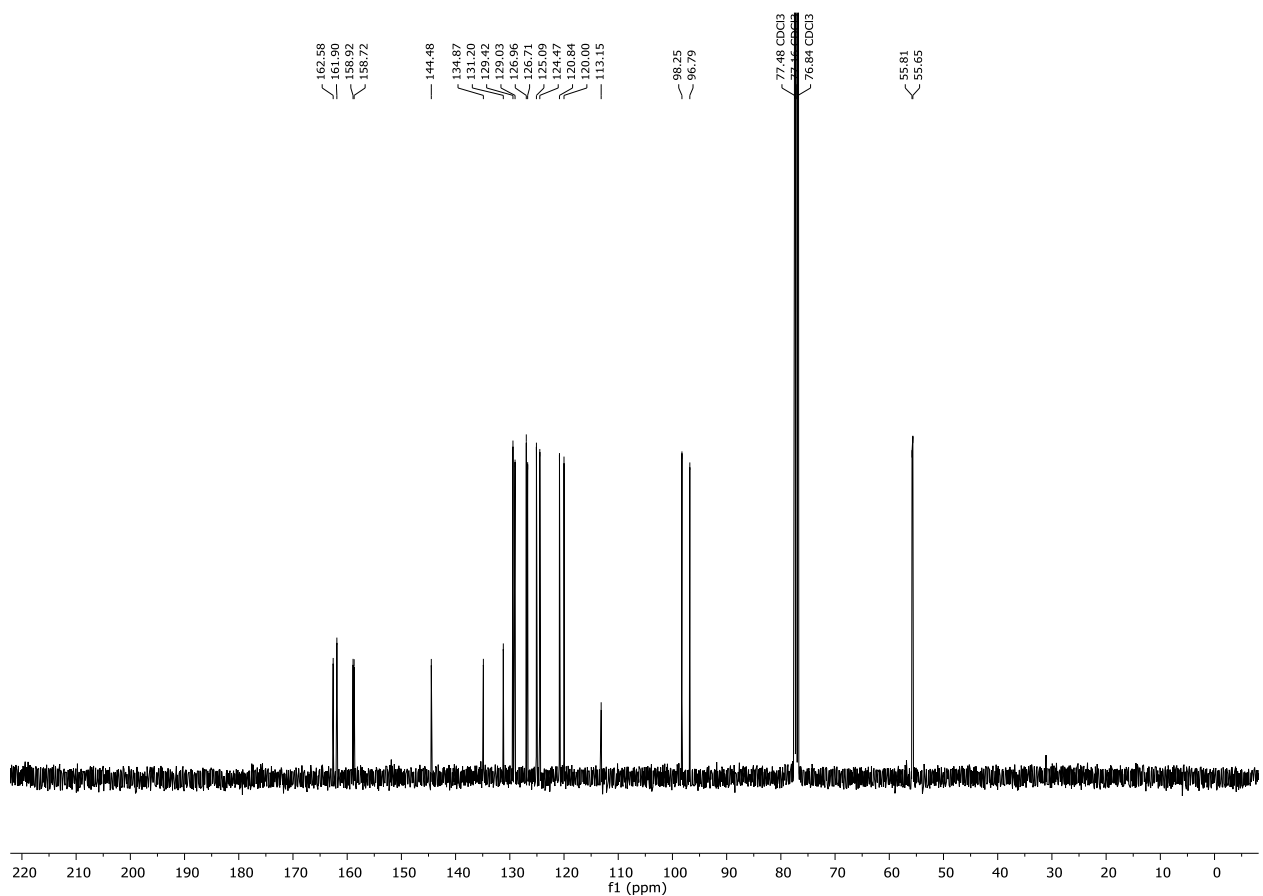


## 7.2 NMR spectra

### $^1\text{H-NMR}$ (400 MHz, $\text{CDCl}_3$ ) Compound **147k**

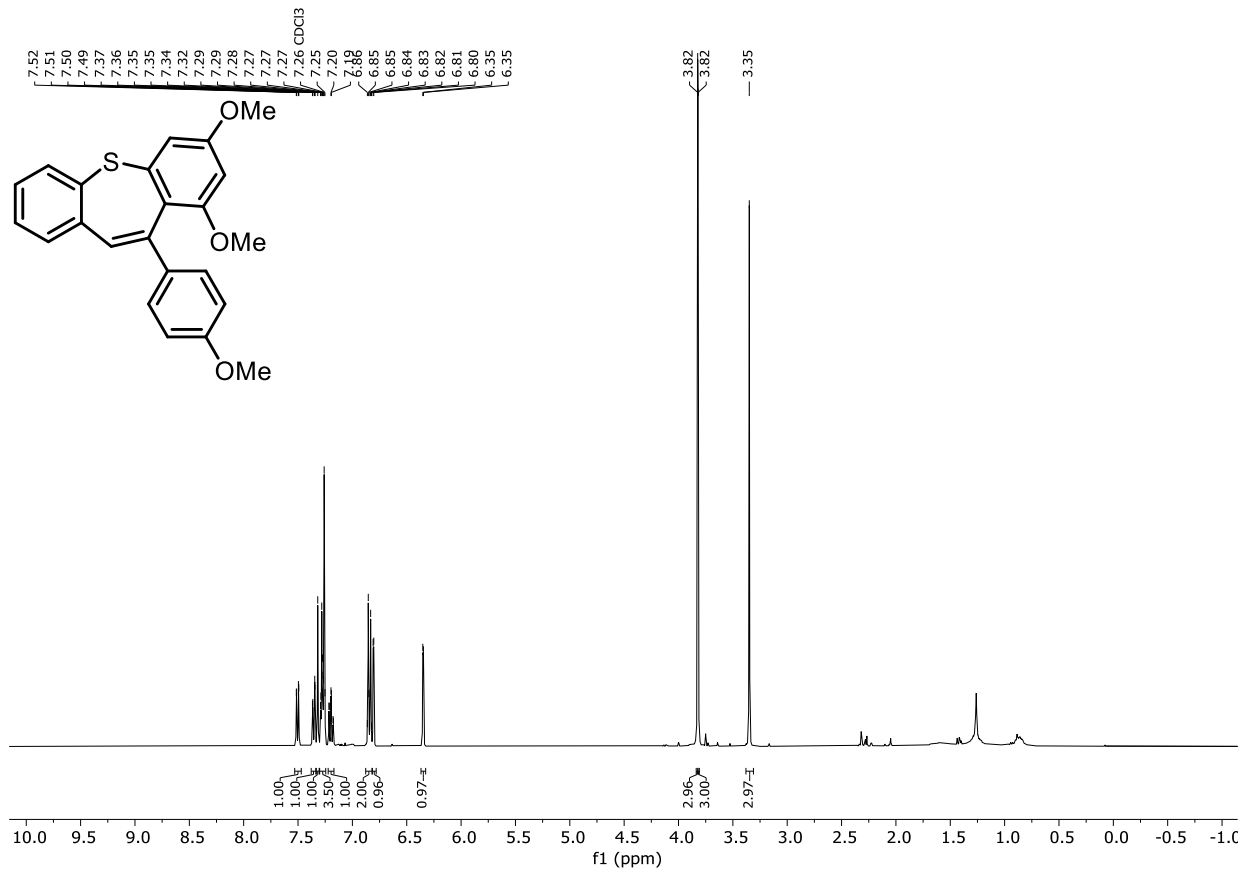


### $^{13}\text{C}\{^1\text{H}\}$ -NMR (101 MHz, $\text{CDCl}_3$ ) Compound **147k**

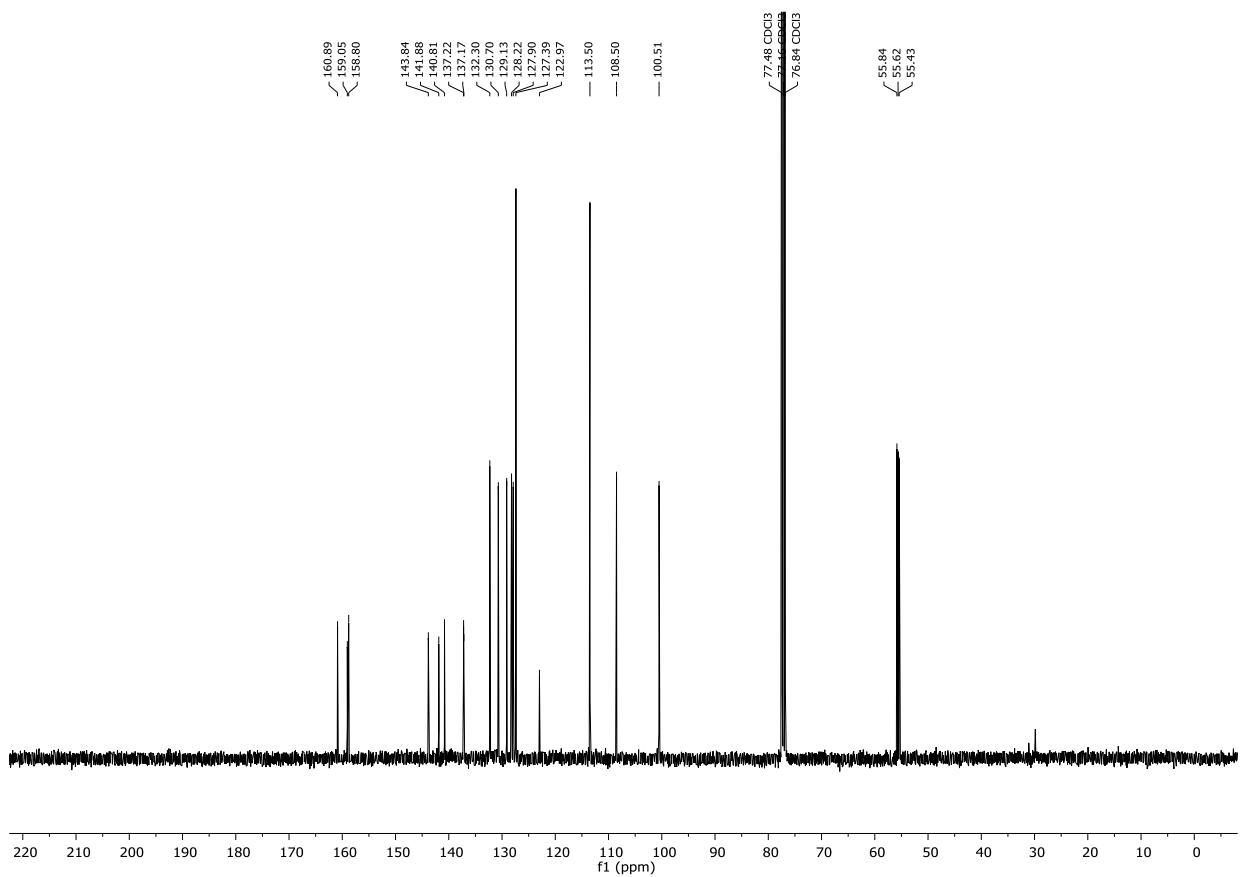


## 7. Appendix

### $^1\text{H-NMR}$ (400 MHz, $\text{CDCl}_3$ ) Compound **148a**

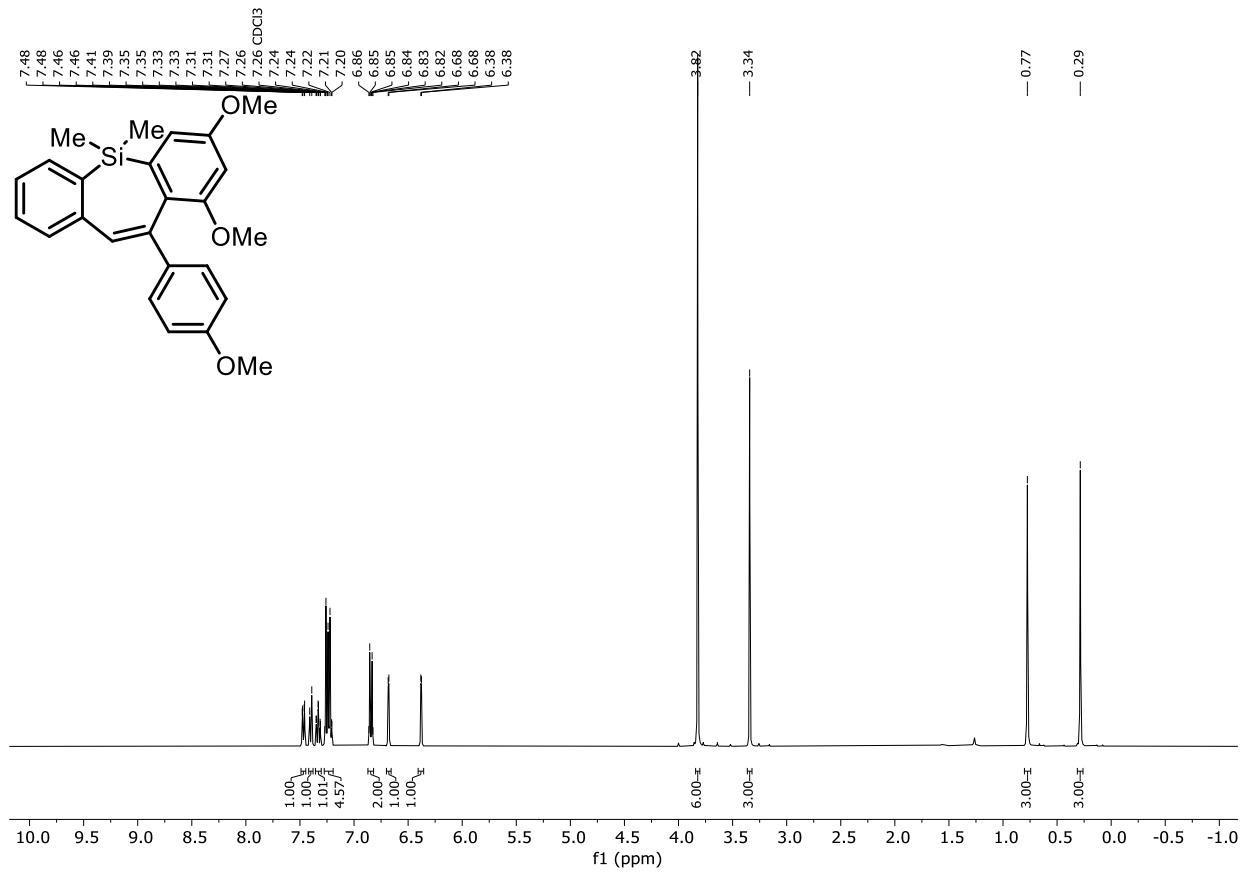


### $^{13}\text{C}\{^1\text{H}\}$ -NMR (101 MHz, $\text{CDCl}_3$ ) Compound **148a**

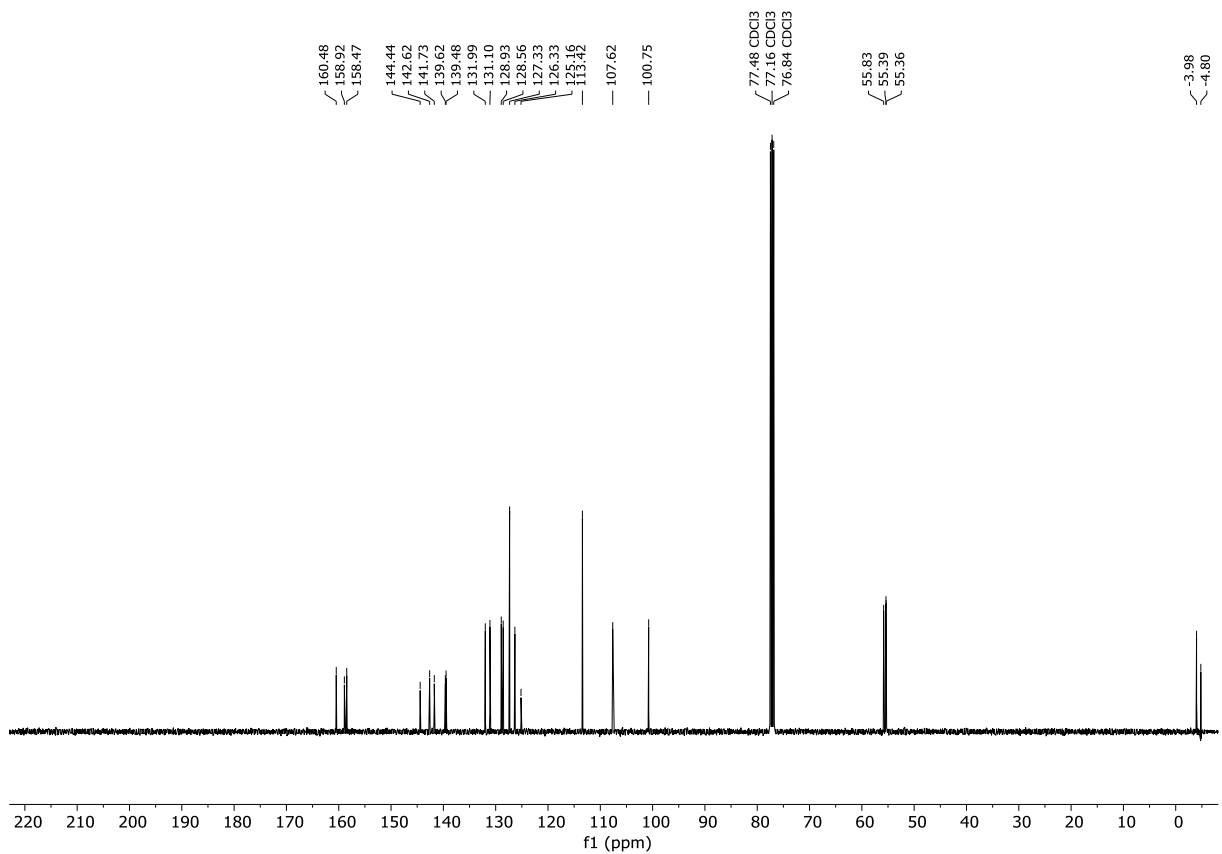


## 7.2 NMR spectra

### $^1\text{H-NMR}$ (400 MHz, $\text{CDCl}_3$ ) Compound **149a**

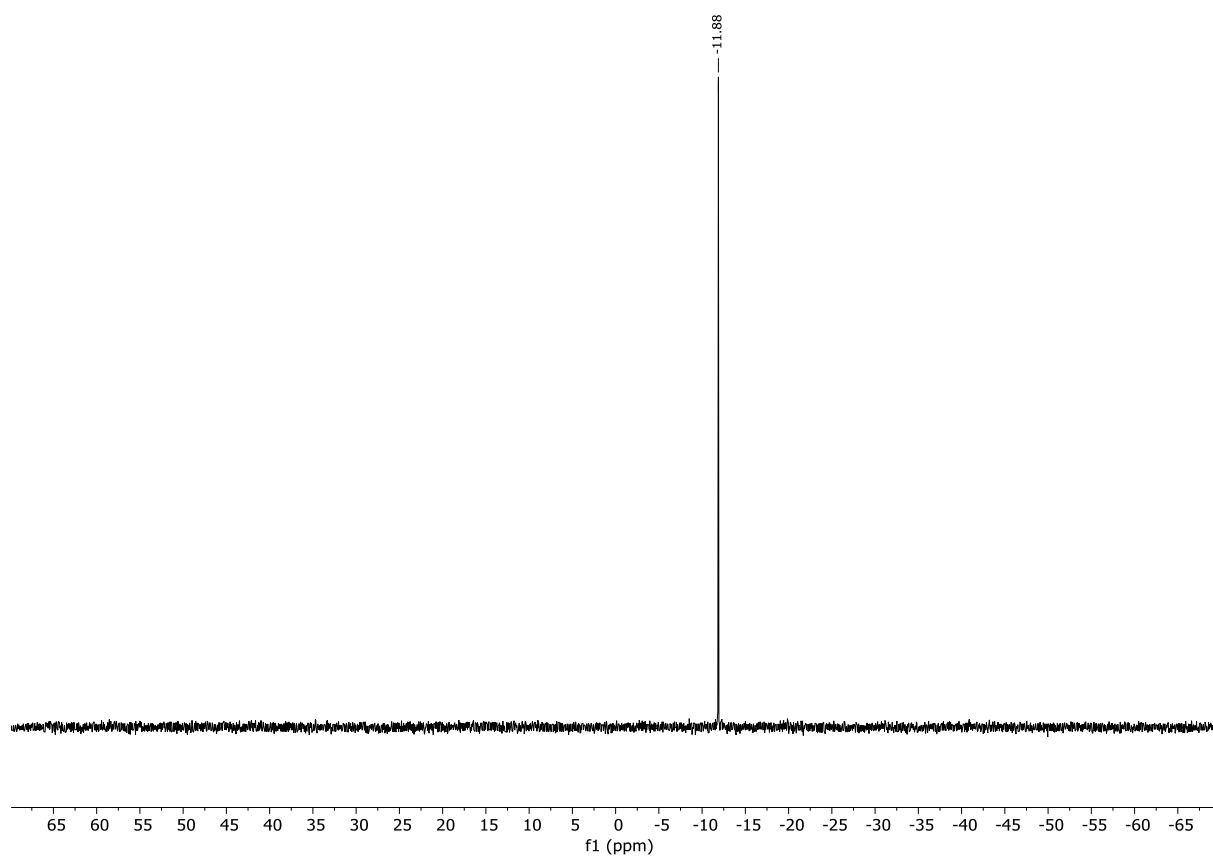


### $^{13}\text{C}\{^1\text{H}\}$ -NMR (101 MHz, $\text{CDCl}_3$ ) Compound **149a**



## 7. Appendix

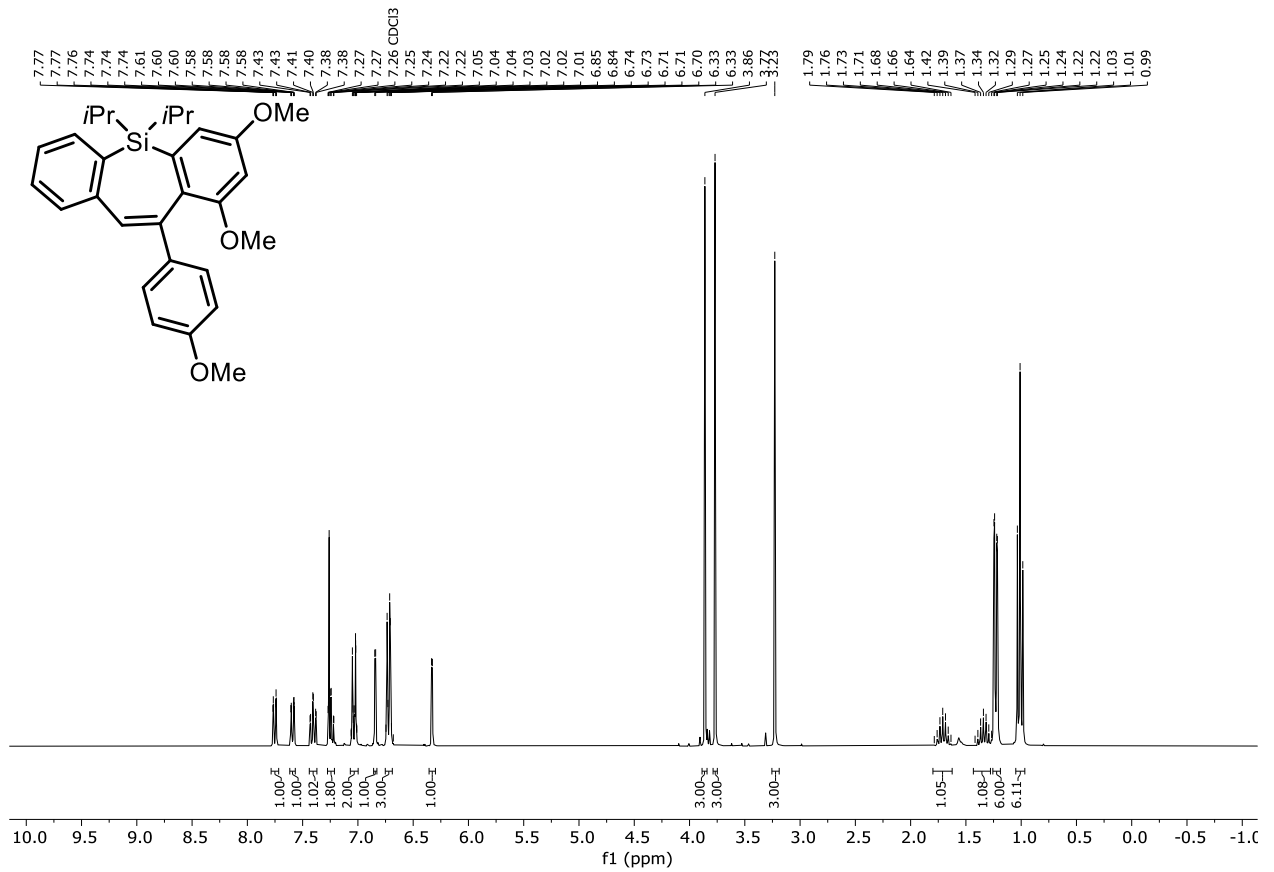
$^{29}\text{Si-NMR}$  (79 MHz,  $\text{CDCl}_3$ ) Compound **149a**



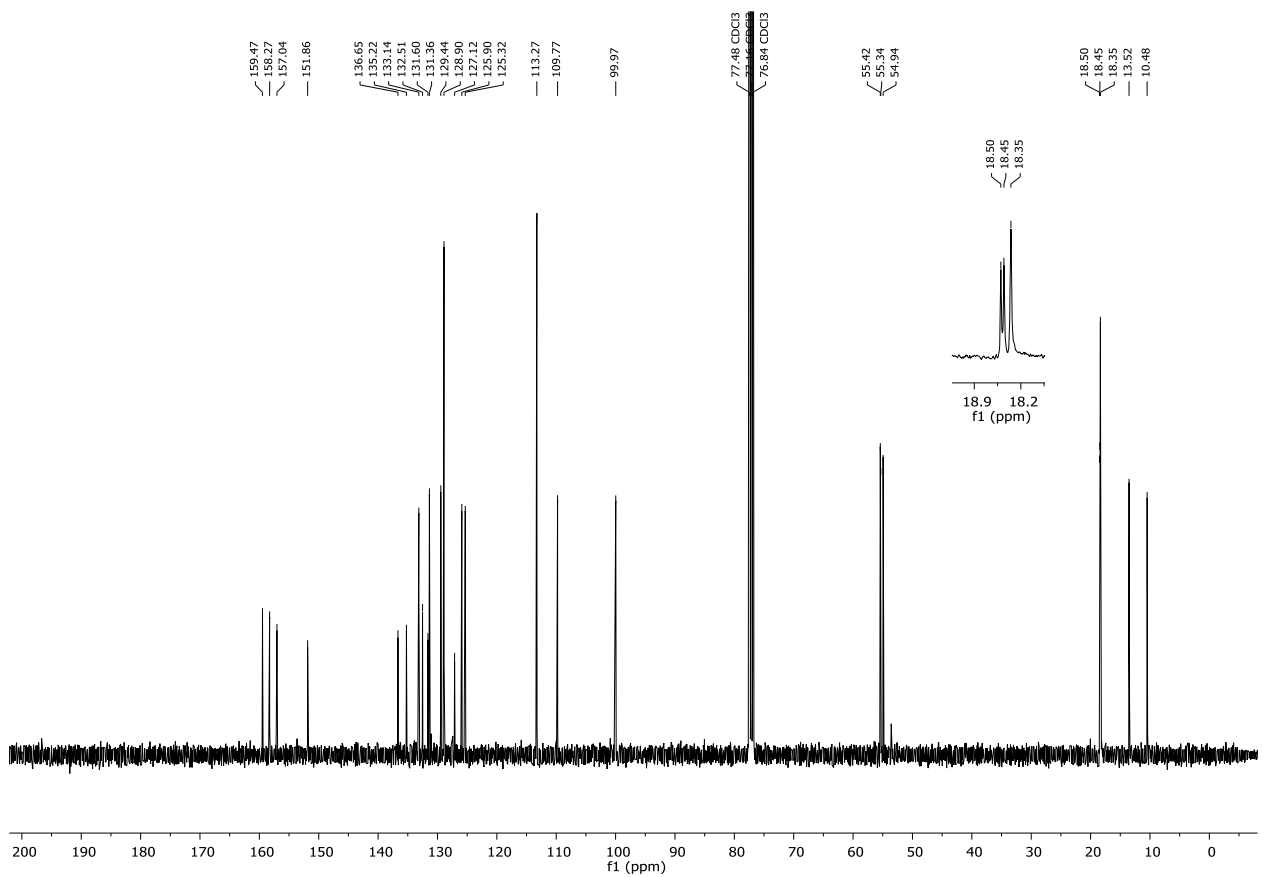


## 7.2 NMR spectra

### $^1\text{H-NMR}$ (300 MHz, $\text{CDCl}_3$ ) Compound **149e**

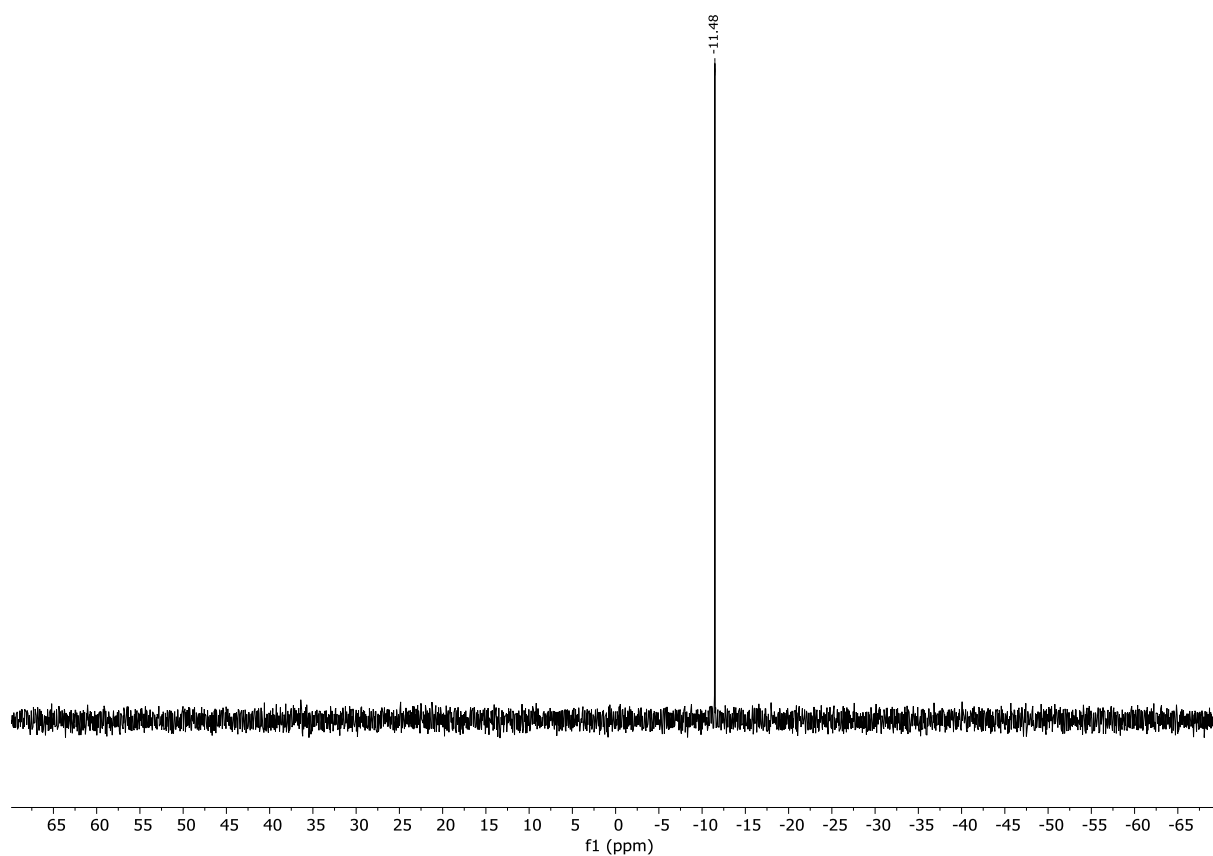


### $^{13}\text{C}\{^1\text{H}\}$ -NMR (101 MHz, $\text{CDCl}_3$ ) Compound **149e**



7. Appendix

$^{29}\text{Si-NMR}$  (79 MHz,  $\text{CDCl}_3$ ) Compound **149e**



## 7.3 Atomic coordinates for DFT calculations

**Table S7:** Atomic coordinates (x, y, z) for optimized minimum and transition state of **146e** at the B3LYP-D3(BJ)/6-31+g(d) level of theory.

Minimum				TS			
Atom	x	y	z	Atom	x	y	z
O	-5.836118	0.173685	-0.798730	O	5.604152	-1.205437	-0.341574
C	-4.517806	-0.111790	-0.565725	C	4.246540	-1.044999	-0.236344
C	-4.062987	-1.092456	0.322550	C	3.459813	-0.327506	-1.145037
H	-4.757092	-1.690782	0.901663	H	3.897822	0.142963	-2.018157
C	-2.688722	-1.294601	0.483157	C	2.081757	-0.223797	-0.932373
H	-2.349013	-2.034458	1.202437	H	1.478957	0.336804	-1.642413
C	-1.746588	-0.542265	-0.225021	C	1.462774	-0.817858	0.171337
C	-2.227647	0.445102	-1.104373	C	2.266932	-1.543839	1.062277
H	-1.516712	1.051299	-1.659185	H	1.809195	-2.004964	1.933159
C	-3.587977	0.658170	-1.279597	C	3.639938	-1.656108	0.868700
H	-3.955224	1.414982	-1.966309	H	4.262193	-2.209052	1.566123
C	-0.282990	-0.772544	-0.087985	C	-0.028607	-0.737974	0.335742
C	1.569657	-2.493202	0.094756	C	-2.026427	-2.380031	0.126255
C	1.889942	-3.604873	0.895659	C	-2.228522	-3.780693	0.110795
H	1.093491	-4.108532	1.438822	H	-1.365845	-4.423673	0.267529
C	3.204032	-4.049259	1.019665	C	-3.474896	-4.352693	-0.106702
H	3.431493	-4.901292	1.654737	H	-3.587995	-5.433335	-0.106036
C	4.226836	-3.395614	0.324632	C	-4.571881	-3.520152	-0.341788
H	5.254687	-3.737422	0.412124	H	-5.557037	-3.938330	-0.529411
C	3.918048	-2.313195	-0.500495	C	-4.387681	-2.139234	-0.336118
H	4.706571	-1.818705	-1.063676	H	-5.243758	-1.491363	-0.515558
C	2.601391	-1.863003	-0.635879	C	-3.139290	-1.545951	-0.093484
C	2.244836	-0.729240	-1.568724	C	-3.165882	-0.033750	-0.011262
H	1.429304	-1.052509	-2.230788	H	-3.675303	0.206995	0.936674
H	3.103749	-0.473419	-2.196986	H	-3.857836	0.314121	-0.787195
C	1.804342	0.477178	-0.774954	C	-1.965118	0.903974	-0.033443
C	2.620349	1.617866	-0.745547	C	-2.340798	2.231079	-0.306620
H	3.535747	1.621475	-1.324924	H	-3.355997	2.420969	-0.634683
C	2.237153	2.720992	0.014738	C	-1.454443	3.289250	-0.115810
C	1.058566	2.681465	0.772191	C	-0.199324	3.041875	0.444562
H	0.812889	3.542869	1.379792	H	0.439218	3.881484	0.687616
C	0.263243	1.540283	0.750697	C	0.171545	1.731018	0.719120
C	0.601480	0.415871	-0.052514	C	-0.642100	0.607219	0.359278
C	-6.816697	-0.586626	-0.109612	C	6.261144	-0.615504	-1.451759
H	-6.733067	-0.454231	0.977372	H	6.141682	0.476504	-1.453291
H	-6.737150	-1.654238	-0.353879	H	5.886873	-1.023100	-2.400396
H	-7.781629	-0.206309	-0.448873	H	7.317793	-0.864961	-1.340716
C	0.178773	-2.048988	-0.010157	C	-0.641577	-1.947693	0.262819
H	-0.564492	-2.844847	-0.004443	H	0.049870	-2.784748	0.195463
O	2.944702	3.886605	0.099594	O	-1.737040	4.596141	-0.386887
O	-0.852387	1.410294	1.519472	O	1.312246	1.449281	1.401266
C	4.168921	3.980677	-0.615305	C	-3.015932	4.912603	-0.920650

## 7. Appendix

H	4.885600	3.221577	-0.276337	H	-3.184959	4.399672	-1.875963
H	4.006987	3.875016	-1.695828	H	-3.815988	4.650102	-0.216548
H	4.561965	4.975751	-0.401048	H	-3.011198	5.991839	-1.080528
C	-1.332616	2.537837	2.234789	C	2.360924	2.406277	1.444366
H	-1.531411	3.379165	1.558867	H	2.099456	3.257716	2.085681
H	-2.264755	2.213724	2.700087	H	3.218177	1.879766	1.866687
H	-0.622753	2.849503	3.011998	H	2.606466	2.761626	0.436371

**Table S8:** Atomic coordinates (x, y, z) for optimized minimum of **146g** at the B3LYP-D3(BJ)/6-31+g(d) level of theory.

Minimum			
Atom	x	y	z
O	-3.584216	4.407575	0.459052
C	-2.472501	3.626832	0.316338
C	-2.233646	2.706364	1.348659
H	-2.923459	2.672229	2.186438
C	-1.132965	1.863609	1.289035
H	-0.961791	1.153829	2.093296
C	-0.225888	1.914956	0.212003
C	0.964764	1.022265	0.183174
C	0.734870	-0.407869	0.495194
C	-0.471024	-1.002758	0.084895
H	-1.194962	-0.394360	-0.446456
C	-0.749615	-2.356255	0.299595
C	-2.035431	-2.943871	-0.148182
C	-3.230575	-2.209636	-0.059946
H	-3.212311	-1.208246	0.361243
C	-4.441656	-2.759914	-0.480345
H	-5.354921	-2.176547	-0.396359
C	-4.484107	-4.058196	-0.995862
H	-5.427410	-4.487509	-1.322459
C	-3.303216	-4.799514	-1.088448
H	-3.322578	-5.806740	-1.496585
C	-2.092130	-4.247108	-0.669980
H	-1.175662	-4.821851	-0.771448
C	0.220420	-3.134472	0.953389
H	0.020817	-4.180841	1.166233
C	1.418857	-2.561550	1.368243
H	2.153356	-3.171933	1.888656
C	1.692278	-1.205496	1.157626
C	2.989671	-0.596398	1.626339
H	3.522800	-1.302326	2.271086
H	2.775524	0.302017	2.223458
C	3.857648	-0.208952	0.453809
C	3.439367	0.845147	-0.388034
C	2.163368	1.536601	-0.204438

## 7.3 Atomic coordinates for DFT calculations

H	2.173745	2.590383	-0.478948
C	4.299020	1.266691	-1.420728
H	3.992058	2.095677	-2.054456
C	5.513285	0.627585	-1.655597
H	6.154544	0.961020	-2.467015
C	5.902184	-0.442568	-0.843376
H	6.849757	-0.945831	-1.015506
C	5.076399	-0.847743	0.205986
H	5.388062	-1.661073	0.857496
C	-0.486748	2.833260	-0.811318
H	0.172329	2.870013	-1.674228
C	-1.593998	3.686886	-0.770881
H	-1.763321	4.373496	-1.592264
C	-3.870419	5.360005	-0.555485
H	-4.780926	5.869428	-0.236443
H	-4.044124	4.870593	-1.522748
H	-3.057071	6.090563	-0.655410

**Table S9:** Atomic coordinates (x, y, z) for optimized minimum and transition state of **146h** at the B3LYP/6-31+g(d) level of theory.

Minimum				TS			
Atom	x	y	z	Atom	x	y	z
O	5.401697	-1.846732	-0.074628	O	4.677690	-2.876197	-0.190549
C	4.074666	-1.518759	-0.094919	C	3.471453	-2.231836	-0.133061
C	3.286786	-2.086619	0.918357	C	2.678713	-2.511492	0.989304
H	3.763893	-2.730027	1.652005	H	3.055625	-3.203360	1.737122
C	1.926351	-1.812317	0.982620	C	1.436152	-1.903096	1.135615
H	1.343956	-2.243526	1.792733	H	0.840617	-2.123170	2.018569
C	1.298423	-0.966500	0.045586	C	0.943599	-0.993142	0.181325
C	2.107402	-0.399227	-0.949287	C	1.751312	-0.727600	-0.931912
H	1.660688	0.264189	-1.684919	H	1.402405	-0.035457	-1.693531
C	3.476793	-0.668403	-1.032675	C	2.999012	-1.335922	-1.100119
H	4.057189	-0.210845	-1.826246	H	3.583854	-1.103402	-1.983307
C	-0.172718	-0.708775	0.061998	C	-0.440995	-0.407688	0.290241
C	-1.012224	-1.731381	0.383363	C	-1.405454	-1.367718	0.374333
C	-2.478812	-1.743529	0.359934	C	-2.859068	-1.392717	0.248952
C	-3.194110	-1.113423	-0.684395	C	-3.673301	-0.307508	-0.127857
C	-4.592343	-1.168106	-0.692829	C	-5.040883	-0.532928	-0.345750
H	-5.138020	-0.681221	-1.498621	H	-5.665791	0.305236	-0.649246
C	-5.291318	-1.853308	0.303199	C	-5.627080	-1.786473	-0.171194
H	-6.377447	-1.890472	0.277306	H	-6.692233	-1.918510	-0.342666
C	-4.587252	-2.506645	1.320332	C	-4.828684	-2.863366	0.222175
H	-5.122080	-3.052348	2.093514	H	-5.259248	-3.851152	0.363950
C	-3.194695	-2.458948	1.338406	C	-3.467076	-2.660512	0.413367
H	-2.645894	-2.967666	2.128291	H	-2.836327	-3.502457	0.689803
C	-2.412233	-0.421533	-1.781335	C	-3.224989	1.135373	-0.236497

## 7. Appendix

H	-3.084906	-0.126737	-2.593596	H	-3.577258	1.636349	0.682418
H	-1.679546	-1.126685	-2.199716	H	-3.819312	1.593061	-1.035725
C	-1.703193	0.796389	-1.229049	C	-1.792650	1.634355	-0.403194
C	-0.664034	0.651960	-0.307646	C	-0.609780	1.059632	0.088308
C	-0.099181	1.836258	0.300823	C	0.514699	1.957402	0.331013
C	-0.545679	3.130955	-0.129748	C	0.521858	3.277182	-0.231983
C	0.008745	4.301879	0.457137	C	1.631982	4.142191	-0.026292
H	-0.338147	5.271152	0.104841	H	1.614136	5.124277	-0.494262
C	0.947460	4.218291	1.461074	C	2.682989	3.768425	0.779725
H	1.359312	5.120105	1.906797	H	3.519755	4.441891	0.946272
C	1.359114	2.946105	1.923778	C	2.641970	2.509680	1.422625
H	2.079706	2.874272	2.734673	H	3.436393	2.226849	2.108738
C	0.851450	1.793006	1.361377	C	1.599295	1.633536	1.198548
H	1.179966	0.835229	1.744804	H	1.599613	0.690524	1.726845
C	-1.562326	3.223660	-1.116585	C	-0.619329	3.721305	-0.942492
H	-1.891468	4.206999	-1.445474	H	-0.613400	4.703702	-1.409225
C	-2.139485	2.087441	-1.626652	C	-1.748507	2.942950	-0.961580
H	-2.939120	2.165285	-2.359833	H	-2.654719	3.336401	-1.416437
C	6.253303	-1.292011	-1.068485	C	5.526474	-2.627281	-1.302539
H	7.249775	-1.683761	-0.857052	H	6.418770	-3.233519	-1.136227
H	6.271877	-0.195669	-1.011410	H	5.810105	-1.567940	-1.359743
H	5.945516	-1.601636	-2.075955	H	5.050468	-2.929990	-2.244723
H	-0.554165	-2.671542	0.688611	H	-1.005247	-2.376267	0.449405

**Table S10:** Atomic coordinates (x, y, z) for optimized minimum and transition state of **146h** at the B3LYP/6-31+g(d) level of theory using the "tight" option and the superfine grid.

Minimum				TS			
Atom	x	y	z	Atom	x	y	z
O	5.400853	-1.848222	-0.074328	O	4.677529	-2.876348	-0.190764
C	4.073892	-1.519983	-0.094867	C	3.471324	-2.231927	-0.133198
C	3.285950	-2.086776	0.918941	C	2.678913	-2.511053	0.989526
H	3.762992	-2.729528	1.653205	H	3.056035	-3.202565	1.737565
C	1.925563	-1.812144	0.982959	C	1.436429	-1.902526	1.135927
H	1.343051	-2.242319	1.793541	H	0.841138	-2.122140	2.019155
C	1.297819	-0.967041	0.045177	C	0.943651	-0.992967	0.181380
C	2.106847	-0.400931	-0.950337	C	1.751071	-0.727867	-0.932183
H	1.660182	0.261791	-1.686626	H	1.402064	-0.035872	-1.693900
C	3.476158	-0.670486	-1.033518	C	2.998685	-1.336354	-1.100484
H	4.056622	-0.214023	-1.827676	H	3.583343	-1.104260	-1.983906
C	-0.173249	-0.708765	0.061732	C	-0.440976	-0.407549	0.290311
C	-1.012953	-1.731334	0.382732	C	-1.405363	-1.367619	0.374525
C	-2.479541	-1.743143	0.359647	C	-2.858965	-1.392712	0.249050
C	-3.194976	-1.112114	-0.684033	C	-3.673221	-0.307630	-0.128084
C	-4.593238	-1.166298	-0.692026	C	-5.040735	-0.533232	-0.346228
H	-5.139011	-0.678698	-1.497316	H	-5.665675	0.304800	-0.650020
C	-5.292087	-1.852071	0.303681	C	-5.626841	-1.786809	-0.171560

## 7.3 Atomic coordinates for DFT calculations

H	-6.378231	-1.888927	0.278100	H	-6.691941	-1.918987	-0.343240
C	-4.587890	-2.506519	1.320033	C	-4.828432	-2.863546	0.222209
H	-5.122656	-3.052749	2.092884	H	-5.258933	-3.851342	0.364103
C	-3.195329	-2.459183	1.337761	C	-3.466880	-2.660529	0.413607
H	-2.646410	-2.968721	2.127036	H	-2.836099	-3.502370	0.690284
C	-2.413150	-0.420193	-1.781007	C	-3.225026	1.135299	-0.236841
H	-3.085969	-0.124935	-2.592981	H	-3.577663	1.636356	0.681885
H	-1.680924	-1.125585	-2.199769	H	-3.819156	1.592787	-1.036328
C	-1.703363	0.797260	-1.228649	C	-1.792711	1.634461	-0.403154
C	-0.664033	0.652219	-0.307564	C	-0.609848	1.059758	0.088370
C	-0.098335	1.836248	0.300770	C	0.514603	1.957535	0.331176
C	-0.544140	3.131183	-0.129806	C	0.521804	3.277347	-0.231727
C	0.011135	4.301833	0.456777	C	1.631967	4.142299	-0.025974
H	-0.335289	5.271263	0.104457	H	1.614126	5.124452	-0.493796
C	0.950092	4.217801	1.460458	C	2.683068	3.768335	0.779840
H	1.362632	5.119418	1.905938	H	3.519915	4.441710	0.946347
C	1.361046	2.945426	1.923218	C	2.642024	2.509523	1.422618
H	2.081772	2.873233	2.733958	H	3.436505	2.226512	2.108583
C	0.852454	1.792553	1.361151	C	1.599169	1.633574	1.198675
H	1.180449	0.834668	1.744728	H	1.599240	0.690649	1.727104
C	-1.561013	3.224445	-1.116379	C	-0.619421	3.721536	-0.942140
H	-1.889626	4.207963	-1.445248	H	-0.613559	4.704001	-1.408727
C	-2.138974	2.088563	-1.626228	C	-1.748575	2.943146	-0.961338
H	-2.938713	2.166812	-2.359248	H	-2.654783	3.336655	-1.416155
C	6.253051	-1.292370	-1.067059	C	5.526243	-2.627427	-1.302812
H	7.249730	-1.682929	-0.854409	H	6.418623	-3.233530	-1.136470
H	6.270159	-0.196015	-1.009875	H	5.809720	-1.568050	-1.360115
H	5.946963	-1.602286	-2.074960	H	5.050253	-2.930291	-2.244953
H	-0.554976	-2.671728	0.687498	H	-1.005131	-2.376138	0.449746

**Table S11:** Atomic coordinates (x, y, z) for optimized minimum and transition state of **146h** at the B3LYP-D3(BJ)/6-31+g(d) level of theory.

Minimum				TS			
Atom	x	y	z	Atom	x	y	z
O	5.364132	-1.855775	-0.081888	O	4.654788	-2.848323	-0.202496
C	4.035016	-1.541317	-0.109352	C	3.438648	-2.224673	-0.148223
C	3.238744	-2.156134	0.868316	C	2.624409	-2.560388	0.941851
H	3.712167	-2.822796	1.582671	H	2.993925	-3.276916	1.669180
C	1.876251	-1.895023	0.923464	C	1.373132	-1.971268	1.083970
H	1.283985	-2.356783	1.708439	H	0.760285	-2.225612	1.944876
C	1.259286	-1.017498	0.011684	C	0.897549	-1.027624	0.157374
C	2.074122	-0.405638	-0.949316	C	1.723037	-0.709469	-0.926826
H	1.629399	0.286820	-1.657979	H	1.384054	0.016614	-1.659766
C	3.445180	-0.660262	-1.022986	C	2.979098	-1.297121	-1.090748
H	4.034017	-0.166755	-1.787422	H	3.582621	-1.021837	-1.947892
C	-0.202816	-0.744224	0.034227	C	-0.473652	-0.428860	0.278815

## 7. Appendix

C	-1.063274	-1.749063	0.347443	C	-1.457484	-1.366226	0.349493
C	-2.526713	-1.708000	0.338131	C	-2.908770	-1.344851	0.231716
C	-3.227213	-1.040532	-0.691300	C	-3.690575	-0.232065	-0.128922
C	-4.624889	-1.028606	-0.679283	C	-5.064496	-0.413487	-0.341507
H	-5.157117	-0.509365	-1.473159	H	-5.663977	0.446954	-0.632195
C	-5.339382	-1.687720	0.322379	C	-5.687353	-1.649809	-0.177794
H	-6.425929	-1.673881	0.313689	H	-6.756472	-1.747593	-0.344923
C	-4.651380	-2.381107	1.323454	C	-4.920207	-2.754543	0.198894
H	-5.199474	-2.906923	2.100553	H	-5.379649	-3.730067	0.331595
C	-3.258594	-2.397369	1.321479	C	-3.553003	-2.594929	0.384915
H	-2.720787	-2.934130	2.099680	H	-2.945153	-3.457179	0.648133
C	-2.431988	-0.371990	-1.788830	C	-3.205551	1.197179	-0.227956
H	-3.097211	-0.054620	-2.597896	H	-3.547736	1.701342	0.692378
H	-1.716871	-1.093989	-2.207081	H	-3.784144	1.674177	-1.026903
C	-1.693659	0.818447	-1.224922	C	-1.763361	1.656609	-0.384828
C	-0.658818	0.629464	-0.310686	C	-0.603218	1.040361	0.102019
C	-0.051569	1.781448	0.310118	C	0.550368	1.891765	0.353085
C	-0.458246	3.094525	-0.097852	C	0.608382	3.210409	-0.203872
C	0.143706	4.236182	0.496951	C	1.756494	4.024069	-0.004595
H	-0.173370	5.221365	0.162467	H	1.778130	5.007626	-0.468285
C	1.092437	4.104545	1.485588	C	2.796812	3.598577	0.788788
H	1.542692	4.984427	1.937016	H	3.665169	4.231863	0.948602
C	1.464309	2.812702	1.926353	C	2.704422	2.341809	1.430064
H	2.192560	2.704531	2.725732	H	3.490931	2.021304	2.107958
C	0.908054	1.686907	1.357177	C	1.621491	1.516086	1.214115
H	1.205595	0.712625	1.721679	H	1.580784	0.572811	1.739005
C	-1.481198	3.234842	-1.071595	C	-0.517850	3.703409	-0.904656
H	-1.781835	4.233383	-1.379876	H	-0.475151	4.688325	-1.363088
C	-2.096835	2.126099	-1.596279	C	-1.675408	2.968396	-0.927125
H	-2.899670	2.238206	-2.320779	H	-2.568219	3.397687	-1.375035
C	6.217856	-1.243888	-1.038532	C	5.522226	-2.530343	-1.280738
H	7.218267	-1.627206	-0.832071	H	6.423320	-3.125159	-1.123050
H	6.214320	-0.151187	-0.932750	H	5.782235	-1.463579	-1.281015
H	5.926048	-1.513631	-2.061912	H	5.072188	-2.796825	-2.246140
H	-0.630162	-2.704629	0.639120	H	-1.082272	-2.385431	0.402676

**Table S12:** Atomic coordinates (x, y, z) for optimized minimum and transition state of **146h** at the B3LYP/6-31+g(d) level of theory with scrf=(cpcm,solvent=chloroform).

Minimum				TS			
Atom	x	y	z	Atom	x	y	z
O	5.406508	-1.839472	-0.073949	O	4.676706	-2.878272	-0.195983
C	4.078738	-1.514560	-0.092483	C	3.470796	-2.233441	-0.133321
C	3.291982	-2.079776	0.924342	C	2.682962	-2.507779	0.994803
H	3.767088	-2.720241	1.662207	H	3.059903	-3.196215	1.746137
C	1.930262	-1.807845	0.989677	C	1.440521	-1.898475	1.145703
H	1.350856	-2.238620	1.801899	H	0.851097	-2.116726	2.032935



## 7.3 Atomic coordinates for DFT calculations

C	1.300759	-0.966327	0.049538	C	0.943562	-0.992522	0.189860
C	2.108049	-0.402743	-0.950015	C	1.746093	-0.732405	-0.929475
H	1.660331	0.253802	-1.691303	H	1.394184	-0.044944	-1.694139
C	3.478374	-0.669340	-1.034444	C	2.993548	-1.341308	-1.102613
H	4.056497	-0.216283	-1.831893	H	3.572857	-1.113765	-1.990517
C	-0.171143	-0.710785	0.065315	C	-0.441328	-0.406374	0.300350
C	-1.010266	-1.732733	0.390625	C	-1.406666	-1.365896	0.389705
C	-2.477207	-1.744006	0.362323	C	-2.860414	-1.390694	0.256861
C	-3.189725	-1.116948	-0.686966	C	-3.672295	-0.305367	-0.127829
C	-4.588951	-1.170552	-0.698449	C	-5.038655	-0.531741	-0.356636
H	-5.132304	-0.686727	-1.507353	H	-5.661595	0.305236	-0.666138
C	-5.290773	-1.852010	0.299421	C	-5.625437	-1.786226	-0.183633
H	-6.376775	-1.888677	0.271013	H	-6.689129	-1.918964	-0.362804
C	-4.589145	-2.502922	1.321142	C	-4.829627	-2.862786	0.218831
H	-5.126098	-3.046141	2.094490	H	-5.261168	-3.850159	0.359735
C	-3.195710	-2.456434	1.342456	C	-3.468593	-2.659495	0.419944
H	-2.649125	-2.964778	2.133923	H	-2.840363	-3.501141	0.702630
C	-2.406653	-0.428875	-1.786050	C	-3.224289	1.137931	-0.231195
H	-3.077715	-0.136939	-2.599705	H	-3.569574	1.633697	0.692797
H	-1.671955	-1.134106	-2.200399	H	-3.823239	1.601605	-1.022398
C	-1.700013	0.790687	-1.234221	C	-1.791907	1.634165	-0.403227
C	-0.663931	0.648503	-0.308617	C	-0.609394	1.060191	0.091196
C	-0.103494	1.834414	0.301419	C	0.515313	1.958084	0.332161
C	-0.547913	3.128633	-0.134470	C	0.525041	3.275228	-0.237847
C	0.002956	4.301542	0.453953	C	1.635900	4.140941	-0.033140
H	-0.340706	5.270115	0.097254	H	1.621171	5.120140	-0.506769
C	0.934813	4.219688	1.465617	C	2.684174	3.770477	0.779445
H	1.343752	5.122135	1.912355	H	3.520988	4.443834	0.945282
C	1.342807	2.947754	1.934925	C	2.639407	2.514993	1.430514
H	2.056179	2.878033	2.752251	H	3.430211	2.237107	2.122787
C	0.839209	1.793034	1.370085	C	1.596256	1.638022	1.206703
H	1.163629	0.835870	1.759260	H	1.592307	0.698600	1.741924
C	-1.559808	3.219602	-1.127681	C	-0.614421	3.717022	-0.954333
H	-1.886777	4.201778	-1.461474	H	-0.606749	4.696365	-1.426892
C	-2.135210	2.081359	-1.637295	C	-1.745303	2.939796	-0.970169
H	-2.931126	2.157162	-2.374407	H	-2.650207	3.332193	-1.427817
C	6.258744	-1.283168	-1.075407	C	5.521505	-2.633973	-1.319841
H	7.255832	-1.671395	-0.863377	H	6.413726	-3.240025	-1.156350
H	6.271600	-0.187951	-1.019573	H	5.803260	-1.575672	-1.380912
H	5.948086	-1.598517	-2.078821	H	5.036363	-2.941001	-2.254445
H	-0.553838	-2.669895	0.706805	H	-1.008167	-2.374210	0.475919

## 7. Appendix

**Table S13:** Atomic coordinates (x, y, z) for optimized minimum and transition state of **146h** at the B3LYP-D3(BJ)/6-31+g(d) level of theory with scrf=(cpcm,solvent=chloroform).

Minimum				TS			
Atom	x	y	z	Atom	x	y	z
O	5.369210	-1.847712	-0.080883	O	4.653478	-2.851342	-0.208950
C	4.039311	-1.536483	-0.106725	C	3.437896	-2.226752	-0.148844
C	3.244195	-2.148989	0.874532	C	2.628291	-2.557620	0.947157
H	3.715676	-2.812783	1.593190	H	2.997433	-3.271447	1.677705
C	1.880397	-1.890525	0.930623	C	1.377334	-1.967247	1.094310
H	1.291112	-2.351957	1.717762	H	0.770294	-2.220275	1.959446
C	1.261848	-1.017279	0.015547	C	0.897841	-1.026716	0.166514
C	2.075007	-0.408558	-0.950040	C	1.718530	-0.713378	-0.923810
H	1.629267	0.277503	-1.664383	H	1.376962	0.008865	-1.659524
C	3.447026	-0.660319	-1.024646	C	2.974050	-1.302107	-1.093230
H	4.033697	-0.170941	-1.793030	H	3.572278	-1.031632	-1.955397
C	-0.201044	-0.746490	0.037097	C	-0.473706	-0.427354	0.289315
C	-1.060923	-1.750794	0.354538	C	-1.458262	-1.364387	0.365667
C	-2.524711	-1.708756	0.340485	C	-2.909686	-1.342962	0.239995
C	-3.222715	-1.044616	-0.694014	C	-3.689252	-0.230377	-0.129431
C	-4.621334	-1.031454	-0.685002	C	-5.061859	-0.413118	-0.353649
H	-5.151342	-0.515349	-1.482094	H	-5.659492	0.445854	-0.651090
C	-5.338497	-1.686537	0.318666	C	-5.685199	-1.650378	-0.191185
H	-6.424939	-1.672183	0.307510	H	-6.752811	-1.749111	-0.366568
C	-4.652711	-2.377247	1.324460	C	-4.920567	-2.754397	0.195721
H	-5.202781	-2.900354	2.101890	H	-5.380802	-3.729499	0.327988
C	-3.259054	-2.394779	1.325682	C	-3.553998	-2.594032	0.392272
H	-2.723419	-2.930879	2.105635	H	-2.948638	-3.455710	0.662666
C	-2.426532	-0.379897	-1.793715	C	-3.204785	1.199342	-0.223096
H	-3.090256	-0.065605	-2.604271	H	-3.540146	1.697872	0.702414
H	-1.709194	-1.101924	-2.207767	H	-3.787990	1.682485	-1.013893
C	-1.690918	0.812404	-1.230152	C	-1.762672	1.656285	-0.385306
C	-0.658732	0.625801	-0.312039	C	-0.602841	1.041089	0.104738
C	-0.055961	1.779520	0.310411	C	0.550725	1.892833	0.354202
C	-0.461575	3.092062	-0.102027	C	0.610997	3.208842	-0.209511
C	0.136710	4.235867	0.494417	C	1.759503	4.023474	-0.010554
H	-0.177956	5.220252	0.155986	H	1.783959	5.004124	-0.479765
C	1.079598	4.106147	1.490081	C	2.797091	3.601445	0.789756
H	1.527001	4.986768	1.942538	H	3.665297	4.234760	0.949352
C	1.448912	2.814581	1.936639	C	2.701269	2.347861	1.438810
H	2.170951	2.708785	2.741842	H	3.484353	2.032431	2.123023
C	0.896777	1.687039	1.364878	C	1.618189	1.521089	1.222392
H	1.191526	0.713352	1.734019	H	1.573619	0.581179	1.753561
C	-1.480540	3.230529	-1.081494	C	-0.513501	3.699241	-0.916618
H	-1.779868	4.227954	-1.393890	H	-0.469288	4.681139	-1.380818
C	-2.094010	2.119637	-1.606145	C	-1.672527	2.965118	-0.936210
H	-2.893758	2.229593	-2.334052	H	-2.564088	3.393100	-1.387112
C	6.223293	-1.235274	-1.046068	C	5.517611	-2.536190	-1.298915

## 7.3 Atomic coordinates for DFT calculations

H	7.223993	-1.616410	-0.839991	H	6.418554	-3.131081	-1.144737
H	6.215814	-0.143714	-0.941781	H	5.776040	-1.470350	-1.301611
H	5.927141	-1.510618	-2.065334	H	5.058363	-2.806159	-2.257538
H	-0.629233	-2.703333	0.657337	H	-1.084559	-2.383436	0.430557

**Table S14:** Atomic coordinates (x, y, z) for optimized minimum and transition state of **146h** at the B3LYP/def2-TZVP level of theory.

Minimum				TS			
Atom	x	y	z	Atom	x	y	z
O	5.386556	-1.829256	-0.073839	O	4.658034	-2.866141	-0.190466
C	4.064639	-1.505332	-0.091755	C	3.457434	-2.224087	-0.129148
C	3.279755	-2.071383	0.916379	C	2.671043	-2.496095	0.991770
H	3.755870	-2.712501	1.646833	H	3.048599	-3.182680	1.738382
C	1.925997	-1.801617	0.980201	C	1.435548	-1.890361	1.139419
H	1.346180	-2.233387	1.786111	H	0.845093	-2.106840	2.021396
C	1.299152	-0.959710	0.049058	C	0.941945	-0.988255	0.188479
C	2.103610	-0.393790	-0.940442	C	1.741939	-0.729063	-0.922909
H	1.657908	0.266776	-1.673073	H	1.392434	-0.042518	-1.683337
C	3.466447	-0.659759	-1.023837	C	2.982364	-1.335705	-1.092390
H	4.044201	-0.203757	-1.814548	H	3.561533	-1.109300	-1.975773
C	-0.168197	-0.706917	0.064074	C	-0.438812	-0.404404	0.297661
C	-1.001363	-1.722923	0.387781	C	-1.397681	-1.358625	0.386963
C	-2.462653	-1.740090	0.360424	C	-2.845331	-1.388258	0.254192
C	-3.174585	-1.118973	-0.682680	C	-3.657764	-0.309639	-0.120855
C	-4.565778	-1.177539	-0.693377	C	-5.015701	-0.538858	-0.350330
H	-5.109660	-0.698148	-1.499111	H	-5.638888	0.294485	-0.655341
C	-5.261079	-1.856348	0.299335	C	-5.594751	-1.789120	-0.186965
H	-6.342730	-1.896543	0.271962	H	-6.653570	-1.924647	-0.367351
C	-4.561070	-2.499565	1.315517	C	-4.799802	-2.858594	0.207401
H	-5.094332	-3.041075	2.086661	H	-5.226498	-3.844424	0.341155
C	-3.176042	-2.449291	1.335804	C	-3.447647	-2.652722	0.409180
H	-2.630077	-2.952156	2.125543	H	-2.817719	-3.489722	0.685733
C	-2.397123	-0.429823	-1.777433	C	-3.212910	1.128913	-0.218666
H	-3.068160	-0.138242	-2.585686	H	-3.557033	1.618419	0.704716
H	-1.664807	-1.131382	-2.190757	H	-3.811146	1.592564	-1.005266
C	-1.693498	0.786228	-1.228240	C	-1.787686	1.629121	-0.390905
C	-0.661743	0.647231	-0.308693	C	-0.607911	1.057421	0.091522
C	-0.106488	1.829869	0.297535	C	0.512387	1.953571	0.325307
C	-0.554457	3.116580	-0.134427	C	0.515234	3.266425	-0.237692
C	-0.010944	4.284862	0.453279	C	1.619884	4.129733	-0.037442
H	-0.358369	5.248739	0.099933	H	1.599580	5.106608	-0.506261
C	0.916281	4.205827	1.457542	C	2.666968	3.761811	0.762905
H	1.319830	5.105805	1.904132	H	3.499707	4.434253	0.925688
C	1.328743	2.941740	1.921742	C	2.629697	2.510801	1.406726
H	2.040948	2.874833	2.734766	H	3.422521	2.233860	2.090315
C	0.833731	1.792325	1.359472	C	1.595209	1.635995	1.187165

## 7. Appendix

H	1.162629	0.839802	1.744363	H	1.598850	0.697654	1.715431
C	-1.562276	3.202694	-1.122118	C	-0.624764	3.704923	-0.941313
H	-1.892001	4.180419	-1.453073	H	-0.621880	4.682125	-1.409020
C	-2.130041	2.069597	-1.628888	C	-1.747251	2.930467	-0.950653
H	-2.923885	2.142626	-2.362595	H	-2.653222	3.318772	-1.400363
C	6.234746	-1.273862	-1.064967	C	5.499717	-2.623064	-1.304346
H	7.230106	-1.660315	-0.858148	H	6.390958	-3.225645	-1.144032
H	6.252473	-0.181309	-1.010204	H	5.783724	-1.568350	-1.369783
H	5.930104	-1.580215	-2.070141	H	5.022927	-2.926589	-2.241324
H	-0.543247	-2.656093	0.700021	H	-0.998381	-2.362887	0.468311

**Table S15:** Atomic coordinates (x, y, z) for optimized minimum and transition state of **146h** at the B3LYP/def2-TZVP level of theory using the "tight" option and the superfine grid.

Minimum				TS			
Atom	x	y	z	Atom	x	y	z
O	5.385766	-1.830223	-0.073294	O	4.657667	-2.866448	-0.190974
C	4.063856	-1.506287	-0.091553	C	3.457127	-2.224302	-0.129428
C	3.27891	-2.071636	0.916917	C	2.671196	-2.495825	0.991922
H	3.754967	-2.712271	1.647823	H	3.049035	-3.182106	1.738667
C	1.925162	-1.801706	0.980509	C	1.435819	-1.889915	1.139868
H	1.345246	-2.232804	1.786706	H	0.845732	-2.105955	2.022195
C	1.298462	-0.960316	0.048823	C	0.941898	-0.988142	0.188783
C	2.10296	-0.395237	-0.941137	C	1.741465	-0.729371	-0.923020
H	1.657285	0.264751	-1.674292	H	1.391777	-0.042931	-1.683466
C	3.465762	-0.661408	-1.024337	C	2.981765	-1.336204	-1.092792
H	4.043604	-0.206155	-1.815420	H	3.560652	-1.110194	-1.976463
C	-0.168770	-0.707049	0.063952	C	-0.438845	-0.404220	0.298060
C	-1.002254	-1.722851	0.387467	C	-1.397710	-1.358396	0.387612
C	-2.463561	-1.739463	0.360294	C	-2.845329	-1.388068	0.254535
C	-3.175426	-1.117567	-0.682407	C	-3.657653	-0.309602	-0.121206
C	-4.566638	-1.175598	-0.692892	C	-5.015462	-0.539010	-0.351277
H	-5.110470	-0.695568	-1.498270	H	-5.638571	0.294167	-0.656897
C	-5.262026	-1.854778	0.299505	C	-5.594509	-1.789255	-0.187739
H	-6.343690	-1.894626	0.272256	H	-6.653225	-1.924918	-0.368617
C	-4.562089	-2.498907	1.315152	C	-4.799695	-2.858527	0.207446
H	-5.095419	-3.040785	2.085990	H	-5.226397	-3.844329	0.341374
C	-3.177050	-2.449035	1.335330	C	-3.447644	-2.652502	0.409736
H	-2.631151	-2.952551	2.124698	H	-2.817782	-3.489377	0.686817
C	-2.397852	-0.428548	-1.777175	C	-3.212855	1.128971	-0.219147
H	-3.068957	-0.136532	-2.585227	H	-3.557444	1.618621	0.703983
H	-1.666057	-1.130492	-2.190775	H	-3.810778	1.592416	-1.006105
C	-1.693424	0.787022	-1.228012	C	-1.787613	1.629286	-0.390855
C	-0.661711	0.647384	-0.308555	C	-0.607921	1.057588	0.091750
C	-0.105650	1.829688	0.297611	C	0.51240	1.953691	0.325621
C	-0.552687	3.116654	-0.134509	C	0.515413	3.266523	-0.237406
C	-0.008222	4.284630	0.452899	C	1.620174	4.129691	-0.037146

## 7.3 Atomic coordinates for DFT calculations

H	-0.354969	5.248703	0.099429	H	1.599980	5.106591	-0.505910
C	0.919104	4.205069	1.457024	C	2.667313	3.761537	0.763036
H	1.323453	5.104813	1.903354	H	3.500198	4.433820	0.925720
C	1.330622	2.940760	1.921427	C	2.629896	2.510520	1.406847
H	2.042853	2.873492	2.734396	H	3.422755	2.233374	2.090305
C	0.834570	1.791611	1.359526	C	1.595139	1.635995	1.187495
H	1.162705	0.838920	1.744639	H	1.598415	0.697790	1.715981
C	-1.560506	3.203389	-1.122140	C	-0.624555	3.705102	-0.941033
H	-1.889539	4.181305	-1.453208	H	-0.621643	4.682330	-1.408683
C	-2.129068	2.070651	-1.628802	C	-1.747066	2.930678	-0.950499
H	-2.922888	2.144159	-2.362485	H	-2.652969	3.319057	-1.400281
C	6.234202	-1.274984	-1.064288	C	5.499175	-2.623358	-1.304990
H	7.229614	-1.660993	-0.856891	H	6.390510	-3.225816	-1.144742
H	6.251515	-0.182394	-1.010013	H	5.783031	-1.568610	-1.370530
H	5.930117	-1.581854	-2.069481	H	5.022307	-2.927018	-2.241884
H	-0.544396	-2.656264	0.699348	H	-0.998454	-2.362639	0.469287

**Table S16:** Atomic coordinates (x, y, z) for optimized minimum and transition state of **146h** at the B3LYP-D3(BJ)/def2-TZVP level of theory.

Minimum				TS			
Atom	x	y	z	Atom	x	y	z
O	5.348847	-1.839136	-0.080812	O	4.634633	-2.838987	-0.203252
C	4.024842	-1.528612	-0.106026	C	3.424134	-2.217677	-0.144647
C	3.231485	-2.141427	0.866545	C	2.616292	-2.545848	0.944547
H	3.703763	-2.805923	1.577652	H	2.986377	-3.257377	1.670568
C	1.875659	-1.884609	0.921094	C	1.372052	-1.959312	1.088321
H	1.285767	-2.346824	1.701658	H	0.764232	-2.210166	1.948401
C	1.259940	-1.010840	0.015144	C	0.895456	-1.023119	0.165101
C	2.070333	-0.400693	-0.940662	C	1.713042	-0.711499	-0.917974
H	1.626639	0.289064	-1.646181	H	1.373364	0.009193	-1.649698
C	3.434862	-0.652291	-1.014179	C	2.961822	-1.297575	-1.083557
H	4.021288	-0.160547	-1.775680	H	3.559702	-1.028492	-1.941325
C	-0.198470	-0.742484	0.035933	C	-0.471812	-0.425704	0.286951
C	-1.052573	-1.740949	0.351433	C	-1.450429	-1.356934	0.363591
C	-2.510981	-1.704704	0.338392	C	-2.895899	-1.339472	0.237875
C	-3.208637	-1.045665	-0.689555	C	-3.675302	-0.233204	-0.122834
C	-4.599517	-1.037284	-0.679455	C	-5.039773	-0.418134	-0.347871
H	-5.130342	-0.524994	-1.472920	H	-5.636975	0.437445	-0.641586
C	-5.310088	-1.690253	0.318922	C	-5.656256	-1.650778	-0.194347
H	-6.392317	-1.679112	0.309048	H	-6.719112	-1.751747	-0.371132
C	-4.625632	-2.374070	1.318677	C	-4.893184	-2.748044	0.185264
H	-5.171956	-2.895857	2.093693	H	-5.349387	-3.721225	0.310727
C	-3.240154	-2.388088	1.318608	C	-3.535275	-2.585833	0.382639
H	-2.704943	-2.919349	2.096417	H	-2.928745	-3.443177	0.647299
C	-2.417918	-0.379594	-1.784876	C	-3.193104	1.191444	-0.212310
H	-3.081668	-0.065252	-2.589778	H	-3.528449	1.685162	0.711413

## 7. Appendix

H	-1.703161	-1.098051	-2.198117	H	-3.774379	1.673619	-0.999969
C	-1.684607	0.808908	-1.223992	C	-1.757604	1.651704	-0.373435
C	-0.656473	0.624993	-0.311990	C	-0.600980	1.038131	0.105188
C	-0.058122	1.775378	0.306602	C	0.548866	1.887544	0.347895
C	-0.466544	3.080936	-0.102193	C	0.603210	3.199551	-0.209122
C	0.125274	4.219971	0.493544	C	1.746246	4.011104	-0.014834
H	-0.192425	5.200015	0.158508	H	1.765977	4.989539	-0.479376
C	1.063418	4.092642	1.482034	C	2.782442	3.590921	0.773206
H	1.505922	4.970691	1.934374	H	3.647075	4.222802	0.929460
C	1.436337	2.808541	1.923784	C	2.693233	2.341716	1.415435
H	2.156920	2.705129	2.724946	H	3.478021	2.026709	2.091020
C	0.892091	1.686286	1.354621	C	1.617995	1.517645	1.203777
H	1.190201	0.716892	1.719825	H	1.580158	0.578772	1.728365
C	-1.481601	3.214948	-1.076282	C	-0.521544	3.687404	-0.903680
H	-1.783149	4.208104	-1.386027	H	-0.481343	4.667242	-1.363069
C	-2.088315	2.109213	-1.597763	C	-1.672631	2.956454	-0.917183
H	-2.886001	2.216816	-2.322284	H	-2.564861	3.380932	-1.360623
C	6.198944	-1.228133	-1.035835	C	5.494745	-2.526921	-1.284332
H	7.197991	-1.606817	-0.834365	H	6.394795	-3.117959	-1.132917
H	6.195692	-0.139063	-0.933141	H	5.755388	-1.464365	-1.293012
H	5.908924	-1.494931	-2.056310	H	5.043164	-2.794288	-2.244336
H	-0.619231	-2.689620	0.650024	H	-1.076507	-2.372107	0.423823

**Table S17:** Atomic coordinates (x, y, z) for optimized minimum and transition state of **146h** at the B3LYP/def2-TZVP level of theory with scrf=(cpcm,solvent=chloroform).

Minimum				TS			
Atom	x	y	z	Atom	x	y	z
O	5.390179	-1.822819	-0.073016	O	4.657143	-2.867422	-0.194684
C	4.068023	-1.501999	-0.089719	C	3.457150	-2.225421	-0.129224
C	3.283843	-2.066242	0.921286	C	2.675062	-2.492247	0.996975
H	3.758088	-2.704957	1.655439	H	3.052911	-3.175314	1.747031
C	1.928893	-1.798595	0.985975	C	1.439595	-1.885781	1.148542
H	1.351415	-2.230673	1.793205	H	0.854669	-2.100418	2.034465
C	1.300965	-0.960108	0.052105	C	0.941883	-0.987791	0.195842
C	2.104037	-0.397101	-0.941336	C	1.737139	-0.733846	-0.921138
H	1.657608	0.257364	-1.679164	H	1.384688	-0.052045	-1.684702
C	3.467830	-0.660669	-1.025538	C	2.977400	-1.340979	-1.094889
H	4.043924	-0.208379	-1.819320	H	3.551679	-1.119328	-1.982555
C	-0.166954	-0.708946	0.066778	C	-0.439161	-0.403308	0.306419
C	-1.000054	-1.724136	0.393985	C	-1.398779	-1.357105	0.400199
C	-2.461718	-1.739827	0.362566	C	-2.846540	-1.386568	0.260965
C	-3.171110	-1.121209	-0.684943	C	-3.656958	-0.307681	-0.120318
C	-4.563236	-1.178769	-0.698460	C	-5.013748	-0.537677	-0.359414
H	-5.104876	-0.701948	-1.507000	H	-5.635164	0.294833	-0.669326
C	-5.261201	-1.854370	0.295910	C	-5.593120	-1.788977	-0.198113
H	-6.342793	-1.894159	0.266196	H	-6.650655	-1.925118	-0.385278

## 7.3 Atomic coordinates for DFT calculations

C	-4.563367	-2.495571	1.316227	C	-4.800337	-2.858416	0.203599
H	-5.098565	-3.034984	2.087485	H	-5.227809	-3.844036	0.336163
C	-3.177417	-2.446442	1.339430	C	-3.448760	-2.652103	0.414248
H	-2.633385	-2.949338	2.130366	H	-2.820855	-3.488935	0.695799
C	-2.392592	-0.435511	-1.781639	C	-3.212532	1.131242	-0.212995
H	-3.062197	-0.146047	-2.590961	H	-3.550069	1.615663	0.715177
H	-1.658748	-1.137269	-2.191553	H	-3.815142	1.600477	-0.991992
C	-1.690696	0.781559	-1.232568	C	-1.787367	1.629021	-0.390128
C	-0.661589	0.644124	-0.309431	C	-0.607712	1.057862	0.094243
C	-0.109917	1.827898	0.298270	C	0.512827	1.954094	0.326275
C	-0.555474	3.114395	-0.138371	C	0.517798	3.264557	-0.242878
C	-0.014626	4.284316	0.450647	C	1.623224	4.128465	-0.044042
H	-0.358818	5.247713	0.093268	H	1.605383	5.102749	-0.518072
C	0.906591	4.206454	1.461759	C	2.668374	3.763413	0.761580
H	1.308027	5.106829	1.909204	H	3.501401	4.435656	0.923223
C	1.315289	2.942283	1.931826	C	2.627956	2.515263	1.412697
H	2.021059	2.877000	2.750537	H	3.417875	2.242689	2.101447
C	0.823335	1.791613	1.367355	C	1.592779	1.639851	1.193889
H	1.147963	0.839458	1.757532	H	1.592598	0.704809	1.728533
C	-1.559095	3.199565	-1.131677	C	-0.621001	3.701261	-0.951186
H	-1.886294	4.176483	-1.467035	H	-0.616528	4.675805	-1.424075
C	-2.125916	2.064814	-1.637954	C	-1.745009	2.927834	-0.957332
H	-2.916431	2.136250	-2.375164	H	-2.650096	3.315152	-1.409151
C	6.239065	-1.266442	-1.070964	C	5.495514	-2.628432	-1.319150
H	7.234814	-1.650421	-0.864057	H	6.386826	-3.230523	-1.160923
H	6.252650	-0.174861	-1.017317	H	5.777323	-1.574528	-1.388177
H	5.931587	-1.577244	-2.072703	H	5.010839	-2.936194	-2.249346
H	-0.543899	-2.654763	0.716056	H	-1.001090	-2.361191	0.491230

**Table S18:** Atomic coordinates (x, y, z) for optimized minimum and transition state of **146h** at the B3LYP-D3(BJ)/def2-TZVP level of theory with scrf=(cpcm,solvent=chloroform).

Minimum				TS			
Atom	x	y	z	Atom	x	y	z
O	5.352849	-1.832036	-0.079700	O	4.633392	-2.841117	-0.208432
C	4.028729	-1.524656	-0.103898	C	3.423675	-2.219511	-0.145113
C	3.235935	-2.135922	0.871381	C	2.619851	-2.543101	0.949448
H	3.706391	-2.798122	1.586193	H	2.989851	-3.251846	1.678612
C	1.878944	-1.881456	0.926621	C	1.375816	-1.955554	1.097571
H	1.291502	-2.344065	1.708632	H	0.773216	-2.205156	1.961502
C	1.262015	-1.011054	0.017993	C	0.895592	-1.022545	0.172982
C	2.071183	-0.403284	-0.941487	C	1.708816	-0.715491	-0.915662
H	1.626803	0.280996	-1.652052	H	1.366577	0.001318	-1.650230
C	3.436574	-0.652313	-1.015692	C	2.957173	-1.302456	-1.086050
H	4.021342	-0.163809	-1.780332	H	3.550410	-1.037841	-1.948323
C	-0.196979	-0.744710	0.038106	C	-0.471955	-0.424493	0.296097
C	-1.050859	-1.742351	0.357591	C	-1.451256	-1.355380	0.377615

## 7. Appendix

C	-2.509565	-1.704743	0.340538	C	-2.896832	-1.337818	0.244991
C	-3.204974	-1.048599	-0.691843	C	-3.674222	-0.231496	-0.122692
C	-4.596718	-1.039174	-0.684470	C	-5.037449	-0.417409	-0.358068
H	-5.125435	-0.529580	-1.480863	H	-5.632899	0.437170	-0.657241
C	-5.309711	-1.688660	0.315631	C	-5.654264	-1.651061	-0.206482
H	-6.391910	-1.677096	0.303521	H	-6.715785	-1.752789	-0.390578
C	-4.627194	-2.370153	1.319613	C	-4.893409	-2.748028	0.181389
H	-5.175297	-2.889636	2.094919	H	-5.350313	-3.720970	0.305927
C	-3.240912	-2.385189	1.322411	C	-3.536136	-2.585210	0.388245
H	-2.707507	-2.916061	2.101622	H	-2.931706	-3.442219	0.658650
C	-2.413467	-0.385996	-1.789202	C	-3.192580	1.193556	-0.206620
H	-3.075972	-0.074100	-2.595291	H	-3.521135	1.681522	0.722273
H	-1.696978	-1.104603	-2.198813	H	-3.778430	1.681773	-0.986220
C	-1.682162	0.803865	-1.228556	C	-1.757247	1.651498	-0.372966
C	-0.656344	0.621689	-0.313310	C	-0.600714	1.038669	0.107785
C	-0.061782	1.773351	0.306971	C	0.549199	1.888305	0.348808
C	-0.468858	3.078534	-0.105644	C	0.605431	3.197911	-0.214170
C	0.119961	4.219312	0.491630	C	1.748947	4.010277	-0.020702
H	-0.195411	5.198758	0.153050	H	1.770909	4.986108	-0.490344
C	1.052891	4.093378	1.486354	C	2.783168	3.593092	0.772973
H	1.493146	4.971938	1.939695	H	3.647915	4.224877	0.928511
C	1.423238	2.809305	1.933065	C	2.691065	2.346683	1.422157
H	2.138315	2.707760	2.739356	H	3.473122	2.036152	2.103040
C	0.882397	1.685718	1.361435	C	1.615441	1.521827	1.210583
H	1.177634	0.716700	1.730722	H	1.574121	0.586041	1.740959
C	-1.480334	3.211387	-1.084803	C	-0.518077	3.683747	-0.913744
H	-1.780246	4.203776	-1.398142	H	-0.476434	4.660924	-1.378334
C	-2.085512	2.103948	-1.606296	C	-1.670525	2.953684	-0.924289
H	-2.880457	2.209769	-2.333868	H	-2.561917	3.377009	-1.369955
C	6.203659	-1.220101	-1.041979	C	5.490858	-2.531258	-1.299694
H	7.202831	-1.597110	-0.840726	H	6.390935	-3.121989	-1.150964
H	6.196865	-0.132092	-0.940053	H	5.749499	-1.469384	-1.310443
H	5.909864	-1.491387	-2.058975	H	5.031550	-2.801951	-2.253789
H	-0.619223	-2.688501	0.666044	H	-1.078812	-2.370443	0.448074

**Table S19:** Atomic coordinates (x, y, z) for optimized minimum and transition state of **146i** at the B3LYP-D3(BJ)/6-31+g(d) level of theory.

Minimum				TS			
Atom	x	y	z	Atom	x	y	z
O	5.628205	-0.610879	0.440938	O	5.387473	-1.352489	0.450505
C	4.268925	-0.605069	0.301779	C	4.057068	-1.094602	0.264474
C	3.560336	-1.399096	-0.606392	C	3.361582	-1.331734	-0.924895
H	4.073232	-2.075943	-1.279915	H	3.858741	-1.747158	-1.793883
C	2.165711	-1.307540	-0.660926	C	1.995952	-1.026735	-0.997457
H	1.628775	-1.910489	-1.387938	H	1.460387	-1.209795	-1.925316
C	1.450156	-0.441282	0.173633	C	1.306842	-0.487945	0.090330



## 7.3 Atomic coordinates for DFT calculations

C	2.187619	0.360186	1.067313	C	2.025955	-0.256329	1.276524
H	1.659883	1.050409	1.719156	H	1.510142	0.162373	2.136665
C	3.570977	0.278629	1.139312	C	3.379063	-0.555506	1.368924
H	4.134800	0.888864	1.838278	H	3.932275	-0.384625	2.287475
C	-0.036305	-0.369106	0.143402	C	-0.167219	-0.210249	0.011566
C	-2.191785	-1.710379	-0.057049	C	-2.375125	-1.572747	-0.008244
C	-2.682295	-2.777072	-0.834691	C	-2.749118	-2.937939	0.008206
H	-1.972645	-3.437890	-1.327497	H	-1.959222	-3.684954	0.013007
C	-4.049467	-2.981206	-1.000144	C	-4.074898	-3.349376	0.022225
H	-4.405427	-3.802765	-1.615939	H	-4.319551	-4.407851	0.033792
C	-4.959525	-2.125835	-0.370494	C	-5.082915	-2.382237	0.026226
H	-6.028768	-2.278724	-0.489686	H	-6.130246	-2.671226	0.041471
C	-4.487429	-1.086242	0.431827	C	-4.729976	-1.035275	0.011361
H	-5.191732	-0.435928	0.945830	H	-5.516612	-0.282828	0.012764
C	-3.116543	-0.876109	0.609048	C	-3.394528	-0.602757	-0.009842
C	-2.595678	0.203505	1.525874	C	-3.232241	0.904231	-0.058525
H	-1.903533	-0.248514	2.251220	H	-3.846616	1.306615	0.758742
H	-3.421798	0.647642	2.090459	H	-3.749389	1.234100	-0.971902
C	-1.873637	1.271695	0.742789	C	-1.919664	1.678749	-0.025685
C	-2.410724	2.559118	0.624491	C	-2.128750	3.068533	-0.031046
C	-1.752581	3.556160	-0.089564	C	-1.095109	3.995302	-0.070285
C	-0.526024	3.290054	-0.716864	C	0.230590	3.550900	-0.118544
C	0.007851	2.007741	-0.596586	C	0.447455	2.176699	-0.100156
C	-0.645665	0.981011	0.114126	C	-0.586969	1.209381	-0.035485
C	6.382830	-1.492801	-0.377735	C	6.120506	-1.902709	-0.633938
H	6.253345	-1.256523	-1.442095	H	6.118925	-1.226906	-1.499376
H	6.102751	-2.539109	-0.198428	H	5.716988	-2.879277	-0.932442
H	7.425806	-1.341126	-0.095577	H	7.141895	-2.026423	-0.270564
C	-0.745220	-1.528121	0.061897	C	-0.936937	-1.325923	0.008438
H	-0.166123	-2.449218	0.015591	H	-0.367905	-2.252024	0.057445
H	-2.188940	4.550635	-0.156239	H	-1.320123	5.059725	-0.072501
H	0.955128	1.784708	-1.078844	H	1.471918	1.829022	-0.140776
H	-3.356926	2.781305	1.112880	H	-3.154772	3.431821	-0.012778
C	0.188036	4.361941	-1.505944	C	1.382256	4.524487	-0.190376
H	-0.383196	4.645555	-2.399335	H	1.374414	5.214784	0.662558
H	0.327351	5.271347	-0.908485	H	2.344352	4.002257	-0.190174
H	1.175006	4.021700	-1.835539	H	1.331709	5.134955	-1.101022

**Table S20:** Atomic coordinates (x, y, z) for optimized minimum and transition state of **146j** at the B3LYP-D3(BJ)/6-31+g(d) level of theory.

Minimum				TS			
Atom	x	y	z	Atom	x	y	z
O	-5.850769	0.042866	-0.447822	O	5.769567	-0.419398	0.435768
C	-4.500396	-0.095147	-0.291878	C	4.415069	-0.365774	0.252001
C	-3.887895	-1.083008	0.486950	C	3.766352	-0.648549	-0.953831
H	-4.475457	-1.808801	1.037242	H	4.323345	-0.935535	-1.838281

## 7. Appendix

C	-2.492677	-1.126727	0.573512	C	2.369686	-0.560667	-1.022355
H	-2.030147	-1.882639	1.202033	H	1.870094	-0.779363	-1.962520
C	-1.682582	-0.207008	-0.102471	C	1.604116	-0.194634	0.085707
C	-2.323536	0.788879	-0.865414	C	2.276259	0.086317	1.288124
H	-1.720662	1.524221	-1.390459	H	1.699932	0.373790	2.163621
C	-3.706305	0.844001	-0.967701	C	3.659954	0.001289	1.376627
H	-4.196067	1.605780	-1.566552	H	4.178798	0.210775	2.307146
C	-0.196839	-0.273709	-0.044563	C	0.102813	-0.152986	0.009520
C	1.831470	-1.808660	-0.042211	C	-1.845703	-1.856799	-0.000937
C	2.232602	-3.014506	0.564122	C	-2.003036	-3.262530	0.034576
H	1.471666	-3.680813	0.964241	H	-1.106945	-3.878032	0.049549
C	3.578674	-3.351187	0.678061	C	-3.250206	-3.872167	0.054778
H	3.867052	-4.280115	1.162600	H	-3.330206	-4.955326	0.081236
C	4.555378	-2.491703	0.163864	C	-4.394327	-3.070622	0.045427
H	5.608175	-2.749588	0.241226	H	-5.385046	-3.516421	0.064982
C	4.170185	-1.310547	-0.471508	C	-4.252346	-1.685579	0.011834
H	4.924953	-0.655527	-0.900795	H	-5.145481	-1.063239	0.002761
C	2.820873	-0.963522	-0.591578	C	-2.998710	-1.054050	-0.016253
C	2.381425	0.279667	-1.324147	C	-3.076088	0.459979	-0.088703
H	1.616420	0.003366	-2.063314	H	-3.769588	0.753518	0.709699
H	3.222721	0.708784	-1.871123	H	-3.634161	0.680523	-1.011333
C	1.788853	1.278333	-0.355900	C	-1.925743	1.456082	-0.048944
C	2.477375	2.457597	-0.003340	C	-2.366444	2.805885	-0.066735
C	1.877577	3.356583	0.883720	C	-1.446931	3.859038	-0.096082
C	0.616949	3.099292	1.427060	C	-0.082005	3.601818	-0.119703
H	0.164870	3.807037	2.116743	H	0.636903	4.415607	-0.158604
C	-0.053508	1.930501	1.090156	C	0.356953	2.286697	-0.093528
C	0.525486	0.996620	0.209016	C	-0.531642	1.187446	-0.041582
C	-6.700836	-0.884199	0.212036	C	6.580870	-0.786442	-0.670143
H	-6.579071	-0.829769	1.301828	H	6.471060	-0.074030	-1.498464
H	-6.508828	-1.910668	-0.126886	H	6.338708	-1.797450	-1.023529
H	-7.718787	-0.596506	-0.055224	H	7.608989	-0.764842	-0.305311
C	0.407080	-1.490614	-0.129232	C	-0.468789	-1.381083	0.010810
H	-0.248556	-2.354977	-0.223447	H	0.245613	-2.200265	0.059960
H	2.404147	4.270282	1.149398	H	-1.812670	4.882741	-0.110471
H	-1.026085	1.718711	1.522241	H	1.421439	2.097719	-0.117027
C	3.847131	2.769575	-0.563654	C	-3.837075	3.165146	-0.067112
H	4.569045	1.977103	-0.332244	H	-4.369190	2.744548	-0.929795
H	3.830240	2.885823	-1.654772	H	-4.354788	2.802239	0.830246
H	4.231629	3.702286	-0.139554	H	-3.961500	4.251339	-0.100976

## 7.3 Atomic coordinates for DFT calculations

**Table S21:** Atomic coordinates (x, y, z) for optimized minimum and transition state of **146k** at the B3LYP/6-31+g(d) level of theory.

Minimum				TS			
Atom	x	y	z	Atom	x	y	z
O	5.806680	-1.350527	-1.324290	O	5.385317	-1.386841	-1.655019
C	4.645132	-0.737485	-0.944379	C	4.287118	-0.798215	-1.088965
C	4.565093	0.329169	-0.040384	C	4.324634	0.078123	0.001359
H	5.454029	0.733655	0.431118	H	5.262084	0.344978	0.476971
C	3.317887	0.878269	0.273996	C	3.131790	0.621746	0.494051
H	3.280083	1.695317	0.990134	H	3.183958	1.305005	1.338558
C	2.128340	0.390219	-0.285656	C	1.885368	0.303896	-0.059392
C	2.236406	-0.691063	-1.184604	C	1.875953	-0.580141	-1.157677
H	1.336534	-1.099647	-1.635594	H	0.930908	-0.838577	-1.626194
C	3.467595	-1.243082	-1.515610	C	3.050270	-1.118555	-1.669121
H	3.540293	-2.069895	-2.216252	H	3.032123	-1.790268	-2.522599
C	0.798349	1.020914	-0.031307	C	0.609860	0.993651	0.355909
C	-0.508416	3.184541	0.042766	C	0.689487	2.351357	0.238274
C	-0.609880	4.334622	0.844771	C	-0.275949	3.443145	0.150684
H	0.218343	4.599618	1.498920	H	0.267897	4.742135	0.013258
C	-1.758959	5.124852	0.823264	C	1.347920	4.858699	0.072228
H	-1.826241	6.003341	1.460129	H	-0.527669	5.860710	-0.208218
C	-2.819635	4.784752	-0.022391	C	-0.073237	6.843643	-0.301932
H	-3.716783	5.398174	-0.049626	H	-1.910296	5.700499	-0.329472
C	-2.716736	3.661663	-0.847171	C	-2.553274	6.555923	-0.520013
H	-3.532805	3.410309	-1.521842	H	-2.461573	4.424561	-0.205541
C	-1.570019	2.860352	-0.832709	C	-3.539192	4.301735	-0.297009
C	-1.414546	1.663091	-1.749845	C	-1.674583	3.292713	0.051084
H	-0.473826	1.761387	-2.310323	H	-2.411969	1.998342	0.315545
H	-2.228863	1.646908	-2.481799	H	-3.386426	2.068742	-0.180022
C	-1.422983	0.371869	-0.953207	C	-2.649168	1.993337	1.393643
C	-2.472027	-0.526639	-1.139114	C	-1.869888	0.600288	0.036805
H	-3.216307	-0.295946	-1.897419	H	-2.804878	-0.315229	-0.440797
C	-2.571318	-1.700480	-0.386116	C	-3.740743	0.072052	-0.836304
C	-1.633617	-1.865403	0.636920	C	-2.593704	-1.703073	-0.389357
H	-1.736893	-2.726832	1.279822	H	-1.496700	-2.119779	0.364179
C	-0.578050	-0.971731	0.903096	C	-1.382407	-3.175308	0.574558
C	-0.407804	0.126389	0.009329	C	-0.531686	-1.238546	0.890567
C	0.244995	-1.237381	2.204362	C	-0.599387	0.133694	0.495888
C	1.422281	-2.207539	1.940640	C	0.393669	-1.816366	2.012582
H	1.062104	-3.146539	1.502714	H	1.531524	-2.719335	1.482907
H	1.925027	-2.448952	2.886655	H	1.139687	-3.492502	0.810978
H	2.164748	-1.782279	1.262909	H	2.021580	-3.226305	2.324512
C	0.771605	0.063565	2.853319	C	2.291785	-2.156001	0.940518
H	1.539778	0.557222	2.261137	H	0.967329	-0.717001	2.934934
H	1.216431	-0.174719	3.827404	H	1.672419	-0.056320	2.435668
H	-0.041948	0.779328	3.020339	H	1.500121	-1.190083	3.769224
C	-0.654020	-1.895667	3.288797	C	0.163671	-0.101829	3.357009

## 7. Appendix

H	-1.576274	-1.325638	3.450833	H	-0.490476	-2.695185	2.948183
H	-0.104334	-1.925621	4.236723	H	-1.376328	-2.148881	3.291805
H	-0.926202	-2.929498	3.053479	H	0.095939	-2.980374	3.830030
C	-3.697757	-2.712580	-0.666606	C	-0.825893	-3.622452	2.474344
C	-3.590011	-3.204923	-2.130717	C	-3.593900	-2.672253	-1.041335
H	-3.674410	-2.379186	-2.845555	H	-3.696546	-2.352417	-2.552925
H	-4.390786	-3.922220	-2.351986	H	-4.029253	-1.323777	-2.729348
H	-2.628954	-3.702761	-2.307126	H	-4.415476	-3.025674	-3.037254
C	-3.631572	-3.945498	0.256062	C	-2.725932	-2.478534	-3.047325
H	-2.683938	-4.486651	0.148321	H	-3.167053	-4.145783	-0.892221
H	-4.439651	-4.640454	-0.001745	H	-2.177402	-4.328966	-1.327361
H	-3.755414	-3.676251	1.311693	H	-3.883857	-4.791293	-1.413614
C	-5.072323	-2.030764	-0.458761	C	-3.144829	-4.463695	0.156949
H	-5.180084	-1.672408	0.571890	H	-4.989778	-2.507103	-0.391206
H	-5.884575	-2.741182	-0.659657	H	-4.949843	-2.723421	0.683056
H	-5.207545	-1.172872	-1.126395	H	-5.708219	-3.197571	-0.851493
C	7.032702	-0.879151	-0.781537	C	-5.380330	-1.491008	-0.514048
H	7.054299	-0.988427	0.310886	H	6.665870	-1.090947	-1.115622
H	7.210052	0.171076	-1.048586	H	6.740609	-1.406517	-0.066364
H	7.811763	-1.502609	-1.223695	H	6.894296	-0.019532	-1.192677
C	0.717540	2.374948	0.021794	C	7.379333	-1.657989	-1.716258
H	1.649378	2.939495	-0.007203	H	1.694451	2.707888	0.023756

**Table S22:** Atomic coordinates (x, y, z) for optimized minimum and transition state of **146k** at the B3LYP/6-31+g(d) level of theory using the "tight" option and the superfine grid.

Minimum				TS			
Atom	x	y	z	Atom	x	y	z
O	5.806449	-1.351480	-1.323786	O	5.386071	-1.385413	-1.654834
C	4.645065	-0.738227	-0.943713	C	4.287624	-0.797240	-1.088802
C	4.565553	0.330127	-0.041688	C	4.324722	0.079233	0.001424
H	5.454809	0.735816	0.428169	H	5.262052	0.346574	0.476984
C	3.318490	0.879528	0.272723	C	3.131628	0.622368	0.494034
H	3.281157	1.697983	0.987270	H	3.183451	1.305833	1.338391
C	2.128559	0.390156	-0.285003	C	1.885350	0.303969	-0.059418
C	2.236093	-0.693037	-1.181691	C	1.876340	-0.580332	-1.157497
H	1.335907	-1.102842	-1.630905	H	0.931445	-0.839491	-1.625914
C	3.467122	-1.245413	-1.512684	C	3.050905	-1.118290	-1.668845
H	3.539387	-2.073694	-2.211631	H	3.033034	-1.790240	-2.522138
C	0.798651	1.021301	-0.031093	C	0.609632	0.993421	0.355775
C	-0.508539	3.184608	0.041585	C	0.688981	2.351148	0.237852
C	-0.610754	4.334636	0.843513	C	-0.276631	3.442793	0.150365
H	0.217221	4.600105	1.497787	H	0.266993	4.741769	0.011964
C	-1.760317	5.124168	0.821867	C	1.347050	4.858458	0.070004
H	-1.828172	6.002642	1.458686	H	-0.528873	5.860187	-0.209241
C	-2.820754	4.783331	-0.023775	C	-0.074607	6.843123	-0.303704
H	-3.718322	5.396137	-0.050988	H	-1.911601	5.699824	-0.329154

## 7.3 Atomic coordinates for DFT calculations

C	-2.717122	3.660282	-0.848541	C	-2.554816	6.555141	-0.519364
H	-3.533032	3.408361	-1.523183	H	-2.462675	4.423886	-0.204251
C	-1.569835	2.859812	-0.834095	C	-3.540369	4.300937	-0.294623
C	-1.413571	1.662436	-1.750962	C	-1.675340	3.292217	0.052024
H	-0.472656	1.760901	-2.311053	H	-2.412138	1.997782	0.317650
H	-2.227611	1.645760	-2.483210	H	-3.387373	2.068006	-0.176390
C	-1.421990	0.371467	-0.953881	C	-2.647587	1.992607	1.396132
C	-2.470446	-0.527604	-1.140301	C	-1.870156	0.599913	0.037803
H	-3.214050	-0.297585	-1.899452	H	-2.805273	-0.315488	-0.439696
C	-2.570090	-1.700982	-0.386557	C	-3.741363	0.071876	-0.834586
C	-1.633270	-1.864896	0.637419	C	-2.593867	-1.703344	-0.389009
H	-1.736736	-2.725981	1.280793	H	-1.496504	-2.120236	0.363962
C	-0.578337	-0.970557	0.904056	C	-1.381984	-3.175846	0.573862
C	-0.407540	0.126897	0.009701	C	-0.531427	-1.239064	0.890364
C	0.243379	-1.235251	2.206282	C	-0.599366	0.133274	0.496029
C	1.418252	-2.208900	1.944768	C	0.394273	-1.816725	2.012291
H	1.055826	-3.148116	1.509177	H	1.533126	-2.718501	1.482667
H	1.920816	-2.449265	2.891150	H	1.142178	-3.492273	0.810899
H	2.161442	-1.786808	1.265763	H	2.023740	-3.224864	2.324330
C	0.773437	0.065478	2.852861	C	2.292756	-2.154386	0.940217
H	1.545921	0.553669	2.261730	H	0.966627	-0.717159	2.935164
H	1.214083	-0.171693	3.829104	H	1.670940	-0.055383	2.436242
H	-0.037393	0.785403	3.015024	H	1.499912	-1.190063	3.769230
C	-0.658136	-1.888826	3.291519	C	0.162236	-0.103083	3.357433
H	-1.578638	-1.315555	3.452090	H	-0.489214	-2.696821	2.947272
H	-0.108949	-1.918891	4.239725	H	-1.375584	-2.151512	3.291128
H	-0.933597	-2.922151	3.057928	H	0.097384	-2.982036	3.828991
C	-3.696199	-2.713376	-0.667207	C	-0.823722	-3.624096	2.472817
C	-3.587032	-3.207341	-2.130668	C	-3.593879	-2.672209	-1.041709
H	-3.670308	-2.382363	-2.846505	H	-3.694576	-2.352457	-2.553469
H	-4.387897	-3.924516	-2.352013	H	-4.026820	-1.323724	-2.730230
H	-2.626032	-3.705831	-2.305507	H	-4.413055	-3.025553	-3.038692
C	-3.631048	-3.945266	0.256889	C	-2.723366	-2.478763	-3.046644
H	-2.683138	-4.486308	0.151071	H	-3.167972	-4.145928	-0.891938
H	-4.438574	-4.640724	-0.001274	H	-2.178274	-4.329873	-1.326637
H	-3.756438	-3.674850	1.312034	H	-3.884937	-4.791153	-1.413465
C	-5.070952	-2.031204	-0.461606	C	-3.146349	-4.463554	0.157327
H	-5.179689	-1.671322	0.568415	H	-4.990466	-2.506321	-0.393303
H	-5.883039	-2.741870	-0.662276	H	-4.951981	-2.722777	0.680983
H	-5.205489	-1.174266	-1.130597	H	-5.708675	-3.196396	-0.854537
C	7.032838	-0.878978	-0.782817	C	-5.380410	-1.490051	-0.516584
H	7.055400	-0.986544	0.309752	H	6.666517	-1.089015	-1.115468
H	7.209740	0.170866	-1.051664	H	6.741488	-1.404779	-0.066285
H	7.811653	-1.502961	-1.224663	H	6.894451	-0.017479	-1.192316
C	0.717730	2.375333	0.021062	C	7.380201	-1.655599	-1.716273
H	1.649382	2.940128	-0.008240	H	1.693826	2.707811	0.023041

## 7. Appendix

**Table S 23:** Atomic coordinates (x, y, z) for optimized minimum and transition state of **146k** at the B3LYP-D3(BJ)/6-31+g(d) level of theory.

Minimum				TS			
Atom	x	y	z	Atom	x	y	z
O	5.775242	-1.267787	-1.264168	O	5.415962	-0.936034	-1.635719
C	4.607433	-0.643326	-0.928454	C	4.276781	-0.411502	-1.090371
C	4.515508	0.463402	-0.075838	C	4.251181	0.510914	-0.039019
H	5.398085	0.891686	0.384962	H	5.166758	0.869838	0.416701
C	3.263750	1.018932	0.201681	C	3.022147	0.976106	0.441622
H	3.209562	1.863817	0.882786	H	3.018873	1.691241	1.260170
C	2.086293	0.494107	-0.343982	C	1.806917	0.530029	-0.085569
C	2.204189	-0.622178	-1.194923	C	1.858801	-0.392833	-1.148185
H	1.306835	-1.057226	-1.624214	H	0.932866	-0.750100	-1.587292
C	3.439967	-1.180183	-1.490325	C	3.068478	-0.853139	-1.648808
H	3.525510	-2.038325	-2.149863	H	3.101795	-1.561010	-2.471383
C	0.748588	1.092578	-0.096908	C	0.480674	1.094371	0.335388
C	-0.656489	3.174512	-0.016911	C	0.406828	2.447743	0.205160
C	-0.814957	4.308909	0.795330	C	-0.684280	3.409839	0.119322
H	0.010233	4.624463	1.429846	H	-0.303834	4.763839	-0.025388
C	-2.016517	5.015897	0.810814	C	0.754014	5.009799	0.030131
H	-2.128190	5.883293	1.455903	H	-1.229896	5.775163	-0.250122
C	-3.073979	4.605579	-0.006598	C	-0.899510	6.805479	-0.349524
H	-4.012721	5.153102	-0.002957	H	-2.582216	5.446237	-0.367675
C	-2.915560	3.497675	-0.842017	C	-3.325197	6.215127	-0.561018
H	-3.729999	3.189528	-1.493985	H	-2.972320	4.113678	-0.236685
C	-1.715485	2.782143	-0.865850	C	-4.026260	3.858389	-0.325003
C	-1.508900	1.597730	-1.785141	C	-2.053359	3.088313	0.023460
H	-0.577598	1.738868	-2.350784	H	-2.634285	1.719906	0.294484
H	-2.328837	1.536527	-2.507525	H	-3.605783	1.669679	-0.208428
C	-1.444747	0.320557	-0.976163	C	-2.876021	1.696239	1.370766
C	-2.444703	-0.635722	-1.127182	C	-1.927941	0.398631	0.035129
H	-3.214133	-0.462887	-1.874842	H	-2.736679	-0.636289	-0.425277
C	-2.462016	-1.796297	-0.348991	C	-3.716278	-0.382401	-0.821495
C	-1.500200	-1.894408	0.658115	C	-2.341276	-1.981373	-0.357662
H	-1.543706	-2.748130	1.316539	H	-1.194561	-2.246224	0.388103
C	-0.496307	-0.937079	0.886509	C	-0.939576	-3.274611	0.605072
C	-0.409069	0.149632	-0.024702	C	-0.356191	-1.239054	0.896174
C	0.362325	-1.112404	2.170951	C	-0.612146	0.104289	0.495190
C	1.600931	-1.999370	1.912766	C	0.649049	-1.660442	2.008687
H	1.303525	-2.959385	1.474506	H	1.904742	-2.388650	1.484438
H	2.113111	-2.204315	2.861746	H	1.630288	-3.185220	0.783337
H	2.314883	-1.526461	1.238543	H	2.437358	-2.849844	2.325887
C	0.798812	0.239560	2.775124	C	2.595347	-1.716123	0.977671
H	1.541249	0.755447	2.171051	H	1.051403	-0.477565	2.913138
H	1.245781	0.065466	3.761097	H	1.644357	0.275772	2.401455
H	-0.059672	0.908576	2.902972	H	1.652217	-0.853825	3.749781
C	-0.472945	-1.807601	3.278384	C	0.163146	0.012947	3.327580

## 7.3 Atomic coordinates for DFT calculations

H	-1.431451	-1.300650	3.436824	H	-0.093237	-2.650424	2.951600
H	0.088012	-1.778423	4.219043	H	-1.054569	-2.241160	3.281067
H	-0.672482	-2.861957	3.063921	H	0.524883	-2.831202	3.838691
C	-3.533432	-2.868787	-0.585763	C	-0.278488	-3.622165	2.485170
C	-3.421989	-3.384398	-2.038072	C	-3.206190	-3.077396	-0.988490
H	-3.562806	-2.577920	-2.765245	H	-3.356692	-2.789105	-2.499102
H	-4.184586	-4.149252	-2.231026	H	-3.824175	-1.815531	-2.679493
H	-2.436510	-3.829574	-2.217817	H	-3.980331	-3.556962	-2.973670
C	-3.384424	-4.070900	0.362416	C	-2.378602	-2.787417	-2.993928
H	-2.410396	-4.560462	0.247655	H	-2.587531	-4.476183	-0.824692
H	-4.158421	-4.813597	0.137304	H	-1.585144	-4.528810	-1.265029
H	-3.501695	-3.779447	1.412482	H	-3.215263	-5.217778	-1.331897
C	-4.933751	-2.253031	-0.367847	C	-2.516335	-4.770796	0.228671
H	-5.036297	-1.874000	0.655456	H	-4.603405	-3.085589	-0.328301
H	-5.712238	-3.007988	-0.534695	H	-4.523148	-3.278100	0.747797
H	-5.121563	-1.420450	-1.053803	H	-5.229378	-3.869889	-0.771969
C	6.986550	-0.764466	-0.719255	C	-5.120666	-2.129641	-0.461187
H	6.984563	-0.824073	0.377048	H	6.665080	-0.519177	-1.104959
H	7.160805	0.274247	-1.029219	H	6.754907	-0.784342	-0.043162
H	7.778423	-1.400991	-1.116950	H	6.807551	0.562977	-1.224651
C	0.612090	2.439814	-0.059985	C	7.425098	-1.051969	-1.678634
H	1.514993	3.047512	-0.106508	H	1.361303	2.914998	-0.025975

**Table S 24:** Atomic coordinates (x, y, z) for optimized minimum and transition state of **146k** at the B3LYP/6-31+g(d) level of theory with scrf=(cpcm,solvent=chloroform).

Minimum				TS			
Atom	x	y	z	Atom	x	y	z
O	5.812621	-1.348605	-1.327021	O	5.387518	-1.391143	-1.657176
C	4.649465	-0.738191	-0.947451	C	4.288776	-0.803031	-1.090910
C	4.567858	0.322916	-0.035973	C	4.327715	0.072192	0.001170
H	5.455526	0.724132	0.440040	H	5.265354	0.338224	0.476312
C	3.320024	0.870928	0.278573	C	3.135467	0.616097	0.495154
H	3.282980	1.684021	0.998975	H	3.191245	1.298903	1.339561
C	2.130864	0.387014	-0.287626	C	1.887443	0.299927	-0.057725
C	2.240130	-0.686861	-1.195192	C	1.876489	-0.581799	-1.157795
H	1.342580	-1.091108	-1.654753	H	0.932035	-0.840385	-1.627607
C	3.472552	-1.238045	-1.526895	C	3.050781	-1.120782	-1.671521
H	3.542361	-2.059304	-2.234767	H	3.026908	-1.791132	-2.526324
C	0.800504	1.017230	-0.031749	C	0.612165	0.990593	0.359358
C	-0.503371	3.182617	0.048950	C	0.694764	2.349293	0.245544
C	-0.602571	4.331942	0.854001	C	-0.269419	3.442922	0.155176
H	0.226553	4.595480	1.507373	H	0.278177	4.740930	0.013634
C	-1.751078	5.124609	0.833804	C	1.358259	4.856223	0.072194
H	-1.816650	6.001954	1.472288	H	-0.516057	5.860833	-0.211492
C	-2.812814	4.788158	-0.013599	C	-0.059763	6.842523	-0.308155
H	-3.708660	5.403394	-0.039898	H	-1.899930	5.702699	-0.332238

7. Appendix

C	-2.711696	3.666354	-0.842014	C	-2.541136	6.558821	-0.525085
H	-3.527487	3.418884	-1.518202	H	-2.454607	4.427697	-0.203748
C	-1.565601	2.862362	-0.828658	C	-3.532290	4.306954	-0.293863
C	-1.412924	1.666952	-1.749033	C	-1.669196	3.294686	0.056917
H	-0.471681	1.763623	-2.308776	H	-2.408308	2.002586	0.327373
H	-2.227145	1.653605	-2.480324	H	-3.386728	2.075390	-0.158773
C	-1.424043	0.375035	-0.953067	C	-2.635233	1.997534	1.407405
C	-2.478285	-0.518650	-1.138452	C	-1.869500	0.604241	0.041841
H	-3.222677	-0.283253	-1.894913	H	-2.808137	-0.307512	-0.437544
C	-2.580623	-1.693906	-0.386695	C	-3.744600	0.083159	-0.827724
C	-1.640735	-1.864605	0.634390	C	-2.599413	-1.696762	-0.391094
H	-1.746674	-2.726949	1.275536	H	-1.502249	-2.118739	0.360475
C	-0.579795	-0.976013	0.899710	C	-1.391262	-3.175225	0.567956
C	-0.407259	0.124126	0.007352	C	-0.534234	-1.241094	0.888531
C	0.246504	-1.249732	2.197754	C	-0.598948	0.132574	0.497394
C	1.426200	-2.214503	1.924031	C	0.389783	-1.823891	2.009326
H	1.066785	-3.152459	1.483179	H	1.522170	-2.732101	1.476807
H	1.932659	-2.458818	2.867139	H	1.123579	-3.507531	0.811471
H	2.164015	-1.781746	1.245743	H	2.016073	-3.235876	2.317894
C	0.770849	0.047511	2.855891	C	2.279536	-2.171067	0.927335
H	1.527632	0.556007	2.261424	H	0.970843	-0.728866	2.932364
H	1.227616	-0.199100	3.822162	H	1.680266	-0.071753	2.434025
H	-0.047512	0.753594	3.041724	H	1.500329	-1.206734	3.765880
C	-0.645858	-1.920634	3.279827	C	0.170417	-0.110156	3.355788
H	-1.568401	-1.353893	3.452413	H	-0.497014	-2.699543	2.945434
H	-0.090517	-1.957523	4.224108	H	-1.375081	-2.145645	3.297336
H	-0.917187	-2.952356	3.035429	H	0.092402	-2.993466	3.822305
C	-3.711720	-2.701311	-0.666074	C	-0.843891	-3.620794	2.468638
C	-3.611662	-3.188171	-2.132757	C	-3.603024	-2.661901	-1.044055
H	-3.697714	-2.359401	-2.843937	H	-3.710546	-2.334509	-2.553890
H	-4.416144	-3.901873	-2.351165	H	-4.045872	-1.305520	-2.723825
H	-2.653490	-3.690084	-2.314579	H	-4.430811	-3.006646	-3.037349
C	-3.646076	-3.937490	0.252281	C	-2.741536	-2.459537	-3.052247
H	-2.700365	-4.481038	0.139659	H	-3.177561	-4.136603	-0.902597
H	-4.457492	-4.627956	-0.006579	H	-2.190049	-4.319381	-1.342920
H	-3.765568	-3.671568	1.309256	H	-3.898434	-4.777433	-1.423923
C	-5.082990	-2.014565	-0.451442	C	-3.150955	-4.458614	0.145143
H	-5.187249	-1.662732	0.582098	H	-4.996742	-2.496441	-0.388931
H	-5.897190	-2.722031	-0.653795	H	-4.954387	-2.720920	0.683756
H	-5.216470	-1.153557	-1.115474	H	-5.716594	-3.183169	-0.852190
C	7.041954	-0.878515	-0.773628	C	-5.384963	-1.478715	-0.505700
H	7.055519	-0.995597	0.316780	H	6.673285	-1.095886	-1.112964
H	7.216932	0.172228	-1.034732	H	6.742401	-1.413161	-0.065236
H	7.821731	-1.499414	-1.216708	H	6.899582	-0.025329	-1.189830
C	0.721910	2.371479	0.027192	C	7.385978	-1.663158	-1.713256
H	1.654137	2.935442	0.008719	H	1.701252	2.705888	0.038462



## 7.3 Atomic coordinates for DFT calculations

**Table S25:** Atomic coordinates (x, y, z) for optimized minimum and transition state of **146k** at the B3LYP-D3(BJ)/6-31+g(d) level of theory with scrf=(cpcm,solvent=chloroform).

Minimum				TS			
Atom	x	y	z	Atom	x	y	z
O	5.780441	-1.265281	-1.266531	O	5.416895	-0.946349	-1.639210
C	4.611190	-0.642677	-0.931947	C	4.278061	-0.421156	-1.092880
C	4.517844	0.458845	-0.071616	C	4.255607	0.498196	-0.037892
H	5.399231	0.883558	0.394114	H	5.172021	0.853467	0.418406
C	3.265627	1.013815	0.205737	C	3.028019	0.965358	0.444648
H	3.212302	1.854975	0.891243	H	3.029596	1.679037	1.264228
C	2.088572	0.493175	-0.347004	C	1.810313	0.523975	-0.082915
C	2.207636	-0.615887	-1.207076	C	1.858844	-0.394919	-1.149039
H	1.312473	-1.046709	-1.645205	H	0.932780	-0.750221	-1.589634
C	3.444507	-1.173453	-1.502990	C	3.067700	-0.856981	-1.652870
H	3.527118	-2.026384	-2.170092	H	3.093949	-1.562741	-2.477923
C	0.750244	1.090443	-0.098339	C	0.485071	1.090915	0.340315
C	-0.653056	3.173516	-0.011206	C	0.416118	2.445817	0.214026
C	-0.809458	4.307472	0.803781	C	-0.672576	3.411449	0.124751
H	0.016939	4.622491	1.436764	H	-0.286583	4.764269	-0.025592
C	-2.011325	5.015617	0.821656	C	0.771765	5.007906	0.029221
H	-2.121493	5.881999	1.468255	H	-1.210266	5.777941	-0.255157
C	-3.070599	4.607596	0.003705	C	-0.876591	6.806715	-0.358668
H	-4.008745	5.155998	0.009187	H	-2.564482	5.452553	-0.371906
C	-2.913745	3.500955	-0.835292	C	-3.304831	6.223043	-0.568500
H	-3.728470	3.195731	-1.488039	H	-2.959809	4.121215	-0.234627
C	-1.713346	2.784085	-0.861352	C	-4.014448	3.869293	-0.321125
C	-1.509433	1.601634	-1.784022	C	-2.043556	3.093761	0.030874
H	-0.577836	1.741755	-2.349335	H	-2.627829	1.728605	0.310399
H	-2.329748	1.542908	-2.505363	H	-3.605180	1.681777	-0.180091
C	-1.446678	0.323621	-0.975882	C	-2.855886	1.706862	1.389415
C	-2.451633	-0.628657	-1.125724	C	-1.927369	0.405666	0.042035
H	-3.222254	-0.451322	-1.870812	H	-2.741923	-0.624273	-0.420947
C	-2.470494	-1.791054	-0.349053	C	-3.722602	-0.365270	-0.810753
C	-1.505061	-1.894766	0.654981	C	-2.350250	-1.971679	-0.360434
H	-1.549862	-2.750013	1.311284	H	-1.202791	-2.244237	0.382510
C	-0.496163	-0.941492	0.882062	C	-0.952239	-3.274708	0.594922
C	-0.408259	0.147861	-0.027382	C	-0.359632	-1.242002	0.893452
C	0.367128	-1.124792	2.162722	C	-0.611078	0.103929	0.497574
C	1.606894	-2.007225	1.893680	C	0.644076	-1.670860	2.004653
H	1.308711	-2.966326	1.453823	H	1.893384	-2.407779	1.477497
H	2.124111	-2.214342	2.839298	H	1.610046	-3.209537	0.785801
H	2.315027	-1.528316	1.217366	H	2.430199	-2.863375	2.319156
C	0.802905	0.223400	2.775624	C	2.581400	-1.740232	0.960019
H	1.532868	0.752867	2.168031	H	1.057150	-0.492335	2.910150
H	1.263096	0.041221	3.753860	H	1.659159	0.255372	2.400375
H	-0.059584	0.883704	2.923056	H	1.652194	-0.875869	3.747457
C	-0.460493	-1.831328	3.268697	C	0.172649	0.005904	3.323794

## 7. Appendix

H	-1.418484	-1.326683	3.438248	H	-0.103742	-2.656462	2.947859
H	0.107143	-1.809139	4.205446	H	-1.057184	-2.235665	3.286212
H	-0.660590	-2.883506	3.045322	H	0.518620	-2.847969	3.829649
C	-3.546618	-2.859383	-0.583811	C	-0.304673	-3.623056	2.477812
C	-3.444871	-3.369463	-2.038971	C	-3.221181	-3.062477	-0.992154
H	-3.588911	-2.559772	-2.762000	H	-3.385795	-2.762234	-2.499137
H	-4.211151	-4.131247	-2.228304	H	-3.858140	-1.788747	-2.667460
H	-2.462076	-3.818295	-2.225495	H	-4.012354	-3.528399	-2.972150
C	-3.396520	-4.065150	0.359576	C	-2.412054	-2.756656	-3.002960
H	-2.424543	-4.557265	0.238371	H	-2.601691	-4.462748	-0.844524
H	-4.174504	-4.803492	0.134424	H	-1.602954	-4.512054	-1.293651
H	-3.507507	-3.776978	1.411229	H	-3.235088	-5.198582	-1.352858
C	-4.943705	-2.238925	-0.357371	C	-2.521660	-4.765742	0.205730
H	-5.041398	-1.867085	0.669336	H	-4.612605	-3.073688	-0.319461
H	-5.724282	-2.991134	-0.525598	H	-4.522842	-3.278869	0.753740
H	-5.130698	-1.402474	-1.038900	H	-5.242746	-3.852662	-0.766214
C	6.994322	-0.764605	-0.708434	C	-5.128470	-2.115198	-0.438942
H	6.982084	-0.832350	0.386003	H	6.671745	-0.533493	-1.101979
H	7.168181	0.274717	-1.011846	H	6.755363	-0.804513	-0.042520
H	7.786866	-1.399590	-1.105688	H	6.814229	0.547768	-1.217833
C	0.615245	2.438024	-0.055480	C	7.430276	-1.066077	-1.676741
H	1.518524	3.045516	-0.091336	H	1.372954	2.911829	-0.009610

**Table S26:** Atomic coordinates (x, y, z) for optimized minimum and transition state of **146k** at the B3LYP/def2-TZVP level of theory.

Minimum				TS			
Atom	x	y	z	Atom	x	y	z
O	5.787214	-1.346746	-1.317385	O	5.367267	-1.383329	-1.653731
C	4.629628	-0.738214	-0.939843	C	4.273798	-0.802880	-1.084487
C	4.548071	0.324071	-0.040714	C	4.310609	0.054304	0.012748
H	5.434259	0.727079	0.427660	H	5.245177	0.309583	0.490870
C	3.307540	0.870622	0.272008	C	3.125323	0.593147	0.508566
H	3.269818	1.685742	0.983808	H	3.178405	1.263301	1.357956
C	2.123375	0.385050	-0.284039	C	1.884880	0.290311	-0.048684
C	2.231352	-0.691968	-1.177231	C	1.874213	-0.575076	-1.152708
H	1.335321	-1.099812	-1.626533	H	0.932906	-0.822553	-1.624979
C	3.456257	-1.240957	-1.506669	C	3.041310	-1.108031	-1.666974
H	3.528072	-2.064767	-2.204802	H	3.021406	-1.764762	-2.526994
C	0.797713	1.014884	-0.031660	C	0.614683	0.979653	0.369466
C	-0.501769	3.170320	0.045385	C	0.701243	2.330378	0.259496
C	-0.601979	4.313259	0.846097	C	-0.251250	3.425517	0.165367
H	0.222633	4.574939	1.499033	C	0.299407	4.712361	0.008658
C	-1.743570	5.101346	0.825232	H	1.376539	4.819711	0.058213
H	-1.809969	5.975093	1.461316	C	-0.484696	5.828248	-0.221300
C	-2.797930	4.767826	-0.018613	H	-0.025228	6.802336	-0.331207
H	-3.689773	5.381331	-0.045327	C	-1.862083	5.678842	-0.330704

## 7.3 Atomic coordinates for DFT calculations

C	-2.697176	3.652569	-0.841926	H	-2.496149	6.533948	-0.527770
H	-3.509792	3.406681	-1.515862	C	-2.420910	4.416443	-0.185139
C	-1.558421	2.851877	-0.827442	H	-3.495869	4.301617	-0.267076
C	-1.407308	1.659516	-1.743037	C	-1.645454	3.287526	0.080628
H	-0.469526	1.755967	-2.300113	C	-2.383096	2.005113	0.365879
H	-2.219863	1.645151	-2.469729	H	-3.367044	2.083311	-0.098598
C	-1.417275	0.372313	-0.949814	H	-2.585442	2.000227	1.446853
C	-2.463338	-0.518851	-1.135108	C	-1.861614	0.609567	0.066407
H	-3.204324	-0.286421	-1.890051	C	-2.803488	-0.285217	-0.415032
C	-2.565552	-1.686662	-0.385798	H	-3.736417	0.115626	-0.792057
C	-1.634223	-1.853446	0.632575	C	-2.603694	-1.668669	-0.389071
H	-1.740620	-2.710715	1.274114	C	-1.510948	-2.104111	0.345962
C	-0.580350	-0.967722	0.896525	H	-1.405989	-3.159477	0.540721
C	-0.406249	0.124480	0.007137	C	-0.539068	-1.243555	0.875754
C	0.240004	-1.239089	2.193209	C	-0.595115	0.128471	0.502931
C	1.399886	-2.221078	1.927432	C	0.383578	-1.846341	1.980887
H	1.027174	-3.152921	1.496858	C	1.503519	-2.751318	1.432826
H	1.903040	-2.464257	2.867186	H	1.099375	-3.509092	0.758492
H	2.140356	-1.808607	1.246610	H	1.993304	-3.271020	2.260448
C	0.782697	0.050908	2.837558	H	2.261527	-2.191428	0.892736
H	1.554421	0.530268	2.246561	C	0.972436	-0.771175	2.912987
H	1.221366	-0.192017	3.807895	H	1.681272	-0.115847	2.421841
H	-0.017766	0.774482	3.003411	H	1.498757	-1.261457	3.735076
C	-0.662535	-1.881623	3.276279	H	0.181102	-0.155131	3.344686
H	-1.568627	-1.296471	3.443468	C	-0.502917	-2.725425	2.905006
H	-0.109889	-1.923420	4.216511	H	-1.372066	-2.172921	3.265898
H	-0.954424	-2.904216	3.038849	H	0.086084	-3.034058	3.771098
C	-3.691336	-2.692954	-0.666108	H	-0.856487	-3.632993	2.417801
C	-3.583183	-3.184329	-2.124894	C	-3.613355	-2.616106	-1.047716
H	-3.663779	-2.361236	-2.835827	C	-3.720297	-2.273079	-2.548501
H	-4.382058	-3.896472	-2.345950	H	-4.042965	-1.243129	-2.705013
H	-2.627174	-3.682597	-2.298316	H	-4.444350	-2.929567	-3.037335
C	-3.628139	-3.920389	0.254942	H	-2.757122	-2.399750	-3.046882
H	-2.685539	-4.460694	0.147584	C	-3.199196	-4.089755	-0.922740
H	-4.434763	-4.610430	-0.000404	H	-2.218691	-4.273260	-1.366300
H	-3.749373	-3.649177	1.305371	H	-3.922563	-4.719219	-1.444714
C	-5.059257	-2.009199	-0.460794	H	-3.170860	-4.419240	0.117631
H	-5.166649	-1.653474	0.565795	C	-4.999142	-2.448258	-0.389513
H	-5.869801	-2.713808	-0.662937	H	-4.955390	-2.682967	0.675882
H	-5.188548	-1.154019	-1.125134	H	-5.723908	-3.120217	-0.855839
C	7.009982	-0.875383	-0.776981	H	-5.376648	-1.430278	-0.492468
H	7.034859	-0.982765	0.311635	C	6.644492	-1.100193	-1.109446
H	7.187371	0.171579	-1.040745	H	6.718647	-1.428654	-0.068220
H	7.789731	-1.493396	-1.216209	H	6.877798	-0.032668	-1.168064
C	0.717903	2.360479	0.025054	H	7.358018	-1.657007	-1.712683
H	1.647221	2.921408	0.000779	H	1.705720	2.679522	0.050529

## 7. Appendix

**Table S27:** Atomic coordinates (x, y, z) for optimized minimum and transition state of **146k** at the B3LYP/def2-TZVP level of theory using the "tight" option and the superfine grid.

Minimum				TS			
Atom	x	y	z	Atom	x	y	z
O	5.786872	-1.347696	-1.316894	O	5.367499	-1.383714	-1.654078
C	4.629442	-0.738885	-0.939226	C	4.274048	-0.803606	-1.084460
C	4.548381	0.324701	-0.041606	C	4.310794	0.052616	0.013520
H	5.434867	0.728546	0.425478	H	5.245324	0.307326	0.492002
C	3.307997	0.871579	0.271150	C	3.125506	0.591204	0.509596
H	3.270679	1.687795	0.981714	H	3.178536	1.260733	1.359477
C	2.123505	0.385048	-0.283391	C	1.885120	0.289144	-0.048194
C	2.230988	-0.693483	-1.174812	C	1.874496	-0.575409	-1.152868
H	1.334679	-1.102208	-1.622700	H	0.933249	-0.822486	-1.625480
C	3.455734	-1.242824	-1.504264	C	3.041594	-1.108138	-1.667356
H	3.527153	-2.067783	-2.201074	H	3.021705	-1.764241	-2.527853
C	0.797932	1.015277	-0.031446	C	0.615070	0.978742	0.370043
C	-0.501933	3.170379	0.044180	C	0.702265	2.329476	0.260172
C	-0.602849	4.313345	0.844744	C	-0.249622	3.425121	0.165854
H	0.221564	4.575576	1.497706	C	0.301740	4.711518	0.007985
C	-1.744962	5.100683	0.823788	H	1.378965	4.818247	0.056774
H	-1.811929	5.974454	1.459776	C	-0.481847	5.827736	-0.222148
C	-2.799165	4.766296	-0.019910	H	-0.021858	6.801474	-0.332967
H	-3.691465	5.379137	-0.046562	C	-1.859408	5.679126	-0.330431
C	-2.697697	3.651029	-0.843144	H	-2.493075	6.534524	-0.527503
H	-3.510197	3.404510	-1.516982	C	-2.418943	4.417162	-0.183669
C	-1.558321	2.851245	-0.828757	H	-3.494035	4.302951	-0.264677
C	-1.406400	1.658780	-1.744077	C	-1.643969	3.287950	0.082157
H	-0.468392	1.755405	-2.300720	C	-2.381805	2.005999	0.368750
H	-2.218626	1.643977	-2.471132	H	-3.366580	2.084791	-0.093855
C	-1.416363	0.371824	-0.950460	H	-2.582027	2.000954	1.450115
C	-2.461818	-0.519925	-1.136225	C	-1.861495	0.610326	0.067819
H	-3.202176	-0.288150	-1.891963	C	-2.804212	-0.283473	-0.413748
C	-2.564355	-1.687243	-0.386108	H	-3.737055	0.118257	-0.790030
C	-1.633804	-1.853026	0.633132	C	-2.605342	-1.667085	-0.388792
H	-1.740347	-2.709944	1.275151	C	-1.512513	-2.103755	0.345434
C	-0.580525	-0.966652	0.897424	H	-1.408174	-3.159323	0.539423
C	-0.406002	0.124924	0.007440	C	-0.539790	-1.244207	0.875329
C	0.238691	-1.236930	2.194989	C	-0.595057	0.128108	0.503324
C	1.397245	-2.221026	1.931218	C	0.383048	-1.848065	1.979794
H	1.023349	-3.153166	1.502327	C	1.503609	-2.751869	1.430956
H	1.900101	-2.463241	2.871382	H	1.099909	-3.509797	0.756510
H	2.138286	-1.810704	1.249661	H	1.994071	-3.271512	2.258236
C	0.783171	0.053166	2.837669	H	2.260985	-2.191160	0.890849
H	1.558013	0.528865	2.247749	C	0.971119	-0.773624	2.913220
H	1.218531	-0.188665	3.809756	H	1.678851	-0.116562	2.422789
H	-0.015642	0.779406	2.999651	H	1.498441	-1.264593	3.734249
C	-0.665600	-1.876314	3.278502	H	0.179230	-0.159202	3.346221

## 7.3 Atomic coordinates for DFT calculations

H	-1.570578	-1.289108	3.444516	C	-0.502857	-2.728859	2.902806
H	-0.113430	-1.918051	4.219006	H	-1.372448	-2.177463	3.264313
H	-0.959513	-2.898574	3.042266	H	0.086401	-3.038051	3.768520
C	-3.689826	-2.693787	-0.666572	H	-0.855632	-3.636142	2.414499
C	-3.579352	-3.187832	-2.124291	C	-3.615630	-2.613308	-1.048210
H	-3.658175	-2.365960	-2.836824	C	-3.719828	-2.270706	-2.549309
H	-4.378298	-3.899852	-2.345480	H	-4.040738	-1.240314	-2.706566
H	-2.623380	-3.687041	-2.295145	H	-4.444123	-2.926283	-3.039012
C	-3.628572	-3.919523	0.256842	H	-2.756099	-2.398933	-3.046220
H	-2.685767	-4.460035	0.152410	C	-3.203993	-4.087549	-0.922006
H	-4.434648	-4.610054	0.001125	H	-2.223483	-4.272984	-1.364745
H	-3.751948	-3.646317	1.306498	H	-3.927995	-4.716132	-1.444159
C	-5.057949	-2.009260	-0.464957	H	-3.176960	-4.416436	0.118583
H	-5.166935	-1.651163	0.560642	C	-5.002152	-2.443081	-0.392196
H	-5.868308	-2.714142	-0.666856	H	-4.960363	-2.677380	0.673362
H	-5.185993	-1.155549	-1.131414	H	-5.727152	-3.114238	-0.859306
C	7.010044	-0.875063	-0.778434	H	-5.378127	-1.424655	-0.496264
H	7.036210	-0.981133	0.310271	C	6.644737	-1.101172	-1.109523
H	7.186620	0.171651	-1.043687	H	6.718949	-1.430813	-0.068674
H	7.789572	-1.493251	-1.217801	H	6.878047	-0.033583	-1.166952
C	0.718019	2.360891	0.024361	H	7.358239	-1.657310	-1.713411
H	1.647225	2.921961	-0.000156	H	1.706923	2.678109	0.051291

**Table S28:** Atomic coordinates (x, y, z) for optimized minimum and transition state of **146k** at the B3LYP-D3(BJ)/def2-TZVP level of theory.

Minimum				TS			
Atom	x	y	z	Atom	x	y	z
O	5.757438	-1.261732	-1.258527	O	5.391493	-0.958733	-1.637066
C	4.593202	-0.642679	-0.924856	C	4.260626	-0.436030	-1.087644
C	4.498467	0.454949	-0.071180	C	4.240990	0.465556	-0.026675
H	5.377512	0.878150	0.391276	H	5.156594	0.806130	0.433091
C	3.253043	1.007569	0.204406	C	3.022491	0.933181	0.457803
H	3.197597	1.846540	0.885870	H	3.025173	1.633743	1.283191
C	2.081994	0.489113	-0.343614	C	1.809550	0.510251	-0.074911
C	2.201089	-0.618112	-1.194955	C	1.853587	-0.392437	-1.145934
H	1.308163	-1.049261	-1.626936	H	0.928267	-0.732662	-1.589579
C	3.430907	-1.172486	-1.488689	C	3.053013	-0.853986	-1.650329
H	3.516704	-2.023973	-2.150287	H	3.079443	-1.545958	-2.481385
C	0.748248	1.085996	-0.098578	C	0.491246	1.080487	0.349228
C	-0.649375	3.160152	-0.013112	C	0.430752	2.428107	0.227836
C	-0.805852	4.286775	0.798983	C	-0.644274	3.399194	0.134614
H	0.016279	4.598293	1.432119	C	-0.250392	4.740743	-0.026929
C	-2.000083	4.991719	0.816567	H	0.806391	4.973304	0.022248
H	-2.110365	5.853757	1.461770	C	-1.160528	5.754274	-0.261700
C	-3.052233	4.588846	0.001250	H	-0.820129	6.775247	-0.375304
H	-3.985844	5.136516	0.006555	C	-2.509796	5.441637	-0.371754

7. Appendix

C	-2.896773	3.489430	-0.833853	H	-3.240580	6.214028	-0.573122
H	-3.708570	3.187337	-1.484779	C	-2.914149	4.122943	-0.221586
C	-1.704411	2.774355	-0.859148	H	-3.967024	3.879725	-0.303868
C	-1.502799	1.595269	-1.777878	C	-2.011454	3.095540	0.049491
H	-0.574315	1.734673	-2.340018	C	-2.600413	1.741131	0.338382
H	-2.321220	1.536706	-2.494839	H	-3.580760	1.701920	-0.137574
C	-1.440156	0.321419	-0.973146	H	-2.812073	1.722429	1.416878
C	-2.438747	-0.626478	-1.122443	C	-1.918920	0.416701	0.061431
H	-3.206119	-0.450748	-1.865379	C	-2.740447	-0.596526	-0.402498
C	-2.459317	-1.781459	-0.348088	H	-3.717266	-0.325702	-0.782553
C	-1.501966	-1.883405	0.652770	C	-2.362239	-1.940564	-0.356991
H	-1.548950	-2.733261	1.309612	C	-1.219101	-2.227878	0.372069
C	-0.497749	-0.935317	0.877607	H	-0.977852	-3.258071	0.575502
C	-0.406985	0.146491	-0.028899	C	-0.367815	-1.242442	0.882724
C	0.361287	-1.117612	2.155709	C	-0.606981	0.102939	0.501381
C	1.590267	-2.006729	1.890397	C	0.636059	-1.690529	1.980084
H	1.286893	-2.959749	1.453024	C	1.875053	-2.423805	1.439409
H	2.103579	-2.215876	2.832239	H	1.586891	-3.206520	0.735688
H	2.300209	-1.537173	1.216747	H	2.407359	-2.897503	2.267720
C	0.803704	0.225599	2.761107	H	2.565048	-1.755485	0.935888
H	1.541551	0.739042	2.157433	C	1.055911	-0.529159	2.895188
H	1.251707	0.045745	3.740209	H	1.651968	0.220778	2.391694
H	-0.048925	0.893229	2.895438	H	1.653691	-0.923192	3.719437
C	-0.471092	-1.810031	3.259265	H	0.178995	-0.037206	3.319482
H	-1.418934	-1.296066	3.426206	C	-0.110077	-2.681184	2.910263
H	0.094919	-1.791999	4.191565	H	-1.056608	-2.262858	3.255148
H	-0.681882	-2.855540	3.037730	H	0.512913	-2.884756	3.782886
C	-3.532090	-2.846786	-0.583164	H	-0.315336	-3.636376	2.429761
C	-3.422279	-3.361999	-2.030118	C	-3.242672	-3.014401	-0.993630
H	-3.558744	-2.557780	-2.753357	C	-3.395248	-2.707127	-2.494924
H	-4.184373	-4.120709	-2.222010	H	-3.847732	-1.729002	-2.659124
H	-2.442428	-3.808980	-2.207472	H	-4.028588	-3.457410	-2.973625
C	-3.386908	-4.043327	0.363817	H	-2.423132	-2.713055	-2.991095
H	-2.418727	-4.533619	0.248493	C	-2.643072	-4.417513	-0.848278
H	-4.161021	-4.779968	0.142456	H	-1.648932	-4.477266	-1.294445
H	-3.499823	-3.748972	1.408524	H	-3.281410	-5.142867	-1.355442
C	-4.924896	-2.226825	-0.366832	H	-2.567904	-4.719863	0.197569
H	-5.025327	-1.849881	0.652401	C	-4.631799	-3.010589	-0.328901
H	-5.703163	-2.974942	-0.533959	H	-4.548777	-3.217923	0.739386
H	-5.105974	-1.396652	-1.049773	H	-5.268573	-3.776224	-0.777897
C	6.964476	-0.762266	-0.710110	H	-5.131781	-2.049040	-0.446408
H	6.962842	-0.826292	0.382024	C	6.640490	-0.563885	-1.099142
H	7.139921	0.274975	-1.010312	H	6.727975	-0.845000	-0.045324
H	7.757559	-1.391431	-1.106651	H	6.795013	0.514776	-1.197811
C	0.613028	2.424979	-0.056554	H	7.396771	-1.090368	-1.676318
H	1.513744	3.028876	-0.097675	H	1.387684	2.884330	0.003374

## 7.3 Atomic coordinates for DFT calculations

**Table S29:** Atomic coordinates (x, y, z) for optimized minimum and transition state of **146k** at the B3LYP/def2-TZVP level of theory with scrf=(cpcm,solvent=chloroform).

Minimum				TS			
Atom	x	y	z	Atom	x	y	z
O	5.791898	-1.344227	-1.319045	O	5.369259	-1.386402	-1.655162
C	4.633281	-0.737984	-0.942628	C	4.275592	-0.806569	-1.086218
C	4.549883	0.319683	-0.037067	C	4.313297	0.050141	0.012295
H	5.434865	0.719840	0.435589	H	5.248042	0.305076	0.489915
C	3.308669	0.865347	0.275192	C	3.128389	0.589172	0.508937
H	3.271477	1.677415	0.990366	H	3.184654	1.259277	1.358019
C	2.124996	0.383179	-0.286860	C	1.886565	0.287257	-0.047673
C	2.234365	-0.687400	-1.187548	C	1.874777	-0.576545	-1.152858
H	1.340621	-1.091502	-1.644846	H	0.934095	-0.824578	-1.626284
C	3.460522	-1.235598	-1.517194	C	3.042055	-1.109790	-1.669011
H	3.530091	-2.054621	-2.221593	H	3.017263	-1.765752	-2.529873
C	0.798872	1.012244	-0.033134	C	0.616400	0.977114	0.372048
C	-0.498727	3.168722	0.050480	C	0.705293	2.328739	0.265638
C	-0.596683	4.311084	0.853865	C	-0.246443	3.425223	0.169281
H	0.229239	4.571817	1.505407	C	0.307218	4.711350	0.009467
C	-1.737958	5.101135	0.834771	H	1.384420	4.817778	0.058919
H	-1.802632	5.974006	1.472230	C	-0.475989	5.828206	-0.223736
C	-2.793840	4.770402	-0.009851	H	-0.015160	6.801393	-0.335809
H	-3.684739	5.385335	-0.035278	C	-1.854493	5.680259	-0.332944
C	-2.694902	3.656138	-0.836263	H	-2.487273	6.535835	-0.531999
H	-3.507610	3.413235	-1.511026	C	-2.415936	4.418530	-0.183770
C	-1.556452	2.853368	-0.823426	H	-3.490910	4.305140	-0.264879
C	-1.408119	1.662727	-1.741981	C	-1.641538	3.288782	0.085420
H	-0.470266	1.758128	-2.298974	C	-2.380494	2.008197	0.375215
H	-2.221141	1.650604	-2.467524	H	-3.367269	2.088284	-0.081889
C	-1.419377	0.374899	-0.949336	H	-2.574655	2.003157	1.457463
C	-2.469802	-0.512433	-1.133458	C	-1.861349	0.612547	0.070492
H	-3.211522	-0.276124	-1.886286	C	-2.806214	-0.279197	-0.412266
C	-2.573294	-1.681824	-0.385542	H	-3.739586	0.124273	-0.784998
C	-1.639110	-1.853490	0.630367	C	-2.608290	-1.663750	-0.390228
H	-1.746555	-2.712149	1.269863	C	-1.515462	-2.103402	0.343288
C	-0.580955	-0.971608	0.893001	H	-1.413279	-3.159499	0.535890
C	-0.406156	0.122696	0.004933	C	-0.541138	-1.245693	0.874167
C	0.243603	-1.249658	2.186043	C	-0.594846	0.127437	0.504163
C	1.406973	-2.225097	1.910319	C	0.380558	-1.852489	1.978104
H	1.035875	-3.156533	1.477328	C	1.495763	-2.761804	1.427392
H	1.914252	-2.470148	2.847237	H	1.085495	-3.522033	0.759492
H	2.142196	-1.804713	1.228425	H	1.989472	-3.278073	2.254714
C	0.782632	0.037717	2.838759	H	2.250529	-2.203704	0.880291
H	1.542795	0.532430	2.245227	C	0.975681	-0.781116	2.910752
H	1.233242	-0.212728	3.801557	H	1.687550	-0.128210	2.420243
H	-0.023467	0.751068	3.022569	H	1.499733	-1.275662	3.731650
C	-0.651326	-1.905262	3.267501	H	0.186905	-0.162785	3.344228

## 7. Appendix

H	-1.558090	-1.324048	3.445444	C	-0.507780	-2.729110	2.902866
H	-0.092586	-1.953276	4.203784	H	-1.369720	-2.170184	3.271613
H	-0.941607	-2.926140	3.021590	H	0.084218	-3.045514	3.764069
C	-3.702718	-2.684588	-0.664340	H	-0.871451	-3.631066	2.413022
C	-3.603263	-3.169349	-2.126148	C	-3.620486	-2.607902	-1.049796
H	-3.687419	-2.342791	-2.832750	C	-3.731350	-2.258255	-2.548984
H	-4.405190	-3.878821	-2.343896	H	-4.056820	-1.228183	-2.699678
H	-2.649593	-3.670162	-2.306371	H	-4.456205	-2.914194	-3.037032
C	-3.637641	-3.915965	0.251340	H	-2.769335	-2.383602	-3.050471
H	-2.696369	-4.457384	0.137690	C	-3.207302	-4.082392	-0.931379
H	-4.447041	-4.602326	-0.004779	H	-2.228703	-4.265276	-1.379609
H	-3.753751	-3.649066	1.303482	H	-3.934281	-4.707773	-1.453095
C	-5.067982	-1.997786	-0.450234	H	-3.174871	-4.415304	0.107748
H	-5.171106	-1.649393	0.579590	C	-5.004628	-2.440074	-0.387685
H	-5.879842	-2.700304	-0.653548	H	-4.959111	-2.682070	0.676206
H	-5.197183	-1.139123	-1.110230	H	-5.730151	-3.108928	-0.856993
C	7.017609	-0.873434	-0.769120	H	-5.380116	-1.420780	-0.485595
H	7.035062	-0.987261	0.317789	C	6.651258	-1.102679	-1.106998
H	7.192595	0.173904	-1.028059	H	6.720831	-1.432073	-0.066996
H	7.798071	-1.489313	-1.208819	H	6.881757	-0.035734	-1.165982
C	0.720582	2.358006	0.028816	H	7.364275	-1.659506	-1.709924
H	1.650067	2.918716	0.013624	H	1.710940	2.678352	0.063059

**Table S30:** Atomic coordinates (x, y, z) for optimized minimum and transition state of **146k** at the B3LYP-D3(BJ)/def2-TZVP level of theory with scrf=(cpcm,solvent=chloroform).

Minimum				TS			
Atom	x	y	z	Atom	x	y	z
O	5.760220	-1.259635	-1.260383	O	5.392208	-0.968438	-1.639376
C	4.595369	-0.641996	-0.928076	C	4.262010	-0.444969	-1.089744
C	4.499644	0.452391	-0.069138	C	4.244829	0.454947	-0.026387
H	5.377942	0.873205	0.396520	H	5.161166	0.792978	0.433443
C	3.253933	1.004854	0.206163	C	3.027519	0.924380	0.459387
H	3.199769	1.841940	0.889917	H	3.034480	1.624403	1.285070
C	2.082915	0.489096	-0.346526	C	1.812447	0.504862	-0.073166
C	2.202657	-0.612917	-1.204385	C	1.853723	-0.395248	-1.146369
H	1.311512	-1.040935	-1.643183	H	0.928407	-0.734340	-1.591063
C	3.433339	-1.167197	-1.498612	C	3.052562	-0.858388	-1.653320
H	3.516210	-2.015051	-2.165673	H	3.072894	-1.549268	-2.485847
C	0.748641	1.085055	-0.100018	C	0.495001	1.077440	0.352799
C	-0.647720	3.160038	-0.008941	C	0.438850	2.426374	0.235083
C	-0.801736	4.287188	0.804466	C	-0.634144	3.400456	0.139111
H	0.021978	4.598850	1.435354	C	-0.235455	4.741053	-0.026223
C	-1.996012	4.993624	0.823786	H	0.821764	4.971602	0.022881
H	-2.104419	5.855615	1.469379	C	-1.143497	5.756648	-0.265052
C	-3.050326	4.592043	0.008961	H	-0.800284	6.776375	-0.381345
H	-3.983322	5.140756	0.015665	C	-2.494411	5.447041	-0.375116



## 7.3 Atomic coordinates for DFT calculations

C	-2.896892	3.492655	-0.828062	H	-3.222930	6.220847	-0.579195
H	-3.709268	3.192424	-1.478987	C	-2.903185	4.129350	-0.220544
C	-1.704386	2.776095	-0.855065	H	-3.956582	3.888900	-0.302006
C	-1.505673	1.598175	-1.776060	C	-2.002838	3.100089	0.054925
H	-0.577429	1.736724	-2.338707	C	-2.595007	1.748425	0.349633
H	-2.325051	1.541152	-2.491377	H	-3.579229	1.712346	-0.117437
C	-1.443069	0.323857	-0.971646	H	-2.796742	1.731020	1.429817
C	-2.444984	-0.621654	-1.119974	C	-1.918194	0.422655	0.066233
H	-3.213887	-0.442595	-1.860335	C	-2.744548	-0.586422	-0.399644
C	-2.464716	-1.778947	-0.347927	H	-3.722042	-0.311444	-0.774686
C	-1.503819	-1.885044	0.650002	C	-2.369596	-1.932325	-0.359452
H	-1.550031	-2.737024	1.304208	C	-1.226223	-2.225972	0.367737
C	-0.496964	-0.938862	0.874288	H	-0.988928	-3.257820	0.567827
C	-0.407047	0.145597	-0.030455	C	-0.371088	-1.244595	0.880596
C	0.365911	-1.126798	2.149376	C	-0.606189	0.102758	0.503022
C	1.595424	-2.013020	1.876070	C	0.631070	-1.698675	1.977145
H	1.290747	-2.966352	1.440106	C	1.863991	-2.440503	1.434396
H	2.113650	-2.221540	2.815248	H	1.567379	-3.229021	0.740589
H	2.299713	-1.539977	1.198640	H	2.400484	-2.907797	2.263547
C	0.808725	0.213518	2.760771	H	2.551117	-1.777270	0.919642
H	1.537452	0.736719	2.154301	C	1.060853	-0.540897	2.892384
H	1.266470	0.027361	3.734074	H	1.665439	0.203316	2.390135
H	-0.046636	0.874961	2.909731	H	1.653014	-0.941324	3.717522
C	-0.460783	-1.826876	3.252406	H	0.187423	-0.041462	3.315482
H	-1.407368	-1.313273	3.428380	C	-0.120327	-2.684451	2.908378
H	0.111102	-1.814710	4.181180	H	-1.059115	-2.255089	3.261360
H	-0.673744	-2.870331	3.024196	H	0.506470	-2.897550	3.775984
C	-3.540201	-2.841960	-0.581360	H	-0.340345	-3.634816	2.425251
C	-3.443235	-3.347303	-2.032882	C	-3.255056	-3.001817	-0.996423
H	-3.586846	-2.538243	-2.749393	C	-3.421957	-2.683372	-2.494043
H	-4.207991	-4.104067	-2.220911	H	-3.880527	-1.706059	-2.646597
H	-2.465622	-3.795239	-2.221126	H	-4.057249	-3.433054	-2.970751
C	-3.388430	-4.044749	0.356656	H	-2.454122	-2.684151	-2.999059
H	-2.420805	-4.533866	0.231648	C	-2.653582	-4.405714	-0.866657
H	-4.164477	-4.778907	0.134179	H	-1.663147	-4.461367	-1.321764
H	-3.494300	-3.757512	1.404103	H	-3.297036	-5.126095	-1.374315
C	-4.930493	-2.221102	-0.350537	H	-2.569154	-4.715835	0.176147
H	-5.023651	-1.854188	0.673333	C	-4.638351	-3.002029	-0.319180
H	-5.709756	-2.967741	-0.518725	H	-4.545765	-3.221623	0.746075
H	-5.114406	-1.385573	-1.026303	H	-5.278805	-3.762792	-0.770949
C	6.969987	-0.761510	-0.701620	H	-5.137363	-2.038388	-0.423602
H	6.959567	-0.830691	0.388969	C	6.646395	-0.575814	-1.096559
H	7.144846	0.275694	-0.998016	H	6.728738	-0.860633	-0.044533
H	7.763393	-1.390161	-1.096950	H	6.800134	0.501978	-1.193250
C	0.614523	2.424317	-0.053449	H	7.401421	-1.102447	-1.674316
H	1.515405	3.028244	-0.085642	H	1.397765	2.881671	0.017245

## 7. Appendix

**Table S31:** Atomic coordinates (x, y, z) for optimized minimum of **147b** at the B3LYP-D3(BJ)/6-31+g(d) level of theory.

<b>Minimum</b>			
Atom	x	y	z
O	-1.818221	-0.474709	-1.310328
O	1.722158	1.232536	1.383025
O	-1.822518	4.120340	0.086096
C	-1.205955	0.562002	-0.618763
C	0.039769	0.361668	-0.014953
C	0.765611	-0.923671	-0.103619
C	0.146020	-2.127270	-0.031460
H	0.766606	-3.019500	-0.085588
C	-1.288308	-2.366642	0.108664
C	-2.237292	-1.527908	-0.500496
C	0.574584	1.472489	0.695750
C	-0.062172	2.710267	0.701637
H	0.343233	3.561780	1.232413
C	-1.282497	2.869598	0.029294
C	-1.874824	1.787992	-0.621905
H	-2.823893	1.854288	-1.136635
C	-3.604055	-1.770540	-0.399872
H	-4.292992	-1.097348	-0.900600
C	-4.057978	-2.881752	0.313722
H	-5.123813	-3.078947	0.386931
C	-3.136508	-3.743673	0.917097
H	-3.481942	-4.614694	1.466814
C	-1.770937	-3.488391	0.807357
H	-1.053294	-4.161695	1.270032
C	2.237785	-0.883470	-0.322467
C	3.106228	-1.741900	0.367195
H	2.703849	-2.409534	1.124012
C	4.479739	-1.718658	0.119992
H	5.137215	-2.385372	0.672305
C	5.010410	-0.833695	-0.822154
H	6.079960	-0.813618	-1.013835
C	4.153712	0.028847	-1.513221
H	4.554731	0.718967	-2.251335
C	2.782580	0.005990	-1.262265
H	2.119798	0.678136	-1.800619
C	2.420265	2.323333	1.965767
H	1.837981	2.781882	2.775206
H	2.665532	3.081413	1.211563
H	3.339255	1.898050	2.371467
C	-3.071884	4.340598	-0.556799
H	-3.857481	3.710862	-0.120308
H	-3.001862	4.146856	-1.634587
H	-3.309996	5.391845	-0.388595

## 7.3 Atomic coordinates for DFT calculations

**Table S32:** Atomic coordinates (x, y, z) for optimized minimum and transition state of **147c** at the B3LYP-D3(BJ)/6-31+g(d) level of theory.

Minimum				TS			
Atom	x	y	z	Atom	x	y	z
O	2.280795	0.680522	-1.344024	O	-5.790621	-0.760877	0.108269
O	-5.832675	-0.137140	-0.821653	C	-4.421228	-0.711940	0.069022
O	-0.897276	-1.472098	1.482172	C	-3.614874	-0.243461	1.114030
O	2.932205	-3.876847	0.021988	H	-4.048010	0.104906	2.044852
C	2.595971	1.775088	-0.541637	C	-2.225769	-0.235056	0.961279
C	1.572639	2.484560	0.109997	H	-1.605880	0.133385	1.775022
C	0.176071	2.066322	0.018007	C	-1.616864	-0.677770	-0.215727
H	-0.553180	2.873459	-0.012635	C	-2.438702	-1.158124	-1.243868
C	-0.290076	0.793882	-0.036757	H	-1.984262	-1.506663	-2.167207
C	-1.750285	0.562896	-0.193714	C	-3.824231	-1.173815	-1.110454
C	-2.697550	1.309890	0.512419	H	-4.461677	-1.539222	-1.910017
H	-2.363024	2.041857	1.242249	C	-0.119440	-0.719003	-0.325131
C	-4.070641	1.112636	0.334069	C	1.733196	-2.495669	-0.109929
H	-4.770059	1.706329	0.911480	C	1.882976	-3.888338	0.050762
C	-4.516915	0.143438	-0.570624	H	0.987251	-4.502796	0.004454
C	-3.580579	-0.619301	-1.284508	C	3.120281	-4.491276	0.264850
H	-3.941919	-1.364899	-1.986413	H	3.188547	-5.569419	0.376140
C	-2.222116	-0.411833	-1.091896	C	4.262735	-3.693337	0.339170
H	-1.506206	-1.008993	-1.650003	H	5.239907	-4.136702	0.508050
C	0.598346	-0.388215	0.019160	C	4.145341	-2.310313	0.192527
C	0.241712	-1.559272	0.745450	H	5.015619	-1.663210	0.237427
C	1.032632	-2.704572	0.717837	C	2.901539	-1.721698	-0.035281
H	0.762850	-3.601449	1.259959	C	2.044004	0.639367	-0.107240
C	2.233980	-2.705688	-0.005321	C	2.692897	1.850946	0.149671
C	2.654483	-1.556586	-0.673753	H	3.761353	1.815328	0.312997
H	3.582339	-1.499129	-1.226787	C	1.974158	3.044490	0.133152
C	1.833805	-0.427048	-0.636049	C	0.620606	3.028450	-0.204109
C	1.937252	3.655388	0.799858	H	0.098461	3.970796	-0.300969
H	1.159074	4.231104	1.295316	C	-0.007613	1.811283	-0.460351
C	3.263191	4.080104	0.860622	C	0.648320	0.546229	-0.309867
H	3.517136	4.985456	1.404794	C	-6.441128	-0.318959	1.289004
C	4.262196	3.343597	0.215841	H	-6.227997	0.739561	1.490933
H	5.296834	3.673038	0.251184	H	-6.144695	-0.921498	2.157992
C	3.924396	2.186874	-0.489918	H	-7.509593	-0.445635	1.106418
H	4.672780	1.607548	-1.021799	C	0.380811	-1.978847	-0.266583
C	-6.820047	0.619065	-0.137509	H	-0.370411	-2.763988	-0.229969
H	-7.781510	0.244557	-0.492633	O	2.515814	4.269109	0.380497
H	-6.734632	1.688706	-0.370476	O	-1.282018	1.772799	-0.924647
H	-6.750443	0.475844	0.949081	C	3.902006	4.341700	0.693371
C	-1.418627	-2.644932	2.089426	H	4.133877	3.765204	1.597527
H	-1.595682	-3.429435	1.343145	H	4.515324	3.979706	-0.141283
H	-2.366656	-2.344540	2.537882	H	4.110099	5.398138	0.868541
H	-0.745681	-3.022460	2.869996	C	-2.108846	2.922842	-0.831470

## 7. Appendix

C	4.171115	-3.934157	-0.673784	H	-1.773666	3.712432	-1.515989
H	4.031449	-3.750225	-1.746536	H	-3.104876	2.585094	-1.121489
H	4.549295	-4.946165	-0.522178	H	-2.132938	3.308672	0.195102
H	4.887132	-3.208902	-0.266778	O	2.978388	-0.364818	-0.252806

**Table S 33:** Atomic coordinates (x, y, z) for optimized minimum and transition state of **147i** at the B3LYP-D3(BJ)/6-31+g(d) level of theory.

Minimum				TS			
Atom	x	y	z	Atom	x	y	z
O	5.762762	-1.168571	-1.338865	O	-6.199181	-0.098531	-0.471842
C	4.595870	-0.562441	-0.968666	C	-4.859020	0.113338	-0.306514
C	4.508721	0.516040	-0.080296	C	-3.923219	0.124921	-1.347439
H	5.394735	0.935964	0.381536	H	-4.223744	-0.034540	-2.376458
C	3.257011	1.054384	0.230587	C	-2.574406	0.342846	-1.053746
H	3.204587	1.878434	0.937117	H	-1.850143	0.349676	-1.863789
C	2.077161	0.537842	-0.316285	C	-2.127208	0.540195	0.256337
C	2.189409	-0.548560	-1.205220	C	-3.087058	0.567822	1.278418
H	1.289452	-0.971387	-1.641036	H	-2.778739	0.779018	2.298172
C	3.424626	-1.088411	-1.533619	C	-4.433509	0.345929	1.008985
H	3.507462	-1.922692	-2.223361	H	-5.174905	0.361913	1.801892
C	0.741442	1.123888	-0.036333	C	-0.688945	0.919128	0.477871
C	-0.692821	3.169135	0.027115	C	0.669180	3.088499	0.078615
C	-0.880461	4.371147	0.729325	C	0.595085	4.308432	-0.623606
H	-0.056068	4.769772	1.315839	H	-0.350014	4.592444	-1.080344
C	-2.098791	5.048248	0.685251	C	1.702565	5.145111	-0.735594
H	-2.225068	5.972567	1.241990	H	1.622279	6.079971	-1.282893
C	-3.152909	4.540610	-0.081346	C	2.913934	4.785810	-0.132188
H	-4.101504	5.068426	-0.125435	H	3.776916	5.441831	-0.204595
C	-2.983302	3.356608	-0.802911	C	3.012579	3.584345	0.572841
H	-3.776677	2.950574	-1.422794	H	3.933125	3.285622	1.064628
C	-1.763795	2.688352	-0.746177	C	1.898225	2.755808	0.663589
C	-1.486953	0.375310	-0.823190	C	1.730073	0.426022	0.715757
C	-2.472085	-0.572844	-1.048438	C	2.856987	-0.234825	0.262717
H	-3.245046	-0.339969	-1.772922	H	3.815158	0.262139	0.373640
C	-2.440060	-1.785097	-0.352887	C	2.736884	-1.511702	-0.290453
C	-1.455563	-1.928470	0.629047	C	1.485202	-2.119661	-0.159902
H	-1.469422	-2.823825	1.231051	H	1.408206	-3.160369	-0.431715
C	-0.463218	-0.970369	0.899995	C	0.335036	-1.500114	0.359454
C	-0.407816	0.176272	0.060718	C	0.407758	-0.076700	0.583416
C	0.424771	-1.203500	2.153528	C	-6.682635	-0.338280	-1.785717
C	1.666946	-2.063209	1.829632	H	-6.227294	-1.238566	-2.218865
H	1.372229	-2.998888	1.340109	H	-6.492364	0.520340	-2.442926
H	2.191172	-2.317913	2.759640	H	-7.758716	-0.487033	-1.683829
H	2.369357	-1.546190	1.176307	C	-0.511256	2.253275	0.216694
C	0.856882	0.123624	2.812167	H	-1.427937	2.791111	-0.014784
H	1.561946	0.688909	2.207172	O	1.959474	1.609368	1.424567

## 7.3 Atomic coordinates for DFT calculations

H	1.347147	-0.091627	3.768943	C	-0.782705	-2.465261	0.873149
H	-0.010626	0.763570	3.009918	C	3.957015	-2.218422	-0.888478
C	-0.384441	-1.960961	3.239017	C	3.608284	-3.599355	-1.469477
H	-1.344679	-1.472366	3.438808	H	3.261425	-4.293487	-0.695431
H	0.192907	-1.972501	4.170132	H	2.833288	-3.529451	-2.241537
H	-0.577784	-3.005190	2.975009	H	4.500227	-4.039482	-1.929849
C	-3.492414	-2.862811	-0.642994	C	5.032826	-2.407563	0.204457
C	-3.402716	-3.267980	-2.131315	H	5.914057	-2.911288	-0.212021
H	-3.577372	-2.414276	-2.794262	H	5.359737	-1.448856	0.620524
H	-4.153154	-4.033910	-2.363061	H	4.646234	-3.017265	1.029163
H	-2.412526	-3.676379	-2.364248	C	4.532955	-1.345535	-2.026094
C	-3.293299	-4.125768	0.212204	H	5.415608	-1.826459	-2.465713
H	-2.310646	-4.580697	0.042200	H	3.790315	-1.200018	-2.819005
H	-4.054041	-4.869580	-0.050759	H	4.833190	-0.356802	-1.663781
H	-3.394722	-3.914250	1.282867	C	-1.191997	-2.013782	2.293055
C	-4.900232	-2.297254	-0.350511	H	-1.536211	-0.983670	2.321844
H	-4.987095	-1.994262	0.699267	H	-2.002654	-2.650441	2.668291
H	-5.665073	-3.057104	-0.553543	H	-0.340959	-2.101383	2.978574
H	-5.122583	-1.423258	-0.971501	C	-0.214878	-3.898474	1.059273
C	6.978485	-0.672623	-0.796982	H	-0.055073	-4.418056	0.107867
H	6.993417	-0.765231	0.296941	H	0.723224	-3.903314	1.623663
H	7.140459	0.376226	-1.078043	H	-0.949413	-4.485380	1.622030
H	7.768825	-1.290806	-1.225441	C	-2.021631	-2.633606	-0.036769
C	0.589941	2.467377	-0.012098	H	-2.743355	-1.831154	0.071737
H	1.477406	3.092468	-0.093910	H	-1.727625	-2.694064	-1.090642
O	-1.583931	1.562840	-1.544941	H	-2.532922	-3.568894	0.222450

**Table S 34:** Atomic coordinates (x, y, z) for optimized minimum of **147k** at the B3LYP-D3(BJ)/6-31+g(d) level of theory.

Minimum			
Atom	x	y	z
O	1.828493	-0.449352	-1.334168
O	1.734401	4.158799	0.023748
O	-1.652314	1.163503	1.488427
C	1.205533	0.579058	-0.639257
C	-0.011331	0.345129	0.008116
C	-0.032361	-2.145358	0.038512
H	-0.618934	-3.061744	0.018676
C	1.412889	-2.325992	0.144887
C	2.310768	-1.468590	-0.515433
C	-0.549796	1.438489	0.743016
C	0.047965	2.695804	0.717405
H	-0.359522	3.536331	1.263764
C	1.233712	2.890835	-0.005922
C	1.835509	1.825021	-0.674167
H	2.763612	1.917361	-1.222021

## 7. Appendix

C	3.688012	-1.659290	-0.453654
H	4.335290	-0.974222	-0.992384
C	4.205333	-2.735092	0.270901
H	5.279515	-2.891573	0.313862
C	3.336148	-3.614151	0.925118
H	3.731033	-4.457759	1.484169
C	1.959355	-3.411434	0.854181
H	1.282458	-4.098480	1.356342
C	2.949621	4.415538	-0.669070
H	3.159096	5.475226	-0.516555
H	2.843968	4.211804	-1.742102
H	3.772218	3.815227	-0.260135
C	-2.337284	2.230749	2.127463
H	-1.713903	2.698478	2.900210
H	-3.215469	1.778428	2.590218
H	-2.653238	2.988610	1.399628
C	-0.695181	-0.965597	-0.052961
C	-2.160159	-0.974071	-0.258629
C	-3.069418	-1.924150	0.321497
C	-2.817917	-0.079771	-1.070491
C	-4.369142	-1.727036	-0.055138
H	-2.760956	-2.697825	1.015946
S	-4.522139	-0.376028	-1.136806
H	-2.383943	0.738068	-1.629806
H	-5.245177	-2.285635	0.246768

**Table S35:** Atomic coordinates (x, y, z) for optimized minimum and transition state of **148a** at the B3LYP-D3(BJ)/6-31+g(d) level of theory.

Minimum				TS			
Atom	x	y	z	Atom	x	y	z
S	2.240080	-0.443785	-1.834845	O	5.649135	-1.388810	-0.336760
O	2.058877	4.313179	0.193214	C	4.299446	-1.176382	-0.229009
O	-0.971442	1.056193	1.866328	C	3.533463	-0.455890	-1.152733
O	-5.896612	-0.809832	-0.397253	H	3.982286	-0.026316	-2.041238
C	2.776875	-1.649298	-0.622839	C	2.161213	-0.296104	-0.935442
C	1.833142	-2.334188	0.171900	H	1.574410	0.265778	-1.657717
C	0.393413	-2.068885	0.099477	C	1.529428	-0.837131	0.187532
H	-0.233269	-2.959402	0.098874	C	2.311490	-1.567878	1.093852
C	-0.238320	-0.871518	0.053793	H	1.842675	-1.988068	1.979409
C	0.456951	0.437832	0.098435	C	3.678061	-1.734920	0.895876
C	1.542936	0.772666	-0.721613	H	4.284328	-2.291122	1.604647
C	2.118435	2.053028	-0.724600	C	0.039531	-0.696879	0.355247
H	2.958443	2.247006	-1.378333	C	-1.973387	-2.372609	0.126262
C	1.598198	3.030463	0.121702	C	-2.120097	-3.776756	0.066827
C	0.548655	2.721149	0.998775	H	-1.230719	-4.386095	0.206168
H	0.204797	3.492910	1.675398	C	-3.341775	-4.400816	-0.164427

## 7.3 Atomic coordinates for DFT calculations

C	0.003666	1.441435	0.999811	H	-3.402924	-5.484971	-0.188294
C	-1.721594	-0.834796	-0.051565	C	-4.475123	-3.617327	-0.383085
C	-2.343140	0.098337	-0.888865	H	-5.439141	-4.075347	-0.585262
H	-1.730652	0.803620	-1.443742	C	-4.360872	-2.228113	-0.350636
C	-3.731638	0.140351	-1.040204	H	-5.238213	-1.612313	-0.531006
H	-4.169502	0.872410	-1.709091	C	-3.135510	-1.603521	-0.076918
C	-4.530708	-0.764375	-0.331990	C	-1.790600	1.076120	-0.014054
C	-3.926353	-1.699423	0.520750	C	-2.097420	2.409973	-0.326440
H	-4.560214	-2.382939	1.077624	H	-3.094013	2.647536	-0.676541
C	-2.544493	-1.729018	0.655329	C	-1.144041	3.413334	-0.138507
H	-2.094334	-2.436345	1.345981	C	0.087569	3.095038	0.432663
C	2.304015	-3.356021	1.017615	H	0.776154	3.895266	0.670921
H	1.585976	-3.901352	1.625463	C	0.381438	1.764030	0.722039
C	3.658486	-3.671014	1.094003	C	-0.491266	0.684642	0.378158
H	3.993278	-4.461678	1.759976	C	6.320597	-0.854262	-1.466560
C	4.582643	-2.969767	0.313358	H	6.240963	0.240871	-1.497767
H	5.640988	-3.210244	0.364857	H	5.925863	-1.274216	-2.401329
C	4.139107	-1.959437	-0.540161	H	7.368000	-1.139121	-1.353754
H	4.843877	-1.409774	-1.156931	C	-0.601002	-1.894742	0.278500
C	3.144434	4.682445	-0.648008	H	0.092874	-2.729287	0.212691
H	2.881777	4.566488	-1.707167	O	-1.347053	4.727727	-0.431609
H	4.038732	4.087058	-0.424487	O	1.502194	1.429377	1.410595
H	3.341492	5.733624	-0.432647	C	-2.607044	5.114996	-0.968233
C	-1.595704	2.036659	2.681773	H	-2.806643	4.603981	-1.918292
H	-2.031714	2.837331	2.071089	H	-3.419179	4.907458	-0.260255
H	-0.887322	2.465835	3.402045	H	-2.536836	6.190183	-1.138409
H	-2.387575	1.510766	3.217041	C	2.621725	2.306019	1.406835
C	-6.556956	0.115514	-1.247626	H	2.437116	3.191546	2.027831
H	-6.251954	-0.017380	-2.293966	H	3.444427	1.727371	1.829456
H	-6.360333	1.150930	-0.939075	H	2.873117	2.611995	0.384660
H	-7.622639	-0.097458	-1.149182	S	-3.316481	0.154599	0.110611

**Table S36:** Atomic coordinates (x, y, z) for optimized minimum and transition state of **149a** at the B3LYP-D3(BJ)/6-31+g(d) level of theory.

Minimum				TS			
Atom	x	y	z	Atom	x	y	z
Si	-2.355902	-0.587001	1.458931	Si	-3.118538	0.303544	0.161240
O	-1.990416	4.428711	0.177980	O	-0.833573	4.714897	-0.831875
O	1.242659	1.363380	-1.748562	O	1.815635	1.300404	1.319303
O	5.878389	-0.610355	1.017533	O	5.732509	-1.924509	-0.129944
C	-1.475050	0.849393	0.623243	C	-1.491362	1.186575	-0.175853
C	-0.340559	0.595282	-0.180373	C	-0.220392	0.699340	0.249859
C	0.206688	1.670819	-0.916142	C	0.748786	1.692808	0.571859
C	-0.312201	2.967045	-0.819328	C	0.598969	3.034963	0.202182
H	0.124216	3.769612	-1.396539	H	1.382322	3.743371	0.433014
C	-1.415331	3.199909	0.009035	C	-0.587422	3.443307	-0.404202

7. Appendix

C	-2.000465	2.143105	0.710083	C	-1.641581	2.530663	-0.526666
H	-2.869300	2.359303	1.323251	H	-2.590812	2.917146	-0.880539
C	0.339999	-0.726668	-0.245110	C	0.175144	-0.726450	0.277546
C	-0.253532	-1.918124	-0.502624	C	-0.543769	-1.886795	0.174572
H	0.410400	-2.782032	-0.526190	H	0.116787	-2.750342	0.149160
C	-1.664592	-2.250833	-0.761911	C	-1.923769	-2.333906	-0.025390
C	-1.945675	-3.167212	-1.792412	C	-2.062371	-3.737791	-0.157804
H	-1.124113	-3.563240	-2.385483	H	-1.176560	-4.360104	-0.056637
C	-3.253126	-3.555628	-2.074863	C	-3.284574	-4.341509	-0.424772
H	-3.448378	-4.253190	-2.885399	H	-3.345992	-5.422720	-0.517584
C	-4.308685	-3.047982	-1.312052	C	-4.424047	-3.549392	-0.581678
H	-5.331942	-3.348573	-1.522197	H	-5.388258	-4.001086	-0.799261
C	-4.037026	-2.163301	-0.267320	C	-4.307966	-2.166048	-0.450318
H	-4.864211	-1.789245	0.331189	H	-5.204166	-1.562990	-0.567915
C	-2.726850	-1.757227	0.035233	C	-3.084547	-1.533669	-0.164296
C	1.804556	-0.713409	0.034879	C	1.657357	-0.999641	0.186873
C	2.315872	0.097830	1.064484	C	2.342069	-1.728849	1.170036
H	1.634449	0.724082	1.633284	H	1.806735	-2.050434	2.059197
C	3.670059	0.108641	1.373205	C	3.695835	-2.020377	1.040544
H	4.058651	0.727360	2.176586	H	4.226787	-2.576129	1.807779
C	4.563031	-0.691788	0.647119	C	4.402106	-1.594113	-0.092436
C	4.078944	-1.498015	-0.389576	C	3.733374	-0.880332	-1.092888
H	4.747634	-2.112799	-0.981308	H	4.247620	-0.554226	-1.990012
C	2.712267	-1.498665	-0.683279	C	2.371888	-0.593693	-0.942797
H	2.355058	-2.100710	-1.513977	H	1.859053	-0.040412	-1.725562
C	-3.966120	0.009524	2.240636	C	-4.517510	1.104610	-0.825983
H	-4.629097	0.490118	1.512089	H	-4.345413	1.037100	-1.906596
H	-3.765961	0.732007	3.041294	H	-4.636418	2.161857	-0.564136
H	-4.510479	-0.830163	2.690132	H	-5.474808	0.617738	-0.607588
C	-1.293311	-1.396291	2.792315	C	-3.440257	0.557152	2.007576
H	-1.805831	-2.270581	3.212845	H	-4.387576	0.091755	2.307884
H	-1.107984	-0.689128	3.610797	H	-3.482708	1.623995	2.259349
H	-0.325611	-1.724516	2.402211	H	-2.638125	0.101550	2.600381
C	-1.431641	5.538762	-0.507870	C	0.196071	5.683991	-0.693623
H	-0.387270	5.705411	-0.212368	H	0.444168	5.852342	0.362621
H	-2.033389	6.401461	-0.217563	H	-0.201417	6.604242	-1.124147
H	-1.487801	5.404867	-1.596348	H	1.099629	5.382974	-1.239497
C	1.991332	2.411234	-2.342159	C	3.036570	2.024278	1.249888
H	2.822807	1.924628	-2.854607	H	3.783298	1.383331	1.721313
H	2.381806	3.098931	-1.580934	H	2.971694	2.973789	1.797202
H	1.391431	2.970183	-3.072848	H	3.320522	2.211194	0.207588
C	6.819831	-1.413389	0.322350	C	6.483647	-1.536175	-1.268782
H	6.586714	-2.481342	0.426738	H	6.083522	-1.990369	-2.185131
H	7.787024	-1.205085	0.782764	H	7.498091	-1.899563	-1.095857
H	6.858264	-1.151306	-0.743464	H	6.501493	-0.443666	-1.382948



## 7.3 Atomic coordinates for DFT calculations

**Table S37:** Atomic coordinates (x, y, z) for optimized minimum and transition state of **149a** at the B3LYP-D3(BJ)/6-31+g(d) level of theory with scrf=(cpcm,solvent=chloroform).

Minimum				TS			
Atom	x	y	z	Atom	x	y	z
Si	-2.318814	-0.630890	1.478811	Si	-3.119243	0.314719	0.175884
O	-2.050054	4.400530	0.229625	O	-0.813362	4.709360	-0.848979
O	1.197999	1.404546	-1.774678	O	1.819394	1.297484	1.322677
O	5.889832	-0.568711	1.018749	O	5.723554	-1.968348	-0.140181
C	-1.468535	0.826015	0.643408	C	-1.487930	1.187432	-0.175105
C	-0.343697	0.596962	-0.181492	C	-0.216852	0.697335	0.249838
C	0.171777	1.686797	-0.921692	C	0.754957	1.690159	0.572907
C	-0.368352	2.973288	-0.807891	C	0.609190	3.031338	0.197184
H	0.043796	3.787772	-1.385563	H	1.394273	3.739363	0.420857
C	-1.459254	3.182296	0.043022	C	-0.575030	3.440576	-0.413200
C	-2.014720	2.110529	0.747734	C	-1.634433	2.531003	-0.529999
H	-2.876626	2.304618	1.378332	H	-2.585392	2.918295	-0.878941
C	0.354860	-0.715550	-0.264043	C	0.173435	-0.730126	0.272072
C	-0.227860	-1.910164	-0.533629	C	-0.552926	-1.887264	0.164509
H	0.442068	-2.768425	-0.574785	H	0.101790	-2.754914	0.134828
C	-1.639213	-2.251708	-0.782822	C	-1.935608	-2.327054	-0.036733
C	-1.924199	-3.153996	-1.825780	C	-2.079142	-3.730363	-0.181443
H	-1.106831	-3.534168	-2.434619	H	-1.196060	-4.357609	-0.087599
C	-3.232330	-3.550968	-2.097593	C	-3.304927	-4.327435	-0.450996
H	-3.431401	-4.236944	-2.916838	H	-3.370407	-5.407417	-0.553222
C	-4.283024	-3.067105	-1.311295	C	-4.442691	-3.529310	-0.597970
H	-5.305760	-3.375082	-1.512528	H	-5.408996	-3.975608	-0.816653
C	-4.006259	-2.197527	-0.254007	C	-4.321625	-2.146803	-0.454012
H	-4.828972	-1.844135	0.362674	H	-5.216367	-1.540223	-0.562167
C	-2.695613	-1.782280	0.037903	C	-3.094493	-1.521123	-0.165182
C	1.819301	-0.690577	0.016708	C	1.654167	-1.011650	0.181877
C	2.324396	0.136790	1.037061	C	2.320745	-1.793539	1.136776
H	1.640915	0.770743	1.594503	H	1.774774	-2.153477	2.004729
C	3.677660	0.153898	1.353322	C	3.673307	-2.095534	1.006942
H	4.056957	0.788192	2.149296	H	4.186435	-2.691236	1.756518
C	4.576692	-0.656121	0.643930	C	4.396311	-1.626003	-0.098427
C	4.098876	-1.479205	-0.383458	C	3.745280	-0.859289	-1.072128
H	4.771105	-2.102066	-0.961958	H	4.273120	-0.494183	-1.945589
C	2.733555	-1.486460	-0.684051	C	2.386459	-0.563479	-0.921608
H	2.384928	-2.107374	-1.504408	H	1.892374	0.035822	-1.682129
C	-3.922244	-0.067641	2.293185	C	-4.525369	1.129238	-0.785696
H	-4.604396	0.412785	1.582538	H	-4.369070	1.067748	-1.869108
H	-3.715677	0.646272	3.099770	H	-4.632654	2.185130	-0.513860
H	-4.444868	-0.922857	2.738915	H	-5.480664	0.644707	-0.554231
C	-1.223347	-1.449167	2.779359	C	-3.413130	0.552408	2.029179
H	-1.723606	-2.331820	3.197192	H	-4.362539	0.093790	2.333378
H	-1.031729	-0.748997	3.602332	H	-3.444708	1.617832	2.288746
H	-0.259910	-1.763520	2.367657	H	-2.608450	0.084393	2.609082

## 7. Appendix

C	-1.517114	5.529033	-0.461145	C	0.228249	5.677525	-0.720677
H	-0.471740	5.705599	-0.180771	H	0.475569	5.851204	0.333295
H	-2.126796	6.379287	-0.153542	H	-0.164753	6.594869	-1.159789
H	-1.591524	5.398308	-1.547418	H	1.125982	5.361914	-1.265010
C	1.872957	2.474945	-2.428881	C	3.026206	2.057593	1.295812
H	2.693573	2.011768	-2.978128	H	3.774726	1.433038	1.784895
H	2.274095	3.190216	-1.701019	H	2.917285	2.998341	1.848112
H	1.209885	2.993371	-3.131988	H	3.333517	2.261292	0.264287
C	6.840915	-1.376855	0.328940	C	6.497437	-1.513465	-1.246865
H	6.611373	-2.442950	0.445676	H	6.109556	-1.912951	-2.192034
H	7.805423	-1.157678	0.788428	H	7.507345	-1.889670	-1.078603
H	6.875543	-1.122741	-0.737427	H	6.516501	-0.417512	-1.292602

**Table S38:** Atomic coordinates (x, y, z) for optimized minimum of **149e** at the B3LYP-D3(BJ)/6-31+g(d) level of theory.

Minimum			
Atom	x	y	z
Si	-2.187711	-0.470969	0.715012
O	-1.303717	4.578573	-0.121512
O	1.927989	1.414778	-1.876875
O	6.112976	-0.724676	1.366781
C	-1.102747	0.944233	0.093409
C	0.121310	0.666976	-0.560675
C	0.819175	1.744548	-1.153926
C	0.379746	3.066848	-1.032433
H	0.935801	3.868545	-1.497341
C	-0.796156	3.325188	-0.322320
C	-1.535562	2.269413	0.214744
H	-2.448417	2.519089	0.739329
C	0.770155	-0.671002	-0.574806
C	0.195544	-1.845479	-0.928195
H	0.846796	-2.717720	-0.879254
C	-1.169350	-2.171291	-1.369149
C	-1.293915	-3.128179	-2.395603
H	-0.391282	-3.525374	-2.854977
C	-2.540637	-3.562965	-2.834721
H	-2.610815	-4.291870	-3.638067
C	-3.696135	-3.067412	-2.225557
H	-4.676939	-3.411296	-2.543879
C	-3.582224	-2.138472	-1.190925
H	-4.492673	-1.788677	-0.714272
C	-2.336344	-1.665192	-0.742294
C	2.189231	-0.700622	-0.112250
C	2.590110	0.077097	0.989504
H	1.861104	0.711936	1.483961
C	3.895459	0.046360	1.462908

## 7.3 Atomic coordinates for DFT calculations

H	4.195663	0.639367	2.321667
C	4.851965	-0.763953	0.835463
C	4.479998	-1.537208	-0.270154
H	5.201365	-2.158426	-0.788789
C	3.160416	-1.495504	-0.729888
H	2.895196	-2.071018	-1.612189
C	-3.948503	0.107774	1.184380
H	-4.487840	-0.843840	1.318614
C	-1.343252	-1.392421	2.156574
H	-0.501906	-1.916776	1.684819
C	-0.587128	5.689626	-0.638705
H	0.422107	5.747244	-0.209948
H	-1.157100	6.573194	-0.347181
H	-0.518542	5.645137	-1.733761
C	2.852719	2.430593	-2.231024
H	3.712706	1.910348	-2.655960
H	3.168086	3.000887	-1.348004
H	2.433774	3.112502	-2.983067
C	7.113043	-1.540244	0.775807
H	6.842352	-2.603143	0.827809
H	8.020725	-1.366742	1.356179
H	7.289453	-1.259956	-0.271311
C	-2.267262	-2.459647	2.769110
H	-3.128650	-2.008610	3.277504
H	-2.653141	-3.147606	2.006918
H	-1.729136	-3.060408	3.515459
C	-0.753616	-0.462205	3.230281
H	-0.178289	-1.037949	3.968494
H	-0.080039	0.282106	2.792256
H	-1.533251	0.081300	3.776021
C	-4.049341	0.855875	2.527951
H	-5.092765	1.133152	2.733416
H	-3.702133	0.244327	3.366049
H	-3.461661	1.781111	2.531909
C	-4.684200	0.892880	0.077581
H	-5.758227	0.952622	0.302474
H	-4.313604	1.919231	-0.001232
H	-4.573750	0.437785	-0.911510

**Table S 39:** Atomic coordinates (x, y, z) for optimized minimum and transition state of **202a** at the B3LYP-D3(BJ)/6-31+g(d) level of theory.

Minimum				TS			
Atom	x	y	z	Atom	x	y	z
O	0.000017	-0.780602	1.072761	C	-0.672304	1.916794	-0.000045
C	-1.185223	-0.495942	0.406756	C	1.607297	0.793458	0.000006
C	-1.556868	0.831862	0.125624	C	2.981634	1.104053	0.000026

## 7. Appendix

C	-0.675286	1.972859	0.364885	H	3.260541	2.154930	0.000035
H	-1.177575	2.932770	0.470468	C	3.978288	0.131419	0.000031
C	0.675173	1.972996	0.364760	H	5.024726	0.421059	0.000048
C	1.556730	0.831908	0.125362	C	3.607499	-1.213057	0.000008
C	2.839320	1.043058	-0.414465	H	4.359484	-1.996911	0.000006
C	3.703220	-0.016536	-0.683449	C	2.255448	-1.554706	-0.000011
H	4.686525	0.178566	-1.101597	H	1.939641	-2.592987	-0.000026
C	3.300767	-1.326366	-0.408105	C	1.261693	-0.573147	-0.000009
C	2.038273	-1.563042	0.139792	C	-1.261690	-0.573146	-0.000019
H	1.708069	-2.566455	0.389469	C	-2.255445	-1.554705	-0.000027
C	1.185222	-0.495872	0.406843	H	-1.939636	-2.592986	-0.000048
C	-2.839534	1.043028	-0.414024	C	-3.607497	-1.213059	0.000002
H	-3.150946	2.062811	-0.627227	C	-3.978288	0.131417	0.000040
C	-3.703262	-0.016635	-0.683276	H	-5.024726	0.421057	0.000070
H	-4.686665	0.178411	-1.101224	C	-2.981634	1.104049	0.000038
C	-3.300565	-1.326507	-0.408463	C	-1.607296	0.793457	0.000002
H	-3.968445	-2.160092	-0.606392	C	0.672294	1.916799	-0.000031
C	-2.038006	-1.563198	0.139295	H	1.156768	2.890882	-0.000076
H	-1.707631	-2.566647	0.388590	O	0.000001	-1.126463	-0.000004
H	3.968786	-2.159929	-0.605652	H	-4.359480	-1.996915	-0.000004
H	3.150589	2.062812	-0.628006	H	-3.260542	2.154926	0.000056
H	1.177393	2.932882	0.470278	H	-1.156782	2.890871	-0.000095

**Table S40:** Atomic coordinates (x, y, z) for optimized minimum and transition state of **202b** at the B3LYP-D3(BJ)/6-31+g(d) level of theory.

Minimum				TS			
Atom	x	y	z	Atom	x	y	z
C	4.857446	-1.212415	-0.233125	C	-4.647880	-1.700672	0.065616
C	4.030309	-1.959562	0.60868	C	-3.892626	-1.811770	-1.103422
H	4.448308	-2.758793	1.21515	H	-4.324752	-2.265677	-1.991400
C	2.665627	-1.67455	0.68537	C	-2.577411	-1.338820	-1.136508
H	2.030958	-2.24264	1.359872	H	-1.989312	-1.420658	-2.046693
C	2.102067	-0.640907	-0.079426	C	-2.001165	-0.750053	-0.003694
C	2.947557	0.112195	-0.912048	C	-2.768819	-0.641349	1.165958
H	2.526352	0.918552	-1.505599	H	-2.328362	-0.186342	2.049312
C	4.309677	-0.17456	-0.993509	C	-4.080813	-1.114869	1.202109
H	4.944471	0.411746	-1.652667	H	-4.659660	-1.030191	2.118120
C	0.641486	-0.355438	-0.035318	C	-0.576095	-0.285076	-0.031089
C	-0.231168	-1.392779	-0.090528	C	0.350307	-1.268427	-0.025203
C	-1.689013	-1.343074	-0.028385	C	1.808746	-1.231884	0.002691
C	-2.429886	-0.262068	-0.53716	C	2.610133	-0.076678	-0.000121
C	-3.820814	-0.240505	-0.490544	C	4.002462	-0.174482	0.052315
H	-4.343635	0.613035	-0.910557	H	4.575743	0.746999	0.046974
C	-4.512141	-1.319008	0.064978	C	4.633157	-1.417084	0.104596
H	-5.598018	-1.307663	0.094094	H	5.717521	-1.468142	0.143066
C	-3.80302	-2.414918	0.566737	C	3.863830	-2.581095	0.106428

## 7.3 Atomic coordinates for DFT calculations

H	-4.333868	-3.261264	0.993144	H	4.333825	-3.559079	0.146455
C	-2.410981	-2.424033	0.512105	C	2.476541	-2.472151	0.058002
H	-1.858622	-3.278839	0.895063	H	1.868250	-3.373216	0.063038
C	-0.970482	1.563769	-0.391774	C	0.932098	1.804187	-0.046039
C	0.228015	1.054141	0.137842	C	-0.334473	1.175740	-0.049353
C	1.026953	1.942849	0.883782	C	-1.452160	2.037541	-0.090288
C	0.653049	3.269328	1.085445	C	-1.350338	3.426347	-0.099225
C	-0.539366	3.749528	0.536624	C	-0.088378	4.014951	-0.068857
H	-0.833579	4.785662	0.678455	H	0.026864	5.095097	-0.070677
C	-1.353218	2.889684	-0.20086	C	1.039124	3.197991	-0.045764
H	-2.281443	3.230296	-0.648724	H	2.038354	3.621117	-0.036753
H	0.190483	-2.393976	-0.154537	H	-0.046989	-2.280767	-0.005965
H	5.920003	-1.431927	-0.292194	H	-5.670087	-2.068321	0.093309
H	1.955027	1.575795	1.309792	H	-2.438237	1.591585	-0.119840
H	1.292776	3.926827	1.667157	H	-2.249964	4.033604	-0.130948
O	-1.783974	0.775891	-1.197723	O	2.183671	1.226237	-0.075865

**Table S41:** Atomic coordinates (x, y, z) for optimized minimum and transition state of **202c** at the B3LYP-D3(BJ)/6-31+g(d) level of theory.

Minimum				TS			
Atom	x	y	z	Atom	x	y	z
O	-2.590993	0.576928	-1.187346	O	5.535402	-0.997332	0.329436
O	5.659019	-0.269295	-0.408121	C	4.198650	-0.743682	0.198196
C	-3.053189	-0.558055	-0.531918	C	3.592068	-0.277452	-0.975235
C	-2.140608	-1.507377	-0.039730	H	4.172000	-0.093903	-1.872318
C	-0.695031	-1.317323	-0.115717	C	2.212938	-0.049835	-0.994377
H	-0.116260	-2.235280	-0.197842	H	1.749071	0.311550	-1.908541
C	-0.002073	-0.152075	-0.050893	C	1.417198	-0.280464	0.132400
C	1.483459	-0.190663	-0.097484	C	2.044135	-0.748348	1.297985
C	2.217039	-1.126935	0.640031	H	1.444106	-0.929268	2.185726
H	1.693392	-1.809025	1.304179	C	3.415855	-0.978506	1.336408
C	3.612189	-1.191579	0.567040	H	3.900840	-1.339416	2.238218
H	4.140352	-1.926040	1.164006	C	-0.067020	-0.078979	0.090042
C	4.301632	-0.298526	-0.260490	C	-2.243208	-1.437803	-0.010745
C	3.584279	0.654324	-1.000453	C	-2.675869	-2.778398	-0.065818
H	4.133599	1.339147	-1.639175	H	-1.916293	-3.555535	-0.032837
C	2.200638	0.707769	-0.911881	C	-4.018478	-3.135474	-0.159785
H	1.657710	1.448564	-1.491694	H	-4.303813	-4.182462	-0.197422
C	-0.642150	1.168277	0.140386	C	-4.983496	-2.128815	-0.206053
C	0.004280	2.169070	0.892182	H	-6.039023	-2.374312	-0.280631
C	-0.580578	3.414407	1.109509	C	-4.587733	-0.792618	-0.155321
H	-0.053653	4.162226	1.695297	H	-5.316492	0.010983	-0.186613
C	-1.838593	3.698170	0.570594	C	-3.238305	-0.445759	-0.056823
C	-2.504827	2.723436	-0.172132	C	-1.926507	1.705872	0.010653
H	-3.479108	2.911325	-0.612248	C	-2.281676	3.057602	-0.021962
C	-1.911353	1.479886	-0.378351	H	-3.339588	3.293713	-0.073852

## 7. Appendix

C	-2.672059	-2.696372	0.495071	C	-1.320804	4.064515	0.023269
H	-1.984200	-3.452934	0.865232	C	0.024050	3.712763	0.109589
C	-4.046404	-2.915290	0.560229	H	0.798461	4.472304	0.160579
H	-4.427900	-3.840870	0.981907	C	0.373251	2.364815	0.132978
C	-4.929797	-1.945414	0.075774	C	-0.568883	1.315035	0.070980
H	-6.002678	-2.111604	0.113647	C	6.375043	-0.773838	-0.794202
C	-4.428557	-0.763694	-0.473837	H	6.351031	0.278630	-1.105978
H	-5.087216	-0.002816	-0.880746	H	6.087425	-1.412571	-1.639569
C	6.433302	-1.219380	0.310252	H	7.383220	-1.033929	-0.468114
H	7.471429	-1.023592	0.037776	C	-0.803707	-1.211614	0.067778
H	6.166560	-2.245634	0.025895	H	-0.231751	-2.136648	0.080741
H	6.309414	-1.095511	1.394061	O	-3.055057	0.913314	0.009863
H	-2.297600	4.670795	0.724171	H	-1.627911	5.106228	-0.000886
H	0.982347	1.954251	1.310162	H	1.420963	2.102678	0.207368

**Table S42:** Atomic coordinates (x, y, z) for optimized minimum and transition state of **203a** at the B3LYP-D3(BJ)/6-31+g(d) level of theory.

Minimum				TS			
Atom	x	y	z	Atom	x	y	z
C	-0.675669	1.871853	0.648554	C	-0.674271	-1.888415	-0.000042
C	1.607663	0.842417	0.181611	C	1.703399	-0.847856	-0.000019
C	2.805152	1.266695	-0.427041	C	3.034899	-1.316205	-0.000029
H	2.995330	2.333776	-0.513656	H	3.193353	-2.391666	-0.000053
C	3.734636	0.357215	-0.924466	C	4.137395	-0.467787	-0.000010
H	4.648161	0.716572	-1.389920	H	5.142864	-0.877862	-0.000019
C	3.487495	-1.014387	-0.821223	C	3.926215	0.910455	0.000020
H	4.206226	-1.733788	-1.203644	H	4.763384	1.602599	0.000036
C	2.312925	-1.459874	-0.214347	C	2.623237	1.405005	0.000031
H	2.112340	-2.522687	-0.118723	H	2.461893	2.480159	0.000055
C	1.384116	-0.546408	0.297779	C	1.511297	0.548805	0.000012
C	-1.384104	-0.546281	0.297742	C	-1.511297	0.548805	0.000012
C	-2.313286	-1.459692	-0.213687	C	-2.623237	1.405005	0.000031
H	-2.112999	-2.522525	-0.117636	H	-2.461893	2.480159	0.000055
C	-3.487901	-1.014204	-0.820543	C	-3.926215	0.910455	0.000020
C	-3.734649	0.357382	-0.924510	C	-4.137395	-0.467787	-0.000011
H	-4.648157	0.716753	-1.389987	H	-5.142864	-0.877862	-0.000020
C	-2.804814	1.266856	-0.427724	C	-3.034899	-1.316205	-0.000029
C	-1.607347	0.842678	0.181014	C	-1.703399	-0.847856	-0.000019
C	0.676018	1.871638	0.649396	C	0.674271	-1.888415	-0.000042
H	1.154029	2.806151	0.940368	H	1.110559	-2.885618	-0.000064
S	-0.000065	-1.188530	1.229775	H	-4.763384	1.602599	0.000035
H	-4.206900	-1.733617	-1.202440	H	-3.193353	-2.391666	-0.000053
H	-2.994712	2.333943	-0.514888	H	-1.110559	-2.885618	-0.000064
H	-1.153690	2.806558	0.938794	S	0.000000	1.501048	0.000033

## 7.3 Atomic coordinates for DFT calculations

**Table S43:** Atomic coordinates (x, y, z) for optimized minimum and transition state of **203b** at the B3LYP-D3(BJ)/6-31+g(d) level of theory.

Minimum				TS			
Atom	x	y	z	Atom	x	y	z
C	-0.722007	1.708763	0.329291	C	-0.599168	1.994401	-0.004253
C	0.359299	1.034637	-0.274221	C	0.571499	1.201199	-0.040516
C	1.152299	1.756197	-1.188533	C	1.799295	1.901725	-0.095216
C	0.888786	3.088934	-1.490967	C	1.893149	3.289894	-0.093594
H	1.518866	3.614879	-2.202884	H	2.868778	3.764756	-0.137652
C	-0.182234	3.744584	-0.877223	C	0.727936	4.048904	-0.032475
C	-0.987655	3.049817	0.023257	C	-0.500217	3.395548	0.009596
H	-1.829992	3.540109	0.501630	H	-1.413091	3.984872	0.048129
C	0.698217	-0.385504	-0.014580	C	0.644494	-0.280502	-0.025915
C	-0.199028	-1.399671	0.062372	C	-0.323125	-1.229731	-0.021454
H	0.213883	-2.400702	0.176429	H	0.083066	-2.238760	-0.009072
C	-1.658817	-1.368118	-0.056886	C	-1.785632	-1.271847	-0.007273
C	-2.297244	-2.416258	-0.748079	C	-2.343909	-2.569344	-0.000165
H	-1.684848	-3.199200	-1.189056	H	-1.661526	-3.415231	-0.016738
C	-3.682339	-2.463889	-0.881010	C	-3.714615	-2.803897	0.028064
H	-4.145982	-3.282920	-1.423846	H	-4.094585	-3.821131	0.030774
C	-4.471109	-1.458899	-0.312978	C	-4.585225	-1.714460	0.055953
H	-5.552999	-1.489136	-0.407794	H	-5.661167	-1.861569	0.081660
C	-3.862748	-0.416070	0.385567	C	-4.065703	-0.421628	0.052293
H	-4.462508	0.367932	0.837967	H	-4.744474	0.427322	0.075216
C	-2.470929	-0.372177	0.525176	C	-2.682256	-0.188163	0.017738
C	2.149848	-0.709551	0.082353	C	2.032466	-0.866477	-0.001128
C	2.996401	0.087651	0.871623	C	2.738631	-0.973748	1.205157
H	2.582682	0.947997	1.389717	H	2.284000	-0.603364	2.120379
C	4.349099	-0.222474	1.006137	C	4.010426	-1.548764	1.235580
H	4.984115	0.399235	1.631754	H	4.543102	-1.630534	2.179460
C	4.887220	-1.328305	0.340838	C	4.595457	-2.021347	0.056755
C	4.059914	-2.119459	-0.459770	C	3.899003	-1.917986	-1.149541
H	4.471296	-2.971532	-0.994602	H	4.344987	-2.284870	-2.070316
C	2.704307	-1.811351	-0.588279	C	2.624814	-1.343726	-1.176800
H	2.071956	-2.415446	-1.232986	H	2.082087	-1.260145	-2.114756
H	5.942767	-1.566349	0.440170	H	0.762994	5.134555	-0.021755
H	1.988000	1.252592	-1.664309	H	2.716016	1.329251	-0.141426
H	-0.392080	4.786926	-1.100941	H	5.585598	-2.468498	0.079689
S	-1.748302	0.901405	1.552139	S	-2.332481	1.553940	-0.011277

**Table S 44:** Atomic coordinates (x, y, z) for optimized minimum and transition state of **203c** at the B3LYP-D3(BJ)/6-31+g(d) level of theory.

Minimum				TS			
Atom	x	y	z	Atom	x	y	z
O	5.743083	-0.298702	0.463451	O	5.648565	-0.847318	0.442206
C	4.389082	-0.329289	0.288662	C	4.308324	-0.652164	0.256448
C	3.710071	-1.274894	-0.487774	C	3.634523	-0.869502	-0.949453

## 7. Appendix

H	4.244993	-2.053056	-1.019803	H	4.159087	-1.216732	-1.832075
C	2.317511	-1.206863	-0.595614	C	2.255094	-0.635382	-1.020315
H	1.804548	-1.931292	-1.222112	H	1.735989	-0.803423	-1.960321
C	1.575742	-0.215282	0.056711	C	1.532322	-0.186874	0.086036
C	2.283237	0.735768	0.818235	C	2.228237	0.027149	1.288531
H	1.734056	1.521228	1.329091	H	1.684607	0.377014	2.162237
C	3.663996	0.679869	0.941124	C	3.595082	-0.203001	1.378886
H	4.205022	1.405932	1.540094	H	4.132285	-0.046003	2.309251
C	0.090694	-0.160014	-0.022976	C	0.043270	0.017865	0.007291
C	-2.054049	-1.547281	-0.050982	C	-2.050524	-1.568183	0.005332
C	-2.498976	-2.693355	-0.738589	C	-2.253759	-2.965864	0.035226
H	-1.758703	-3.355072	-1.182128	H	-1.375239	-3.605774	0.048896
C	-3.853927	-2.987381	-0.865429	C	-3.517017	-3.547750	0.049640
H	-4.166277	-3.876787	-1.405761	H	-3.620095	-4.628573	0.070284
C	-4.807140	-2.138083	-0.295256	C	-4.640947	-2.721617	0.042447
H	-5.866735	-2.360482	-0.385878	H	-5.642193	-3.142611	0.058262
C	-4.391221	-1.002595	0.399900	C	-4.474283	-1.338572	0.017239
H	-5.119054	-0.337046	0.854208	H	-5.350090	-0.694413	0.013697
C	-3.028809	-0.711918	0.534237	C	-3.198209	-0.754783	-0.006254
C	-1.680833	1.646910	0.329166	C	-1.751229	1.891655	-0.041677
C	-2.183690	2.918825	0.025304	C	-2.020113	3.270484	-0.049653
H	-3.095752	3.251875	0.511148	H	-3.055155	3.602445	-0.024698
C	-1.523242	3.744468	-0.882584	C	-1.003960	4.220132	-0.100630
C	-0.358503	3.288505	-1.506356	C	0.318484	3.788871	-0.151416
H	0.161337	3.916633	-2.224511	H	1.137402	4.499953	-0.207245
C	0.141059	2.024780	-1.205487	C	0.588599	2.424165	-0.125705
C	-0.501657	1.175077	-0.283292	C	-0.414257	1.429179	-0.052967
C	6.524895	-1.303807	-0.166455	C	6.418953	-1.301436	-0.661209
H	6.426581	-1.257787	-1.258957	H	6.385354	-0.584277	-1.491896
H	6.242807	-2.304846	0.185009	H	6.072787	-2.282857	-1.011110
H	7.558316	-1.096241	0.115034	H	7.442962	-1.386028	-0.294259
C	-0.611917	-1.317519	0.064188	C	-0.648859	-1.148542	0.019099
H	-0.026861	-2.228283	0.182019	H	0.002926	-2.017195	0.077289
S	-2.539649	0.670626	1.557937	H	-1.252335	5.277631	-0.107226
H	-1.917412	4.732456	-1.104246	H	1.622281	2.107851	-0.164185
H	1.048922	1.676838	-1.688199	S	-3.310467	1.016660	-0.084120

**Table S45:** Atomic coordinates (x, y, z) for optimized minimum and transition state of **204a** at the B3LYP-D3(BJ)/6-31+g(d) level of theory.

Minimum				TS			
Atom	x	y	z	Atom	x	y	z
C	-0.677393	1.922728	0.442980	C	-0.673963	1.846645	-0.000167
C	1.579721	0.805143	0.163511	C	1.649819	0.760139	-0.000028
C	2.813867	1.077611	-0.457857	C	3.005388	1.163982	0.000081
H	3.072849	2.110274	-0.680102	H	3.221306	2.229599	0.000104
C	3.686579	0.053192	-0.813618	C	4.056648	0.256980	0.000153



## 7.3 Atomic coordinates for DFT calculations

H	4.628593	0.286741	-1.302171	H	5.084386	0.609066	0.000242
C	3.343240	-1.274263	-0.539589	C	3.768161	-1.109265	0.000097
H	4.017382	-2.082481	-0.809935	H	4.566885	-1.845894	0.000135
C	2.138340	-1.556220	0.105434	C	2.438067	-1.522250	-0.000007
H	1.882338	-2.585487	0.346335	H	2.218058	-2.588314	-0.000044
C	1.257669	-0.534876	0.475724	C	1.361548	-0.620705	-0.000062
C	-0.000025	-0.839401	1.253747	C	0.000002	-1.303933	-0.000109
H	-0.000085	-0.234961	2.173169	H	-0.000013	-1.979213	0.867468
H	-0.000025	-1.891325	1.556880	H	0.000007	-1.979233	-0.867670
C	-1.257726	-0.534856	0.475715	C	-1.361540	-0.620695	-0.000102
C	-2.138654	-1.556079	0.105845	C	-2.438053	-1.522246	-0.000098
H	-1.882863	-2.585335	0.347026	H	-2.218038	-2.588308	-0.000192
C	-3.343552	-1.274053	-0.539176	C	-3.768152	-1.109275	0.000042
C	-3.686550	0.053378	-0.813691	C	-4.056649	0.256969	0.000195
H	-4.628520	0.286964	-1.302312	H	-5.084388	0.609051	0.000327
C	-2.813590	1.077708	-0.458304	C	-3.005393	1.163972	0.000163
C	-1.579508	0.805226	0.163204	C	-1.649819	0.760140	0.000001
C	0.677636	1.922694	0.443359	C	0.673938	1.846650	-0.000162
H	1.165211	2.889911	0.559133	H	1.133830	2.833464	-0.000322
H	-4.017926	-2.082190	-0.809182	H	-4.566869	-1.845912	0.000036
H	-3.072305	2.110354	-0.680932	H	-3.221321	2.229588	0.000246
H	-1.164981	2.889946	0.558392	H	-1.133858	2.833453	-0.000317

**Table S46:** Atomic coordinates (x, y, z) for optimized minimum and transition state of **204b** at the B3LYP-D3(BJ)/6-31+g(d) level of theory.

Minimum				TS			
Atom	x	y	z	Atom	x	y	z
C	-4.833179	-1.254166	0.226085	C	-4.513135	-1.935295	0.081746
C	-3.983476	-2.015336	-0.580058	C	-3.961455	-1.354286	1.228151
H	-4.381858	-2.838109	-1.168056	H	-4.525452	-1.340010	2.157233
C	-2.621707	-1.714400	-0.645789	C	-2.683817	-0.794567	1.184721
H	-1.971093	-2.294241	-1.294513	H	-2.255937	-0.341186	2.075145
C	-2.081937	-0.650265	0.094284	C	-1.934994	-0.810586	-0.001473
C	-2.951066	0.117267	0.888710	C	-2.495376	-1.396043	-1.143734
H	-2.550522	0.951278	1.457950	H	-1.921711	-1.408148	-2.066766
C	-4.310417	-0.185067	0.960180	C	-3.776329	-1.954974	-1.104246
H	-4.962838	0.414409	1.589707	H	-4.196177	-2.405005	-2.000165
C	-0.624490	-0.340073	0.062560	C	-0.540533	-0.249391	-0.035297
C	0.260413	-1.371254	0.128732	C	1.887416	-1.157671	-0.007033
C	1.720678	-1.330175	0.055190	C	2.520172	-2.423650	0.007594
C	2.477425	-0.282934	0.625094	H	1.891786	-3.310534	-0.014221
C	3.869531	-0.288621	0.495544	C	3.900166	-2.568019	0.051571
H	4.443966	0.523914	0.934662	H	4.347035	-3.558198	0.060654
C	4.527317	-1.327348	-0.164426	C	4.698812	-1.422509	0.087841
H	5.610678	-1.318716	-0.248207	H	5.781803	-1.501398	0.126287
C	3.786778	-2.388077	-0.696114	C	4.089847	-0.170242	0.074735

## 7. Appendix

H	4.289533	-3.209181	-1.199827	H	4.714062	0.721134	0.101253
C	2.399796	-2.389558	-0.576798	C	2.696411	-0.006983	0.024542
H	1.821196	-3.210987	-0.993272	C	2.244329	1.440294	-0.012030
C	1.761619	0.801488	1.392747	H	2.715833	1.881575	-0.902406
H	2.487436	1.436471	1.910566	H	2.741645	1.939040	0.831249
H	1.123328	0.335556	2.157416	C	0.806336	1.948268	-0.014909
C	0.908478	1.639103	0.472309	C	0.749140	3.352311	-0.009143
C	-0.239907	1.077683	-0.127747	H	1.687787	3.901795	0.032224
C	-1.025131	1.891573	-0.968075	C	-0.443334	4.066208	-0.064830
C	-0.677133	3.213808	-1.228078	C	-1.642665	3.359577	-0.138038
C	0.467141	3.759654	-0.639146	H	-2.594812	3.879362	-0.197953
H	0.744352	4.793064	-0.829245	C	-1.611486	1.971220	-0.133215
C	1.248370	2.969970	0.202974	C	-0.409200	1.224610	-0.057070
H	2.134938	3.390799	0.671710	C	0.429003	-1.195466	-0.028986
H	-0.163548	-2.372608	0.185600	H	0.049195	-2.215049	-0.011036
H	-5.893560	-1.486151	0.276423	H	-0.431540	5.152711	-0.058818
H	-1.911260	1.469310	-1.431336	H	-2.550887	1.437303	-0.192814
H	-1.295351	3.815572	-1.888653	H	-5.508468	-2.370238	0.114744

**Table S47:** Atomic coordinates (x, y, z) for optimized minimum and transition state of **204c** at the B3LYP-D3(BJ)/6-31+g(d) level of theory.

Minimum				TS			
Atom	x	y	z	Atom	x	y	z
O	5.648621	-0.278732	0.391941	O	5.484941	-1.082319	0.325029
C	4.289493	-0.304023	0.256142	C	4.153715	-0.796012	0.195045
C	3.587440	-1.220429	-0.534442	C	3.548895	-0.360749	-0.990795
H	4.106098	-1.977715	-1.110938	H	4.124917	-0.229498	-1.899566
C	2.192152	-1.149700	-0.598148	C	2.176110	-0.095072	-1.006770
H	1.660306	-1.850655	-1.235455	H	1.713472	0.244447	-1.929966
C	1.469291	-0.184533	0.112633	C	1.385213	-0.257116	0.134631
C	2.200039	0.737681	0.887455	C	2.010448	-0.695588	1.312184
H	1.666871	1.505271	1.440934	H	1.414135	-0.825011	2.211480
C	3.584148	0.679059	0.967100	C	3.375804	-0.962541	1.348463
H	4.142794	1.383808	1.575388	H	3.859151	-1.301186	2.259817
C	-0.017709	-0.131714	0.077089	C	-0.097117	-0.013084	0.094619
C	-2.160596	-1.507173	0.065494	C	-2.269074	-1.427883	-0.000608
C	-2.644368	-2.672046	-0.560702	C	-2.610773	-2.801469	-0.007326
H	-1.930784	-3.386279	-0.965352	H	-1.805941	-3.529522	0.056777
C	-4.010294	-2.908268	-0.689441	C	-3.923685	-3.244010	-0.094556
H	-4.361338	-3.807414	-1.188567	H	-4.143882	-4.307875	-0.095496
C	-4.925561	-1.984853	-0.173734	C	-4.950446	-2.301067	-0.184292
H	-5.993807	-2.161686	-0.265301	H	-5.988152	-2.614842	-0.257228
C	-4.459806	-0.843680	0.480520	C	-4.629051	-0.946135	-0.179718
H	-5.167889	-0.137041	0.907582	H	-5.430551	-0.212711	-0.247903
C	-3.090140	-0.600008	0.619935	C	-3.307306	-0.482301	-0.086356
C	-2.575378	0.596505	1.382005	C	-3.181943	1.028953	-0.068989

## 7.3 Atomic coordinates for DFT calculations

H	-1.871918	0.252020	2.153837	H	-3.772999	1.371248	0.793187
H	-3.402296	1.102682	1.890166	H	-3.741754	1.393959	-0.941151
C	-1.871301	1.559397	0.458158	C	-1.889553	1.837764	-0.027528
C	-2.432241	2.809909	0.173852	C	-2.139066	3.220182	-0.066382
H	-3.380370	3.077248	0.634758	H	-3.172344	3.550576	-0.155501
C	-1.793050	3.713754	-0.673367	C	-1.133993	4.178277	0.014896
C	-0.569405	3.365817	-1.252677	C	0.186167	3.751657	0.149816
H	-0.059500	4.058090	-1.917133	H	0.999155	4.467711	0.232245
C	-0.001819	2.125121	-0.977374	C	0.457915	2.390040	0.178441
C	-0.640275	1.196761	-0.131443	C	-0.548445	1.397230	0.076796
C	6.410835	-1.256295	-0.301707	C	6.318515	-0.927424	-0.814013
H	6.278262	-1.166995	-1.387913	H	6.320563	0.112057	-1.167792
H	6.140559	-2.271227	0.017916	H	6.004686	-1.590736	-1.630767
H	7.452532	-1.058345	-0.044700	H	7.322596	-1.202585	-0.487386
C	-0.715568	-1.297741	0.152554	C	-0.839159	-1.146618	0.072567
H	-0.127899	-2.211453	0.227453	H	-0.247031	-2.059358	0.090545
H	-2.241732	4.682770	-0.874898	H	-1.381733	5.235743	-0.018611
H	0.945822	1.855530	-1.432721	H	1.487156	2.073923	0.286333

**Table S48:** Atomic coordinates (x, y, z) for optimized minimum and transition state of **205a** at the B3LYP-D3(BJ)/6-31+g(d) level of theory.

Minimum				TS			
Atom	x	y	z	Atom	x	y	z
Si	0.000020	1.243559	0.534287	Si	0.000000	-1.218126	-0.000001
C	1.506496	0.311200	-0.081881	C	1.591666	-0.220642	-0.000001
C	1.671735	-1.068455	0.200784	C	1.744516	1.187696	-0.000001
C	2.874524	-1.703316	-0.173064	C	3.054145	1.723996	0.000000
C	3.873968	-1.020675	-0.859544	C	4.186212	0.918688	0.000002
H	4.785376	-1.538364	-1.146866	H	5.174723	1.370166	0.000002
C	3.698393	0.329323	-1.174568	C	4.038915	-0.469778	0.000002
C	2.527777	0.977909	-0.779328	C	2.755263	-1.013486	0.000001
H	2.414063	2.034193	-1.009522	H	2.659926	-2.097576	0.000002
C	0.677688	-1.914312	0.874895	C	0.677999	2.191297	-0.000001
C	-0.677780	-1.914253	0.875056	C	-0.677999	2.191297	-0.000002
H	-1.125855	-2.758729	1.398661	H	-1.090853	3.199377	-0.000002
C	-1.671814	-1.068401	0.200898	C	-1.744516	1.187696	-0.000001
C	-2.874604	-1.703248	-0.172950	C	-3.054145	1.723996	0.000000
H	-3.010095	-2.756025	0.064611	H	-3.173590	2.804770	0.000000
C	-3.873970	-1.020622	-0.859569	C	-4.186212	0.918688	0.000001
H	-4.785377	-1.538300	-1.146914	H	-5.174723	1.370166	0.000002
C	-3.698295	0.329336	-1.174706	C	-4.038915	-0.469778	0.000002
H	-4.471987	0.874573	-1.708956	H	-4.909774	-1.119786	0.000004
C	-2.527684	0.977909	-0.779424	C	-2.755263	-1.013486	0.000001
H	-2.413933	2.034169	-1.009699	H	-2.659926	-2.097576	0.000002
C	-1.506489	0.311211	-0.081823	C	-1.591666	-0.220642	-0.000001
C	-0.000006	3.003179	-0.146866	C	0.000000	-2.317340	1.540206

## 7. Appendix

H	0.000213	3.026266	-1.242961	H	0.000000	-1.705737	2.450199
H	0.881815	3.553692	0.202641	H	0.885673	-2.963457	1.571072
H	-0.882109	3.553484	0.202269	H	-0.885674	-2.963456	1.571072
C	0.000015	1.304421	2.420646	C	0.000000	-2.317342	-1.540207
H	-0.888572	1.830412	2.791294	H	-0.885673	-2.963458	-1.571072
H	0.888094	1.831212	2.791370	H	0.885673	-2.963459	-1.571071
H	0.000442	0.296750	2.848608	H	0.000001	-1.705741	-2.450202
H	4.472173	0.874562	-1.708688	H	4.909774	-1.119786	0.000003
H	3.009948	-2.756121	0.064409	H	3.173590	2.804770	0.000000
H	1.125793	-2.758838	1.398393	H	1.090854	3.199377	-0.000002

**Table S49:** Atomic coordinates (x, y, z) for optimized minimum and transition state of **205b** at the B3LYP-D3(BJ)/6-31+g(d) level of theory.

Minimum				TS			
Atom	x	y	z	Atom	x	y	z
Si	-1.754883	0.857994	1.065420	Si	2.271581	0.981953	0.000005
C	-0.560649	1.661429	-0.138867	C	0.561854	1.760982	-0.000004
C	0.560646	0.948703	-0.626710	C	-0.726936	1.162407	0.000000
C	1.413272	1.569758	-1.561018	C	-1.850562	2.027002	0.000005
C	1.161375	2.856561	-2.027625	C	-1.733366	3.412190	0.000002
H	1.828587	3.306418	-2.758187	H	-2.630282	4.025912	0.000005
C	0.054719	3.563965	-1.550978	C	-0.469620	3.998585	-0.000006
C	-0.790022	2.963310	-0.618480	C	0.647772	3.167246	-0.000008
H	-1.647221	3.522676	-0.252442	H	1.629049	3.637465	-0.000013
C	0.915538	-0.433111	-0.200284	C	-1.014893	-0.293365	0.000000
C	0.077442	-1.494513	-0.076674	C	-0.224530	-1.404226	-0.000002
H	0.561774	-2.434964	0.184245	H	-0.823507	-2.312859	-0.000002
C	-1.373209	-1.634703	-0.277636	C	1.197362	-1.760027	-0.000004
C	-1.819189	-2.823007	-0.889500	C	1.440156	-3.155811	-0.000009
H	-1.085678	-3.561022	-1.206864	H	0.589276	-3.832522	-0.000011
C	-3.173229	-3.056640	-1.112660	C	2.723910	-3.685966	-0.000011
H	-3.491789	-3.973823	-1.601147	H	2.866187	-4.763353	-0.000015
C	-4.117182	-2.110655	-0.702806	C	3.822892	-2.823959	-0.000008
H	-5.177178	-2.286007	-0.867168	H	4.836030	-3.216972	-0.000009
C	-3.688651	-0.946676	-0.063669	C	3.600893	-1.448212	-0.000003
H	-4.433106	-0.227872	0.269914	H	4.466490	-0.788601	-0.000001
C	-2.327808	-0.688334	0.169549	C	2.309748	-0.887520	-0.000002
C	2.366425	-0.668058	0.065969	C	-2.480614	-0.658250	0.000000
C	3.091267	0.245132	0.850963	C	-3.168082	-0.845550	-1.206058
H	2.589615	1.129314	1.233615	H	-2.639716	-0.699913	-2.144792
C	4.435715	0.024206	1.147826	C	-4.516119	-1.212536	-1.207878
H	4.974208	0.736825	1.767144	H	-5.034693	-1.357129	-2.152174
C	5.089491	-1.107464	0.650974	C	-5.194759	-1.395829	0.000000
C	4.385550	-2.013758	-0.145624	C	-4.516109	-1.212572	1.207878
H	4.888384	-2.887417	-0.552240	H	-5.034676	-1.357194	2.152173
C	3.037441	-1.794680	-0.435424	C	-3.168072	-0.845587	1.206059

## 7.3 Atomic coordinates for DFT calculations

H	2.502458	-2.490576	-1.075753	H	-2.639699	-0.699978	2.144792
C	-3.220630	1.999555	1.393285	C	3.192357	1.582890	1.540477
H	-3.753451	2.268648	0.473886	H	2.677652	1.251870	2.450275
H	-2.891242	2.927626	1.876306	H	3.258801	2.676869	1.572560
H	-3.938471	1.519855	2.069915	H	4.214186	1.185368	1.571193
C	-0.916514	0.443495	2.704765	C	3.192383	1.582900	-1.540449
H	-1.614492	-0.073851	3.374721	H	4.214209	1.185372	-1.571154
H	-0.584315	1.361024	3.206720	H	3.258834	2.676879	-1.572520
H	-0.043400	-0.200548	2.562989	H	2.677688	1.251891	-2.450257
H	6.139169	-1.276169	0.875618	H	-0.352951	5.079026	-0.000009
H	2.279129	1.027368	-1.928735	H	-2.845793	1.603403	0.000011
H	-0.145412	4.573498	-1.900677	H	-6.243215	-1.681624	0.000000

**Table S50:** Atomic coordinates (x, y, z) for optimized minimum and transition state of **205c** at the B3LYP-D3(BJ)/6-31+g(d) level of theory.

Minimum				TS			
Atom	x	y	z	Atom	x	y	z
Si	-2.444388	0.633428	1.121169	Si	-3.026196	0.701494	-0.078083
O	5.939309	-0.168523	0.664909	O	6.067142	-0.672646	0.375263
C	-1.438225	1.630934	-0.109606	C	-1.454112	1.727854	-0.012626
C	-0.243285	1.106366	-0.657922	C	-0.090930	1.329420	0.040288
C	0.462630	1.865906	-1.612095	C	0.889091	2.353645	0.066954
C	-0.002927	3.105902	-2.039549	C	0.565466	3.705461	0.047030
H	0.555446	3.664334	-2.786356	H	1.359623	4.447071	0.070335
C	-1.182716	3.627631	-1.502717	C	-0.771099	4.095299	-0.002974
C	-1.884416	2.889601	-0.550417	C	-1.750133	3.105234	-0.032448
H	-2.800254	3.304922	-0.137524	H	-2.790154	3.422516	-0.073617
C	0.337833	-0.210569	-0.275013	C	0.413835	-0.066652	0.069275
C	-0.325680	-1.388530	-0.141279	C	-0.203804	-1.282515	0.063354
H	0.304543	-2.247882	0.085739	H	0.523367	-2.091308	0.096259
C	-1.744737	-1.744894	-0.295871	C	-1.556338	-1.846973	0.031358
C	-2.030041	-2.975524	-0.920173	C	-1.588114	-3.263171	0.060186
H	-1.206472	-3.586607	-1.283248	H	-0.646167	-3.804332	0.102872
C	-3.340834	-3.409187	-1.098045	C	-2.777548	-3.979918	0.036559
H	-3.535862	-4.355032	-1.596839	H	-2.757185	-5.066234	0.060460
C	-4.400443	-2.626509	-0.630291	C	-3.992456	-3.292948	-0.018117
H	-5.427270	-2.958674	-0.759460	H	-4.934959	-3.833543	-0.037988
C	-4.127920	-1.422812	0.020661	C	-3.978479	-1.899805	-0.046941
H	-4.958578	-0.832215	0.399440	H	-4.932437	-1.377771	-0.089971
C	-2.813632	-0.964707	0.209938	C	-2.786169	-1.151844	-0.023387
C	1.816249	-0.222458	-0.077399	C	1.916109	-0.206419	0.120716
C	2.438232	0.788115	0.681981	C	2.594620	-0.242176	1.349279
H	1.832456	1.588411	1.096925	H	2.027940	-0.143504	2.271558
C	3.805537	0.776930	0.918577	C	3.975190	-0.399195	1.405155
H	4.279252	1.550375	1.515369	H	4.500472	-0.431075	2.354888
C	4.604333	-0.245626	0.384298	C	4.716044	-0.523428	0.220848

## 7. Appendix

C	4.012574	-1.249760	-0.389851	C	4.057860	-0.491261	-1.013474
H	4.606833	-2.040122	-0.833744	H	4.604275	-0.589238	-1.944464
C	2.631837	-1.226446	-0.611618	C	2.667063	-0.333097	-1.048987
H	2.187748	-1.997953	-1.234564	H	2.160825	-0.305779	-2.010578
C	-4.051084	1.532364	1.534188	C	-3.939308	1.123351	-1.681338
H	-4.658209	1.732131	0.643612	H	-3.331105	0.854161	-2.553067
H	-3.845866	2.491749	2.024737	H	-4.166255	2.194025	-1.748831
H	-4.657591	0.937405	2.228061	H	-4.886715	0.575082	-1.752453
C	-1.484890	0.322552	2.716529	C	-4.111351	1.190227	1.393819
H	-2.067782	-0.306627	3.400706	H	-5.061705	0.642794	1.384451
H	-1.274534	1.271014	3.226777	H	-4.344377	2.261563	1.389583
H	-0.531280	-0.178532	2.524973	H	-3.603649	0.961731	2.338412
C	6.792591	-1.181048	0.151013	C	6.864691	-0.798877	-0.792670
H	6.508726	-2.171019	0.531476	H	6.584772	-1.688579	-1.372066
H	7.795395	-0.930170	0.500080	H	7.892593	-0.901945	-0.441432
H	6.779359	-1.193219	-0.946770	H	6.782670	0.092134	-1.429134
H	-1.549474	4.600089	-1.821151	H	-1.048626	5.145881	-0.019668
H	1.384458	1.468428	-2.025915	H	1.935663	2.083338	0.104359